Reducing Energy Demand and CO_2 Emissions from Industrial Ceramic Manufacture using Novel Raw Materials and Additives

GLORIA WIE-ADDO

A thesis submitted in partial fulfilment of the requirements of
Sheffield Hallam University
for the degree of Doctor of Philosophy

October 2022

"The production of ceramic products is not possible without the consumption of raw materials and energy and the associated CO_2 emissions."

Vogl, "Ceramic roadmap 2050 - Whitewares' contribution,2013

Declaration

I hereby declare that:

1. I have not been enrolled for another award from the University, or other academic or professional organisation, whilst undertaking my research degree.
2. None of the material contained in the thesis has been used in any other submission for an academic award.
3. I am aware of and understand the University's policy on plagiarism and certify that this thesis is my work. The use of all published or other sources of material consulted has been properly and fully acknowledged.
4. The work undertaken towards the thesis has been conducted following the SHU Principles of Integrity in Research and the SHU Research Ethics Policy.
5. The word count of the thesis is 83,046.

Name	GLORIA WIE- ADDO
Date	October 2022
Award	PhD: Reducing Energy Demand and CO_2 Emissions from Industrial Ceramic Manufacture using Novel Raw Materials and Additives
Faculty	College of Business Technology and Engineering
Director(s) of Studies	Professor Paul. A. Bingham Dr Alan Hywel Jones
Industrial Supervisors	John Renshaw and Stephanie Palmer

Acknowledgement

I am grateful to God Almighty for the successful completion of this work.

I express my profound gratitude to Wienerberger Ltd for Co-sponsoring my Education with the Sheffield Hallam VC- Scholarship.

I am sincerely grateful to my supervisors, Prof. Bingham, Dr Hywel Jones, John Renshaw and Stephanie Palmer, for their guidance and constructive criticism, enabling me to complete this study successfully.

I am very thankful to Dr A.M.T Bell, Dr Francis Clegg, Dr Vincenzo Starinieri, Dr Alex Scrimshire and Paul Allender, who gave me proper laboratory training on equipment usage and advice throughout my studies Prof. Elizabeth Laycock, who read my thesis and provided feedback. I am grateful for the Bingham research group (both past and present), the second family I had away from home and shared great memories with and obtained countless support from.

Lastly, but by far the most important, I wish to say a massive thank you to my Family and Friends, especially my Dad, Rev. Kow Agyapanyin Wie-Addo, an Environmentalist and a retired Senior Lecturer in Biology and Science Education from the University of Cape Coast and Dr Anthony Koomson, a chemistry lecturer at the University of Cape Coast for their support, encouragement and gifts of love throughout my PhD journey.

.

Abstract

This study of reducing energy demand and CO_2 emissions from industrial ceramic manufacture using novel raw materials and additives was undertaken to contribute to the industry's requirement to decrease energy inputs and CO_2 emissions and increase material efficiency when manufacturing structural ceramic products whilst maintaining product quality. Weald clay was replaced with additive levels 1-4wt% alkali and alkaline earth carbonates, industrial and inorganic mineral additives and shaped into cylindrical pellets. The admixtures were fired to 850°C, 900°C, 1000°C and 1040°C. Ten characterisation techniques (XRF, XRD, TG/MS, MIP, dilatometry, volumetric shrinkage testing, boiling water absorption testing, compressive strength testing, Mössbauer spectroscopy and Raman spectroscopy) were used to determine the chemistry, microstructure and changes to the resulting ceramics in comparison to a reference standard and existing products.

Mineralogically, the additive K_2CO_3 and Na_2CO_3 admixtures do not promote new firing phases not already present in the Weald clay ceramics fired to 900°C, 1000°C and 1040°C, as opposed to the effects of the other 12 additives studied. Alkali additives, however, promoted stronger bonds on firing, so the mechanical strength obtained for K_2CO_3 doped samples was over 85MPa compared to 81.5MPa for the control sample. Of the industrial waste additives, 2wt% container glass and 4wt% mineral wool were promising candidate for other products with resulting ceramic compressive strengths of 58MPa and ~54MPa, respectively. Only 4wt% wollastonite and talc additions for inorganic additives increased ceramic strength to 72MPa and 60MPa for ceramics fired to 1040°C, respectively. Nepheline syenite and colemanite additives functioned as pore formers, resulting in ceramics with lower compressive strengths of below 50MPa. Technologically, boiling water absorption, strength, mercury intrusion porosity (MIP), pore size, and shrinkage depended on firing temperature, additive type and proportion of additive. Volatiles in all cases were

found to be CO_2, re-absorbed water and chemical water. Pore sizes moved towards larger pores (> 1μm) with increased firing temperature (~1040°C). The alkaline earth additives controlled excessive expansion caused by carbonate decomposition and promoted reduced sintering temperatures of between 4- 41°C. Meanwhile, adding alkali carbonate additives (Li, K) at levels ~ >2wt% caused the clay body to expand again above the quartz transition temperature.

The surface scum observed was found to be $CaSO_4$ on 12 samples except for the samples doped with $BaCO_3$ and greater than 2wt% $MgCO_3$, both of which prevented the formation of the scum (whitish stains) on fired ceramic bodies. Fired ceramics with alkali carbonate additives added at 1wt% (Li, Na, and K) were free from surface scum. Surface defects such as patches and darker rims on ceramic surfaces were noticed in the >2wt% Li, Na, and K carbonate ceramic samples. Changes in fired ceramic colour were found due to differences in iron in the paramagnetic and magnetic iron sites. Iron is present in all admixtures as Fe^{3+} hematite (Fe_2O_3) except for the unfired Weald clay, which contained iron as Fe^{2+} and Fe^{3+}. By firing ceramics at 1000°C and 1040°C, 90°C and 50°C temperature reductions have been obtained compared to industrial firing of bricks at 1090°C. This implies that ceramics fired to 1000°C and 1040°C resulted in reduced energy of 64kWh and 23kWh, respectively. Moreover, the additive 1wt% K_2CO_3 gives better CO_2 savings than 1wt% Li_2CO_3 fired at a lower temperature yet retains the quality of a class B engineering brick. The replaced additives can save about 80,000-320,000 tonnes of clay. It is recommended that direct durability testing is conducted on all samples, but mainly on 2wt% $MgCO_3$, 4wt% Wollastonite, 4wt% Talc, 1wt% K_2CO_3 samples fired to 1040°C and 1wt% Li_2CO_3 samples fired to 1000°C, to validate the modified frost resistance for heavy clay ceramic manufacturers. Pilot-scale testing for dopants to prevent efflorescence and scummingformed on fired ceramic products of $MgCO_3$ as an alternative to $BaCO_3$ is also recommended.

List of Publications and Conferences

1. Janani R, Deng W, Backhouse DJ, Kabir-Kazi F, Wie-Addo G, Jones AH, Jackson CM, Holcroft C, Bingham PA.“Paving the way to net zero by repurposing waste. Glass International”. 2022 Jan 19;45(1):39-43.

2. Wie-Addo. G, A. H. Jones, S. Palmer, A.Scrimshire, J. Renshaw, P. A. Bingham, The Influence Of Mineral Additives On Firing Behaviour And Properties Of Clay Ceramics (POSTER) 14th Pacific Rim Conference on Ceramic and Glass Technology (PACRIM 14) including Glass & Optical Materials Division 2021 Annual Meeting (GOMD 2021) ARCHIVE –

3. Wie-Addo. G, A. H. Jones, S. Palmer, A. Scrimshire, J. Renshaw, P. A. Bingham**.** Effects Of Additives On Heavy Clay Ceramic Materials Examined By Mössbauer Spectroscopy, for a contributed oral presentation Minerals in the Natural and Built Environment A Research in Progress meeting clay mineral conference, Newcastle, UK-2021**.**

4. Wie-Addo.G, A. H. Jones, S. Palmer, ATM Bell, J. Renshaw, P. A. Bingham**.** Recycling Of Waste Mineral Wool And Quarry Wastes In Clay Brick Manufacturing for a contributed oral presentation, 57th Clay Mineral Conference, Newcastle, UK, 2020**.**

5. Wie-Addo. G, A. H. Jones, S. Palmer, V. Starinieri, J. Renshaw, P. A. Bingham, Reformulating Ceramic Body Composition to Improve Energy Efficiency Brick Manufacture. for a contributed oral presentation ICESF Hatfield Hertfordshire /UK/10-11 September 2020 2nd ICESF- The International Conference of Energy and sustainable futures**.**

6. Wie-Addo.G, A. H. Jones, S. Palmer, V. Starinieri, J. Renshaw, P. A. Bingham**.** Reformulating Ceramic Body Composition to Improve Energy Efficiency Brick Manufacture. ICESF Hatfield Hertfordshire /UK/10-11 September 2020 2nd ICESF- The International Conference of Energy and sustainable futures (BOOK CHAPTER)**.**

7. Bell, A.M., Backhouse, D.J., Deng, W., Eales, J.D., Kilinc, E., Love, K., Rautiyal, P., Rigby, J.C., Stone, A.H., Vaishnav, S. and Wie-Addo, G., 2020. X-ray fluorescence analysis of feldspars and silicate glass: effects of melting time on fused bead consistency and volatilisation. Minerals, 10(5), p.442.

Contents

List of Figures

List of Tables

Definition of Terms

B1	1wt% $BaCO_3$
B2	2wt% $BaCO_3$
B3	3wt% $BaCO_3$
B4	4wt% $BaCO_3$
Body	A mixture of two or more compositions
Bone-dry state	Removal of formation water until constantly dried before firing
Brick	Rectangular-shaped clay fired into a dense or hard product for structural applications
BWA	Boiling Water Absorption
C1	1wt% $CaCO_3$
C2	2wt% $CaCO_3$
C2GW	2wt% Container glass
C3	2wt% $CaCO_3$
C4	4wt% $CaCO_3$
C4W	4wt% Colemanite
Clamp Kiln	Temporary kilns produced by setting clay bricks and dismantling them after firing.
Cullet	A waste glass that can be recycled into body compositions
CTE	Coefficient of linear thermal expansion
Dehacking	Packing of fired clay brick
DIL	Dilatometry
DTGA	Derivative of Thermal Analysis
EDS	Elemental Dispersive Spectroscopy

Efflorescence	Flaky or visible salt crystals appear on fired clay products at a later stage when the clay product is exposed to extreme climate conditions.
F4W	4wt% Filter cake
Flux	A substance that lowers the melting temperature of a composition. These are the oxides of the RO group like K_2O, Na_2O, CaO, Li_2O, MgO, and B_2O_3, also known as a glass former.
Heavy Clay Products	e.g., Tiles, clay bricks, table ware, sanitary wares
K1	1wt% K_2CO_3
K2	2wt% K_2CO_3
K3	3wt% K_2CO_3
K4	4wt% K_2CO_3
kWh	Kilowatt-hour (s)
L1	1wt% Li_2CO_3
L2	2wt% Li_2CO_3
L3	3wt% Li_2CO_3
L4	4wt% Li_2CO_3
MO	Mass of oxide
MCO_3	Mass of carbonate
M1	1wt% $MgCO_3$
M2	2wt% $MgCO_3$
M3	3wt% $MgCO_3$
M4	4wt% $MgCO_3$
M4W	4wt% Mineral wool
MIP	Mercury Intrusion Porosimetry
Ms	Mass Spectroscopy

N1	1wt% Na_2CO_3
N2	2wt% Na_2CO_3
N3	3wt% Na_2CO_3
N4	4wt% Na_2CO_3
N4W	4wt% Nepheline Syenite
Plasticity	The ability to deform, shape or draw clay without breaking or cracking
Preheating stage	Gradual removal of physical water from clay product on firing to prevent bloating from water expansion
RMM	Relative molecular mass
S4W	4wt% Slurry dust
Scumming	A whitish stain on a ceramic surface on drying and firing caused by soluble salts.
SEM	Scanning Electron Microscopy
T4W	4wt% Talc
TGA	Thermogravimetry Analysis
W4W	4wt% Wollastonite

Chapter 1 Introduction

Fireproof construction materials were first legislated in the United Kingdom (UK) following the great fire in London in the 16th Century[1,2]. Clay-based bricks can withstand high temperatures, so they have become the material of choice for the building industry. Fired ceramic bricks have high compressive strength and good resistance to natural weathering[3,4] and pollutants[5]. Following the industrial revolution, demand for clay bricks grew from a few hundred tonnes to thousands of tonnes with technological improvements in manufacture [2,6]. High production levels are not without environmental impact, and the manufacture of clay bricks in 2015 emitted 23.3kg CO_2/m^2 brick [7].

The heavy clay ceramic industry uses about 92% more fuel (typically natural gas) in production than the technical, whitewares and refractory sectors due to the high volume of product produced[8]. Four factors should be considered to decarbonise the heavy clay ceramic sector. These are switching to greener fuels, changes in body composition to reduce carbonates and organics in the clay, clay brick weight, kiln efficiency and removal by carbon capture[8–11]. In this present study, the ceramic body modification approach is explored.

There is already evidence in the literature of clay bricks produced at a lower firing temperature by introducing alkaline earth carbonates, feldspars, organic materials, and inorganic materials such as clay minerals, granites and even industrial wastes substituted into virgin clays. Al-Fakih et al. [12], Green[13], Zhang[14], Dondi et al. [15]. and Velasco et.al[16] give the most prominent compilation review. These are also detailed in **Chapter 2, section 2.14** of this study. However, these studies did not consider modifying ceramic recipes for an engineering class B brick with low water absorption of ~7.0% and compressive strength of 75MPa or greater.

1.1 Statement of the problem

While there has been prior research on certain ceramic body modifications, this has not been fully utilised within the heavy clay ceramic industries, which still face the challenges of minimising fuel use and CO_2 emissions. This is because a specified ceramic product has yet to be defined for the appropriate additives to be considered. Secondly, raw materials and their chemical transformations when heat is applied have yet to be entirely understood, particularly when considering wastes from one process as future raw materials for another, whilst the heterogeneity of clays is also a factor.

Hence a choice of 14 unique components with alkali / alkaline earth- primarily based oxides as a sintering aid to assist in acquiring reduced energy and achieve a Class B engineering property due to their early melts between 722- 891°C. These chosen substances are grouped into three series: sequence one composition consists of carbonates of Ca, Ba, Mg, K, Na and Li; sequence two composition components had been industrial wastes of a quarry, mineral wool from a tomato's plantation and waste glass and finally, Series three composition components are inorganic minerals like Nepheline syenite, colemanite, wollastonite and talc.

1.2 Aims and Objectives of the Study

This study prioritises understanding existing clay-based ceramic brick products and changes to their chemistry by laboratory scale material optimization, incorporating 14 different additives to reduce firing times and/or temperatures (energy cost) and thereby reducing CO_2 emissions for ceramic products (i.e., clay-based bricks). Secondly, this project aims to develop a laboratory analogy which allows benchmarking of the formulation at an industrial scale.

Hence this research aims to:

- Understand the raw materials, mineralogy and chemical changes associated with manufacturing "Engineering brick Class B" used for structural applications, with a maximum water absorption limit of 7% and a compressive strength of >75Mpa. This was achieved through physical, thermal, chemical, and mechanical analysis characterisation studies developed laboratory scale products that will benchmark new materials requirements (compositions and fire regimes).

- Reduce fuel use in heavy clay ceramic manufacturing by re-formulating ceramic compositions by introducing substances into the raw clay that promote sintering at lower temperatures while maintaining the ceramic properties and functions. Reduction of fuel use will be made possible with the introduction of inorganic minerals and industrial wastes at up to 4wt% addition levels, fired to just above the clay sintering temperature of 950°C to 1040°C, and substituting 1-4wt% alkali carbonates firing at 850°C -1040°C instead of the range 900°C and 2750°C[17]. These additives could improve the clay drying time from 36 hours to 24 hours or even less, act as fillers, provide adequate density particle packing, and decrease the temperature required to form the required phases and properties while maintaining product quality.

- Achieve reductions in CO_2 emissions from heavy clay ceramic manufacture using the methods described above through the reduction of both time and temperatures required to dry and fire ceramics that could be used to manufacture Engineering Class B bricks.

1.3 Research questions

1 Would the addition of different fluxing additives to Ewhurst Weald clay:

   i. Affect the outcome of the product obtained?

   ii. Change its chemistry and hence affect the product formed?

   iii. Reduce the firing time and also temperature.

   iv. Reduce carbon dioxide emissions?

2 Would mimicking the industrial product by making samples on a laboratory scale serve as a benchmark for all new formulations?

1.4 Significance of the study

This study is relevant to heavy clay ceramic industries, researchers, the UK, and international government(s), and all interested in decarbonising the ceramic sector through material modifications.

The study will enable a proper understanding of the raw materials, mineralogies, and chemical changes to the manufacture of “Engineering brick Class B” used for structural applications. Re-formulating ceramic compositions by introducing substances into the raw clay that promote sintering at lower temperatures and/or times while maintaining the final ceramic properties and functions with lower fuel use, contributing to reductions in carbon dioxide emissions.

1.5 Scope

This study's scope is limited to reforming Wealden clay-based ceramics by introducing additives that decrease firing temperatures/times and help reduce overall process emissions, with the reference being ceramics for Class B Engineering brick properties.

1.6 Limitations

Firing temperature and clay body recipes is one of many companies' trade secrets worldwide. Mimicking the industrial shaping of engineering brick, specifically a Class B brick, with a hydraulic press rated at 7 tonnes pressure instead of an extruder, impacted the fired ceramics' boiling water absorption and mechanical strength. However, the method enabled the shaping of reasonably sized samples of a known weight of 8.34g of clay balls before shaping them into 20mm x 5mm with the hydraulic press. Issues with the hydraulic press included the inability to reach 7 tonnes of pressure and problems in demoulding the shaped samples of varying compositions. These issues were improved by ensuring that all samples (over 600 test pieces) were subjected to a given forming pressure and, for demoulding, used a mould release agent supported with gentle but uniform manual protocols. Small cylindrical-sized samples for compressive strength testing obtained significant uncertainties due to the sample sizes, although all samples were weighed to 8.34g before shaping to obtain the same pressed sample size. The industrial firing temperature for a class B engineering brick produced from Weald clay was initially declared 1050°C by personal communication from John Renshaw, the Group Technical Manager Wienerberger Kingbury factory.

Furthermore, as the study progressed, 1055°C was found to be the firing/sintering temperature of Weald clay (see **Table 1-1**) provided by Nick Mikulski, Laboratory team leader at Wienerberger. However, when developing the estimation for energy and CO_2 models, the thermal profiling system, which recorded the firing of 6336 brick pieces in real-time, was found to be 1090°C. In this study, a firing temperature of 1100°C was used as a reference recommended by the Brick Development Association (BDA). The maximum temperature (~1090°C), as read from the thermal profiling system, was close to that

temperature given by BDA. The Control material was clay without additives, and 2wt% $BaCO_3$ was fired at 1040°C.

Table 1-1: Catalogue of Wienerberger products, especially Ewhurst Weald clay for producing a Class B Engineering brick fired to 1055°C obtained by personal communication from Nick Mikulski, Laboratory team leader Wienerberger, in December 2017.

Factory	Brick Name	Body composition	Firing Temperature	Length of Firing	Moisture content (average)
Sandown	**Class B Engineering**	10% Sandown,40% Campions Wood, 50% Holly Bank	1070°C	33.5hrs	0.7% before firing
Warnham	Red Stock	90% Weald clay, 10% Body Sand	1035°C	64hrs	2% before firing
Ewhurst	**Class B Engineering**	**Weald clay**	**1055°C**	**50hrs**	**15%**

1.7 The organisation of the thesis

The thesis consists of 7 chapters.

- **Chapter 1** gives background information on the relevance and scope of the study.
- **Chapter 2** discusses critical aspects of past and current clay ceramic brick production, focusing on existing research on past clay modification and its effects on ceramic properties. The chapter also reports on energy and CO_2 policies and targets achieved by the heavy clay ceramic sectors.

- **Chapter 3** gives the methodological procedure for process modification and how modified bodies have been analysed.
- **Chapter 4** reports on obtained results and discussions on the base material Weald clay.
- **Chapter 5 – Chapter 7** reports on obtained results and discussions for the 14 additives incorporated into Weald clay for Class B Engineering brick ceramics, subdivided into three topics, namely Series 1-3, using nine analytical techniques.
- **Chapter 8** also contains a detailed evaluation of additive effects and causes of surface stains (efflorescence and scum) on ceramic samples using XRD, Raman spectroscopy and SEM-EDX as the main tools. It also presents Mössbauer spectroscopy used to help explain changes in ceramic colours (brownish red to a darker hue).
- **Chapter 9** reports on industrial products and raw material tests with their discussions.
- **Chapter 10** presents simple energy and CO_2 estimation model on ceramics produced using selected additives based on modified body porosity and mechanical strength.
- **Chapter 11** is the final chapter summarising the study's important findings and providing recommendations for future works.

Chapter 2 Literature Review

This study seeks to understand existing heavy clay ceramics and the changes in their chemistry by laboratory scale material optimization: incorporating 14 different fluxing additives to reduce firing times and temperatures (energy cost) and thereby reduce carbon emissions for construction material, referred to as a ceramic product (i.e., clay brick). Moreover, mimic the industrial product by making laboratory scale samples that will serve as benchmarks for all new formulations; this chapter will consider the following:

- Historic manufacture of masonry bricks and how technology has evolved
- Modern brick manufacture
- Raw materials for brick making
- Clay compositions (what is in clay?)
- Impurities and role of clay minerals and their effect on brick properties
- Clay bricks and types for structural applications
- Emissions and energy use associated with manufacturing heavy clay ceramic products
- Current fuel and emissions reductions within the heavy clay ceramics sector
- Impact of firing techniques and firing atmosphere on energy consumption and mineralogy
- Rate of firing on mineralogy, microstructure and phase transformations in brick manufacture
- Forms and transitions of Fe_2O_3 in clays on thermal treatment
- Clay brick properties
- Additives used in heavy clay ceramic manufacturing and unfired brick products compared with fired clay bricks in terms of energy reduction

2.1 Historic manufacture of masonry bricks and how technology has evolved

In this context, brick refers to prism-shaped clay fired into a dense or hard product for structural applications such as road pavements and building blocks. These materials are highly resistant to climatic changes[17,18]. Historical constructions made from bricks have stood the test of time, for example, Roman bricks, the Great Wall of China, the Kings Bench Walk, the Temple, London built in 1677 and other notable structures across the globe[19,20]. The term "heavy clay products" is used to distinguish from hydrated products[21] (e.g., cement or concrete) and describes clay products such as tiles, facing bricks, common bricks, engineering bricks and sewage pipes used in construction.

These ancient products, now used globally for structural applications, were developed by humans using earth or clay, water, air, heat from the sun and, later, fire. In ancient Egypt civilization, straws were incorporated into the mix to aid in faster drying times and to produce lighter bricks (Exodus 5:7-8)[22]. **Figure 2-1** illustrates historical brick production. In making clay bricks, humans seek to convert an unconsolidated material into a hardened stone. It is postulated that the historical discovery of clay-based bricks was accidental[23] and originally the brick was dried in the sun to achieve the required hardness after hand-shaping plastic clay[19,21]. Clay particles in sun-baked are not chemically bonded by sintering, so the shaped product lacks the strength, durability, scratch resistance and improved porosity of a fired ceramic [24].

Plasticity, as used in this context, refers to the ability to deform, shape or draw clay without breaking or cracking[25]. Fernandes et al.,[26] reported the differences in clay bricks manufactured between the 12th and the 18th Centuries in Portugal as a material type and shaping method. Most raw materials are named according to the locations from which they are obtained (referred to as "winning" the clay). The processing of clay bricks begins with selecting the best clays, which limit adverse effects such as shrinkage, cracking and warping

during drying and firing [27,28]. The ancient production of brick clays was simple but time-consuming in that clays were excavated and shaped by hand and hardened by the excessive heat of the sun's rays[6]. Production rates were low[29] compared to the modern manufactured ceramic bricks using kiln cars (over 6000 bricks per kiln car)[8].

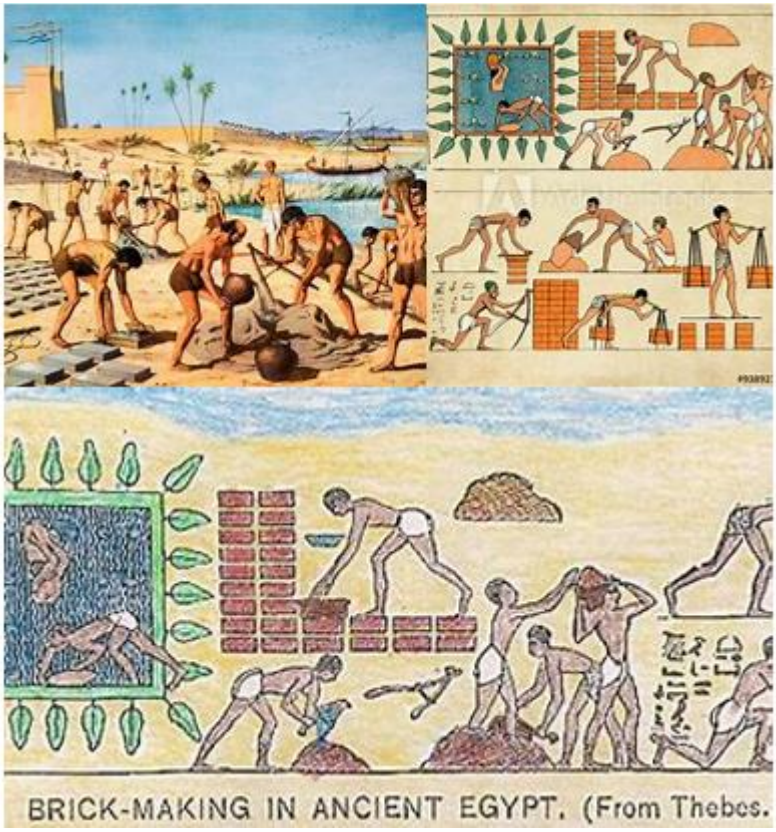

Figure 2-1: Illustration of historical brick production[30]

Between 1840 and 1968, bricks produced at Ashburnham in the UK were produced manually[6]. Clays were by digging and then stored and which allowed the clay to break down further over weeks, months, and, in some cases, years, improved the workability of the clay or how plastic the clay is. Leslie[6] further explained some tools used in the historical winning, preparation and shaping of clay bricks. For example, the mattock was used to break mined clays into lumps. Shovels were used to mix clay and water to the correct consistency, the use of the "naked feet" or horses for kneading or pugging stiff and soft clay for even consistency[5] (**Figure 2-2**), as well as normally removing air pockets, unwanted materials

such as twigs, stones, lime, and other contamination which were known to affect clay processing adversely. In the modern era, contaminants such as these have been identified as causing significant deleterious effects on clay brick products, mainly if the clay contains higher levels of soluble salts [31]. The stiff clay was then thrown into a rectangular wooden box without a base or lid, lubricated with water or sand to demould-shaped clay [5,18]. The surface of the clay was mostly smoothed with a wire mesh or plywood. The process is adopted universally as it gives a more uniform shape. Drying is reported to take at least 24 months in the sun before firing clay bricks for wall construction[5,32].

Figure 2-2: Clay preparation- "the naked feet" approach[33] and shaping clay brick in a wooden mould[6]

In the 18th Century at Ashburnham, UK, firewood was the common fuel used, until the discovery of gas and coal firing, in an intermittent kiln built (clamp kiln) with brick earth, which was dismantled after firing bricks for over 50 hours. Packing bricks in the kiln was time-consuming, taking not less than three days, and required skills to prevent damage due to dimensional shrinkage changes during heating and create an even heat distribution within the temporary kiln where the firing of about 20,000 clay bricks[6,18] took place. In Ghana, a similar method is used with palm kernel and firewood to fire clay bricks in a clamp kiln

producing over 11,000 bricks with less product damage than firewood alone [34]. After the clamp or intermittent kiln firing of clay bricks, the kiln was dismantled, and the fired bricks were packed off or de-hacked for structural applications[34,35]. During construction, clay slip was used as the binding material for many cultures until cement (lime mortars/gypsum mortars) was discovered. Kilns for firing were designed based on their functionality[33], as shown in **Figure 2-3**.

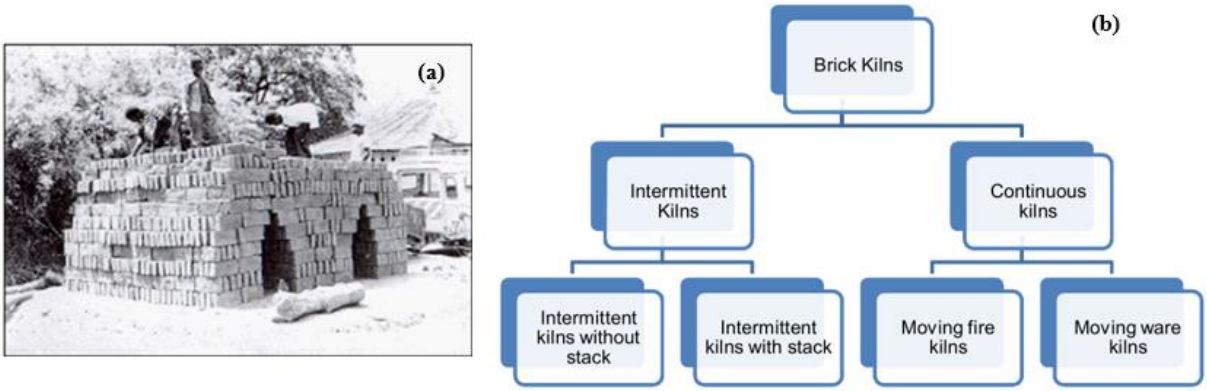

Figure 2-3: Firing of clay bricks (a) clamp firing[35] and (b) different functionalities of kilns designed from the prehistoric era to the 21st Century[33].

Now, there is a paradigm shift in the clay brick process. The driving force for these was from both economic and environmental viewpoints[6]. Despite mechanisation, sometimes large pieces of lime can still be present in the clay. Press moulding, dry pressing and extrusion or wire cut methods have been employed as forming methods[6]. Their selection is essentially a function of water content or plasticity. Instead of drying naturally for 48-50 days, heat recovered from firing is transferred to the drying zone for faster and more efficient production[6,24]. Despite the increased use of continuous kilns, periodic kilns are still used, and cooled fired products are removed after firing, even to the current day[6]. Permanent kilns

using gas as the primary fuel, with wall insulation to control excessive heat loss, are now common. Further research on kiln heat loss needs to be addressed.

World War I and II had a tremendous effect on the advancement of the industrial era, urbanization, technological advancement in kilns (continuous firing)[36], extrusion of clay-based products, scientific discoveries of X-rays (X-ray diffraction of clay mineral crystal structures), microstructure, thermal studies, spectroscopic studies[36,37], schools and research facilities[36] have helped pushed the understanding of clay ceramic science. The rise of cement production also affected changes and advancements in brickmaking in the 1920s. By 1960, five significant improvements had been accomplished through scientific research and are still being used in 2022. These improvement starts with raw material preparation, firing and product packaging using AI-assisted technologies and established standards to ensure durable products[36].

2.2 Modern brick manufacture

Heavy clay ceramic brick production can be summarised into six stages: (1) winning of clays and stockpiling, (2) preparation clays which involve crushing, (3) forming methods, (4) drying, (5) firing, (6) sorting (quality control), packing and distribution [7,24,29]. Firing is the most crucial stage by Wood[38] ,although brickmakers accept that all stages of the process play essential roles in producing the final ceramic (e.g., brick) and determining its properties. For example, if clay preparation is poor, the final product may be full of voids and prone to cracks, affecting strength. Each step is relevant to the production of brick and tiles, and all are summarized below.

Winning of clays and stockpiling: modern production uses equipment for clay drilling and stockpiling **(Figure 2-4).** The essence of the stockpiling is for a homogenous and consistent

composition of the “won” or “winned” clay and further weathering by exposing it to rain, wind, and snow to improve workability[39]. This period is known as clay ageing[24].

Figure 2-4: Clay stockpiling at a UK quarry site

Crushing larger aggregates of clays: within the clay preparation stages, jaw crushers and mill pans are used to obtain the correct and uniform particle sizes needed for brickmaking. Depending on the shaping method for the product, exceptionally fine particles (1mm) are needed for dust pressing. In contrast, a 2-15 mm particle size is usually used for the wire-cut method [39,40]. Sometimes water may be added to minimise dust pollution.

Mixing: Blending clays with or without additives and water occurs at this stage. This mixture is placed in a pug mill which rotates to mix the clay homogenously to avoid an uneven mixture that could distort drying and firing. The blends of clays or additives are mostly incorporated to promote product properties on drying and firing [39].

Shaping methods in heavy clay ceramic manufacture: the microstructure and packing of clay particles to form the initial green strength is obtained at this stage. Product names are influenced by the shaping techniques used. There are three principal methods for forming

clay bricks. These are the machine or wire-cut or extrusion method, pressing, and hand moulding[2,39,41]. Water/ sand struck forming methods were developed based on their demoulding or lubricant characteristics and their effect on surface finish[39]. Individual forming techniques are described below.

Wire-cut or extrusion: method requires sufficient plasticity of clay. The method forces a stiff clay with a moisture content of about 20-23% into a metal die with or without perforations or complex shapes with embossed designs to create textures on brick surfaces [7,41] (see **Figure 2-5**). One key advantage of this process is the removal of trapped air from the clay mix and that it can also accommodate intricate shapes[7,24]. This entire process is often automated. Examples of bricks produced in the UK by extrusion are engineering, perforated and complex-shaped bricks[7]. Plasticizers are added to non-plastic clays to aid extrusion[42].

Figure 2-5: Extrusion of clay brick at Wienerberger's factory site (Ewhurst, UK)

Pressing: Plasticity is not required when pressing as a finer particle size ranging from 1mm-dust and high tonnage hydraulic press can form a very dense product. In the semi-dry method, a small amount of water is added to force particles to bond to promote sintering[43–45]; an example produced by the semi-dry method is the Fletton brick[7,25]. This method is also fully automated.

Hand moulding: this is based on the ancient technique used before the introduction of industrialization. Usually, a high moisture content is needed (>23%)[46]. Soft mouldings fall within this category where a wooden, plastic or metallic mould is used, and kneaded clay is thrown into the mould with excess clay cut off the formed brick and allowed to dry to retain its shape[7,24,39,46]. The mould-release agent can be water or sand. It is suggested that body fuels for hearted bricks are best achieved with soft mould processes[47].

Water/sand struck method: Bricks produced from this method are also fully automated. It has been modified in a way that involves less handling by human labour, uses water and sand as a mould release, and finally adds a texture to the product[7].

Drying: The drying for the three (3) different forming processes (wire cut, pressing, hand moulding) used in heavy clay ceramic production differs mainly because of the water content. For example, bricks may be fired right after forming with the dry press, while the semi-dry press will require a few hours for the added water to evaporate. In the soft mud process, several days of drying clay in the mould are needed to reach even a leather-hard state, from which the bone-dry state is achieved by preheating to drive out all traces of water of formation[7,24,48]. “Bone dry” describes greenware (unfired clay) ready for firing. For the wire–cut or extrusion method, formed with approximately 20% moisture content of added

water[46] ,the low air void needs exceptional care to get the ware into a bone-dry state. Even drying is vital to prevent cracking and distortion of shape due to the initial shrinkage from the loss of physical water[7,49–51]. Drying is commonly conducted in a chamber where waste heat from kiln chambers is directed to dry ceramics – waste heat recovery. A laboratory study on the formulation of a "new brick" or tile making has proven the necessity for removing formation water by drying to constant mass before firing[52]. Inadequate removal of added water to shaped clay prior to the heating will cause the water to expand, resulting in cracks. The firing profile is regulated during thermal treatment to remove the added water of formation and chemical water. The decomposition of organic and carbonate compounds occurs around 600^{o}C depending on the associated clay mineral[49,53,54]. The initial stage of firing is known as the pre-heating zone.

Firing: Firing and cooling are paramount in clay manufacturing, ensuring the key properties of desired bricks since heating affects clay mineralogy, shrinkage, porosity, strength, microstructure and chemical properties of the unfired-shaped clay[46,54,55]. For example, Temuujin et al.,[56] showed that the chemical compounds, the composition of clay mineralogy, and the firing atmospheres account for the reactions during firing, affecting the product, e.g., yellow bricks and blue bricks, porosity and ceramic density. Brownell[36] describes the effect of mineralogy being controlled by the shaping method, drying, and firing. A case in point is when clays obtained from the primary rock are non-plastic, making it challenging to form unless pressing is deployed, which directly affects the bonding of clay particles during sintering into a denser product and compact microstructure with lower porosity compared to ceramic-shaped by hands. Cooling profiles are equally essential to minimise or stop unnecessary cracking of ceramics by expansion[24]. The entire brick process is illustrated in **Figure 2-6**.

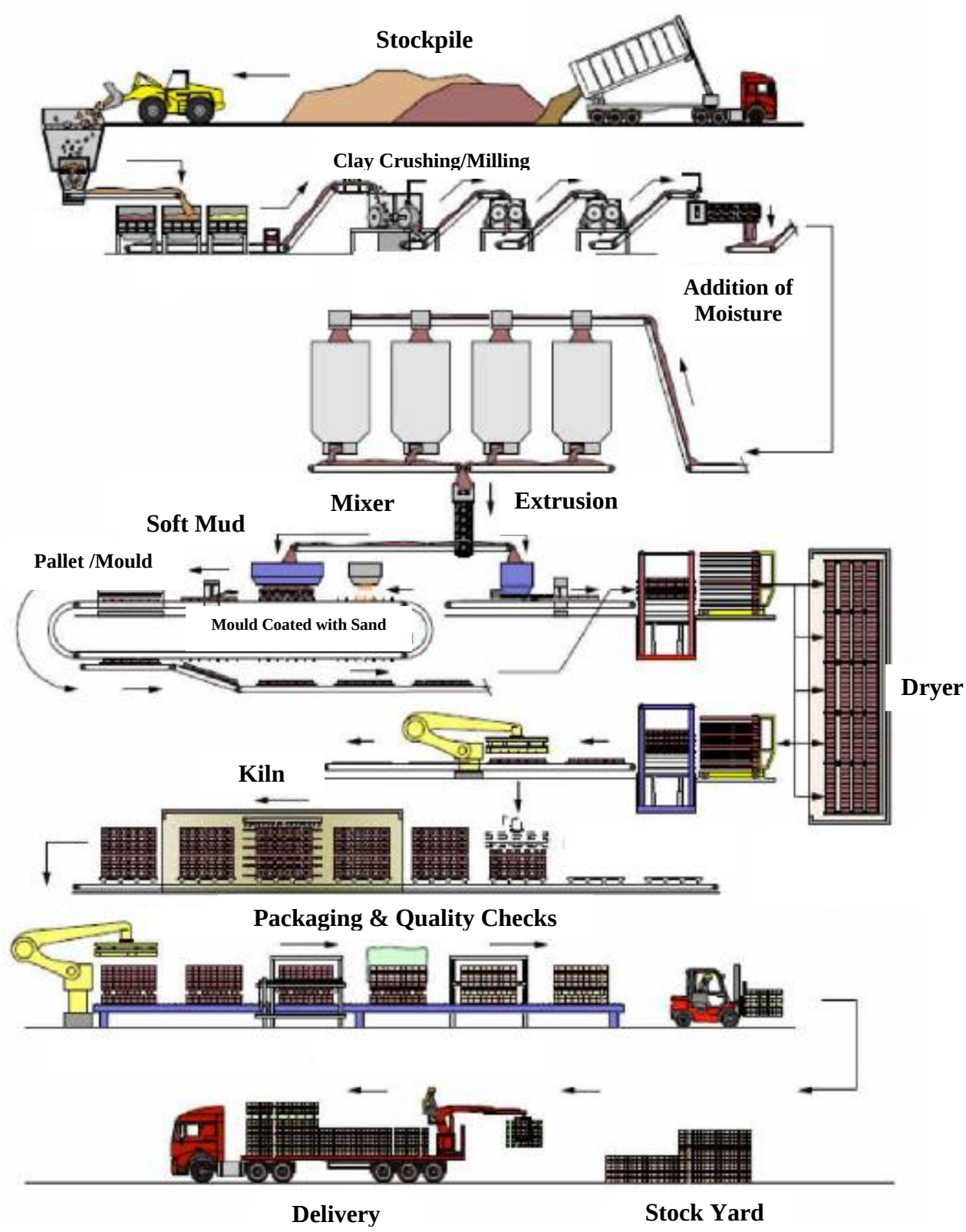

Figure 2-6: Schematic diagram of a typical modern clay brick ceramic manufacturing process (modified after [39]).

2.3 Raw materials for brick making

Natural clay is the most abundant raw material close to the earth's surface and the most widely used material by man, including the global use in ceramic manufacture[58]. The theoretical formula of clay is $Al_2O_3.2SiO_2.2H_2O$[25], but additionally, natural clay contains colourants Fe_2O_3 and minor alkali/ alkaline earth compounds usually of less than 2wt%, but compositions vary based on the region and dept[23,57]. Organic and carbonate matter are associated with every clay deposit, an inevitable part of the clay formation deposition[28].

Clay is widely known for its diverse electrical, aerospace, health and structural applications and important properties such as high resistance to climatic change, elevated temperatures, high strength and low cost[58,59]. Shale, clay, water, sand, colourants, and other additives are added to clay to improve body composition for any specific function. Over 26 materials from waste streams are incorporated in ceramic manufacture, of which 15 are currently in use because of the functionality and longevity of waste; however, high carbonates in the form of body fuels (e.g. coke breeze, coal) does contribute to the overall CO_2 released into the atmosphere[60]. A summary of inorganic raw materials and wastes currently used in brick manufacture and the functions of the materials are explained in **Table 2-1**. The use of other additive type [61,62] and their effects on firing is further discussed in **section 2.14,** derived from industrial trials and journal publications.

Table 2-1: Raw materials and their function used in the brick industry.

Material	Material description	Function
Shale / clay[63]	Alumina silicate material with grain size 0.02-2mm with enough plasticity to shape	Main raw material
Foundry sand[60,64]	Obtained from steel plants with sand grain size depending on the sand type (from white (31.5-0.063mm), pale and dark grey colour (1- 0.063mm)	Control shrinkage, reduce plasticity, as a lubricant for hand moulding or soft mould bricks and texture to fired ceramic
Carbonate minerals[47,65]	E.g., Lime, Talc or chalk	Replacement additive
Perlite[66]	Expandable rock from a volcanic region	Improve plasticity
Barium carbonate[67]		Anti- Scumming additives and binder Crack prevention during extrusion and firing with great strength Reduce shrinkage and improve sintering
Ligno sulphate[68]		
Molasses[69]	A non-mineral-based additive	
Borates[70]	Inorganic material flux	
Sawdust[47,71]	Fine wood chippings	Open ceramic body function as body fuel and promote colour change
Coke breeze[47]	Organic material	
Coal fines	Inorganic wastes from coal mines	
Grog[60]	Recycled fired brick ground down to powder	Reduce shrinkage and improve drying and fired strength. Moreover, it is introduced as a filler.
Quarry fines[72]	Has comparable properties to clay but contains a more significant amount of feldspar	Additive flux and improve shrinkage and density (function as filler)
Mining wastes[73]	Contains fluxes, metals and sulphates	Potential raw material replacement but may be detrimental to sulphate attack
Water-treated residue[47]	Waste additives	Plasticity
Incinerated sewage sludge ash [74–77]	Si, Al, Ca and Fe P_2O_5	Production of insulating materials. Leaching of metals
Waste glaze[78]	Waste glaze composition for tiles	Additive flux and improve sintering and stop efflorescence
Slag[60]	Industrial wastes containing alkali and alkaline earth fluxes	Clay supplement, filler, and flux. With occasional colour modification
Pulverized fly ash[47,79,80]		
Town ash[60]		

2.4 What is clay?

Clay is a "naturally occurring material composed primarily of fine-grained minerals, which is generally plastic at appropriate water contents and will harden when dried or fired"[59]. Clays are weathered rocks transported from the parent or found in situ with the parent rock[19]. A transported clay is referred to as the secondary clay[25]. Transported clays contain impurities such as Fe, Mg, and Na and possess high plasticity linked to their fine constituent particle size[19,24,25,81]. Clays used in the production of fired bricks are required to be plastic. However, Konta[58] describes clay as a poly mineral consisting of illite, kaolinite, chlorite, vermiculite, smectite and mixed layer structures of earlier clay minerals with a chemical composition of SiO_2 in larger quantities, Fe_2O_3, and other associated fluxes, often CaO, Na_2O, K_2O, minimizing fuel cost.

These associated minerals are chiefly impurities. Christie et al.,[82] explain that particle sizes for brick clays consist of a high amount of silt ranging from 0.004-0.0063 mm with clay particles well below 0.004-0.002 mm and sand as high as 2 mm. This gives clarity in explaining the sort of material under discussion. Additives such as industrial inorganic materials like the feldspars (potash- $KAlSi_3O_8$, soda- $NaAlSi_3O_8$ and lime- $CaAl_2Si_2O_8$) are introduced into the body to function as flux and aid in sintering[81]; the chemical analysis for most clays reveals the presence of feldspar types in small percentages in the raw material composition. Furthermore, Aydin Aras[83] affirm from his studies that the main minerals found in the heavy clay industry are quartz, kaolinites, illites, and feldspars, of which quartz is the principal constituent. Christie et al.,[82] also agree that these main clay minerals are primarily found in brick clay.

Dunham[84] outlines four (4) categories of clay minerals present in most British clays, shown in **Table 2-2**.

The table shows that some brick clays can contain up to four different clay minerals and a minimum of two, at least illite and kaolinite or illite and chlorite. Moore and Reynolds[37] reported on four clay types of kaolin envisaged in ceramic manufacture: ball clays, fireclays, flint clay and underclays used for ceramic application.

Table 2-2: Category of clay minerals in brick clay (adapted from source:[84]).

No	**Clay Minerals**			
I	**Illite** $(K,H_3O)Al_2Si_3AlO_{10}(OH)_2)$	**Kaolinite** $Al_2Si_2O_5(OH)_4$	**Chlorite** $(Mg,Fe)_3(Si,Al)_4O_{10}(OH)_6$	**Smectite** $(1/2Ca,Na)(Al,Mg,Fe)4(Si,Al)_8O_{20}(OH)4nH_2O)$
II	**Illite**	**Kaolinite**	**Chlorite**	-
III	**Illite**	**Kaolinite**	-	**Smectite**
IV	**Illite**	**Kaolinite**	-	-
V	**Illite**	-	**Chlorite**	**Smectite**
VI	**Illite**	-	**Chlorite**	-

Dunham[84] explains the changes in these minerals when allowed to age (geological age). For example, non-clay minerals such as quartz (SiO_2) decrease as it ages while alumina (Al_2O_3), fluxing oxides: Fe_2O_3, MgO, Na_2O, and K_2O increase when left for extended periods. Hence there is a change in chemical and mineralogical composition with time and even with firing (i.e., a stockpile). This has been confirmed with the use of X-ray fluorescence (XRF). These minerals present in clays are further explained in **sections 2.5.2 and 2.5.3**.

Another material that is chiefly used in the heavy clay industry is shales (a sedimentary rock). While this raw material is being used as one of the main commodities in brick production, Shaw and Weaver[85] present the mineralogy of shales as similar to clays having quartz 31%, feldspar 4.5%, organic materials 1%, carbonates less than 0.5%, clay minerals as high as 61% and 2% of other materials but non-plastic. The composition of the clay-stone shale is mainly due to the environmental conditions associated with its formation[85,86]. Pyrite,

siderites and gypsum are non-clay minerals commonly found, with certain clays posing a detriment to the production[87].

In summary, clays are defined or characterised by their chemical and mineralogical constituents, which could vary from region to region or even with depth from the Earth's surface. The chemical history of clays provides relevant information on how long the clay can be fired, to which temperatures, fired colour and sulphate content are detrimental to fired clay strength and aesthetics[5].

2.5 Impurities, the role of clay minerals and their effect on ceramic properties

The heterogeneity of clays, in general, is complex and presents challenges in assigning neo-crystalline phases[88]. Impurities commonly found in clays are quartz, feldspar, micas, sulphates and carbonates (such as $FeCO_3$, $CaCO_3$ and $MgCO_3$)[46,89].

The mineralogy of clays profoundly influences the outcome of the ceramic product- bricks[84]. The minerals found in clays are formed in two stages, during clay formation and the firing of clays, where new phases emerge by the conversion and fusion of clay particles. Clay minerals differ because their physical and chemical properties depend on their structure and composition[90]. Clay minerals have different crystal structures and sizes, which, when thermally treated, metamorphose into different forms and decompose at several temperatures. The application of several thermal techniques discussed by[91,92] explains this by the temperature at which the material begins to sinter, (re)crystallise and melt. Though much research has been published on single clay minerals, these minerals, especially illite/muscovite, have not been used as an additive in clay brick manufacture to reduce fuel cost despite melting at 950°C[93].

Kaolinite and illite are predominant in most UK clays. Illite (s) tend to function as a flux at elevated temperatures with kaolinite, forming mullite, an important phase contributing to

ceramic strength[59,84]. A well-ordered or disordered structure can take place in the formation of kaolinites with the chemical formula $Al_2Si_2O_5(OH)_4$. The crystal structure of kaolinite groups is held together by hydrogen bonds[81]. At temperatures above 950^{o}C, kaolinite forms an interlocking layer (mullite), contributing to a robust product. Dilatometry studies conducted by Flank[94] revealed that bond breaking of the mineral kaolinite happens at 450^{o}C-550^{o}C as the hydroxyl group is removed, resulting in shrinkage, and temperatures exceeding 900^{o}C promote the formation of the mullite structure (see **Figure 2-7**).

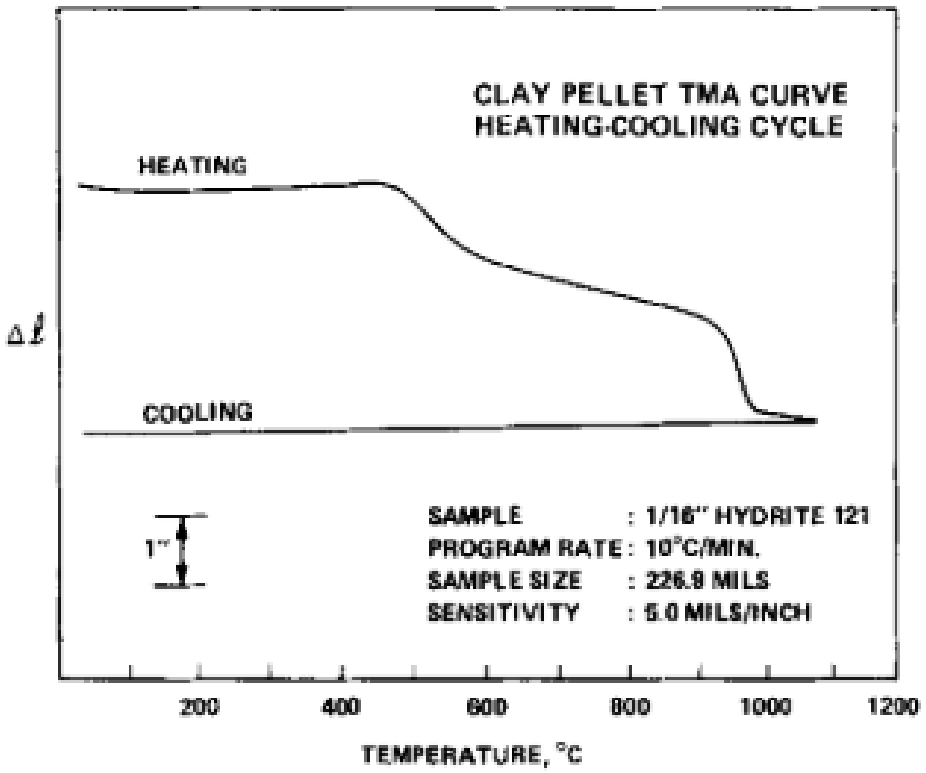

:

Figure 2-7: Thermomechanical analysis of clay [94]

Peters and Iberg [95] also made similar observations of the structural breakdown of kaolinite at 500^{o}C-550^{o}C. They also revealed that dolomite $CaMg(CO_3)_2$ and calcite ($CaCO_3$) decompose at 650^{o}C and 700^{o}C, respectively. Illite and montmorillonite decompose slowly within 650^{o}C - 700^{o}C and the entire structure has been transformed at 950^{o}C when analysed with the X-ray diffraction technique.

Illite $(K,H_3O).(Al_2Si_3AlO_{10}(OH)_2)$ a micaceous mineral with a 2:1 layer like the smectite groups, and is remarkably similar to muscovite $(KAl_3Si_3O_{10}(OH)_2)$, with the difference being the amount of potassium or chemical water present in the system[83]. Worrall[81] highlights that the compact nature of illite can only be broken down by chemical means. McConville and Lee [96] state the significance of illite as a mineral that encourages fusion on heating because of the amount of liquid phase it produces.

Grim and Bradley[93] show that chemical water from illites is lost between 350ºC and 600ºC; a complete collapse of the structure occurs above 700ºC. The new structure formed above 700ºC is spinel, which combines with any alkalis or fluxes to form mullite above 950ºC when the liquid phase cools and crystallises. Meanwhile, Araújo et al.,[97] support the view that the tetrahedral layer of illite also loses water at about 850ºC, transforming into the new phase[93]. They also noted that cristobalite does not form with the decomposition of illite at higher temperatures.

Bentonite clays are classed as smectites[46]. Smectites have been widely used in the medical sector in healing and binding materials for in vivo applications. Bentonite clays swell in contact with fluid: an example is the montmorillonite group rich in Na / K (Wyoming / Chatite clays in the USA). Murray[98] describes the smectite group as one that substitutes both the octahedral and tetrahedral layers with a large surface area. Traditional ceramics (heavy clay product) is mostly in mixed layers with other types of clay mineral or as the dominant constituent described by Durham [84]. Thermal analysis conducted by Schomburg,[99] reveals that complete layer breakdown occurs in smectites at 840ºC - 900ºC of the hydroxyl group (OH) is removed from within the mineral, forming spinel and cristobalite phases. See **Table 2-3**. Clays containing >8wt % of CaO are considered Ca-rich material. When Ca-rich clay is heated, it is expected to transform into gehlenite, anorthite and wollastonite phases as any calcite present decomposes at 850ºC[100].

Table 2-3: Thermal analysis of clay minerals and their thermal reactions[95,97,99]

Clay Minerals	Temperature Range	New phases / thermal reactions
Kaolinite $Al_2Si_2O_5(OH)_4$	920°C -1000°C	Alumina silica spinel phase
Talc (non-swelling group) $(Mg_3Si4O_{10}(OH)_2)$	800°C -900°C	Dehydroxylation of chemical water
Illite $(K, H_3O) Al_2Si_3AlO_{10}(OH)_2)$	850°C -950°C	Spinel and mullite formation
Montmorillonite $(1/2Ca,Na)(Al,Mg,Fe)4(Si,Al)_8O_{20}(OH)_4.nH_2O$	840°C - 900°C	Decomposition of structure Spinel and Cristobalite phase
Mg-Chlorite $(Mg,Fe,Li)_6AlSi_3O_{10}(OH)_8$.	650°C -850°C 800°C -830°C	Dehydroxylation of the Mg sheet Forsterite formation
Palygorskite $(Mg,Al)_2Si_4O_{10}(OH)•4(H_2O)$	800°C -830°C 1000°C - 1030°C	Dehydroxylation of clay mineral Cristobalite phase

2.5.1 *Structure and characteristics of common clay minerals in clays for ceramics*

Section 2.4 described clays as a composition of clay minerals and non-clay minerals[90]. These are commonly distinguished and identified using X-ray diffraction (XRD). XRD is the most widely used technique for clay mineral identification and essential for a clay mineralogist [90,101–104] when coupled with X-ray fluorescence (XRF) to determine chemical constituents[105,106]. The quantity of each mineral percentage can also be examined using Rietveld refinement.

2.5.2 *Kaolin group*

The kaolin group belong to the 1:1 dioctahedral layer with four polytypes (nacrite, dickite, halloysite and kaolinite) having similar structure ($Al_2(OH)_4Si_2O_5$) but different octahedral layers in adjacent layers[102]. **Figure 2-8** shows the structure of two stacked sheets of a clay mineral, kaolinite.

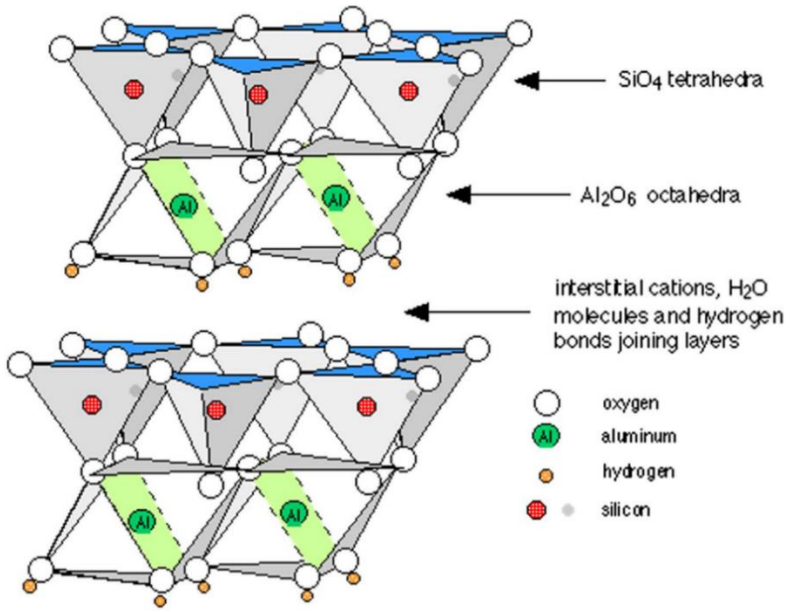

Figure 2-8: Diagram of Kaolinite[107]

The distinction between these diverse groups is with their unit cell being orthorhombic, monoclinic, and triclinic, respectively. Another difference is the structure's excess water, especially with halloysite ($Al_2Si_2O_5(OH)_42H_2O$)[102,108]. Moreover, the physical and chemical characteristics can change due to crystal perfection and particle size. Morphology-wise, hexagonal plate-like shapes are readily identified as kaolin, even though other minerals may have the same microstructural characteristics[25]. Therefore, multi-techniques are often used to confirm the identified mineral[81]. Kaolin is an important mineral for the ceramic industry to produce porcelain, medical applications, fire-proof, and refractory products. Kaolin, in its purest form, is white and can appear as ordered or disordered, and this can be identified by

how sharp or broad the XRD peak shape is. Serpentine is another mineral commonly associated with kaolin and has a similar structure to kaolin but of different octahedral ions [102,108,109].

2.5.3 *Mica group minerals*

Haldar and Tišljar[101] named seven classes of minerals under the group of 2:1 phyllosilicates. These are: muscovite ($KAl_2(OH)_2AlSi_3O_{10}$), celadonite ($Kfe^{3+}(Mg, Fe^{2+})(OH)_2Si_4O_{10}$), paragonite ($NaAl_2(OH)_2AlSi_3O_{10}$), biotite ($K(Mg,Fe)_3(OH)_2AlSi_3O_{10}$), illite $K_{0.65}Al_2(OH)_2Al_{0.65}Si_{3.35}O_{10}$) and glauconite $(K, Na)(Fe^{3+}, Al, Mg)_2(Si,Al)_4O_{10}(OH)_2$ [102]. It is further grouped into finer and coarse-grained minerals. The schematic diagram of the crystal structure of illite is shown in **Figure 2-9**.

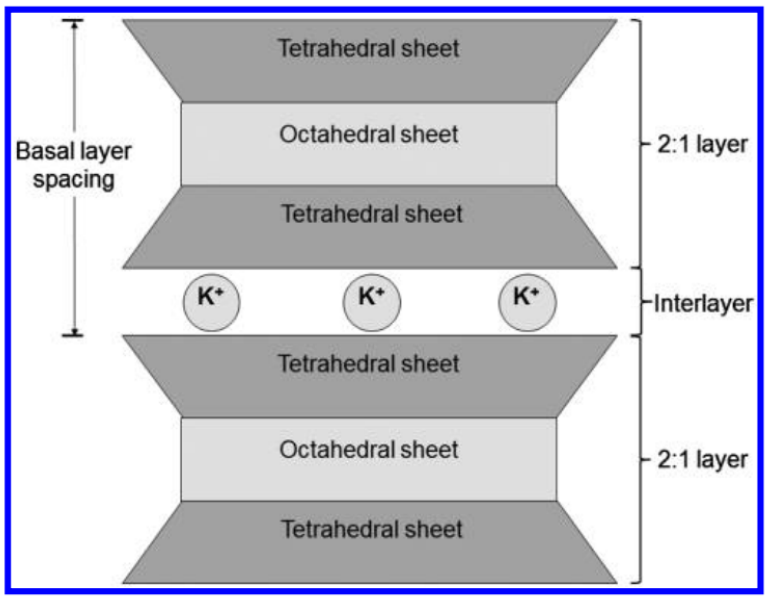

Figure 2-9: The crystal structure of illite[110]

Muscovite is the commonest coarse-grained mineral in the mica group which does not contain iron (Fe)110. However, other mica minerals exist with the replacement of K with Na or Mg by isomorphous substitution. Only muscovite illite and kaolinite are important to this study because these clay minerals were present in the Weald clay. Muscovite is known

for its high alumina (Al_2O_3) content but could also be rich in silica (SiO_2) and will be of the 3- layer trigonal (3T) ordered species. It can also be a 2- layer monoclinic 2M while 1M is a fabricated structure[102].

Illite derives its name from Illinois, a state in the USA[101] and is a non-expandable clay mineral structurally similar to muscovite but containing more H_2O and Si and less Al and K than muscovite. In clays and soils, illite can be present in a mixed layer making its identification difficult to distinguish[109]. Changes in the fingerprint of 1M muscovite and montmorillonite clay mineral patterns are shown in **Figures 2-10** when mechanically mixed or with OH layers in the mix. The advantage of the mixed layer series is that it enables geologists to trace its historical sedimentary rock pattern [109].

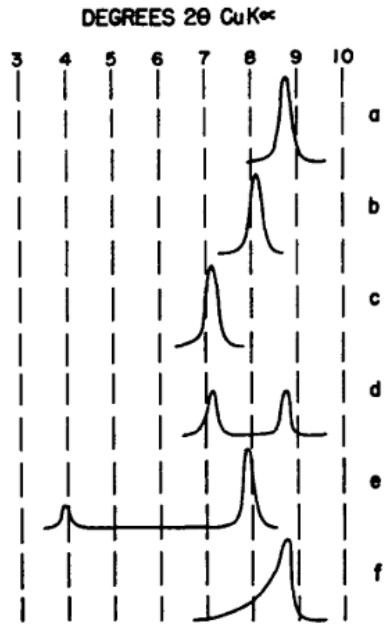

Figure 2-10: Powder diffraction of low angle 1M muscovite and montmorillonite clay mineral (taken from Yoder and Eugster [104])

a) 1M muscovite
b) Mixed layer of muscovite and montmorillonite
c) Montmorillonite has just one layer of water in its matrix
d) Mechanically mix muscovite and montmorillonite
e) Ratio of 1:1 muscovite and montmorillonite
f) High muscovite content with random montmorillonite arranged in an alternative pattern.

Smectites belong to the 2:1 minerals but with physically expandable behaviour when the interlayer comes into contact with water. Odom[108] and other researchers[81,101,102] show that in the small crystal structure, exchangeable ions of both tetrahedral and octahedral sites of smectite minerals give its unique property of having a larger surface area for easy absorption and as small as 0.2µm particle size. Minerals such as montmorillonite, saponite and hectorite belong to this class of mineral[108]. Applications of smectite include as a binder in paints, to improve the plasticity of non-plastic clays, or in cosmetics, medicinal drugs, clay catalysts and adhesives. Naturally, Ca, Mg, and Na cations are the leading influencers of the swelling property of smectites. The rarest form of smectites is Na ion exchange. Crystallographic, chemical, environmental, and physical mineralogy has been identified and well discussed by[101]. Hydrogen bonds are removed on drying and firing[111].

2.6 Clay ceramics and types for structural applications

Products of clay ceramics (e.g., bricks, tiles) are named based on the performance, function, method of shaping and materials used for the production. The 2009 sector report by Ecofys[43] states that differentiating products based on colour alone is ambiguous; therefore, using their technical qualification or brick characteristics is most suitable, e.g., the porosity of the masonry product[43]. According to the BS EN 771-1:2011112, only two groups of fired clay masonry are classified based on dry gross density, these being low density (LD) (less than 1000 kg/m^3) and high density (HD) (greater than 1000 kg/m^3) units. The LD clay brick types need protection from moisture, whilst the HD does not. In the UK, two brick types are readily identified and commonly used. These are facing bricks; clay blocks common clay bricks (unprotected), and Engineering bricks- protected) listed in the British standard (EN 771).

2.7 Emissions and Energy Use on Heavy Clay Products

2.7.1 *Emissions policy in the UK and Europe*

A policy is a carefully researched set of principles to guide actions to achieve a specified goal backed mainly by law or legislation[113]. Reducing energy demand from industrial manufacturing results from a human behavioural change in doing the right things to ensure energy efficiency[114]. Five (5) main benefits of energy efficiency are mentioned by Malinauskaite et al.,[114]: security in energy supply, cost competition, job creation, reduction in energy use and emission control. These changes are then enforced in policies which become laws that govern industrial sectors. The UK government has laid down 44 action plans for the 2021-2022 calendar year for the industrial decarbonization strategy[115].

Figure 2-11 shows the UK's plan to abate global warming through technology and carefully shared costs across the nation.

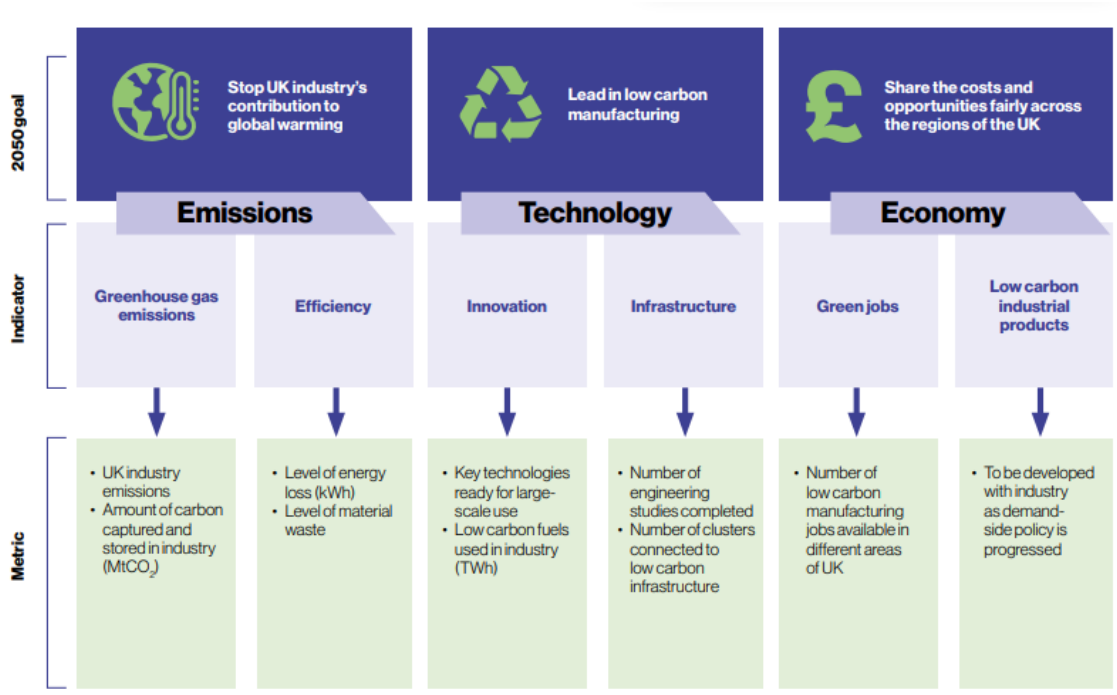

Figure 2-11: UK Industrial plan for a decarbonized economy[115].

Emissions policies are summarised into four main streams governed by their funded organisation, described in **Table 2-4**. The funded organisation ensures and reviews set policies against investment pushed into the bill.

Table 2-4: UK policies and funding groups to improve energy efficiencies[114,115]

	Policies	Funding Group
1	Carbon pricing	Climate Change Levy (CCL), UK Emissions Trading Scheme (UK ETS)
2	Competitiveness support	Climate Change Agreements (CCAs), Emissions Trading Scheme (ETS) Free Allowances, Financial relief for Energy Intensive Industries (electricity costs)
3	Demonstration of funding	Energy Innovation Programme (EIP) (2016 – 2021), Net Zero Innovation Portfolio, Industrial Decarbonisation Challenge (IDC), Transforming Foundation Industries (TFI)
4	Deployment and Infrastructure Funding	CCUS Infrastructure Fund, Clean Steel Fund, Heat Network Improvement Programme (HNIP), Industrial Energy Efficiency Accelerator part of the Energy Innovation Programme, Industrial Energy Transformation Fund (IETF), Industrial Heat Recovery Fund), Net Zero Hydrogen Fund, Renewable Heat Incentive (Non-Domestic)

The building industry contributes half (50%) of global CO_2 emissions into the atmosphere[116,117]. Climate change has influenced the UK to target 80% emissions by 2050. The UK calculates its emissions on three (3) streams territorial, resident and consumption base[118]. Emissions declined between the 1950s and 1980s due to the decline from switching coal to natural gas has been reported[119]. Undoubtedly, the 1970s fuel crises led to the technological advancement for energy efficiency in the ceramic sector, which comprises tiles, tableware, sanitary wares, and heavy clay products. Until the 1990s, the ceramic industry focused chiefly on energy conservation through kiln innovations, clay processing modifications, automated plants, and novel drying technologies[15]. Most of these listed

innovations began with the tile sector due to its competitiveness through high production demands.

By 2008, CO_2 emissions rose from 620 Mt to 81,071 Mt compared to the 1990 Mt CO_2e, which was approximately a 20% increase. Although the problem persisted, production was still in full swing despite not having an adequate robust database that would serve as a guide globally[119]. In the UK, it has been reported that cement, ceramics, chemicals, food & drink, glass, iron & steel, oil refining, and pulp & paper are the most energy-intensive sectors emitting a quarter of the total Greenhouse Gas (GHG.) The policy under the Kyoto Protocol commenced the climate change levy intended to control energy usage for all sectors[117,120].

According to IFS report R84 [118], emissions policies only favour household emissions since taxes on energy usage are subsidised. At the same time, the industrial sector pays premium charges[118]. The policy of the manufacturing industries having to pay high rolls for emissions release has brought about the recent innovative re-formulation of clay body compositions from industrial wastes for ceramic production[117]. Many such additives from other streams are captured in **section 2.14**. Another technological adjustment in kiln efficiency and fuel switching is being discussed and reviewed.

The question is, how would this fuel reduction be beneficial to the heavy clay industry and the environment? Is there any link between energy reduction and CO_2 emissions? The ceramic industry is an energy-intensive sector, meaning the resource is "thermally activated physical-mineralogical transformation processes" of the product by extensive firing times[8]. The 2050 decarbonization plan delivered by the ceramic sector in 2017 addresses three major categories for minimising GHG associated with the sector[8]. This includes breakthrough technologies in material processing and firing (e.g., use of syngas /biogas), energy efficiency and CO_2 reduction, carbon capture storage (CCS) and kiln electrification[117,121,122].

2.8 Current fuel and emissions reduction within the heavy clay ceramic production

Spain is the largest producer and exporter of ceramic tiles in Europe, accounting for 3.4% of global tile production; Africa, the Middle East and Europe are the major importers of tile[123]. Ros-Dosdá, Teresa, et al.,[121,122] modelled simulations Life cycle Assessment (LCA) of ceramic stoneware tile production a representative of production in Europe[81]. At the end of the LCA simulations, they reported[122] that innovative technological improvements in the use of waste additives and weight reduction of products will significantly minimise the CO_2 targets for 2020. Their studies (Ros-Dosdá et al.,[122]) also pointed to the possibility of developing an energy-efficient glaze for tile coating.

Change in clay mixing from wet to semi-dry grinding has minimised water content to 6% and saved 0.7GJ/t on energy. 0.6GJ/t energy savings have been obtained by changing the programme process by automation even though there is about 15% energy usage [121]. This continuous wet grinding is highly productive. Shaping a single-stage press glaze for tile products has been successful[48]. Isostatic pressing, commonly used in the tableware subs-sector to produce complex or intricate shapes, has been adopted to eliminate prolonged drying and increase energy saving by not using porous moulds that require drying[121,123]. Similarly, pressure casting and capillary vacuum (CVC) have been adopted for the sanitary ware sector to save energy through casting time and mould drying.

The energy savings for CVC in mould drying is about 1 GJ/t. Steam extrusion has a net saving of 0.17-0.21 GJ/t for extruding plastic tile[122]. Product weight reduction[124] in heavy clay products is another effective energy and raw materials reduction method by creating 3-10 holes in a standard brick (see **Figure 12**).

Figure 2-12: Created holes and frogs in some Wienerberger-fired brick products for material reduction.

Energy savings routes developed include heat recovery from cooling zones to the drying zone to achieve 1% drying before firing. Heat is also recovered to preheating green wares up to 400^{o}C and 600^{o}C. It has a 17% and 28% reduction in energy usage, respectively [121,122]. This technology is used in all ceramic sectors. Aside from waste heat recovery, using electromagnetic waves and warm air allows for rapid drying of tiles within 3-4mins. Controlled humidification is commonly used in sanitary industries where heat for drying is contained in a room with the products[121].

Development of ceramic firing included the replacement of heavy refractories that take time to heat up with low thermal mass refractory cars. Improvement of kiln insulation to prevent heat loss[33,121] and the development of fast-firing and roller kilns have been adopted in all sectors. For the tile industry, an integral thermal process was developed where firing zones were controlled at specific temperatures up to the maximum to reduce energy cost[114]. It is reported that microwave-assisted firing has eight times higher production gains due to the controlled temperature gradient supplemented by the microwave, which heats the internal body, whilst gas -controlled aid in the outer part of the product in the kiln123. There is also the alternative use of high calorific waste fuel like palm kernel[34] sawdust[71] and paper pulp[125]

to reduce the costly traditional fuels like coal and gas. Finally, the use of high-speed burners has been explored as well. Alternative fuels like hydrogen and biomass[123] and fuel mix[121] studies are ongoing to address fuel efficiency in the heavy clay ceramic sector. It has been reported that 2,774,366,458 kWh account for 92% of energy usage from the burning of fossil fuel (Natural Gas & LPG) for sintering ceramics and 253,826,481 kWh for 8% from electricity[126]. Out of this fuel usage in the kiln, technology has made it possible to recover about 48% of total waste heat from the kilns to the dryers, which aids in faster drying of the bricks before they get to the preheating zone by kiln cars. **Figure 2-13** shows the distribution of fuel types used in the heavy clay industry and heat recovered. 8% electricity helps power equipment, including conveyor belts for clay transportation, crushers, and the ball mill for mixing raw materials into a homogenous mix, as well as light for production, all administrative works and all automated accessories for dehacking and packaging.

Re-formulations of body composition for shorter firing times have gained much attention over the past decades with fluxing additives from waste streams and inorganic materials[15,20,126–131].

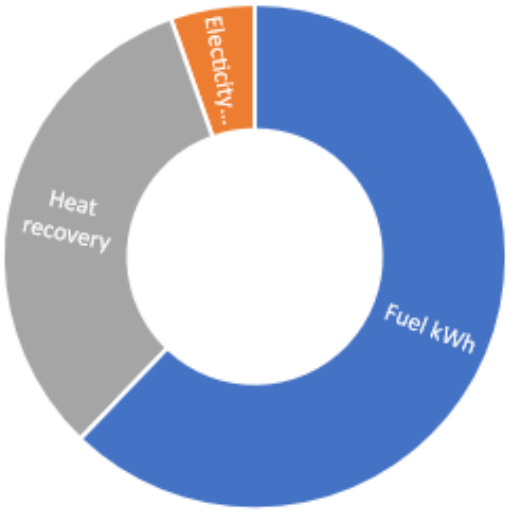

Figure 2-13: Heavy clay ceramic heat demand and heat recovery[126]

2.9 Impact of firing techniques and firing atmosphere on energy consumption and mineralogy.

Firing types used in ceramic applications are classified based on the fuel type (gas[7], firewood[55], palm kernel[34], electric kiln[7] or even kiln type[24,46]) or the final aesthetic quality of the product / special product effect. In heavy clay manufacture, especially with commercial firms, the choice of firing technique depends on the availability of the (general fossil) fuel, the amount of energy it can generate, its ease of operation, and its cost implications[7,24,55].

Generally, firing atmospheres are vital to the material quality and physical appearance of fired products132. The two most talked about atmospheres in firing pottery and heavy clay products are oxidation and reduction firing. In oxidation firing, there is enough oxygen in the kiln to ensure the burning of the product with the help of the flue, gas chamber and any other opening that pushes air into the firing chamber. This type of firing environment produces vibrant and true colours of the fired products[133–135]. The reduction firing, in contrast, is where lack of oxygen creates a deficiency in the oxides present in the clay product and a formation of sooth in a combination of carbon monoxide that settles on the surface, usually promoting darker shades. This effect typically changes the microstructure by increasing closed pores as opposed to larger pore sizes and the colour of the ware mostly in a positive way[56,134–136]. Similar reactions happen with the reduced atmosphere. A typical reaction on firing in an oxidated atmosphere is described by Ferrer et al.,137 shown in **Figure 2-14** and a more detailed summary of stages of clay behaviour and transformations on heating in an oxidative environment is provided by Moedinger[35] and Mutsago[46].

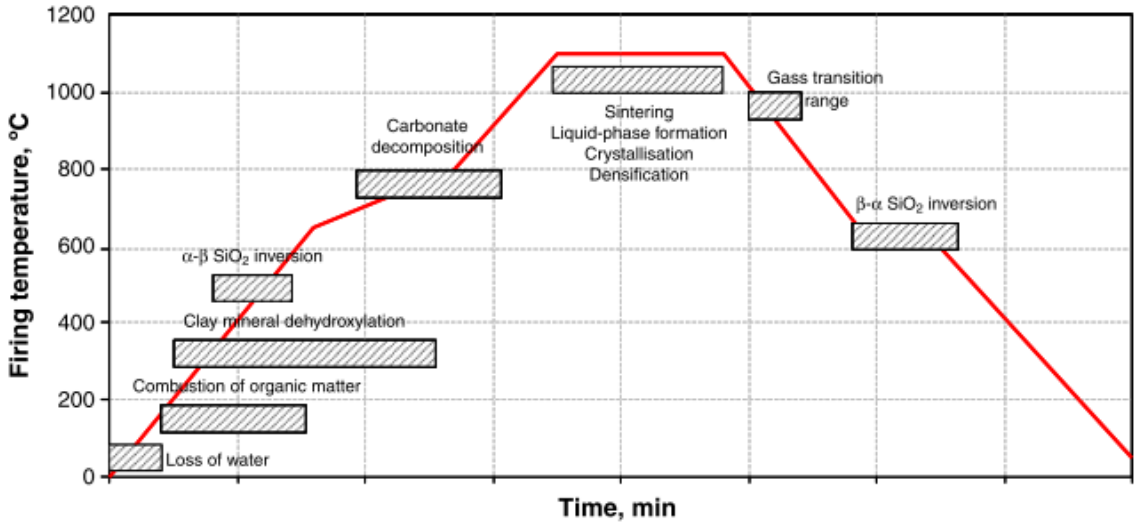

Figure 2-14: Reaction of firing clay in an oxidative firing137

Studies suggest that firing atmospheres have no direct influence over the durability and compressive strength of the brick ware because results obtained for reduced atmosphere and oxidation did not vary extensively 138,139. However, Pontikes and Angelopoulos138 explain that the outer shell of a brick fired under reducing atmospheres increases in strength with more closed pores resulting in a 4.5% increase in strength compared to the strength of 25.9MPa of the same ceramics fired in an oxidising atmosphere at a heating and cooling rate of 3°C/mins soaked for 4hrs at the maximum temperature (1000°C). However, in terms of energy consumption, in experimentation, irrespective of the firing atmospheres as products are subjected to the same firing temperature and soaking time by researchers, the difference in energy usage becomes impossible to figure out, however in terms of a denser product, a reduced atmosphere promises to be the best [38,139]. However, this choice strongly depends on the product required, especially the physical appearance. Nonetheless, Denissen[140] cautions about the re-oxidation of the brick product during the cooling stage and relates the energy consumption to the reduction of the kiln design. Therefore, his study re-designed a kiln that saves fuel usage by 60%.

In terms of the effect of the mineralogy and fired colour, for example, hematite (Fe_2O_3) oxidation state changes to magnetite (Fe_3O_4) because of the firing atmosphere, has been

reported by various authors141–144 the importance of running a Mössbauer spectroscopy has been used to help explain changes in ceramic colours (brownish red to a darker hue). A firing atmosphere is reported to be a minor function of strength but a function of maturity. Moreso, neither heavy clay products' oxidation nor reduction firing was said to have similar strength145.

In ancient China, adding water vapour to a kiln was a frequent practice and believed to have reduced energy consumption by 12% and sintering temperature by 150^{o}C[56]. According to Houseman [146], water vapour ~ 23% introduced through the burners and nozzles improves heat transfer mechanisms within the burning zone, increases uniformity in temperature and finally helps obtain a better product and brings down the temperature by 4.4°C in an oxidizing atmosphere. In contrast, 82.2°C is achieved under a reducing atmosphere when ceramic is fired to 1138°C.

2.10 Rate of firing on ceramics

As used in literature, it means the rate in minutes above 30 minutes at which a product is fired[147]. A historical account of how this slow and fast firing has been practised is given by Dondi et.al[148]. This is believed to shorten the firing cycles to about one – three hours of firing and is primarily applicable and continuously used in the ceramic tile sector, whose density and volume are thinner than heavy structural products like bricks. A higher heating temperature (10°C/min) has been found to significantly control gas emissions (CO, CO_2, Cl_2 and NO) from ceramic manufacture at a shorter time whilst at slow firing < 2°C/min increases gas release with the lower mechanical strength of modified ceramics[149]. Studies conducted by Ukwatta and Mohajerani150 on waste biosolids in fired brick-making fired to 1050°C for 3 hours with different heating rates of 0.7, 1.0, 1.5, and 2.0 °C min^{-1} looked at how the different heating rates affect the effect the modified clay brick property (i.e.,

physical and mechanical). Their findings showed that 5 °C min^{-1} reduced the sintering time by 47% compared to 0.7 °C min^{-1}; a higher heating rate led to lower glassy phase formation. We can, therefore, infer that slow heating rates promote gas emissions. However, the reduced compressive strength reported to be caused by the high heating rate could be affected by several factors ranging from additive level, shaping type and firing temperature. Also, due to the clays' organics and carbonates, firing encourages the formation of black coring[151]. Restrictions on some ceramic compositions containing MgO cannot promote densification and shorten firing time when faster firing is used instead of a slow rate[152].

In a dilatometry study, quartz transition temperatures have been found to shift to higher temperatures when the heating rate was increased above 5°/min [47]. The heating rate checks internal stresses caused by the free quartz transition and expulsion of gases from carbonates in clays. Changes to the α-β quartz transition temperature are given by [147]. Clay minerals undergo structural changes when thermally treated. This is because of weakly bonded minerals with hydrogen and oxygen gas which come off during heating giving rise to the reactivity of clay microstructure through the formation of new phases. However, there has not been a clear distinction to prove otherwise, the slow heating or the fast-firing hindering fired clay microstructure on cooling. What causes changes in clay microstructure is temperature dependant and dwell/ holding time which positively affects the "physicomechanical" property of ceramic samples produced.

2.11 Microstructure and phase transformations in ceramic manufacture

During thermal treatment of clay ceramics, clay minerals lose both surface water and chemical bond water convert and undergo partial melting, and in most cases, release carbon dioxide gas from the decomposition of carbonates. The loose particles transform into a robust structure suitable for a functional application[153,154.] Factors that affect the

microstructure or texture are clay minerals, chemical composition, shaping method, firing temperature and atmospheric conditions20,155,156. Techniques commonly used to study microstructure are optical microscopy, scanning electron microscopy coupled with energy dispersive x-ray (SEM-EDX) and other times indirectly with water absorption test. For mineralogical analysis, X-ray diffraction (XRD) is used [24,81]. In 2012, Rasmussen et al.,[157] combined XRD and SEM to determine the firing temperature of pottery. It is well known from studies that temperatures below vitrification temperatures of clays (900^{o}C) have a permeable body 158,159. In pottery, any ceramics produced below 900°C is called biscuit firing.

Rekecki et al.160 report on the role and effect of high carbonate clay ceramic on product microstructure and strength. Likewise, interlocking mullite crystal96,161 that forms on firing clays to temperatures above 1000°C provides mechanical strength to ceramics[162].

Dondi et al.,148 make a compelling case for different compositions, fast or slow firing affecting ceramic strength. Nigay et al.,163 propose a trade-off in brick properties; thus, thermal insulation products are obtained by adding organic wastes into brick clay, decreasing the bulk density and the mechanical strength. This is true as most studies trying to combat energy reduction in ceramic manufacture have predominately researched organic waste; see **section 2.14.1.**

Franke and Schumann[164], in the "brief history of brick making in northern Europe", also justified with micrographs that the processing route influenced the microstructure of the final product. For example, it was determined by them that the hand mould shaping introduced "large pores and streaks", which is associated with non-uniform hand mixing by kneading, compared to mechanical mixing and shaping, which uses the wire-cut method through de-airing auger forces clay into a die, therefore, causing clay minerals and particles to be in layers as shown in **Figure 2-15**.

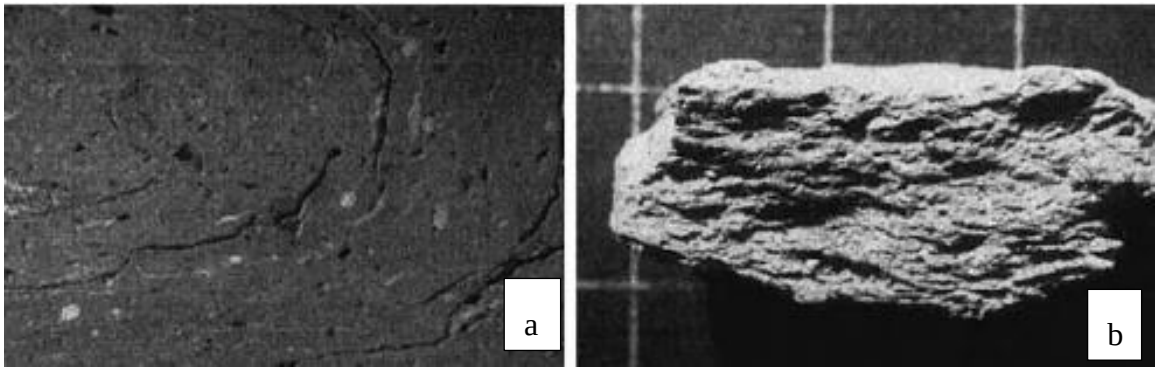

Figure 2-15: (a) fired ceramic produced by hand mould, (b) unfired ceramic shaped by wire-cut method [164]

Assessing firing temperatures using new phases formed by experimentation conducted by Viani et al.,165 was unsuccessful because the thermal decomposition of individual clay minerals shown in **Table 2-2** was not considered. Ignorance of clay mineral thermal analysis is not ideal for understanding clay brick microstructure.

Overall, phase transformations in fired clay products are chiefly related to the thermal decomposition of the clay mineral present and the sintering temperature[166–168]. At the same time, the microstructure is affected by the processing route or shaping method, the chemical composition of the raw material and the type of clay mineral(s) present and finally, the firing temperature and atmosphere.

2.12 Transformations of Fe_2O_3 in clays upon thermal treatment

Iron oxide (Fe_2O_3) is one of the primary colourants required in fired clay brick products. This iron in clays could be changed during firing to produce either red, yellow, grey or blue brick by interfering with the firing atmosphere or the colourant concentration. The intensity of the brick colour is a function of firing temperature mostly above 1000°C[134,135,157,169] and colourant in clay greater than 6wt%. It has been reported that iron is developed from iron-bearing minerals such as pyrites, goethite, siderite etc., from the decomposition of clay

minerals such as chlorites and illite recrystallization of hydroxides or oxyhydroxides (Fe^{2+} and Fe^{3+})169.

Structurally, the iron formation has been found to sit either at the tetrahedral or the octahedral sites when studied with transmission Mössbauer spectroscopy at room temperature. The Mössbauer technique is extremely sensitive for even lighter hues for ceramics fired to 950°C170.

2.13 Heavy clay ceramic properties

Standardisation of structural products is the key to ensuring quality to evaluate and validate new or novel manufacturing processes and products (see **section 2.2** for the manufacturing process). Several nations have their standards based on their raw materials and climatic conditions. These create differences and sometimes similarities among the standards. However, the most globally used standards are the European (EN)[17,112] and American Standard Testing Materials (ASTM)63,171 for bricks and structural clays.

For brick manufacture, irrespective of the type of brick, the most crucial property or parameters mostly looked out for are the strength, durability, required colour, water absorption, porosity test and physical characteristics of the fired products[5,24]. The durability is linked to the strength and absorption rate of the product. These properties will be discussed as subheadings thoroughly.

2.13.1 *Compressive strength*

The strength test is one of the most important measurements and properties needed for a structural application. Compressive strength testing has been preceded by the European standard EN 772-1, which requires that the surface is filed to flatness before applying force.

However, the BS standard 3921:1985[112] stress to failure is conducted on wet samples between plywood. The total number of test pieces should be an average of 10 samples. Each brick failure is recorded individually and then calculated to a percentage over the mean.

Murmu & Patel[21] relate the two principal factors that directly affect the crushing strength of heavy clay products as the choice of forming method and the raw material composition. A case in point is in the utilization of 10% bottom ash of olive pomace, which resulted in 33 MPa lower than the base material (47.96 MPa) and increased additive level up to 20 wt% obtained even lower compressive strength of the ceramic (14.2 MPa) when ceramics was fired to 950°C172. Another study[150] suggests that the firing temperature, rate of holding or even the firing atmosphere have a significant role in the final strength of brick and tiles. Engineering bricks have high strengths, and manufacturers are expected to achieve the limit or exceed it for a class A or B masonry type (125 MPa/75MPa, respectively)[17].

The discrepancies in recent literature on brick and tile strength for masonry result from product developers not adhering to one standard or clarifying the type of brick being altered, especially with additive incorporated articles. This scenario does not help keep track of specified problems being tackled with a brick type in terms of durability or strength.

2.13.2 *Water absorption test*

This test determines the clay brick's open porosity, significantly affecting durability[168]. Wu et al. [173] investigated the use of red mud in a ceramic application and obtained 45.64% water absorption when ceramics were fired to 1100°C by pressing. The authors[173] did not provide the pressure of the forming technique. Meanwhile, ceramics containing 2.5-10wt% charcoal fired to 950°C were found to be 19-40% by soft mud shaping technique[174]. Engineering bricks (formerly Class A and B) produced by extrusion are expected to achieve a limit of

4.5% and 7.0[17]. The method is achieved by immersing fired clay masonry into cold water for 24hrs or 5hrs in boiling water in BS EN 772-7[17,175].

2.13.3 *Durability test*

The durability of clay brick is related to the size or micropores of the brick, and the crushing strength test is related to product porosity and firing temperature, which determines the afore properties[5,176,177]. The direct measurement is determined by freezing and thawing engineering bricks for 100 cycles to check for cracks and falling apart of brick pieces due to environmental changes causing the brick's water to expand and contract[17]. Durability is reported eighter as fail, moderate or pass based on the effect of the test described above. Instead of direct durability testing, the Maage[177] equation uses the pore size distribution obtained by mercury intrusion porosimetry measurement. Winslow[178] explains the Maage equation in two halves: the first equation reports on larger pore volume, which produces a non-durable ceramic product, whilst the second part of the equation considers pore size >3μm that makes up the overall pore volume but does not retain water due to its ease in expelling water from the system. This should mean that a larger pore size should promote brick durability because water is quickly drained from the system. The equation is (3.2/PV) +(2.4 × P3). PV is defined as the pore volume, and P3 is the percentage of PV >3μm. For durability studies, the ASTM Standard C67/C67M-21 uses 24-hour cold soaking versus 5 hours of boiling water testing to predict heavy ceramic durability accessment[179].

Aside from porosity, high strength and high firing temperature have been reported to produce products which withstand the freeze and thaw process[180]. Also, with durability, other destructive conditions such as acid rain-related attack and dissolution, crystallisation of salt can be conducted[176]. However, it is advised to measure by direct exposure to severe weather for certainty.

2.13.4 *Efflorescence and scum on clay ceramic surface*

In past times, attention to the crystallization of sulphates or surface stains appearing on ceramic surfaces of unfired and fired clay bricks has been looked into, and investigations have been conducted to understand its causes and effect on structural works. Brownell's works have brought much clarification[2,181–187]. The terminologies efflorescence and scumming are two different surface defects that affect clay brick. Scumming is the whitish stain on the ceramic surface during drying (dryer scum) or firing. It is exceedingly difficult to remove, whilst efflorescence appears at the latter stages on fired clay products when exposed to extreme climate conditions causing the formation of visible salt crystals or flaky stains and deterioration over time[2,188,189.] **Figure 2-16** shows an example of effloresced brick of clay composition containing sulphidic mine waste fired to 965°C.

Figure 2-16*:* Effloresced ceramic containing sulphidic mine waste fired to 965°C[73].

In the 1940s, Brownell [182] investigated the primary cause of the whitish deposits found on clay products and reported that the salts are formed during the thermal treatment by the reaction of sulphur gas and the solid-state reactions involving SO_4^{2-} ions. Tourneret et al. [168] also suggest that the temperature for firing, oxides present in the raw material, and mineralogy are significant parameters. Merrigan [190] confirms this by describing three basic conditions that cause the soluble salt formation on the brick surface (Efflorescence). These conditions are the presence of sulphates in the brick, moisture to evaporate the salts and a path to transport the soluble salts to the surface during hot temperate seasons. Scum is scarcely described or talked about in the literature compared to efflorescence.

Impurities that promote the crystallization of sulphates on drying and the fired product have been identified. These impurities are pyrite (FeS_2) and siderite found in some clays, the fuel type, and additives to improve product function[49,87,186]. Palmer[189] commented that even lower levels (<1wt%) of sulphates in clays can cause scum but are less likely to efflorescence. Sulphate or salt restrictions or limitations are given in the European Standards [112] and American standard testing of materials (ASTM)[63]. Fly ash (Class F)[191], slags[192], and calcium-rich wastes are common sulphate inducers to structural products[190,193].

Various colour stains, brown or green, can appear on a brick surface other than white stains, based on chemical elements found in the composition, such as vanadium, molybdenum, and manganese[190,193].

Efflorescence found on clay bricks is sometimes caused by “backup materials” at the joints filled with cement-based mortar through pores of the body by the mechanism of evaporation[194]. Sandblasting is the most common means of removing efflorescence[190]. Stains caused by the reaction of CO_2 and $Ca(OH)_2$ or KOH are impossible to be removed because of the hard coatings it forms on the body forming part of the surface. According to Broken and Nijland[195], soil and environmental conditions are another cause of

Efflorescence. Moreover, particle sizes of soluble salt, an atmospheric condition in the kiln, firing times and temperature and incomplete $CaCO_3$, but in compositions where $BaCO_3$ and $CaCO_3$ both exist, Barium carbonates fail to stop efflorescence[182]. Gredmaier et al.,[151] reported a phenomenon called "black coring," denoting a description of a fired clay product having a colour scheme of the interior different from the outer shell caused by SO_4^{2-} in clay.

To destroy pyrites silicates, react with sulphates at 1034°C[181]. Also, sulphur is removed at temperatures less than 400°C in clays. However, it depends equally on clay mineralogy, composition, and atmospheric condition in the kiln and around the product[196].

To date, eight preventive measures for reducing or eliminating scumming/ efflorescence via modifications prior to firing; and two after-firing remedies have been described in the literature. These include (i). reduction of soluble salt contents from building products[63,112], (ii) longer firing times at matured temperatures (1200°C; most bricks products do not get to this temperature[197]) with improved draft systems to remove sulphur-rich gases[181] Although it may successfully prevent the appearance of whitish stains on ceramic products, it is not economical for manufacturers as consuming more fuel will impact the overall cost of the fired product and increase CO_2 emissions and sulphur-rich gaseous emissions, which are detrimental to the environment. (iii). Firing under a reducing atmosphere[198] (iv). Optimization of additives with the use of ammonium chloride affects the clay body by opening pores for oxygen exchange and release of sulphurous gases from within the ceramic body at lower temperatures during firing (<400°C)[184,196], (v). Adding < 1% ammonium phosphate to high carbonate clays[199], (vi). Silica and flint sand additions have been suggested to reduce efflorescence by reacting with sulphates at elevated temperatures, stopping its formation[184], (vii). 4wt % grog (crushed fired ceramics) and $BaCO_3$[67,182,200];(viii). Ceramic sludge from the whiteware industry can convert soluble salts to insoluble salts[201]. Post-preventive measures: (i) immersing high-content carbonaceous fired ceramics in water for a maximum of two hours to wash away soluble salts caused by

lime and minimise the rate of effloresce after firing[202] (ii). reduced water absorption rate (0-6%) due to higher densification stops efflorescence caused by backup materials such as mortars[182].

Testing for efflorescence is captured in structural application standards where: (i) product soluble content is declared[112] or (ii) products stated as either effloresced or non – efflorescend[171]. For over 50 years now, $BaCO_3$ and sometimes a mixture of ammonium lignosulphonate have been used as scum and effloresce inhibitors in large-scale industrial production of brick-purpose products[203]. The additive $MgCO_3$ has been discussed in **Chapter 5** as an alternative additive in brick manufacture to lower sintering temperature and stop scum formation.

Recent publications of cement and concrete researchers use $BaCO_3$ for the same purpose in products [204–207]. The use of $MgCO_3$ as a sulphate resistance has never been looked at in literature.

2.13.5 *Defects associated with the manufacture of clay bricks*

Lynch[208] gives a good description of the general brick properties highlighted in the pages above. Defects associated with fired clay bricks can be controlled if the firing profile and clay chemistry or composition are understood. This section describes and explains the common defects associated with brick manufacture.

"Black core" is caused by trapped sulphur within a fired brick resulting in a distinct colour difference in the core and the outer section of the brick, which cannot be removed and is caused by excess sulphur in the furnace and a fast-firing approach of [84,151], as shown in **Figure 2-17**.

Figure 2-17: source Gredmaier et al.,[151] Black core a significant problem in heavy clay brick manufacture.

Bloating is another common flaw in firing clay bricks, as **Figure 2-18** shows. Bloating occurs when gases are trapped in the shaped clay and cannot readily escape during firing. Iron compounds, carbon, sulphates, alkalis, and alkaline earth are said to instigate the defect[209]. Overfiring, another defect, causes excessive swelling and expansion of the baked/fired material affecting product dimensions. An overfired product is simply a waste of fuel and product. Dilatometry is the routine tool used to predict the firing temperature of clays and bodies to avoid underfiring and overfiring, which sometimes results in complete melting affecting kiln elements and refractories. **Figure 2-16** shows an example of an overfired clay product.

Figure 2-18: Bloated ceramic distorting ceramic shape[210]

Alkaline earth oxides also cause lime blowing; it has been mainly observed that larger particle sizes of lime ($CaCO_3$) and dolomite ($MgCO_3$) leave physical pores on the surface as a result of the blow [208]. Essential remedies to lime blowing are reduced particle sizes of the carbonate-containing substances and soaking brick in water after firing[11–213].

Figure 2-19: Overfired heavy clay product

Distortion in shape is another fault in heavy clay production caused by inhomogeneous drying or the clay blend containing excessive flux content resulting in an increased shrinkage from over-burning; these are also colloquially known as 'crozzles'[208]. Scumming and efflorescence have been reviewed in **section 2.13.4**, and research findings are presented in **Chapter 8**

2.14 Additives used in heavy clay ceramic manufacturing

Substituting solid wastes or other materials into clay brick-making has been promoted since the discovery of fired clays. Clays are mixed with other additives to enhance or alter clay brick properties. In Egypt, straws were added to air-dried clays for easy drying and to produce lighter-weight bricks[214]. Reprocessing or reusing wastes is influenced by the availability of preferred or appropriate quality clays, fuel reduction, product enhancement

and landfill levy, as 8 Mt have been recovered for manufacturing over the last 30 decades[20,57]. Clews[24] reports the low levels of preferred clays causing industries to find and move to other new sites for clay extraction. However, unlike other ceramic products concerned with 100% purity, the heavy clay product manufacturing industries are not so concerned about impurities. Rather, clays are the best containers of other industrial waste [12,14,15,45,211–214]. So ceramic research for development has switched from kiln development to body-mix recipes (Clay bodies) specifically to minimize fuel costs and conserve clay deposit sites.

The main reviewed journal articles on waste additives are [12,15,47], and the most important works are [20,214]. They are important because authors [20,214] show the role of industrial waste discussed, but waste codes regulations and their off gases in great detail.

The addition of secondary materials introduced to clay brick to alter a specific property is described by manufacturers and researchers[14,15,39,57,60,211,214]. Several types of additives can be identified and grouped as follows: (1) fuel or pore former types, (2) fluxing types, (3) non-fluxing or fillers, and (4) colourants[15]. Dondi et al.[15] grouped additives into four groups but with an added category of; fly ash wastes, plasticiser and non-plasticiser. These four categorized sections of additives used in the heavy clay industry could broadly be grouped into two organic and inorganic additives. However, both could be sourced from industrial waste streams or mined. Regulations to particular waste streams like glass[215] and others are in place. Greenwood [13] outlines nine (9) fluxing materials used in clay masonry bricks with factors contributing to an early melt. These categorised additive types and their effect on microstructure and brick properties are mentioned in the **sub-sections** below (**2.14.1-2.14.4**). Overall, four main factors affect the use of additives: additive level, firing temperature, clay

mineralogy and chemical composition. The general effects of additives in body compositions are summarized in **Table 2-5** below.

Table2-5: Additive effects on clay body compositions for heavy clay production[15,16,20,35,51,57]

Additive Type	General Effect
Organic wastes	Odour and lower densities may act as body fuels and even fillers if ashes are used, improving thermal properties in the form of micro -pores
Inorganic wastes	provide fluxing properties, emissions, energy reducing
Industrial wastes	Leaching of metals improves strength, fluxing property, improves compression strength or decreases density, colour change, improves the microstructure
Fuel wastes	Colour effects, body fuels, emissions, damage to refractories and kiln linings

2.14.1 *Organic pore-formers additive type*

Organic additives are fuel-type because of their high calorific value, depending on the additive type[216]. Some carbon-containing fuels added to heavy clay ceramics are palm kernel shell, bagasse (crushed sugarcane fibre)[217–220], petrol, coal or coke, cigarette butts[221,222], olive oil residue[216], sawdust[61,62,223], paper industry waste[125,224–227] and other agricultural wastes[228]. The benefit of these additives is to produce lighter or more porous bricks with less mechanical strength, high insulating or thermal properties, and cost reduction on firing. Polymeric wastes are also pore-reducing additives[229]. Moreover, how light clay ceramic

product is is highly dependent on the level of organic waste in body composition, usually levels greater than 5wt%[59,214,225,234].

Díaz-García et al.[216] studied the effect of industrial waste olive oil residue incorporated into clay bricks to minimise the waste sent to the landfill. This study showed that 3-10wt% additive improved strength at 850ºC (the highest strength was 33MPa at 3w% additive levels). However, an increment in waste (10wt%) addition introduces pores which negatively impact the strength 17MPa compared to 53 MPa for the control as the residue decomposes during the initial firing stages.

Other studies were conducted on the 0-50wt% replacement of olive pomace bottom ash into clay and semi-dry pressed using a uniaxial laboratory press of 54.5 MPa load. Samples were then fired to 950°C at a 3°/min heating rate for 4hrs. It was shown that additive levels greater than 30wt% produced a less dense (1.481 -1.278 kg/m^3) product compared to the control (1.757 kg/m^3) product with higher porosity (26 to 33%) and lower strength (14 to 12 MPa). However, 10-20wt% replacement fulfilled the UNE-EN 772-1 standard strength with 33 MPa and 15 MPa, respectively[172].

Aouba et al. [230]. characterized the inclusion of olive stone flour (2, 4, 5 and 8 wt%.) and wheat straw (1, 3, 5 and 7 wt%) from agricultural waste streams. For this study, sand was also introduced into the mix as an original constituent of the base composition and extruded with dimensions mimicking the actual industrial parameters, then fired in an industrial kiln at 920°C for 1hr. The heating rate was not given. Results obtained from using the agricultural wastes again reduced thermal conductivity from 0.50 to 0.35 Wm/K and mechanical strength 44.4-24.8MPa[230].

5wt% and 10% olive mill waste were added to brick clay to produce a porous fired body. Cylindrical pellets were produced from the semi-dried body at a force of 20MPa. Samples for firing were heated to 600°C at 2.5°/min, then raised to the top temperatures (850°C,

950°C and 1050°C) for 2hrs at a heating rate of 10°/min. Results show that higher percentages of organic additive introduce more significant pores (~47%)than 5wt% and 0% additive[231].

The toxicity level of cigarette butts with their unhealthy ways of disposing into the environment and the dangers it poses after 2 years on soil has been discussed by Kurmus et al.,[222] and propelled the study of the impact of cigarette butts in brick production. Actual experimentation at the lab with cigarette butt into clay brick for structural applications reported that 1wt% of cigarette butt tended to reduce 58% of the energy (due to the unburnt carbon from the waste) needed for clay brick vitrification and to get rid of environmental pollutants by incorporating the waste into clay brick making[159]. It was estimated that 1-2wt% cigarette butt could save 10.20% and 14.71% fuel cost, respectively, whilst reducing density and environmental nuisance[221].

Goel and Kalamdhad[159] studied the incorporation of seaweed or freshwater floating plants Hyacinth of the genus Eichohornia of the Pontederiaceae family, doped in varying percentages (0-20wt%) to either laterite soil or alluvial soil in brick making. They obtained from their research that 10wt% seaweed has the potential to reduce 7% fuel consumption to reduce density (i.e., 1.56 to 1.31 g/cm^3) due to pores created by the aquatic weed and with no physical defects like black coring or cracks and efflorescence where ceramics were fired to 900°C. Except for higher water absorption percentages recording 25% and 41% with additives greater than 10wt% in soils used and fired to 900°C they also explained that this organic waste increased the release of greenhouse gas by 153% for laterite ceramics and 205% for alluvial ceramics fired to 900°C, although its fuel consumption was minimised by 7%. The use of bagasse ash waste from sugarcane plantation[217–219,232], although organic, promises to be an excellent filler in clay bricks because of its high silicon (85.58%) and alumina content depending on the soil in which it was grown and the correct ratios of ash

added to the clay[217,233]. While the only setback to this waste (bagasse) is strength reduction attained at 1000°C without shape distortion. Efflorescence caused by soluble salt-rich clays can be reduced or removed with sugarcane ash replacemen[234]. Consequently, studies reveal the harmful effects of the bagasse on fired samples, such as black coring caused by the unburnt carbon, efflorescence or even with colour change which is an important technological and consumer requirement[218]. Interestingly, according to Teixeira et al.,[218], the crystallinity of the bagasse ash and the main mineral phase wollastonite, which forms at temperatures below 900°C, makes it an excellent substitution for glass–ceramics.

Moreover, in the presence of limestone and K_2CO_3, energy consumption is minimised to produce glass ceramic at temperatures <900°C. So, it can be inferred that using bagasse in brick-making provides more than one advantage: fuel reduction, filler and minimising efflorescence. Like all other studies on fired bricks, compressive strength testing and absorption tests were conducted; however, freeze and thaw should be conducted for this formulation of bagasse ash inclusion to see whether this new body meets up with the standards of durability. The fine raw bagasse in ceramic body formulations has not been studied yet.

Waste sewage sludge, classed as organic bio-solids, has been successfully used as an additive in making fired clay bricks due to its availability[235]. Ukwatta and Mohajerani [235] concluded that bio-solids incorporated into clay bricks could only be useful in non-load-

bearing structures because of the lower density obtained by adding that waste. At the same time, a 1.5°C / minute heating rate was believed to minimise energy consumption in obtaining a sintered-fired clay brick. Sawdust has also been accessed as a potential sustainable, cost-effective waste to produce insulating products[236]. Sawdust is said to contain 61% carbon, 1% nitrogen, 34% oxygen and 5% hydrogen[61,71]. Cultrone et al.,[71] examined how the firing temperature and additive level affect the brick property. They concluded that

up to 10wt% sawdust as an additive increased porosity (~60%) with lower density (1 g /cm^3) even at temperatures above 1000°C. Moreover, the addition of sawdust does not affect the fired colour of the ceramic product and crystalline phases.

Assessment of petroleum wax with a calorific value of 31,000 kJ/kg in the brick-making was examined by Dondi et al.,[15], and it was stated that 1-2wt% increased porosity and significantly decreased fuel cost due to the additions. Almeida and Carvalho[237] observed improved drying with this petroleum wax, a body fuel.

Charcoal is produced by reduction firing[174]. The physical and mechanical properties of charcoal additions at 2.5%, 5%, 7.5% and 10wt% incorporated into brick manufacture were studied by Phonphuak et al. [174]. Rectangular hand-shaped soft mud technique of 5.0cm x 9.5cm x 3.0cm sizes was dried and fired in a gas furnace, holding the temperature at 2hrs at the maximum temperatures at 50°C intervals (900°C-1100°C). The findings of this examination showed that particle sizes of 0.5mm with the lowest additive level as temperature peaks and improved compressive strength of 143 MPa for 2.5% additive level is achieved with lower levels of water permeability of ~18%. Meanwhile, particle sizes of 2-3mm charcoal in high proportions increased porosity (34%-54%). Fired sample images also showed a reduced section caused by the charcoal additions, especially with samples with the smallest particle size fired to 950°C shown in **Figure 2-20** as an unburnt carbon.

The properties and results obtained are not so different from the density reduction obtained with the fuel additive.

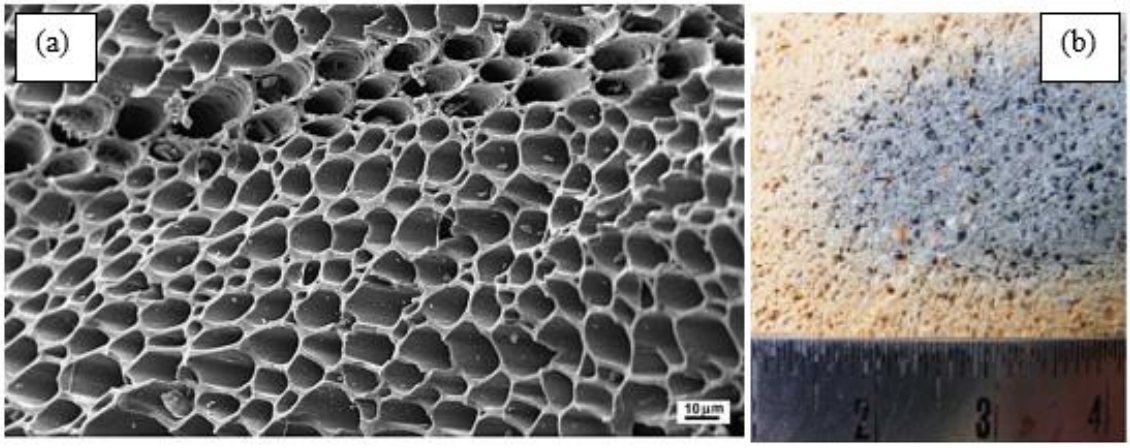

Figure 2-20: (a)SEM image of charcoal and (b) fired image of clay mixed with clay fired to 950°C [174].

The use of plastics in clay brick making has been explored, and it has been found to leave no residual ashes behind, therefore an excellent pore former and weight-reducing additive. Veiseh S.et al.[238] reported that 1.5wt% plastics recycled into clay and fired to 1050°C improved ceramic strength (125 MPa) and water absorption (22.5%) due to the formation of mullite from melt species as well as the additive's potential fuel savings which the authors did not quantify. Moreover, they demonstrated that polystyrene foam of 3.35mm sieve reached a density of 0.98 g/cm^3 higher than 0.89 g/cm^3 of non-sieved polystyrene.

Finer particle sizes (0.6mm) of rubber tires compared to chopped bottles of 1.18mm and 2.26mm were reported to slightly affect compressive strength (11.88 N/mm^2) and water absorption percentage (22.32%) positively when 2wt% is added. Different particle sizes (1.18mm and 2.26mm) of polymeric wastes affect surface texture with flaky shapes promoting high porosity, whiles high levels (10wt%) of the rubber tire additives cause black coring and even surface texture[239]. These are shown in **Figure 2-21**.

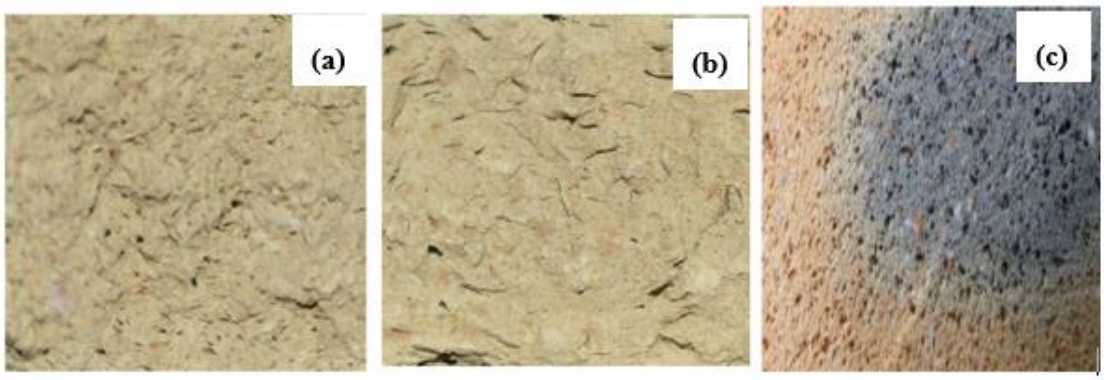

Figure 2-21: Effect of additives particle size on clay brick composition extruded and fired to 1000°C (a) plastic bottle 1.18mm (b) plastic bottle 2.26mm and (c) rubber waste 0.6mm added in 10wt%[239]

Plastics sourced from automotive waste (in 1mm-2mm) were added to clay at 1wt%, 2wt% and 5wt% and fired to 1200°C to produce a low-density pellet in 20mins. The fast firing caused trapped gases from the plastic melts to escape resulting in reduced density. It was, reported that the decomposition of the plastics occurred between 380°C- 520°C, with recorded volatiles being methane, carbon monoxide and carbon dioxide. Black coring followed the fast firing of the plastics incorporation. Plastics in clay affected volume change (expansion) and promoted the amorphous phase of FeO and Fayalite on firing. The author has only reported strength for the control (5 MPa) and stated a reduction in strength for the admixtures without quantification. Water absorption was affected by the additive. It is reported to increase from 19.2% (control) to 22% with 1wt% levels and 23% for 2wt% additive levels[240].

2.14.2 *Industrial wastes additives*

Industrial wastes fall under inorganic wastes and organic wastes. Due to the melting flux traces, the inorganic wastes are said to improve the thermal conductivity of heavy clay products more than the organic waste, which reduces the closed pores in the ceramic[241].

The substitution of pulverised fuel ash, also known as fly ash, from the waste of thermal power plants has been widely investigated as one of the efficient means of contributing to the green production of fired clay bricks, especially if they are not thermally treated[241]. The incorporation of this waste material (fly ash) was investigated in two ways; by adding a proportional amount with a plasticizer and firing or activating with an alkaline aqueous solution without firing[80]. The non -conventional shaping and firing of bricks with fly addition was looked at by Lingling et al. [241], who were convinced that incorporating fly ash into ceramics promotes material efficiency and reduce CO_2 emissions on firing. The researchers [241], report that the carbon content in the fly ash can reduce energy reduction as the carbon will aid in the burning process. Cultrone and Sebastian[127] also confirmed the benefits of adding fly ash to solid bricks to reduce cost and the negative effect of decreasing density. However, Cultrone and Sebastian found that >5wt% of the waste alters the brick's physical (colour) characteristics. Both researchers recommend using a plasticizer when a high dosage of fly ash (75% by mass) is introduced into a mix. It should be noted that these bricks were fired at 1000^{o}C and 1050^{o}C. At the same time, the efflorescence test was positive, which means that with fly ash in the fired clay body, progressive wear is expected to occur. **Figure 2-22** below shows the morphology of how pulverised ash behaves under an oxidising atmosphere at 800^{o}C and 1000^{o}C. The sample fired to 1000°C shows a more vitrified structure than the sample fired to 800°C.

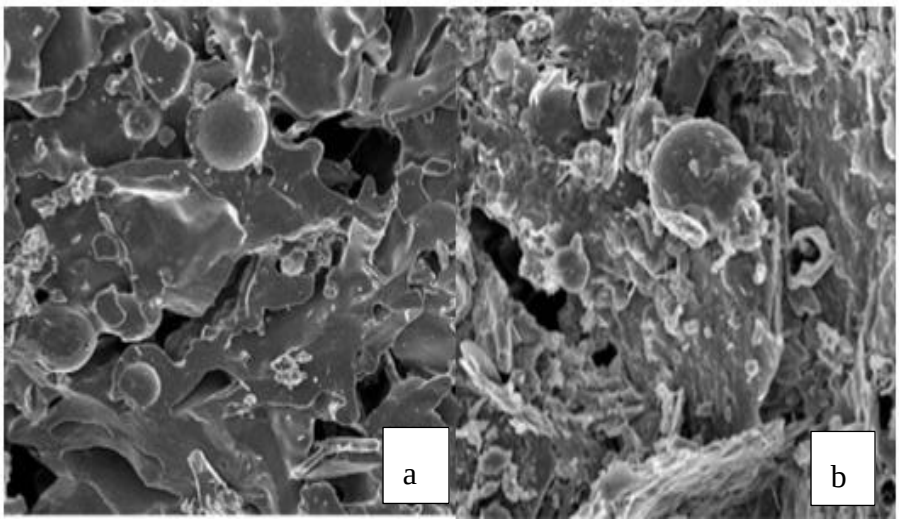

Figure 2-22: Source: Cultrone and Sebastian [127], Fly ash additive at (a) 1000ºC and (b) 800ºC.

Although the plasticiser used was not named in either paper, it suggests that the pulverised ash rich in SiO_2 content reduces the plasticity/workability needed to extrude the ceramics/bricks. The load applied to samples for the strength test was not recorded; therefore, repeating this study will be difficult despite the possibility of recycling fly ash into heavy clay production; the type of fly ash used, whether class F or C, was not stated. Secondly, there have not been any studies on the waste material (whether the class F / C) in a reducing atmosphere to see if there will be changes in the microstructure or improvement in strength.

YalcË õn and SevincË[242] demonstrate that bauxite waste, red mud, contains high Fe between 30-60%. The by-product from the aluminium industry was successfully used as raw material (37wt %) in making a glaze for ceramic wares, including porcelain and sanitary ware, because its chemical composition is a mixture of SiO_2, Na_2O, CaO, Al_2O_3, Fe_2O_3, MgO, K_2O and TiO_2. The experimental study revealed that red mud alone produced matt-craze glaze at 1100ºC. So, it could be inferred that adding bauxite wastes in brick-making can produce a liquid phase, binding particles together for a stronger body.

The benefit of replacing 50wt% clay with bauxite waste to improve physical and mechanical properties has been demonstrated by Pérez-Villarejo et al.[243]. They show that bauxite waste increases vitreous phase closing micro pores whilst it decreases water absorption rate in ceramics and improves compressive strength to 50MPa for a 60mm x 30mmx 12mm slab fired at 950ºC at a heating rate of 5ºC.

Foundry sand is used in the automobile industry for casting metal shapes. Clay brick manufacturers have explored this additive cause of its high SiO_2 content, which controls shrinkage, cost-effective when introduced to reduce plasticity (like smectites), sometimes foundry sand may contain organic binders and leaching metals like Pb, Cr and Mo[244–246]. Organic binders for sand casting are given by Tittarelli [246]. Fluxing species like Na, Ca, Mg and Fe in the range of >0.6% -5.2% have been present in the additive[247].

A combination of foundry sand and ferric slag (Waelz), a waste from an electric arc furnace containing CaO and Fe_2O_3, was found to minimize CO_2 and NOx emissions in the brick making, but HF and HCL increased with the additive use. It was stated that sulfur retention was prominent in the presence of alkali and alkaline earth oxides when temperatures were below 900°C. Additions of foundry sand in ceramic products produced 16%-10% and open porosity of 35.4% -0.18% when ceramics were fired in a tunnel kiln for 1hr at a temperature of 850°C. Density and flexural strength increased by the combined additives with 1.90g/cm^3 and 6MPa (for 15wt% Waelz), respectively[244].

Alonso-Santurde et al.[245] described two types of foundry waste (green and core sand wastes) incorporated into ceramic production. The green sand contains silica, bentonite, bituminous coal and water, and the core sand is a mixture of silica, binders and catalyst (given names of binder and catalyst not mentioned in the study). They reported that using sand wastes does not alter the clay mineralogy but shows slight changes in shrinkage (5.2% vs 4.9%) and water absorption (7.5% vs 8.1%). Meanwhile, the compressive strength testing was ~

10MPa, and the density for the core sand waste increased to 153 kg/m^3 for the green sand waste. Also, due to the high levels added (0-50wt%), lignosulphonate was added to the admixture to improve plasticity. The authors affirm that the modification of foundry sand meets the limit requirements.

Waste from the Belgaum foundry was added to a brick composition and was found to increase composition moisture content (i.e., from 9-11% to 12-14%) when 50wt% sand is added to make hand-made bricks of dimension 225mm x 110mm x 75mm then fired to 900°C after 15 days drying under a shed. This body was found to reduce mechanical strength from 5.68 MPa- 3.34 MPa with no impact on brick colour[248].

In previous work by Lin, Deng-Fong et al.[249], 15% waste foundry sands incorporated in tile manufacture were found to contain alkaline earth (CaO -2.35%, MgO-1.19%), Fe -7.21% and a high C content (7.65%) which aided in sintering as well minimized the firing temperature by 50°C significantly reducing cost and fuel use. However, the authors did not give the exact figures for cost and fuel cost. The authors stated that firing the composition to 1000^{o}C produced a homogeneous pore within the tile structure. Finally, waste sand from the foundry is viable in ceramic applications; only levels of the additions should be low not to affect workability. If fluxes in clay brick body composition are enough, leaching metals like Mo, Cr etc., from the foundry sand can be locked up in the fired clay matrix. Leaching metals like Pb, Zn, Cu, and V is a challenging problem with mine tailing waste. Heavy clay products can be the best receptacle for immobilising the leaching metals into metal-bearing minerals by chemical reaction during firing, replacing a parent atom with another (Al^{3+} / Ca^{2+}) with $Pb^{2+,}$ Cu^{2+} [250]. According to Suárez-Macías et al. [251], mining waste creates a porous structure due to its higher weight loss, lower shrinkage, and reduced density. Notwithstanding, the authors recorded colour variations as additive levels increased from 0-

100%, as shown in the diagram below (**Figure 2-23**).

Figure 2- 1: The effect of mining waste on brick colour as levels increased from 10-100% and the mixture fired to 950°C for 1hr at a heating rate of 4°/min[251].

Tungsten mine tailing's chemical composition can vary from region to region with high SiO_2 content (40-91%), low Al_2O_3 content (2-9%) and Fe_2O_3 (0.5-10%). Alkali oxides (K_2O + Na_2O_3) are low (1-6%), but alkaline earth oxides (CaO / MgO) could reach 28%. Tungsten tailings have been successfully used as a raw material in glass-ceramic making[252] and geopolymer applications as supplementary cementitious material and have been found to improve early strength[253–255]. In ceramic applications, the tailings waste (70%) was added to pure alumina and magnesium oxide and fired over six temperatures (1000°C,1050°C, 1100°C, 1150°C, 1200°C and 1250°C) for 2hrs. Findings show that the newly found waste can be incorporated into ceramic applications to obtain suitable properties and complex mineralogy (cordierite ($Mg_2Al_4Si_5O_{18}$, ringwoodite (Mg, Fe)$_2SiO_4$, corundum (Al_2O_3), enstatite ($MgSiO_3$), but there is no record of the additive in clay brick manufacture[253].

Chamotte, also known as grog, was used; a fired brick waste was added to clay and uniaxially pressed at 20MPa. Adding >5wt% grog increased porosity from 22% for the control to 23.6% for the 20wt% grog addition. The authors reported that >5wt% lowered the unfired and fired strength, partly because of the shaping technique and partly because the clay body was fired at 700°C [256].

Glass cullet types are widely studied as an additive in brick production mainly because of spinel's (A_2BO_3) formation, which has low thermal conductivity and high chemical resistance and reduces landfill waste[255]. Studies conducted by Mao et al.,[257] reveal the ability of cullet (waste crushed glass) to increase the strength of clay bricks from 20 MPa - 32.7 MPa because of the formation of the liquid phases that seal up most pores during thermal treatment. Galán-Arboledas et al.,[258] experimentation supports the use of glass cullet improving strength. Lin et al.[259] reports on incorporating 30-40% of solar panel glass waste into the ceramic tile of particle size 10µm -100µm to promote a glassy phase which seals up the micro-pore, enhancing strength. **Figure 2-24** shows the microstructures incorporating 30-40wt% SPG in the ceramic making with well-defined pores.

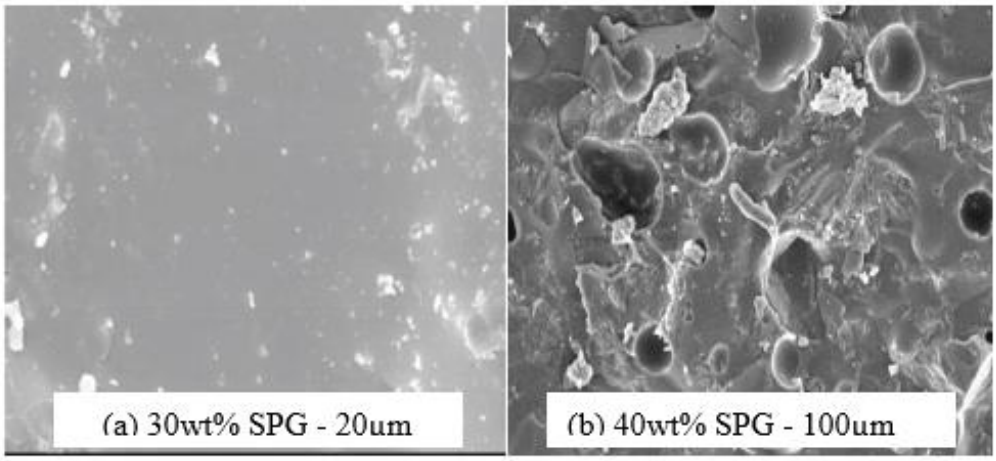

Figure 2-23: Effect of 30wt% and 40wt% solar panel waste glass in ceramic production[259]

Hwang et al.,[260] demonstrated that supplementing coloured glass waste can reduce the melting temperature by 50°C- 150°C when samples are fired at 900°C. Matteucci et al.,[261] reported that soda lime glass as an additive to ceramic products promotes liquid phase sintering at lower temperatures in porcelain stoneware tiles. Whilst supplementing for feldspar with electronic components (LCD) glass panel waste to produce ceramic tiles fired at 1100°C, improving strength and saving 50°C of energy cost[262]. Additions of glass waste

in ceramic applications improved drying shrinkage whiles increasing firing shrinkage positively due to its glassy phase formation[263].

Smith[264] explains that the reactivity of glass cullet recycled into bricks depends highly on its particle size. A brick manufacturing company in the UK conducted pilot testing on the possibility of waste glass as an efficient energy saver and a better-quality product. The result indicates that 5wt%- 10wt % of the waste glass, depending on the minerals present in the clay body mix, can reduce the energy by about 16% and improve physical properties. Nevertheless, processing waste glass to the finest particle size for production is expensive for industries [264]; therefore, optimising and exploring other materials or minerals that will be cost-effective for companies to use is a principal concern.

2.14.3 *Inorganic minerals as an additive in ceramic production*

Naturally occurring minerals as an additive have also been explored as a cheap material that could be used in clay brick products mainly because they contain alkali & alkaline oxides which function as a flux aid in sintering. For example, Souza et al.,[265] used gneiss, a metamorphic rock which is remarkably high in potash oxide (K_2O) flux, along with Na_2O, K_2O, MgO, CaO, Fe_2O_3, quartz and mica for floor tile body. Their study improved floor tile strength (from 28MPa ->50 MPa) by blending 47.5wt% to the gneiss rock to clay. They concluded that the additive enhanced the vitrification by behaving as a flux and lowered water absorption in bricks to 0.5% for 50 wt% additive levels compared to 6.5% for the control. However, because the study looked at the reformulation of floor tile whose shaping method (pressing) and high firing (1210^{o}C) temperature are higher than for most brick products, it may be possible to achieve the same or better results with an extrusion technique with bricks bearing in mind the effect of the additive on plasticity.

In 2006, Ibrahim et al.,[265] examined the effect of granite waste, whose main constituents were quartz and feldspar, by adding 5-10 wt.% of local potash feldspar to manufacture an acid-resistant sewage brick. The combination of granite waste and the local potash reduced the firing temperature because of its high flux content. It was obtained that granite alone in the formation without the local potash improved densification and mineralogy.

Vieira et al.,[266] obtained comparable results by incorporating granite waste in clay which fires red due to its high iron content. They observed a faster drying time (1.5% compared to 4.8 % of the base ceramics and no change in strength (8.5 MPa) with 40wt% of the granite addition at a temperature of 970^{o}C. The diagram below **(Figure 2-25)** shows the effect of granite waste on red ceramics.

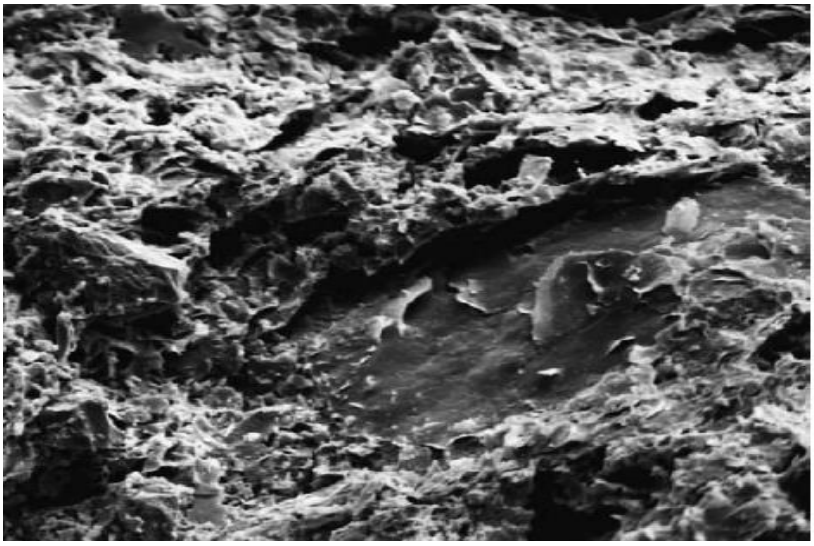

Figure 2-24: Effect of 40wt% granite waste in a clay bod[266]

Replacement of feldspars by natural zeolites in producing porcelain tiles was conducted by de' Gennaro et al.[267]. They show that dried zeolite provides better workability and produces more melt to densify the product. Despite this, the main drawback of this material is its high shrinkage rate (4.6%-8.7%) because of the liquid phase obtained at elevated temperatures for porcelain tiles[268].

Wollastonite ($CaO.SiO_2$) has a needle-like shape; when viewed under a microscope, it is advantageous in clay body addition as a filler, functions as a flux in ceramics, has dielectric properties, promotes drying, reduces cracking and excessive shrinkage mostly seen in fired products, as well as giving the same strength that glass waste provides[269]. Wollastonite has been used extensively in bio-ceramic applications due to its compatibility with body tissues, reduced colour effect and degradable properties[270–272].

The use of colemanite ($2CaO.3B_2O_3.5H_2O$) in ceramic compositions has numerous advantages beneficial to the metallurgist [273], as a filer in polymer applications[274], radiation shield in concrete applications[70], glaze and glass manufacture of which one of its benefits is with its early low melts above 300°C to enable the ceramic bond formation and falls under the category of calcium borates with main oxides being B_2O_3 (50·81%) and CaO (27·28%) [275]. Colemanite comprises infinite boron-oxygen chains joined by Ca^{2+}cations to form planes parallel to (010). Chemical information on colemanite from Turkey had 41% boron, 26% calcite, 5% silica and less than 2% (alumina oxide, magnesium oxide and strontium oxide)[70]. This result is slightly lower than what [53,273,275–277] reported. One interesting characteristic of lattice disordering through grinding and heating was that the large surface area caused an initial moisture release at lower temperatures[278].

For masonry applications (tiles), colemanite waste (5,10 -20 % by mass) has been added to the porcelain tile body as a new sintering additive, a source of flux to replace Na-Feldspar. The study revealed that waste colemanite in porcelain bodies starts to sinter at 915°C with continuous contraction, but as temperature increases, above 1050°C bloating occurs due to the decomposition of colemanite when fast firing is used. Slow decomposition of colemanite was observed at lower temperatures between 350°C-450°C. The main phases obtained at 1210°C in the colemanite body are mullite and crystabollite. Note that this compositional result still included Na, K feldspar and sand[66].

Celik et al.,[66] produced a low density (i.e. lower than 1000 kg/$m^{3,}$ which is 20–55% lighter) and better-insulating neutron shielding masonry material by incorporating 10% by

mass colemanite into perlite, carboxymethyl cellulose and coal dust body mix and fired the shaped ceramics with dimensions 50 x 100x 100mm^3 at 400°C.

1wt% partial substitution of colemanite and K-feldspar in the porcelain body reduced the temperature by 50°C in kaolin, k-felspar and quartz composition without compromising quality. New phases obtained from the colemanite addition included anorthite, mullite and quartz at elevated temperatures (1250-1300°C). Anorthite was visible only with samples with greater than 3wt% colemanite. The researchers also found that partial melting of colemanite occurred at 700°C on conventional firing and recorded even lower temperatures with microwave firing at 595°C[279]. This means that microwave firing can help with fuel reduction. Karasu[280] explored the use of solid waste borax in several ceramic applications, including bricks and found that 10wt% in a brick body could be fired to 950°C to obtain a satisfactory brick with no characterized study to prove the claim "satisfactory".

According to Uslu and Arol [281], waste tailing from borax extraction from the earth's crust contained clay minerals rich in borate. 30% of the tailing was added to the brick clay, shaped in a cylindrical mould (26mm x 38.8mm) and fired to temperatures of 700ºC-900ºC. Results showed that 30% of the tailing at 900ºC formed viscous glass and filled up pores, and improved ceramic strength (229 Kg /cm^2 compared to the reference brick 211.70 kg /cm^2), a change in colour from dark red to brown whilst conserving fuel cost of 200 or 100°C if ceramic samples are fired to 700°C and 800°C but which will yield a lower compressive strength test. Kurama et al.[282] point out that combining waste feldspar from the sanitary ware plant and boron (dewatering sieve waste) is an excellent means of obtaining vitreous ware. However, increased boron content produces blisters on the surface of the brick when fired. Kavas[283] confirms that using boron from Turkey in red mud bricks can only obtain a strong,

dense product at lower temperatures (900°C) by introducing 15wt % of the boron waste. Interestingly, Christogerou et al.,[284] obtained a distorted or warped rectangular pressed shape of 101mm x 20mm x 8mm when the temperature was raised >900°C for a body containing 15wt% boron. More so, without any bulk chemical analysis, Christogerou et al.[284] found out that the addition of boron increased porosity (23.6%) if the ceramic was fired to 800°C by 5wt% additive and increased strength from 26.4 MPa- 27.8 MPa for ceramics fired to 950°C because of the presence of fluxing additive for the bodies prepared after Kavas[283].

As a replacement additive to heavy clay ceramic ware, Boron promises to promote sintering and reduce fuel costs; although it is hard to burn contains more energy than petroleum and coal[284]. Conversely, the right fluxing content is needed to achieve the standard brick.

Borogypsum doped bricks have been explored by Emrullahoglu Abi[285] who found that 10wt % of this waste could improve strength when bricks are fired to 1000°C and 1100°C with recorded strength of 38 MPa and 48 MPa, respectively, as opposed to the controlled brick strength of 28 MPa and 38 MPa. The true benefit of this waste is its ability to reduce density to provide both technical and economic costs. However, transportation costs will make it impossible to use throughout the globe[13].

Greenwood[13] demonstrated that limestone ($CaCO_3$) and dolomite ($CaMg(CO_3)_2$) give rapid vitrification, while Chalk and Talc are considered an expensive alternative fluxing additive for clay brick manufacture. He also stated that phosphorous pentoxide (P_2O_3) as an additive is not a flux for brick temperatures (1000^{o}C -1200^{o}C) as it fires above 1115^{o}C.

30wt% of laterite soil, an inorganic material rich in iron and alumina oxides, was added to clay and fired to 1000^{o}C. The results showed that the additive improved the mechanical strength of 22.93 MPa with a decreased shrinkage of 4% compared to 7.5% and minimized the thermal conductivity of the product from 0.64 W / m. K of the unfired to 0.34 W / m K

for the fired ceramics containing 30wt% laterite. Moreover, the TG/DTG of the laterite shows no thermal reaction after 650ºC; this is shown in **Figure 2-26**.

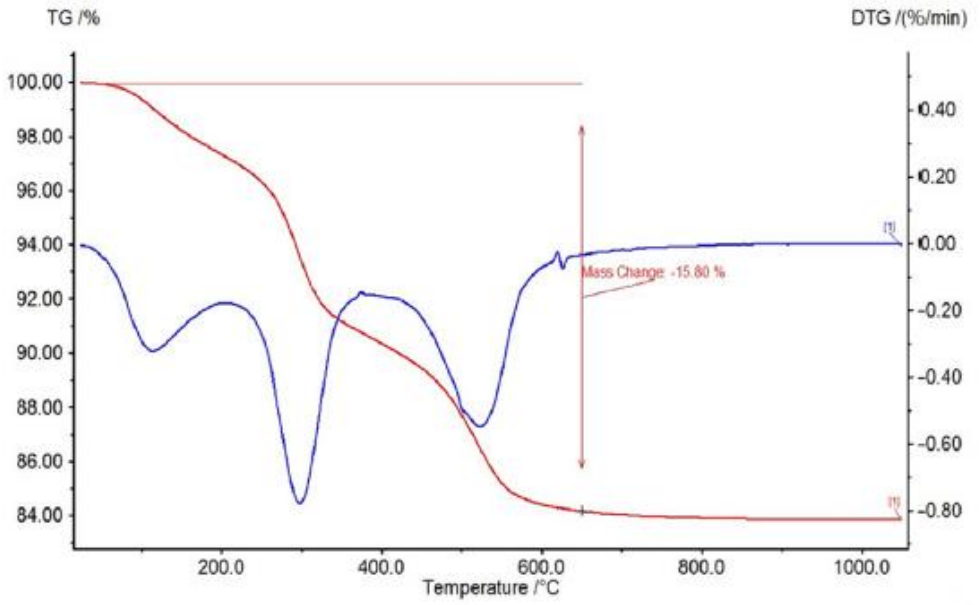

Figure 2-25: Thermogravimetric and derivative curves of laterite soil fired to 1000ºC at a heating rate of 10ºC/min [286]

Nepheline syenite ($K_{1.37}Na_6(AlSiO_4)_8$) is an igneous rock mined for industrial applications [287–290]. The rock has been distinguished from feldspar as a low silica material rich with alkali and alkaline earth oxide and other impurities such as clay fines and iron[287,291]. For this reason, nepheline syenite is processed to separate the actual ore from the impurities. However, suppose it is used in clay brick production. In that case, the beneficiation processing will not be necessary as purity is not required in clay brickmaking. For ceramic applications, only 15% of nepheline syenite is used, while 70% is utilized in glass making, and the remaining 15% is sourced for plastics and paint applications[292,293]. The principal fluxing oxides in nepheline syenites are the Na and K, which are mostly more than 14wt% compared to about 12wt% in feldspars[287,294,295]. However, what seems confusing in the literature is what researchers term low silica content without quantifying the amount. For example, studies conducted by Salem[296] recorded a value of 60.14% of SiO_2 for the chemical

content, yet stated that nepheline syenite is deprived of silica (SiO_2); meanwhile, Pranckevičienė.et al.,[295] records 44.80% SiO_2 for nepheline syenite used, as shown in **Table 2-6**.

Oxide	References			
	[292]	[295]	[296]	[297]
SiO_2	60.14	44.80	60.1	60.02
Al_2O_3	23.50	28.60	23.5	23.01
Fe_2O_3	0.09	2.60	0.1	0.46
CaO	0.40	1.20	0.4	0.27
MgO	0.03	0.60	0.0	0.01
K_2O	5.00	19.50	5.0	6.32
Na_2O	10.40	-	10.4	9.69
Ti_2O	0.00	-	0.0	0.01
L.O. I	0.55	0.90	0..6	1.09

Table 2-6: Published chemical analyses of nepheline syenite as a fluxing additive in wt.%

Although 15% of the nepheline syenite is heavily used in the ceramic sector, it is consumed mainly by the stoneware and porcelain manufacturers because of : (i) the additive's energy savings on elevated temperatures beyond 1200°C, (ii) promote early melt and semi-vitreous phase, (iii) vitrification, (iv) reduce internal stress caused free quartz and (v) facilitate ceramic bond[81,298]. The nepheline syenite processing makes it unattractive for the clay brick industry mainly because of cost implications. However, as mentioned earlier, clay brick could effectively use un-refined rock ore. Talc is an inorganic mineral that is soft and hydrophilic with the chemical formula $Mg_3Si_4O_{10}(OH)_2$, commonly referred to as magnesium silicate low in Fe[299,300]. This material has been extensively used in the body compositions for bioactive material[299], papers[301], ceramic, glaze, glass, cosmetics[302], paints[303], polymers[304] and in the pharmaceutical industry[305] due to its low cost and specific

property obtained from product to product. **Table 2-7** summarises some industrial applications of Talc and its chief role.

Table 2-7: Summary of industrial applications of Talc

Industrial Applications	Role
Plastic/rubber/	Stabilizer
Paper industry	Filler, stabilizer, sticky control agent, smooth surface, chemically stable, and minimize surface friction
Cosmetics	The Microcrystalline feature allows it to be used, skin-friendly
Paints	Thickener in paints
Pharmaceutical	Agent in drugs
Food (confectionary)	Filler, stabilizer, and non-sticky
Animal feed	Additive to improving weight gain in livestock
ceramics	Mechanical strength, filler, stop crazing, cracks,

2.14.4 *Alkaline earth as a fluxing agent*

High carbonated clays are excellent energy savings and deliver workable plasticity, which is significant in shaping / extrusion[258,306]. In contrast, its high plasticity makes the product prone to excessive shrinkage during drying and firing, and it can absorb more moisture during forming due to the surface area[258]. Another shortcoming will be an increase in porosity, but this effect also depends on the levels of carbonates present in the material. While higher temperatures are needed for non-carbonated, the opposite is said about carbonated clays[57]. For example, studies conducted by Trindade et al.,[306], with magnesium and calcite-rich clays prove this trend. **Figure 2-27** shows the microstructural effect of high calcareous content in brick production, resulting in a highly porous structure.

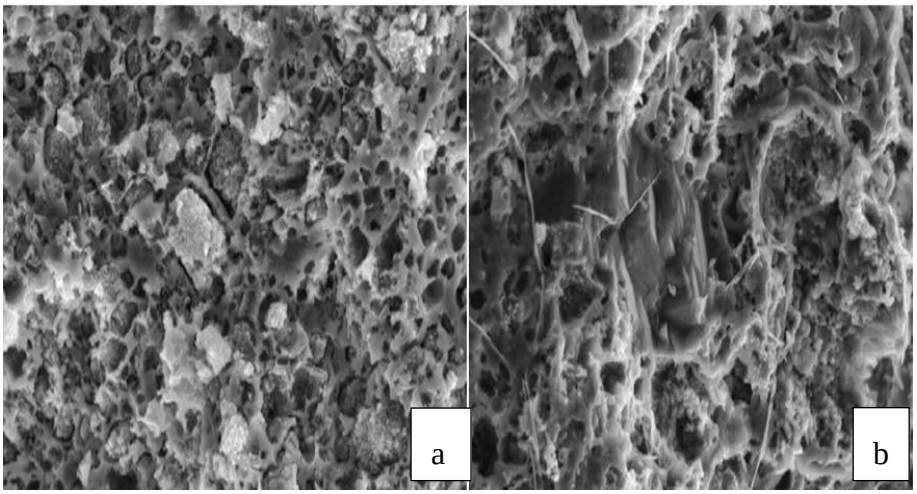

Figure 2-26: Source: M.J. Trindade et al. [306], Effect of Magnesium Oxide (MgO [a]) and Calcium oxide (CaO [b]) flux in a brick composition.

In dielectric application, 10wt% $BaCO_3$ was introduced to a mixture containing talc, kaolin and bentonite clay and fired to 1000°C and 1250°C[44]. The additive promoted new crystalline phases, such as $BaAl_2Si_2O_8$, Ba_2SiO_4, and $BaSiO_3$, at 1250°C; no barium-forming compound was obtained and promoted porosity due to the decomposition of the clay[44]. An additive % of $BaCO_3$ greater than 6wt% in porcelain body having initial constituents as clay, Na feldspar and $NaSiO_3$ as a deflocculant fired to 1210°C was found to increase porosity from 0- 7%[307].

Therefore, although less energy may be required to fire ceramics between 700 and 800°C, using fluxing oxide may be the smartest or best option. However, CO_2 emissions released during firing could still threaten the environment; therefore, newer routes and a thorough understanding of brick clays and specified brick types should be established.

2.15 Unfired brick products compete with fired clay bricks in terms of energy reduction

Unfired brick products have been debated as the ideal solution for energy consumption and zero greenhouse gas products. An example is the Adobe bricks, also known as compressed earth bricks or mud bricks, made from clays and used as structural material[308]. As the name suggests, the processing of Adobe brick requires no firing for its strength; therefore, researchers [127,309] believe the use of unfired brick such as Adobe is an effective alternative for energy savings to fired brick products since it does not depend on fuel heat to determine its properties but takes heat from the sunlight to dry just as in ancient times. Hence, it has zero emissions, costs less labour, and saves energy required to obtain a rigid and dense product. Although adobe brick may be an excellent alternative to fired clay brick products, Zhang [309] states that fired bricks have versatile advantages such as strength, resistance to wear and water, compared to unfired bricks, even though the energy cost may be high. Again, products are designed to fit their intended purpose; thus, product properties and characteristics enable them to perform their function. Therefore, for clay bricks or tiles to serve their intended use, it is thermally treated to be durable.

Nevertheless, although the compressed earth bricks are mainly used for structural purposes, additional treatments are added to the surface to resist wet-weather conditions. Adobe brick is mostly stabilized with cement as a binder, a significant contributor to CO_2 emissions (8%) produced annually[310]. Therefore, the firing of bricks must be understood by changing/altering their physical and chemical characteristics to provide the service intended for them. Secondly, the mechanical strength of unfired bricks, whether un-stabilised or stabilized, is lower than fired clay bricks. Oti and Kinuthia [311] examined the use of blast furnace fly ash into unfired clay, just like the geoplymerization of cement, to combat the

energy usage and CO_2 emission facing the heavy clay industry. However, the sustainability of the substituted blended material may be questionable as the same material is derived from steel processing, which is also energy intensive.

About 95% of studies on brick clay modification focused on the additive effect on the ceramic property. Moreover, only a few studies reported on energy savings and CO_2 reduction. This is summarised in **Table 2-8**.

Table 2-8: Summarises some additives used in heavy clay manufacture and their associated energy and CO_2 reduction.

Reference	Additive	Levels (wt%)	Temp (°C)	CO_2 reduced	Fuel reduced	Effect
[312]	Steel slag	30	950	17.6%	24%	High water absorption and reduced strength
[264,313,314]	Soda-lime glass and Container glass waste	5-10	960,1000-1120	20%	15-40°C for six different UK clays	Improved strength water absorption and zero efflorescence
[222]	Cigarette Butt	1-2.5	1050	unspecified	16.70-18.37%	Reduction in strength and high porosity with mild efflorescence
[315]	Waste marble sludge	5% - 25%	800	unspecified	unspecified	Reduction in strength and high porosity with an additive increase
[316]	A blend of biomass and granite waste into ceramic production	2.5	550-1050	unspecified	7.7%	Energy savings from the biomass and sintering aid from the granite Increased or decreased strength based on additive levels.

Reference	Additive	Levels (wt%)	Temp (°C)	CO_2 reduced	Fuel reduced	Effect
317	Kraft pulp	2.5,5 & 10	900	unspecified	unspecified	No black coring. Low-density bricks, low strength and high porosity. Energy contribution
159	Water hyacinth	5-20	850 & 900	unspecified	7%	Increased CO_2, energy savings decreased strength and high porosity as additive levels increase
234	Waste rice husk and sugarcane bagasse ashes	5	-	unspecified	unspecified	Prevent efflorescence, and promote low density and compressive strength. High porosity
238	Polystyrene foam	0.5-2	900-1050	unspecified	unspecified	Lightweight bricks
41	Waste from granite sawing	20-60	1150-1200	unspecified	unspecified	Increased water absorption is proportional to additive waste. Non-plasticiser and contains fluxing oxides

Reference	Additive	Levels (wt%)	Temp (°C)	CO_2 reduced	Fuel reduced	Effect
[174,318]	Charcoal	2.5-10 5,15&30	900, 1000, or 1100 °C	unspecified	unspecified	Low strength, increased porosity and shrinkage Particle sizes affect brick property
[245,248]	Foundry sand	0-50,	850-1050	unspecified	unspecified	Lower strength and shrinkage with increased water absorption
[244]	Blend of foundry sand and Waelz slag	20-40	850	unspecified	unspecified	No interruption to the forming method (extrusion), reduction in water absorption and emissions (CO_2, NOx) Additives reduce the leaching of heavy metals
[312]	Electric arc furnace stainless steel	10,20 & 30	850-1050	24%	17%	Reduction of fuel and CO_2 emissions Reduced moisture content for extrusion and low strength

2.16 Summary of Chapter 2

The study objectives required that **sections 2.1- 2.15** be addressed thoroughly, and these can be summarised below:

1. Heavy clay brick is an energy-intensive sector that releases greenhouse gases from manufacture from batch materials and fuel use. Policies have been created to limit the emissions rate by discouraging manufacturers with high-rate carbon taxes greater than domestic rates. Manufacturing processes have been modified over the years to meet the current demands. These modifications to brick manufacture have concurrently been driven by economic, material, environmental and scientific approaches.
2. Incorporating waste is not a problem with heavy clay products, and existing recycling already minimizes landfill waste and promotes virgin materials' sustainability. Altering standard body compositions and microstructure of clay brick by introducing additives seems to be one of the ideal means for improving brick quality and reducing CO_2 emissions. To achieve this, the specified brick type must be chosen to select a suitable material for the new composition.
3. Clays for brick production contain clay minerals which influence the material's behaviour on firing. Clay minerals such as illite and muscovite of the micaceous minerals produce liquid phases after 750^{o}C encouraging fusion, but no study of its inclusion in heavy clay bricks has been found the exception for reformulating with zeolite.
4. Industrial (inorganic) and agricultural (organic) wastes such as fly ash and sawdust/plastics affect workability per the amount of additive added, affecting both durability and economic value. Organic wastes do not function as fillers and may not be ideal for certain heavy clay products where durability is vital. Nonetheless, these wastes are excellent for lightweight brick manufacturing like insulators and a source

of body fuel, although the ignition point of organic wastes may vary from low to high. Secondly, the conversions of these organic ashes from the raw state were not explained: the temperatures needed to convert the organic waste material into ash.

5. Magnesium and calcium carbonates aid in sintering, but percentages greater than 10% increase porosity deleterious in manufacturing engineering brick.
6. Inorganic waste additives could assist in obtaining clay vitrification at lower temperatures and function as a filler. For example, laterite, gneiss and granite may have the potential to be formulated in brick clays used in the heavy clay industries to acquire shorter firing times and improve strength, but the percentage ratio to be added must be calculated, taking into consideration the functionality of the brick.
7. Leaching metals from industrial wastes from mines and automobile industries used in ceramics needs careful monitoring.
8. While brick packing and density are not vital factors considered in literature but are necessary for the commercial sectors, most studies will give a different result when piloted at an industrial scale. A case in point is the experiment conducted by Gredmaier et al.,[149], where a subsided brick thickness was used to assess why two distinct colours were obtained when bricks were fired. Their findings or claims could be flawed because the heat transfer through the two media (a brick block vs a section of brick less than 8cm) in some electric kin with similar firing conditions will be automatically different from what they were claiming to be the remedy for black core problems during the firing of clay bricks. Body fuels (coke breeze, bitumen coal or fly ash) also encourage the production of multi-coloured bricks. Additionally, a correct body composition needs to be derived from achieving lower

   firing times and strength for clay brick, bearing in mind the functionality of the clay brick.

9. Glass cullet initially seemed very promising in obtaining a semi-vitreous clay brick, but the cost of reducing glass into finer particle sizes is costly.
10. The additive's choice affects not only brick or ceramic microstructure after firing but also the refractory and kiln lining; therefore, careful examinations are needed to protect kiln elements.
11. The clay composition, particle sizes, heating rate and firing atmosphere affect the formation of new phases that induce strength.
12. Fired bricks are of better durability than unfired bricks because of the additional properties, such as resistance to fire and severe climate changes.

Chapter 3 Experimental Procedures

3.1 Research Design

The design used for the study was mostly experimental, conducted in laboratories at Sheffield Hallam University. Only Raman Spectroscopy was conducted at the Henry Royce Institute for Advanced Materials- University of Sheffield. The raw material, Cretaceous Wealden Clay, from the Ewhurst Factory and all industrial wastes were provided by Wienerberger Ltd. and brought to the laboratory. This chapter describes the experimental method, ten (10) characterization techniques used to analyse ceramics samples, and the principles behind each technique.

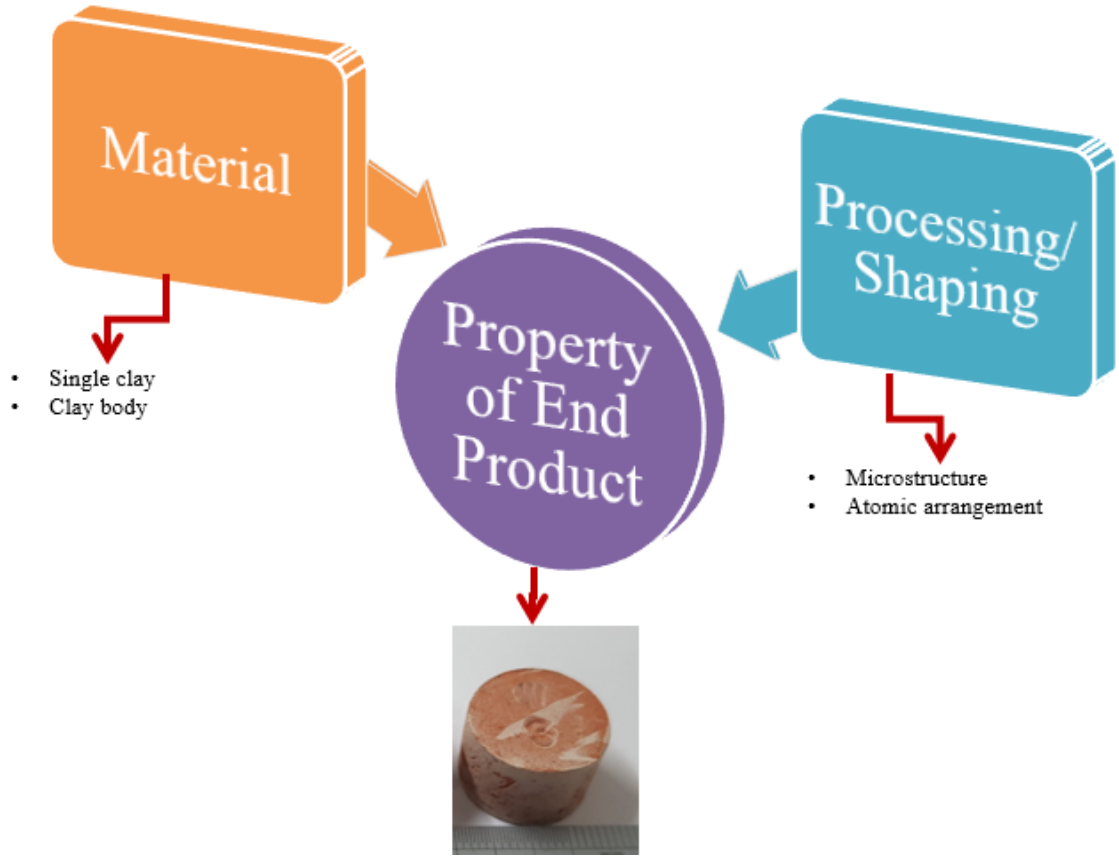

Figure 3-1: Converging radial chart illustrating the general procedure for the study

3.2 Background of Control material (Weald Clay)

Cretaceous Weald Clay is the chief raw material used for this study in the southeastern UK[319]. It is over 120-130 million years old. The raw material is extracted about 3km from the factory and is transported chiefly on conveyor belts. One of the significant disadvantages of this clay is a surface defect obtained on drying and firing (termed dryer scum and fired scum) due to the pyrite (FeS_2) impurity often accruing at concentrations of 0.02%[320]. On heating, sulfide in the clay reacts, crystallises, and forms the scum as a whitish deposit on the brick surface. This defect (scum/efflorescence) has traditionally been removed with the addition of BaCO[42,67], which prevents scum formation by causing soluble salts to become insoluble sulphates. Weald clay has been successfully used to produce Class B brick and tiles within the UK, which have been exported to other nations. The raw material from Wienerberger Ltd is greyish with occasional red stones in the clay. Weald clay is plastic, meaning it can be formed or shaped easily without any plasticiser. The reported average fired shrinkage of Weald clay is 9.2%[6].

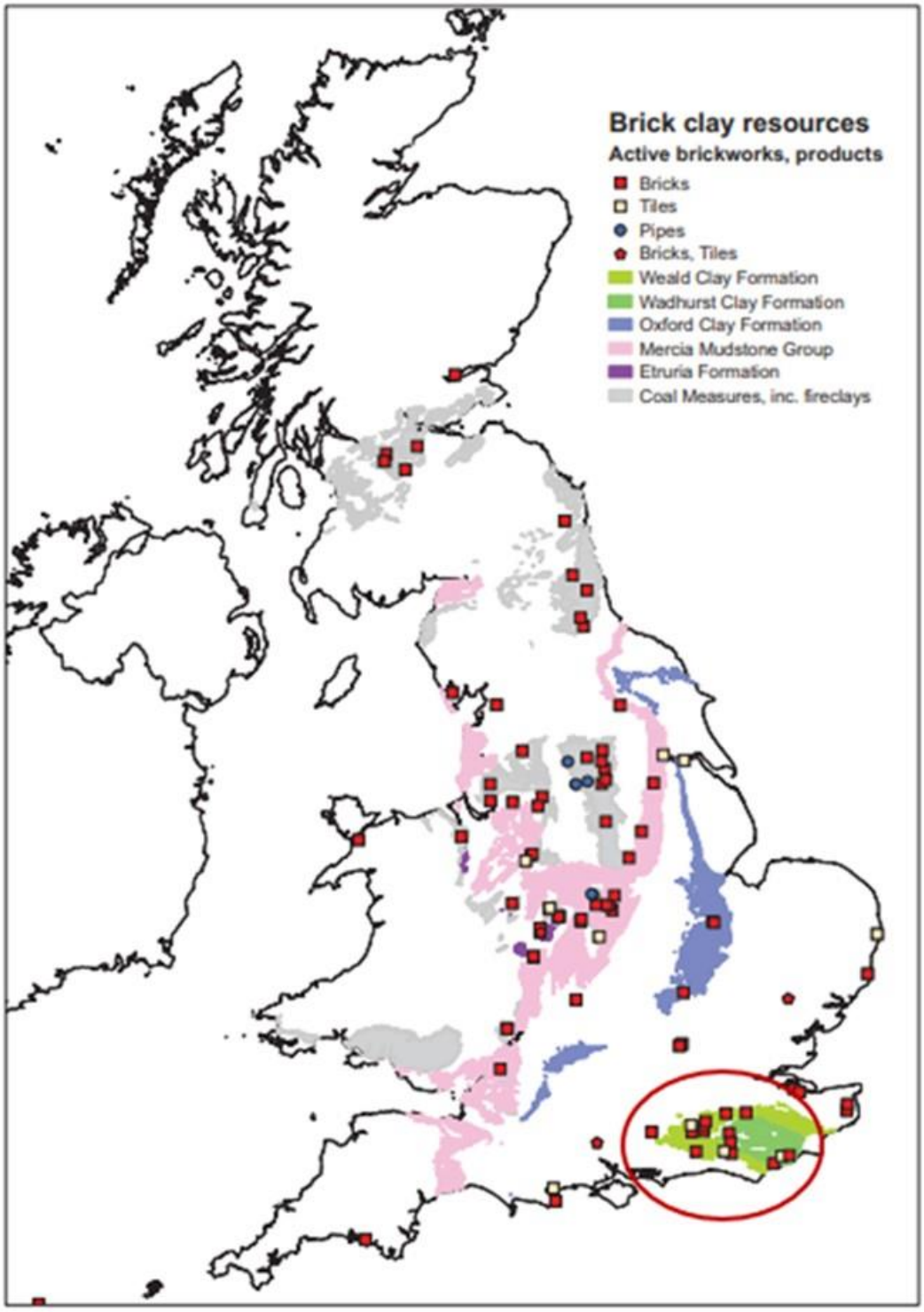

Figure 3-2: Weald clay is situated and mined in the Southeastern part of the UK map[319]

3.3 Criteria for material and additive selection for energy and CO_2 reduction

Material selection is vital in body reformulation to understand the changes the additives produce (worse or better) on brick properties. In this case, a clay ceramic for a class B engineering brick according to the EN standard BS EN771-1 2011[321], whose water absorption and compressive strength test is 7% and 75 MPa. Materials were selected based on their ability to produce melts at lower temperatures, reduce stresses caused by free quartz in clays, be environmentally friendly (thus health and safety approved), have low cost, and have the potential to improve strength and colour and to improve the chemical reaction in clays by forming an interlocking network so reducing porosity.

3.4 Making a cylindrical ceramic pellet with a simple hydraulic press

Clay and additives (Series 1-3), as summarised in **Table 3-1**, were separately dried in an oven at 120°C for 48hrs. Each 1- 4 wt% additive level was weighed and mixed with 99-96wt% dried clay, then milled in Retzsch vibratory disc mill for 1 minute at 800 rpm to produce a fine powder. This powder was mixed with 20-23ml distilled water (21%) to provide sufficient plasticity for shaping. A hydraulic press with 7 tonnes of pressure was applied to the 8.3g wet weight of the composition to form a 20 mm x 5 mm cylindrical pellet. After shaping, the green body dimensions were recorded in the "as-pressed" condition. Samples were left on a bench and dried in an electric laboratory oven (105°C) for approximately 36 hrs to eliminate free water gradually. The effect of additives on the brick property was studied by firing samples to 850°C, 900°C, 950°C, 1000°C, and 1040°C at a 1°C/minute heating rate and holding for 2hrs at the maximum temperatures before cooling at the same rate in an electric laboratory furnace. However, Series 2 and 3 (industrial waste and inorganic mineral additives) were fired to only 950°C and 1040°C.

Table 3-1: Clay body composition design

Body Compositions			
Clay	Series 1	Series 2	Series 3
100% **Weald Clay**	1-4wt.% alkali and alkaline earth carbonate oxides. ($CaCO_3$, $MgCO_3$, $BaCO_3$, Li_2CO_3, K_2CO_3 and Na_2CO_3)	4wt.% Industrial wastes. (Rockwool or mineral wool, granite wastes and 2wt% container glass waste (100µm)	4wt.% Inorganic Minerals. (Colemanite, nepheline syenite, wollastonite, talc and Great Tew clay)

Note: series 2 samples were obtained from Wienerberger Ltd., and chemical information was required for Tew clay.

3.5 Batch calculations for Alkali and alkaline earth flux doped clays

Consider the general reaction

$MCO_3 \longrightarrow MO + CO_2$

Supposing the mass of carbonate = y and that of the oxide = x

Then $$\frac{Y}{\text{RMM of } MCO_3} = \frac{x}{\text{RMM of MO}}$$

Suppose 1 unit of oxide is produced (fire)

$$\frac{Y}{\text{RMM of } MCO_3} = \frac{1}{\text{RMM of MO}}$$

$$Y = \frac{\text{RMM of } MCO_3}{\text{RMM of MO}}$$

$\frac{\text{RMM of } MCO_3}{\text{RMM of MO}}$ = constant

The Batch Factor is, therefore, the amount of the carbonate required to fire 1 unit of the oxide.

However, From

$$\frac{Y}{\text{RMM of } MCO_3} = \frac{x}{\text{RMM of MO}}$$

Supposing a unit of raw material is used, y = 1

$$x = \frac{\text{RMM of } MCO_3}{\text{RMM of MO}}$$

(1/BF) is the Unit Factor (UF), which is the amount of oxide fired when one unit of the carbonate is used. **Table 3-2** shows the BF and UF values of the various carbonates used.

Table 3-2: Batch and unit factors of carbonates

Raw material (RM)(Formula)	Molar mass	Oxide (Formula)	Molar mass	Batch Factor (BF)	Unit Factor (UF)
$BaCO_3$	197.335	BaO	153.326	1.2870	0.7770
$CaCO_3$	100.086	CaO	56.077	1.7848	0.5603
$MgCO_3$	84.313	MgO	40.304	2.0919	0.4780
K_2CO_3	138.204	K_2O	94.195	1.4672	0.6816
Na_2CO_3	105.988	Na_2O	61.979	1.7101	0.5848
Li_2CO_3	73.888	Li_2O	29.879	2.4729	0.4044

The composition of carbonates for the experiment varied based on the BF and UF values. This is shown in **Table 3-3.** The reader must note that the samples marked for 1wt% were calculated using the unit factor calculations.

Table 3-3: Batch calculation compositions for alkali and alkaline earth additives

Batch	Amt. of carbonates used(g)	Mole	Amt of Clay used(g)	Batch Size	Molality
B1	1.368	0.007	174.632	176.000	0.040
B2	4.530	0.023	171.470	176.000	0.134
B3	6.795	0.034	169.205	176.000	0.204
B4	9.060	0.046	166.940	176.000	0.275
C1	0.986	0.010	175.014	176.000	0.056
C2	6.282	0.063	169.718	176.000	0.370
C3	9.424	0.094	166.576	176.000	0.565
C4	12.565	0.126	163.435	176.000	0.768
M1	0.841	0.010	175.159	176.000	0.057
M2	7.364	0.087	168.636	176.000	0.518
M3	11.045	0.131	164.955	176.000	0.794
M4	14.727	0.175	161.273	176.000	1.083
L1	0.712	0.010	175.288	176.000	0.055
L2	8.705	0.118	167.295	176.000	0.704
L3	13.057	0.177	162.943	176.000	1.114
L4	17.410	0.236	158.591	176.000	1.486
K1	1.200	0.009	174.800	176.000	0.050
K2	5.165	0.037	170.835	176.000	0.219
K3	7.747	0.056	168.253	176.000	0.333
K4	10.329	0.075	165.671	176.000	0.451
N1	1.029	0.010	174.971	176.000	0.055
N2	6.019	0.057	169.981	176.000	0.334
N3	9.029	0.085	166.971	176.000	0.340
N4	12.039	0.114	163.961	176.000	0.693

Mole = mass used/molar mass of carbonate

For B1 = 1.368/197.335= 0.007

Molarity = mole/amount of clay used x 1000

= .007/174.632 x 1000

=.040

For C1 = .986/100.086 = .010

Molarity = .010/175.014x 1000

= .057

Where B-N represent the various carbonates(Ba, Ca, Mg, Li, K and Na) and 1-4 are the levels of additives added to the clay.

Table 3-4: Weight Percentages of oxides expected in batch fired with $BaCO_3$ as raw material

Mass of RM used	Mass of clay used	Mass of oxide	Batch weight	Wt% of oxide
1.37	173.74	1.06	176.00	0.60
4.53	171.47	3.52	176.00	2.00
6.80	169.21	5.28	176.00	3.00
9.06	166.94	7.04	176.00	4.00

Table 3-5: Weight Percentages of oxides expected in batch fired with $CaCO_3$ as raw material

Mass of RM used	Mass of clay used	Mass of oxide	Batch weight	Wt% of oxide
0.99	175.01	0.55	176.00	0.31
6.28	169.72	3.52	176.00	2.00
9.42	166.58	5.28	176.00	3.00
12.57	163.44	7.04	176.00	4.00

Table 3-6: Weight Percentages of oxides expected in batch fired with $MgCO_3$ as raw material

Mass of RM used	Mass of clay used	Mass of oxide	Batch weight	Wt% of oxide
0.84	175.16	0.71	176.00	0.40
7.36	168.64	3.52	176.00	2.00
11.05	164.95	5.28	176.00	3.00
14.73	161.27	7.04	176.00	4.00

Table 3-7: Weight Percentages of oxides expected in batch fired with Li_2CO_3 as raw material

Mass of RM used	Mass of clay used	Mass of oxide	Batch weight	Wt% of oxide
0.71	175.29	0.51	176.00	0.29
8.71	167.30	3.52	176.00	2.00
13.06	162.94	5.28	176.00	3.00
17.41	158.59	7.04	176.00	4.00

Table 3-8: Weight Percentages of oxides expected in batch fired with K_2CO_3 as raw material

Mass of RM used	Mass of clay used	Mass of oxide	Batch weight	Wt% of oxide
1.20	174.80	0.82	176.00	0.47
5.17	170.84	3.52	176.00	2.00
7.75	168.25	5.28	176.00	3.00
10.33	165.67	7.04	176.00	4.00

Table 3-9: Weight Percentages of oxides expected in batch fired with Na_2CO_3 as raw material

Mass of RM used	Mass of clay used	Mass of oxide	Batch weight	Wt% of oxide
1.03	174.97	0.60	176.00	0.34
6.02	169.98	3.52	176.00	2.00
9.03	166.97	5.28	176.00	3.00
12.04	163.96	7.04	176.00	4.00

3.6 Analytical Methods

3.6.1 *X-rays Fluorescence*

X-rays are a high-energy form of electromagnetic radiation. Their energy range for X-rays is approximately 100eV to 100keV; this corresponds to an approximate wavelength range of 0.1 to 100Å, where 1Å = 10"-10m. The technique uses high-energy X-ray photons, which are fired into a material[322]. When that happens, some of the energy is either transmitted by displacing an electron from its shell (K) or gets scattered by inelastic (Compton) or as an elastic characteristic (Rayleigh), producing K_α and K_β radiation. The L or M shell fills the created hole emitting a fluorescence radiation characteristic of its energy distribution for the studied material, which is then collected by the detector. The L and M shells come after the inner shell K with 3 and 5 subshells, respectively (L_I, L_{II}, L_{III} & M_I, M_{II}, M_{III}, M_{IV}, M_V). The L shell has 8 electrons, and 18 for the M -shell[323]. **Figure 3-3** shows a schematic diagram of how X-ray Fluorescence (XRF) is determined.

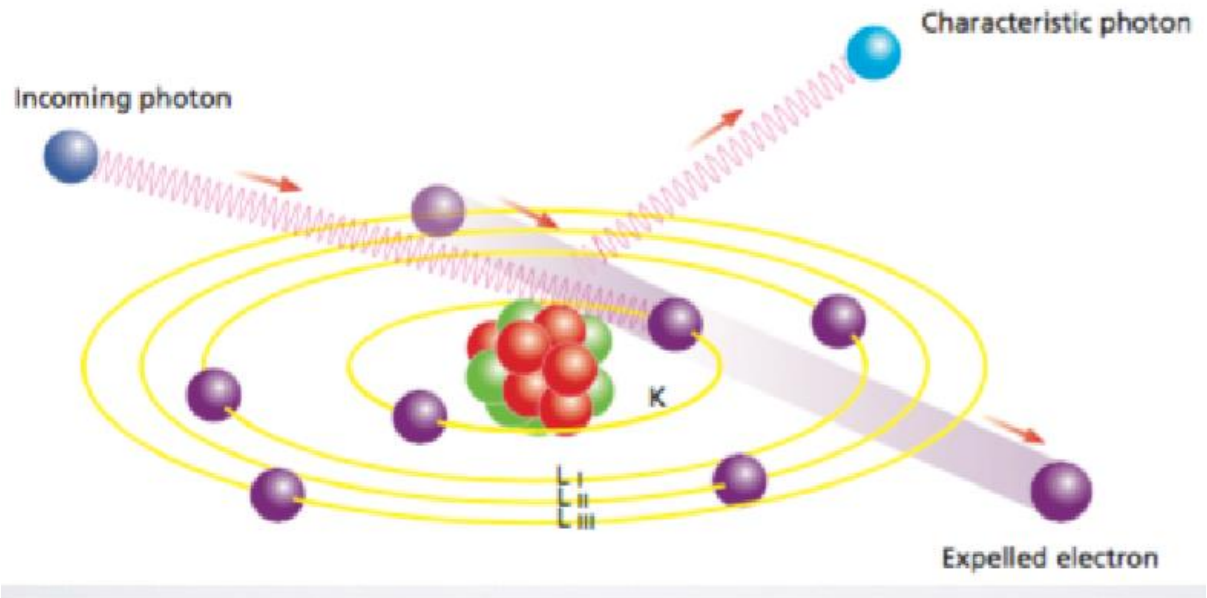

Figure 3-3: Determination of X-ray fluorescence on a material[323]

3.6.2 *Chemical analysis of Weald clay (X-ray Fluorescence)*

The chemical composition of raw materials and fired body compositions were determined using a PANalytical MagiX Pro X-Ray fluorescence spectrometer when the material was bombarded with a high-energy X-ray. The MagiX PRO could detect elements in the range F-Am; lighter elements (H-O) could not be detected as the X-ray photons for these elements are too low in energy to be detected. Analysed elements in the clay are presented in an oxide form (e.g. SiO_2, Fe_2O_3). The method is fast and widely used on most materials. It does not give information on the chemical compounds present. That is why it is supplemented with XRD, which can provide information on crystalline chemical compounds.

Pictures of the equipment are shown in **Figure 3-4**. The sample was made into a homogenous glass disc by mixing approximately 10g of lithium tetraborate ($Li_2B_2O_7$) with approximately 1g of raw material (Clays and additives). The $Li_2B_2O_7$ was doped with 0.5% Lithium Iodide (LiI) to stop the fused bead from cracking on cooling. Adding $Li_2B_2O_7$ will not affect the results on the samples added with Li_2CO_3. The mixture was then loaded into a 95% Pt: 5%Au crucible heated in a LeNeo fluxer at 1065ºC to produce a melt cooled to form glass beads [54,106]. The result is then expressed in wt. % of oxides using the IQ programmer and Oxi[324], while the loss of ignition (L.O.I) is expressed as the difference between the weight of raw material to the fired weight see **Chapter 4 and Chapter 9**.

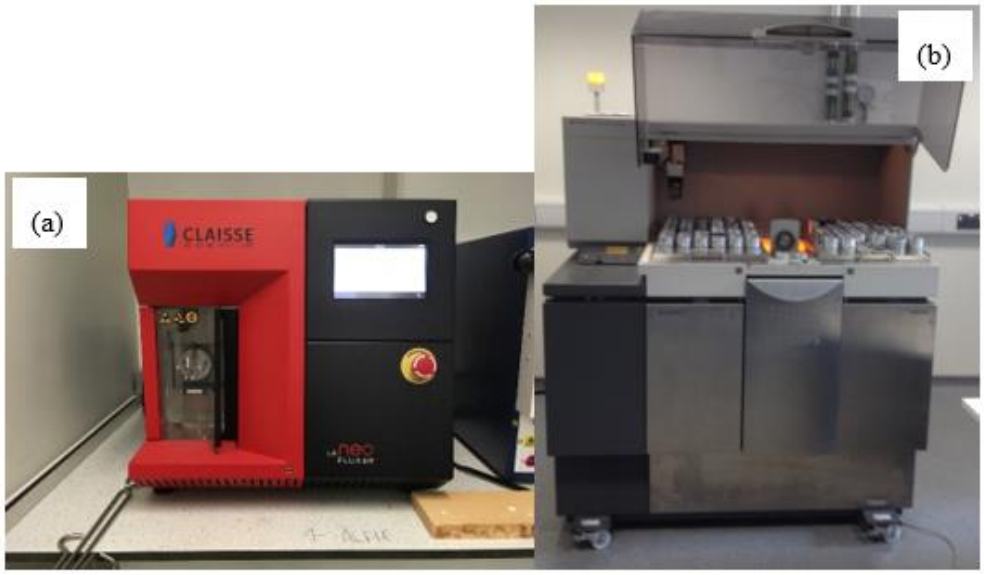

Figure 3-4: (a) XRF fused bead maker and (b) Phillips MagiX Pro X-Ray fluorescence spectrometer analyser at SHU

3.6.3 *X-ray Powder Diffraction (XRD)*

X-ray Powder Diffraction is a technique for identifying and determining lattice parameters for phases present in a crystalline material by firing an X-ray beam onto the crystalline sample, which may be solid or powder form [322,325]. Five components (X-ray source, filter, collimator, sample and detector) are needed to generate XRD patterns. This is illustrated in **Figure 3-5**. With a powder sample, the crystallites lie in orientations so that the diffracted X-rays merge to form diffraction cones by Bragg reflections[325]. The positions of the Bragg reflections in XRD are determined using the Braggs Law equation: $\lambda = 2d \sin \theta$. Where λ is the X-ray wavelength, d is the spacing between atomic layers, n is an integer (usually n = 1), and θ is the angle of incidence of the X-rays. Three types of emitted rays are generated during an electron's ejection and fill the hole created. These are the Kα (1 and 2) and Kβ X-ray radiation. The Kβ has lower intensities with noise, which is usually filtered out using an iron (for Co Ka X-rays) -or nickel (for Cu Ka X-rays) filter. The optical elements divergent silt is used to adjust the beam length on the specimen to determine the X-ray size and reduce

the effect of flat plate and specimen error. The anti-scatter silt reduces background noise and ensures diffracted beams from the sample reach the detector, Soller silts to reduce asymmetry, and the beam mask adjusts the beam width on the sample. The semiconductor-based detector then receives the diffracted beam. The resulting pattern is compared against known X-ray powder diffraction patterns stored in an extensive data base[326].

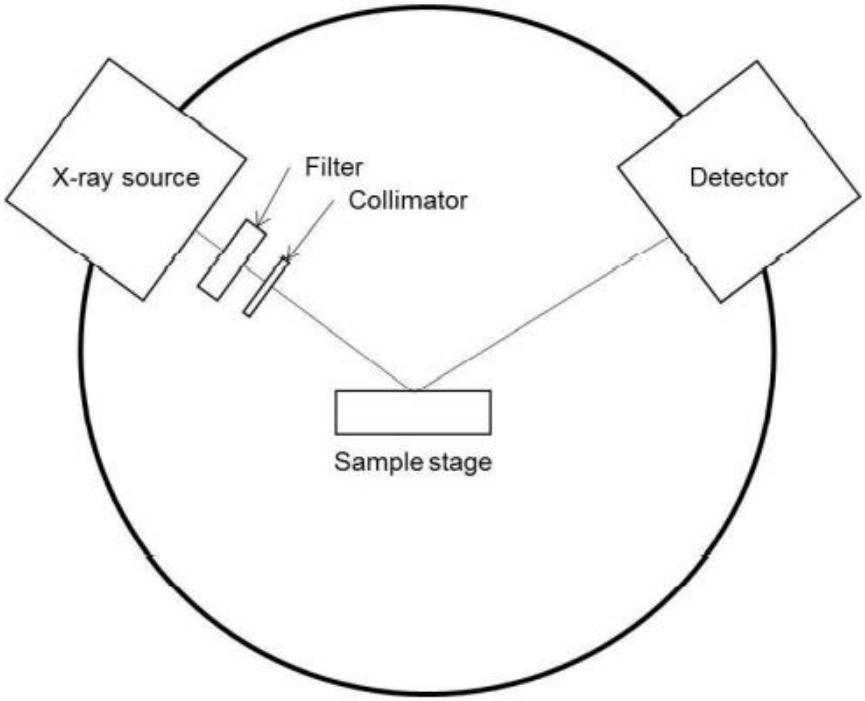

Figure 3-5: Schematic of an X-ray diffractometer

3.6.3.1 *XRD Data Acquisition*

XRD data were obtained from powdered raw material samples operating at 40kV and 40mA, which uses Cu-Kα radiation for the X'Pert / Co-Kα radiation for the Empyrean. The two sources have wavelengths 1.5405 Å and 1.789 Å, respectively. The X'pert and Empyrean are shown in **Figure 3-6**. Measurement was conducted for 120 minutes using the same parameters: 5^{o}- 52^{o} of 2Θ, divergence slit size of ½°, the mask of 15 and anti-scatter slit size of 1° and step size of 0.017^{o}. Phase identification was possible using X'Pert HighScore Plus

software which contained an updated **2019** library database (International Centre for Diffraction Data Powder Diffraction File (ICDD) for matching XRD peaks[327].

Figure 3-6: XRD equipment at SHU **(a)** Empyrean using a Co anode X-ray source and (b) X'Pert using a Cu anode X-ray source.

3.6.4 *Rietveld Refinement with HighScore plus*

The technique was developed by Rietveld [322]. This is a highly / commonly used technique in quantitative material analysis, providing phase proportions for multiphase samples and determining crystal size and microstrain. To obtain satisfactory results, data collected must be crystalline and of decent quality and must have identified crystalline phases that make chemical sense to the material being worked on that is a good fit for all unidentified phases[328]. An already collected diffraction pattern with identified phases is used. The equation below calculates a diffraction pattern for each crystalline phase present.

$$y_i = (|F_{hkl}|^2 \times j_{hkl} \times L_{hkl} \times G_{hkl}) + B_i$$

"*Where y is the profile intensity and i as the powder diffraction. F_{hkl} is the structure factor of each Bragg reflection hkl, this is proportional to the square root of the reflection intensity and is a function of the electron density in the crystal structure for each hkl plane. jhkl is the multiplicity of each reflection, as determined from the crystallographic space group. L_{hkl} is the Lorentz factor, this determines how the overall diffracted intensity varies with diffraction angle and the polarisation of the X-rays. G_{hkl} is the peak shape function. Bi is the non-Bragg scattered background at point i"*[325]. In this method, a diffraction pattern profile is calculated for each phase present, and then a least squares refinement is used to get as good a match as possible between the observed diffraction data and the calculated diffraction profile.

3.6.4.1 *Using HighScore plus for Refinement*

To use HighScore Plus for refinement, the following procedures are to be followed.

1. Convert pattern to phase- from a CIF or ICSD crystal structure information data for the analysis.
2. Change additions to difference plots.
3. Refinement Control ⟶ Default Rietveld ⟶ Automatic/Manual
4. Select and refine the following:
    - Background parameters
    - Lattice parameter
    - Profile parameters (calculate for width peaks-W, U and V)

Unit cell parameter

- Refine Atomic coordinates (Heavy elements first)
- Refine peak shape (Gaussian / Lorentzian)
- Temperature factors (just for heavy atoms) 'B' should be of a positive value.

5. Remember to check for error proportions and save for each stage.

3.6.5 *Thermal analysis*

Two main techniques are described here: thermogravimetric analysis and dilatometry measurement. Thermal measurements are vital on clays to understand their behaviour when heat is applied. Particle size, clay mineralogy, heating rate, material composition, temperature, atmosphere/environment, and sample holder affect reactions that may occur during the heating process[154,322]. The thermal analysis does not give any information on chemical information; therefore, it is mostly combined with other techniques, such as those described in **sections 3.6.2 & 3.6.3,** for a more comprehensive understanding of the material. The thermogravimetric analysis measures a material's weight loss or gains in a regulated temperature environment. The instrument consists of an electromagnetic balance, inlet gas (air, O_2, Nitrogen, CO_2), a control thermocouple (to record actual changes in the sample container), and a balanced thermocouple underneath the sample holder, furnace, and sample container. A small quantity of fine powder (50mg) is weighed into the sample holder (alumina) and then loaded into the closed chamber with the electronically programmed temperature to record weight loss. Volatile materials are recorded using a mass spectrometer (MS)[153,329]. **Figure 3-7** depicts a schematic diagram of the equipment. The equipment has an inbuilt analysing software known as Netsch and Aeolos 32 controlling the TG and Mass spectroscopy, respectively. Results are presented on a graph as weight % versus temperature. The Ms is plotted as ions current versus temperature/time. Common volatiles mostly recorded when heating clays are water (H_2O), carbon mono oxide (CO), carbon dioxide (CO_2), fluorine and sulphur [330,331]. A correction file is necessary for these experiments to check whether instruments are working correctly and for the actual measurement.

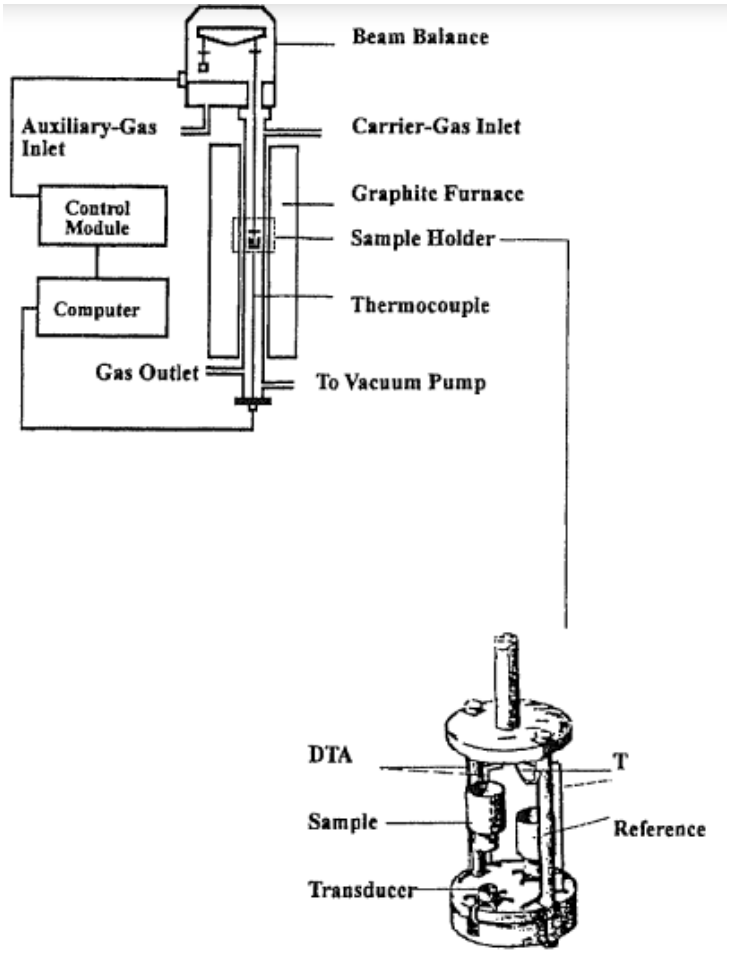

Figure 3-7: Schematic diagram of thermogravimetry analysis analyser[332]

3.6.5.1 *Thermogravimetry analysis coupled with mass spectroscopy analysis (TG/Ms)*

The equipment NETZSCH STA 409 PC/ PG was used for thermogravimetric analysis (TGA-MS) running simultaneously with a mass spectrometer which recorded the evolved gases at a constant heating rate. A powdered sample of 50mg was weighed into an alumina crucible and fired at 35^{o}C – 1100^{o}C at 10^{o}C/minute, with the carrier gas being air. It took approximately 6 hours (i.e., heating and cooling of the sample) for one complete data set to be collected because of the heating rate.

3.6.5.2 *Dilatometry analysis*

The technique measures the change in the dimension of materials as they are heated. It can be used to predict the behaviour of clay bodies on heating and cooling and thus design firing profiles for specific body compositions. There are two forms of this kit. One with a pushrod (with load) to study thermal expansion or shrinkage and phase transition, and one without load is mostly used to determine the mechanical properties of a solid material. Measurement for data collection is obtained from room temperature to top temperature, usually above 1000°C, with a range of heating rates being possible. Results are presented as temperature versus change in dimensional changes (dL/Lo) or the derivative as dL/dt (%/min). The dimensional changes observed in ceramics are related to thermal expansion, densification (shrinkage), quartz transition temperature, other clay constituents' phase changes, and water removal.

Figure 3-8&9 shows a picture of the instrument. The pushrod dilatometer works on the principle of differential while comparing changes in a solid material with a known reference material (alumina) and the actual test piece of the exact measurement, typically 25mm in length and diameter of 6mm, heated from room temperature to top temperature then cooled. The instrument uses a linear displacement sensor (Linear variable differential transducer (LVDT) or a capacitance sensor. Jankula, Miroslav, et al.[333] describe the factors that affect dilatometry measurement. These factors include heating rate, wrong positioning of sample for testing, size (thinner or larger samples affect dilatometry curve and reaction with sample) and finally, impurities left behind in the equipment from the previous measurement.

3.6.5.3 *Dilatometry measurement*

The push-rod dilatometry (NETZSCH DIL 402SE) was used to determine the dimensional changes under a controlled temperature. A “bone dried” clay rod (dried in the oven for 48hrs at 105°C) of 25mm in length was fired using the heating parameters 35ºC - 1040ºC at 5ºC/minute to determine the dimensional change when heated for all samples (control and reformulated mixtures).

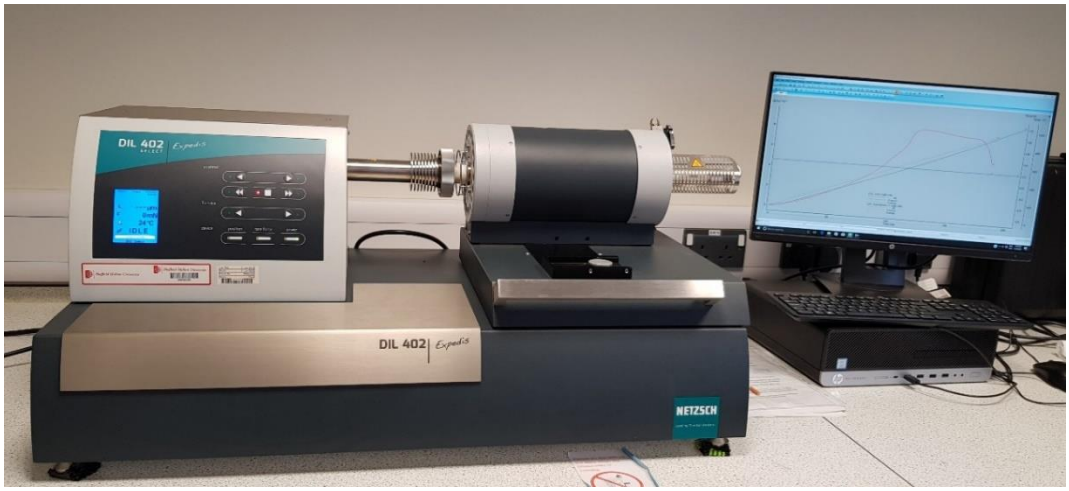

Figure 3-8: Dilatometry analyser

Figure 3-9: Push rod, thermocouple, and furnace

3.6.6 *Mercury intrusion porosimetry (MIP)*

MIP is a physical examination of porous material to determine the pore size distribution in a material, usually ranging from 0.001- 100µm. It is useful for obtaining information such as the pore size distribution, the total pore volume, the skeletal and apparent density, and the specific surface area of a sample. Mercury has a high surface tension with a typical contact angle of 90° and thus does not wet most solid surfaces [331,334] see **Figure 3-10**.

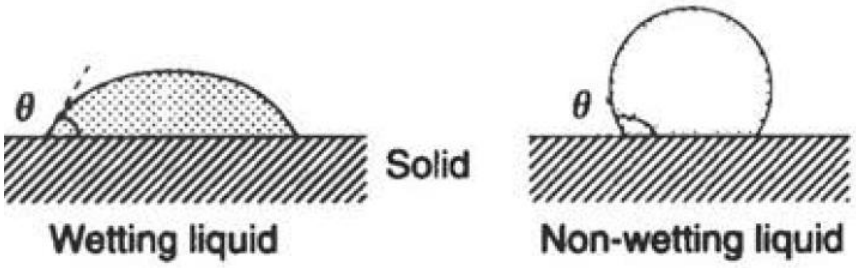

Figure 3-10: Wetting liquid versus non-wetting method [331]

MIP has long been used to determine pore sizes in cement pastes and concrete but is widely used for many porous materials[330,331]. To completely describe the pore nature of a porous system, other analytical techniques such as microstructural studies and the absorption test are used[128]. Data collected for MIP is measured by low and higher pressure for total porosity. Sample preparation is simple. A few cm^3 that will fit the neck of the penetrometer is dried in the oven according to [331].

The mass of the sample is taken prior to the analysis to provide a known weight for calculations. The material is then placed in the dilatometry device for the evacuation procedure, which removes adsorbed dirt or impurities to ensure the correct contact angle of 90° and removes air from the cell to ensure adequate mercury pumping into the pores. This evacuation procedure is conducted at lower and higher-pressure levels.

At the lower pressure, mercury is filled through the penetrometer stem until the bulb, tube, or sample is filled. After this first measurement, the specimen's mass and the mercury are weighed to determine the amount of mercury in the sample. At this stage, the smallest pore sizes are determined.

Two experimental pressure modes can be selected during the higher-pressure test: incremental or continuous. The difference has to do with the equilibrium system of the measurement after each step. However, a continuous mode is preferred for its excellent quality control check on porous material. Incremental modes give a better assurance that the true equilibrium is reached. For the continuous mode, the system does not come to equilibrium. However, the disadvantages encountered with the incremental mode cannot be overlooked. For example, it takes more time to obtain results, the inability to hold pressure constant at every step, and the possibility of missing important data information, as in filling narrow or multimodal pores. This study collected data without compression mode, meaning no temperature fluctuation will affect the results. Six basic tools needed to perform the analysis and test procedure have been detailed by [330,331].

There are theoretical assumptions and experimental errors that affect results obtained from MIP. For example, it is assumed that pore geometry is cylindrical for simplified calculations ($\Delta P = y\left(\frac{1}{r1} + \frac{1}{r2}\right) = \frac{2y\ Cos0}{r\ (pore)}$), surface and contact angles are constant for pore size distribution etc. According to Hearn and Hooten[335], a reduction in sample mass results in lower total intrusion pores and the sample preparation method prior to the experiment, thus either by crushing or a cut-out prism from the bulk specimen. It was concluded that the crush method introduced secondary cracks, and sample size affected pore distribution and not intrudable porosity. The limitations of MIP make it impossible to rely solely on its data, but a useful tool for comparative analysis [330,331,334]. **Figure 3-11** shows a representative pore type present in a solid material, as presented by Herbert Giesche[334].

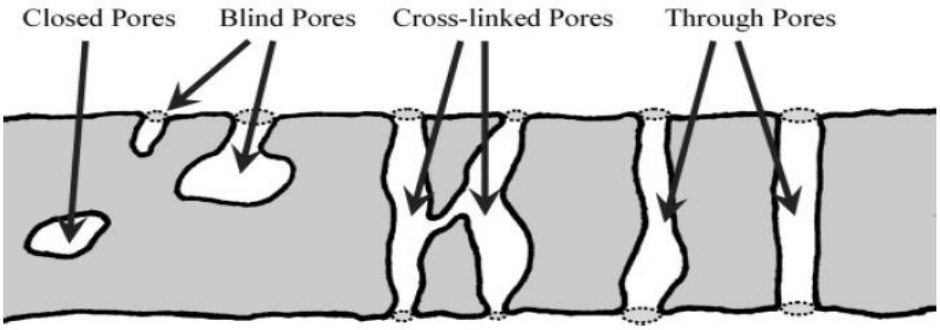

Figure 3-11: Pore types of a typical porous material[334]

Direct interpretation of pore size or diameter distribution by shape has been reported to be unrealistic as it turns to exaggerate larger pore sizes [330,331].

3.6.6.1 *Method/ Procedure*

Samples were cut into wedges – a few cm weighing not more than 1.2g to fit the rim of the dilatometer, then dried in the oven at 105ºC to remove water for 48hrs. Also, the programme parameter was set at 20°C for all measurements.

3.6.7 *Boiling water absorption testing*

Water absorption is an important property for masonry products linked to a material's compressive strength and product durability. The testing is straightforward, assessing the amount of water absorbed. The test is conducted by placing a dried sample of the known ceramic mass in boiling water for 5hrs at 100°C, then allowing it to cool to room temperature in the water. The wet ceramic samples are lightly patted with a cloth to remove excess surface water and weighed with the results are reported as a percentage using the formula (1):

Water absorption = $\frac{wet\ \ weight - dry\ weight}{dry\ weight} x\ 100$ (1)

Factors that readily influence the water absorption of bricks are shaping method, body composition and the degree of firing/densification. The test procedure and method of the result are in the British Standard [112] and ASTM [63] Standards. An average of 3 samples for each experiment is recorded.

3.6.8 *Volumetric Shrinkage testing*

Shrinkage of clay bodies is the contraction of a material due to water loss on the drying and the changes in the clay at elevated temperatures (sintering). The dimensions of ceramic samples were taken in the following conditions: wet pressed, dried, and fired and reported as a volumetric shrinkage%. Measurements were carried out using digital callipers (precision of ±0.01 mm). For this study, since the sample produced was cylindrical, the height (h) and diameter (2r) of the sample were measured, and the volumes calculated using $V = \pi r^2$h.

$$\text{Volumetric Shrinkage (\%)} = \frac{Dry\ Volume - Fired\ Volume}{Dry\ Volume} x\ 100 \qquad (2)$$

3.6.9 *Compression strength testing*

The test determines the maximum compressive load for a given material (ceramic produced 20mm x 5mm). Load is applied to individual samples of size 20mm x 5mm at a constant rate until it fails, using an Instron 6800 series compressive testing machine, and results are presented as MPa (N/mm^2). Sample parameters (height and diameter) and rate of force were computed on the testing machine. Results are reported by taking the mean of samples crushed as specified in EN772-1. A mean of 3 samples was recorded.

3.6.10 *Microstructural studies*

3.6.10.1 *Scanning electron microscopy SEM/EDS*

The technique examines the morphology and composition of solid material at various magnifications. It is a reflective mode imaging where an energy source (electron gun) interacts with the electrons of the object (ceramics) at a working range of 100A°- >10µm using 5-50keV. Imaging modes are collected as secondary electron imaging (SEI) or Backscattered imaging (BSI). In the SEI mode, sample morphology is collected at the sample's surface at lower secondary electron energy using inelastic collisions. However, with BSE imaging, the observed morphology is obtained by the specimen's atomic number contrast (high - low)t a high energy electron beam[336,337]. The compositional elements are determined from the same source using X-rays. Ceramics is a non-conductive material, so samples were coated with a conductive material (carbon) to prevent charge build-up during imaging. In most cases, SEM is used as a complementary technique to XRD, optical imaging, MIP, and other related techniques to understand the morphology and distribution of material composition.

3.6.10.2 *Material preparation and how images are obtained*

For the microstructural studies, a piece of the fired clay brick sample was mounted in resin or bakelite, ground and polished with grades of abrasive paper (320 -1µm) and carbon-coated (15nm in thickness). The surface image of clay samples was obtained using a focused beam at 5.0 KV at a working distance of 10mm. The elemental analysis was conducted on the same sample relying on the X-rays produced as electrons hit the sample. The morphology was determined using Secondary Electrons, backscattered imaging, and elemental analysis with energy dispersive spectroscopy (EDS).

3.6.11 *Infinite focus microscopy (IFM)*

Infinite focus microscopy uses visible light to produce high-resolution topographic anatomy of a material surface in 3D. This 3D optical imaging can detect surface defects and true surface texture using the Alicona infinite focus microscopy (IFM) with a magnification of 5x with a vertical and lateral resolution of 10µm x 23.5µm, respectively. **Figure 3-12** shows the picture of IFM at Sheffield Hallam University. Sample preparations were conducted similarly for SEM analysis except for the carbon coating. This was conducted on the industrial-fired samples only.

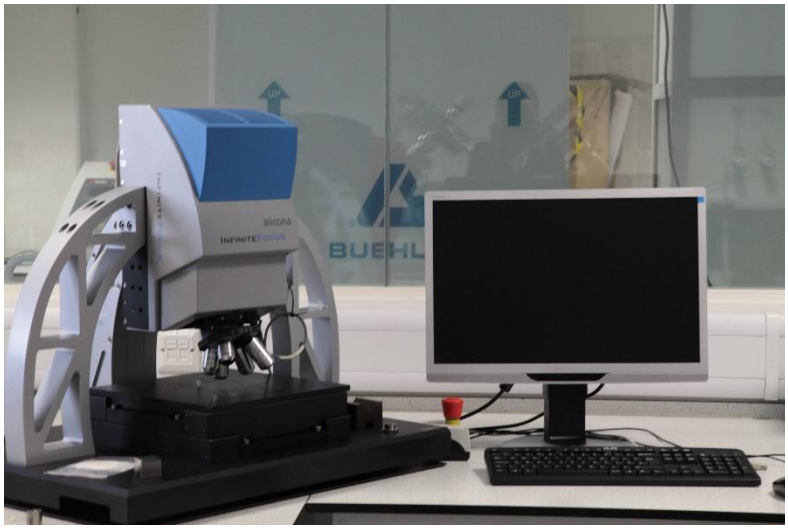

Figure 3-12: Infinite Focus Microscopy at SHU

3.6.12 *Spectroscopic analysis*

3.6.12.1 *Mössbauer spectroscopy*

Mössbauer spectroscopy was used to explain the magnetic properties and coordination/oxidation state of Fe[142,170,338,339] in the fired product as part of the benchmark material characterisation, for example, for Blue Engineering bricks (i.e., brick products shaped by extrusion and fired in a reducing atmosphere) and to understand the role of certain additives in improving colour (see **Chapter 8 Section 8.2**). Powdered unfired and fired samples were loaded onto an acrylic absorber disc without adding graphite. The powdered

sample was measured at room temperature using 14.41 keV gamma rays (^{57}Co source to a ^{57}Fe) with the velocity range ± 12 mm/sec. The calibrations were conducted on natural metallic iron. Recoil software was used to fit the Mössbauer spectra using Lorentzian lineshapes[340].

3.6.12.2 *Raman spectroscopy*

Raman spectroscopy was used to obtain the vibrational changes in bond molecules in sections produced using different firing atmospheres and to understand the structural composition of surface stains obtained after firing weald clay without any additive. The technique is a vibrational spectrographic technique using a monochromatic light source laser. The software Omnic Dispersive enabled data to be collected using the 514nm/532nm lasers at 10mW with a scanning time of 30s. The difference between the two lasers is the overall intensity, but the difference in data is likely to be small or even negligible. Information on the ceramic surface stain was collected.

3.6.12.3 *Attenuated Total Reflectance (ATIR) Spectroscopy*

The technique is useful in identifying clay minerals and any compositional change. Infrared light is passed through an ATR –crystal, which has contact with the material to analyse (solid /liquid). The crystal has a high refractive index, like diamond, germanium or zinc; selenide is often used due to its properties and cost. When the IR light passes through the ATR crystal, it creates an evanescent wave at the reflected light, then sweeps across the contact sample surface and sends chemical information of the analysed material to the detector. Data was collected in the mid-infrared range (400-4000cm^{-1}). The number of scans was set for 32 and 4cm^{-1} using Omnic software to obtain this data. The instrument Nicolet IS50FT-IR detector DTGS-ATR was utilized. This analysis was only conducted on the

control (Weald clay) to certify the presence of carbonates detected by the mass spectroscopy on thermal analysis. The graph is plotted as absorbance and wavenumbers, cm^{-1}.

Chapter 4 Effect Of Weald Clay Without Any Additive On Sintering, Microstructure And Brick Properties

4.1 Results and Discussions

4.1.1 *Background and Sample Preparation*

The background and sample preparation of the starting material, Weald clay, is described in **Chapter 3, Sections 3.2** and **3.4**. Also, individual characterisations are reported in **Sections 3.6. to 3.6.12**

4.1.2 *Chemical and Mineralogical Studies of Weald Clay*

Unfired Weald clay is Ca-poor (0.3wt%). It contains a high amount of silica (SiO_2-74%) and appreciable alumina (Al_2O_3-15%), with 6 % iron oxide responsible for its reddish hue after sintering. Moreover, this clay's total fluxing or impurity content to aid in sintering is approximately 3% (K_2O+ CaO+MgO+Na_2O), excluding the iron. Great Tew clay is also Ca-poor but in a higher amount of K_2O (3.5%) and CaO (2.2%) greater than weald clay. Fluxing oxides in this clay is 15% while Weald clay sums to 9%. SiO_2 is 12wt% lower than weald clay, but the Fe_2O_3 is 2% higher. See **Table 4-1**. According to Munir et al. [315], Muñoz et al.,[16] and Fernandes et al.,[5] most brick clays have SiO_2 and Al_2O_3 in the 50-60% range and 10-20%, respectively. Reported chemical information on Weald clay by Rowden[341] shows that silica content is 55%, Ferric oxide is 10.4% and lime 2.7%, different from the analysed Weald clay for this study. Moreover, in this study, the composition in oxides observed SiO_2 content for Weald clay at 73.5% greater than the suggested range (50-60%). Only Tew clay fitted within the proposed SiO_2 and Al_2O_3 range. This is because clays tend to be chemically different from one region to the other, and even clays of the same pit can vary[23]. The low Ca-content (0.3 and 2.2%) in both Weald and Tew clay allows both to be classed as non-calcareous clay[266]. The

high L.O.I **(see Table 4-1)** values recorded for the unfired Weald clay are attributed to the greater mass of organics and carbonates.

The mineralogical assessment of Weald clay by Rietveld refinement shows that the total clay minerals (Kaolinite ($Al_4(OH)_8(Si_4)_{10}$ - 00-058-2004), 2M1 Muscovite/illite (K, $H_3O)Al_2Si_3AlO_{10}(OH)_2$ - 00-058-2035) and 2M1 Muscovite ferrian ($K_{3.72}Na_{0.28}Si_{12.72}Al_{10.60}Fe_{0.68}Mg_{0.12}O_{48.00}$ - 01-073-9862) sums up to 44% whiles the non-clay mineral, quartz(SiO_2) is 54.8%. Iron sulphate hydroxide (Fe (SO_4) (OH) - 04-012-6256) records 1.1%. This is shown in **Figure 4-1.** Note that the XRF shows the total Si content as SiO_2, but of course, some are present in the other silicate minerals, as revealed by the mineralogical measurement. The mineralogy obtained for the unfired Weald clay corresponds to Dunham's[84] third class category of clay minerals found in British clays. Note that the difference between illite and muscovite is the grain size, and that illite has more water, silicon, and lower potassium than muscovite[342].

Changes in clay mineralogy upon firing Weald clay to 900^{o}C, 950^{o}C 1000^{o}C are plotted as XRD peak intensity vs diffraction angle. The diffraction patterns are displayed in **Figure 4-2.** At lower temperatures (900^{o}C and 950^{o}C), minor reflections of hematite begin to appear while the clay mineral, muscovite ($KAl_3Si_3O_{11}$ - 00-046-0741) in a dehydrated form is still present in the composition, and quartz is present at all temperatures. Mullite ($Al_{2.26}Si_{0.74}O_{4.87}$ - 04-016-1586)), microcline ($KAlSi_3O_8$ - 01-084-0709) and hematite (Fe_2O_3 - 04-005-4630) form at temperatures >1000^{o}C.

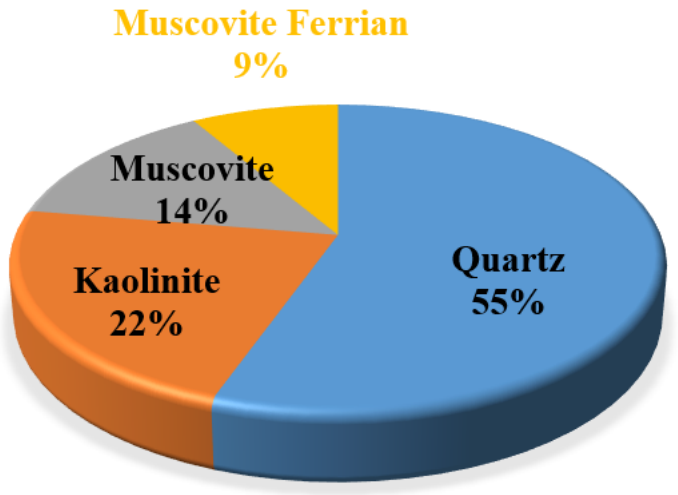

Figure 4-1: Summary of Rietveld refinement of XRD pattern for Weald clay (clay mineral versus non- clay mineral quantities).

Table 4-1: Analysed chemical analysis of weald clay- (Control)in Wt%

100% Weald Clay	**OXIDES**															
Sample date	**SiO_2**	**Al_2O_3**	**Fe_2O_3**	P_2O_3	Cr_2O_3	**Na_2O**	**MgO**	**CaO**	**K_2O**	**Mn_3O_4**	**TiO_2**	**SO_3**	**BaO**	**L.O.I**	**Colour ((Fe/Al)**	**Sum of Flux**	**Firing (°C) Al /(K2O +Na2O)**
	%	**%**	**%**	**%**	**%**	**%**	**%**	**%**	**%**	**%**	**%**	**%**	**%**	**%**	**%**	**%**	
27-Mar-19	**73.5**	**15.4**	**6.1**	**0.1**	**0**	**0**	**0.5**	**0.3**	**2.2**	**0.1**	**1.5**	**0.2**	**0.1**	**16.73**	**0.4**	**9.1**	**7.0**
Great Tew	**62.0**	**20.2**	**8.1**	**0.1**	**-**	**0.3**	**0.1**	**2.2**	**3.5**	**0.1**	**1.1**	**0.1**	**-**	**10.30**	**0.4**	**15**	**5.3**

Table 4-2: Summary data of property of Weald clay

Temperature (°C)	Boiling Water Absorption (%)	Compression strength (MPa)	MIP- Porosity (%)	Fired Volumetric Shrinkage (%)
900	13.3	50.7	22.64	1.38
950	12.2	54.4	20.41	1.96
1000	9.7	78.4	19.26	7.23
1040	8.6	81.5	18.30	9.84

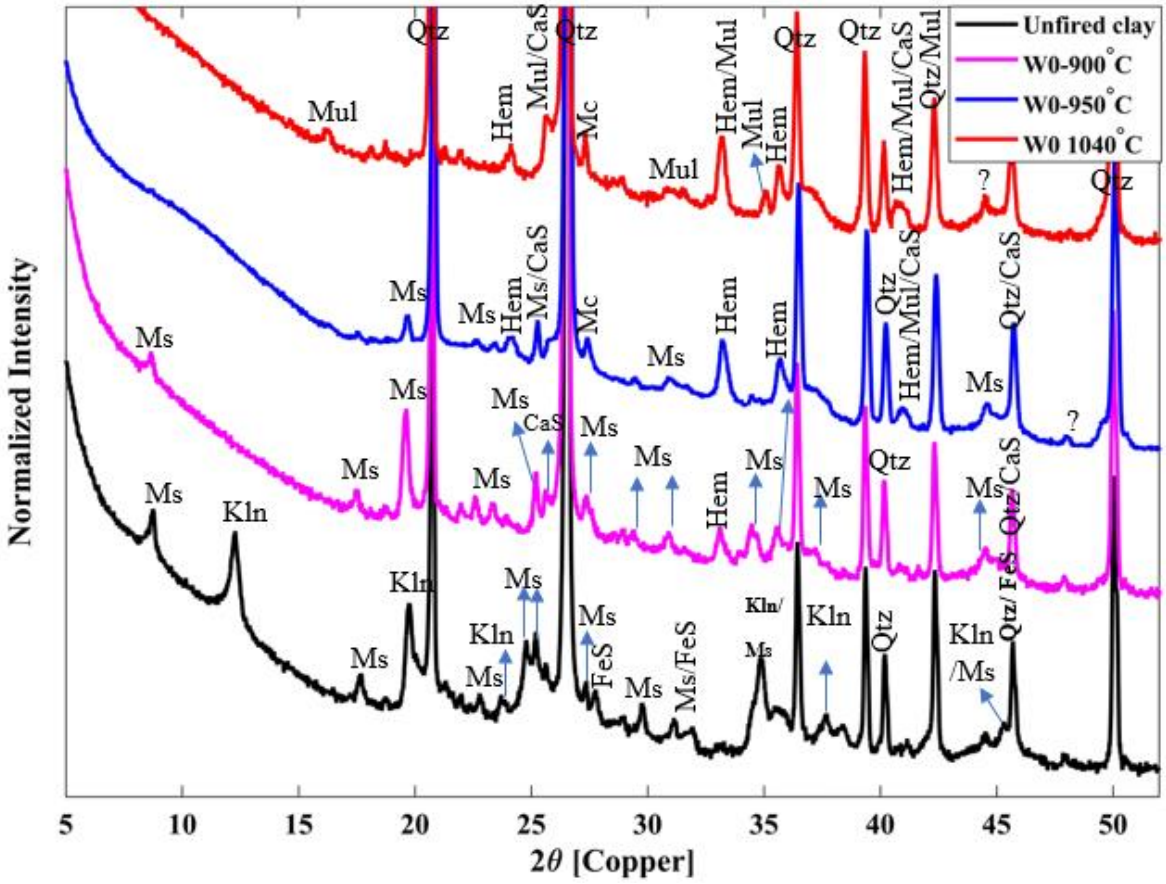

Figure 4-2: Changes in XRD pattern when Weald clay is fired to 900°C, 950°C, 1000°C and 1040°C.

Symbols after Kretz[343] Where Qtz=quartz: Kln=kaolinite; Ms = Muscovite/ dehydrated muscovite; Hem= hematite Mul= Mullite; FeS = iron sulfate hydroxide, CaS-calcium sulphate ($CaSO_4$) and Mc= Microcline.

4.2 Structural composition of Weald clay

The presence of carbonates and organic carbons in Weald clay is obtained using the Attenuated Total Reflection Fourier Transform Infrared –(ATR-FTIR), as shown in **Figure 4-3**. The band 3500-3690cm^{-1} has been assigned to the clay mineral kaolinite, 2000-2950 cm^{-1} depicts the hydrocarbons within the clay, and finally, 1000-1200cm^{-1} is assigned to the quartz region (Si-O) and carbonate region (overlapping region)[344]. The result confirms the presence of hydrocarbons and carbonate in Weald clay. Although organic compounds were not identified in the XRD spectra due to the low quantity being poorly crystalline, these were observed with

the FTIR within the range of 2000-2950cm^{-1} of the unfired Weald clay. This resulted in the release of CO_2 gas on firing around 300-600°C. This is depicted in the thermogravimetry analysis coupled with mass spectroscopy (TG/Ms), **Figure 4-4**. The associated emissions or off-gases from the burning of clays are unavoidable on firing[117,345], and TG/Ms and FTIR analysis confirms this fact. The range observed in Weald clay (2000-2950cm^{-1}) agrees with the band range reported by Manoharan et al.,[346] on the thermal behaviour of red clay (4925 and 2855cm^{-1}).

The specific surface area of organic matter in clays promotes the plasticity of mouldable brick clay. On heating red clay to 1000°C, Manoharan et al.,[346] observed the destruction of terminal OH (peaks around 3500cm^{-1}), the bending (778 and 796cm^{-1}) and stretching of S-0 band (694cm-1) to form mullite whilst quartz and hematite were still present at lower temperatures <900°C. This structural change corresponds to results obtained with the XRD upon heating Weald from 850°C-1040°C, where mullites begin to form at temperatures >1000°C and clay minerals remain as dehydroxylated muscovite at 900°C. Several studies on the mineralogical changes in clays or kaolinite-rich clays agree with these results[92,306,329,347–349].

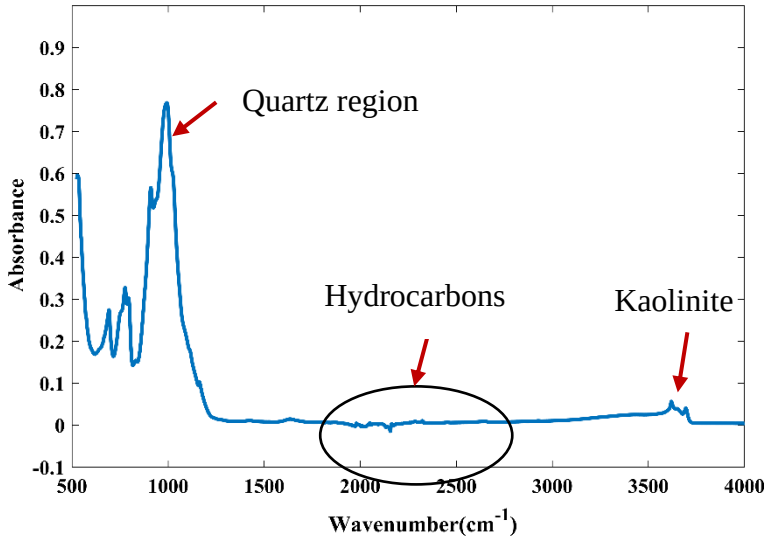

Figure 4-3: Attenuated Total Reflection Fourier Transform Infrared Spectroscopy(ATR-FTIR) of Weald clay.

4.3 Thermal analysis

Thermogravimetry (TGA) was used to examine the behaviour of Weald clay on heating as a function of temperature. **Figure 4-4 (a)** shows the heating behaviour of Weald clay as depicted by the TGA and its derivative of TG (DTG) curves and its corresponding mass spectroscopy (Ms). The derivative curve shows an early mass loss caused by removing physical/hydrated water at temperatures 35°C-200°C. The thermal behaviour of kaolinite occurs as[350]

$Al_2O_3.2SiO_2.2H_2O$ (Kaolinite) → $Al_2O_3.2SiO_2$ (metakaolinite) + $2H_2O$ (400-500°C).

$2(Al_2O_3.2SiO_2)$(metakaolinite) → $Si_3Al_4O_{12}$(spinel)+SiO_2 (~950°C)

$3Si_3Al_4O_{12}$(Al-Si-spinel) → $2(Al_2O_3.2SiO_2)$(mullite)+$5SiO_2$ (>1050°C)

At 300°C-600°C, there is a significant mass loss caused by the release of volatiles from the decomposition of clay minerals and the removal of structural water (OH-groups), which starts above 200°C. The total mass loss recorded is 5.09%. The thermal behaviour is consistent with kaolinitic clay behaviour on heating. The type of gases (Mz) from the burning of Weald clay and its concentration are shown with the mass spectroscopy graph in **Figure 4-4 (b)**. The main volatiles recorded are reabsorbed and chemical water and CO_2.

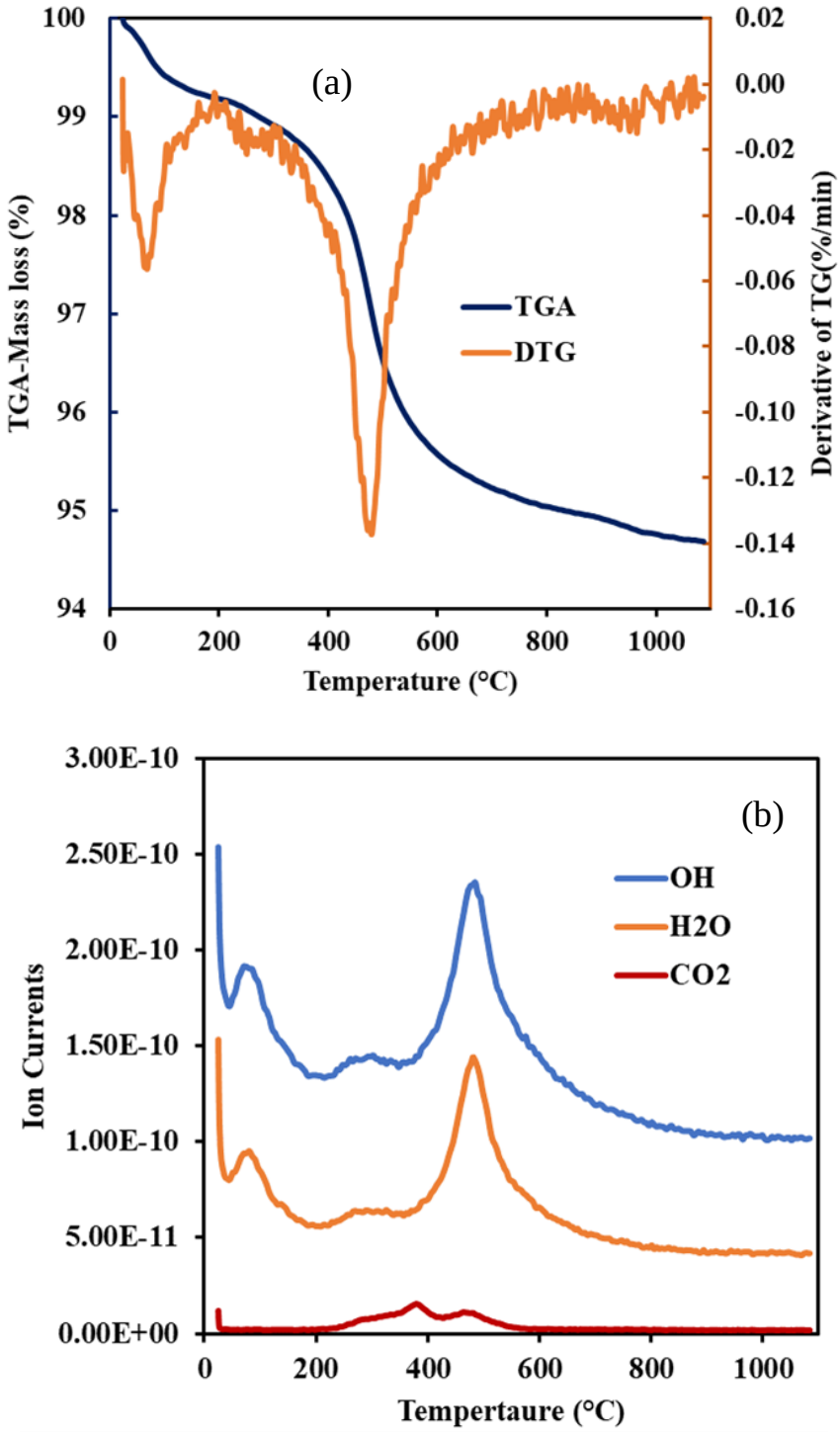

Figure 4-4: (a) Thermogravimetric curve (TG) and its Derivative (DTG) of Weald clay fired to 1200^{o}C at a rate of 10^{o}C/min (b) mass spectroscopy graph of gases released from clay during thermal treatment.

F**igure 4-5(a)** shows the shrinkage of the control at 2.3%. The dilatometry results show three stages of the unmodified clay's thermally induced expansion and shrinkage using the push rod

(Dilatometry). Firstly, clay minerals dehydrate just above the boiling point of water along with the removal of chemical water (250-350°C) and the first shrinkage (See **Figure 4-5b**). After this step, the decomposition of clay minerals between 450 and 550°C takes place. A sharp volume change shortly overtakes this due to quartz inversion from α-β with a difference in CTE as 40.680 $x10^{-6}$ for base clay with an expansion rate of 1%. This is given in **Table 4-3**. There is also a shrinkage mechanism active just above the quartz transition temperature (~600^{o}C) and the more dramatic one active above 800^{o}C till it cuts off after reaching 3% shrinkage beyond 950°C. The final shrinkage indicates vitrification associated with material densification at an intense heat because of the liquid phase formation from the flux (e.g., Ca, Na, K etc.), natural components in the clay.

Table 4-3: Summary of Weald clay linear shrinkage analysis

Sample ID	**Onset temperature before final shrinkage (°C)**	**B-Quartz (°C)**	**Expansion (%)**	**Linear shrinkage (%)**
Weald clay (W0)	820	581	1	2.3

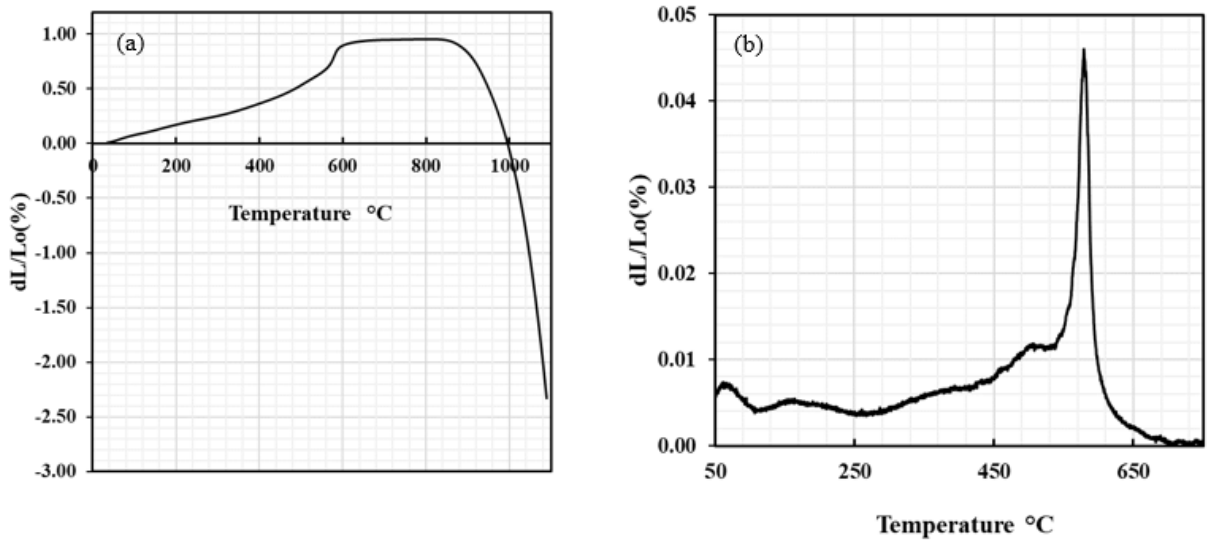

Figure 4-5: Dilatometry curve for Weald clay showing (a) expansion and shrinkage curve (b) the derivative of the dilatometry curve showing the various thermal changes in weald clay fired to 1100°C at a heating rate of 5°/min.

4.4 Physical Properties of Weald Clay

4.4.1 *Visual examination of fired Weald clay*

The control developed a "drier scum", a whitish stain on drying and firing and judging surface colour due to this surface stain after firing was challenging, requiring colour measurements to be done on the base of these stained samples. The whitish stain form from the reaction of sulphate (S) and Ca^{2+} to form $CaSO_4$. This phenomenon is detailed in **Chapter 8, section 8.1.4**. The intensity of the fired clay colour is temperature dependant and is shown in **Figure 4-6.** Clay samples fired at 1040°C produced the darkest hue, reddish brown and the lightest hue for samples fired at 900ºC—no colour difference between 1040ºC and 1000ºC.

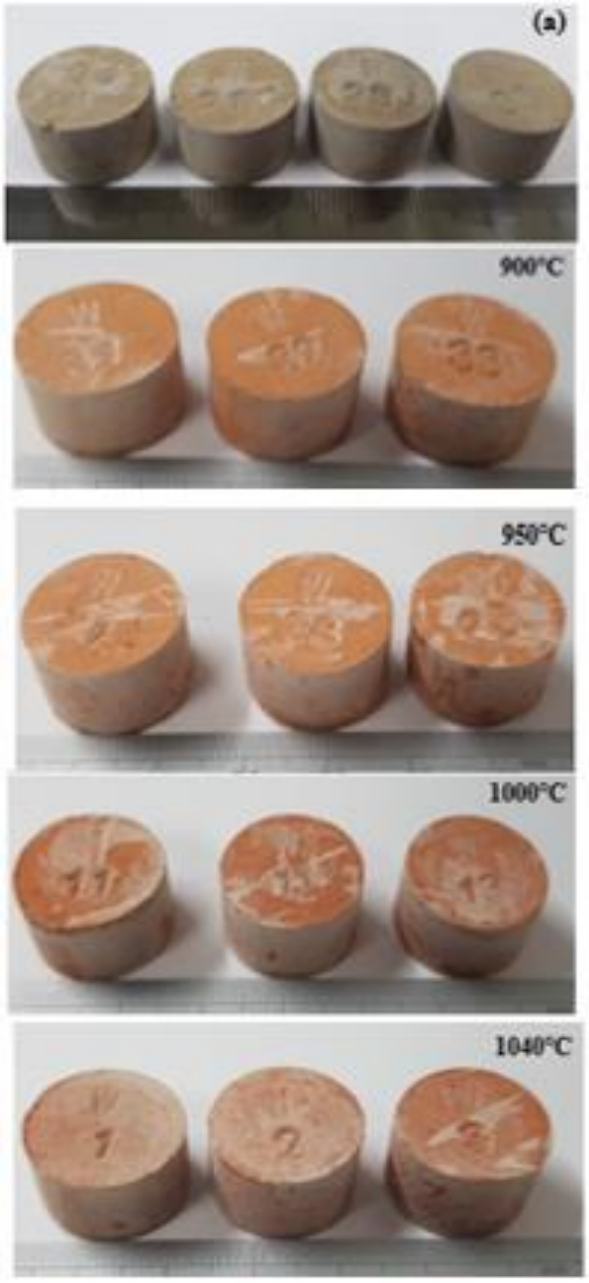

Figure 4-6: Images of (a) Unfired clay and control fired to 900ºC, 950°C, 1000°C and 1040°C

4.4.2 *Volumetric Shrinkage and Boiling Water Absorption*

Volumetric shrinkage (VS%) and boiling water absorption (WA%) percentages of fired clay samples are affected by the temperature, mineralogy, body composition, shaping method and plasticity. The VS results show that, at lower temperatures, 850°C -950°C VS (%) is less than

2%, while samples fired to 1000°C and 1040°C could shrink up to 7 and 9.8%, respectively. Interestingly, the degree of shrinkage is related to the firing temperature, as shown in **Figure 4-7**. Higher temperatures result in higher VS (%), and lower temperatures produce low VS%. Likewise, for the boiling water absorption % (BWA), lower temperatures recorded the highest porosity of 13.5% (850°C-900°C) and 12.2% for 950°C compared to just 8.6% for samples fired to 1040°C. Meanwhile, samples fired to 1000°C marked 9.5%. This agrees with the high shrinkage lower absorption (%), which indicates the degree of strength in clay bricks. However, it does not account for the closed pore. Boiling water absorption (BWA) is a factor used to judge "durability", i.e., the brick's ability to resist water penetration and thus avoid spalling in freezing weather.

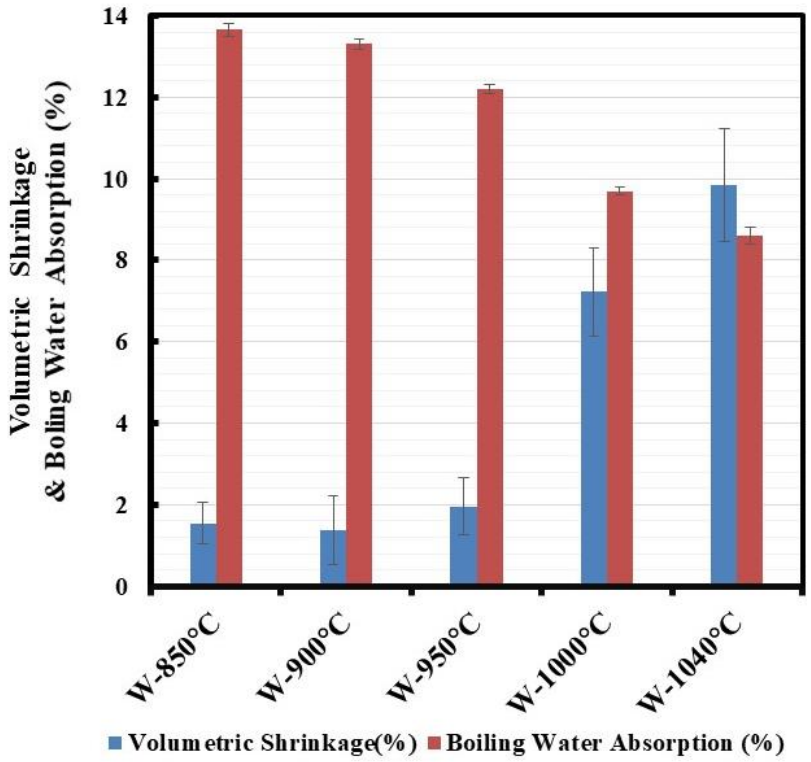

Figure 4-7*:* Volumetric shrinkages and boiling water absorption test on base clay fired to 850°C, 900°C, 950°C,1000°C and 1040°C.

The main parameters that affect the shrinkage of the control (100% fired clay fired to 900°C, 950°C,1000°C and 1040°C) are flux %, the temperature and the removal of chemical and water of formation (OH and H_2O) from shaped clays. Lower temperatures (900 & 950°C) recorded lower shrinkages than ceramics fired at 1040°C, which saw a high volumetric shrinkage due to the melt produced influenced by temperature, as shown in **Figure 4-7.** The boiling water testing (absorption) of ceramic samples also confirms the observations of others that higher shrinkages give lower water absorption. Hence the results were obtained. Other researchers have obtained similar outcomes with temperature effect on permeability, shrinkage and pore size distribution shifts, making it quite clear that ceramic's durability, porosity, and strength depend highly on temperature or the degree of firing[5,54,128,349,351]

4.4.3 *Mercury intrusion porosimetry (MIP)*

Figure 4-8 shows the differential pore size distribution (PSD) of Weald clay (W0) with different laboratory firing temperatures. The shape of the curve suggests a bi-modal pore size distribution of Weald clay fired to 900ºC, 950ºC, 1000ºC and 1040ºC. Samples fired to lower temperatures between 850ºC-950ºC pore size diameter shift towards the micropores (0.001-0.2μm), whilst samples fired to 1000ºC and 1040 ºC pore size diameter move towards the larger pore size (0.001-0.7μm, and 0.001-1μm respectively). The volume range is significant in the intrudable micropores capacity of each temperature**.**

Figure 4-9 shows samples fired to 900°C and 850ºC record the highest Hg % of 22.64 and 23.66%. However, samples fired to 1000°C marked 20.94%, whilst further reduction was obtained when samples reached 1040°C with 18.2%.

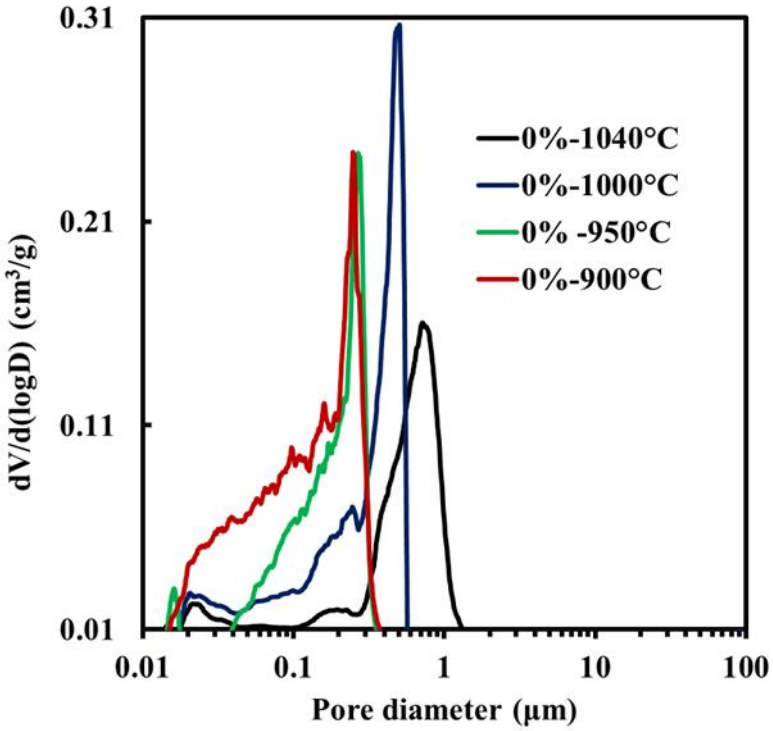

Figure 4-8: Mercury intrusion porosimetry pore diameter of Weald clay fired to 900ºC,950ºC, 1000ºC and 1040ºC.

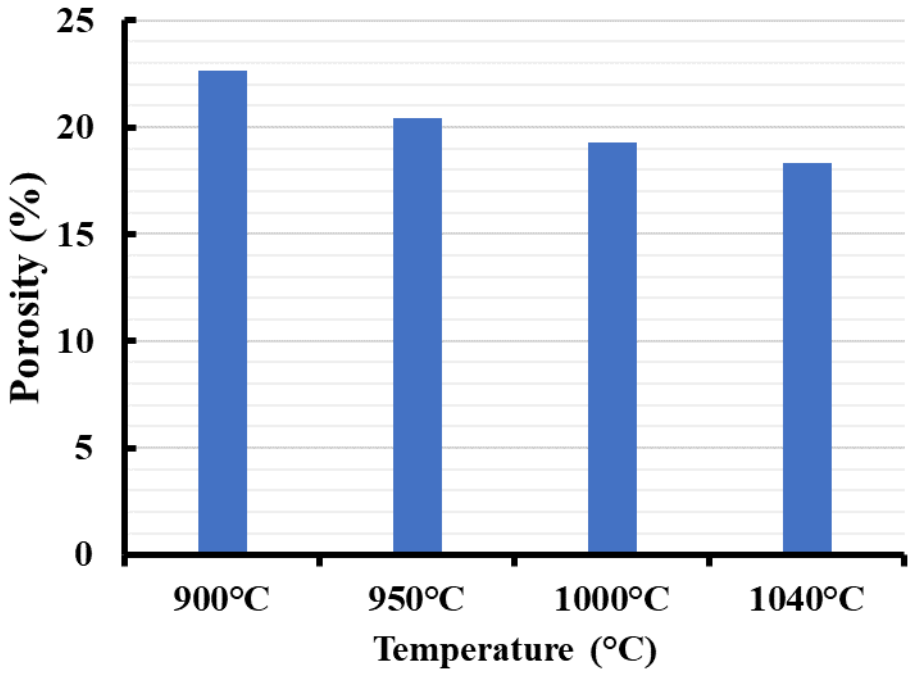

Figure 4-9: Intrudable porosity percentage of Weald clay fired to 900ºC, 950ºC, 1000ºC and 1040ºC (device accuracy 0.25%).

4.4.4 *Predicting ceramic durability using the Maage equation*

Ceramics fired to 900°C, 950°C, and 1000°C failed the durability prediction[175] with a durability factor (DF) less than 55. Only ceramics fired to 1040°C were found to be in the uncertainty region; thus, values between 55 and 70. See Appendix 3 **Table 3**.

4.5 Mechanical Property of Weald Clay

4.5.1 *Compressive strength testing*

Clay samples fired to 900°C record the least compressive strength (51 MPa). However, as the temperature increases to 950°C, strength increases by 3% (54MPa). By the time it reaches 1000°C, 78MPa is obtained. At 1040°C, 81MPa is achieved. Overall, the strength of ceramics is temperature dependant. The properties of Weald clay, including its strength, are summarised in **Table 4-2**.

The load-bearing capacity of clay-based ceramics is associated with the crystalline phases formed on firing, which create stronger bonds between the other structural components in fired clay (e.g.SiO_2 particles). These phases are formed from the liquid phase created by the fluxing additives. The mineralogy in the fired clay is affected by (i) clay chemistry, (ii) clay mineralogy, (iii) degree of firing and (iv) firing atmosphere[20,156]. Phases (quartz, hematite and mullite) obtained on heating were similar to previous studies when samples were fired in an oxidising atmosphere[84]. The formation of melts is enhanced (i.e., the greater amount produced) by temperature. The formation of mullite and hematite promotes fired clay denseness and fired colour[16,352], which complements porosity findings obtained with MIP and BWA. In the case of the XRD, the developed crystalline phase affected the formed microstructure, as shown in **Figure 4-2.** According to BS EN771-1, water absorption for a class B Engineering brick must be 7.0% or less [112] for clay masonry units. The project's initial objective was to maintain

product quality for a class B engineering brick. However, the water absorption for the control (>8%) did not pass the BSI standard. However, the required strength >75MPa was achieved by firing ceramics at 1040°C instead of > 1055°C/ 1100°C[353] reported for the same clay. This effect could be caused by the method of shaping (stiff clay pressing) adopted at the laboratory to mimic industrial production (extrusion) to produce a dense and compact clay brick in the green state. This has, however, revealed the importance and role of shaping methods, boiling water absorption and temperature effect on ceramic strength.

4.6 Microstructure of fired specimens

Changes in specimen morphology on heating are examined using scanning electron microscopy (SEM). The SEM images depict the effect of temperature on the control microstructure, as shown in **Figure 4-10**. Samples fired to 900°C and 950°C show a less sintered body, with fewer individual particles fused to neighbouring particles to form a denser structure. Temperatures above 1000°C quartz particles are visible, with improved porosity with increased temperature. The morphology indicates a more interconnected microstructure compared to samples fired to 900°C.

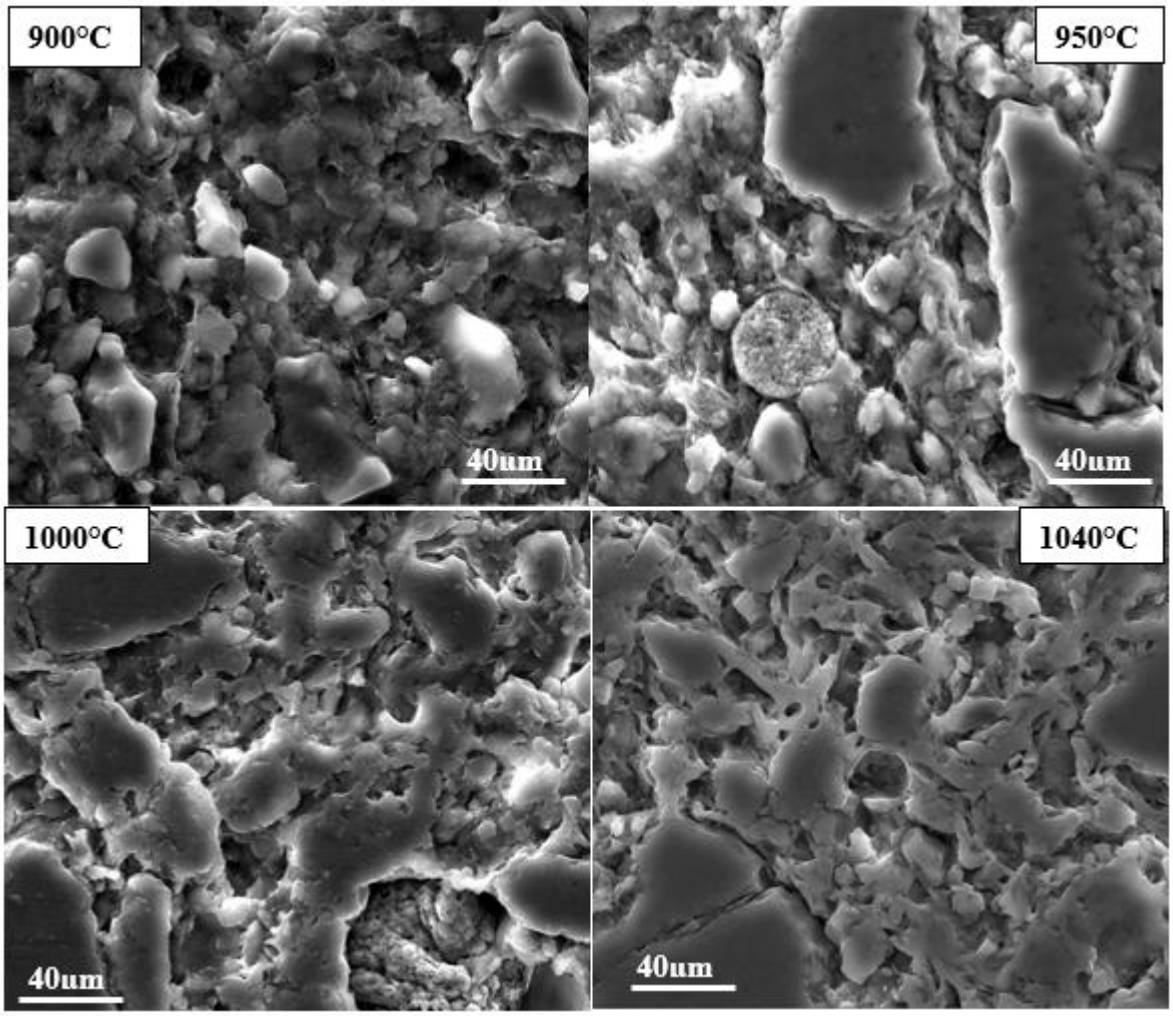

Figure 4-10: Microstructure of Weald clay fired to 900ºC, 950ºC, 1000°C and 1040ºC

4.6.1 *SEM/EDX Maps of Weald clay fired to 1000°C*

EDX mapping of the control fired to 1000°C reveals that Mn and Fe co-exist in the same region and are not evenly distributed within the structure. The ceramic body is rich in SiO_2, whilst constituents such as Na, K, and Mg are homogeneously distributed within the network on cooling, forming part of the composition. This is possible because these alkali and alkaline earth constitute the flux which helps in the liquid-solid solution. Ti and Ca are scarcely scattered in the composition. See **Figure 4-11/12.**

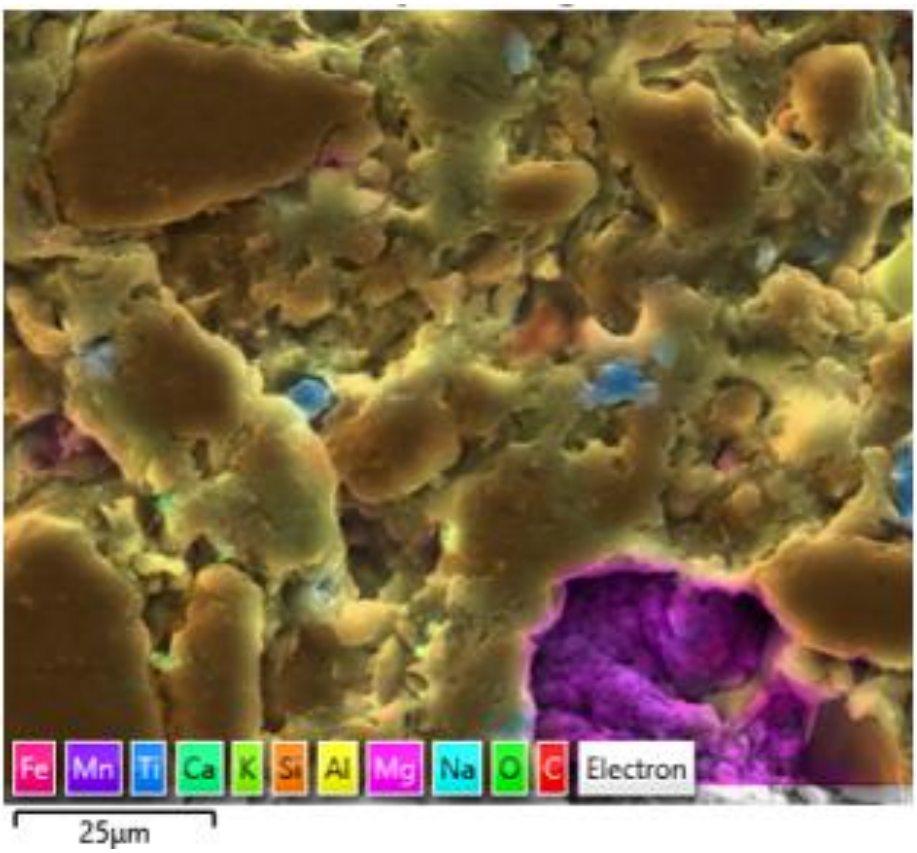

Figure 4-11: Maps of 100% Weald clay fired to 1000°C

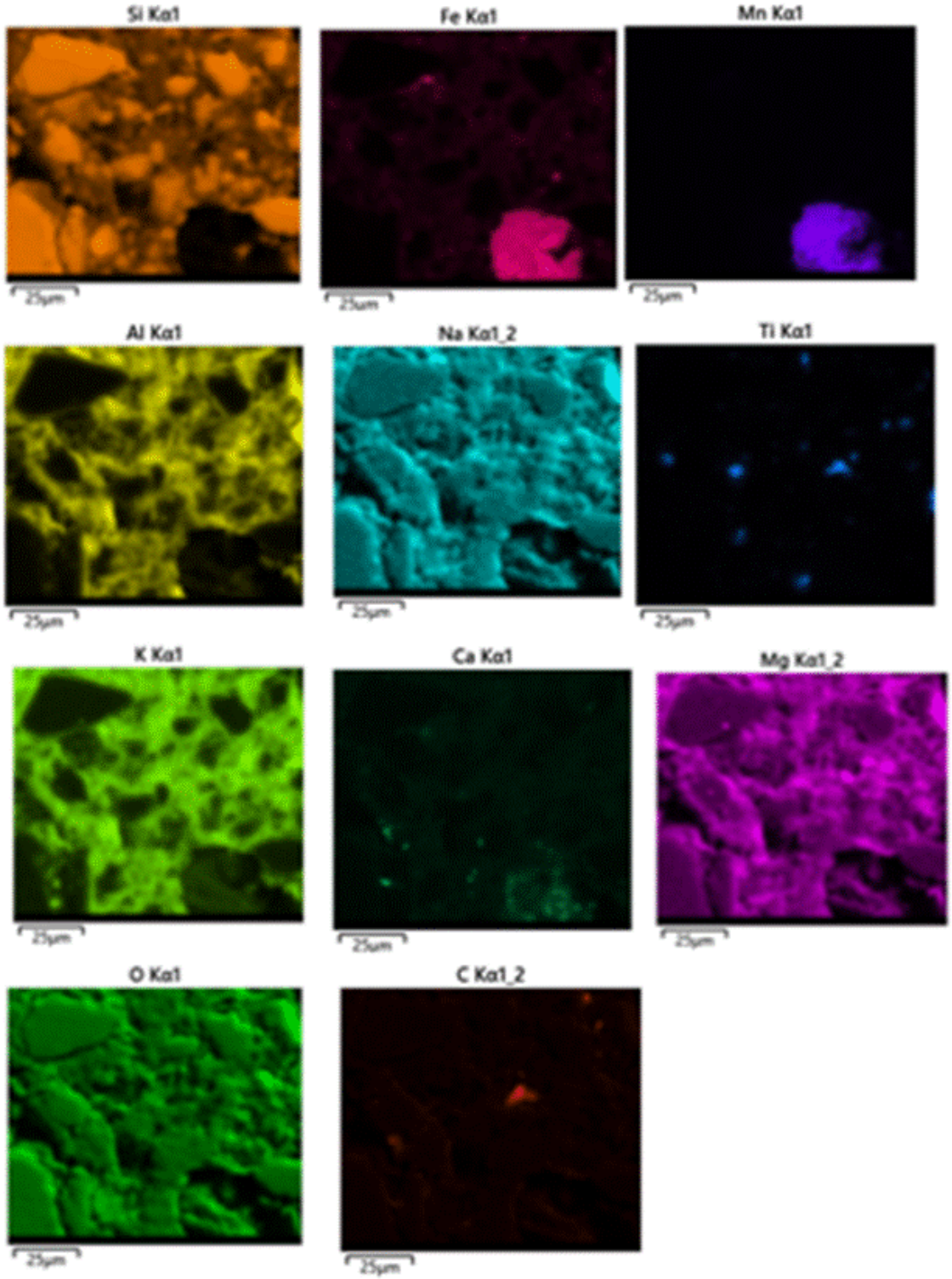

Figure 4-12: Maps of 100% Weald clay fired to 1000°C.

4.7 Main points on Weald clay

In summary, the control contains 44% clay minerals and 54% quartz with no evidence of the amorphous mineral presence in the raw clay. Flux is about 3% in Weald clay. ATIR-FTIR confirms the presence of hydrocarbons in small ratios, while there is indirect evidence for carbonates being the emission of CO_2 observed in the base clay with the TGA. Recorded volatiles from this raw material is CO_2, OH and reabsorbed water. Dried and fired sample surfaces are prone to whitish stains from the reaction of sulphate retention in clay on firing. Finally, fired Weald's Clay boiling water absorption is proportional to the firing temperature, whereas strength and shrinkage increase with temperature.

Chapter 5 Effect Of Alkali And Alkaline Earth Carbonate Additive On The Sintering, Microstructure And Properties Of A Class B Engineering Brick

5.1 Background

This study attempts to reduce industrial ceramic manufacturing's energy and carbon dioxide emissions. This chapter investigates the replacement of 1-4wt% of Series 1 additive (alkali and Alkaline earth carbonate) into Weald clay brick body composition. Various experimental techniques will serve as sub-headings for the individual results to investigate and compare the control and experimental materials analysed to respond to the research questions.

Weald clay is the primary material used for Class B Engineering Brick manufacture. Weald clay contains pyrite (FeS_2) as an impurity in low quantities (0.009%). The average 2020 stockpile of brick clays' total carbon content, provided through private communication by John Renshaw on 27 May 2021, is 0.26%. The low undetected limit of FeS_2 in the clay produces surface stains on drying (drier scum) and firing.

The additives are:

> **Series 1:** Six (6) carbonates from the periodic table group 1 and 2 oxides, also known as alkali and alkaline earth carbonates (Na_2CO_3, K_2CO_3, Li_2CO_3, $CaCO_3$, $BaCO_3$ and $MgCO_3$).

5.1.1 *SERIES 1 Sample Preparation*

Clay and additives (Series 1), as summarised in **Table 3-1**, were separately dried in an oven at 120°C for 48hrs. Each additive level of 1- 4 wt% was weighed and mixed with 99- 96wt% dried clay, then milled in Retzsch vibratory disc mill for 1 minute at 800 rpm to produce a fine powder. This powder was mixed with 20-23ml distilled water (21%) to provide sufficient plasticity for shaping. A hydraulic press with 7 tonnes of pressure was applied to the 8.3g wet

weight of the composition to form a 20 mm x 5 mm cylindrical pellet. After shaping, the green body dimensions were recorded in the "as-pressed" condition. Samples were left on a bench and dried in an electric laboratory oven (105°C) for approximately 36 hrs to eliminate free water gradually. The effect of additives on the brick property was studied by firing samples to 850°C, 900°C, 950°C, 1000°C, and 1040°C at a 1°C/minute heating rate and holding for 2hrs at the maximum temperatures before cooling at the same rate in an electric laboratory furnace. Also, individual characterisations are reported in **sections 3.6.31, 3.6.5.1,3.6.5.2, 3.6.6.1, 3.6.7, 3.6.8, 3.6.9** and **3.6.10.2**.

5.2 Results and Preliminary Discussion

5.2.1 *Chemical Analysis of Series 1 Additives*

The fused bead chemical analysis of Weald clay containing 4wt% alkali and alkaline earth carbonate fired samples is provided in **Table 5-1.** Elements present in the Weald clay were present. The elemental contents of the body composition containing 4wt% of the series 1 additives found include Si, Al, Fe, Ca, Mg, Ti, K, Mn, P and S. The result showed that Na, Ba, Cr and Li were not naturally present in Weald Clay. However, when 4wt% of Na, Ba is added to Weald clay, it becomes part of the element. On the other hand, Li is not detectable as a light element. K_2O content remained constant at 2.2% for all additives (4wt% $MgCO_3$ as M4, 4wt% $CaCO_3$-C4, 4wt% $BaCO_3$- B4, 4wt% Li_2CO_3 L4 and 4wt% Na_2CO_3 N4) except for 4wt% K_2CO_3 (K4) which doubles up to 4.6% as shown in **Table 5-1** due to the replaced additive level. Similar trends are seen with the various additives as they become the main flux supplier in the clay body, but the Ba recording was 1.2%. Also, TiO_2 remains constant at 1.5%, except for K_2CO_3, which marked 1.1%. Moreover, there was no trace of any sulphur content after firing because the fused bead temperature was 1065^{o}C, possibly removing the S – gas. Chemical analyses of samples fired to 900°C are presented in **Appendix 2**.

Chemical results obtained by incorporating alkali and alkaline earth suggest that silica reacted with clay's fluxes to form new phases—the relative amount (%) of alumina and iron content increase on firing during sintering. Sulphur and unburnt carbon were not detected in the reformulated fired bodies, which may cause blackcoring[151].

Findings of this study concur that sulphur in each body primarily arising from the clay was removed at lower temperatures as reported by Brownell[184], A. Andrés et al.[203], Schorr and Everhart[196] and Bell et al.,[106]. Brick setting (i.e., packing style in the furnace), size and spacing of ceramic samples within the furnace and fuel used (electricity) were different in the laboratory from the industrial gas-fired, compact stack packing and the temperature (850°C-1040°C) was such that it enabled the complete removal of sulphur during firing.

5.3 *$CaCO_3$ additive replacement phases*

Minor phases' intensities intensify with the dosage of the additive. At 900°C (**Figure 5-1**), clay mineral muscovite ($KAl_3Si_3O_{11}$ - 00-046-0741 and $CaSO_4$ (04-013-4616) observed phases remain in the composition. Calcium samples fired to 900°C were the same as found with 100% clay, with a significant increase in the peaks associated with the Ca-containing phases when additions were above 2wt%.

Mullite ($Al_{2.22}Si_{0.78}O_{4.89}$ - 04-016-1586), hematite (Fe_2O_3 - 04-005-4630), gehlenite ($Ca_2(Al(AlSi)O_7$- 01-073-2041) or anorthite ($CaAl_2Si_2O_8$ - 00-041-1486) were formed with samples fired above ~1000°C for C1- C4 samples. Additional peaks between 18°, 20° and 30° were found, which could not be identified. The obtained crystalline phase peaks increase in intensity as additive levels rise from 2-4wt%. This is shown in **Figure 5-1**.

Adding 1-4wt% $CaCO_3$ additive produced new crystalline phases, which were absent in the 0% additive. The use of $CaCO_3$ encouraged the formation of gehlenite or anorthite, which

improved the interlocking of clay particles (see **Figure 5-2**) as well as the creation of pores from the decomposition of carbonates at temperatures above 600°C shown in **Figure 4-25** (TG-Ms). This result reflects the findings of Traore´ et al.,[354], in which the calcium compound reacted with kaolin. They discovered that anorthite only forms after gehlenite formation at temperatures over 933°C. In their work, 64.2 wt% kaolinite, 20wt% quartz and 15wt% calcite were sintered at 1100°C at a 1°C/min heating rate. The Ca-rich phase was found heterogeneously mixed in the composite matrix with occasional larger pores forming anorthite at the rim (by SEM study) from the decomposition of calcite. The reaction of the crystalline phase is given by Traore´et al.,[354]

The formation of gehlenite and anorthite is a sign of brick sintering since the formation of anorthite promotes strength[355]. Kaolinite ($Al_2O_3.2SiO_2.2H_2O$) reacts with $CaCO_3$ to form gehelenite ($CaO.\ Al_2O_3.SiO_2$) at 930^oC [89]. Explaining why gehelenite does not form at 900^oC because the critical dissociation only occurs at 930^oC. The effect was most significant with additives containing greater than 2wt%. In the experimental studies, the replacement of alkaline earth was excellent in controlling clay expansion on heating compared to the alkali oxide. Studies present $CaCO_3$ as an excellent material for a perfect body fit between a ceramic body and glaze (stability) with good shrinkage and enhancing the formation of crystalline phases formed from clay minerals. $CaCO_3$ limits the formation of the amorphous phase, which causes expansion due to its high surface area absorbing moisture; the crystalline phases are gehlenite and anorthite-calcium aluminosilicate[354,356]. These phases (gehlenite and anorthite) are consistent results from this study and build upon the existing knowledge on the effect of additive reactivity on firing. Higher admixture (up to 10wt%) is described by Cultrone et al., [176]to cause strength reduction unless the clay body is fired to 1100°C and hence was not considered relevant in this work.

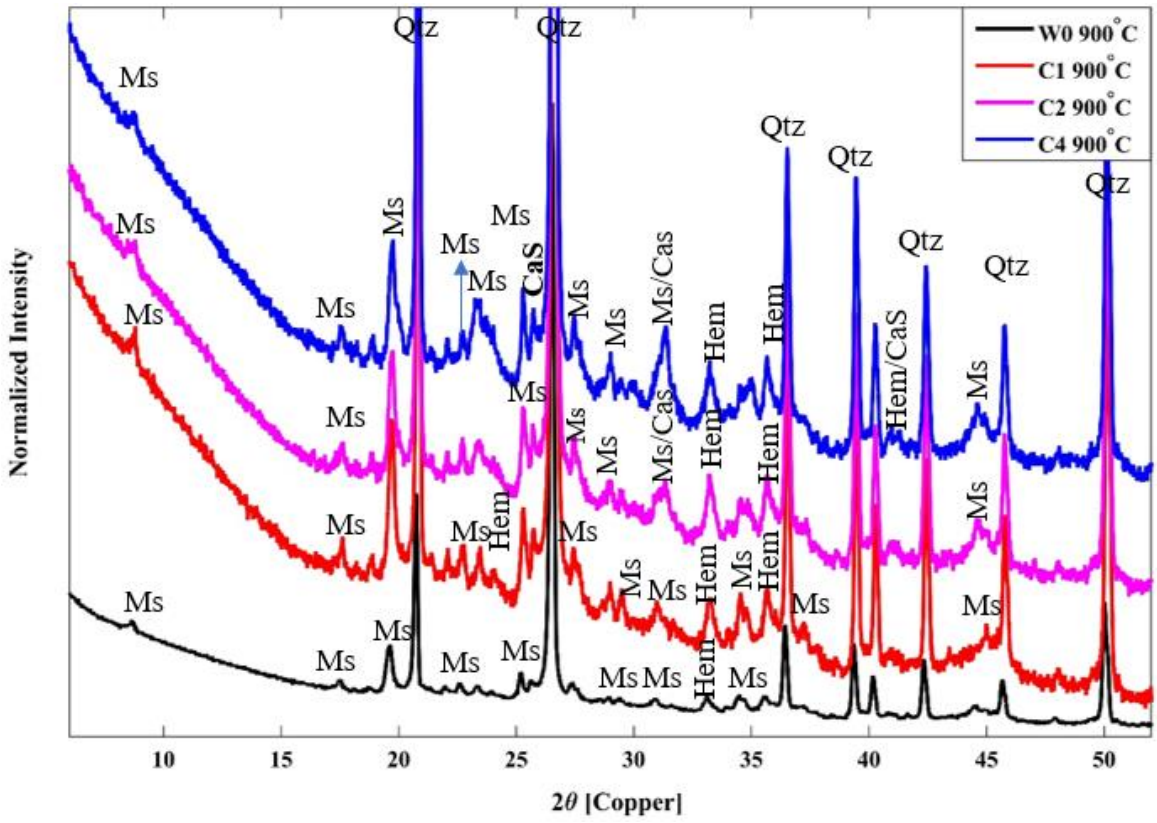

Figure 5-1: Crystalline phases developed in weald clay with 1,2 &4w% replacement of $CaCO_3$ fired to 900°C.

Symbols after Kretz 1983[343] where Qtz=quartz; Hem= hematite; CaS-calcium sulphate and Ms- dehydrated Muscovite

Table 5-1: X-ray fluorescence analyses of unfired clays and fired clay bodies doped with 4wt% of alkali and alkaline earth using the new Oxi programme. Where Mg- magnesium carbonate, Ca=calcium carbonate, Ba=Barium carbonate, K=Potassium carbonate, Na= sodium carbonate and Li=Lithium carbonate.

Oxide	Clays			Alkaline earth and alkali oxide formulations					
	Weald Clay	Tew Clay	Fired Weald Clay (1040°C)	Mg-1040°C	Ca-1040°C	Ba-1040°C	K-1040°C	Na-1040°C	Li-1040°C
SiO_2	73.5	62.0	71.0	68.4	67.6	70.1	67.9	67.7	70.5
Al_2O_3	15.4	20.2	15.9	15.6	15.4	15.8	16.3	15.9	16.2
Fe_2O_3	6.1	8.1	7.7	7.5	7.3	8.0	5.6	7.5	7.8
Mn_3O_4	0.1	0.1	0.1	0.1	0.1	0.1	0.2	0.1	0.1
TiO_2	1.5	1.1	1.5	1.5	1.5	1.5	1.0	1.5	1.5
Na_2O	0.0	0.3	0.2	0.2	0.2	0.2	0.2	3.8	0.2
K_2O	2.2	3.5	2.3	2.2	2.2	2.2	4.8	2.2	2.3
MgO	0.5	0.1	0.6	3.9	0.6	0.6	0.6	0.6	0.6
CaO	0.3	2.2	0.4	0.4	4.7	0.4	0.3	0.4	0.4
P_2O_5	0.1	0.4	0.1	0.1	0.1	0.1	0.1	0.1	0.1
ZnO	0.0	0.0	0.0	0.0	0.0	-0.1	0.0	0.0	0.0
SrO	0.0	0.0	0.0	0.0	0.0	0.0	0.0	0.0	0.0
BaO	0.1	0.1	0.1	0.1	0.1	1.2	0.0	0.1	0.1
ZrO_2	0.0	0.0	0.1	0.1	0.1	0.0	0.0	0.1	0.1
SO_3	0.2	0.1	0.0	0.0	0.0	0.0	0.3	0.0	0.0
Fe/Al	0.4	0.4	0.5	0.5	0.5	0.5	0.2	0.5	0.5
SUM (%)	100	100	100	100	100	100	100	100	100
LOI (%)	16.75	10.30	4.83	8.14	6.93	6.73	0.06	5.71	6.54

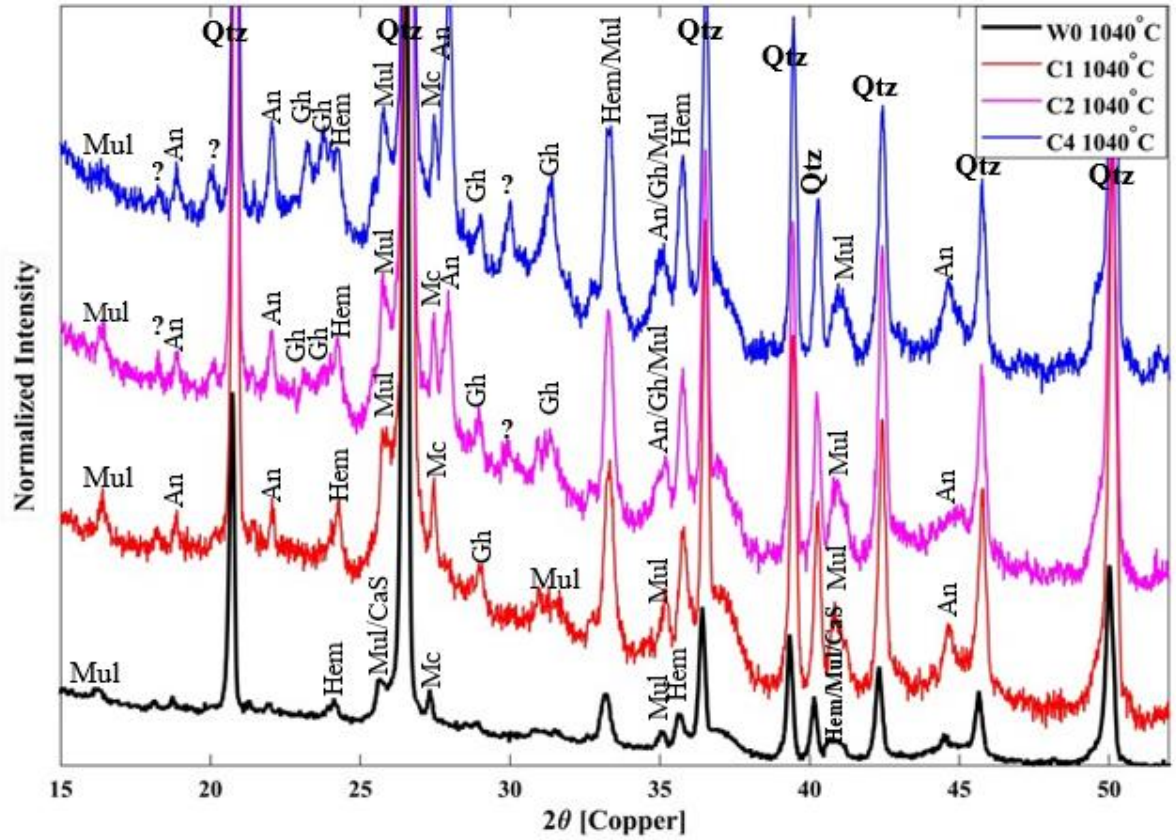

Figure 5-2: Crystalline phases developed in weald clay body composition with 1,2 & 4wt % replacement of $CaCO_3$ fired to 1040°C.

Symbols after Kretz 1983[343]. Where Qtz- quartz, Mul- mullite, Hem- hematite, CaS- calcium sulphate, Mc- microcline, An- anorthite and Gh- gehlenite.

5.3.1 *$CaCO_3$ additive heating behaviour in Weald clay*

$CaCO_3$ additive with Weald clay in 1-4wt% shows a gradual increase in weight loss with temperature as the additive dosage increases **Figure 5-3**. The derivative of TG mass indicates that the initial mass loss results from the dehydration of absorbed water removal at 35°C- 200°C amounting to 0.75%. The second trough stems from the release of the hydroxyl group (OH)- between (200°C -600°C) accounting for 4.05% mass loss from clay minerals due to clay mineral decomposition (see **Figure 4-4** for the base clay). The total weight loss recorded for 1wt% $CaCO_3$ is 6% which is 0.91% higher than the 100% clay. Overall, the thermal behaviour

of the control and C1 is similar, but the difference lies in the additional Ca- producing a higher total weight loss.

The decomposition of $CaCO_3$ occurs between 600°C and 800°C, as illustrated in the derivative of the TGA and volatile type shown with the mass spectroscopy (**Figures 5-4)**. However, at additive masses of 2-4wt%, a third trough develops at 680°C, linked to the breakdown of $CaCO_3$ and release of CO_2 just after the decomposition of carbonates in the clay. The third phase loses weight due to the volatile release and the chemical water. Finally, the derivative of the TGA shows another little trough around 1100°C, which is believed to be the final removal of steam**.** The total weight loss of replacing 1-4wt% $CaCO_3$ is summarised in **Table 5-2.** Pure $CaCO_3$ has been reported to decompose at 820^{o}C**.** However, in a clay body composition, the reaction occurs faster (680^{o}C) at a lower temperature at a 10^o heating rate.

Table 5-2: Summary of thermal behaviour of 1-4 mass (%) $CaCO_3$ additive in weald clay

Additive	**Event 1**		**Event 2**		**Event 3**		**Total weight loss (%)**
	Temperature (°C)	**Weight loss (%)**	**Temperature (°C)**	**Weight loss (%)**	**Temperature (°C)**	**Weight loss (%)**	
C1	**35-200**	**0.75**	**200-600**	**4.05**	**600-800**	**0.86**	**6.00**
C2		**0.85**		**4.09**		**1.96**	**7.23**
C3		**0.69**		**3.81**		**2.63**	**7.22**
C4		**1.15**		**4.09**		**3.37**	**8.73**
Inference	**Dehydration**		**Hydroxyl release**		**Carbonate decomposition**		

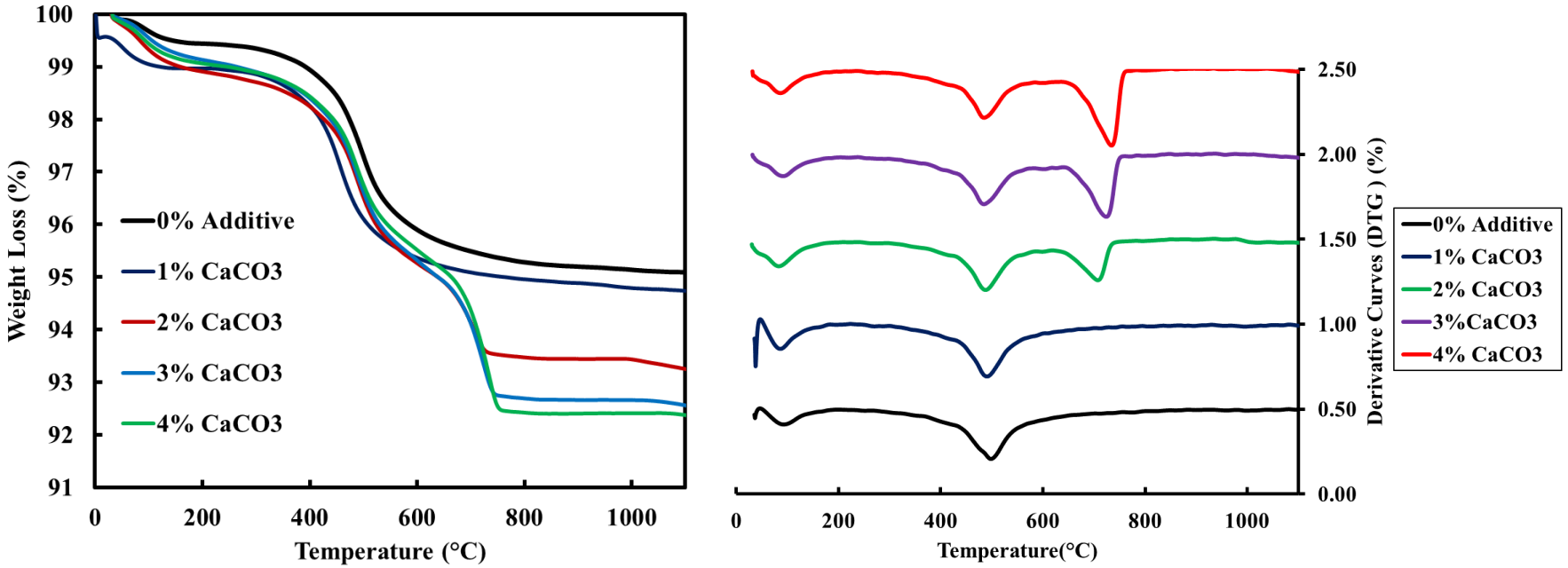

Figure 5-3: Thermogravimetry analysis (TGA) and derivative of TG (DTG) of 1-4wt% $CaCO_3$ in Weald clay fired from 35°C -1200°C at 10°C/min in an alumina crucible.

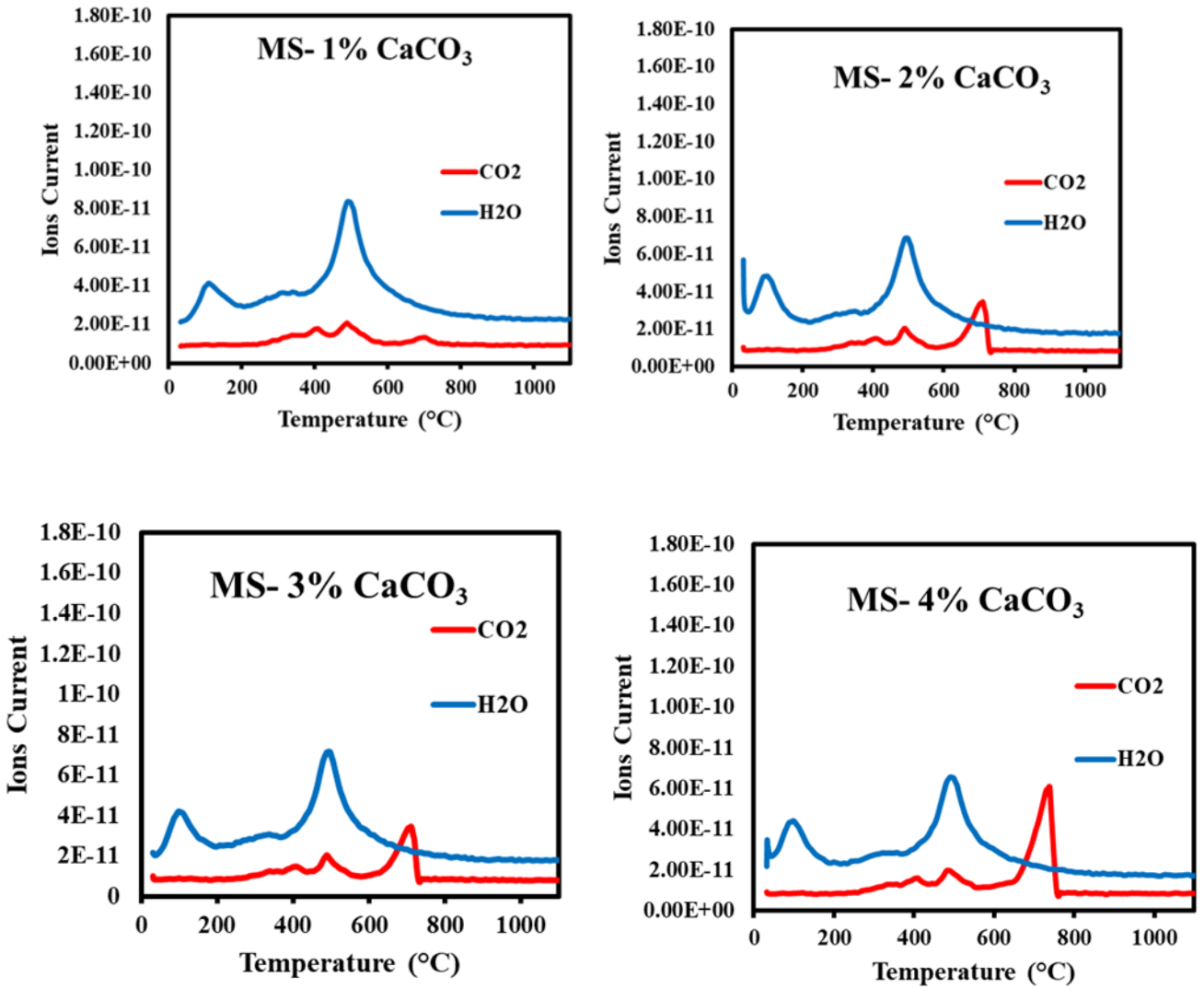

Figure 5-4: Mass spectroscopy of 1-4wt% $CaCO_3$ in Weald clay fired from 35°C -1400°C at 10°C/min in an alumina crucible.

5.3.2 *Dimensional changes in heating for $CaCO_3$ body compositions*

The Dilatometry curve confirmed observations made with TGA/DTGA on the derivative graph. Additions of 1-4wt% of $CaCO_3$ in Weald clay on heating had similar observations for the control. Between 35°-200°C, the clay loses water of formation and then expands linearly up to 550°C due to the β-quartz transition.

The highest linear shrinkage recorded was C3, with 2.5%; the least was C1 due to the additive level. Thermal effects on additives are shown in **Figure 5-5.** Temperature reduction in shrinkage is recorded when the dilatometry curve crosses (the) temperature when the curve passes through dl/L0 = 0%. A summary of additive levels effect in weald clay is shown in **Table 5-3**.

Table 5-3: linear shrinkage and reduced temperature of incorporating 1-4wt% $CaCO_3$ additive in Weald clay

Sample ID	Reduced Temperature (°C)	β-Quartz (°C)	Expansion (%)	Linear shrinkage (%)
Weald clay (W0)	0	581	1	2.3
C1	28	580	0.9	1.5
C2	41	580	0.9	1.7
C3	31	580	0.9	2.5
C4	15	580	0.9	1.6

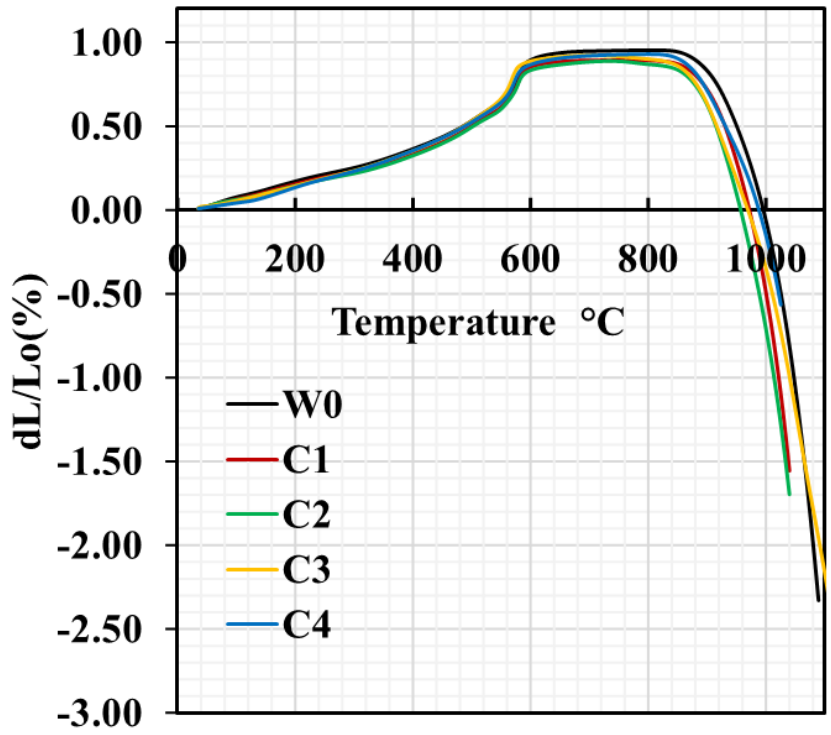

Figure 5-5: Linear shrinkage of 1-4wt% replacement of $CaCO_3$ in weald clay fired to 1040°C at 5°C/ min. Where C1-C4 is 1-4wt% $CaCO_3$

5.3.3 *Calcium carbonate effect on ceramic pore size*

The pore size distribution (PSD) of 1-4wt% calcium-doped samples is shown in **Figure 5-6 to Figure 5-8**. Samples fired to 900°C had smaller PSD ranging between 0.01µm and < 1µm with intrudable mercury porosity (%) lower than the control. For example, additive levels C3 and C4 resulted in 21% and 22%, respectively, lower than the control, which resulted in 23% at 900°C.

Samples fired to 1000°C and 1040°C distribution curves shift towards larger pores (1µm and >1.2µm, respectively). However, additive levels slightly changed the porosity percentages for the top temperatures. The least Hg porosity% was found with the C1 samples (15%), but porosity increased with C4 samples (21%).

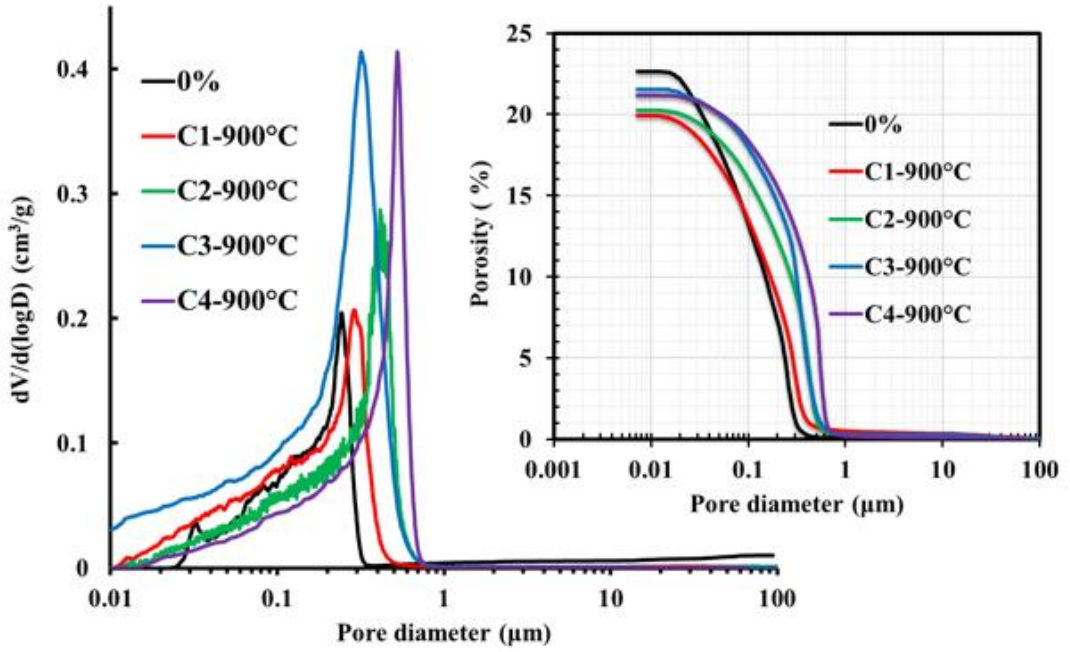

Figure 5-6: Pore size distribution curves and porosity% for 0% additive compared to 1-4wt% $CaCO_3$ fired at 900°C

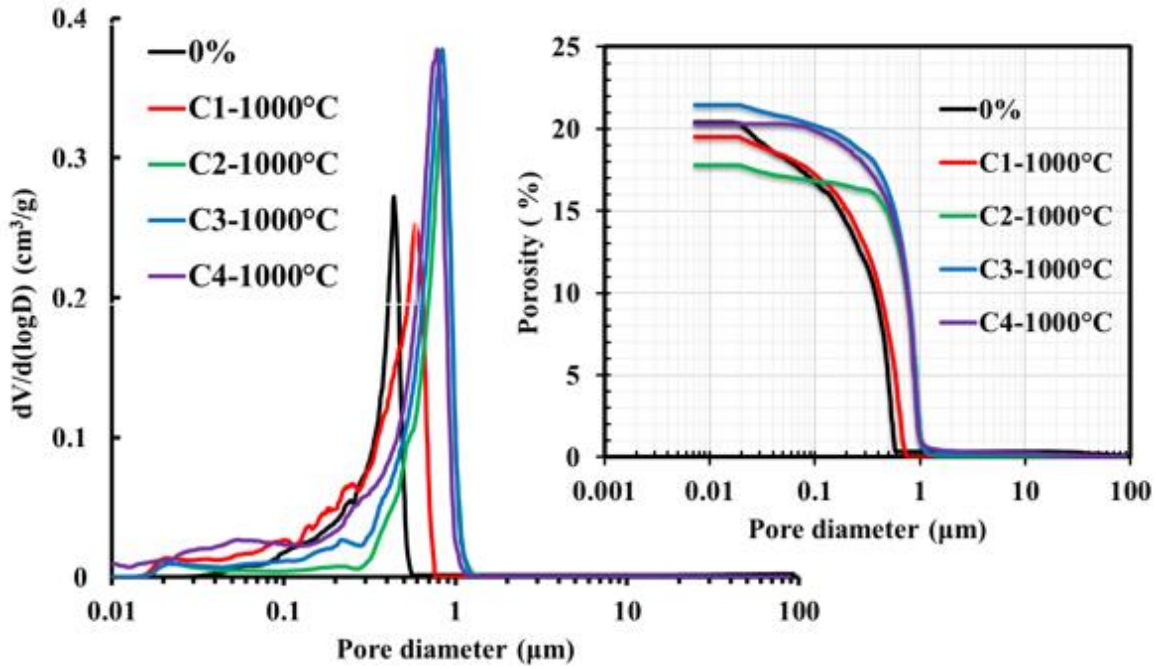

Figure 5-7: Pore size distribution curves and porosity% for 0% additive compared to 1-4wt% $CaCO_3$ fired at 1000°C.

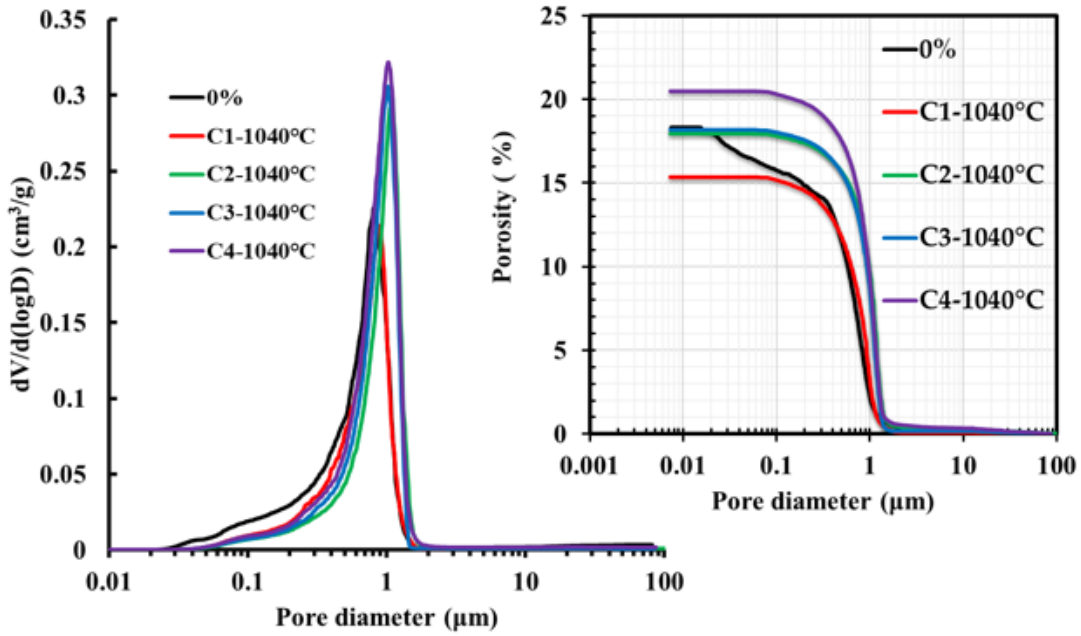

Figure 5-8: Pore size distribution curves and porosity% for 0% additive compared to 1-4wt% $CaCO_3$ fired at 1040°C

5.4 $MgCO_3$ additive replacement phases

Clay samples containing 1wt% $MgCO_3$ fired to 900°C had the same phases as the control at the same temperature. Spinel ferrian ($MgFe_{0.4}Al_{1.6}O_4$ - 04-006-2473) begins with samples containing 2wt% and above, even at 900°C. This is shown in **Figure 5-9.**

Distinct changes are observed in $MgCO_3$ - containing samples with 2wt% and above at 42° at 1040°C, dehydrated muscovite disappears, and mullite ($Al_{2.26}Si_{0.74}O_{4.87}$ - 04-016-1587) forms. Akermanite ($CaMg_{0.9}Al_{0.2}Si_{1.9}O_7$ - 04-014-4688) starts to form in samples containing 2wt% $MgCO_3$ and above, which is not present with the samples with 1wt% additive.

The new phase is akermanite observed in $MgCO_3$ at levels > 2wt% at 43°, on the diffraction pattern shown in **Figure 5-10**.

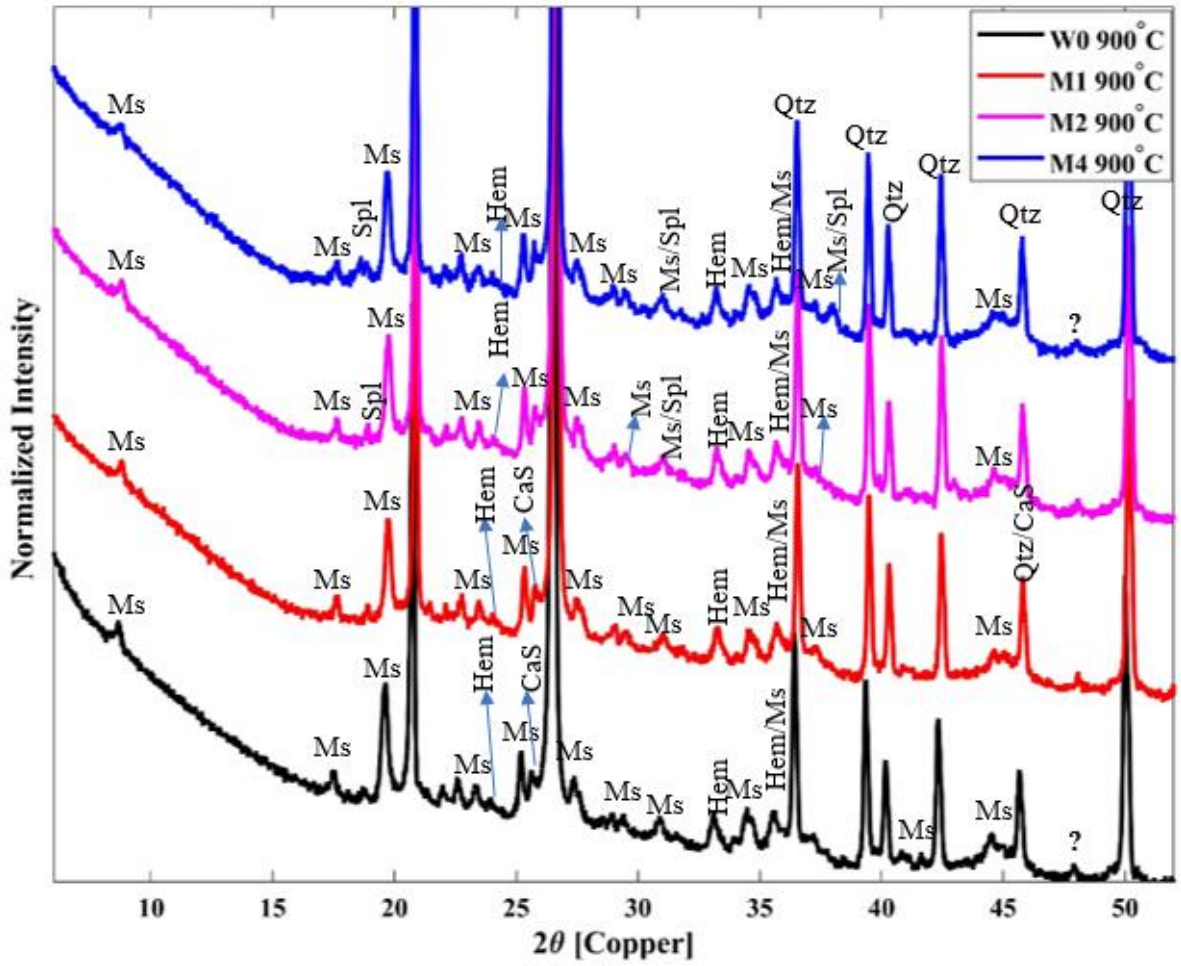

Figure 5-9: Crystalline phases developed in weald clay with 1-4w% replacement of $MgCO_3$ fired to 900°C.

Symbols after Kretz 1983[343] where Qtz=quartz; Ms = Muscovite/ dehydrated muscovite; Hem= hematite; CaS-calcium sulphate, Spl- Spinel ferrian/ Magnesium iron Aluminium Oxide ($MgFe_{0.4}Al_{1.6}O_4$) and Ms- dehydrated Muscovite.

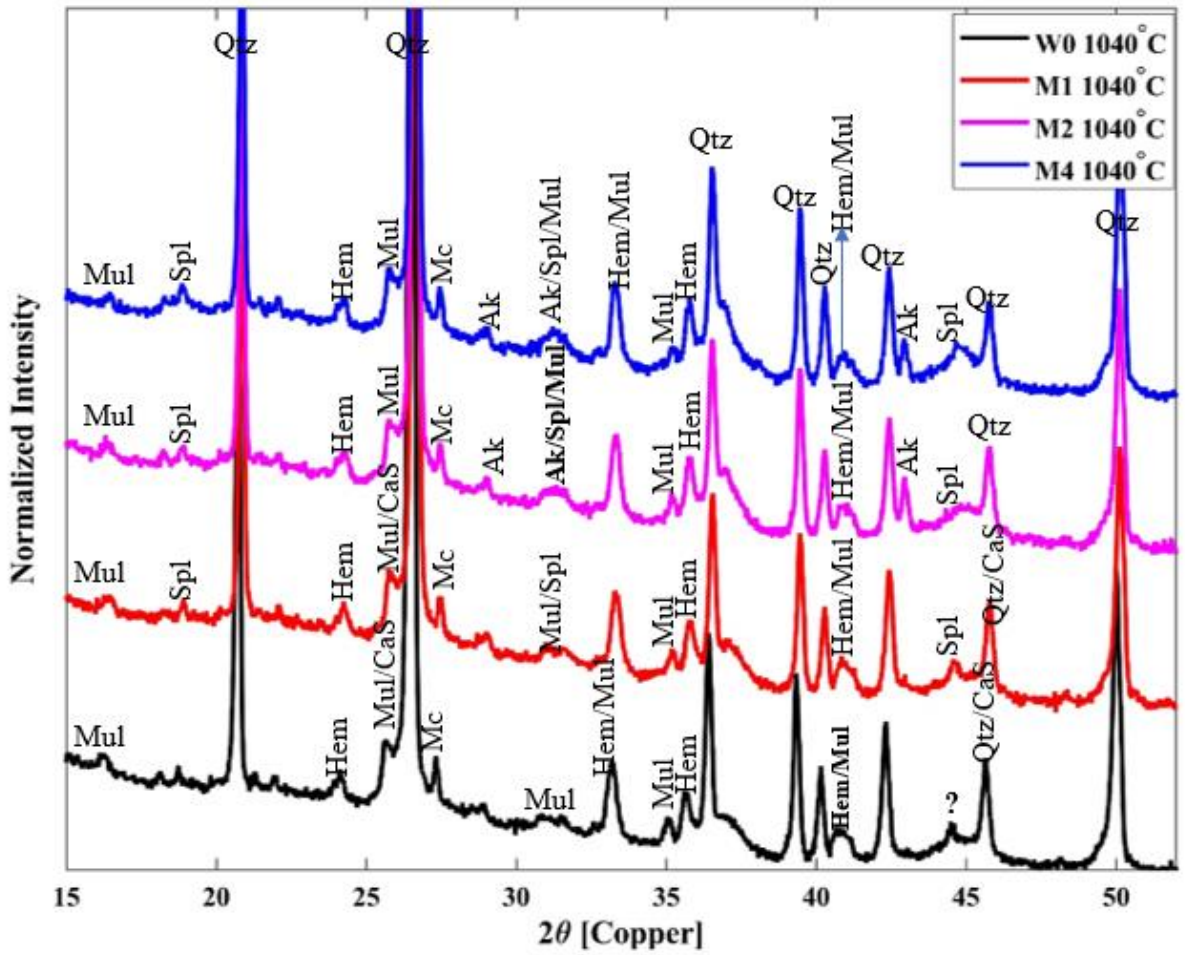

Figure 5-10: Crystalline phases developed in weald clay with 1,2 and 4wt % replacement of $MgCO_3$ fired to 1040°C

Symbols after Kretz 1983[343] where Qtz=quartz, Mul=mullite, Hem= hematite, CaS= calcium silicate, Mc= microcline, Spl= Spinel ferrian/ Magnesium iron Aluminium Oxide($(MgFe_{0.4}Al_{1.6}O_4)$[M1]/ Spinel ferroan/ Magnesium iron Aluminium Oxide ($Mg_{0.588}Fe_{0.188}\ Al_{0.224}$) ($Mg_{0.277}Al_{1.766}Fe_{0.007}$) O_4) [M2]/ Spinel ferroan ($MgAl_2O_4$) [M4] and Ak- Akermanite (Calcium Magnesium silicon Oxide)

5.4.1 *$MgCO_3$ additive heating behaviour in Weald clay*

Like $CaCO_3$ additions, three (3) stages of heating behaviours were observed. The first was the dehydration of water just above the boiling point of water (35°C- 200°C); secondly, the decomposition of $MgCO_3$ and finally, the dehydroxylation of clay minerals (Kaolinte and illite)[357] Beyond 950°C, little additional change occurs, as depicted in the derivative of the TG.

The absorbed water is released between 35°C and 200°C, resulting in the first mass loss. 1-4wt% of the additive is summarized in **Table 5-4.** This corresponds to the endothermic peak in the DTA curves shown in **Appendix 1**. What is interesting about the $MgCO_3$ additive is that the additive decomposes within the same temperature range (300°C-600°C) as the control to give off CO_2 gas shown in **Figures 5-11 and 12** (especially with the derivative DTG). The reaction is $MgCO_3 \longrightarrow MgO + CO_2$. In the DTA curve, exothermic and endothermic reactions are observed within 300-560^oC. At 573^oC, a little endothermic peak is seen as the ά-β structural conversion of quartz also detected with the dilatometry. No melting is detected with such low dopant levels; the formation of liquid phases (i.e. melting) is not separable from the shrinkage effects that occur over a wide temperature range from the DTA curves (> 800^oC). The total weight loss increases considerably with additive levels of 2wt% and above (5.33%, - 9.67% for 1 and 4wt %, respectively).

Table 5-4: Summary of thermal behaviour of 1-4 mass (%) $MgCO_3$ additive in Weald clay

Additive	Event 1		Event 2		Total weight loss (%)
	Temperature (°C)	Weight loss (%)	Temperature (°C)	Weight loss (%)	
M1	35-200	0.78	200-600	3.66	5.33
M2		1.34		6.62	9.33
M3		1.27		6.97	9.55
M4		1.04		7.66	9.67
Inference	Dehydration		Hydroxyl release /Carbonate decomposition		

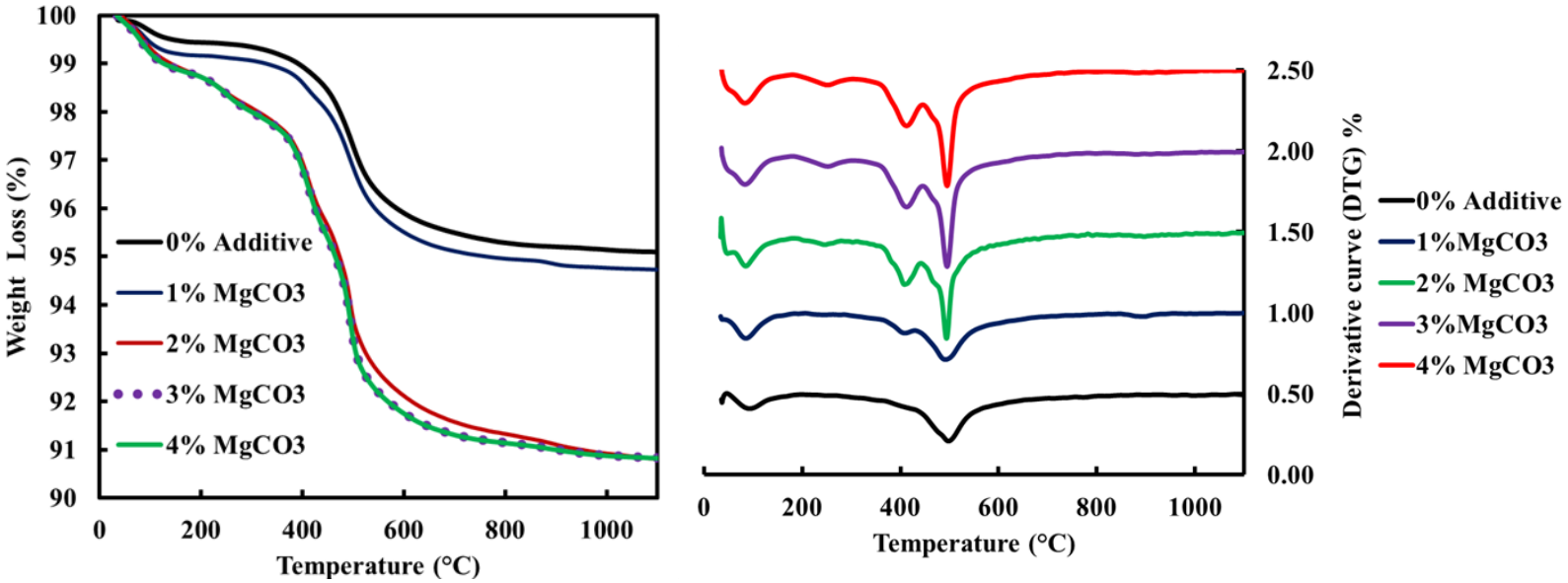

Figure 5-11: TGA and DTG of 1-4wt% doped $MgCO_3$ in Weald clay fired from 35°C -1100°C at 10°C / min in an alumina crucible.

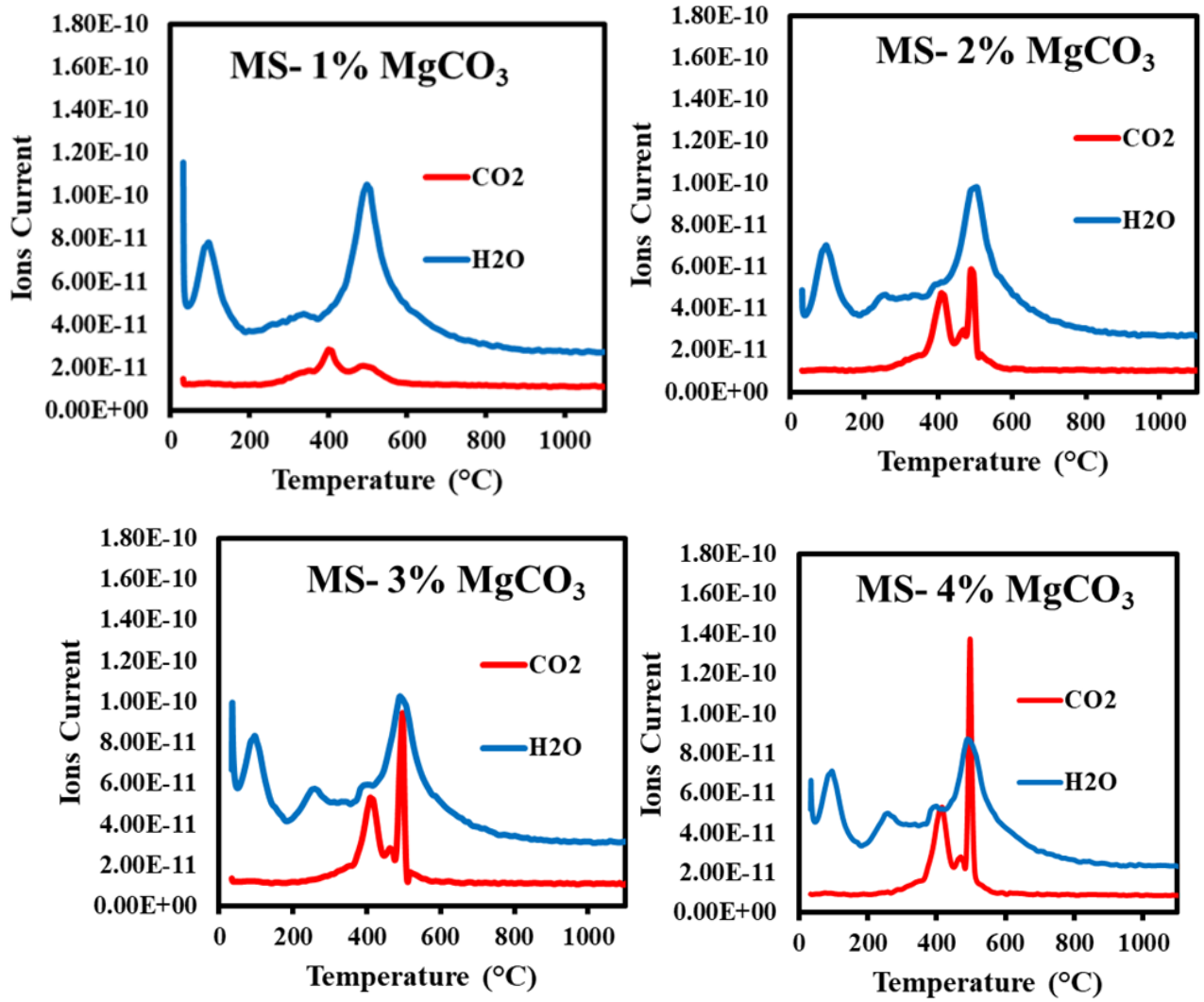

Figure 5-12: Mass spectroscopy of 1-4wt% $MgCO_3$ in Weald clay fired from 35°C to 1100°C at 10°C / min in the alumina crucible.

5.4.2 *Dimensional changes in heating for $MgCO_3$ body compositions*

The effect of 1-4wt % magnesium carbonate (M1-M4) replaced with Weald clay is depicted in **Figure 5-13,** with heating behaviour again comparable to Weald clay control. The linear shrinkage obtained from the concentrations of $MgCO_3$ increased from (M1) 2.1 % - 2.5% with increased dosage. The temperature at which dL/Lo crosses the 0 shows a reduced shrinkage temperature of 4°C, 21°C and 12°C for M1, M2 and M3-M4, respectively. The additive increased shrinkage is 1 -2% compared to the control (2.3%).

Table 5-5*:* linear shrinkage of 1-4wt% $MgCO_3$ additive

Sample ID	**Shrinkage temperature reduction (°C)**	**β-Quartz (°C)**	**Expansion (%)**	**Linear shrinkage (%)**
Weald clay (W0)	0	581	1	2.3
M1	4	580	0.8	2.1
M2	21	580	0.8	2.4
M3	12	580	0.8	2.5
M4	12	580	0.7	2.5

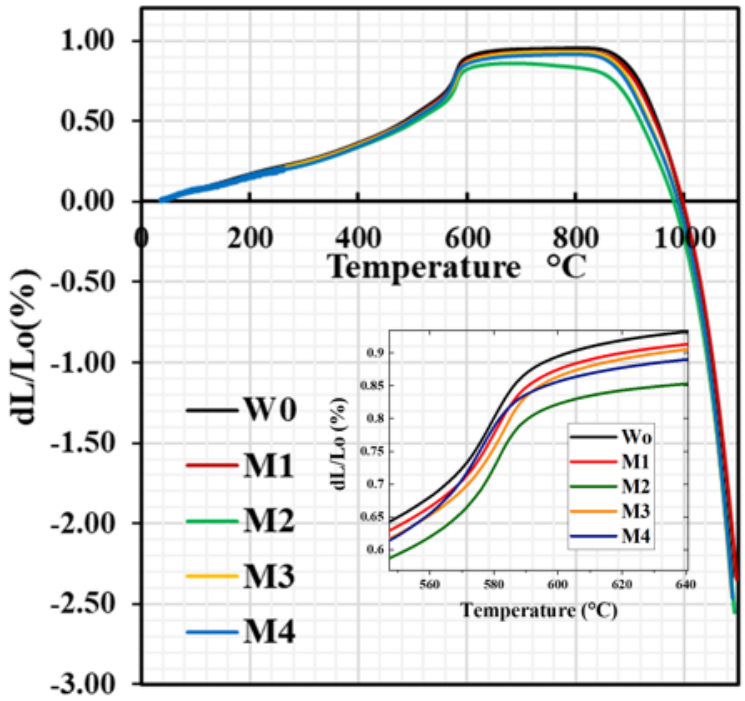

Figure 5-13: Linear shrinkage of 1-4wt% replacement of $MgCO_3$ in Weald clay fired to 1040°C at 5°C/ min.

5.4.3 *Magnesium carbonate effect on ceramic pore size*

The shape and peak height for the porosimetry curves of clay replaced with 1-4wt% $MgCO_3$ is remarkably similar to the 0% additive. The pore size distributions of this alkaline earth additive are bimodal in shape, with shifts in pore sizes changing with temperature and composition see **Figures 5-14 to Figure 5-16**.

1-4wt% $MgCO_3$ fired to 900°C pore diameter ranges from 0.01µm-0.4µm Additive increase produced lower intrudable porosity below 21% except for M1 with 23% attainable mercury. As the temperature increases to 1040°C, the pore size moves towards larger pores (> 1µm), resulting in lower porosity than samples fired to 900°C. This was 2% greater than what was recorded for Ca-containing compositions, and for samples fired to 1040°C, M2 and M4 resulted

in the highest Hg porosity with 20 % and 19%, respectively. Meanwhile, M1 resulted in the lowest intrudable porosity (17%).

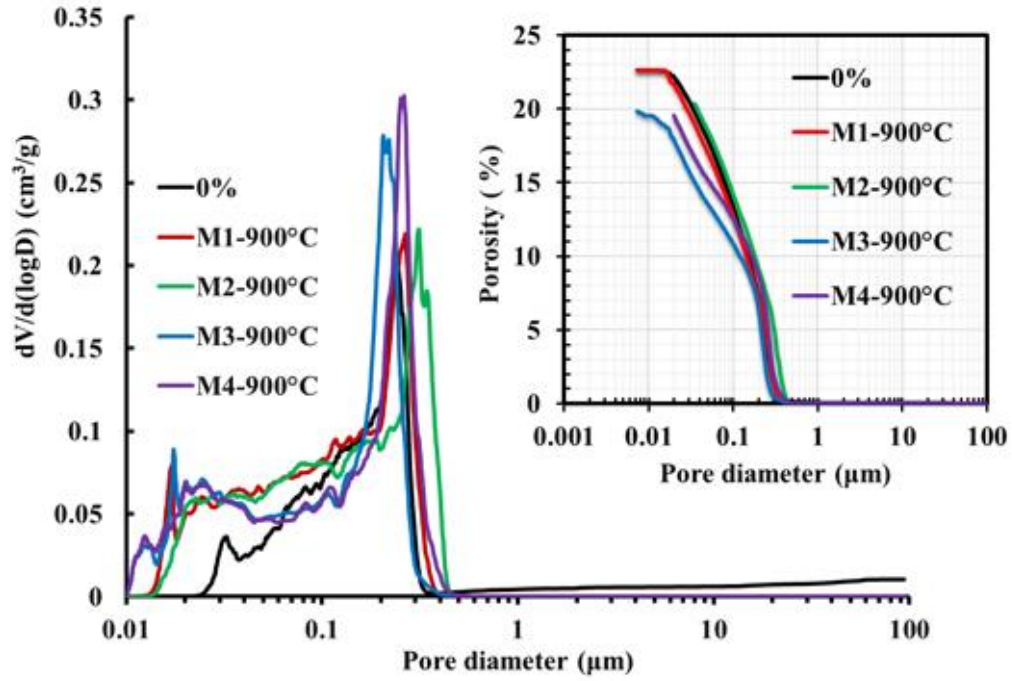

.

Figure 5-14: Pore size distribution and porosity % of 0% additive compared to 1-4wt% $MaCO_3$ fired at 900°C

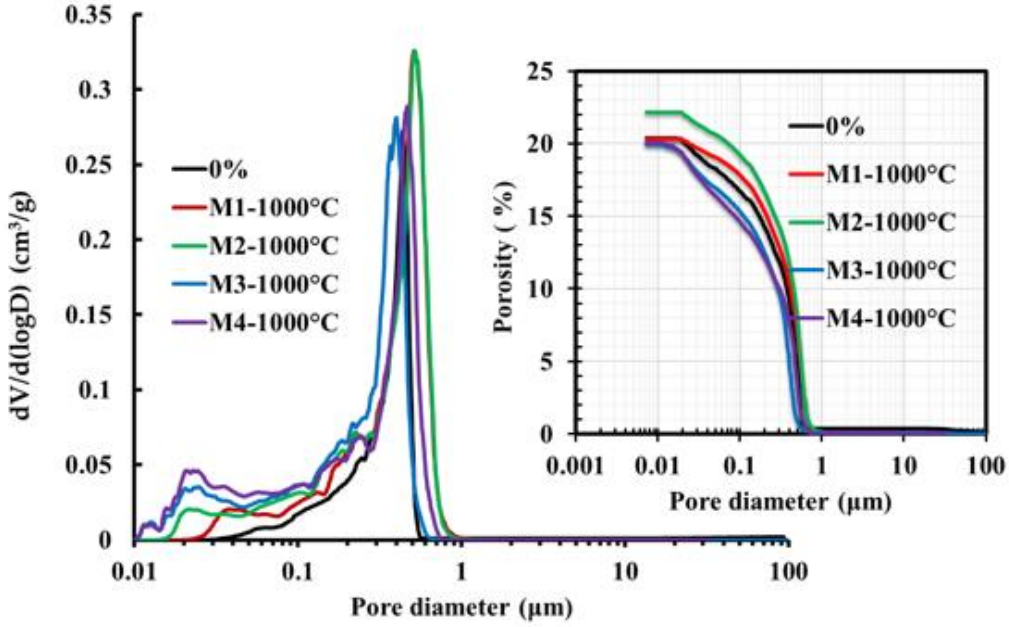

Figure 5-15: Pore size distribution and porosity % of 0% additive compared to 1-4wt% $MaCO_3$ fired at 1000°C

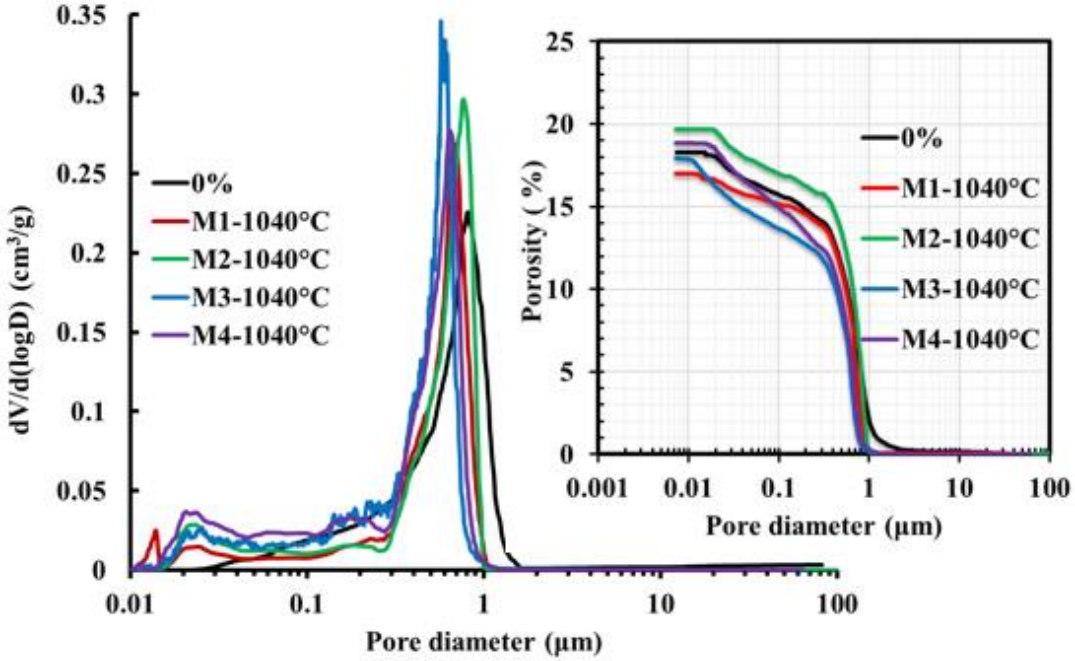

Figure 5-16: Pore size distribution curves and porosity (%) for 0% additive compared to 1-4wt% $MgCO_3$ fired to 1040°C

5.5 $BaCO_3$ replacement phases

Samples fired to 900°C are displayed in **Figure 5-17.** Clay samples replaced with 1wt% $BaCO_3$ show the presence of barium iron oxide sulfide ($BaFe_2Si_2O$ - 04-021-3910), but as levels of additive increase, the locked-up sulfide is not found with 2wt% and above samples. Moreover, SiO_2, Fe_2O_3, and $KAl_3Si_3O_{11}$ are found with all additive levels in the control sample except for $CaSO_4$ (04-013-4616).

At 1040°C (**Figure 5-18**), mullite – ($Al_{2.26}Si_{0.74}O_{4.87}$ 04-016-1586), hematite (Fe_2O_3- 04-005-4630), barium silicate (Ba_2SiO_5 - 01-071-1441) and microcline ($KAlSi_3O_8$-01-084-0709) for samples containing 1wt% and 4wt% $BaCO_3$. 2wt% additive showed the two barium silicates ($Ba_2AlSi_2O_2$ - 01-072-7502) at angle 11.3° and 22.5° / (Ba_2SiO_5 - 01-072-0171). In the B4 sample, the peak at 11.3° disappears, but barium silicate (Ba_2SiO_5 - 01-071-1441) remains in

the composition at a lower intensity. Surprisingly, at 2% (B2), even at 900°C, there are peaks for barium-containing compounds BiS/Bs (also seen at 2% for the 1040°C samples).

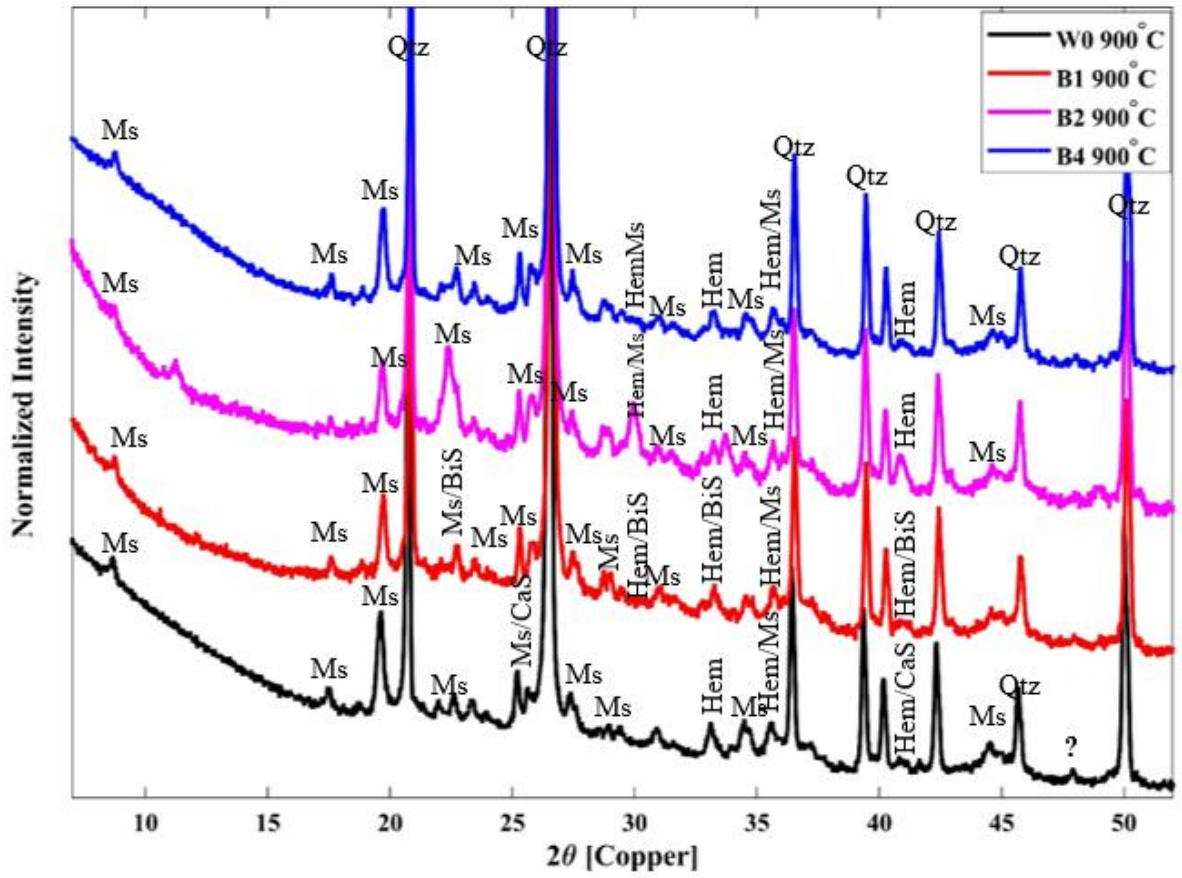

Figure 5-17: Crystalline phases developed in weald clay with 1-4w% replacement of $BaCO_3$ fired to 900°C.

Symbols after Kretz 1983[343] where Qtz- quartz, Ms- dehydrated muscovite, Hem- hematite, BiS- barium iron oxide sulfide and CaS-calcium sulphate.

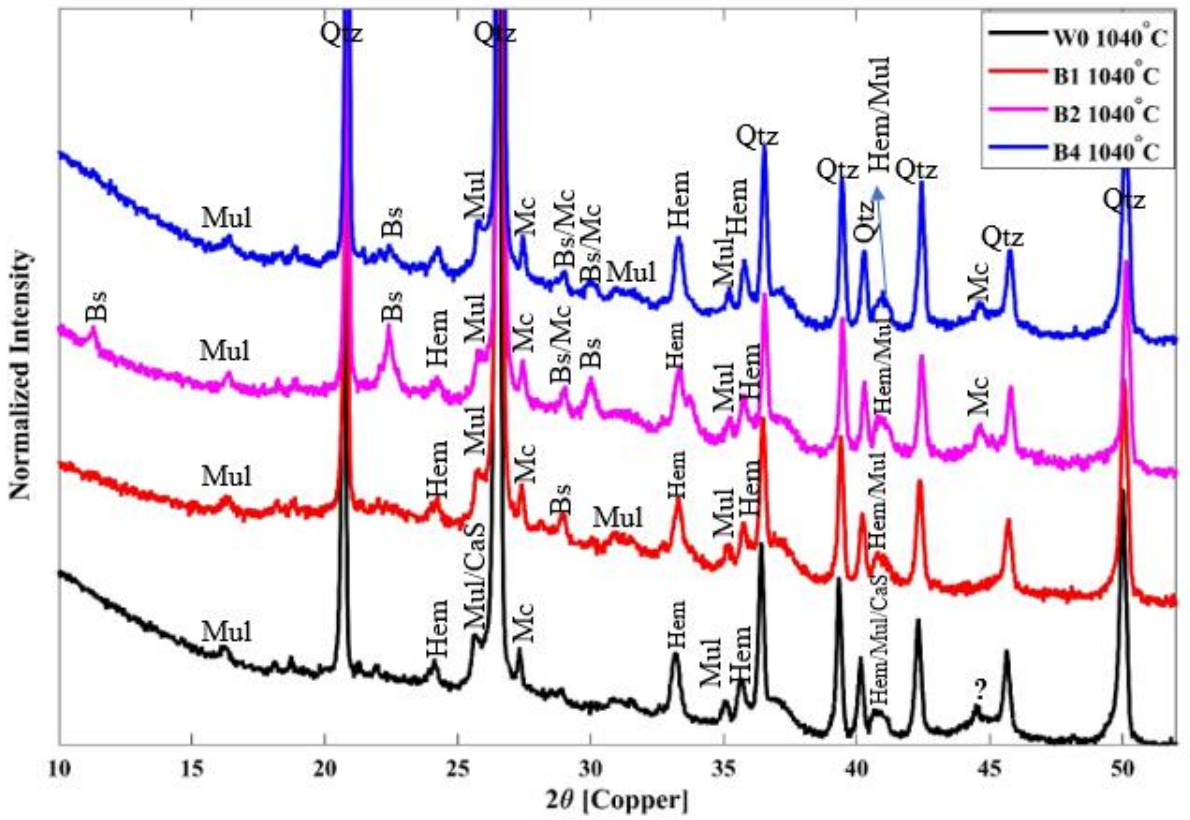

Figure 5-18: Crystalline phases developed in weald clay with 1-4w% replacement of $BaCO_3$ fired to 1040°C

Symbols after Kretz 1983[343] where Qtz=quartz, Mul=mullite, Hem= hematite, CaS= calcium silicate, Mc= microcline, Bs= barium silicate ($Ba_2AlSi_2O_2$- B2 & B4) / Barium Silicate ($BaSi_2O_5$ B1-B4).

5.5.1 *$BaCO_3$ additive heating behaviour in Weald clay*

Reformulated body composition containing 1wt % $BaCO_3$ shows the same thermal behaviour as the base clay but with higher mass loss (5.68%).

From the 2wt% $BaCO_3$ additive, the derivative shows a third (3rd) trough resulting from the decomposition of $BaCO_3$ to form barium Oxide (BaO) and carbon dioxide (CO_2) gas, which occurs beyond 600°C and ends at 800° This corresponds to the DTA curve shown in **Appendix**

1. The TGA curve and its derivative do not reveal the quartz inversion. However, the DTA curves indicate an endothermic peak at 573^{o}C. The quantity of the off-gas released depends on additive levels, as shown in **Figures 5-19 and 20**. The first and second troughs are assigned to absorbed and intrinsic water from clay minerals and the decomposition of carbonates present in the raw material, which are removed on heating between 35°C-600°C; this is an endothermic reaction. Although no more significant change is seen with the derivative curve of 1wt%, the amount of additive resulted in a total weight loss of 0.59% greater than the control. The total body composition weight loss containing barium increases with dosage levels (1-4wt%). 4wt % of replaced additive with Weald clay resulted in a more significant weight loss of 6.44%. A summary of additive replacement levels' thermal behaviour is shown in **Table 5-6**.

Table 5-6: Summary of thermal behaviour of 1-4 mass (%) $MgCO_3$ additive in Weald clay

Additive	Event 1		Event 2		Event 3		Total weight loss (%)
	Temperature (°C)	Weight loss (%)	Temperature (°C)	Weight loss (%)	Temperature (°C)	Weight loss (%)	
B1	35-200	1.03	300-600	3.44	600-800	-	5.69
B2		1.01		3.99		0.99	6.69
B3		0.92		3.39		1.13	6.24
B4		0.93		3.67		1.37	6.44
Inference	Dehydration		Hydroxyl release		Carbonate Decomposition		

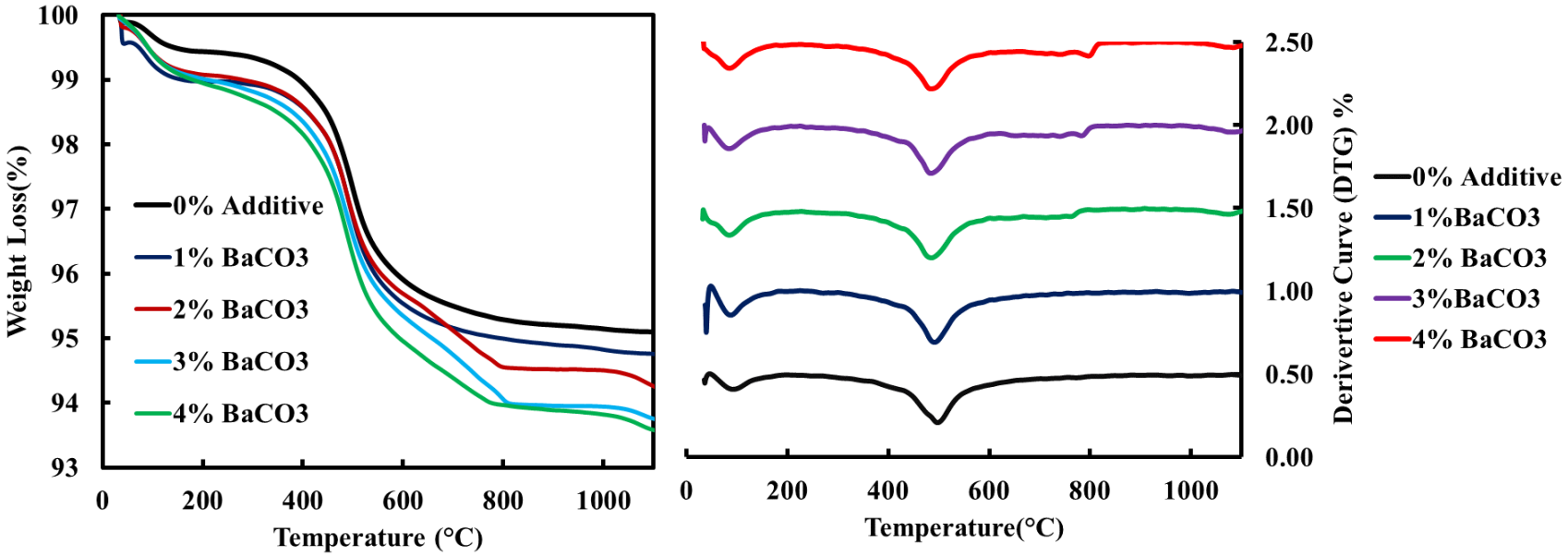

Figure 5-19: The TGA and DTG of 1-4wt% $BaCO_3$ in Weald clay fired from 35°C -1100°C at 10°C/min in alumina crucible.

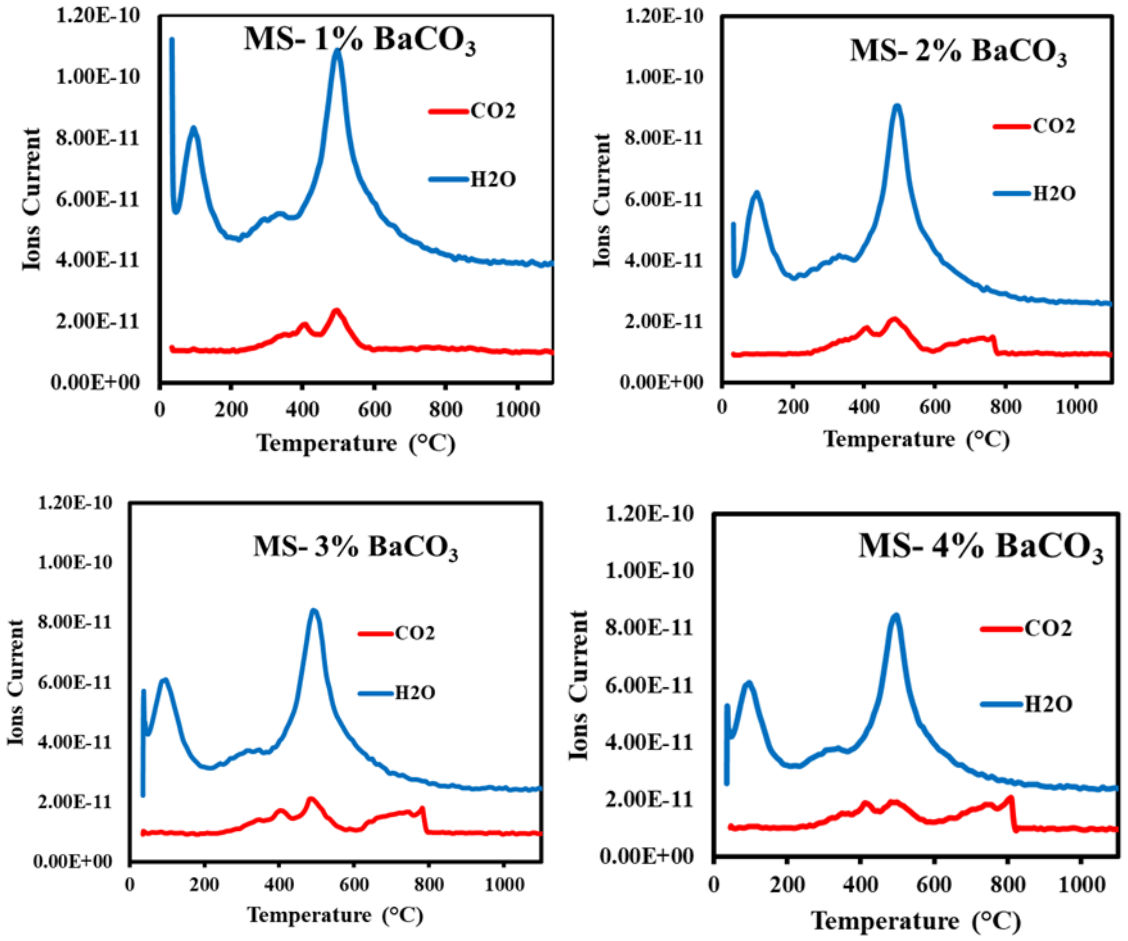

Figure 5-20: Mass spectroscopy of 1-4wt% doped $BaCO_3$ in Weald clay fired from 35°C -1100°C at 10°C/min in alumina crucible.

5.5.2 *Dimensional changes in heating for $BaCO_3$ body compositions*

$BaCO_3$ additive helps positively reduce thermal expansion, especially as the additive levels increase. The expansion is between 0.85-0.9%. The dilatometry curve for samples containing 1-4wt% $BaCO_3$ additive is shown in **Figure 5-21**. The reduced shrinkage temperature is calculated from where the curve crosses 0 at dL/Lo. Maximum shrinkage reduction is 11°C for 4wt% and 2°C for the sample containing 1wt% additive. **Table 5-7** provides the summary for 1-4wt% $BaCO_3$ additive. Forming liquid phases is not separable from the shrinkage outcomes that manifest over a large temperature.

Table 5-7: Onset and linear shrinkage of 1-4wt% $BaCO_3$ with Weald clay sample

Sample ID	Reduced shrinkage temperature	β-Quartz (°C)	Expansion (%)	Linear shrinkage (%)
Weald clay (W0)	0	581	1	2.3
B1	2		0.9	0.8
B2	9		0.9	1.1
B3	10		0.9	1
B4	11		0.85	2.4

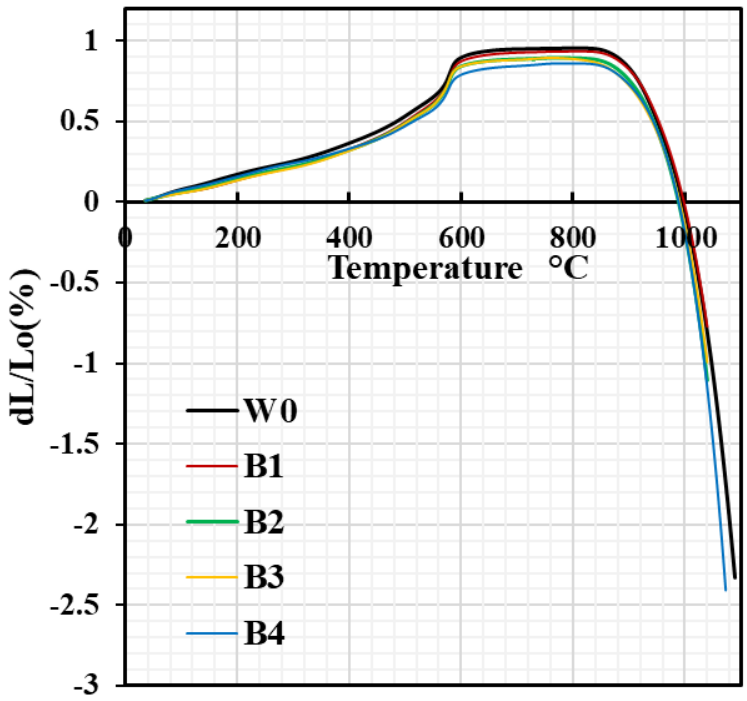

Figure 5-21: Linear shrinkage of 1-4wt% replacement of $BaCO_3$ in Weald clay fired to 1040°C at 5°C/ min.

5.5.3 *Barium carbonate effect on ceramic pore size*

Pore size diameter (PSD) for barium-based samples fired to 900°C ranges from 0.01-0.2µm for B4 fired samples, followed by B2 and B3 with 0.01-0.4µm range and lastly with 0.01-0.5µm. B4 records the highest porosity (24%) when the sample is fired to 900°C compared to 23% of the control. This is shown in **Figure 5-22**.

1-4wt% $BaCO_3$ fired to 1000°C- and 1040°C shift towards 1µm in the distribution curve as shown in **Figures 5-23** & **Figure 5-24.** Ceramics containing 1-3wt% additive pore sizes range from 0.01-1.2µm whilst 4wt% $BaCO_3$(B4) shifts to 1µm. 2 and 3wt% had extra larger pores at 56µm, which were not seen in 1 and 4wt% samples fired at 1040°C. Interestingly, at 1040°C, 4wt% records the least porosity (%) of 14%, while 1wt%, 2wt% and 3wt% resulted in 17% and 18%, respectively. Once again, the Hg porosity (%) was found to be temperature and additive

levels.

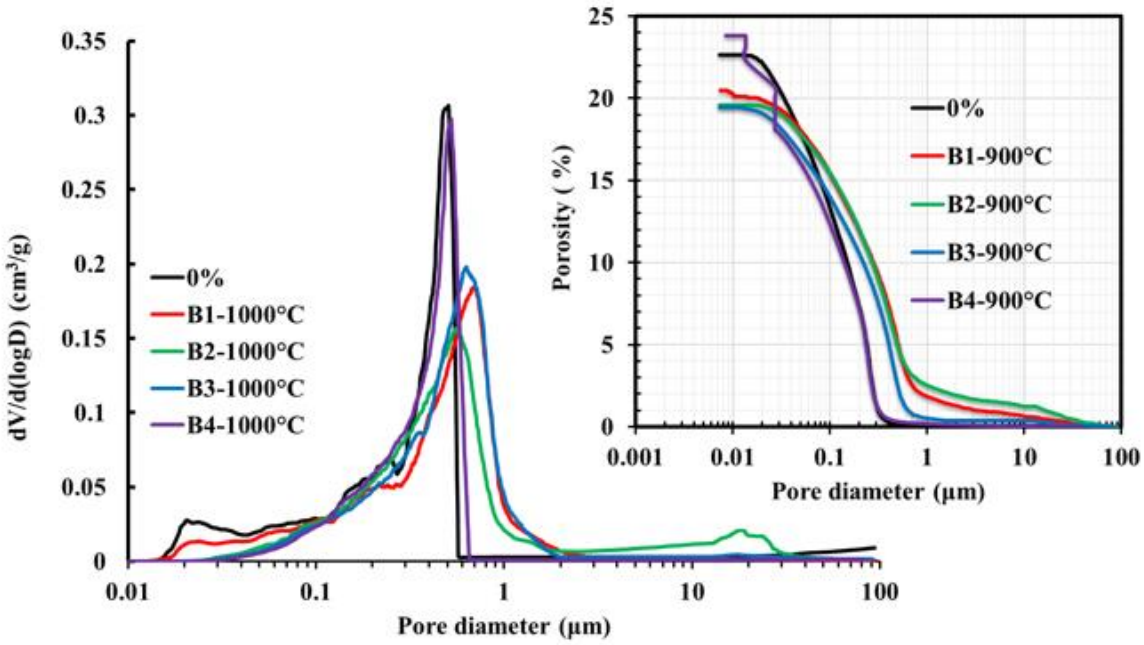

Figure 5-22*:* Pore size distribution curves and porosity% for 0% additive compared to 1-4wt% $BaCO_3$ fired at 900°C

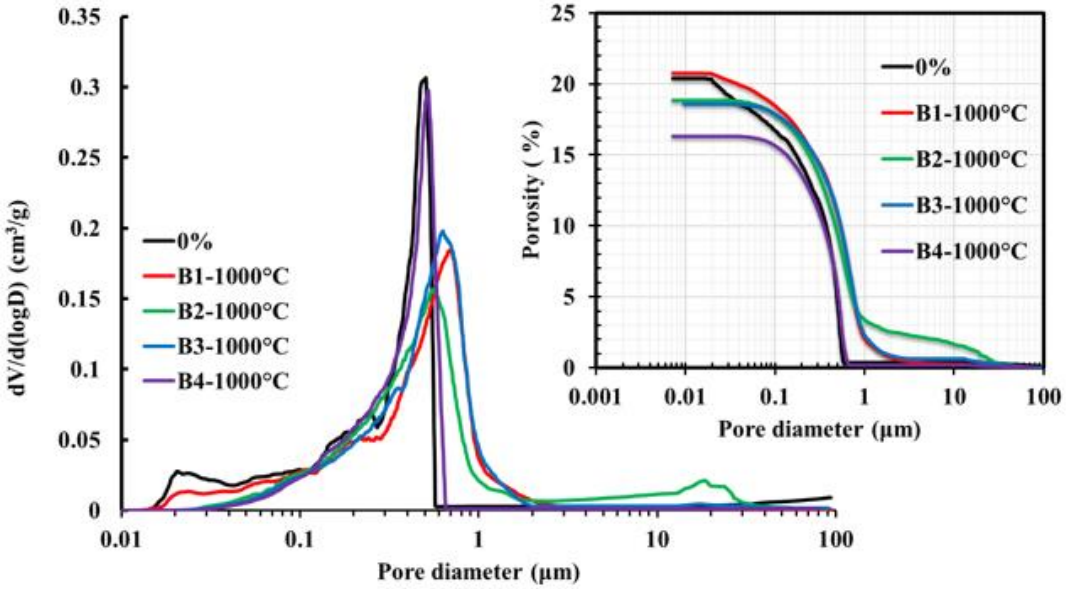

Figure 5-23: Pore size distribution curves and porosity% for 0% additive compared to 1-4wt% $BaCO_3$ fired at 1000°C

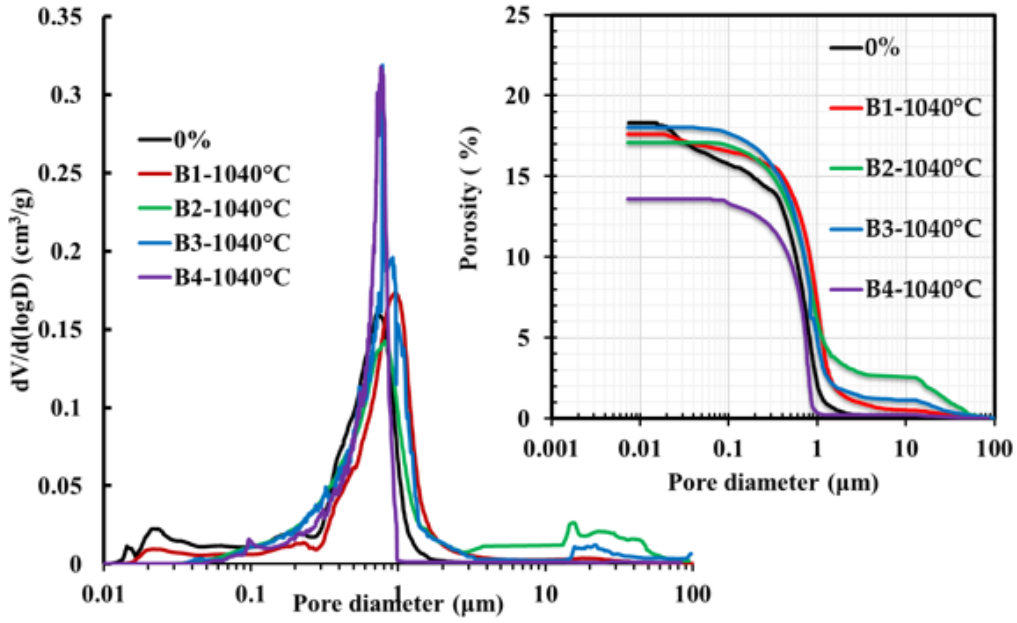

Figure 5-24: Pore size distribution curves and porosity% for 0% additive compared to 1-4wt% $BaCO_3$ fired at 1040°C

5.6 Li_2CO_3 additive replacement phases

At 900°C,1wt % additive shows the same phases obtained with the control as the additive level increased beyond 2wt%, and a new phase, lithium aluminium silicate ($LiAlSi_2O_6$ - 04-020-3038), forms. The hematite (Fe_2O_3 - 04-005-4630) formed in samples with 4wt% levels reveals an intense peak compared to the control, 1 and 2wt%. Additionally, dehydrated muscovite, a clay mineral, does not form in the 4wt% samples; potassium aluminium silicate $K(AlSi_3O_8)$ - 01-071-1543, a monoclinic crystal structure, is seen. The XRD pattern is shown in **Figure 5-25**.

Whilst mullite ($Al_{2.26}Si_{0.74}O_{4.87}$), hematite ($Fe_2O_3$ - 04-005-4630), microcline ($KAlSi_3O_8$) and quartz (SiO_2) form in samples containing 1wt% Li_2CO_3 (L1), L2 and L4 does not promote mullite formation instead $LiAlSi_2O_6$ (04-016-0114) and lithium iron oxide ($Li_{0.63}Fe_{0.37}$ - 01-085-1992) along with the quartz, hematite and microcline found in the control. Interestingly,

microcline ($KAlSi_3O_8$ - 01-084-0709) does not form with L4 samples fired to 1040°C. Moreover, three peaks (28°-34°C) with L2 and L4 samples could not be identified. See **Figure 5- 26**.

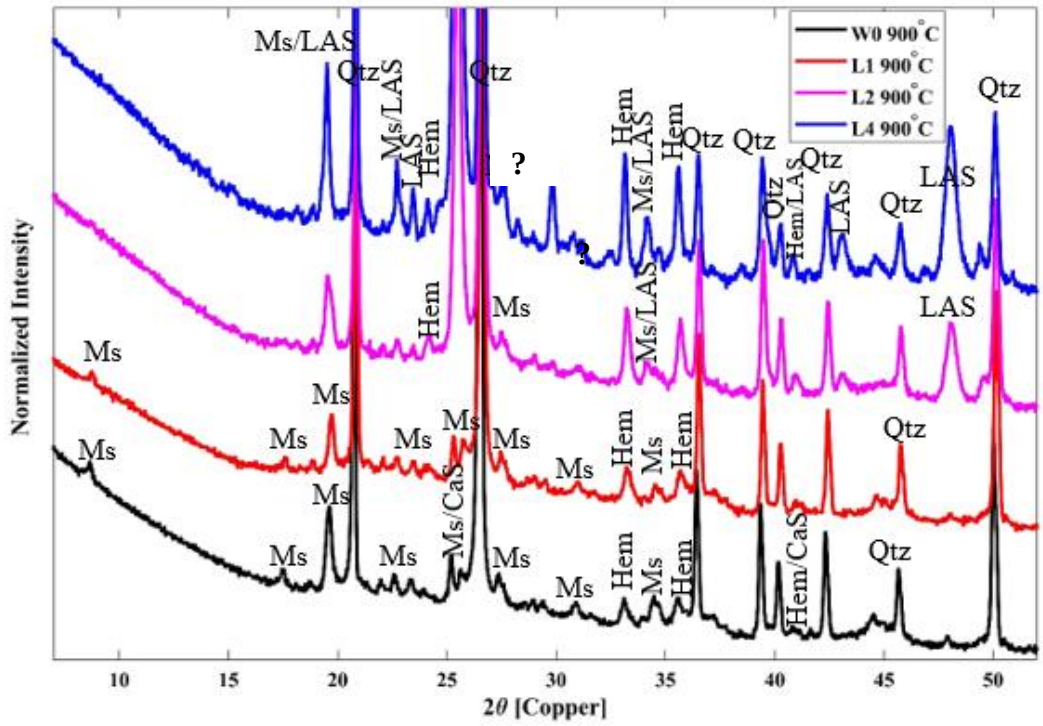

.

Figure 5-25: Crystalline phases developed in weald clay with 1, 2 and 4w% replacement of Li_2CO_3 fired to 900°C. Symbols after Kretz 1983[343]. Where Qtz- quartz, Ms- dehydrated muscovite ($KAl_3Si_3O_{11}$) / Ms- potassium Aluminium Silicate $K(AlSi_3O_8)$ [01-071-1543] for L4, Hem- hematite, CaS-calcium sulphate, and LAS- Lithium Aluminium Silicate ($LiAlSi_2O_6$) [04-020-3038]

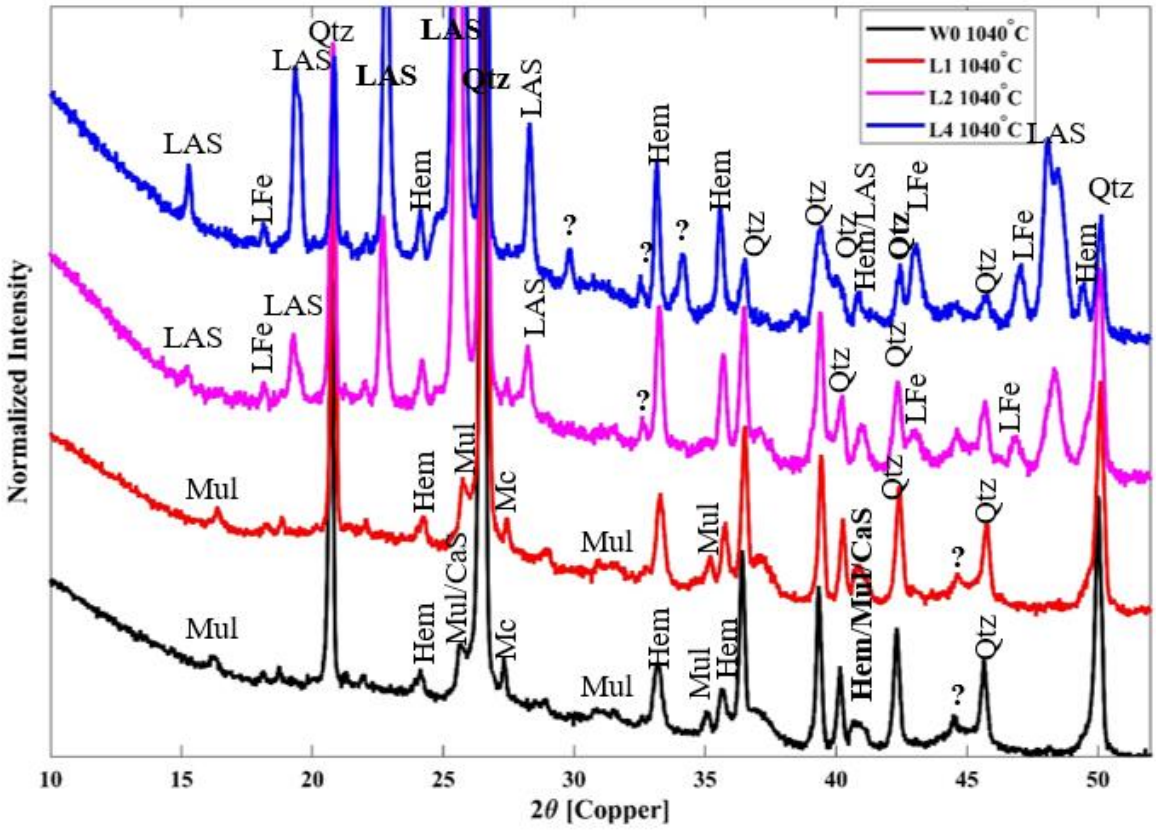

Figure 5-26: Crystalline phases developed in weald clay with 1-4w% replacement of Li_2CO_3 fired to 1040°C.

Symbols after Kretz 1983[343] where Qtz=quartz, Mul=mullite, Hem= hematite, CaS= calcium silicate, Mc= microcline, LAS- Lithium Aluminium silicates [($LiAlSi_2O_6$) - 04-016-0114] and LFe- Lithium iron oxide [($Li_{0.63}Fe_{0.37}$) FeO_2 - 01-085-1992]

5.6.1 *Li_2CO_3 additive heating effect on Weald clay*

Li_2CO_3 additive, the lightest oxide element, causes thermal changes in three (3) phases. First, there is initial water removal between 35-200°C, dehydration of clay minerals at temperatures beyond 200°C-450°C an endothermic reaction depicted in **Appendix** 1, followed by the final weight loss associated with decarbonising Li_2CO_3 to give off CO_2 gas shown in **Figure 5-27**.

Both OH and CO_2 come off from the mass during the dehydroxylation stage. The mass spectroscopy is shown in **Figure 5-28**—the CO_2 gas results from the decomposition of carbonaceous substances in the clay and carbonates of the additive. The CO_2 from the clay comes off gradually between 200°C-600°C. After 600°C, additive decomposition occurs, an endothermic reaction in samples containing >2wt%. Bazhenov et al.[358] reported that the melting point of Li_2CO_3 is 733°C. The total mass loss of Li_2CO_3 replacement from l-4wt% is 5.48%,9.99%,10.88% and 11.83%.

The intensity of CO_2 evolution is associated with additive levels. Overall, Li_2CO_3 has the highest weight loss for all the additive levels compared to the control. Summary details of the Li_2CO_3 thermal behaviour are shown in **Table 5-8**. This decomposition temperature for Li_2CO_3 suggests possibly an early melting of lithium to promote the liquid formation, as reported by Gruverr[359].

Table 5-8: Summary of thermal behaviour of 1-4 mass (%) Li_2CO_3 additive in Weald clay

Additive	Event 1		Event 2		Event 3		Total weight loss (%)
	Temperature (°C)	Weight loss (%)	Temperature (°C)	Weight loss (%)	Temperature (°C)	Weight loss (%)	
L1	35-200	1.12	200-600	3.55	800-1076	0.13	5.48
L2		1.18	400-800	7.12	900-1065	0.27	10.12
L3		1.10		8.48		0.19	10.89
L4		0.94		9.66		0.15	11.77
Inference	Dehydration		Hydroxyl release/ carbonate decomposition		-		

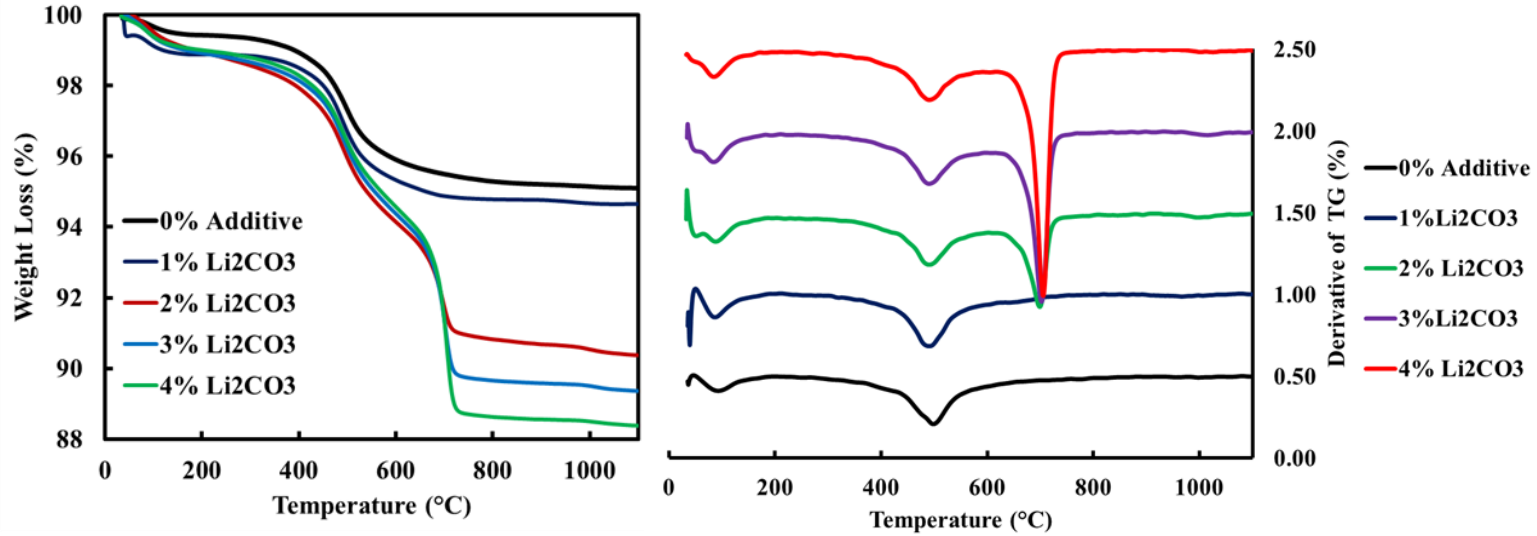

Figure 5-27: TGA and DTG of 1-4wt% Li_2CO_3 in Weald clay fired from 35°C -1100°C at 10°C / min in an alumina crucible.

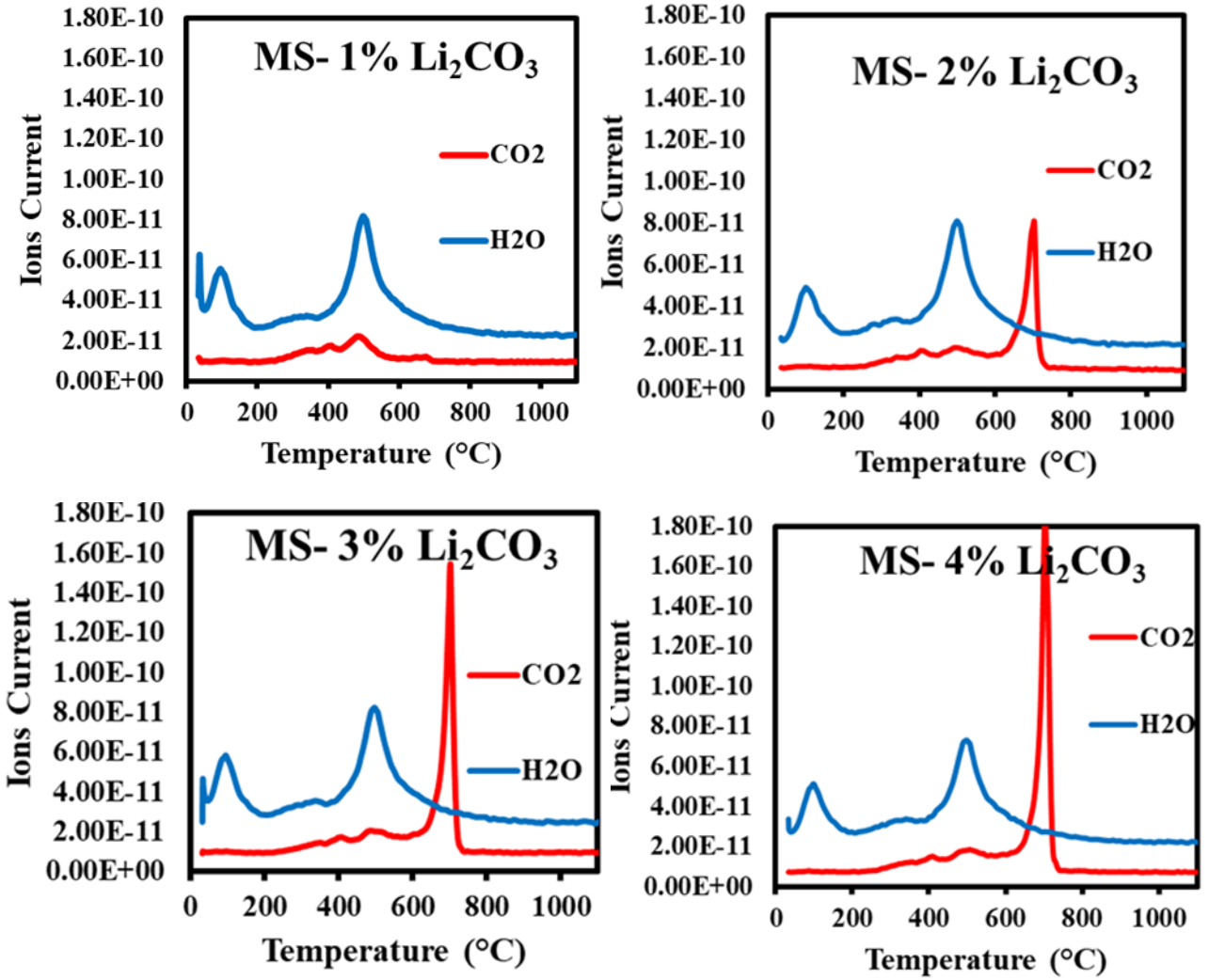

Figure 5-28: Mass spectroscopy of 1-4wt% Li_2CO_3 in Weald clay fired from 35°C -1100°C at 10°C / min in an alumina

5.6.2 *Dimensional changes in heating for Li_2CO_3 body compositions*

The dilatometric curve of the reference (control) composition and Li_2CO_3 1-4wt% addition is shown in **Figure 5-29**. It was observed that expansion increases until a maximum by a sharp change to quartz inversion. After 600°C, the expansion rate gradually decreases, and sintering starts at 820°C. Shrinkage increases more rapidly with temperature. Dilatometric curves for compositions containing 1-4wt% had a different effect on the expansion. It was observed that 1wt% had the same thermal effect as the control with 1% expansion and a shrinkage temperature reduction of 22%. Above 2wt%, the dilatometry curve expands beyond the line where dL/Lo is 0% to 1200°C. This suggests the expansion of the liquid-solid reaction caused by the viscosity of the additive as the temperature exceeds 980°C. The continuous expansion, even after the quartz transition, could be caused by the decomposition of Li_2CO_3, which follows the densification of ceramic from the glassy phase developed as the temperature rises above 720°C. The summary of linear shrinkage reduced firing temperature and change in quartz transition is shown in **Table 5-9.**

Table 5-9: Linear shrinkage of 1-4wt% Li_2CO_3 with Weald Clay sample

Sample ID	B-Quartz (°C)	Shrinkage temperature reduction (°C)	Expansion (%)	Linear shrinkage (%)
Weald clay (W0)	581	0	1	2.3
L1	576	22	1	2.5
L2	561	-42	1	1.7
L3	564	-157	1.2	0.2
L4	575	-160	1.3	0.3

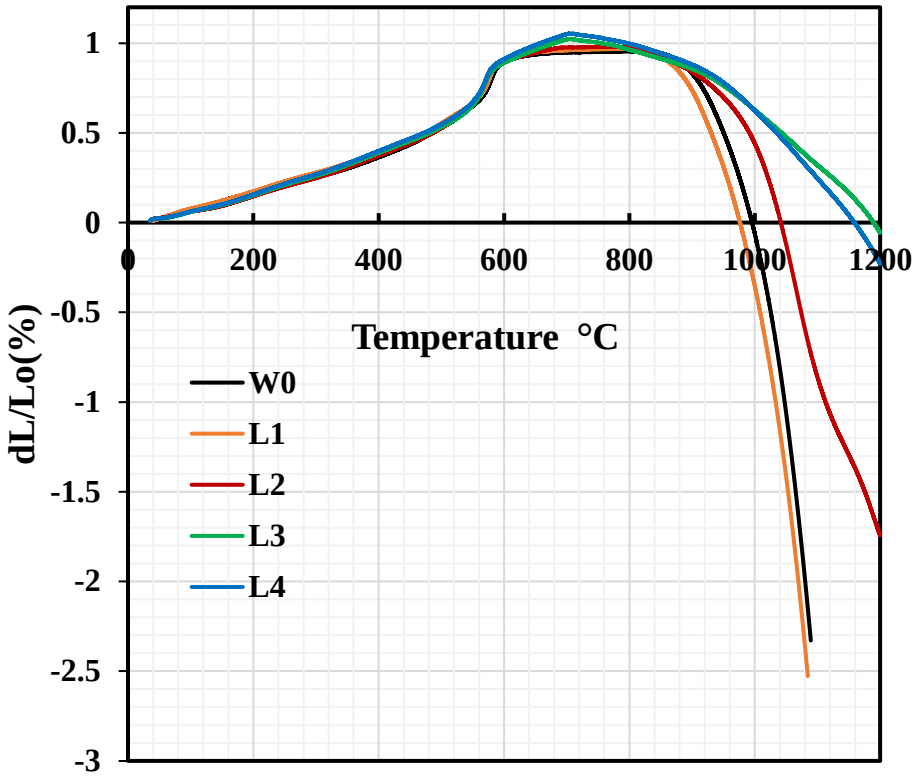

Figure 5-29: Linear shrinkage of 1-4wt% replacement of Li_2CO_3 in Weald clay *fired to 1200°C at 5°C/ min.*

5.6.3 *Lithium carbonate effect on ceramic pore size*

For Li_2CO_3 additive, only samples containing 3wt% and 4wt. % showed a bimodal shape different from the 0% additive. Pore distribution shifted per additive level and temperature as depicted in **Figures 5-30 to 32.** But generally, this analysis shows that Li-carbonate aids in sintering clay particles compared to the 0% additive in porosity percentage. Pore diameter for samples fired to 900°C saw the highest porosity, especially with the highest additive level (L4) of 21%. The least intrudable Hg % was found in samples containing 1% Li_2CO_3 (L1) (18.32%).

As the temperature rises to 1000°C, the intrudable porosity decreases, and pore diameter moves toward larger pores with increasing additive influence. L1 fired to 1000°C recorded the least

porosity of 14.93%, followed by L2 with 17.89%. Interestingly, L3 recorded the highest intrudable percentage at 19.15% at > 1 µm.

When the temperature reaches 1040°C, Hg can only fill fewer pores, but the additive level again influences this. The least Hg % was found to be L1 (12.83%). L3 and L4 showed an unusual pore size distribution (1µm-100µm) towards the macro-porous 15µm, but notwithstanding, L4 recorded lower Hg porosity (~4% less) when compared to L3 (19.12%) fired to the same temperature under the same conditions.

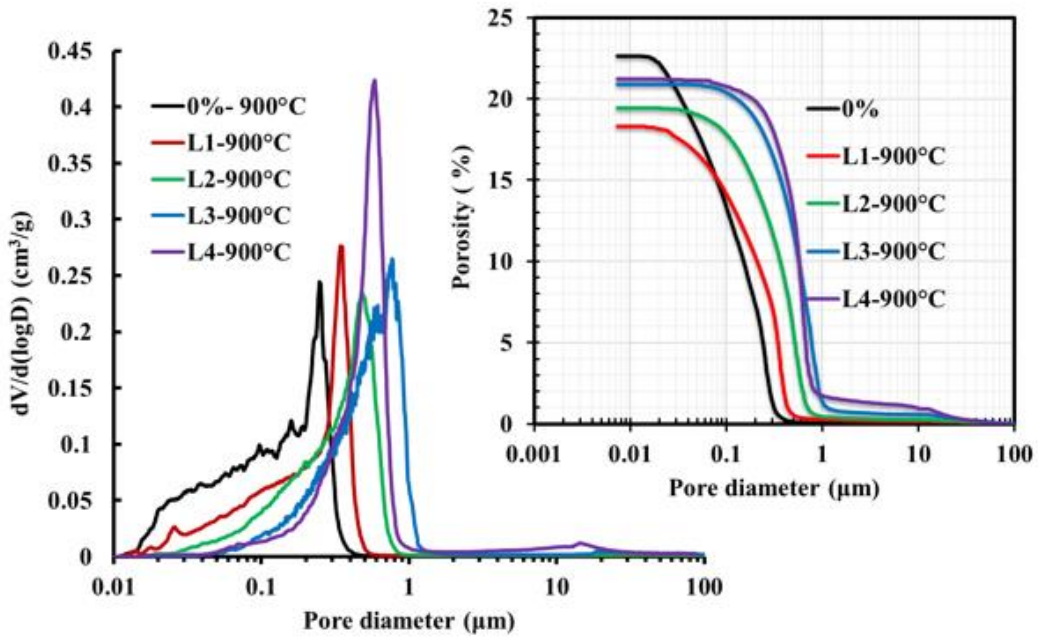

Figure 5-30: Pore size distribution curves and porosity% for 0% Weald clay compared to 1-4wt% Li_2CO_3 fired at 900°C

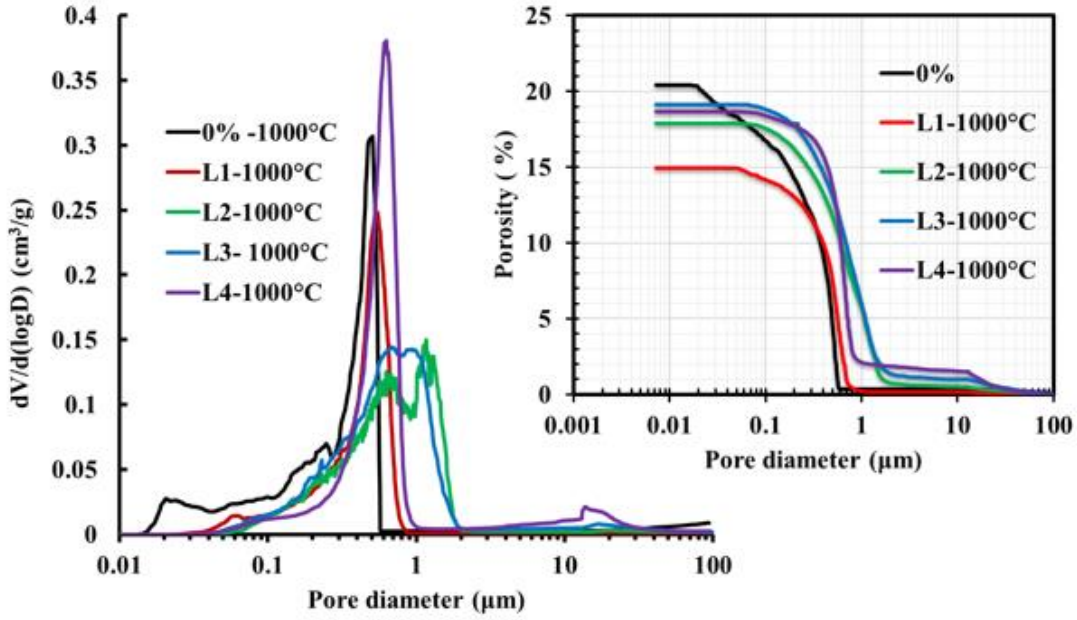

Figure 5-31: Pore size distribution curves and porosity (%) for lithium-based additive (1-4wt%) compared to 0% additive fired at 1000°C.

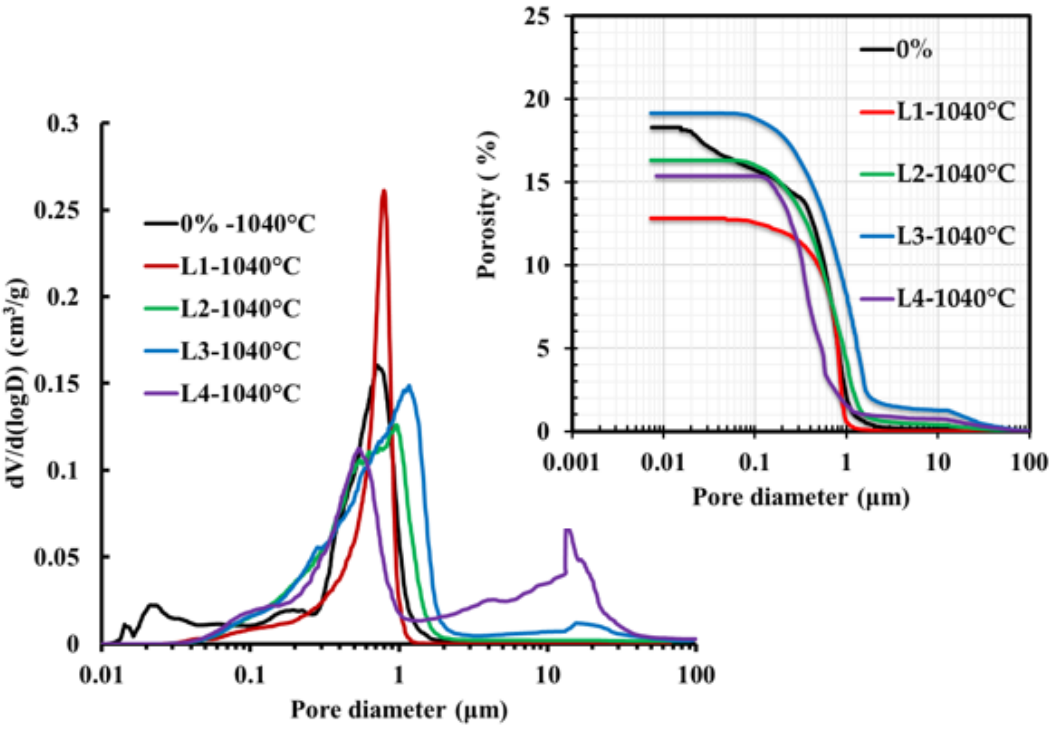

Figure 5-32: Pore size distribution curves and porosity (%) for lithium-based additive (1-4wt%) compared to 0% additive fired at 1040°C.

5.7 K_2CO_3 additive replacement phases

Figures 5-33 & 34 depict the diffraction pattern of K_2CO_3 samples fired to 900°C and 1040°C, showing no difference or significant changes compared to the control.

Phases obtained were quartz- (SiO_2- 01-087-2096), hematite (Fe_2O_3 -01-076-4579) and dehydrated muscovite ($KAl_3Si_3O_{11}$ -00-046-074) for samples fired to 900°C.

In samples fired to 1040°C, dehydrated muscovite was replaced by mullite ($Al_{2.26}Si_{0.74}O_{4.87}$ - 04-016-1586) and microcline ($KAlSi_3O_8$ 01-084-0709 [K1 & K2]. Quartz (SiO_2- 01-087-2096), hematite (Fe_2O_3 -01-076-4579 and microcline ($KAlSi_3O_8$ 01-084-0709) remain in the control. Two forms of microcline, a potassium aluminium silicate formed in a K4 sample fired to 1040°C [$KAlSi_3O_8$ 01-084-0709 / $KAlSiO_4$ 00-048-1028].

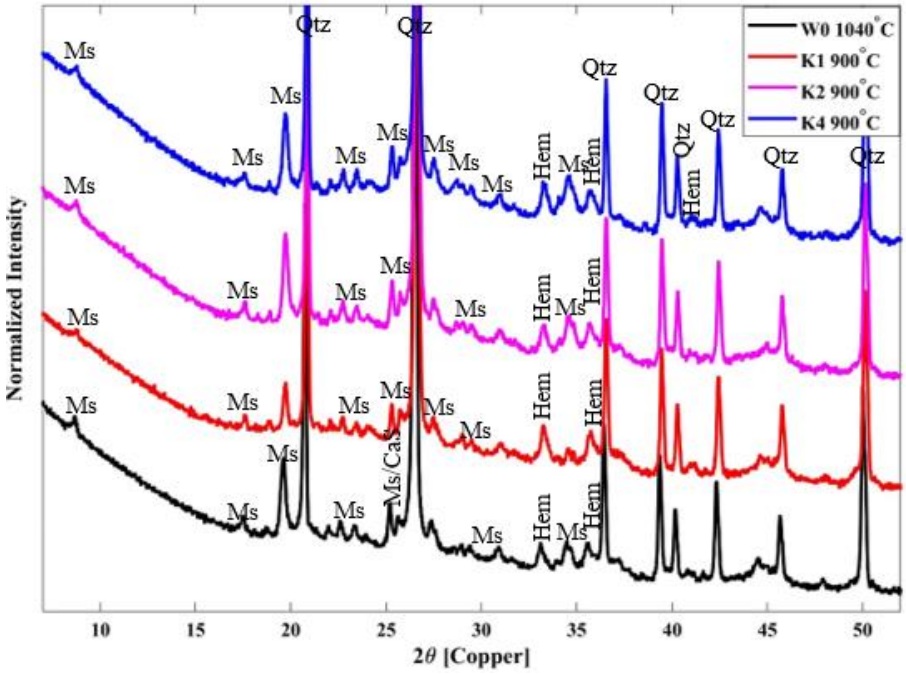

Figure 5-33: Crystalline phases developed in weald clay with 1,2 and 4w% replacement of K_2CO_3 fired to 900°C. Symbols after Kretz 1983[343] where Qtz=quartz; Ms = Muscovite/ dehydrated muscovite; Hem= hematite; CaS-calcium sulphate and Ms- dehydrated Muscovite.

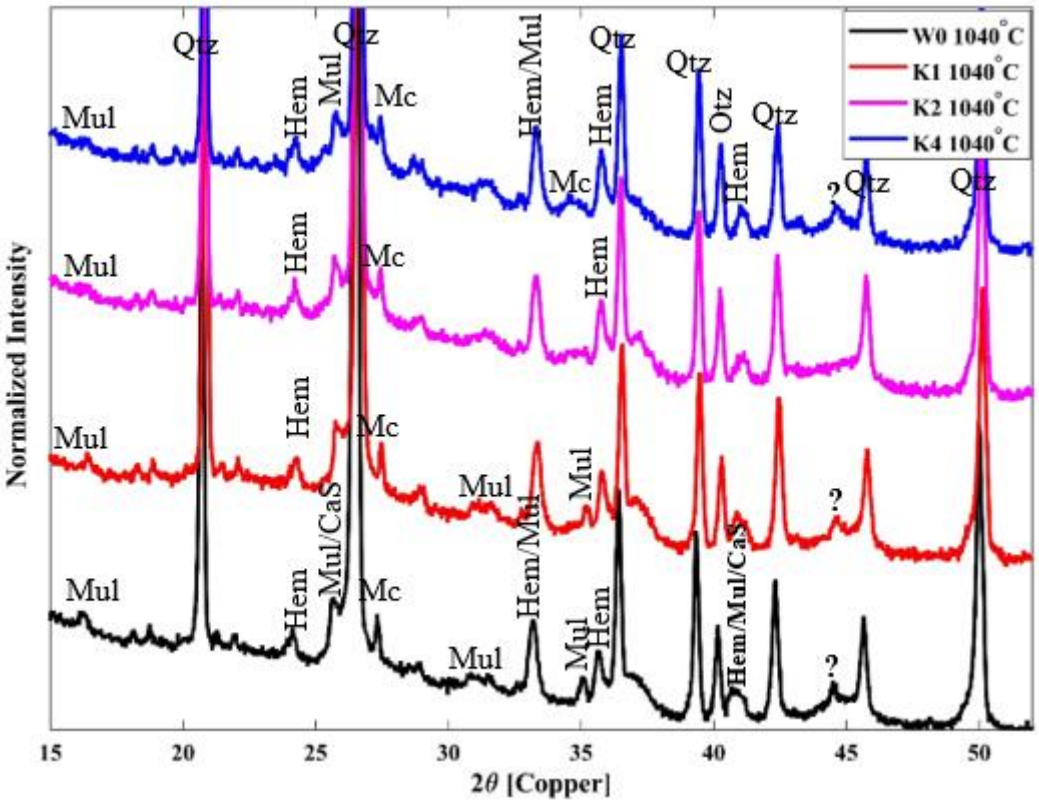

Figure 5-34: Crystalline phases developed in weald clay with 1,2 and 4w% replacement of K_2CO_3 fired to 1040°C.

Symbols after Kretz 1983[343] where Qtz=quartz**,** Hem= hematite**,** Hem= hematite**,** CaS-calcium sulphate and Mul- mullite and Mc- microcline

5.7.1 *K_2CO_3 additive heating behaviour on Weald clay*

K_2CO_3 additive levels have a similar heating effect because of the same base clay, as shown in **Figure 5-35** by the TGA and DTG curves. The only difference in the decomposition temperature of K_2CO_3 is attributed to the potassium compound breaking down between 800°C-920°C (an exothermic reaction – **Appendix 1**) and slight loss beyond 1000°C revealed by the mass spectroscopy as OH/H_2O. The weight loss is attributed to physical and chemical water and CO_2 removal (**Figure 5-36),** an endothermic reaction. The mass loss for 1wt% and the base clay is almost the same (4.84% and 5.09%), respectively. And an endothermic peak at 573ºC as a result of quartz transition.

Table 5-10: Summary of thermal behaviour of 1-4 mass (%) K_2CO_3 additive added to Weald clay

Additive	Event 1		Event 2		Event 3		Event 4		Total weight loss (%)
	Temperature (°C)	Weight loss (%)	Temperature (°C)	Weight loss (%)	Temperature (°C)	Weight loss (%)	Temperature (°C)	Weight loss (%)	
K1	35-200	0.33	200-600	3.61	800-1000	0.20	-	-	4.88
K2		0.79		3.67	700-900	0.69	900-1100	0.36	6.27
K3		1.03		4.46		0.90	900-1100	0.39	7.79
K4		0.83		4.30		1.20	900-1100	0.36	7.85
Inference	Dehydration		Hydroxyl release/ Carbonate decomposition		Carbonate decomposition		-		

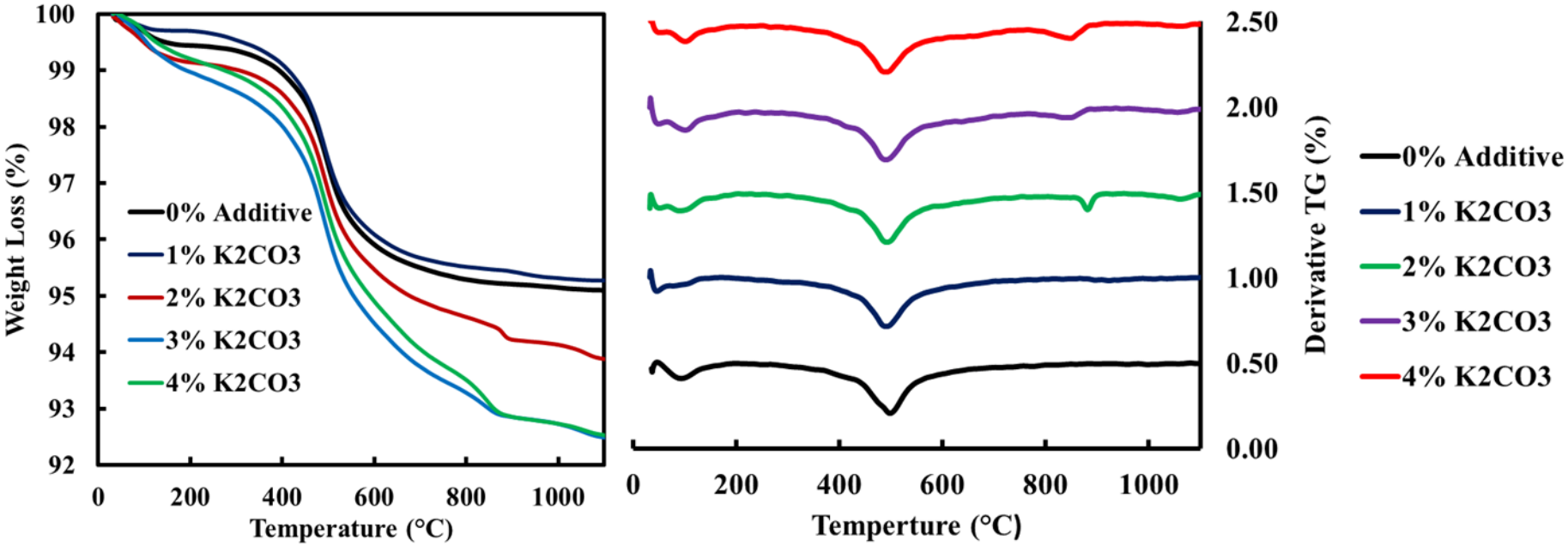

Figure 5-35: TGA and DTG of 1-4wt% K_2CO_3 in Weald clay fired from 35°C -1100°C at 10°C / min in an alumina crucible.

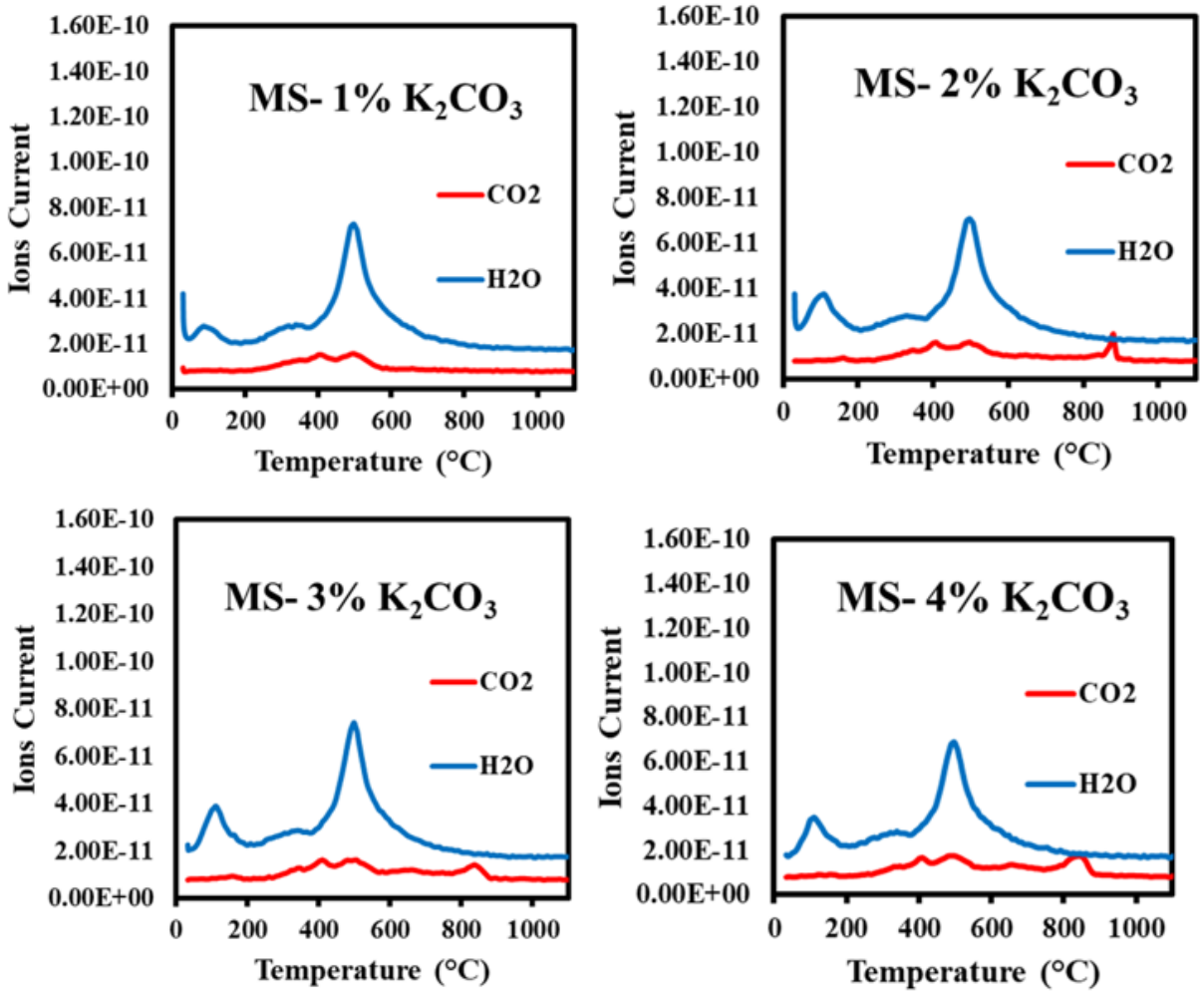

Figure 5-36: Mass spectroscopy of 1-4wt% K_2CO_3 in Weald clay fired from 35°C -1100°C at 10°C / min in an alumina crucible

5.7.2 *Dimensional changes in heating for K_2CO_3 body compositions*

Potassium additive from the dilatometry curve **Figure 5-37** indicates two expansions. One from the (i) conversion of alpha quartz to beta quartz and (ii) breakdown of additive to expel CO_2. After the transition temperature, it begins to plateau. However, it expands from 1% to 1.2% due to additive increase and further decomposition at temperatures above 800°C just before the final shrinkage. This effect was found to be different from the control and 1wt % K_2CO_3.

Table 5-11: linear shrinkage of 1-4wt% K_2CO_3 additive

Sample ID	B-Quartz (°C)	Shrinkage temperature reduction (°C)	Expansion (%)	Linear shrinkage (%)
Weald clay (W0)	581	0	1	2.3
K1	578	5	1	2.3
K2	582	4	1.2	2.0
K3	581	4	1.2	2.0
K4	582	0	1.2	2.0

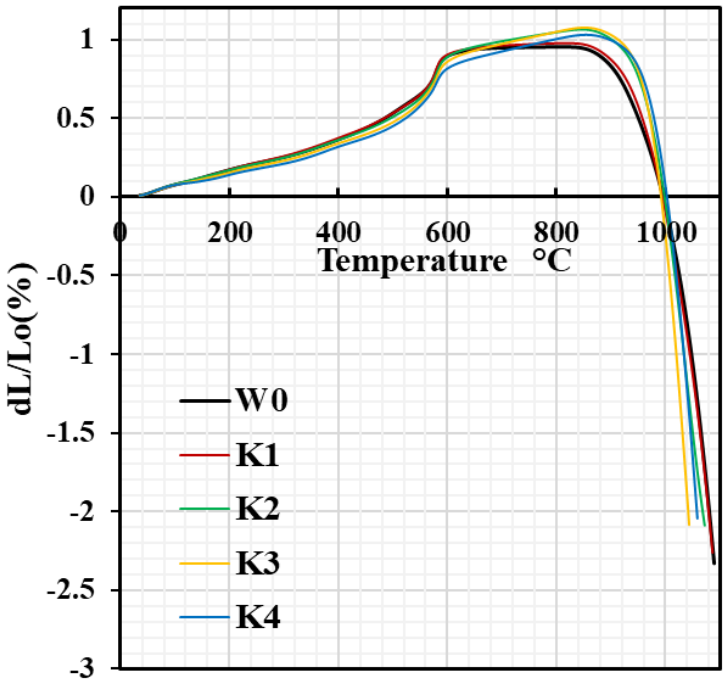

Figure 5-37: Linear shrinkage of 1-4wt% replacement of K_2CO_3 in Weald clay fired to 1040°C at 5°C/ min.

5.7.3 *Potassium carbonate effect on ceramic pore size*

Potassium carbonate-contained samples replaced with 1-4wt% show a unimodal pore. PSD shifts from 0.9 µm (for 900°C) to 0.4 µm (1040°C). It is interesting to point out the effect of additive with its level on fired clay pore sizes compared to the 0% additive and the shifts to macro-pore due to additive increase. Overall, the additive level increase favoured the production of a lower intrudable Hg porosity at all temperatures compared to the control.

Clay samples fired to 900 ºC with 1-4wt% additive level obtained 20.61%-19.66% Hg porosity for K1 and K4, respectively. Further reduction in porosity was recorded for samples fired to 1000°C and 1040°C. However, the least porosity was found to be K4(12.44%) fired to 1040°C. **Figures 5-38 to 40** show the PSD curve and porosity.

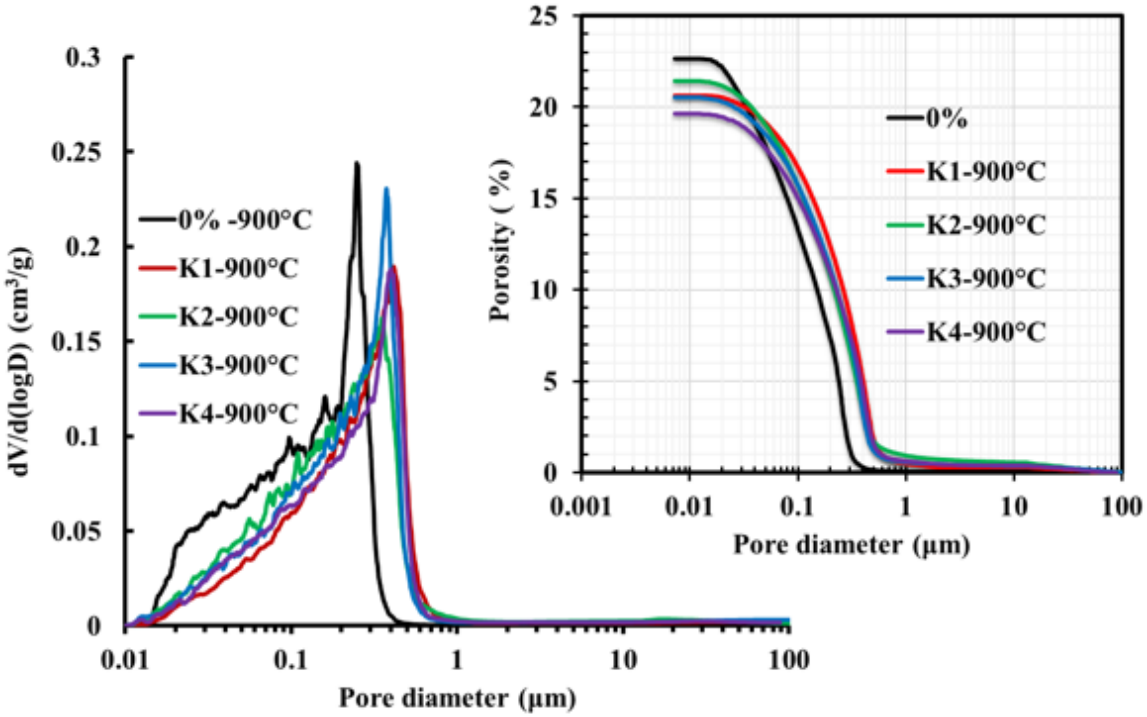

Figure 5-38: Pore size distribution curves and porosity% for 0% Weald clay compared to 1-4wt% K_2CO_3 fired to 900°C

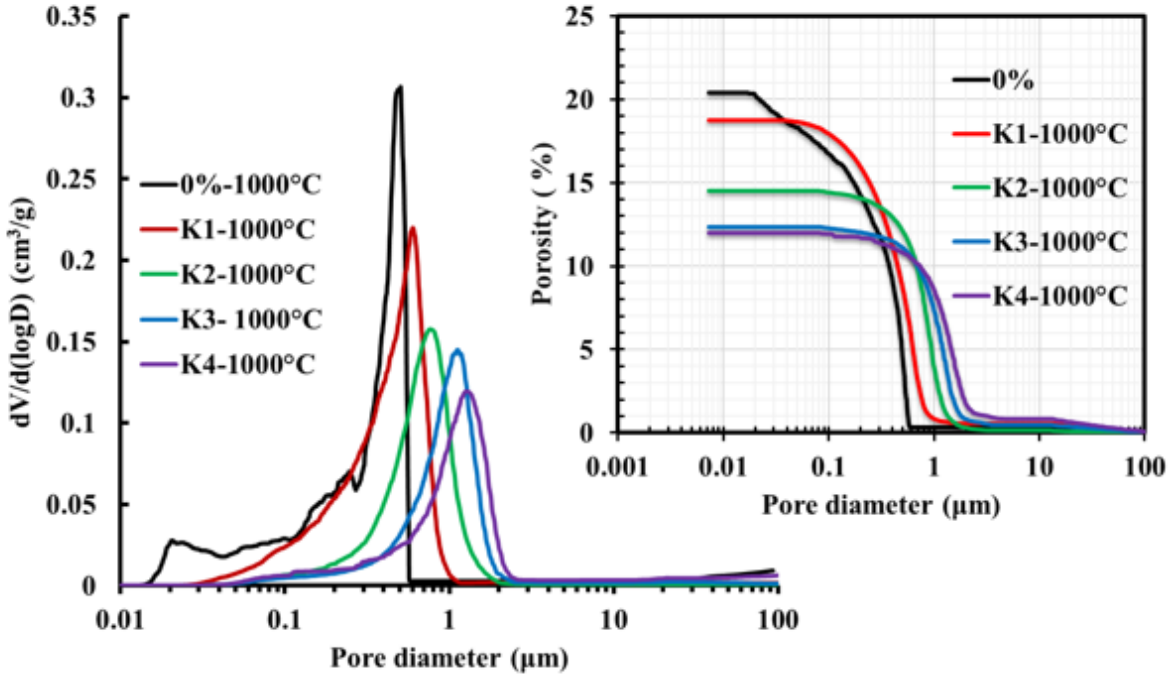

Figure 5-39: Pore size distribution curves and porosity% for 0% Weald clay compared to 1-4wt% K_2CO_3 fired to 1000°C.

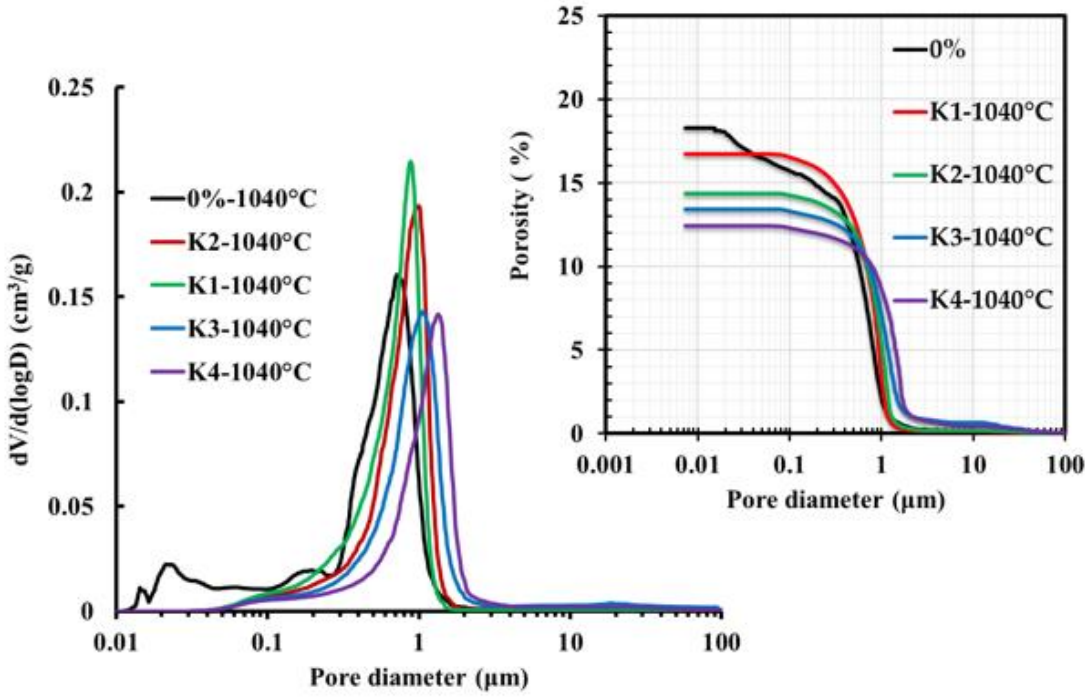

Figure 5-40: Pore size distribution curves and porosity% for 0% Weald clay compared to 1-4wt% K_2CO_3 fired at 1040°C.

5.8 Na_2CO_3 additive replacement phases

Phases obtained with samples fired to 900°C (**Figure 5-41)** are the same as the control specimens. The phases are quartz (SiO_2 - 01-087-2096), hematite (Fe_2O_3 - 04-005-4630) and dehydrated muscovite ($KAl_3Si_3O_{11}$ - 00-046-0741). Samples fired to 1040°C reveal that N1 was the same pattern as the control fired to 1040°C, albeit with a slight hump attached to the quartz peak at 50°. Unknown new peaks at 33°, 42.98°-44.6° were observed in N2 and N4 samples but not in N1 or the control. The mullite phase at 16° obtained with samples containing 2wt% and 4wt% were weak compared to the N1 and the control. Hematite intensity is temperature and additive-level dependent (**Figure 5-42**).

The common phases observed with samples fired to 1040°C are quartz- (SiO_2- 01-087-2096), mullite ($Al_{2.26}Si_{0.74}O_{4.87}$ -04-016-1586), hematite (Fe_2O_3 -04-005-4630 and microcline ($KAlSi_3O_8$ 01-084-0709).

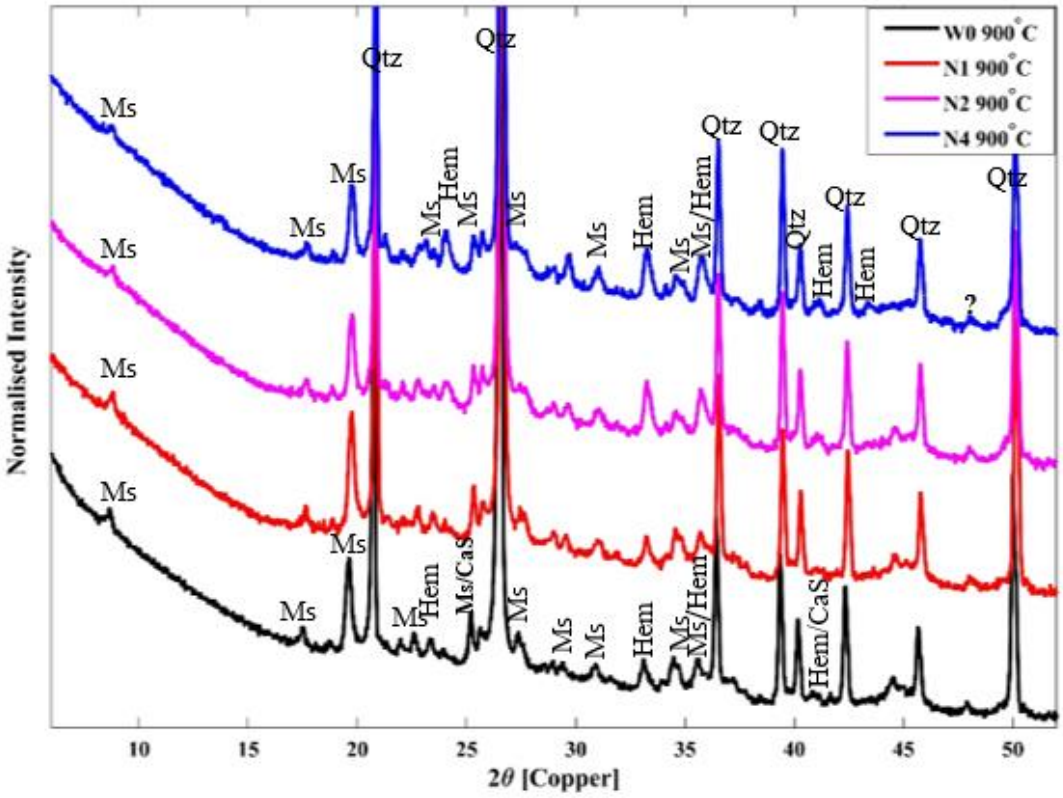

Figure 5-41: Crystalline phases developed in weald clay with 1,2 and 4w% replacement of Na_2CO_3 fired to 900°C.

Symbols after Kretz 1983[343] where Qtz=quartz; Ms = Muscovite/ dehydrated muscovite; Hem= hematite; CaS-calcium sulphate and Ms- dehydrated Muscovite.

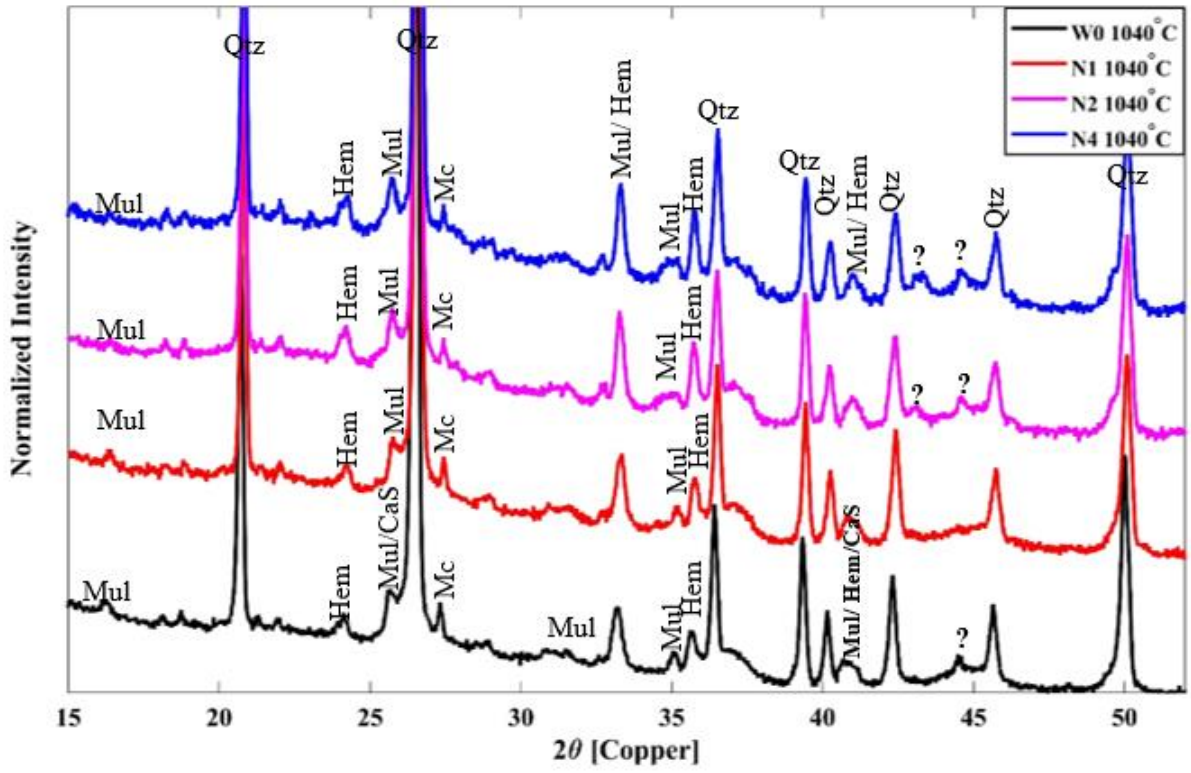

Figure 5-42: Crystalline phases developed in weald clay with 1, 2 & 4w% replacement of Na_2CO_3 fired to 1040°C.

Symbols after Kretz 1983[343] where Qtz=quartz, Hem= hematite, Hem= hematite, CaS-calcium sulphate and Mul- mullite and Mc- microcline

5.8.1 *Na_2CO_3 additive heating behaviour on Weald clay*

This heating behaviour of Na_2CO_3 can be compared to $CaCO_3$, where the breakdown of the Na_2CO_3 occurs at temperatures >600°C-820°C following the dehydroxylation of clay minerals (exothermic reaction) and physical water (endothermic reaction). See **Figure 5-43** to **44**. There is no evidence of melting from the DTA curve shown in **Appendix 1**. The influence of additive level on the overall mass is shown in **Table 5-12**.

Table 5-12: Summary thermal behaviour of 1-4 mass (%) Na_2CO_3 additive in Weald clay

Additive	Event 1		Event 2		Event 3		Total weight loss (%)
	Temperature (°C)	Weight loss (%)	Temperature (°C)	Weight loss (%)	Temperature (°C)	Weight loss (%)	
N1	35-200	1.10	200-600	3.33	600-900	-	5.41
N2		1.11		3.63		1.64	6.62
N3		1.17		4.05		2.34	7.96
N4		1.05		3.95		2.85	8.17
Inference	Dehydration		Hydroxyl release/ Carbonate decomposition		Carbonate decomposition		

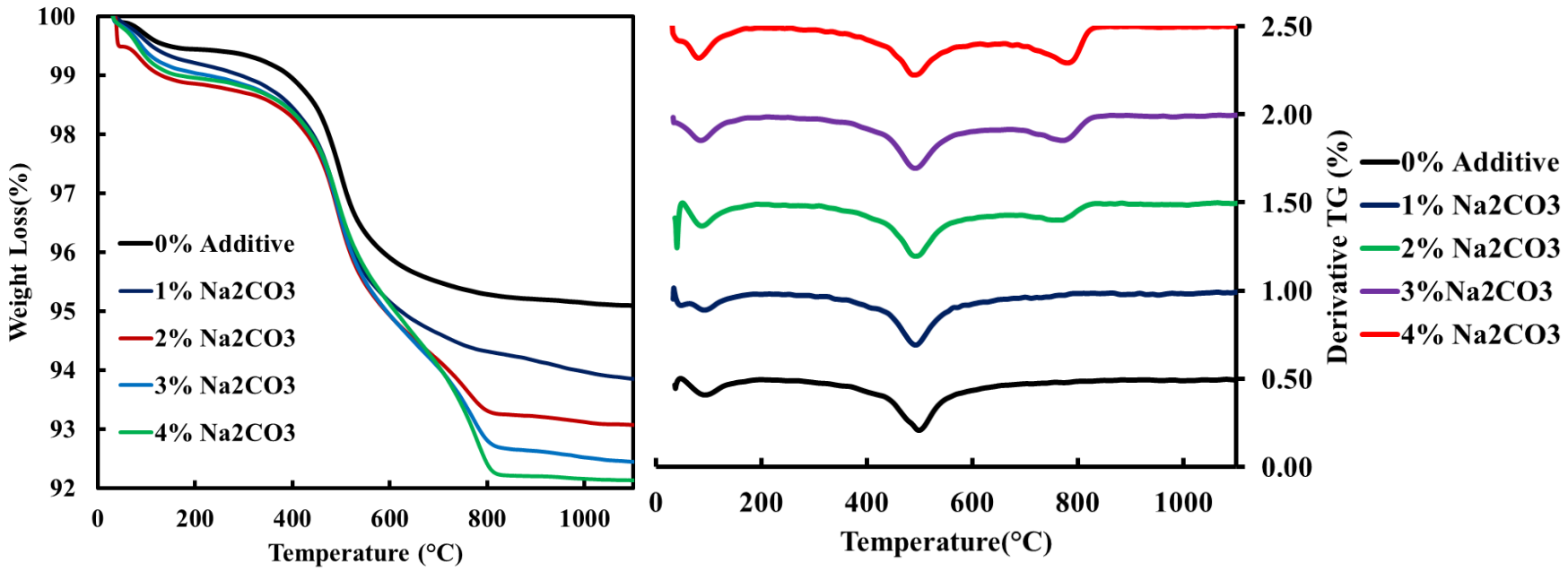

Figure 5-43: TGA and DTG of 1-4wt% Na_2CO_3 in Weald clay fired from 35°C -1400°C at 10°C/min in an alumina crucible

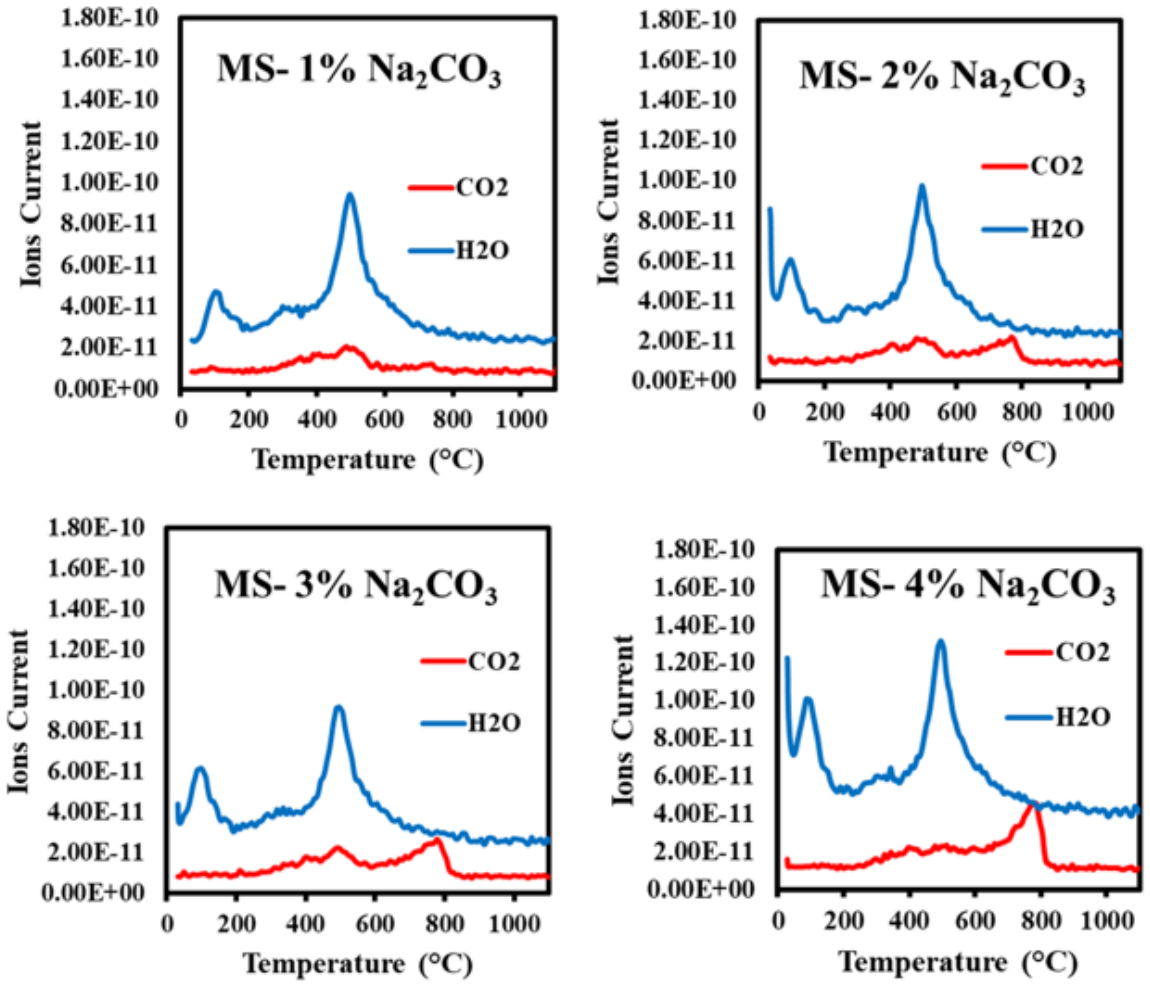

Figure 5-44: Mass spectroscopy of 1-4wt% Na_2CO_3 in Weald clay fired from 35°C -1100°C at 10°C/min in alumina crucible.

5.8.2 *Dimensional changes on heating for $NaCO_3$ body compositions*

Sodium carbonate's linear shrinkage increased from 2.3% to 2.9% as the levels increased with highly reduced shrinkage temperature greater than $CaCO_3$, $MgCO_3$ and $BaCO_3$ and even 100% clay due to the additive's melt. This is summarised in **Table 5-13 and Figure 5-45**. Moreover, as observed with Mg, Ba and Ca doped samples, the linear expansion of samples containing 2-4wt% was in the 1-1.2% expansion range. The differences in these additives are the linear expansion and the amount of shrinkage /contraction on heating. Linear and quartz inversion temperatures for Na_2CO_3 samples decrease with additive level.

Table 5-13: linear shrinkage of 1-4wt% Na_2CO_3 additive

Sample ID	B-Quartz (°C)	Shrinkage temperature reduction (°C)	Expansion (%)	Linear shrinkage (%)
Weald clay (W0)	581	0	1.0	2.3
N1	583	17	0.9	2.2
N2	580	37	1.0	2.6
N3	580	37	1.1	2.7
N4	580	62	1.1	2.9

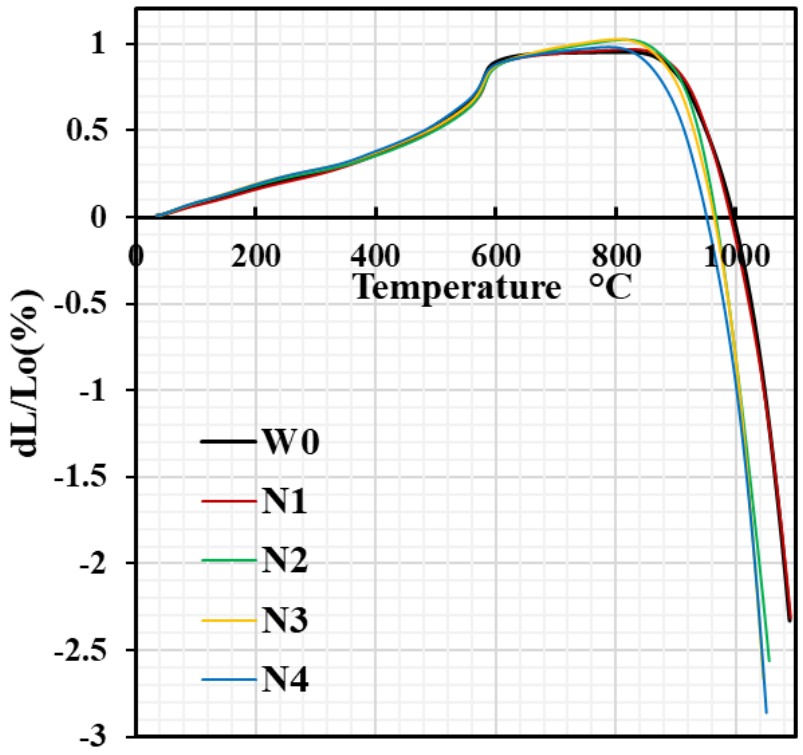

Figure 5-45: Linear shrinkage of 1-4wt% replacement of Na_2CO_3 in Weald clay fired to 1040°C at 5°C/ min.

5.8.3 *Sodium carbonate effect on ceramic pore size*

As with the previously reported, Na_2CO_3 caused pore diameter to shift by temperature and additive level, with 4wt% samples showing a move toward larger pore size (10μm).

The Na-containing additive shows the least porosity % across all the additives reported in the temperature range (900-1040°C). Correlating with the observation that 2-4wt% had a glassy coating on the surface but not the inner section, which the Hg penetrated. Samples fired to 900°C, Hg absorption rose to 18.79%,20.08%,19.05%, and 19.28% for 1-4wt%, respectively (Figure 5-46 to 48**).** However, by 1040°C, porosity had decreased to 10.69, 8.86% and 8.68% for 1-4wt%, respectively.

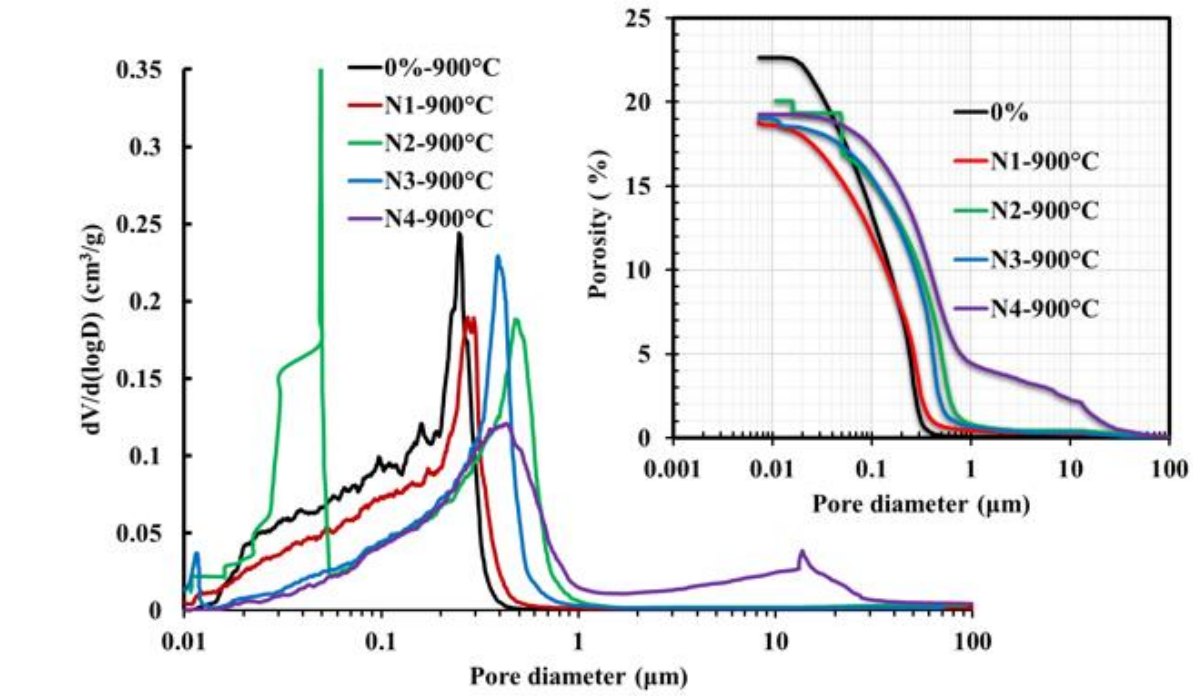

.

Figure 5-46: Pore size distribution curves and porosity% for 0% Weald clay compared to 1-4wt% Na_2CO_3 fired at 900°C

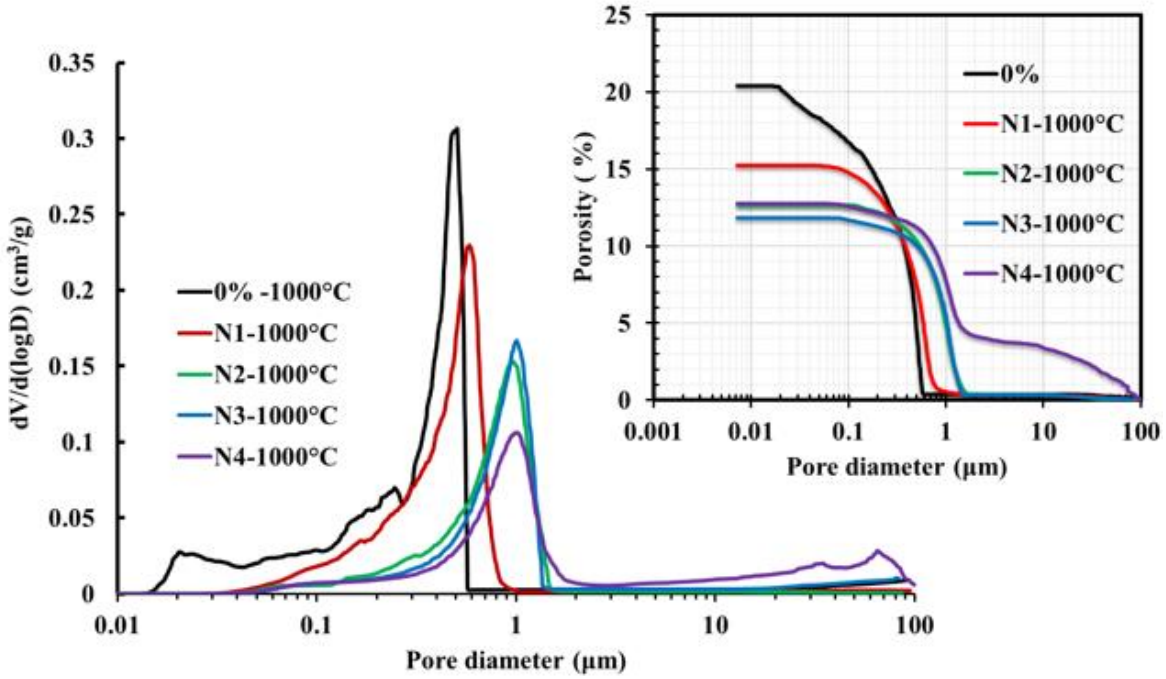

Figure 5-47: Pore size distribution curves for 0% Weald clay compared to 1-4wt% Na_2CO_3 fired at 1000°C

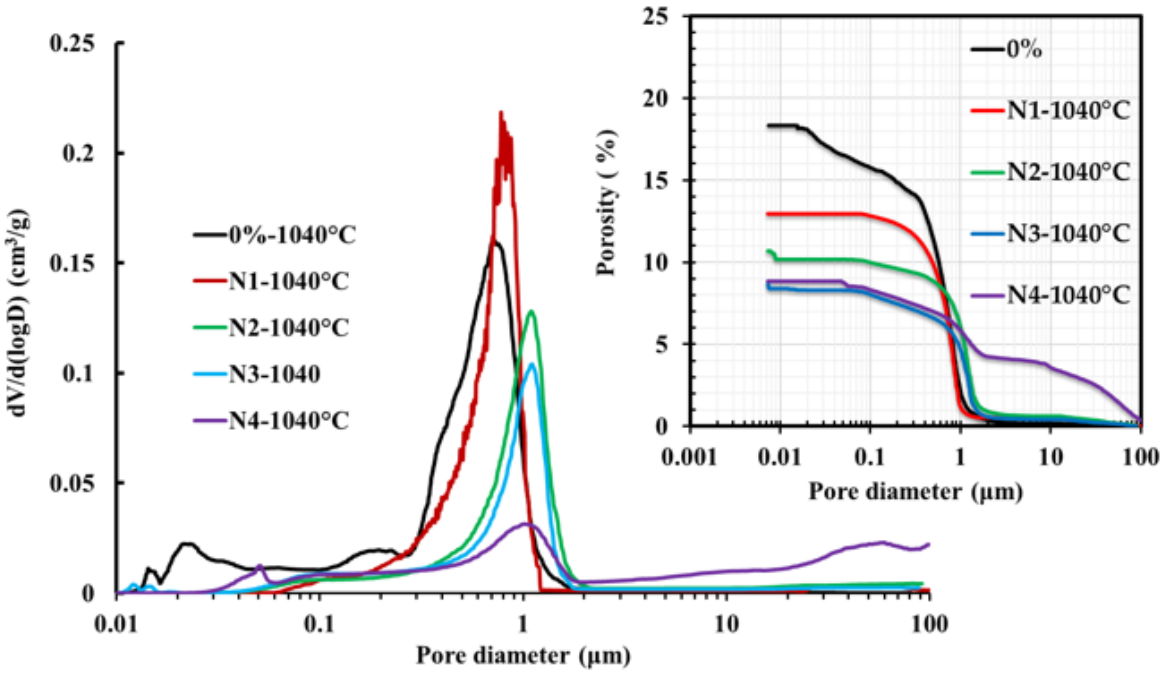

Figure 5-48*:* Pore size distribution curves and porosity% for 0% Weald clay compared to 1-4wt% Na_2CO_3 fired at 1040°C

5.9 Predicting alkaline and alkali admixtures' durability using the Maage equation

Body compositions containing 1-4wt% alkaline earth additives (Ca, Ba and Mg) fired to 900°C and 1040°C were not frost resistant because values did not exceed the uncertainty limit (55-70). Only 2wt% $BaCO_3$ fired to 1040°C was found to be durable value ~76. For alkali-containing ceramics (Li, K and Na), fired to 900°C and 1040°C, only 4wt% Li_2CO_3, 2wt% Na_2CO_3, 3wt% Na_2CO_3 and 4wt% Na_2CO_3 samples were fired to 1040°C were accessed as durable with >80 values. Meanwhile, 3wt% K_2CO_3, 4wt% K_2CO_3 and 1wt% Na_2CO_3 samples were of uncertain durability, with the remaining 16 samples, mostly the low-fired ceramics, being non-durable. (see **Appendix 3**)

5.10 Summary of the thermal behaviour of series 1 additives

In summary, the TGA results show that:

- Li_2CO_3 records the highest weight loss with the decomposition temperature below 800°C, whereas K_2CO_3 breakdown occurs at temperatures between 800-920°C.
- $MgCO_3$ decomposes at the same temperature as the Weald clay. Moreover, the overall weight loss for all levels is slightly greater than that of $BaCO_3$ and $CaCO_3$, which break down after 600°C.
- Na_2CO_3 and K_2CO_3 are very much alike in heating effect, with carbonate compound decomposing between 600°C and 820°C.
- Physical water, chemical water, and the decomposition of carbonates from clay and additives were identified as the cause of weight loss.
- The DTA shown in Appendix 1 does not indicate sudden melting behaviour. The Dilatometry on the additives also shows no sudden melting. With such low dopant levels, the formation of liquid phases (i.e., melting) is not separable from the shrinkage effects that occur over a wide temperature range.

5.10.1 *Summary of dilatometric effect on series 1 additives*

The following trends and differences are a summary of the series 1 additive. Note that the programme was set to stop measurement at 3% shrinkage to stop unnecessary melts, which could damage the instrument.

1. The alkaline earth additives seem to control excessive expansion caused by the decomposition of the additive carbonate and promote a reduction in the sintering temperature of between 4- 41°C calculated from where the curve crosses 0 at dL/Lo.

2. The alkali additives containing ~>2wt% cause the body to expand again after the quartz transition temperature. Reduced shrinkage for 1wt% Li_2CO_3 is 22°C, but negative values are recorded above this additive level (3wt% and 4wt% Li_2CO_3). Samples containing Na_2CO_3 reduced sintering temperature between 17-63°C due to the melt produced. K_2CO_3 recorded the least reduced shrinkage temperature (4-5°C).

5.11 Volumetric fired Shrinkage(VS)

Figure 5-49 (a-f) shows the volumetric Shrinkage of mixed compositions**.** Differences in shrinkage were affected by body composition, temperature, and mineralogy. Overall, lower firing, irrespective of additive and its levels, produced lower levels of Volumetric shrinkage.

The lowest volumetric shrinkages recorded were with samples containing 3, and 4wt% $CaCO_3$ fired to 850°C and 900°C. Shrinkages marked 2% and 3% compared to the clay sample, replaced with 2wt% and the control.

Increased additive levels for samples fired at 1040°C resulted in lower shrinkages, with 3wt% and 4wt% $CaCO_3$ marked 9% and 6% volumetric shrinkages. 1wt% caused the highest shrinkage of 22%, and at 2wt% was halved.

The $MgCO_3$ sample's volumetric shrinkage (VS) increased with additive level increase and temperature. For example, 4wt% recorded the highest shrinkage percentage (11%) compared to the 9.8% shrinkage obtained for the control. At lower temperatures of 850° and 900°C, only 2 and 3% shrinkages were recorded for 1-3wt% additive levels, but 4wt% levels fired at the same temperature shrunk to 3% for samples fired to 900°C and 2% for 850°C ceramics samples.

$BaCO_3$, on the other hand, saw a reduction in volumetric shrinkage with 2 and 3 additive levels fired to 1040°C, obtaining 6 and 7% VS, while the highest obtained shrinkage of 10% was

recorded for 1% and 4wt% levels. Shrinkage for lower firing resulted in 2 or 3% only for samples fired to 850°C and 900°C.

Again, additive level and temperature were the determining factors for the alkali additives obtained for high or low shrinkages. Just as in the Mg samples, the Na-based additive's volumetric shrinkages were found to increase on additive dosages and the degree of firing. Shrinkages (%) increased from 9% to 17% for 1-4wt% dosage of Na_2CO_3. The decline in temperature to 1000°C was recorded at 6% for 1wt% additive level to less than 1% for samples fired to 850°C. Whilst samples containing dosage levels greater than 2wt% fired at 900°C attained only 3% and 4% shrinkages. However, samples fired at 850°C obtained 3% shrinkage.

The shrinkage for K_2CO_3 declined to 2% at all additive levels for samples fired to 850°C and shrunk to 3% with samples fired to 900°C. By the time temperature rises to 1040°C with samples containing 1wt% dosage, 10% shrinkage has been achieved. As the additive level increases to 4wt%, a 15% degree of shrinkage has been attained for the sample fired to 1040°C. 1-2wt% additive samples shrunk to 10 and 12% only.

Overall, volumetric shrinkage % was dependent on both temperature and additive level. The highest shrinkage observed for lithium-based samples was with a 1wt% additive level at 11% for samples fired to 1040°C. As the additive level increased, the shrinkage percentages dropped to 5%,3% and 1.4% for 2-4wt% additive dosage, respectively, when the clay body was fired to the top temperature (1040°C). However, samples fired below 1000°C decreased to 3% for L1. However, a rise in additive levels brought about further reductions of 2% and 1% shrinkages for L2-L4 clay samples fired to 900°C whilst 850°C samples shrunk to 1% except for L4, which recorded less than 1% shrinkage.

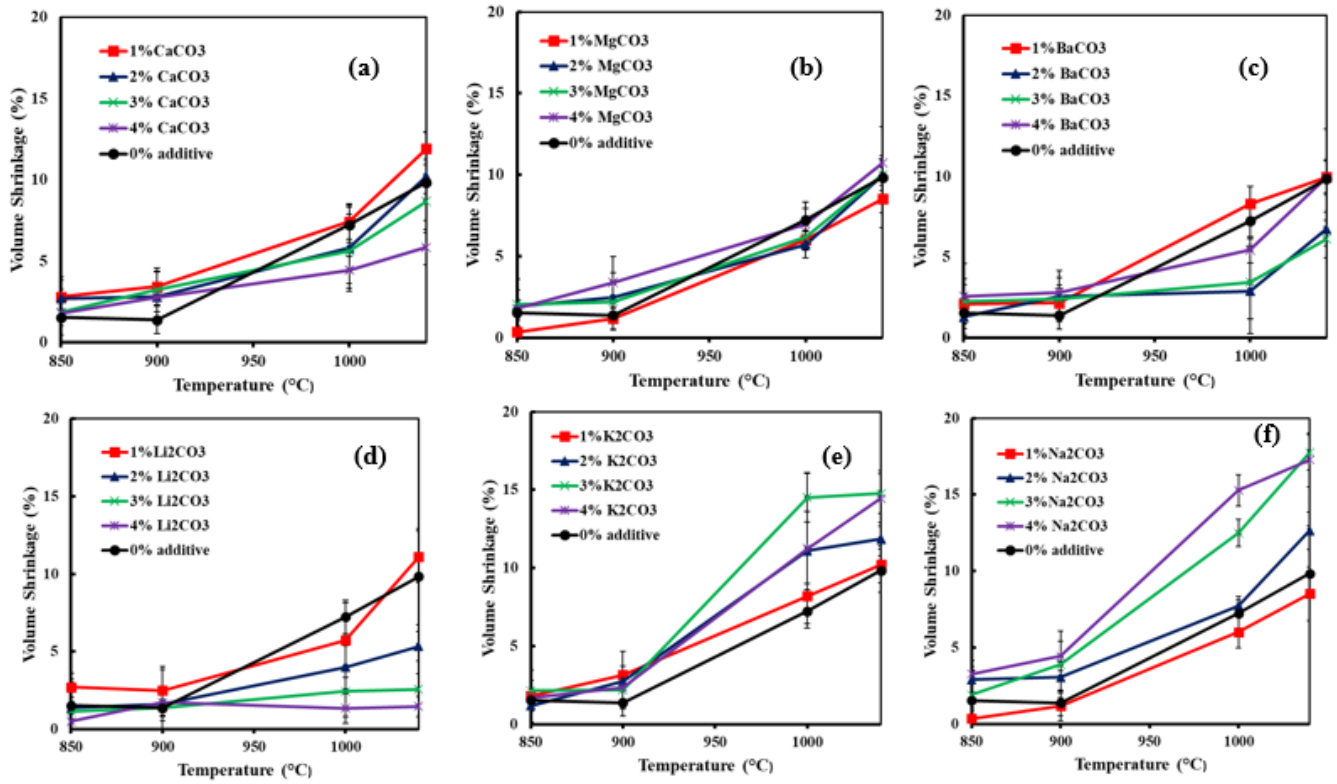

Figure 5-49: Volume metric shrinkage result of alkaline earth carbonates (a-c) and alkali carbonates labelled (d-f) replaced with Weald clay fired to 850°C, 900°C, 1000°C and 1040°C at 1-4wt% additive levels.

5.12 Boiling water absorption test (BWA)

Generally, the drivers that affect the absorption rate of ceramic are the material composition, compaction or shaping method and degree of firing, which affect shrinkage.

Samples fired to 850°C and 900°C recorded the highest BWA of 14% for 1-4wt% $CaCO_3$. In clay mixtures fired to 1000°C, BWA% decreases to 11-13%, with 4wt% levels recording 13%. Moreover, clay bodies fired to 1040°C saw a further reduction. 9%-12% is recorded for 1wt% -4wt% additive fired to 1040°C **(Figure 5-50 (a)).** An interesting trend was seen with $CaCO_3$ substitution to Weald clay is that BWA % increases with a temperature reduction as levels increase.

$MgCO_3$-containing samples follow a similar trend. Samples fired to 850°C and 900°C recorded the highest BWA%, but the additive level also predominantly influenced the water uptake. So, the absorption rate increased from 13% (1wt%) - 17% (4wt%). At 1040°C, the additive level still affected the absorption rate. From the chart, as shown in **Figure 5-50 (b),** 1wt % $MgCO_3$ (M1) fired to 1040°C,1000°C, 900°C, and 850°C had the lowest recording of approximately 10%, 11% and 13%, respectively. It is immediately clear from the $MgCO_3$ fired pieces that the level of additive impact on the ceramic body's porous nature because of its high BWA % irrespective of the temperature, as seen with clay body containing 2-4wt% additive levels.

For $BaCO_3$, 1wt% recorded 14% for both 850°C and 900°C. 15% was recorded for a 3wt% additive increase, and 2wt% samples were fired to 850°C. Samples fired to 1000°C saw a dip in absorption %, particularly with 1wt% samples obtained 13%. However, as the levels reached 2wt% and 3wt%, BWA % rose to 14%. A significant decrease in absorption is obtained with samples fired at 1040°C. 1-4wt % levels, records 11%,12%, 13% and 9% respectively. Another significant observation seen with the $BaCO_3$ trend is the reverse in BWA % for replacing 4wt% $BaCO_3$ (B4) in weald clay, making 4wt% levels the least porosity body among the Ba-set compared to the 1-3wt% additive of the same body mix fired to 850°C-1040°C. **(Figure 5-50 (c)).**

A reverse trend in alkali additives, particularly Na_2CO_3 and K_2CO_3, has been achieved. Higher additive levels (between 2-4wt%) and elevated temperature produces a decline in BWA %. Samples containing 1-4wt% Na_2CO_3 fired to 850°C obtained >12-14% body, but 900°C recorded >12-13%, the lowest BWA% compared to the alkaline earth.

Unlike $MgCO_3$ doped samples, an increase in additive level and elevated temperature improve the permeability of the ceramic. Higher levels of Na_2CO_3 are advantageous for boiling water absorption due to the glassy coating on the clay body. 3 and 4wt% levels of Na_2CO_3 additive to Weald clay fired to 1040°C records the lowest BWA% in this series (5%) compared to 9%

for the control, $MgCO_3$ (11 & 13%), Ca-based (11& 12%) and Ba-additives (9 & 13%) **(Figure 5-50 (d)).**

13% and 14% are recorded for the K_2CO_3 body fired to 850°C and 900°C, respectively, higher than the control, shown in **Figure 5-50 (e).** 3wt% and 4wt% additive levels were beneficial at increased temperatures (1040°C and 1000°C), resulting in a reduced permeable body of 8% for 3wt% levels. 4wt% of the additive fired to 1000°C and 1040°C significantly reduced BWA with 8% and 7%, respectively. Meanwhile, 1wt% K_2CO_3 fired to 1000°C recorded 12% BWA greater than the control (9%). The same values are obtained when samples are fired to lower temperatures (850°C and 900°C).

1-4wt% Li_2CO_3 additions recorded lower levels, 13 and 12% of BWA (%) for samples fired at 850°C and 900°C compared to the control. 1wt% Li_2CO_3 fired to 1040°C had the least BWA % of 6%, 2wt% samples recorded 8%, whiles 9% and 10% were recorded for 3wt% and 4wt% additive levels, respectively. This means there is a BWA increase as dosage levels increase even with temperature **(Figure 5-50 (f)**

In summary, the additive flux (alkaline earth carbonates (a-c) introduces pores and increases water uptake of the body at all firing temperatures. The only exception to this phenomenon is with $BaCO_3$ doped at 4wt%, where we see a decrease in its water up-take (9%) just as the base material at 1040°C. There is a 2% increase with B1 and M2 fired to 1040°C compared to the 100% clay. This suggests a degree of vitrification given by the additive level and temperature. Higher levels of additive (2-4wt%) and degree of firing (1040°C) increase pores within the body as shown with $MgCO_3$ and $CaCO_3$ doped; however,1wt.% replacement records 9% BWA when fired to 1040°C. The result also shows that temperatures below 1040°C have more open pores, providing channels for water absorption into the brick matrix.

For Alkali oxides labelled **Figures 5-50 (d-e),** higher levels of additives 3-4wt % obtained the least water uptake for Na_2CO_3 and K_2CO_3 for samples fired to 1040°C compared to the control. Li_2CO_3 additions show a different trend: above 2wt %, the porosity rate increases with this sample across the four different temperature ranges. Only 1wt% Li_2CO_3 records the least absorption rate of 6%. While Li_2CO_3 samples are very promising, their cost may not be ideal for the building industry, although only 1wt% proves suitable for a class B engineering brick with a water absorption rate limit. Note that the samples used (pellets) are not the standard brick sizes.

Overall, the results for shrinkage correspond to the boiling water absorption percentages. Higher shrinkages recorded lower WA (%), while lower shrinkages encouraged higher WA rates in ceramic bodies.

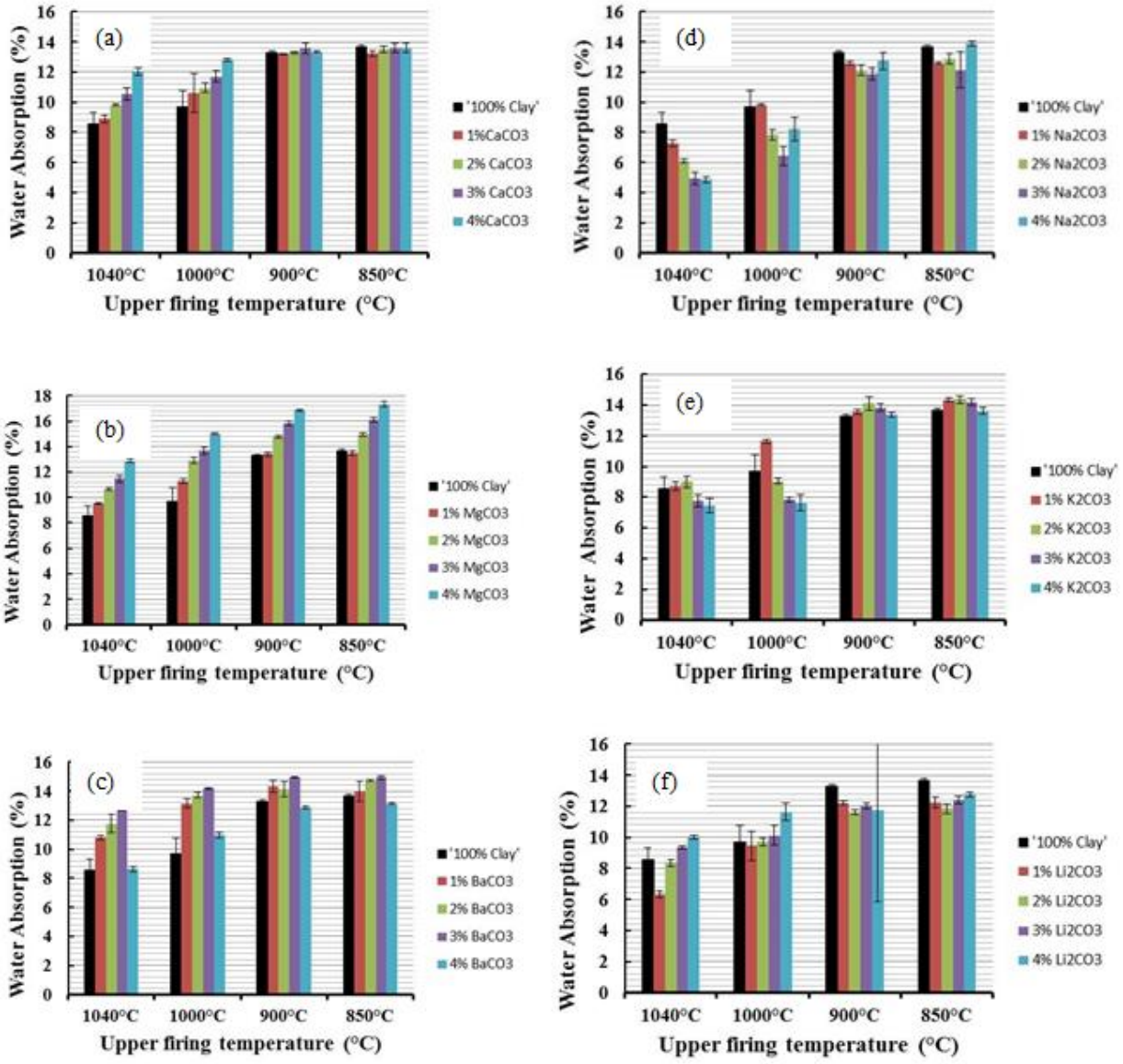

Figure 5-50: Boiling water absorption test for replacing 1-4wt% alkaline earth (a-c) and alkali oxides (d-f) fired to 850°C, 900°C, 1000°C and 1040°C

5.13 Images of additive effects on Series 1 body compositions

The alkaline earth carbonate $CaCO_3$ was found to promote scum on the fired surface **(Figure 5-51),** while $BaCO_3$ **(Figure 5-53)** and greater than 2wt% $MgCO_3$ **(Figure 5-52)** additives

inhibited the formation of scum on the fired sample surface. 1-4wt% of $CaCO_3$ fired at 850°C developed less fired scum on the clay mix surface.

For the alkali oxides replacement, 1wt% Li_2CO_3 and 1wt% Na_2CO_3 **(Figures 5-54 & 56)** also stopped the occurrence of the scum after firing. Li_2CO_3 replacement of >2wt % fired at 1040°C had darker spots on the surface, which showed as white specs at lower temperatures across the additive levels. For the Na_2CO_3 additive, there was a discolouration on the sample rim (a darker hue) for 1% Na_2CO_3. Moreover, 2-4wt% Na_2CO_3 after firing, the surface had a glassy coating at higher temperatures (1000°C and 1040°C), whilst 900°C and 850°C showed a matt, non-glossy surface (**Figure 5-56).**

Potassium carbonate (K_2CO_3) additive restrained the formation of scum deposits. However, it formed patches on the sample surface compared to the control on drying and firing (**Figure 5-55),** along with a darker rim similar to Na_2CO_3. The hue becomes lighter in the shade at lower temperatures (850°C -900°C). This shows that temperature influences how strong the colour obtained from firing ceramics can be. This stained spot may have formed from the retained sulphur in reaction with the solid and liquid phases.

In **Chapter 8**, **section 8.14** and **Figure 8-11**, admixtures coated with whitish stains have been examined and affirmed by Raman spectroscopy as $CaSO_4$ except for $BaCO_3$ and $MgCO_3$ admixtures, which stopped surface scum.

Figure 5-51: Comparison of fired images of baseline to 1-4wt% $CaCO_3$ additives fired to 850°C, 900°C, 1000°C and 1040°C

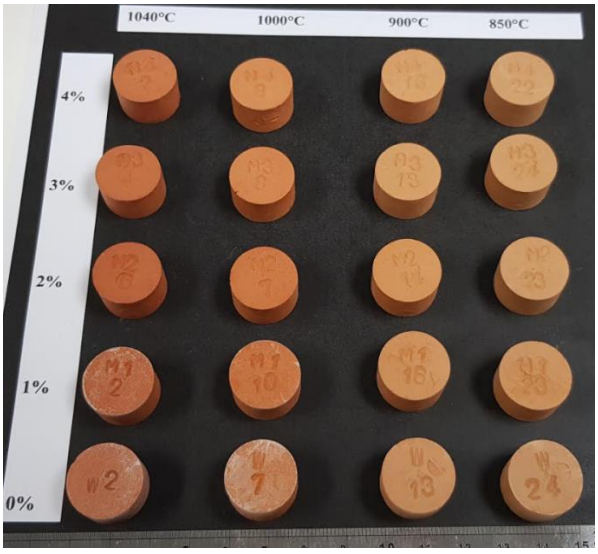

Figure 5-52: Comparison of fired images of baseline to 1-4wt% $MgCO_3$ additives fired to 850°C, 900°C,1000°C and 1040°C

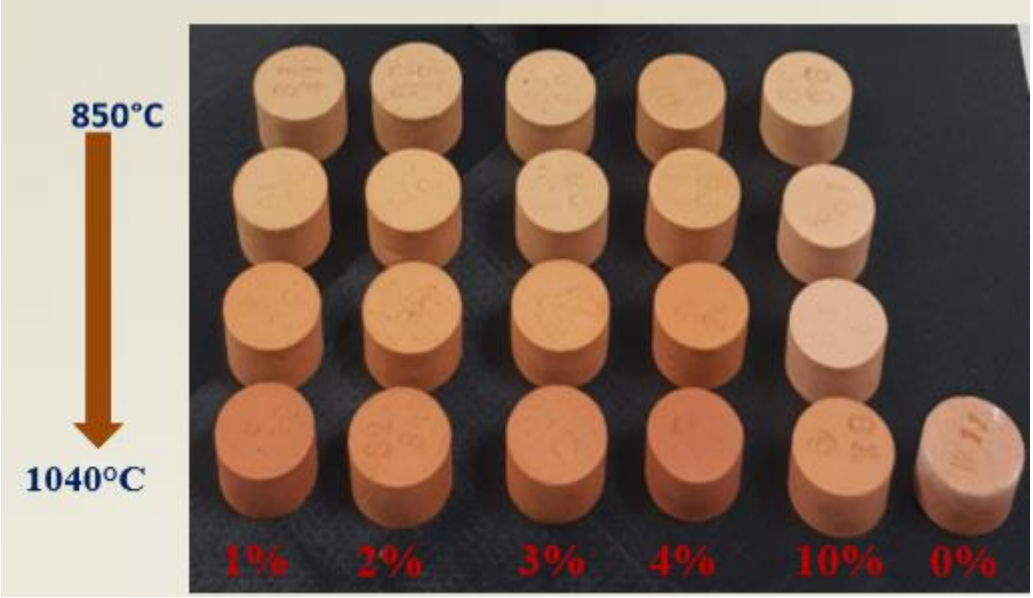

Figure 5-53: Comparison of fired images of baseline to 1-4wt% $BaCO_3$ additives fired to 850°C, 900°C,1000°C and 1040°C

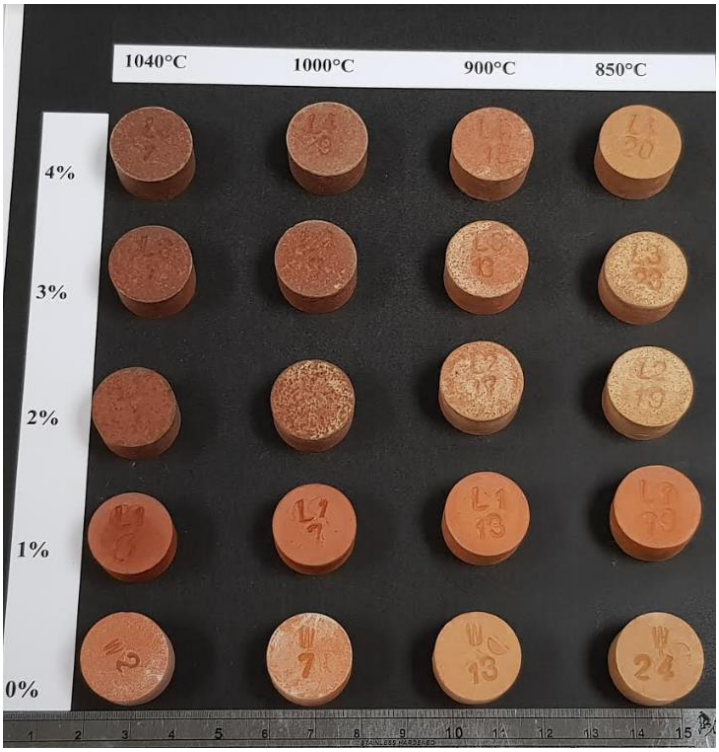

Figure 5-54: Comparison of baseline to Li_2CO_3 additives at different wt. (%) and temperatures

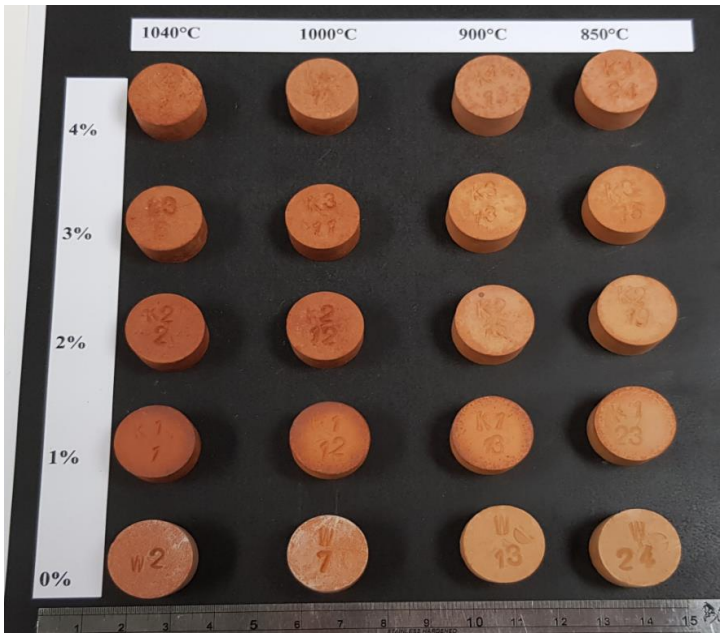

Figure 5-55: Comparison of fired images of baseline to 1-4wt% K_2CO_3 additives fired to 850°C, 900°C, 1000°C and 1040°C

Figure 5-56: Comparison of fired images of baseline to 1-4wt% Na_2CO_3 additives fired to 850°C, 900°C, 1000°C and 1040°C

5.14 Microstructural studies -SEM

5.14.1 *Microstructure of alkaline earth and alkali-containing additive ceramic bodies*

Micrographs obtained from this study clearly show the role of additive level and temperature influence on the morphology of fired specimens. The trends seen with $CaCO_3$ samples show that as the level of additive increases (1-4wt%) at lower temperatures (900°C) interparticle bond created is weak with large pores. However, samples fired to 1040°C were found to have greater bonding between particles. When confirmed with the EDs phases, mullite and other new crystalline phases have developed along with quartz. It was also found that higher additive levels promoted greater sintering to form a strong bond. See **Figures 5-57-66**.

$MgCO_3$-containing samples fired to 900^{o}C show many fine particles with no large quartz particles even with the additive increase. The quartz particles are not defined. >2wt% $MgCO_3$ samples fired to 1040^{o}C, larger quartz crystals develop, hematite (Fe_2CO_3) forms being visible in the sample due to the high sintered body see **Figure 5-69**. At 900°C, even the additive increase could not promote a compact structure. Similar micrographs were obtained for $BaCO_3$ where growth in quartz with additive increase and temperature **(Figures 5-67-73)**.

However, structures observed with the alkali additives were slightly different.

Li_2CO_3 samples fired to 900°C showed less sintering with bigger pores, whilst compositions fired to 1040^{o}C had fewer individual particles and smooth surfaces with defined porosity. There's better sintering with high dosage at higher temperatures. The fired structure was far more improved than the alkaline earth due to its improved sintering **(Figure 5-77 to 80)**.

As for Na_2CO_3 **(Figure 5-81 to 82),** only 1-2wt % was observed under the microscope because >3wt % by mass addition formed a thick, glassy coating on the surface shown in **section 5.13**. SEM images obtained with the sample containing 2wt% fired to 900°C showed greater particles

than 1wt%Na_2CO_3 fired at 900ºC. The samples fired to 1040°C had better sintering, especially the 2wt% dosage due to the sodium salt **(Figure 5-82).**

K_2CO_3 shows many quartz crystals compared to the previous alkali fired to 900ºC with little sintering and less visible quartz. By 1040ºC, quartz grains are visible with better sintering. The additive level and temperature played a significant role in the microstructural pattern. It was found that 4wt% samples fired at 1040°C exhibited the greater high-density surface characteristic with smaller pores than lower levels fired at the same temperature.

1-4wt% K_2CO_3 samples fired at 900°C did not encourage highly dense structure as found with samples fired at 1040°C **(Figure 5-83 to 85).**

This may mean that higher levels of additive only work effectively at temperatures greater than 1000°C to enable better sintering that promotes the bonding of loose particles enhancing compaction of the structure, which does not occur at lower firing temperatures (900°C or less).

C1-1040°C maps

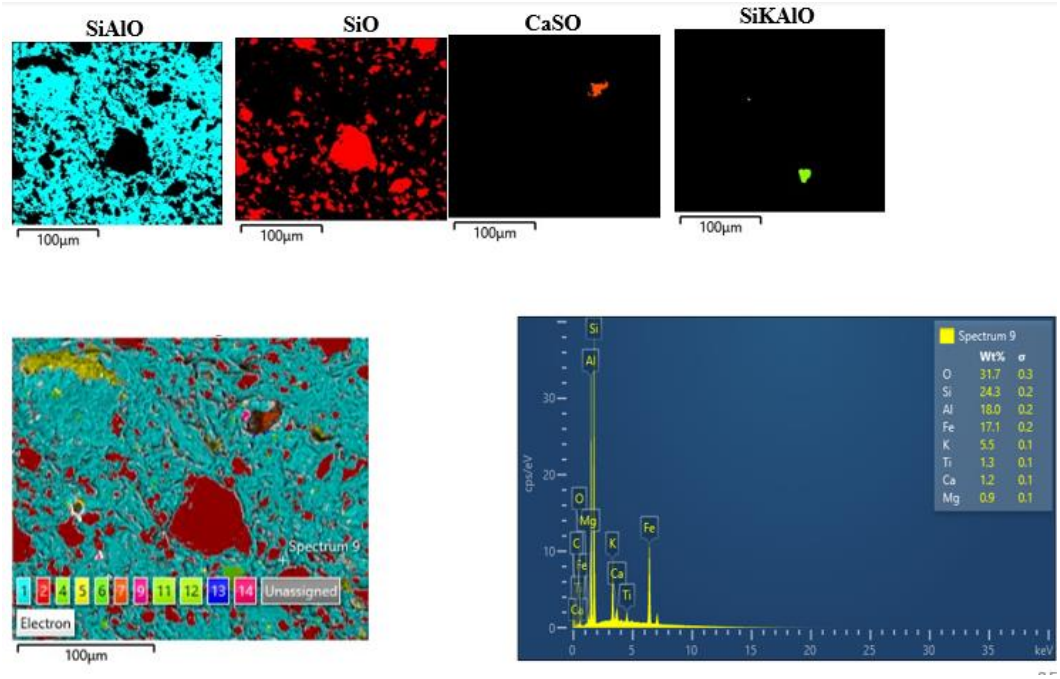

Figure 5-57: EDS mapped images with point analysis of 1wt% $CaCO_3$ replacement fired to 1040°C

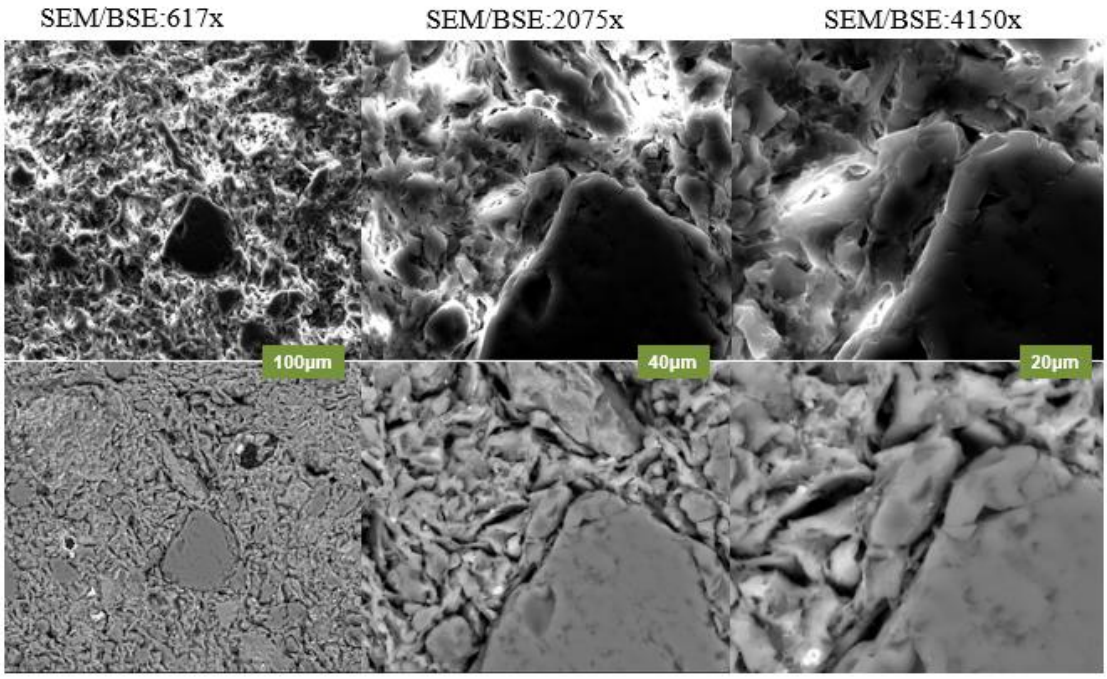

Figure 5-58: Secondary electron and Backscattered images of 1wt% $CaCO_3$ fired to 900°C.

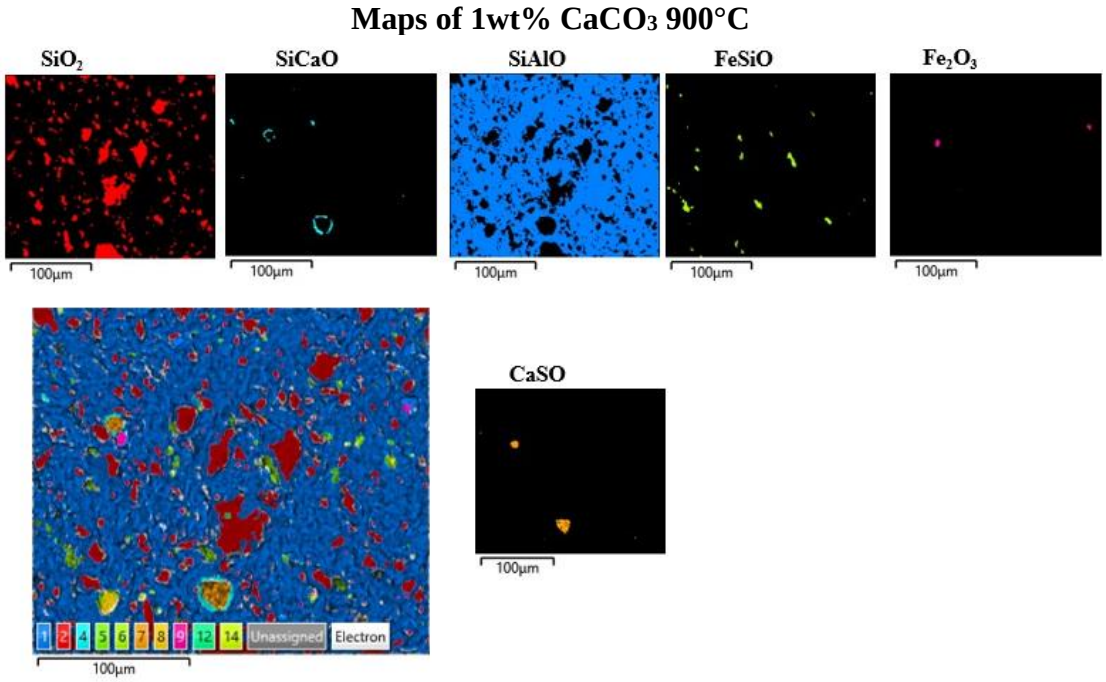

Figure 5-59: EDS mapped images with point analysis of 1wt% $CaCO_3$ replacement fired to 900°C

2wt% $CaCO_3$ at 1040°C

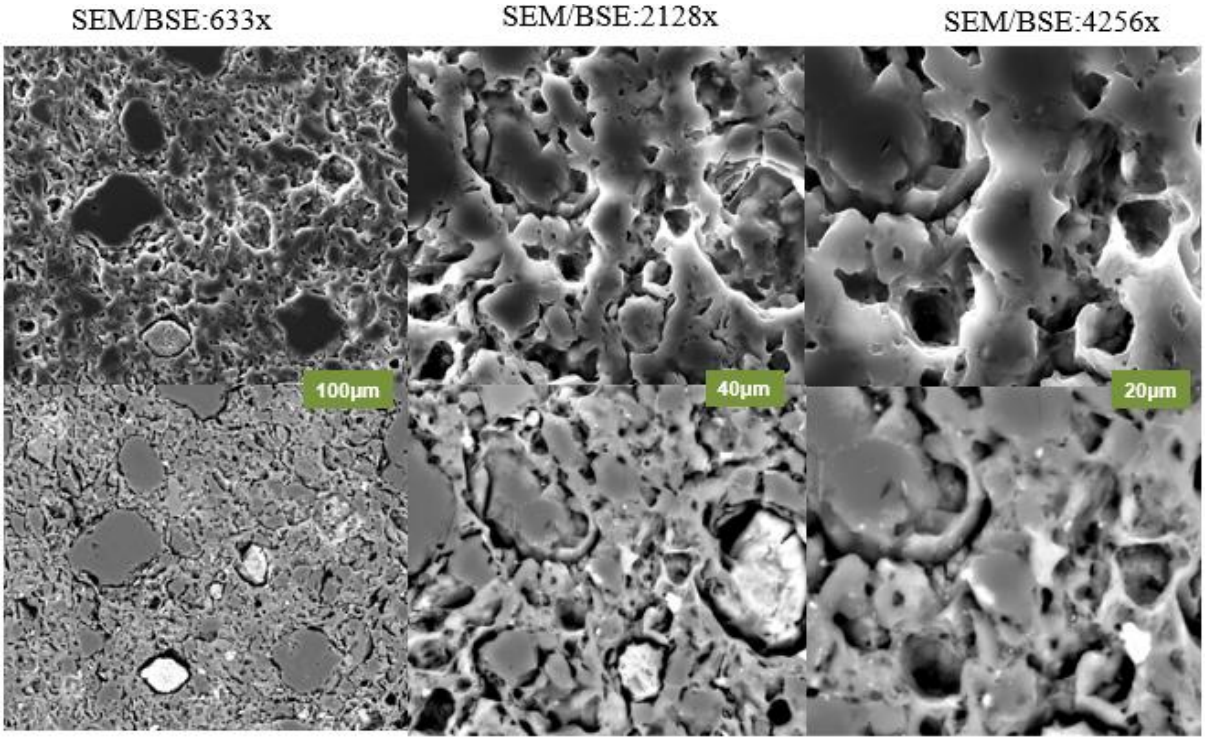

Figure 5-60: Secondary electron and Backscattered images of 2wt% $CaCO_3$ fired to 1040°C.

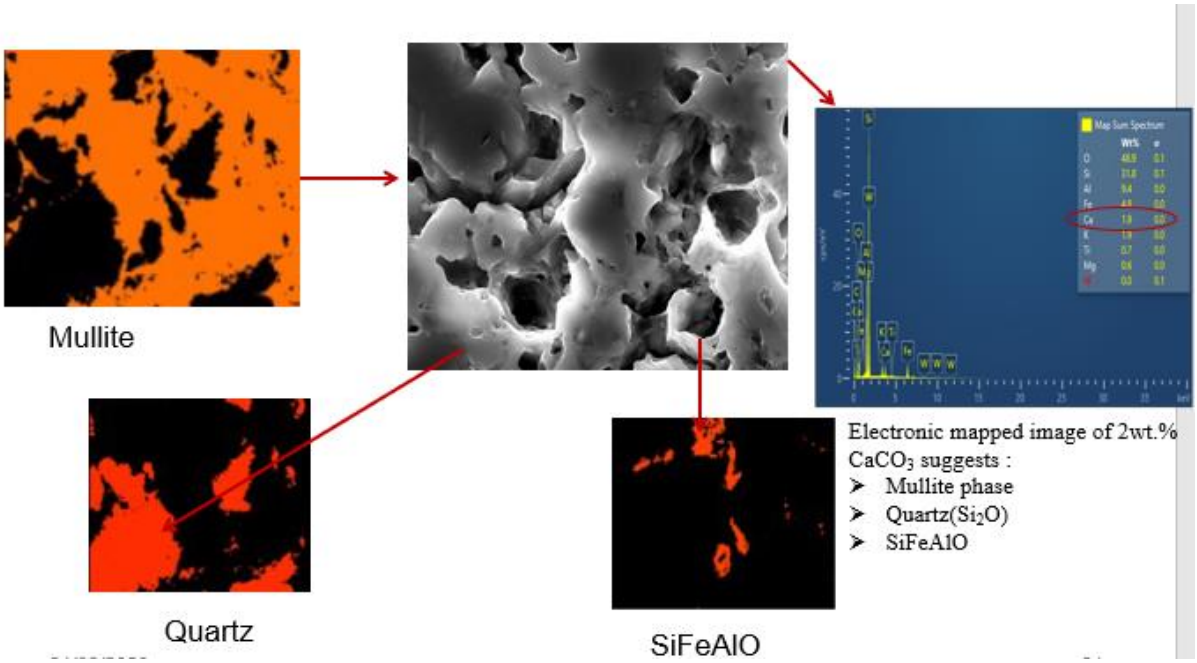

Figure 5-61: EDS mapped phases with point analysis of 2wt% $CaCO_3$ replacement fired to 900°C

2wt.% $CaCO_3$ 900°C

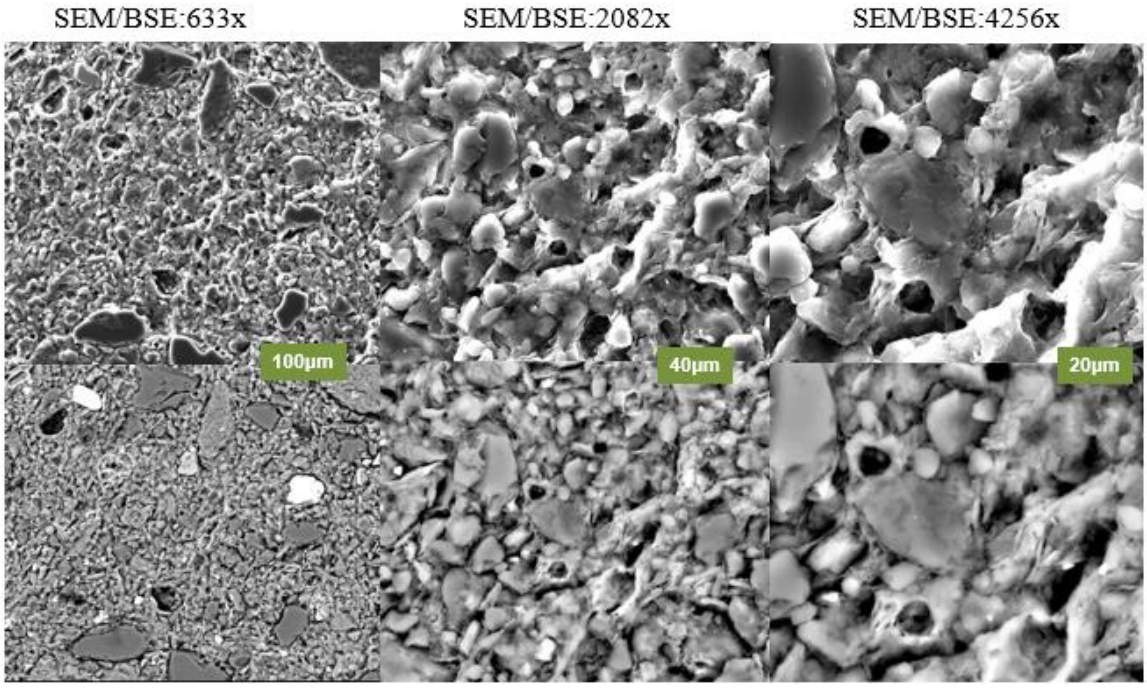

Figure 5-62: Secondary electron and Backscattered images of 2wt% $CaCO_3$ fired to 900°C.

3wt% $CaCO_3$ at 1040°C

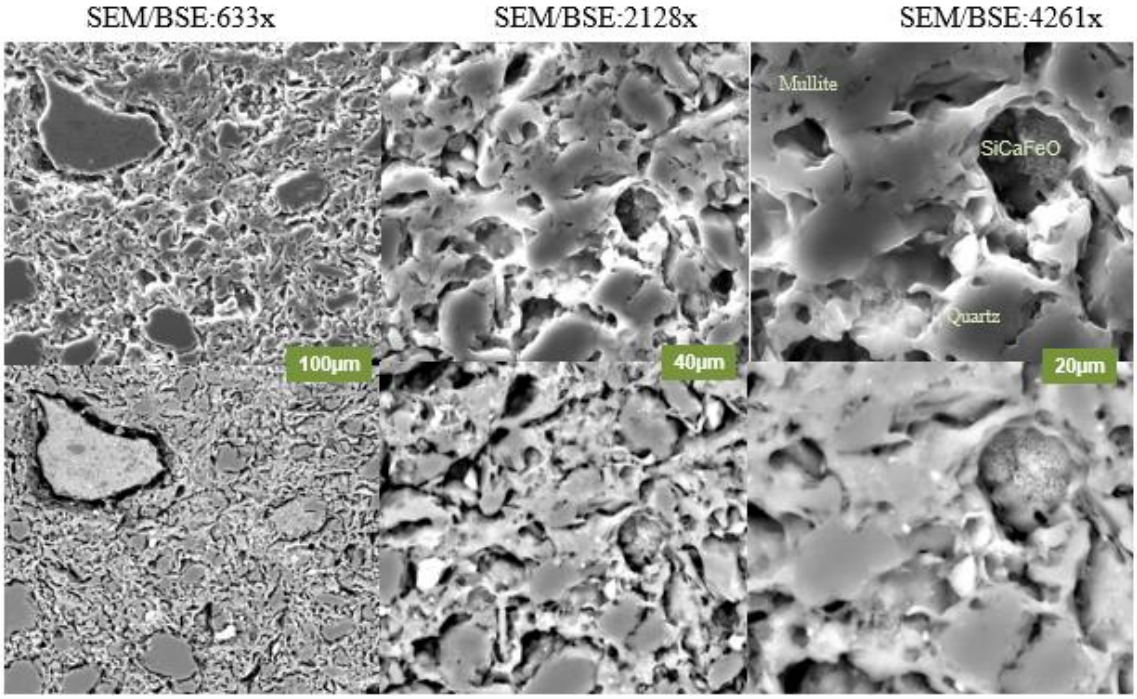

Figure 5-63: Secondary electron and Backscattered images of 3wt% $CaCO_3$ fired to 1040°C.

3wt% $CaCO_3$ at 900°C

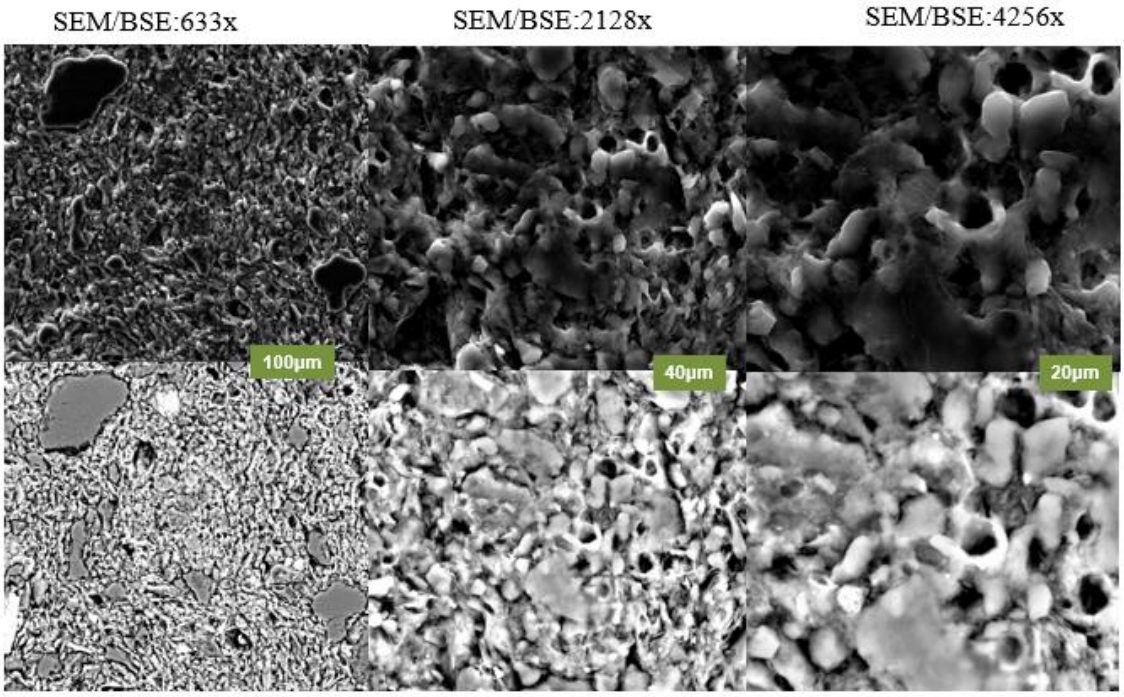

Figure 5-64: Secondary electron and Backscattered images of 3wt% $CaCO_3$ fired to 900°C.

4wt% $CaCO_3$ at 900°C

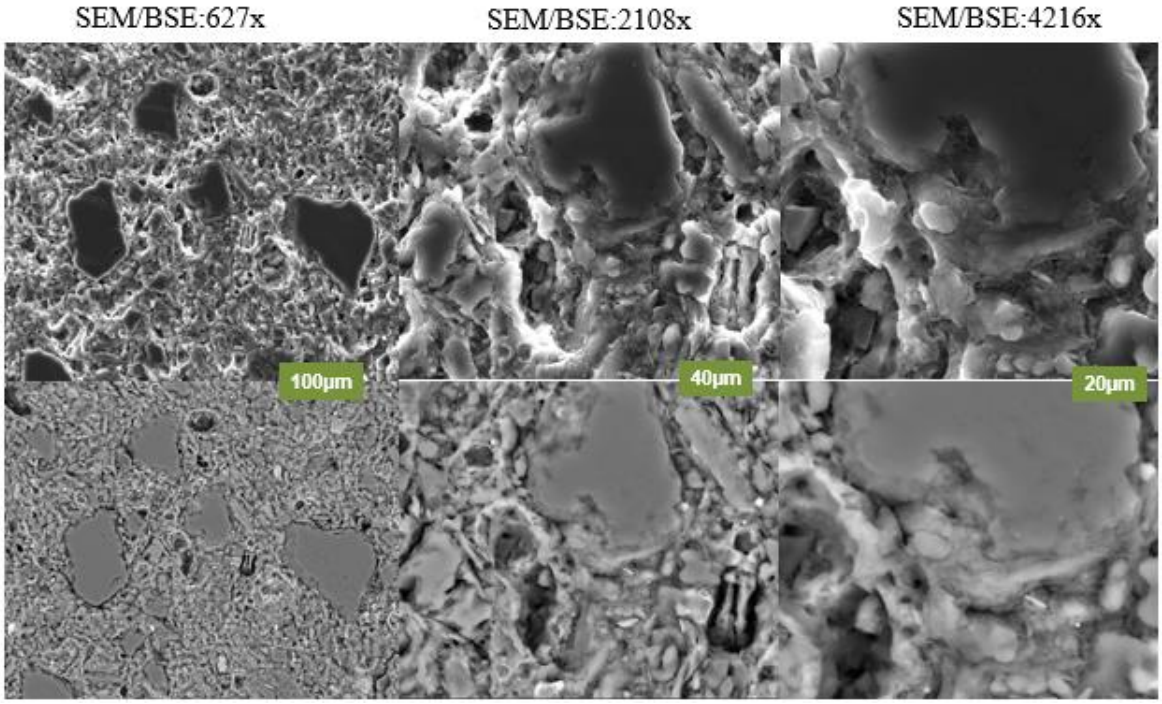

Figure 5-65: Secondary electron and Backscattered images of 4wt% $CaCO_3$ fired to 900°C.

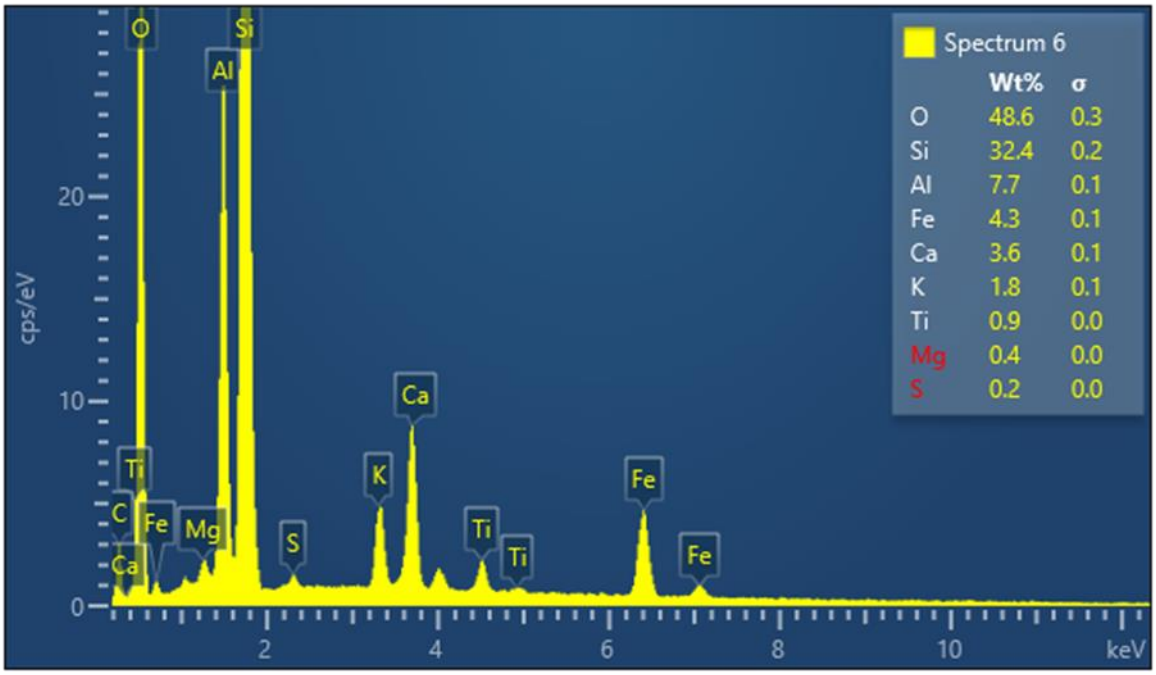

Figure 5-66: EDS of 4wt% $CaCO_3$ fired to 1040°C confirming the approximate Ca content at 3.6% and sulphur at 0.2%

1wt% $MgCO_3$-1040°C

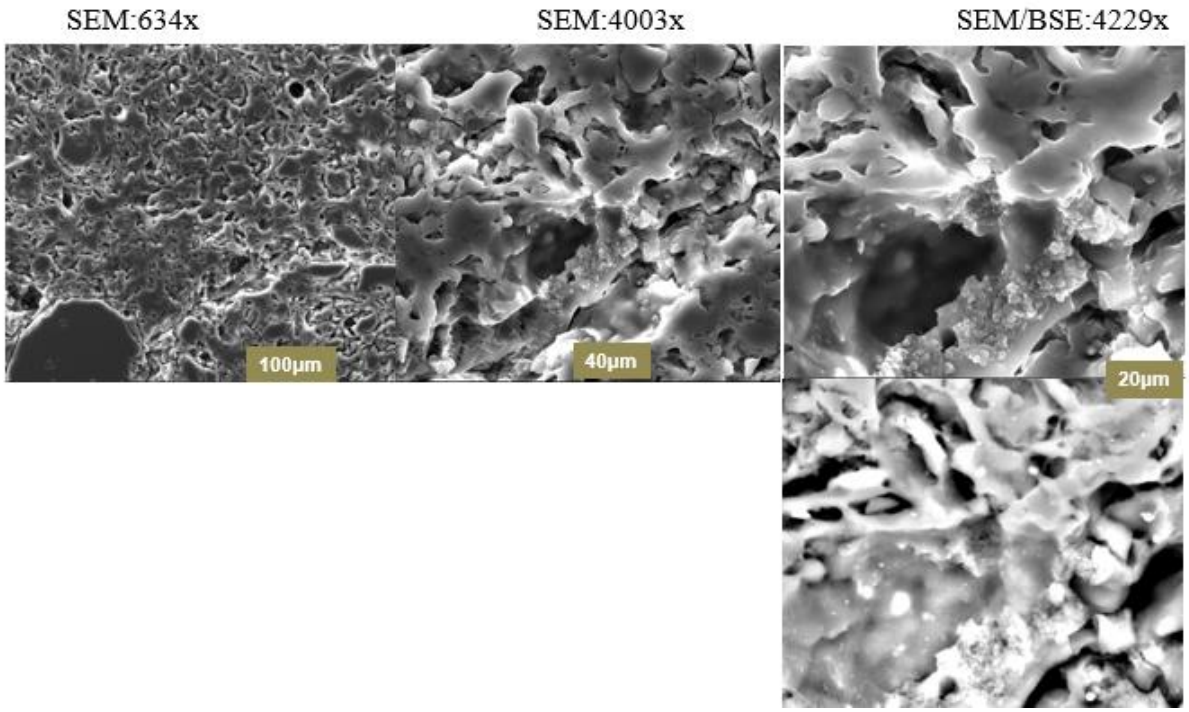

Figure 5-67: Secondary electron and Backscattered images of 1wt% $MgCO_3$ fired to 1040°C.

1wt% $MgCO_3$-900°C

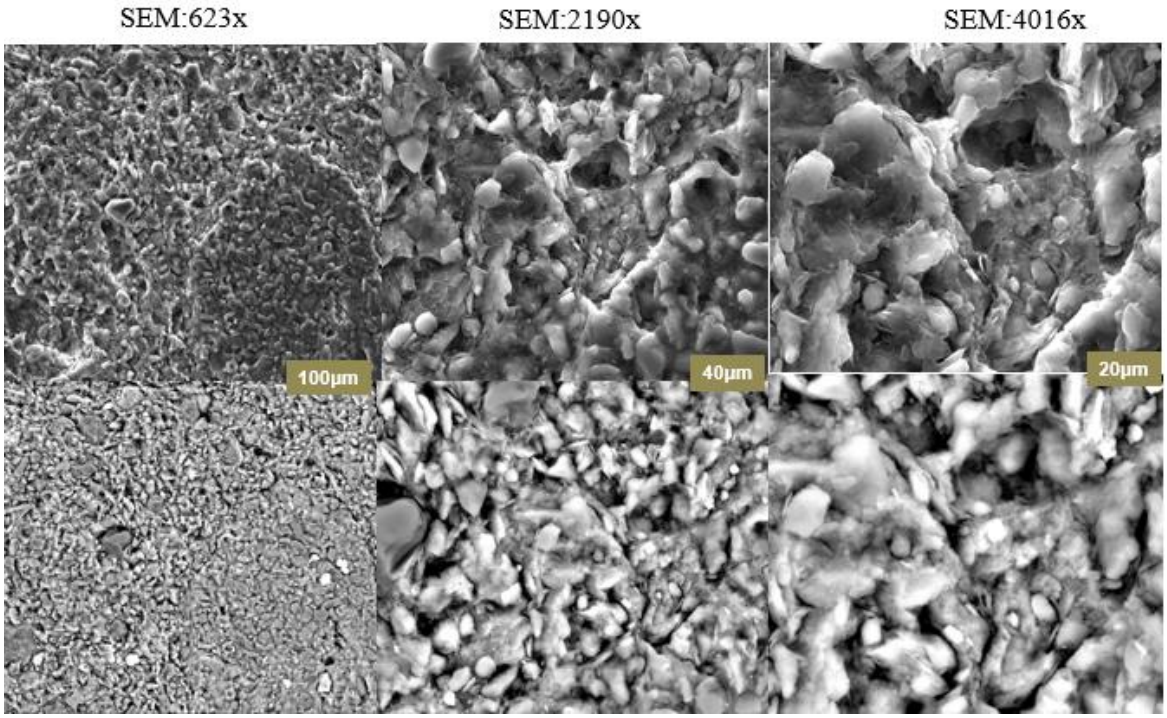

Figure 5-68: Secondary electron and Backscattered images of 1wt% $MgCO_3$ fired to 900°C.

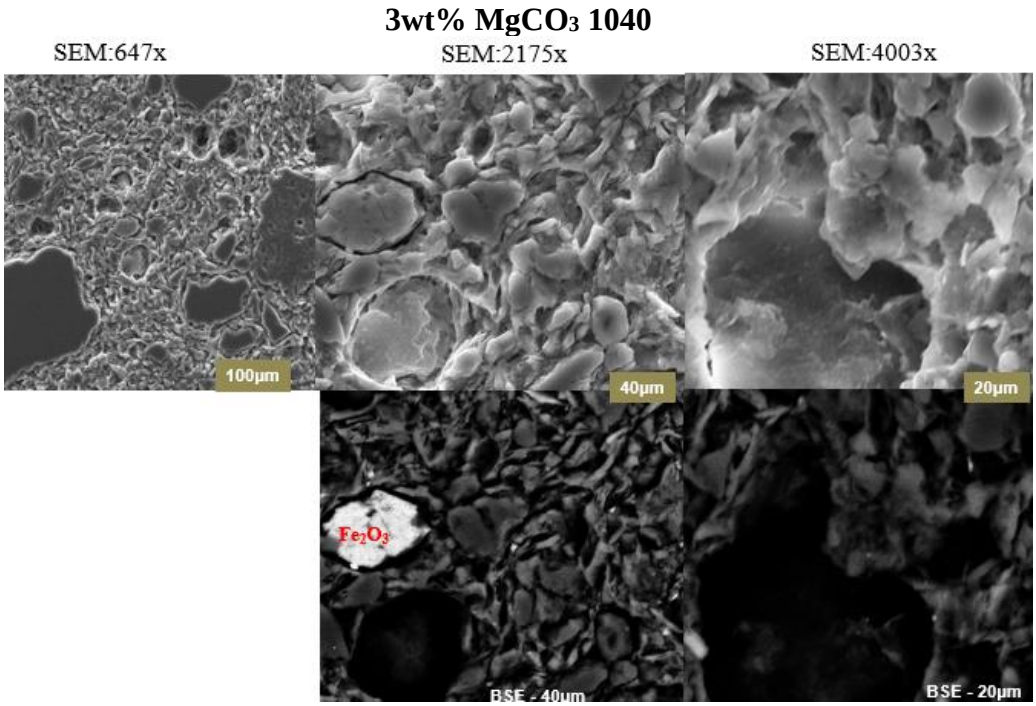

Figure 5-69: Secondary electron and Backscattered images of 3wt% $MgCO_3$ fired to 1040°C

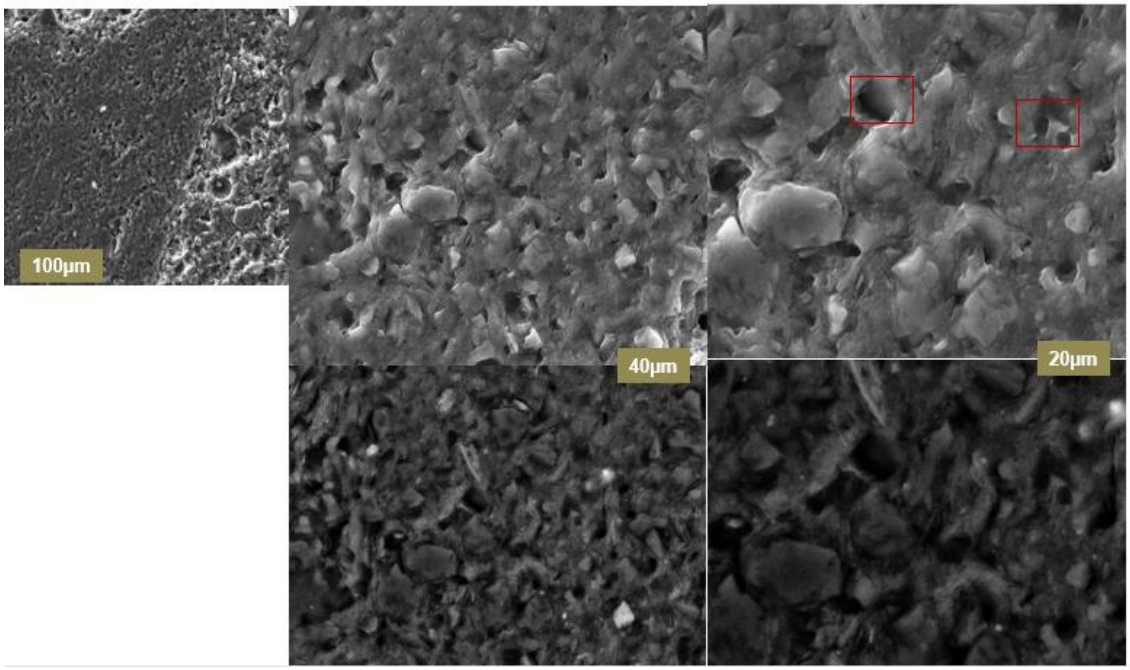

Figure 5-70: Secondary electron and Backscattered images of 3wt% $MgCO_3$ fired to 900°C

4wt% $MgCO_3$-1040°C

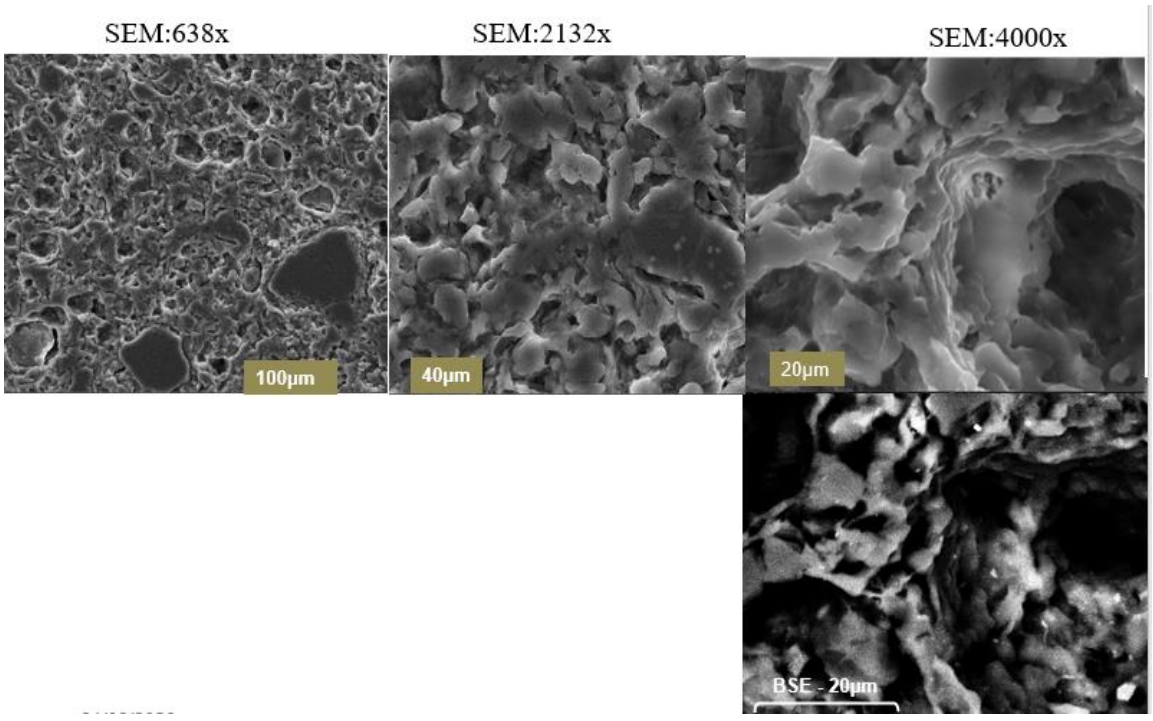

Figure 5-71: Secondary electron and Backscattered images of 4wt% $MgCO_3$ fired to 1040°C.

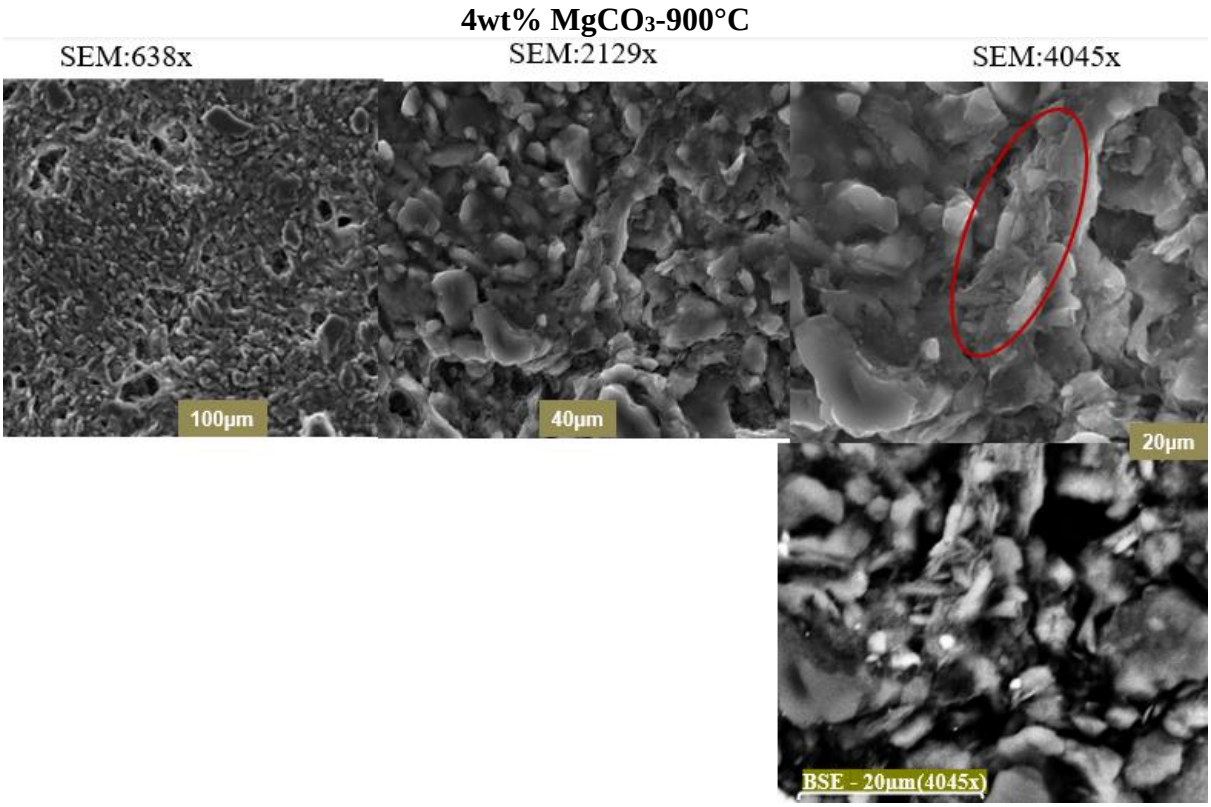

Figure 5-72: Secondary electron and Backscattered images of 4wt% $MgCO_3$ fired to 900°C.

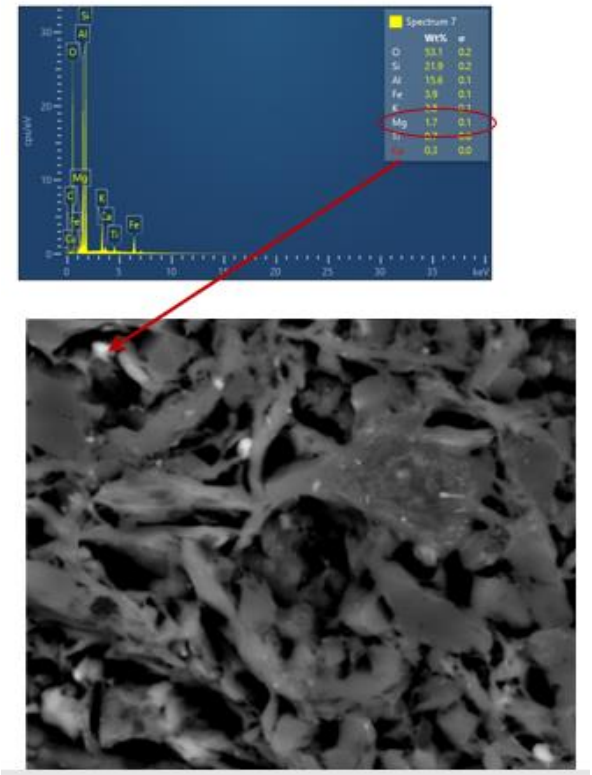

Figure 5-73: SEM/EDS of 2wt% $MgCO_3$ fired to 1040°C.

The image **(Figure 5-73**) shows the placement of MgO in the ceramic structure that prevents the formation of fired scum on the ceramic surface.

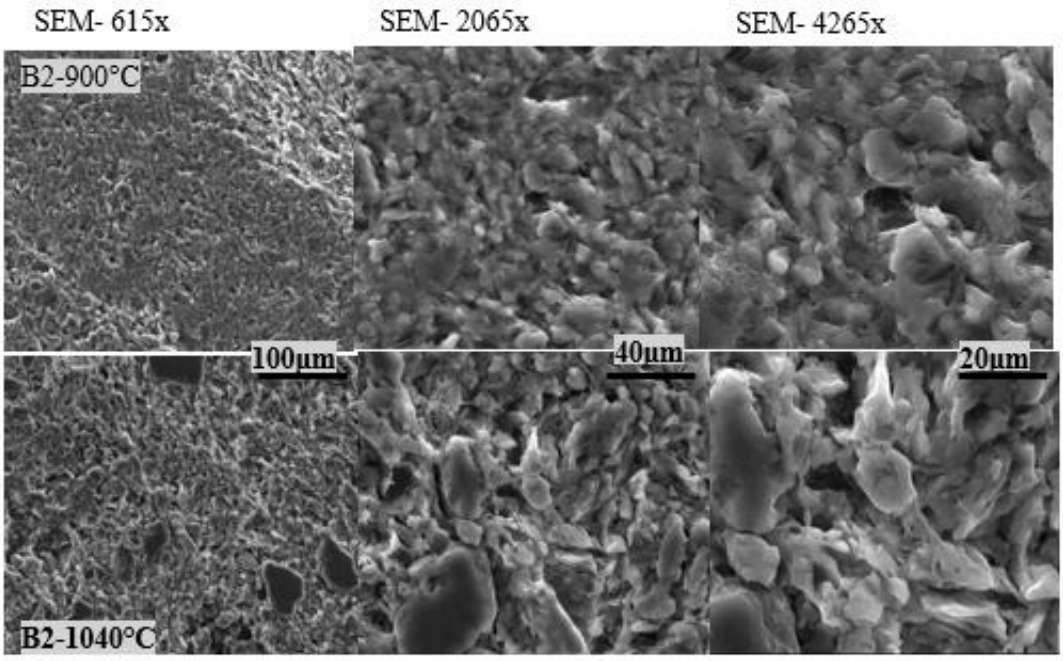

Figure 5-74: Secondary electron (SE) of 2wt% $BaCO_3$ fired to 900°C and 1040°C.

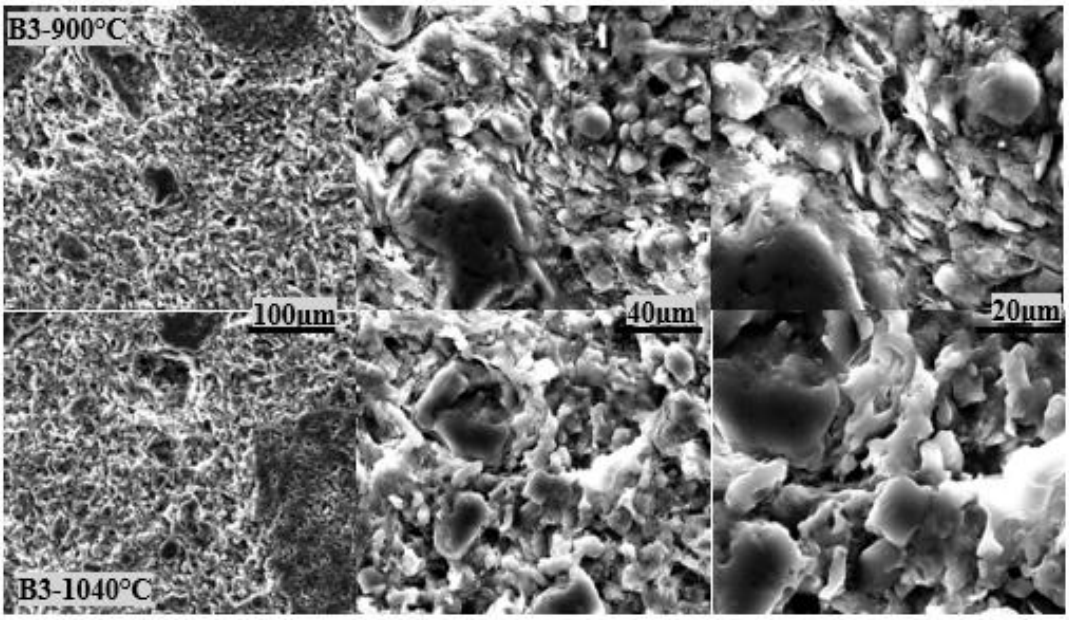

Figure 5-75: Secondary electron (SE) of 3wt% $BaCO_3$ fired to 900°C and 1040°C.

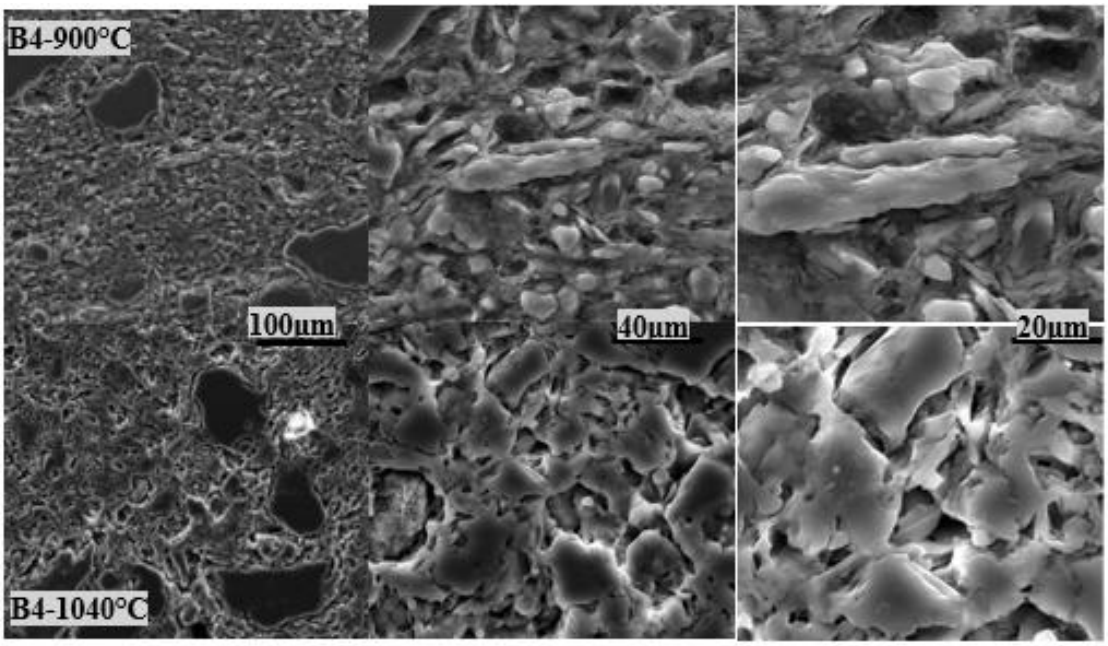

Figure 5-76: Secondary electron (SE) of 4wt% $BaCO_3$ fired to 900°C and 1040°C.

4wt%-Li_2CO_3-1040°C

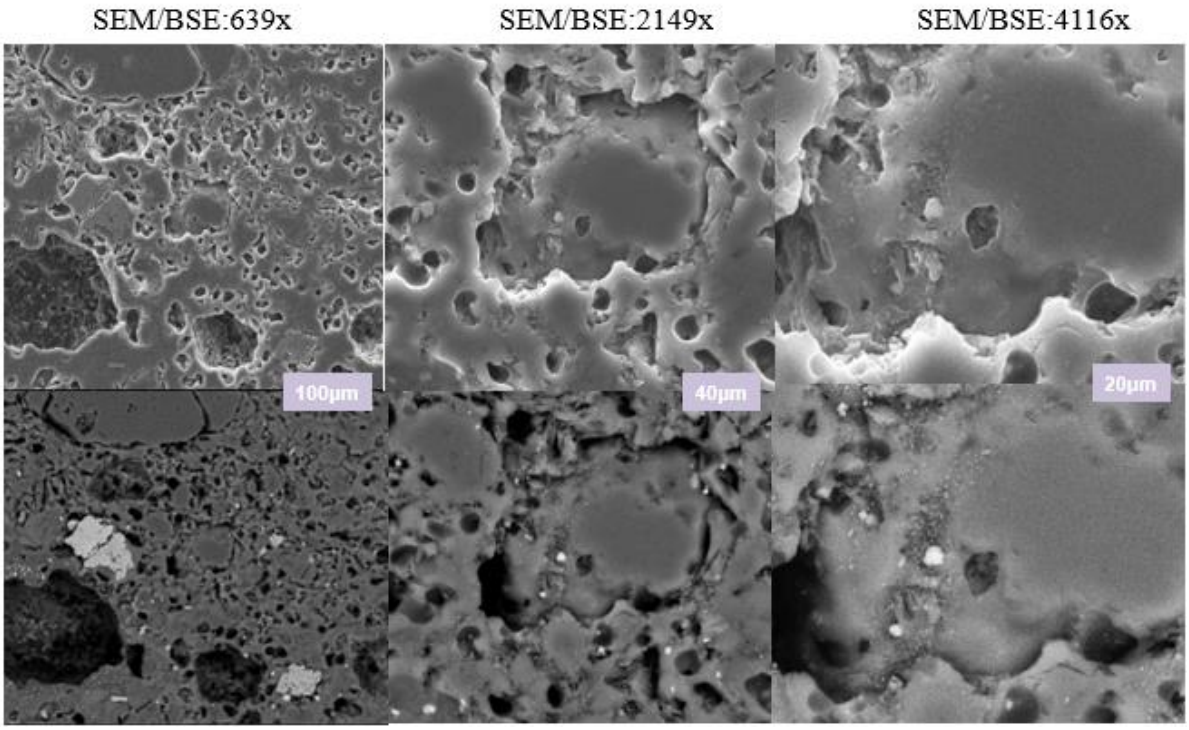

Figure 5-77: Secondary electron (SE) and Backscattered images (BSE) of 4wt% Li_2CO_3 fired to 1040°C.

4wt%-Li_2CO_3-900°C

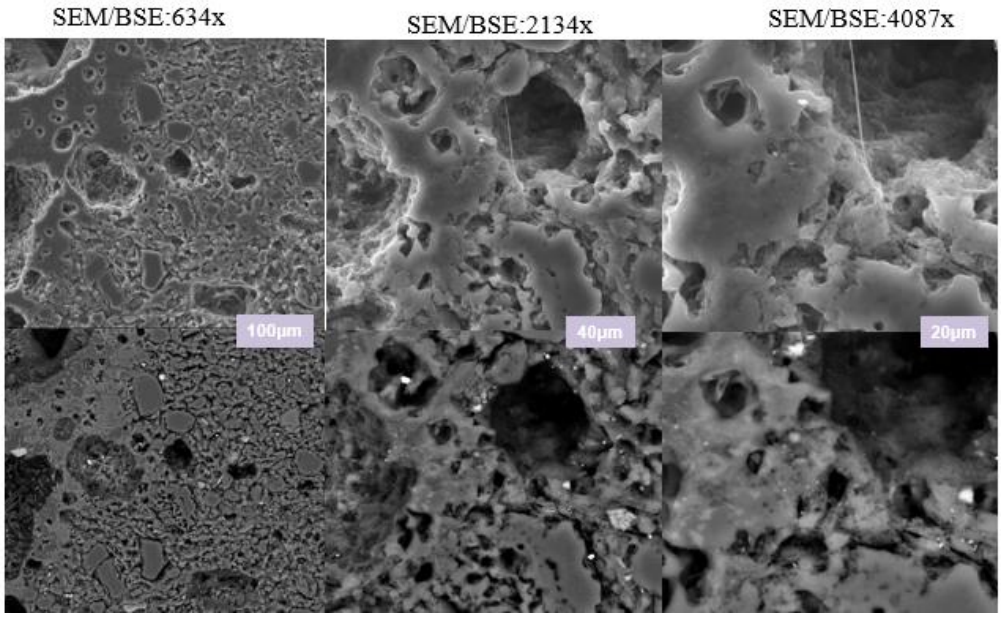

Figure 5-78: Secondary electron (SE)and Backscattered images (BSE) of 4wt% Li_2CO_3 fired to 900°C.

3wt%-Li_2CO_3-1040°C

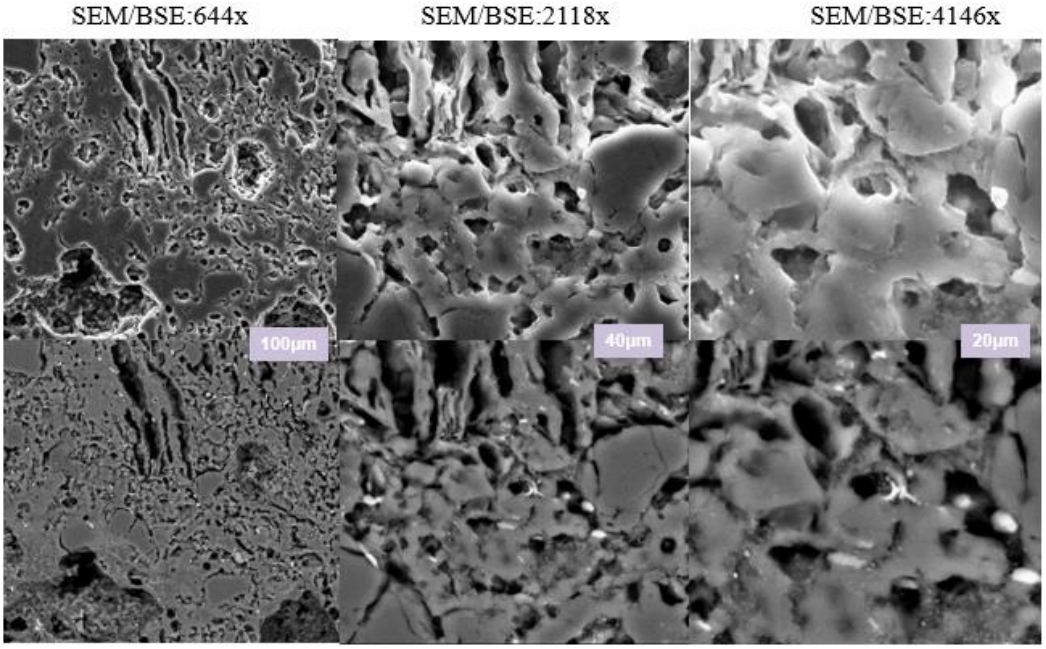

Figure 5-79: Secondary electron (SE)and Backscattered images (BSE) of 3wt% Li_2CO_3 fired to 1040°C.

3wt%-Li_2CO_3-900°C

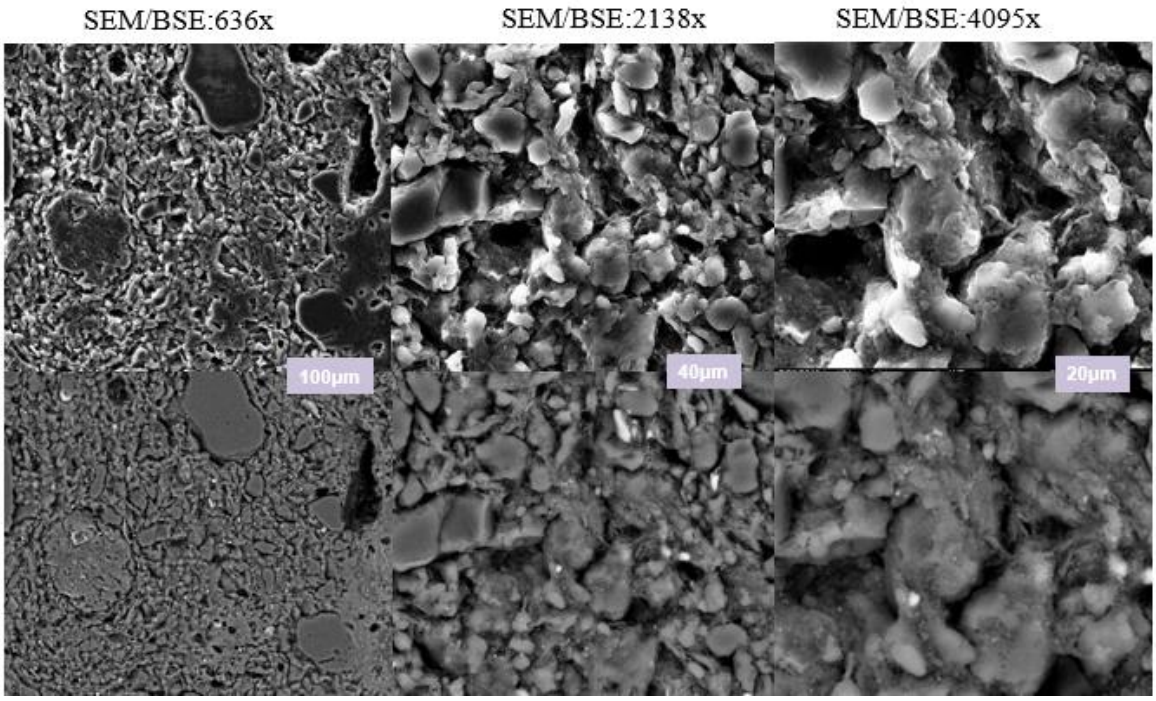

Figure 5-80: Secondary electron (SE)and Backscattered images (BSE) of 3wt% Li_2CO_3 fired to 900°C.

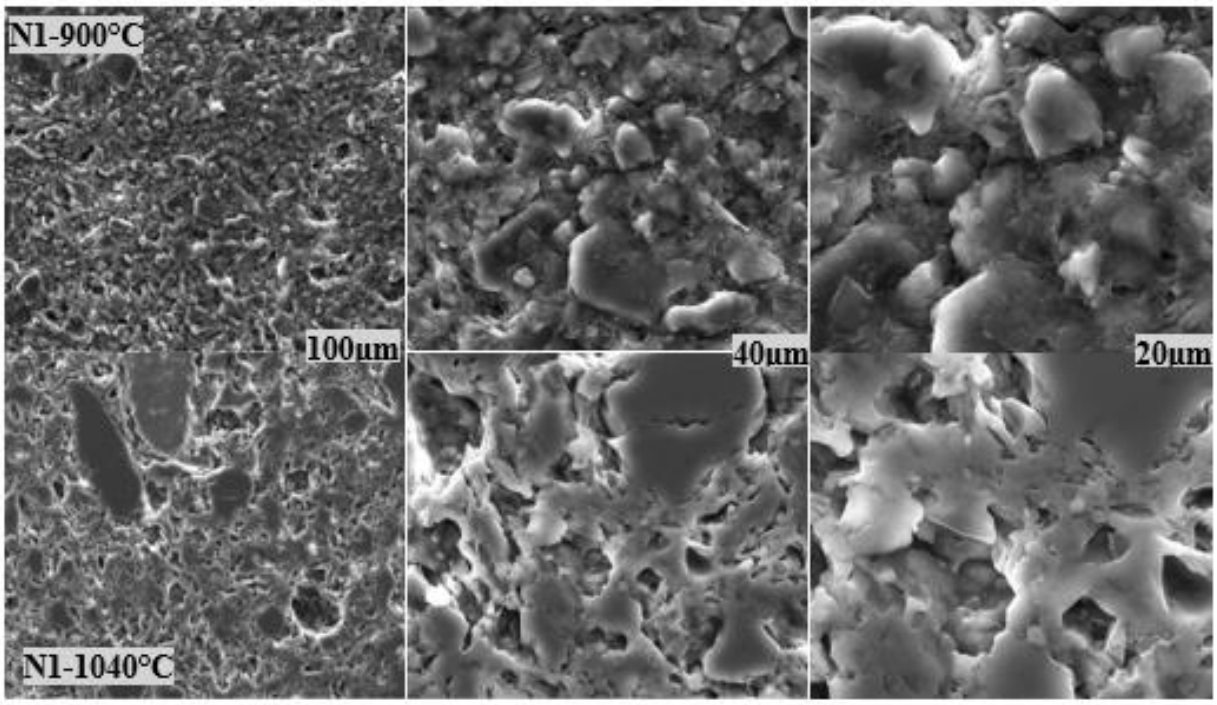

Figure 5-81: Secondary electron (SE) of 1wt% Na_2CO_3 fired to 900°C and 1040°C.

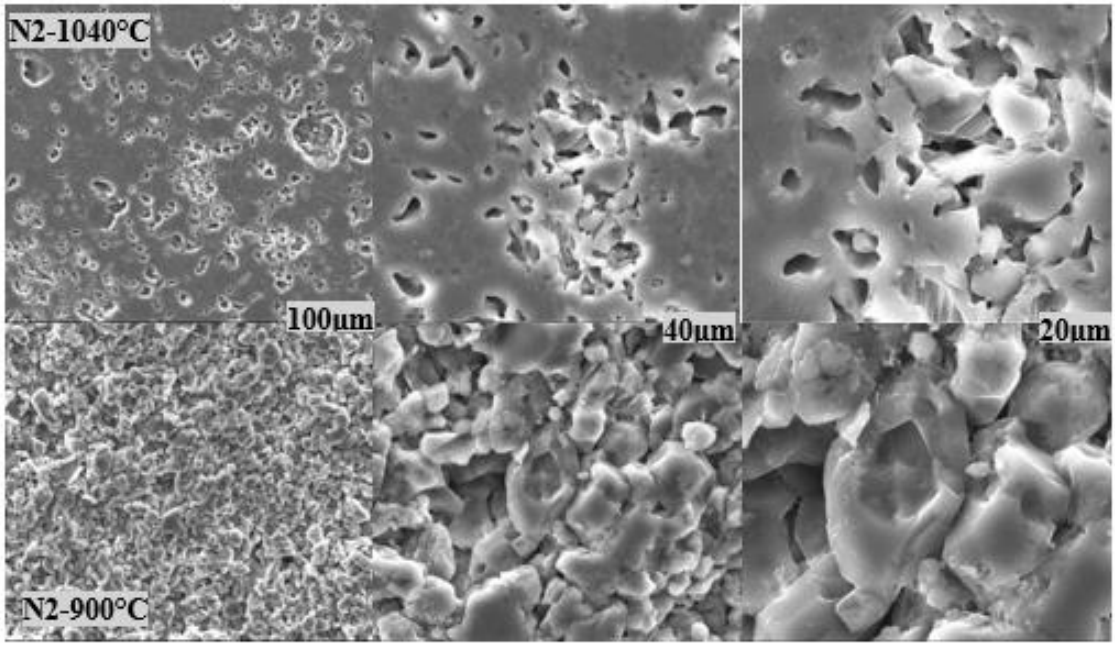

Figure 5-82: Secondary electron (SE) of 2wt% Na_2CO_3 fired to 900°C and 1040°C.

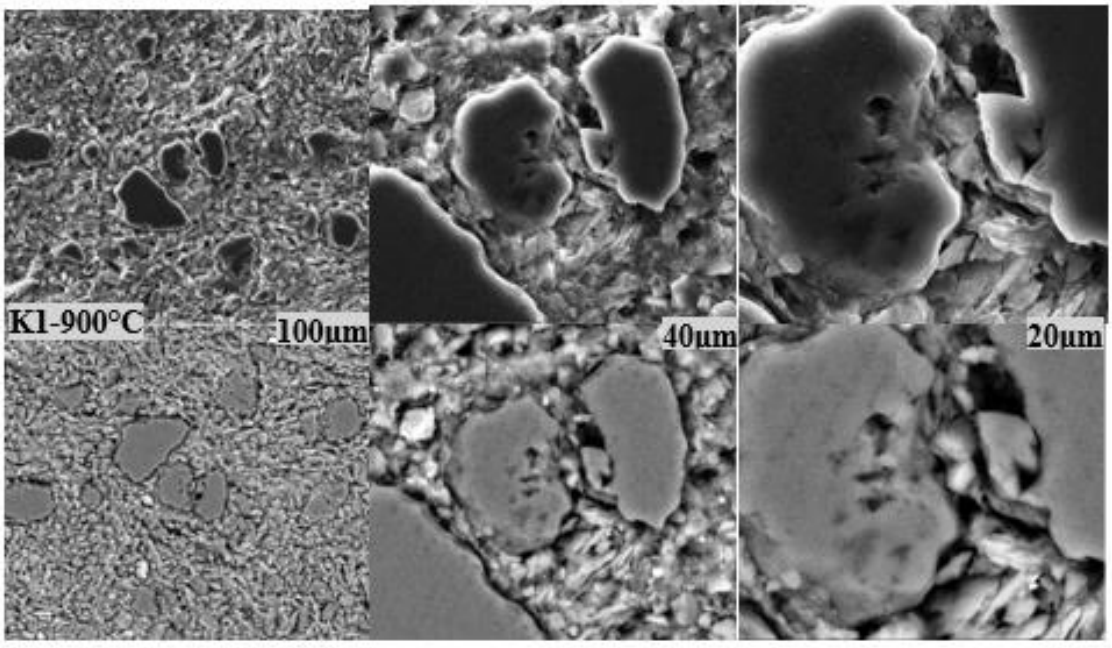

Figure 5-83: Secondary electron (SE)and Backscattered images (BSE) of 1wt% K_2CO_3 fired to 900°C.

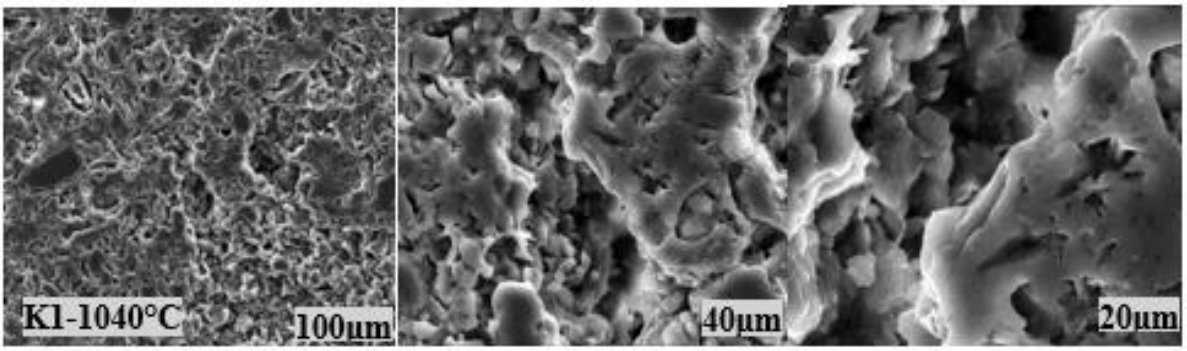

Figure 5-84: Secondary electron (SE) of 1wt% K_2CO_3 fired to 1040°C

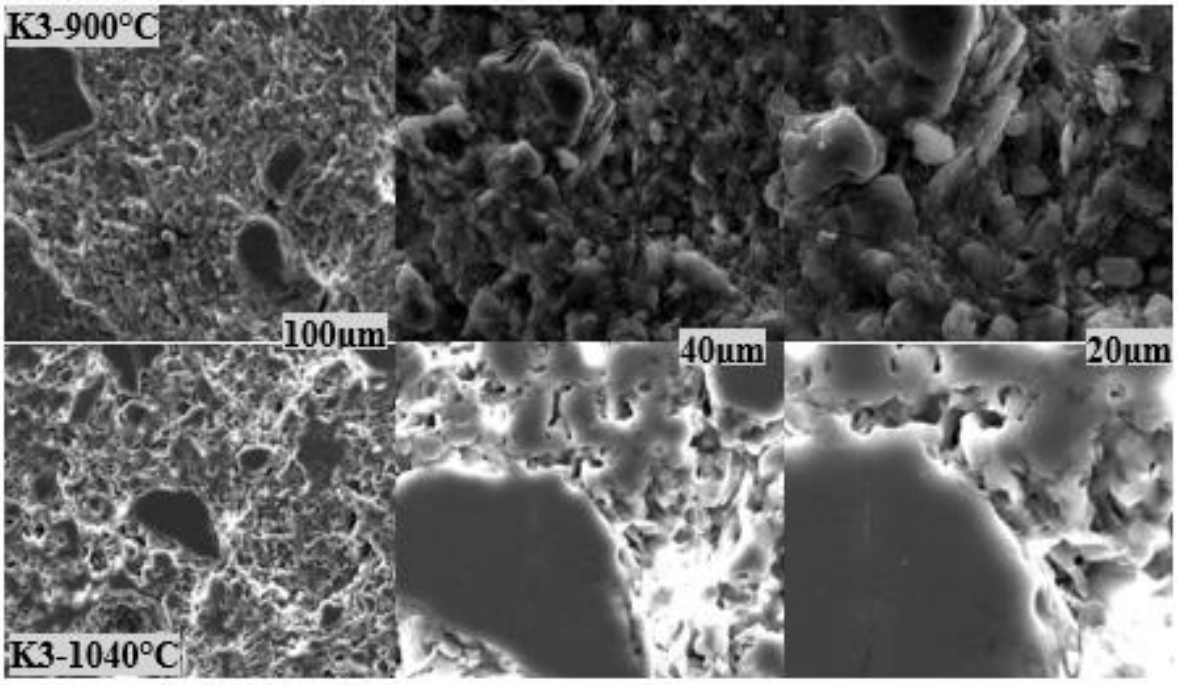

Figure 5-85: Secondary electron (SE) of 3wt% K_2CO_3 fired to 900°C and1040°C

5.15 Compressive strength testing by additive level

Figure 5-86 (a-f) shows the effect of additive levels and temperature on reformulated brick body composition containing 1-4wt% of alkali and alkaline earth carbonates fired to 900°C - 1040°C.

For alkaline earth mixtures fired to 1040°C, it was observed that $CaCO_3$ proportions 1-3wt% recorded higher strength compared to the $MgCO_3$ and $BaCO_3$ with 80MPa, 82MPa and 83MPa, respectively. Also, 4wt% $CaCO_3$ was 2MPa greater than $MgCO_3$.

$BaCO_3$ body strength decreased from 68MPa (1wt%) to 48MPa and 50MPa for 2wt% and 3wt%. But 4wt% $BaCO_3$ additive obtained 85MPa.

$MgCO_3$ body additive level saw a decline in strength as additive increased from 1-4wt% with 74MPa, 72MPa, 68MPa and 60MPa, respectively. However, compared to $BaCO_3$, it was observed that 1-3wt% $MgCO_3$ fired to 1040°C obtained the highest strength compared to $BaCO_3$; at 4wt%, $BaCO_3$ was 25MPa stronger than 4wt% $MgCO_3$.

Trends seen with the alkalies were different and recorded the highest compressive strength among the additives except for 4wt% Na_2CO_3, whose recorded strength was the least.

Li_2CO_3 additive looked promising at 1040^{o}C with only 1wt % additive taking the strength from 81.5MPa to 108MPa. 90MPa was obtained for 2wt% an 18MPa strength reduction. Further reduction is seen as additive levels increased to 4wt% but still greater than the alkaline earth except for 4wt% $BaCO_3$ of 85MPa.

Moreover, this additive and its levels had better strength when compared to alkaline earth. 3wt% K_2CO_3 obtained the highest strength of 120MPa, whilst 4wt% saw an 18MPa reduction. Meanwhile, 94MPa and 74MPa were recorded for 1-2wt% additive, a fall of 20MPa. The gradual reduction in strength as additive increased from 2-3wt% was recorded for Na_2CO_3 (76MPa,70MPa,) at 1040°C whilst samples containing 4wt% recorded 45MPa.

Reduction in strength was recorded for all samples fired to 1000°C compared to 1040°C 1wt% of alkali additive (Na and Li) still showed strength. 71MPa for Na-sample and 96MPa for the Li_2CO_3 body marking the highest strength. Only $BaCO_3$ saw a significant reduction from 68MPa to 41MPa by a 40°C. $CaCO_3$ and $MgCO_3$ recorded strengths were 60MPa and 63MPa, respectively. Samples containing 2wt% for K_2CO_3 and $CaCO_3$ obtained the same strength (71MPa), whilst Na_2CO_3 attained the highest result (76MPa) due to the matt formation on the clay surface. Moreover, Li_2CO_3 records 69MPa. Interestingly, 2wt% $MgCO_3$ samples obtained 58MPa compared to $BaCO_3$ (33MPa). As additive levels increased to 3wt%, K_2CO_3 recorded 93MPa and Li_2CO_3 marked 72MPa, whiles Na_2CO_3 scored 69MPa, just like $CaCO_3$. Meanwhile, 3wt% $MgCO_3$ recorded 63MPa compared to 33MPa for $BaCO_3$. Furthermore, the 4wt% Na_2CO_3 sample marked the lowest strength (26MPa), indicative of a weaker body caused by the ceramic surface's glassy coating, making the body more brittle. The K_2CO_3 ceramic body recorded an increase in strength from 93MPa to 97MPa, whiles the strength obtained for the Li_2CO_3 body was maintained (72MPa). For the alkaline earth, 4wt% $MgCO_3$ recorded the least strength of 44MPa, and $BaCO_3$ and $CaCO_3$ strength increased with the additive increase to 69MPa and 60MPa, respectively.

Samples fired to 900°C saw a further reduction in compressive strength as additive proportion increased, strength decreased, and strength decreased as temperature decreased. Moreover, it was observed that Li_2CO_3, $CaCO_3$ and $BaCO_3$ increased in strength as additive levels increased for samples fired to 900°C. At 4wt%, Li_2CO_3 recorded 65MPa, 59MPa for $CaCO_3$ and $BaCO_3$ marked 53MPa. Also, K_2CO_3, $MgCO_3$, and Na_2CO_3 additives saw a decline in strength as additive levels increased from 1wt% -4wt%. The least recorded strength was 26MPa for 4wt% Na_2CO_3, followed by 38MPa $MgCO_3$ and 41MPa with K_2CO_3.

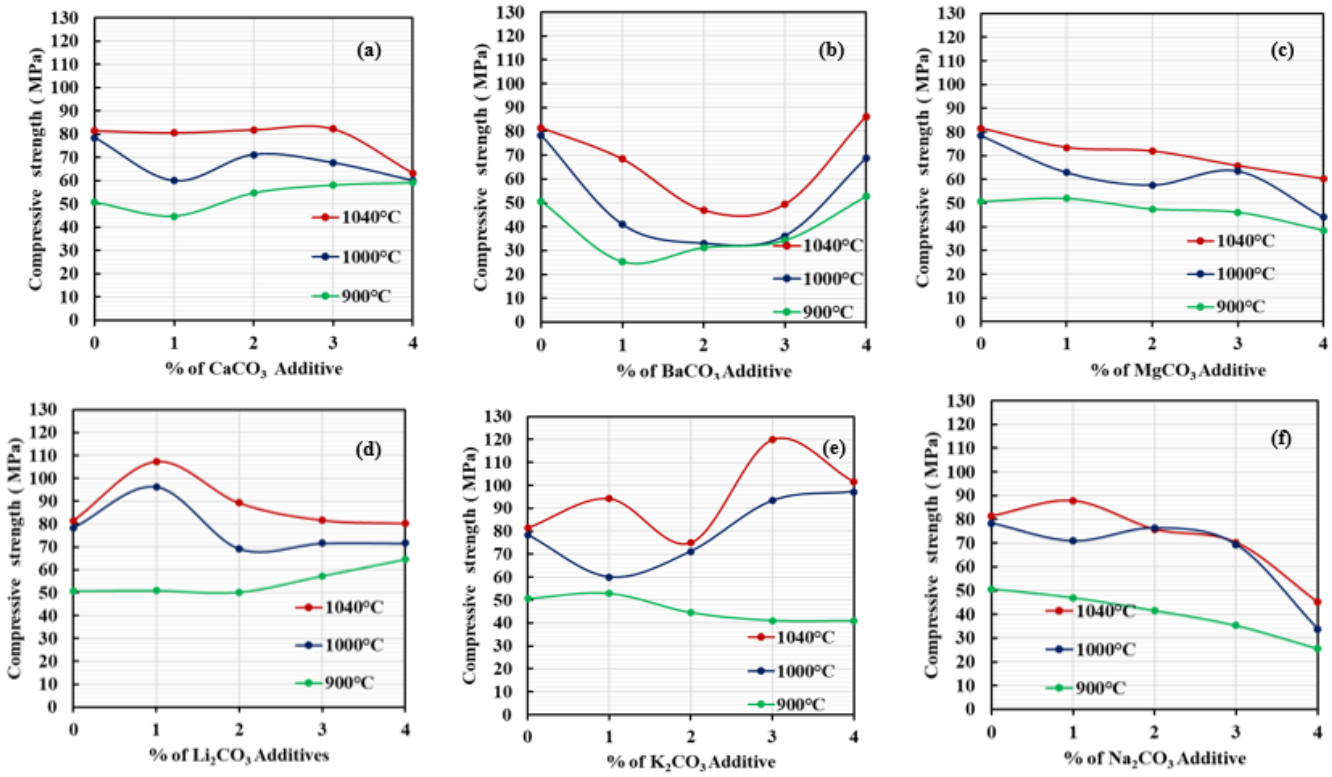

Figure 4-1: Alkaline earth carbonate levels 1-4wt% effect on clay brick strength (a) $CaCO_3$ (b) $BaCO_3$(c) $MgCO_3$ additives (d) Li_2CO_3 (e) K_2CO_3 additives and(f) Na_2CO_3.

5.16 Further Discussions

5.16.1 *Thermal effect of alkaline earth and alkali additive in ceramic applications on low-fired ceramics*

The role of the alkalis and alkaline earth is to react with glass formers (SiO_2) and Al formers (Al_2O_3) in clays to form early melts at eutectic points [316,360].

Dehydroxylated muscovite in alkaline earth-containing samples fired at 900°C confirms that the mineral muscovite[84] decomposes above 980°C and primarily depends on mineral particle size. The presence of muscovite in fired ceramics can be used to determine the degree of firing, especially in understanding historical structures that need to be replaced.

5.16.2 *$CaCO_3$ containing ceramics on mechanical strength*

It has been observed that clays containing lower levels of $CaCO_3$ as an additive (1-2wt%), fired to 900°C are not suitable for high thermal resistance bricks but obtained boiling water absorption of 13%, which was within the Spanish standard UNE 67-019[361]. According to Melhem[350], the clay mineral Kaolinite decomposes into the following reactions:

$Al_2O_3.2SiO_2.2H_2O$ (Kaolinite) → $Al_2O_3.2SiO_2$ (meta kaolinite) + $2H_2O$(400-500°C)

$2(Al_2O_3.2SiO_2)$(meta kaolinite) → $Si_3Al_4O_{12}$(spinel)+SiO_2 (~950°C)

$3Si_3Al4O_{12}$(Al-Si-spinel) → $2(Al_2O_3.2SiO_2)$(mullite)+$5SiO_2$ (>1050°C).

Dehydrated muscovite was the mineral formed as clay composition was heated to 900ºC. Although at 1040ºC, mullite was obtained, the DTA did not show any crystallization as an exothermic peak corresponding to this phase, possibly due to the rapid reaction and the low dosage of the additive. With the low percentage of $CaCO_3$ dosage in the composition 1040ºC, the transformation will change as follows:

$CaSiO_3 + Al_2O_3 + SiO_2 \rightarrow CaAl_2Si_2O_8$ formed from Wollastonite at temperatures 960-980°C by the $CaCO_3 + SiO_2 \rightarrow CaSiO_3 + CO_2$ reaction. Firing transformations of clay containing $CaCO_3$ fired to 950 and 1100ºC were reported to form calcium phases, including anortithe but not mullite[347]

The $CaCO_3$ additive levels and the control fired to 900°C had no considerable influence on BWA. However, samples containing 1wt% -4wt% fired to 1040°C held for 2hrs produced lower BWA (8.4%-12%), which, compared to the Control, is higher (>8.6- 13.3%) see **Figure 5-50a**. This effect resulted from the additive level and temperature, which improved strength for samples containing 1-3wt% fired to 1040°C with >81MPa meeting the British standard EN772-1 for a class B engineering brick (**Figure 5-86a**); however, it fails in the BWA% according to BS EN772-7. Strength reduction and increased porosity have been reported to be the negative effect of the additive[131]. Temperatures below 1040°C also failed in the strength

test. The shaping method used in place of the extrusion could be why the porosity obtained was ~8%. Furthermore, if we consider using the firing temperature of $CaCO_3$ mixtures up to 3wt% fired to 1040°C. This composite mixture can improve brick strength whilst reducing the firing temperature of at least 60°C and thus reduce CO_2 emitted from a gas burn. Okada, Kiyoshi, et al.,[362] reported that particle sizes affect the crystallization on firing above 850°C, corresponding to the dilatometer results (**Figure 5-5**) showing a rapid shrinkage after that same temperature.

Comparing the results from BWA and MIP, the most striking effect from the data is that MIP porosity increases to 15% - 22% compared to 8.4%-12% for the BWA. This is because the non-wetting method of MIP affects the variation in the obtained porosity (%). The pores remained throughout the mass without colliding and collapsing the pores created by the steam in the case of the BWA (%). The shortfall to this additive is the insoluble nature of $CaCO_3$, which reacts with sulphur on heating to form $CaSO_4$, an unwanted stain on the fired brick surface. However, this can be corrected by introducing $BaCO_3$ into the body [2,42,67,184].

5.16.3 *The role of $MgCO_3$ additive effect in ceramic production*

What was notable in using $MgCO_3$ compared to $CaCO_3$, $BaCO_3$, and the alkali additives is its low breakdown temperature (600°C), just as with the control material to promote early sintering. However, the rest of the alkaline and alkali carbonates decomposition is above 800°C consistent with literature [363].

The additive magnesite was observed to increase internal porosity with 1-3wt% $MgCO_3$ obtaining the best mechanical strength (74-68MPa) **Figure 5-86** with its BWA increasing from 9% -12% for 1-4wt% fired to 1040°C **Figure 5-50.** When 2-4wt% magnesite was added to porcelain tiles and fired at 1100°C, 1120°C and 1130°C, they were found to produce lower porosity with good strength and energy reduction up to 30°C [363]. What is interesting about their

formulation is that the body contained 40wt% feldspar in addition to the $MgCO_3$ with reduced porosity.

Previous studies have demonstrated that $BaCO_3$ is the best additive to remove stains (Scum) on heavy clay products[36,67,203]. However, this study clearly shows the effectiveness of 2wt% and above $MgCO_3$ sufficient in removing stains caused by pyrite in Weald clay on drying and firing as well as an additive improving brick strength (highest obtained with 1wt% is 74MPa and 60MPa being the least for 4wt% additive). The immobilised salts expected to remain within the fired body could not be proven with Raman spectroscopy (**Figure 8-11)** or XRD (**Figure 5-10).** The only study which reported on the role of $MgCO_3$ in removing surface stain (efflorescence with levels 0.25-1.5% by mass in a tunnel kiln at 950°C) could also not prove the traces of any sulphate compound locked up in the body as a crystalline phase [364]. Studies have shown that the phase $MgAl_2O_4$ (spinel) possesses excellent strength[365], which was only found with samples containing 4wt% fired to 1040°C with 60 MPa strength. This experimental study suggests that using greater than 2wt% $MgCO_3$ can help prevent clays prone to scum and efflorescence by promoting the presence of Akermanite which stops the whitish stain from appearing on the ceramic surface. The additive dosage levels and temperature strongly affected the significant colour change of the less dark shade of brick colour.

Boiling water absorption obtained for M2 and B4 fired to 1040°C were the same but obtained two different strengths. The obtained strength for M2 samples was 72MPa, 3MPa less than the requirement for a class B engineering brick, and for boiling water absorption, 4% greater than the absorption limit for a class B engineering brick (recorded 11% for M2 fired to 1040°C). According to the indirect equation given by Maage [177] to predict durability with MIP, one of the variances for a frost-resistant product is if the product's pore diameter is greater than 3μm. However, the measured samples' diameter for all $MgCO_3$ samples did not exceed 3μm (**Figure 5-14&16**). Pores accessible to MIP can be as low as 0.0055μm [366]. There is a probability that

if the extrusion method is used for this formulation, then the optimised level of 2wt% will pass the strength and boiling water assessment whilst removing surface stains. If, as stated by Smith [367], heavy clay ceramics are generally fired to 1100°C; the result of using this study, 1-4wt% of $MgCO_3$ containing ceramics fired at 1040°C, would result in 60°C reduction in temperature and associated reduction in CO_2 emissions.

5.16.4 *The role of $BaCO_3$ additive on ceramic properties*

The bulk compositional information given by XRF pre-informs the possible reactions on firing to promote the new phases obtained. Samples containing 1wt% of the additive fired to 900°C showed the presence of barium iron oxide ($BaFe_2Si_2O$) but not in samples with >2wt% fired at 900°C. At 1040°C, the additive promoted the formation of barium silicate phases $Ba_2AlSi_2O_2$ and $BaSiO_3$ in the ceramic samples see **Figure 5-18**. This higher temperature (>1000°C) phase is consistent with a previous study on dielectric ceramic containing 10wt% $BaCO_3$ [44]. This means that on firing, the additive readily reacts with the silicate in the clay to form barium silicate phases and mullite, improving ceramic strength and colour from the hematite formation [155]. In cement and concrete research, the reactivity of $BaCO_3$ has been found to promote barium silicate structures (Ba_3SiO_5) and early tricalcium silicate (C_3S) due to the additive's low firing function as flux [368]. Bennet and Goodrich[200] reported that the additive reactivity to precipitate sulphates is 25% and 32 % in heavy clay ceramics (terracotta). Brownell [180] also demonstrated the precipitation of the additive with sulphates found in clays and from fuel burning becoming one of the main additives ($BaCO_3$) used in heavy clay manufacture principally to prevent drier and firing scum and aids in sintering [42,67,197,369].

$BaCO_3$ has been employed in studying porcelain bodies as an additional flux to replace feldspar by 2-10wt%, then fired to 1210°C for 2hrs. The study supports the effect of the additive promoting mullite formation of which the Ba is uniformly distributed within the clay matrix.

Shrinkage reduction was observed as the additive increased from 2wt% -8wt% but increased again and then decreased at the top temperature of [307]. Another study, with higher levels of $BaCO_3$ (40-60wt%) in clay containing kaolinite and halloysite, fired at 1100 and 1200°C for 3hr, revealed a drastic porosity reduction of fired composite with 40wt% additive levels, and at higher temperatures, mullite disappears [370]. The reactive nature of Ba^{2+}ions with clay particles on sintering improves the dense structure of ceramics[370]. The additive has also been used as a sintering aid and found to stop bloating and impart colour with composites containing fly ash high in $CaSO_4$ when fired at 1150°C with 10wt% additive levels[369]. Evidence in the literature shows the relationship between the additive promoting porosity in dielectric ceramics and porcelain bodies[44,307], which is good. The observed porosity with the incorporation of $BaCO_3$ in this current study resulted from the release of CO_2 from the breakdown of the additive and the formation of melts that fused clay particles, especially for ceramics fired to 1000°C.

Turning now to the experimental findings on strength (**Figure 5-86b**), there was a decline in strength with 2wt% and 3wt% of $BaCO_3$ additive in Weald clay, but at 4wt% additive, the strength was found to be suitable for a class B Engineering brick, although the water absorption was 2% greater than the standard BS EN772-7. This may be due to clay compaction in pressing clay samples before firing. The improved fired ceramic colour supports evidence from the previous observations [353] better than fired ceramics which do not contain $BaCO_3$ and prevent the soluble sulphate-containing salts from being dissolved and then migrating to the surface [371] producing scum or efflorescence.

5.16.5 *Li_2CO_3 additive effect in ceramic production*

The present study was designed to determine the effect of Li_2CO_3 on clay brick body compositions. Lithium carbonate is the most cost-effective and extensively used lithium compound in ceramics applications for glazes, porcelain, enamels and glasses [372–374].

The findings show that the additive promotes new crystalline phases and improves strength even with samples fired to 1000°C. The additive stopped the formation of mullite with lithium aluminium silicate. This is due to the early melt property of lithium over sodium reported by Betz (1938)[372]. Low-grade lithium-bearing minerals with 2.7% Li_2O and silica crucible waste have been replaced with feldspar to produce a low-firing porcelain tile (1070°C), which traditionally fires to >1200°C[374]. Their findings showed that increasing lithium dosage in clay-based compositions decreases the vitreous phase[374] reducing the shrinkage of a clay body containing lithium carbonate. This study is consistent with the laboratory experiment's additive reduction in volumetric shrinkage (6%-1.5% for 1 and 4wt% additive levels). The 2017 report on lithium market research also reported the benefits of incorporating lithium in ceramics to improve strength with decreased shrinkage and minimising energy consumption[373]. The current study found out that the additive improved ceramic strength with 1-4wt% additive fired to 1000 and 1040°C, suitable for a class B engineering brick except for additive levels 2-4wt% fired to 1000°C whose strength is 70MPa, and low fired ceramics ~900°C. However, in terms of the BWA%, per the British standard for Class B Engineering brick, only 1% additive mixture fired to 1040°C passes the standard. This finding suggests that 1wt% of the additive can be fired to 1000°C with a temperature reduction of 100°C.

A challenge to using this additive is that lithium demand is increasing, and its global production, estimated at 175 000 LCE tons (Lithium Carbonate Equivalent tons) in 2015, is expected to reach 650 000 tons in 2025 and 1 Mt by 2029 [375]. However, there is a possibility of using a cheaper product of lithium tailings instead of processed minerals. One unanticipated finding was that samples containing >2wt% additive levels on the dilatometric analysis had continuous expansion after the transition temperature of 561°C, different from the control and the alkaline earth additives. This cause of expansion is due to the low temperature at which Lithium melts.

5.16.6 *K_2CO_3 additive effect in ceramic production*

K_2O is one of the oxides found in the unfired clay and denotes the presence of the clay mineral illite/muscovite. A high amount (>2%) of K_2O is necessary to reduce the refractoriness of a clay (Al/K_2O)[376], therefore, promoting lower firing temperature. Olive pomace ash rich in K_2CO_3 was found to promote sulphate scum on drying and firing, so 1% $BaCO_3$ was added to precipitate salts but was ineffective because scum appeared at the fringes of the ceramic[377]. Meanwhile, in this study, adding 1wt% K_2CO_3 in the body composition removed the scum on both drying and firing and showed darker rims (brick red colour) on samples fired to 1040 and patches with additive increase discussed in **Chapter 8, section 8.1.1**.

One key advantage of using K_2CO_3 over other waste sources (olive pomace and sugarcane ash) of potassium oxide is the mechanical strength obtained. In this study, samples fired to 1000°C with 3wt% and 4wt% attained 95 and 98MPa suitable for a Class B engineering brick according to the BS EN 772-1. Moreover, samples fired to 1040°C, containing 1-4wt% of the additive, obtained 90 MPa,75 MPa,120MPa and 103MPa, respectively, all passing the class B engineering brick requirement. This identifies 1wt% K_2CO_3 could be the optimised limit for brick manufacturers. Although the olive pomace is a rich source of K_2CO_3, it is a fuel/ organic pore former[236,377] which means higher additive levels >5wt% will significantly decrease density and strength and promote high porosity. Mineralogically, the additive K_2CO_3 did not promote new phases not already identified in the Weald clay fired to 900°C and 1040°C (see **Figure 5-33 & 34**). This is because the alkali best works as a flux, and its reaction only promotes vitrification or the fusion of clay particles into a stronger bond on firing.

The literature has not reported the volume change using K_2CO_3 additive in clay bodies. This is not surprising because this phenomenon was only revealed by the dilatometry measurement of the second expansive change, which occurred in the clay body at temperatures above the quartz transition temperature of ~800°C (**Figure 5-37**). This was the same temperature the TG/Ms

revealed (**Figure 5-36**) on the CO_2 evolution from clay and K_2CO_3 mixture from 800-920°C. Therefore, we can infer that the expansion could be caused by releasing CO_2 from K_2CO_3 to form K_2O. There was no evidence from the microstructural studies (SEM- **Figure 5-85**) of micro-cracks caused by the volume change recorded with the dilatometry; this is possible due to the careful choice of the heating rate 60°/hr for the firing of the ceramics.

In place of using pure K_2CO_3, other waste streams from incinerators, olive pomace and sugarcane ash can be incorporated, but levels less than <5wt% are recommended for ceramic manufacture that requires increased strength [377,378].

5.16.7 *Na_2CO_3 additive effect in ceramic production*

One advantage of using the additive Na_2CO_3 other than the volatilization of CO_2 and H_2O is its non-destructive nature on kiln refractories and its vibrant colour on firing[379].

Findings from the study suggest that only 1wt% of the additive is useful for heavy clay ceramics. This is because 2-4wt% effloresced on drying and firing developed a matt and/or glossy coating on the ceramic surface(**Figure 5-56**). The water absorption for the matt and glossy surface ceramics was deficient (**Figure 5-50d**) because water could only be absorbed in the base of the ceramic not covered in glass. The coating also affected the compressive strength testing in that the brittle nature of the glass after the impact gave way to the complete collapse of the ceramic with low strengths. The unexpected finding obtained with the 1wt% additive was its non-surface stain after firing ceramics to 900 -1040°C, and the vibrant colour was achieved. This is consistent with the findings of Wasanapiarnpong et a.,l [380] reported that 1% Na_2CO_3 has the potential to stop scum by reacting with $CaSO_4$ to form insoluble salt; the reaction:

$$CaSO_4\,(aq) + Na_2CO_3\,(aq) \longrightarrow CaCO_3\,(s) + Na_2SO_4\,(aq)$$

Lower water absorption and increased strength were obtained with the Na_2CO_3 additive.

The additive's melting point is reportedly 851^oC[380], and the transformed phases were no different from the Weald clay Na_2SO_4 was also not identified with XRD. However, on visual examination, 1% Na_2CO_3 stopped surface scum.

This study has proved that incorporating 1wt% Na_2CO_3 fired to 1040°C in ceramic production may be the allowable or optimised level. Because it passed the BWA test and compression test for a class B engineering brick (BS EN 771-2011) because it causes molten materials to be created during the firing of bricks, which reduces porosity and compresses the interspaces[381] Since there is no change in the mineralogy, we could conclude that the introduction of Na_2CO_3 only functioned as a sintering aid.

Chapter 6 Additives Effect Of Industrial Waste Additive On The Sintering, Microstructure And Properties Of A Class B Engineering Brick

6.1 Series 2 Industrial waste additives (Background)

Industrial wastes introduced at 4wt% filter cake (F4W), 4wt% slurry dust (S4W), 4wt% Mineral wool (M4W), and 2wt% container glass powder (CG2W) were examined; using Chemical information, Thermal studies, Mercury intrusion porosimetry (MIP), Physical assessment (boiling water absorption) and Mechanical testing were conducted. Methods and experimental procedures are discussed in Chapter 3.

6.2 Sample Preparation

Series 2 additive composition is summarised in **Table 3-1.** Raw materials were separately dried in an oven at 120°C for 48hrs. 4 wt% was weighed and mixed with 96wt% dried clay, then milled in Retzsch vibratory disc mill for 1 minute at 800 rpm to produce a fine powder. This powder was mixed with 20-23ml distilled water (21%) to provide sufficient plasticity for shaping. A hydraulic press with 7 tonnes of pressure was applied to the 8.3g wet weight of the composition to form a 20 mm x 5 mm cylindrical pellet. After shaping, the green body dimensions were recorded in the "as-pressed" condition. Samples were left on a bench and dried in an electric laboratory oven (105°C) for approximately 36 hrs to eliminate free water gradually. The effect of additives on the brick property was studied by firing samples to 950°C and 1040°C at a 1°C/minute heating rate and holding for 2hrs at the maximum temperatures before cooling at the same rate in an electric laboratory furnace.

6.3 Chemical compositions of additives and fired clay bodies

In Series 2, four (4) industrial wastes were examined: container glass/cullet, mineral wool, slurry dust and filter cake. The analysed chemical compositions of industrial waste additives and the reformulated fired body have been obtained using X-Ray Fluorescence (XRF- fused bead technique), and the respective additive is shown in **Table 6-1**. Low-fired samples are summarised in **Appendix 2**. The result shows that the replacement additives do not contain chlorine which destroys kiln elements and promote greenhouse gas, except for oxide constituents present in the control material but in higher ratios (>6%)**.**

Container glass powder was rich in alkali and alkaline earth oxides that could help reduce sintering temperature (12% Na_2O, 11.5% CaO and 1.2% MgO) with less colourant - iron <0.3%. The total flux in container glass comes to 26%. The melting point of a simple soda lime silica glass is formed by melting batch materials between 1500-1600^oC [382]. Mineral wool, on the other hand, was high in CaO (23%) and MgO (8%) content with a total flux amounting to 33% (Na_2O+ MgO+ K_2O+ CaO) with low SiO_2 (39%). Slurry and filter cake supplied similar oxides to those indicated in mineral wool with 12% and 16% flux. Iron is responsible for the fired brick brownish red colour was found to be greater in filter cake (10.5%), slurry dust (8.5%), and mineral wool (7.6%) than in the control sample.

There was a decline in Fe in CG2W by 0.8%, 0.5% in M4W, and 0.4% in S4W and F4W when replaced with 2wt% or 4wt% Weald clay fired at 1040°C. 2wt% container glass tripled in iron content (i.e., from 0.4% -7.7%) from the clay minerals since only 2wt% was substituted for 98% of clay. SiO_2 increased by 2% (72.7%), whilst K_2O and TiO_2 remained constant at 2.2% and 1.5%, respectively.

The difference between mineral wool and the quarry wastes lies within the greater portion of CaO quantity (1.5%) due to the waste's original high CaO content of 24%. The ignition loss is

between 5.4% and 6% for mineral wool and quarry wastes, respectively. The total fluxing (K_2O+ CaO+ BaO+MgO+Ti_2O) content for each body (M4W, S4W and F4W) increases slightly, recording 6.4%. 5.5% and 5.4%, respectively. Oxides such as TiO_2 and K_2O remain stable for the three wastes.

Table 6-1: Analysed chemical information of weald clay, industrial additives and reformulated bodies fired to 1040°C.

Oxide	Clay	Industrial waste without Wealden clay				Industrial wastes in Wealden clay				
	Weald clay	Container glass	Mineral wool	Slurry dust	Filter cake	Fired Weald clay (1040°C)	CG2W (1040°C)	M4W (1040°C)	S4W (1040°C)	F4W (1040°C)
SiO_2	73.5	71.6	39.4	63.1	54.8	71.0	72.7	71.0	72.1	71.8
Al_2O_3	15.4	1.9	17.6	15.5	17.7	15.9	15.1	15.3	15.3	15.2
Fe_2O_3	6.1	0.4	7.5	8.6	10.1	7.7	6.90	7.2	7.1	7.1
Mn_3O_4	0.1	0.0	0.7	0.2	0.2	0.1	0.1	0.2	0.2	0.2
TiO_2	1.5	0.2	1.0	0.6	0.6	1.5	1.5	1.5	1.5	1.4
Na_2O	0.0	12.4	1.8	2.4	1.9	0.2	0.4	0.2	0.3	0.2
K_2O	2.2	0.7	0.4	1.1	2.2	2.3	2.2	2.0	2.1	2.1
MgO	0.5	1.2	7.3	3.2	4.6	0.6	0.5	0.9	0.7	0.7
CaO	0.3	11.5	23.7	5.3	7.6	0.4	0.6	1.5	0.6	0.7
P_2O_5	0.1	0.0	0.2	0.0	0.0	0.1	0.1	0.1	0.1	0.1
SrO	0.0	0.0	0.0	0.0	0.0	0.0	0.1	0.0	0.0	0.0
BaO	0.1	0.1	0.0	0.0	0.1	0.1	0.1	0.1	0.1	0.1
ZrO_2	0.0	0.0	0.0	0.0	0.0	0.1	0.0	0.1	0.1	0.1
SO_3	0.2	0.1	0.1	0.0	0.0	0.0	0.0	0.0	0.0	0.0
SUM (%)	100	100	100	100	100	100	100	100	100	100
LOI (%)	16.75	4.95	8.97	8.22	13.46	4.83	7.16	5.39	5.71	5.79

6.4 Crystalline phases present in the reformulated body containing 2wt% or 4wt% industrial additives compared to the control.

Reformulated body compositions containing 4wt% industrial waste additives (M4W, S4W and F4W) fired to 950°C and 1040°C are presented in **Figures 6-1 to Figures 6-2**.

Phases present in samples fired to 950°C generally contain quartz (SiO_2- 01-087-2096), dehydroxylated muscovite ($KAl_3Si_3O_{11}$ -00-046-0741) and hematite (Fe_2O_3-01-076-4579) for M4W, S4W and F4W. However, diopside ferroan ($Ca_{0.92}Fe_{0.08}Al_{0.14}Fe_{0.33}Mg_{0.53}Si_2O_6$- 01-074-2424) was not present with F4W and S4W samples except for microcline ($Al_1K_1O_8Si_3$ -01-084-0709).

The diffraction pattern of samples (M4W, S4W and F4W) fired to 1040°C were found to be present with mullite ($Al_{2.25}Si_{0.75}O_{4.875}$ -04-016-1586), hematite (Fe_2O_3-01-076-4579), microcline ($KAlSi_3O_8$ 01-084-0709) and quartz (SiO_2- 01-087-2096). Diopside ferroan ($Ca_{0.92}Fe_{0.08}Al_{0.14}Fe_{0.33}Mg_{0.53}Si_2$ O_6- 01-074-2424) remains even at 1040°C but with increased intensity for M4W. Anorthite ($CaAl_2Si_2O_8$) was only present in the M4W sample. See **Figure 6-2**. Hematite peak increases in intensity for all samples.

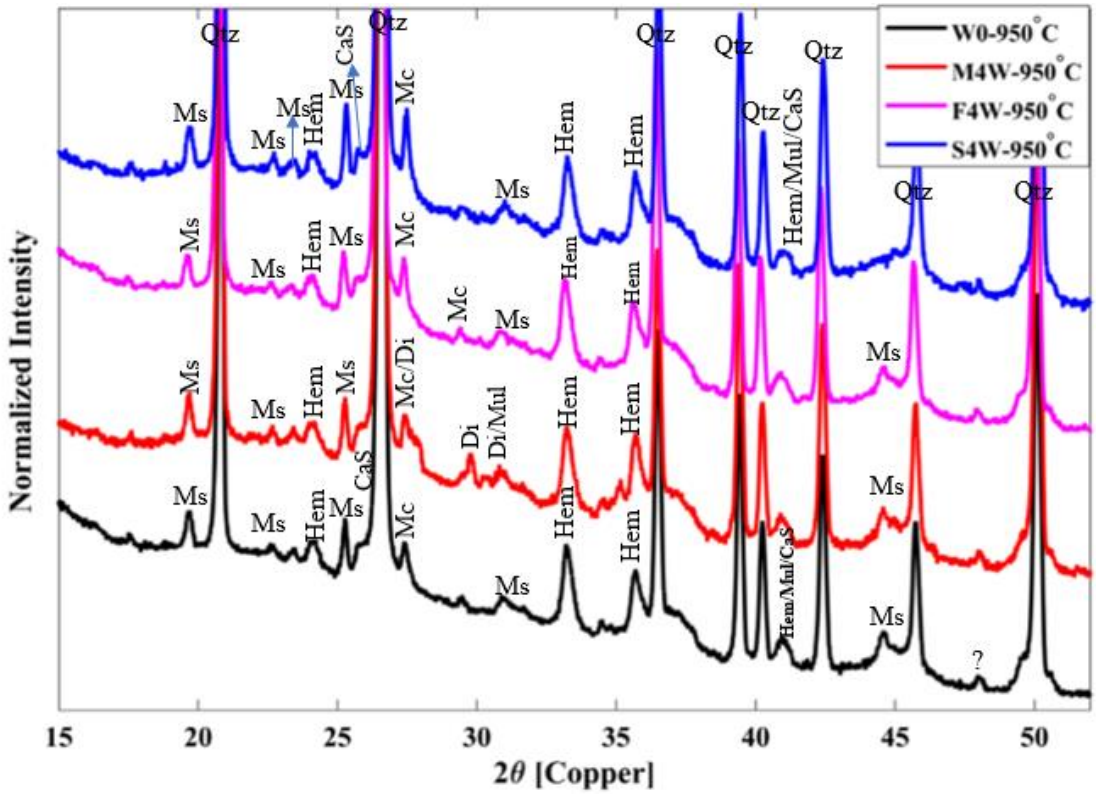

Figure 6-1: XRD pattern of 4wt% industrial waste additives compared to 100% Weald clay fired at 950ºC. Mineral symbols after Kretz, 1983: Qtz=Quartz (SiO_2), Ms=Muscovite ($KAl_3Si_3O_{11}$), Hematite (Fe_2O_3), Mc=Microcline ($Al_1K_1O_8Si_3$) Di=Diopside ferroan ($Ca_{0.92}Fe_{0.08}Al_{0.14}Fe_{0.33}Mg_{0.53}Si_2\ O_6$) CuKa X-ray radiation 1= 1.5406 Å.

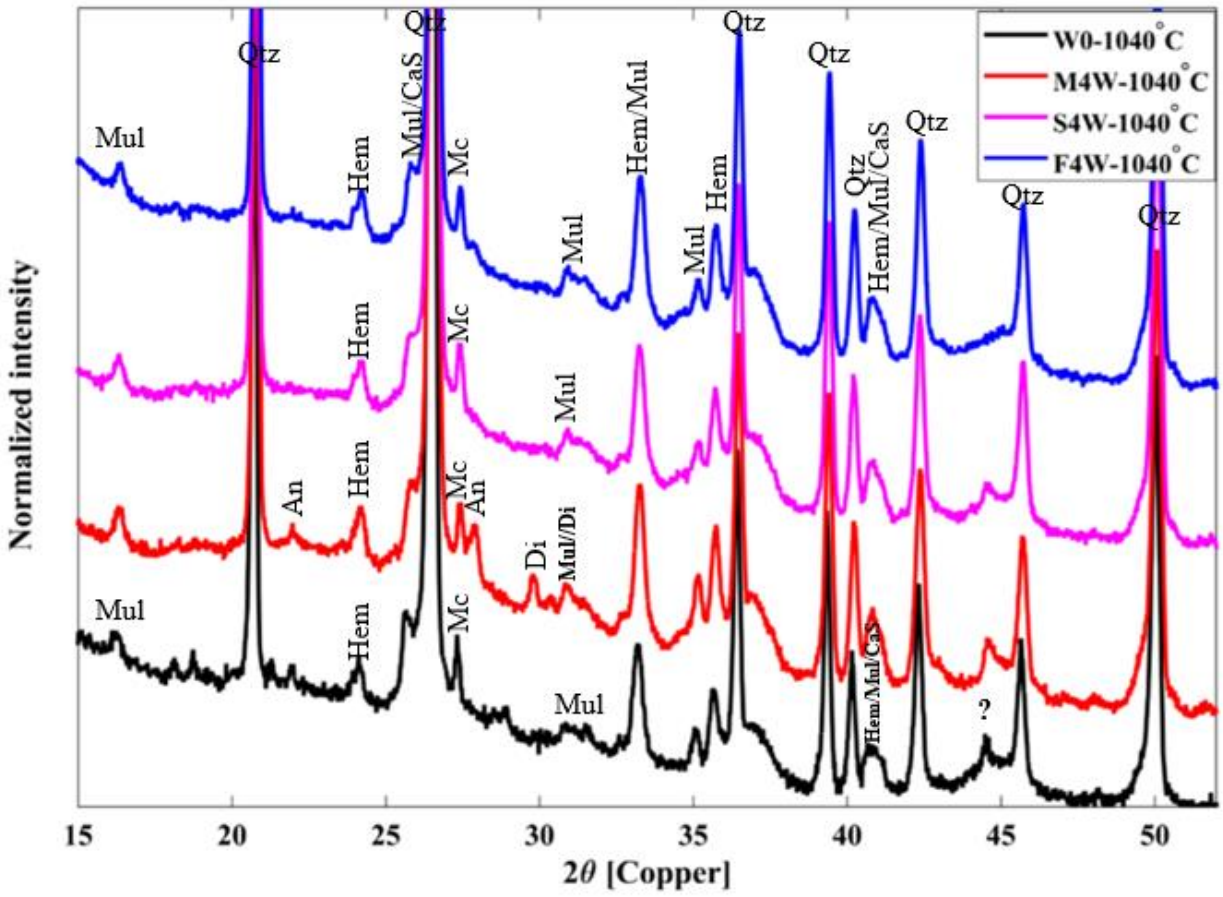

Figure 6-2: XRD pattern of 4wt% industrial waste additives (M4W, S4W and F4W) fired to 1040°C compared to 100% clay. Mineral symbols after Kretz 1983[343]: Qtz=Quartz (SiO_2), Hematite (Fe_2O_3), Di= Diopside ferroan ($Ca_{0.92}Fe_{0.08}Al_{0.14}Fe_{0.33}Mg_{0.53}Si_2\ O_6$), Mul=Mullite ($Al_{2.25}Si_{0.75}O_{4.875}$), An=Anorthite($CaAl_2Si_2O_8$)and Microcline ($Al_1K_1O_8Si_3$) CuKa X-ray radiation 1= 1.5406 Å.

6.4.1 *The container glass waste*

As the name suggests, waste from crushed bottled glass with <150µm powder particles was analysed using the cobalt tube, whose wavelength was 1.79Å longer than that of copper (1.54Å). The data collected in **Figure 6-3** shows the material is amorphous. The two peaks between 32°-38° may be impurities which could not be detected. The phases obtained with clay samples containing 2wt% cullet fired to 950°C are albite calcian ($Al_{1.46}Ca_{0.347}Na_{0.685}O_8Si_{2.54}$ - 01-083-

1939), dehydrated muscovite ($KAl_3Si_3O_{11}$ - 00-046-0741), hematite (Fe_2O_3- 04-005-4630), mullite ($Al_{2.26}Si_{0.74}O_{4.87}$ -04-016-1587) and quartz (SiO_2 - 01-087-2096).

Samples fired at 1040°C show the presence of quartz (SiO_2 - 01-087-2096), hematite (Fe_2O_3- 04-005-4630) and mullite ($Al_{2.26}Si_{0.74}O_{4.87}$ - 04-016-1587) meaning the waste glass promotes the formation of mullite at lower temperatures which was not observed with the other industrial wastes. Sahar et al.[383] reported that cullet-clay ceramics doped with high levels of cullet (>40-80%) fired to 900°C phases developed were Aluminium oxide, tridymite and quartz different from the composition reported in this current study, possibly due to its higher cullet.

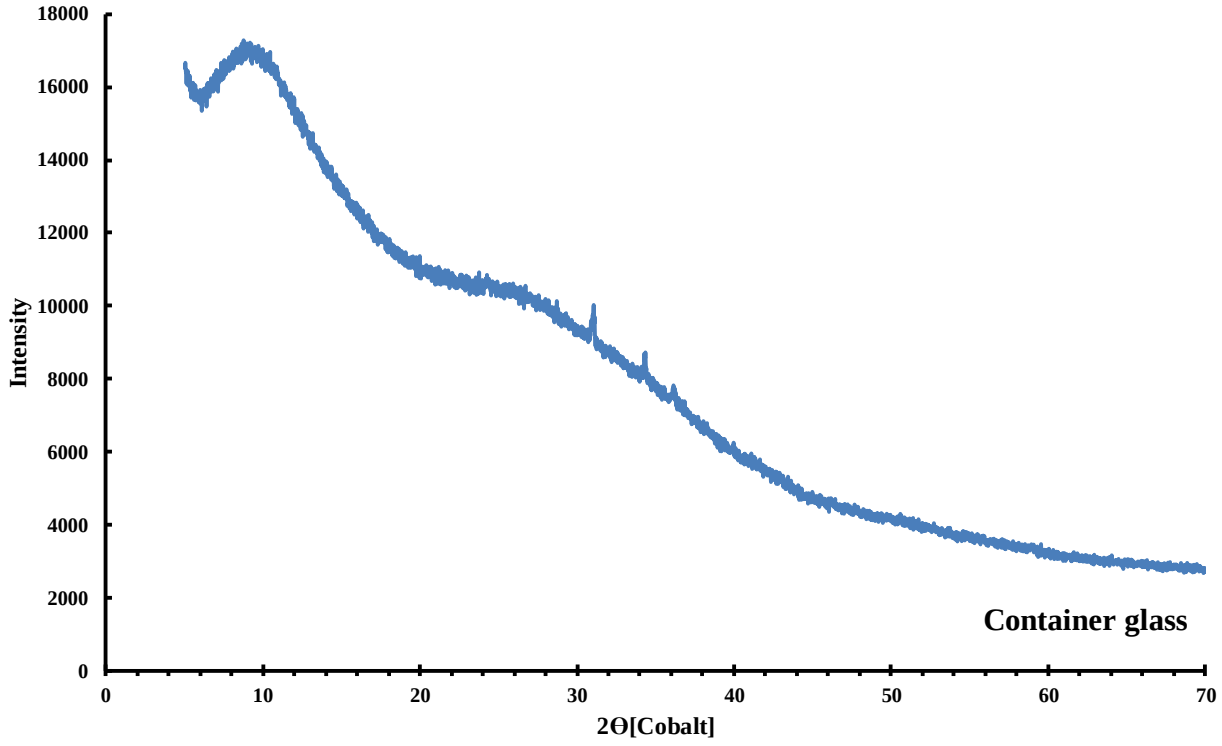

Figure 6-3: XRD pattern of container glass powder collected using cobalt source.

6.5 Thermal behaviour of Industrial wastes additives without clay

Figures 6-4 and **Figure 6-5** show the changes in heating industrial wastes and the volatiles in the replacement material. Total weight loss is summarised in **Table 6-2.**

The industrial wastes show three main stages in the derivative of the TG curves compared to the control (dehydration and dehydroxylation of clay minerals along with the decomposition of carbonates and organics). The reaction becomes irreversible once measured additives hit the decomposition temperature (above 600°C).

The mineral wool's temperature for decomposition is between 230°C-620°C, which falls slightly above the decomposition of carbonaceous matter in control see mass spectroscopy (**Figure 6-6**) analysis for mineral wool. At 750°C, there seems to be a phase change attributed to the melting of mineral wool. The total mass loss recorded is 2.98%. The thermal behaviours of the quarry wastes (slurry dust and filter cake) are different, i.e., the big peaks are at different temperatures. After the first phase of absorbed water removal, the gradual decomposition of the chemical constituents in the quarry wastes occurs at temperatures greater than 450°C and is completed at 780°C. The mass change was associated with physical water, chemical water (OH) and CO_2 shown with the Mass spectroscopy. Total weight loss recorded is 3.77% and 7.08% for slurry dust and filter cake, respectively. The difference in this mass loss lies within the total flux obtained from the chemical analysis. Moreover, further removal of the OH groups comes off at 900°C for the quarry wastes, slurry dust and filter cake only. This suggests carefully removing moisture from the composition when Weald clay is replaced with slurry dust.

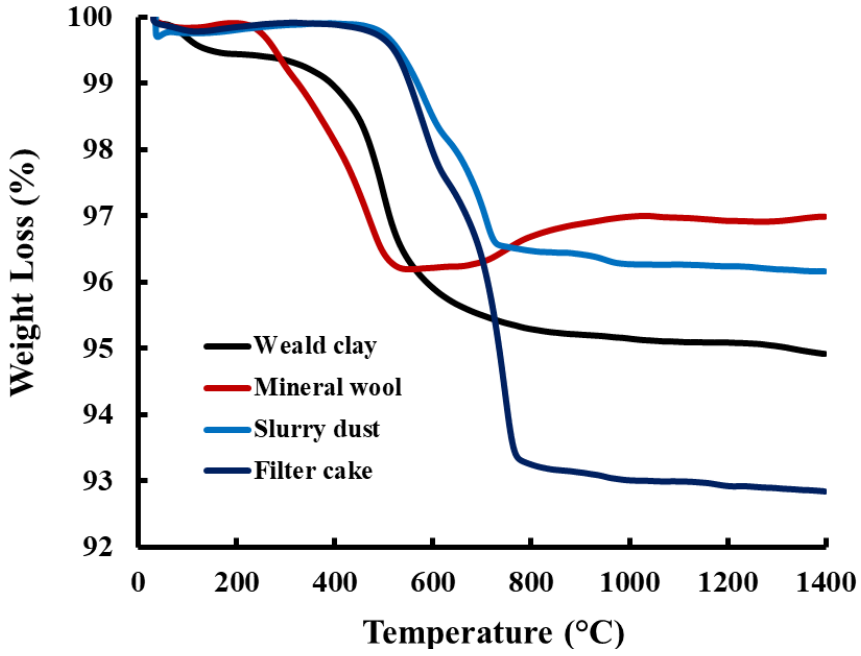

Figure 6-4: Thermogravimetry analysis (TGA) of industrial wastes compared to Weald clay fired from 35°C -1400°C at 10°/min in an alumina crucible.

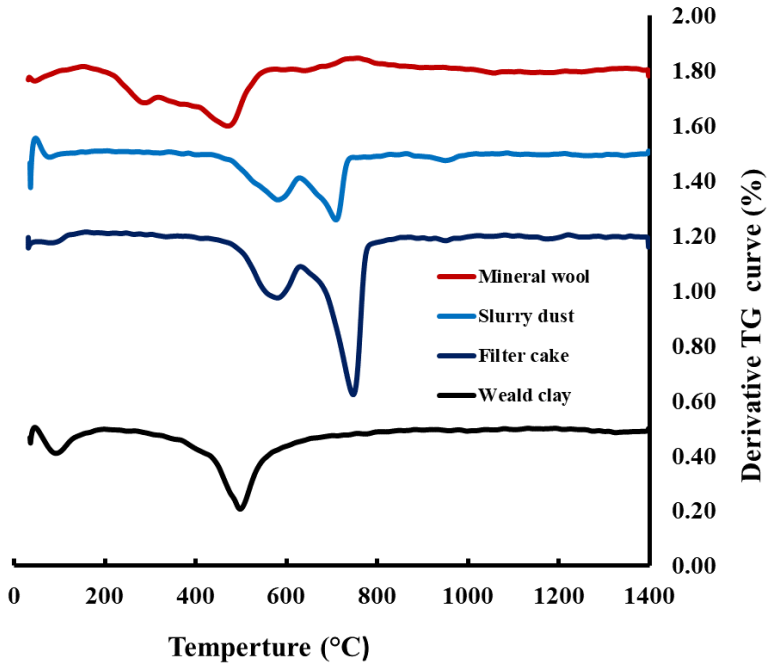

Figure 6-5: Derivative of thermogravimetry analysis (DTG) of industrial wastes compared to Weald clay fired from 35°C -1400°C at 10°/min in an alumina crucible.

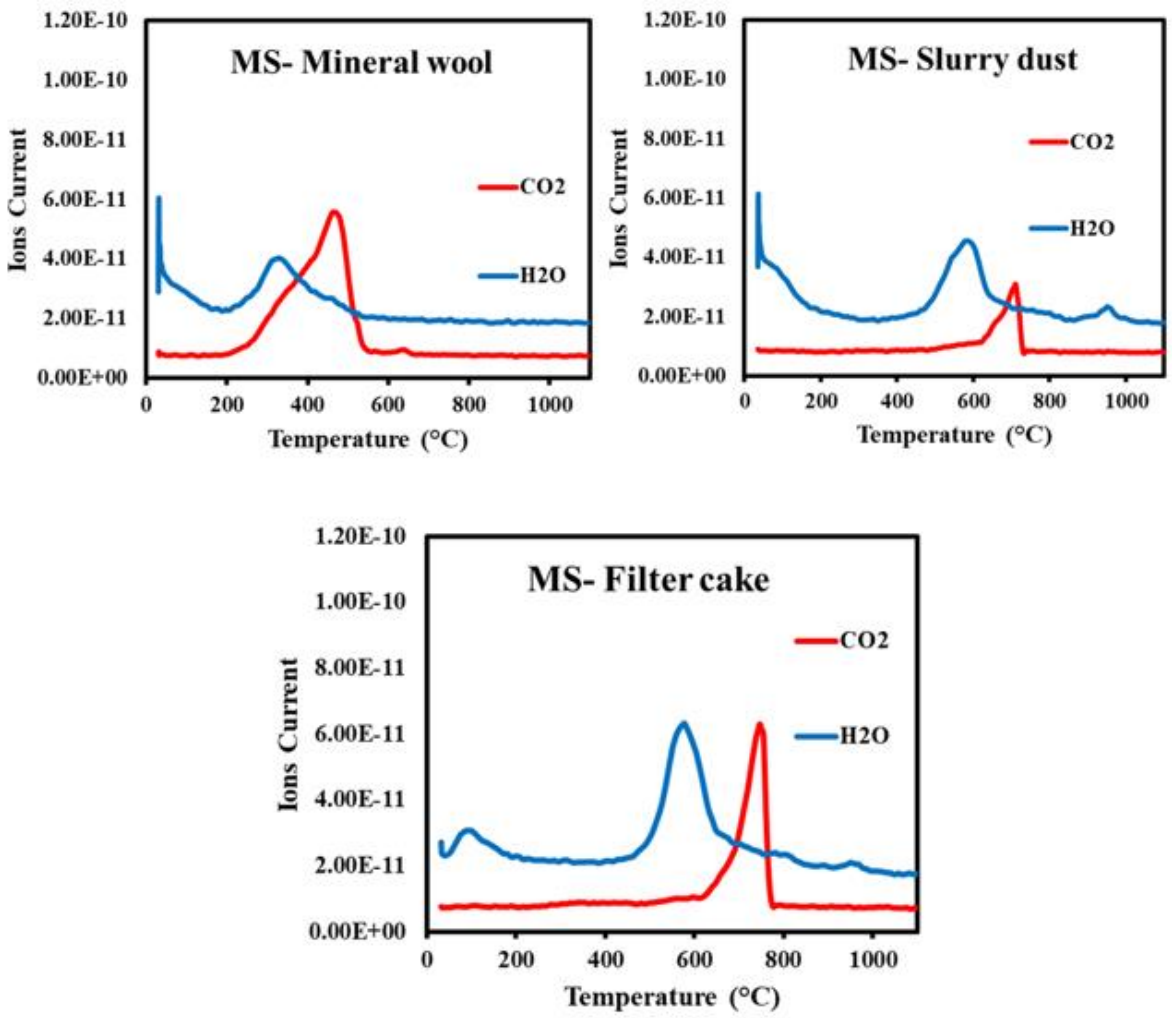

Figure 6-6: Mass spectroscopy of 4wt% industrial waste composition fired from 35°C -1400°C at 5°/min in an alumina crucible.

Table 6-2: Summary of additive weight loss

Sample ID	T. Weight Loss (%)
Mineral wool	**2.98**
Slurry dust	**3.77**
Filter cake	**7.08**

6.5.1 *Thermal behaviour of 4wt% industrial wastes replaced with weald clay*

When 4wt % quarry wastes are added to Weald clay, the thermal curve does not change compared to base clay. **Figure 6-7**; the total weight loss differs with quarry wastes and mineral wool. Filter cake (F4W) marked the highest mass loss of 7.43% and 6.91% for slurry dust (S4W). However, a loss of 5.09% was recorded for mineral wool due to the airy texture of the additive. The light weight of the additive means that the weighted volume of 4wt%, in a practical sense, is more than the quarry wastes for its high SiO_2 content.

2wt% container glass additive (CG2W) recorded the lowest weight loss of 4.95%, explained as the volatiles in CG2W were already burnt off during glass making. The mass spectroscopy result illustrated in **Figure 6-8** shows three different volatiles: absorbed, chemical water removal (endothermic reaction) and CO_2. It should be noted that extra CO_2 is removed from the mass after 600°C for the quarry wastes.

The DTA curves in **Appendix 1b** show a broad exothermic peak between 300-560^{o}C corresponding to the dehydroxylation of clay mineral kaolinite and illite[357] and an endothermic peak at 573^{o}C is a result of quartz transition, which was not present in the DTG.

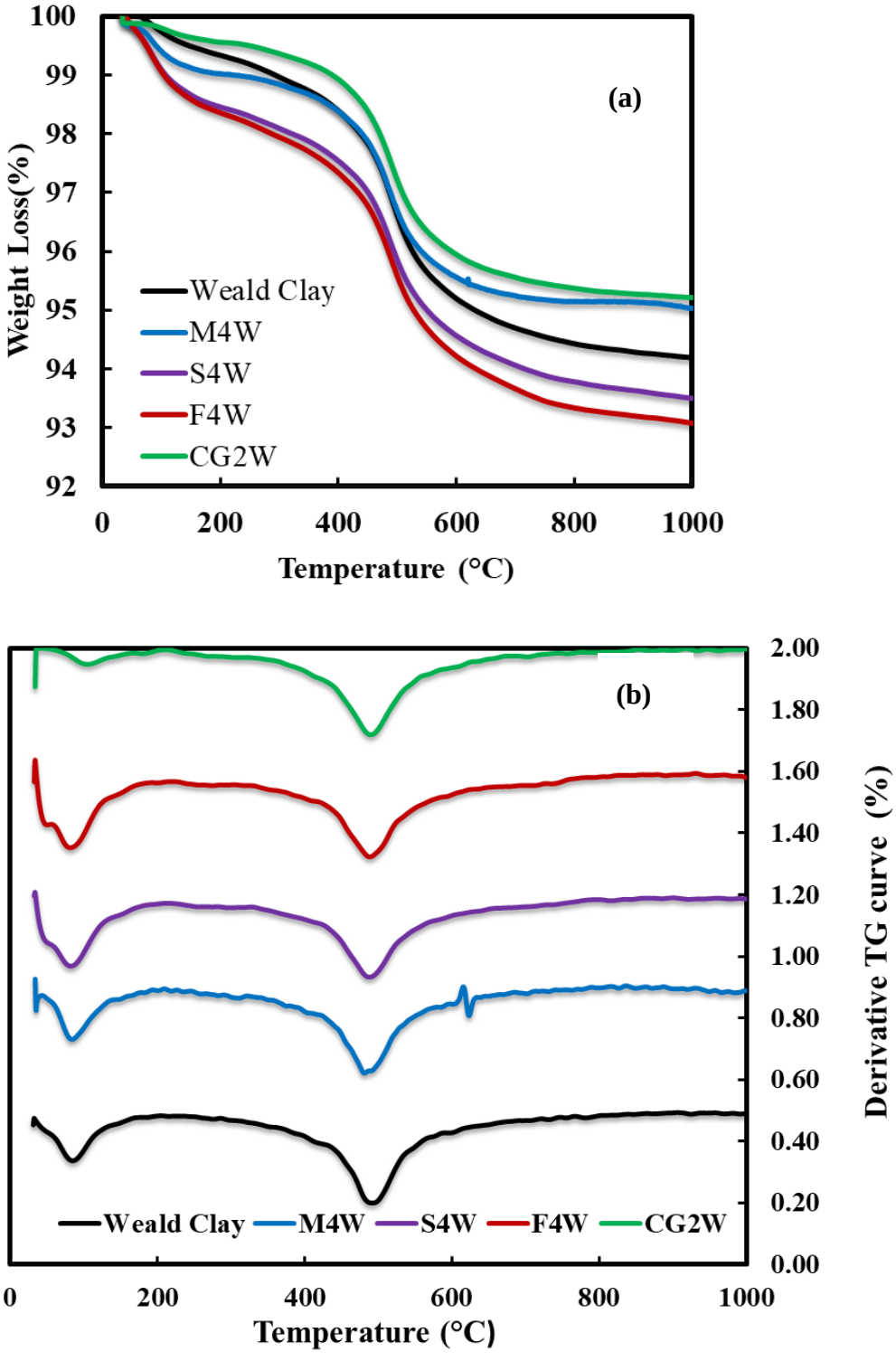

Figure 6-7: TGA and DTG of 4wt% industrial wastes (filter cake-F4W, slurry dust -S4W, mineral wool-M4W) and 2wt% container glass powder- CG2W compared to the control fired from 35°C -1400°C at 10°/min in an alumina crucible.

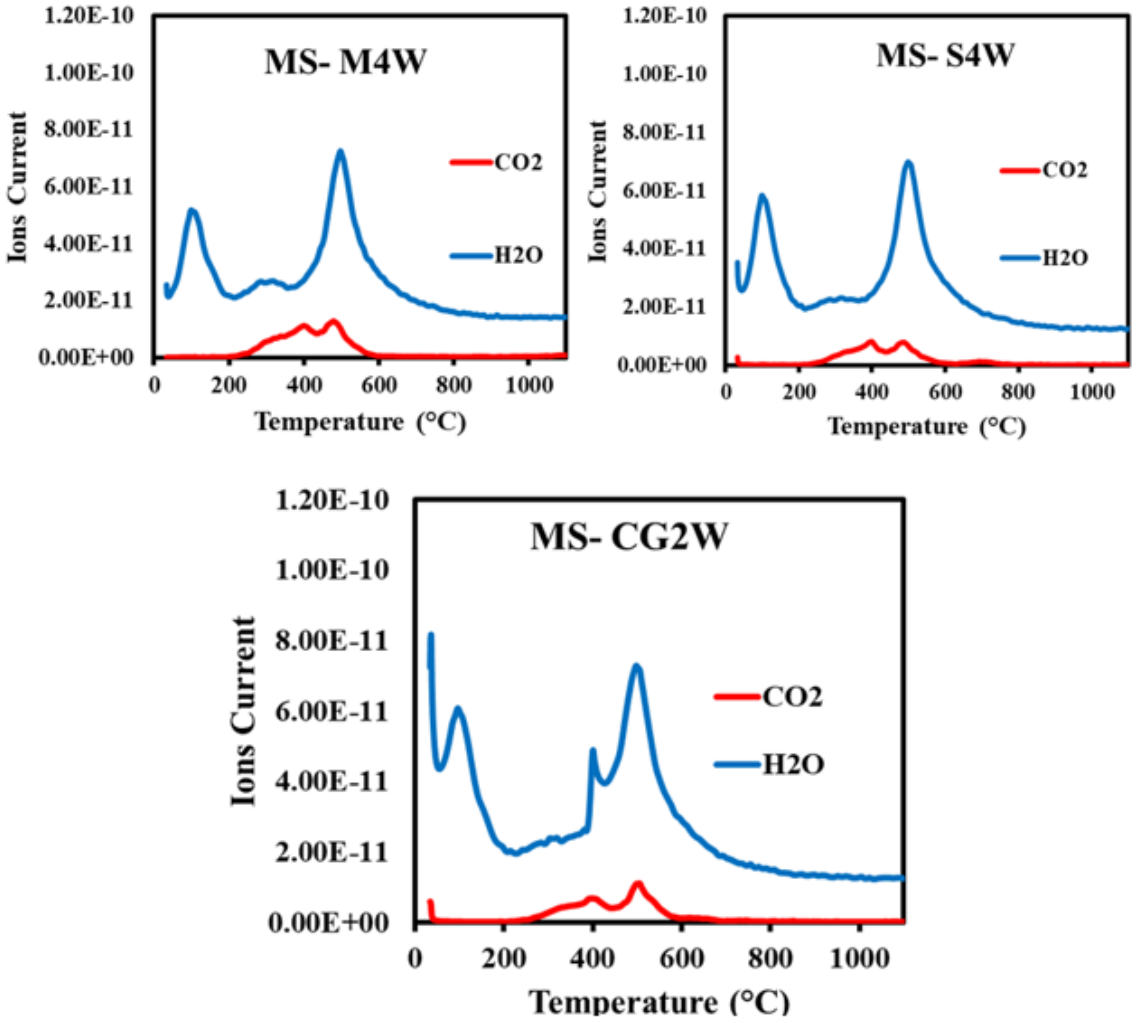

Figure 6-8: Mass spectroscopy of reformulated bodies containing industrial wastes fired from 35°C -1400°C at 10°C/min in an alumina crucible.

6.5.2 *Dilatometry analyses of industrial wastes*

Dimensional changes in additive effect with 2wt% or 4wt.% of industrial waste replacement in Weald clay are presented in **Figures 6-9** and **6-10**.

The reformulated body loses water at lower temperatures (35-300°C), causing the first shrinkage followed by the decomposition of clay minerals (450°C-550°C), then a gradual but sharp distinctive expansion due to α-β quartz inversion at 581°C. After this expansion plateaus,

the sample begins to shrink due to sintering effects. This was similar for the three (3) wastes, but the difference is more visible than the control. Shrinkage is active at 600°C with rapid shrinkage starting at 820°C to 1000°C, at dL/Lo, which is at zero (0°C) for the control. Rapid shrinkage or second shrinkage temperatures recorded for the additives began at 992°C for M4W, 822°C for S4W and finally 820°C for F4W with its linear shrinkages given in **Table 6-3**.

It is also interesting to note that M4W has the potential to reduce firing temperature by 20°C and up to 22°C and 35°C for filter cake and slurry dust.

For the sample containing 2wt% container glass, the linear shrinkage was found to be 2.7% and the reduction in sintering temperature to be 34°C. This means the body can be fired to 34°C lower but may not get the same mechanical strength as the control.

Table 6-3: Linear shrinkage and reduction in sintering temperature with 2wt% or 4wt% additive in weald clay at a heating rate of 5°/min.

Sample ID	Reduction in Sintering Temp (°C)	Linear shrinkage (%)
W0	0	2.3
M4W	20	2.5
F4W	22	2.7
S4W	35	2.5
CG2W	34	2.7

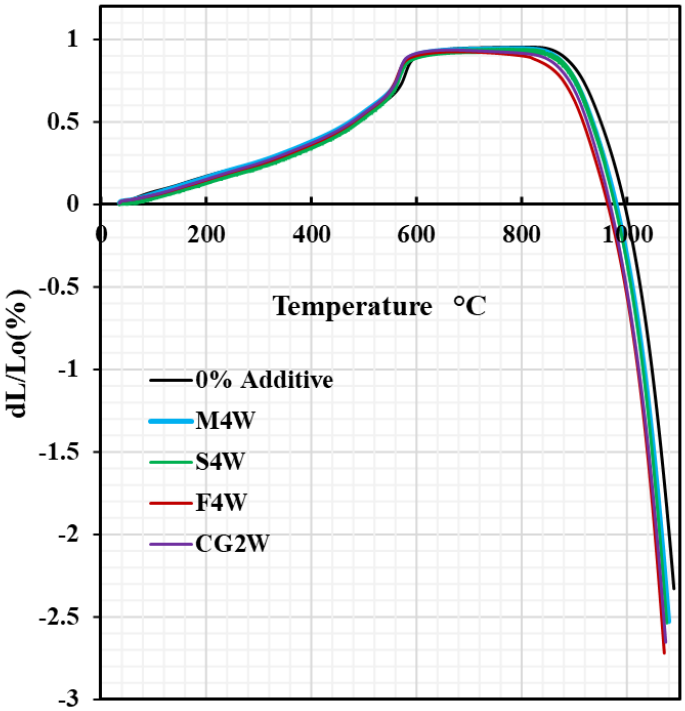

Figure 6-9*:* Comparable dilatometry curves of 100% Weald clay, 2wt% container glass wastes,4wt% quarry wastes and 4wt% mineral wool fired at a heating rate of 5°C/min.

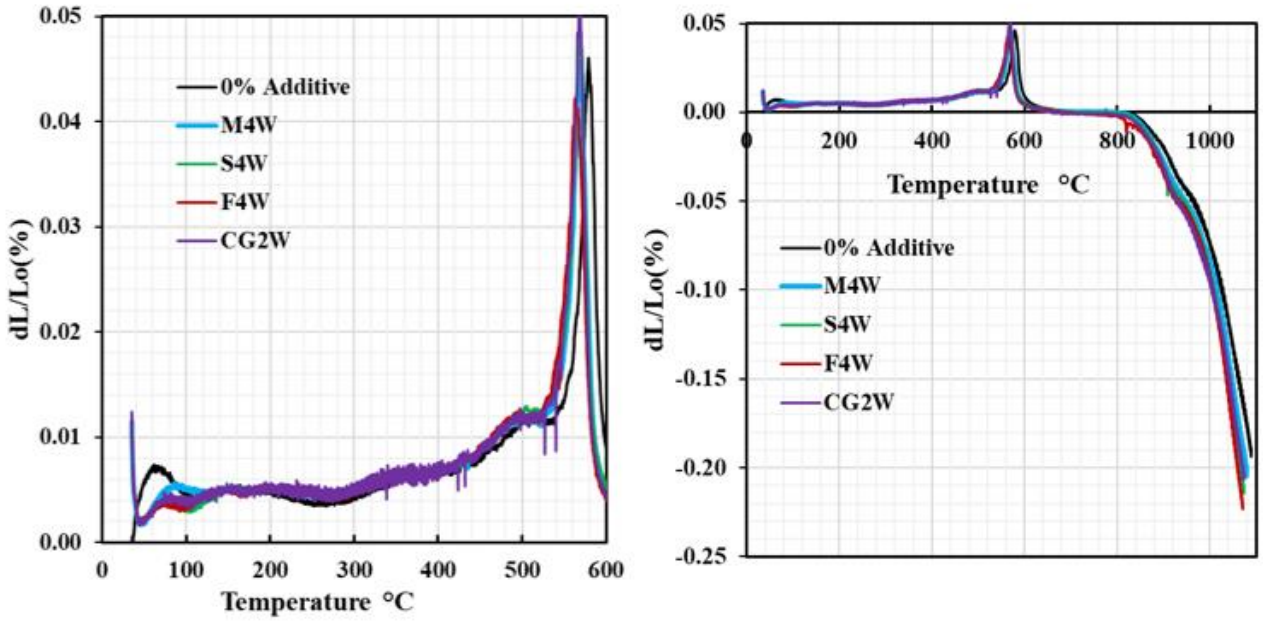

Figure 6-10: Comparable derivative dilatometry curves of 100% Weald clay, 2wt% container glass waste, 4wt% quarry wastes and mineral wool fired at a heating rate of 5°C/min.

6.6 Images of fired specimen

After firing reformulated bodies with industrial wastes, all the fired ceramic bodies had fixed scum on the sample surface. The intensity of the scum was seen to be dependent on the temperature, as presented in **Table 6-4**. Mineral wool provided the most staining whitish scum because of the body's high CaO (1.5%) compared to slurry dust, filter cake, container glass, and base clay.

.

Table 6-4: Fired images of industrial wastes compared to the control

Body Composition(s)	Firing temperature (°C)	
	1040°C	950°C
100% Clay (W0)	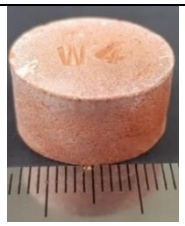	
4wt% Mineral wool waste (M4W)		
4wt% Slurry dust waste (S4W)		
4wt% Filter cake waste (F4W)		
2wt% Container glass waste (CG2W)		

6.7 Technological properties of additive effects

6.7.1 *Volumetric shrinkage*

Generally, higher temperatures provide a higher degree of shrinkage, although replacements can influence shrinkage.

Figure 6-11 shows shrinkage is higher than the control when clay with additives is fired to 950°C. Except for the 2wt% container glass (CG2W), shrinkages for M4W, F4W and S4W levels are lower than the raw clay when fired at 1040°C.

For samples fired to 1040°C, 2wt.% container glass (CG2W) records the highest shrinkage due to the ground glass's low viscosity and higher flux content. The container glass volumetric shrinkage is at least twice that of the base clay, the mineral wool (M4W) and the quarry wastes (S4W and F4W). The second highest shrinkage recorded was the base clay scoring 9.8%, followed by M4W with 9% volumetric shrinkage and 8% for the quarry wastes.

6.7.2 *Boiling water absorption testing (BWA).*

In **Figure 6-12,** for samples fired to 950°C, the boiling water absorption is around 12% for M4W, S4W and F4W, with container glass(CG2W) being 0.3% higher than the base clay (12.2%). For samples fired to 1040°C, F4W records the lowest absorption of 8.4%, followed by CG2W and F4W with 8.6%, and the highest absorbed sample was S4W (8.7%).

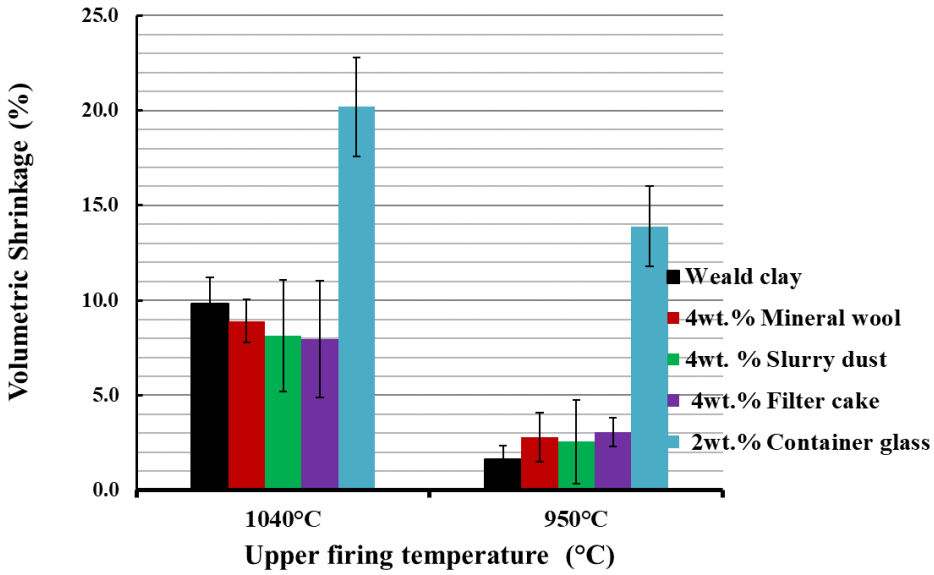

Figure 6-11: Volumetric shrinkage of 4wt.% industrial wastes (mineral wool (M4W), slurry dust (S4W) and filter cake (F4W) and 2wt% Container glass (CG2W).

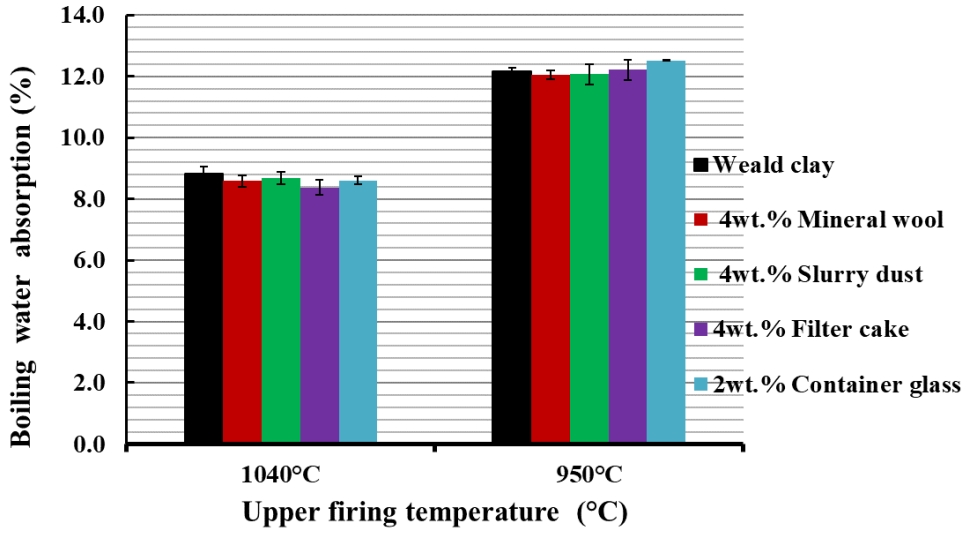

Figure 6-12: Boiling water absorption of 4wt.% industrial wastes (Mineral wool (M4W), Slurry dust (S4W) and filter cake (F4W) and 2wt% Container glass (CG2W).

6.8 MIP analyses

The differential intruded volume vs pore diameter is shown in **Figures 6-13** and **Figure 6-14.** The pore size distribution of reformulated body composition fired at 950°C was high in total Hg (%) compared to samples fired at 1040°C (**Figure 6-15)**. At 950°C, CG2W pore size was 0.01 µm – 0.07µm with 17.66% of the total intrudable mercury. M4W, S4W and F4W have a critical pore size (maximum continuous pores) of 0.05 µm, just like the base clay. Although the remaining additives showed more small pores, the total attainable porosity % recorded was >18.26%, except for M4W at 18.02%.

Samples fired to 1040°C showed pore sizes shifting towards the larger pore or (macro) pore sizes up to 1 µm for Weald clay and > 1 µm for the additives. This shift was attributed to the temperature at which ceramics were fired (900 /1040ºC).

Interestingly, F4W recorded the least intrudable percentage at 1040°C with 13.82%, followed by 14.12% CG2W. The remaining additives, M4W and S4W, total intrudable porosity, were above 14.19%, summarised in **Table 6-5.**

Table 6-5: Summary of intrudable porosity of reformulated body containing industrial waste.

Sample ID	Samples fired to 950°C Total Porosity (%)	Samples fired to 1040°C Total Porosity (%)
W0	20.41	18.30
CG2W	17.66	14.12
M4W	18.02	14.55
F4W	18.26	13.82
S4W	18.32	14.36

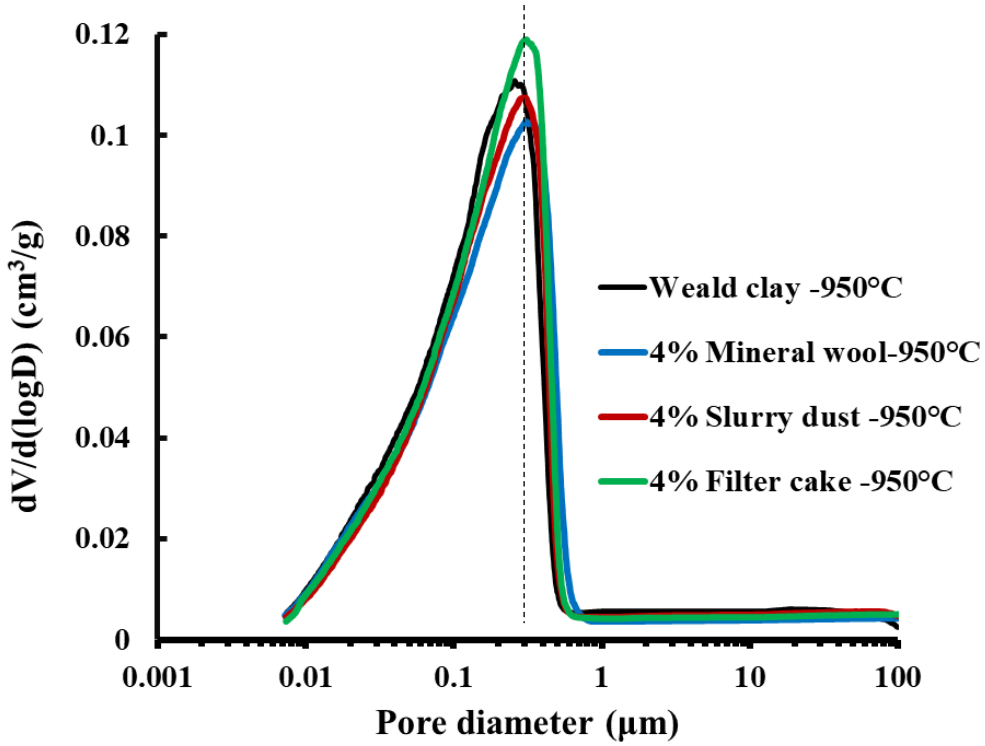

Figure 6-13: Mercury intrusion porosity of 4wt % mineral wool, filter cake and slurry dust fired to 950°C.

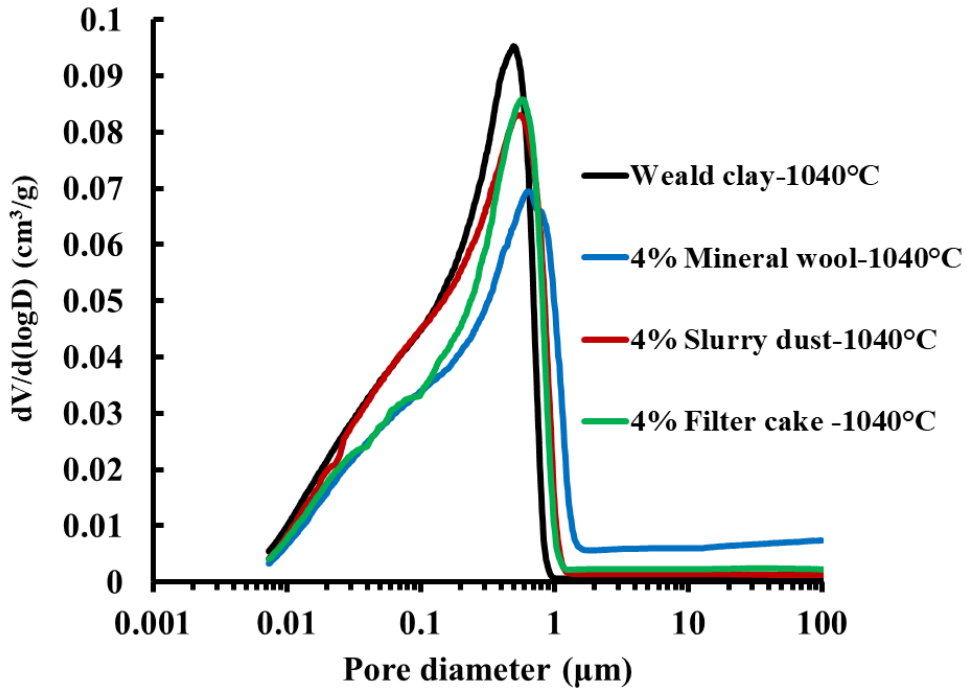

Figure 6-14: Mercury intrusion porosity of 4wt % mineral wool, filter cake and slurry dust fired to 1040°C

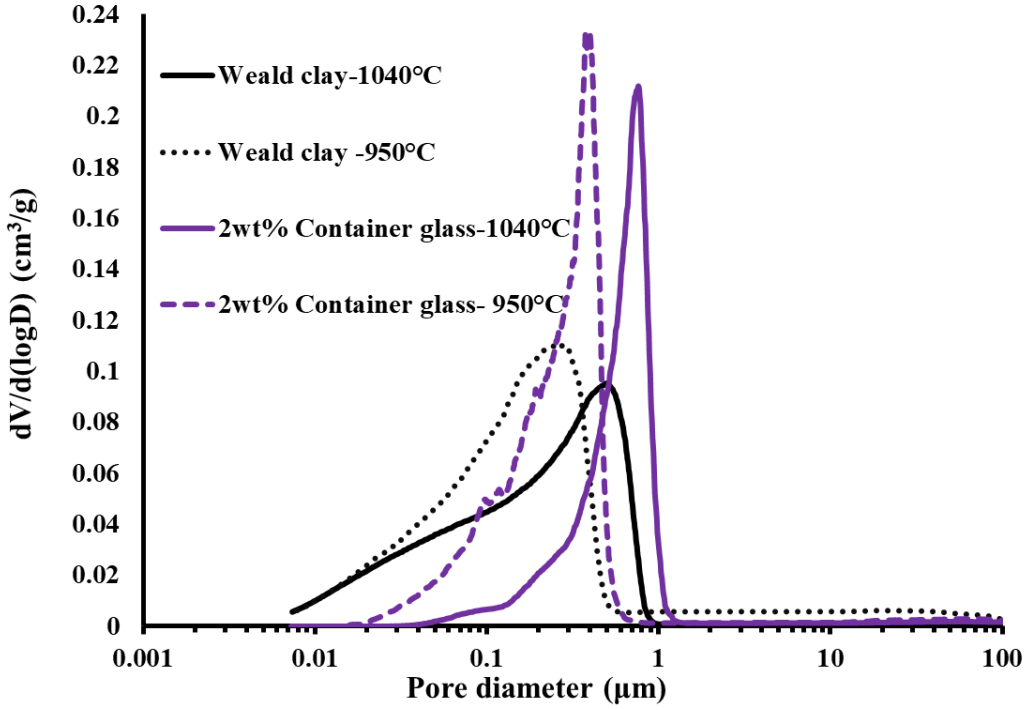

Figure 6-15: Mercury intrusion porosity of 2wt % container glass fired to 950°C and 1040°C.

6.8.1 *Predicting industrial wastes admixture durability using the Maage equation*

Durability factor prediction for industrial waste additives (mineral wool, slurry dust, filter cake and 2wt% container glass) fired to 950°C and 1040°C failed with values below 55 except for 4wt% filter cake fired to 1040°C, which lies in the uncertainty region. The results are shown in **Appendix 3**.

6.9 Mechanical assessment of industrial wastes additive samples.

Mechanical strength (compression) obtained by incorporating 4wt% mineral wool, quarry wastes (S4W and F4W) and 2wt% container glass waste fired to 950°C and 1040°C is shown in **Figure 6-16**. The graph shows a reduction in strength from 54 MPa (Control) to 49MPa and 42MPa for mineral wool and quarry waste (F4W and S4W), respectively, compared to the control for samples fired to 950°C. Meanwhile, CG2W had the least strength, 39MPa, compared to the remaining additives and the control.

Samples fired to 1040°C also saw a significant decline in strength when compared to the control. CG2W sample marked the highest compressive strength with 58MPa, followed by M4W (53MPa), but S4W and F4W scored 46MPa and 43MPa, respectively, compared to 81.5% for the control.

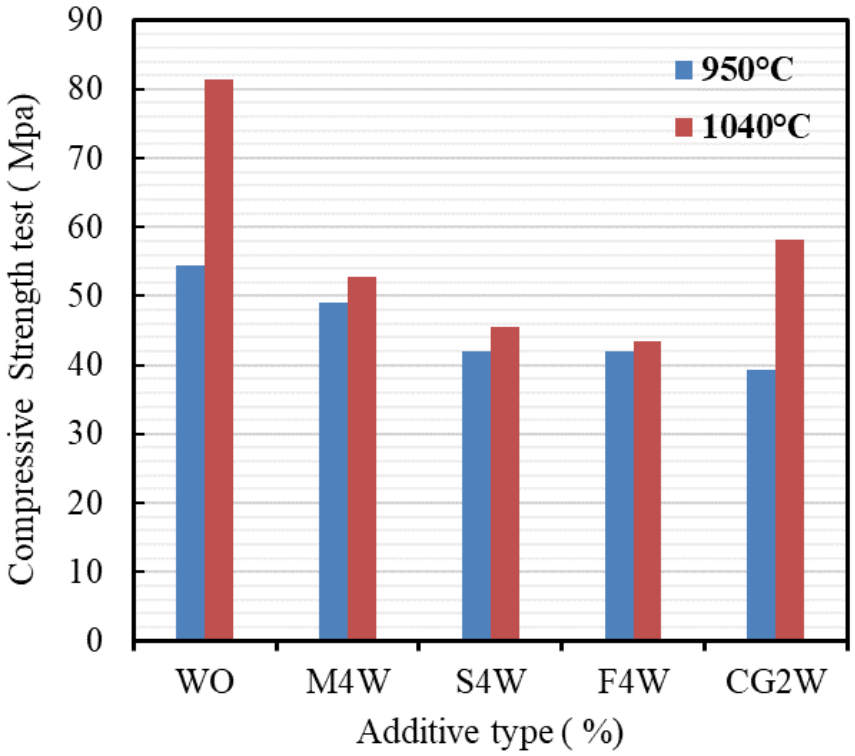

Figure 6-16: Effect of temperature and additive on Weald clay body strength incorporated with 2wt% and 4wt% industrial wastes additives fired to 950°C and 1040°C. where WO= Control, M4W= 4wt% mineral wool, S4W= 4wt% Slurry dust, F4W= 4wt% filter cake and CG2W= 2wt% Container glass waste. Error margin ±2-8 (MPa) and ±0.2 (Boiling water absorption test)

6.10 Scanning electron microscopy -SEM

Container glass examined using the SEM shows 3 different particle sizes. A low concentration particle ranging from 100-150µm, a high concentration ranging from 25-100µm and a small concentration of medium particles ranging from 10-25µm. Larger particles are platelet with fewer sharp shards. This is shown in **Figure 6-17.**

Reformulated bodies, including 2wt% and 4wt% industrial wastes (mineral wool, slurry, filter cake and cullet wastes) fired to 950°C and 1040°C **(Figure 6-18** and **Figure 6-19)** were examined to see the effect on the microstructure; the following was discovered:

At 950^{o}C, 2wt% Container glass (GC2W) has sintered. Composition containing 4wt% mineral wool (c) has started sintering with few individual particles compared with the control, 4wt% Slurry dust (d) and 4wt% Filter cake (e). At 1040^{o}C, the 4wt% mineral wool sample (Figure 6-19c) has compressed pores sharper at the ends at the top/ bottom than container glass (b), slurry dust and filter cake sample. What is familiar with samples fired to 1040°C are the well-defined pore and a well-interconnected structure.

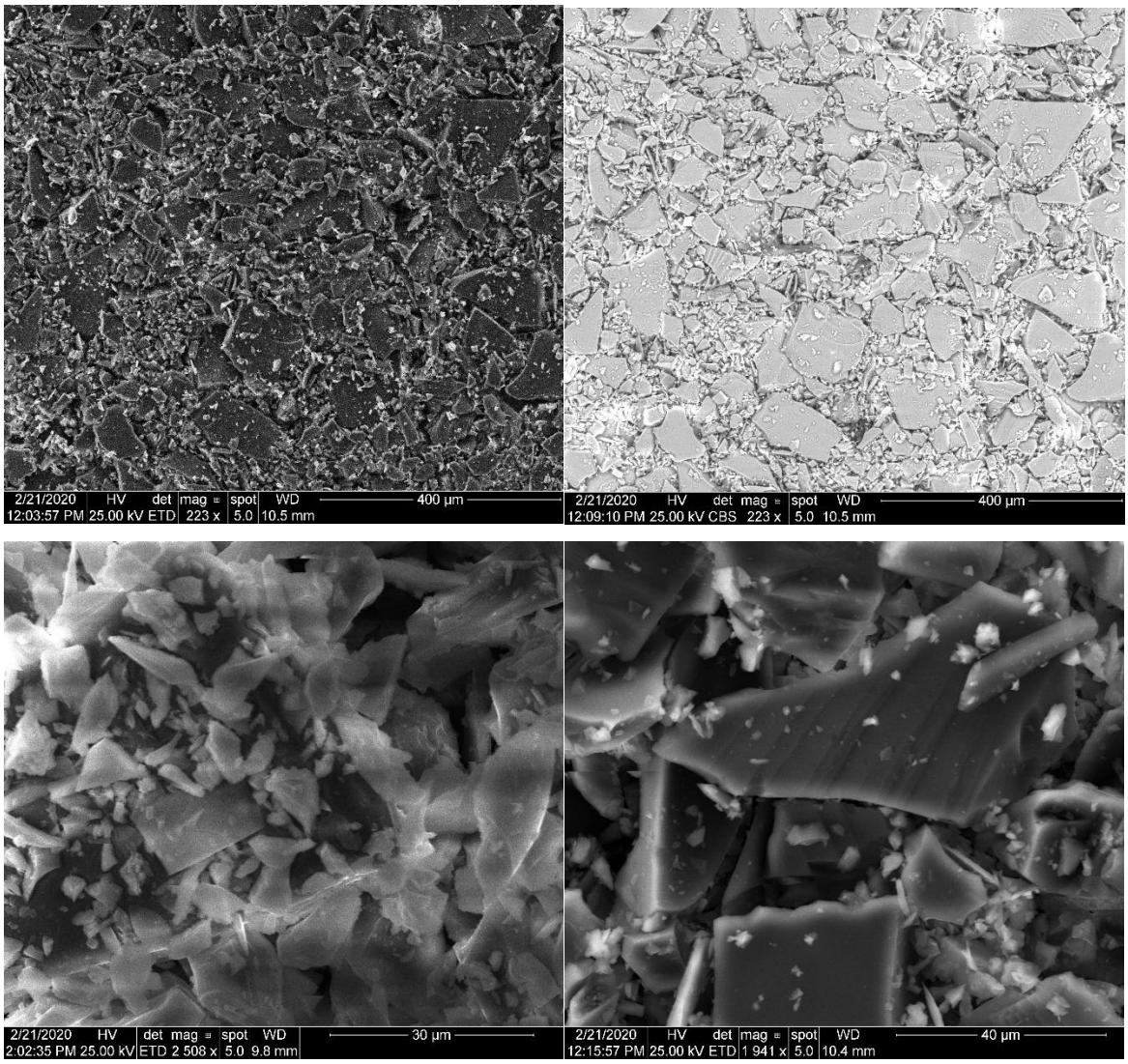

Figure 6-17: SEM and BSE of <150µm particle size container glass.

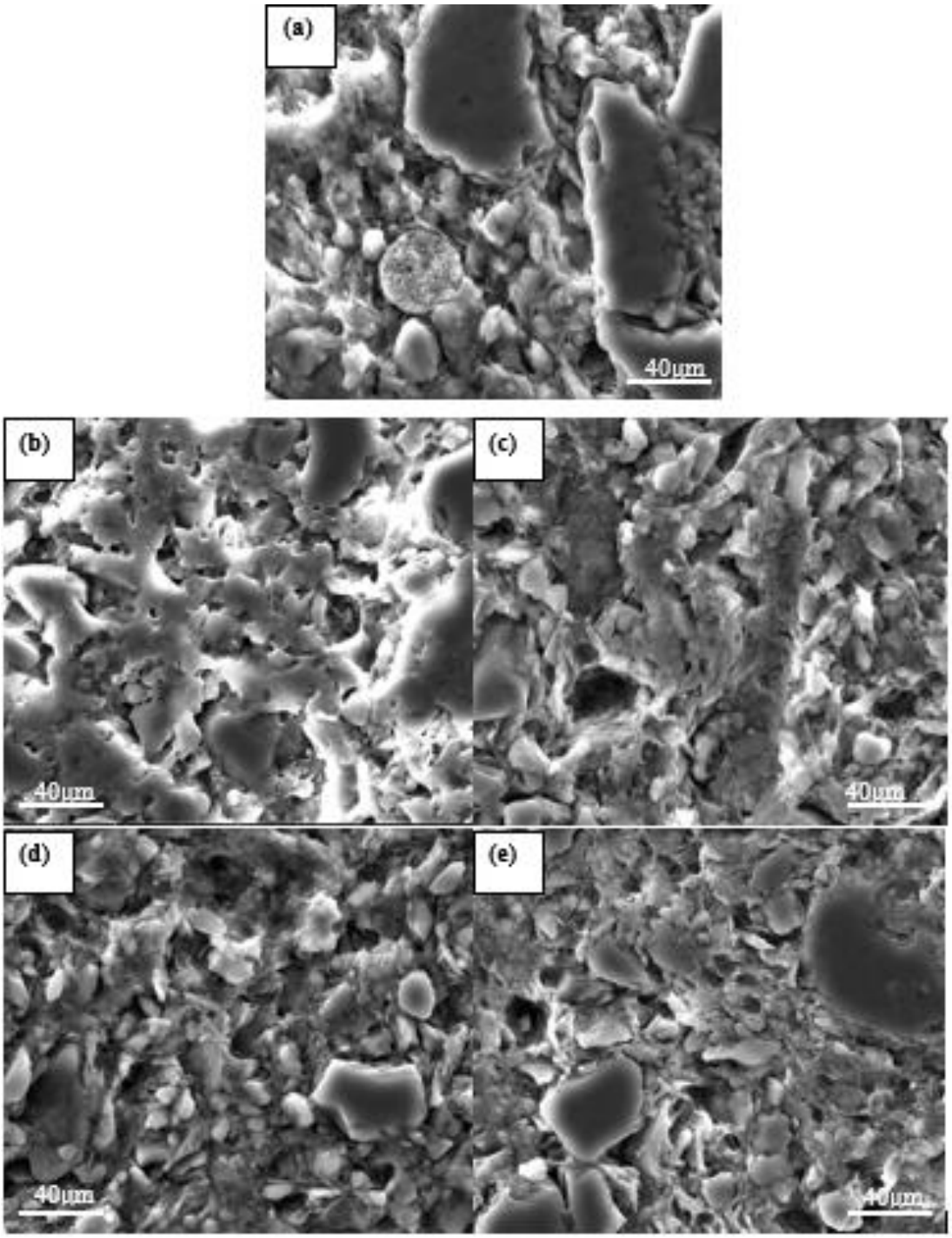

Figure 6-18: SEM images on (a) control (b) 2wt% container glass(c) 4wt% mineral wool (d) 4wt% slurry dust (e) 4wt% filter cake body fired to 950°C.

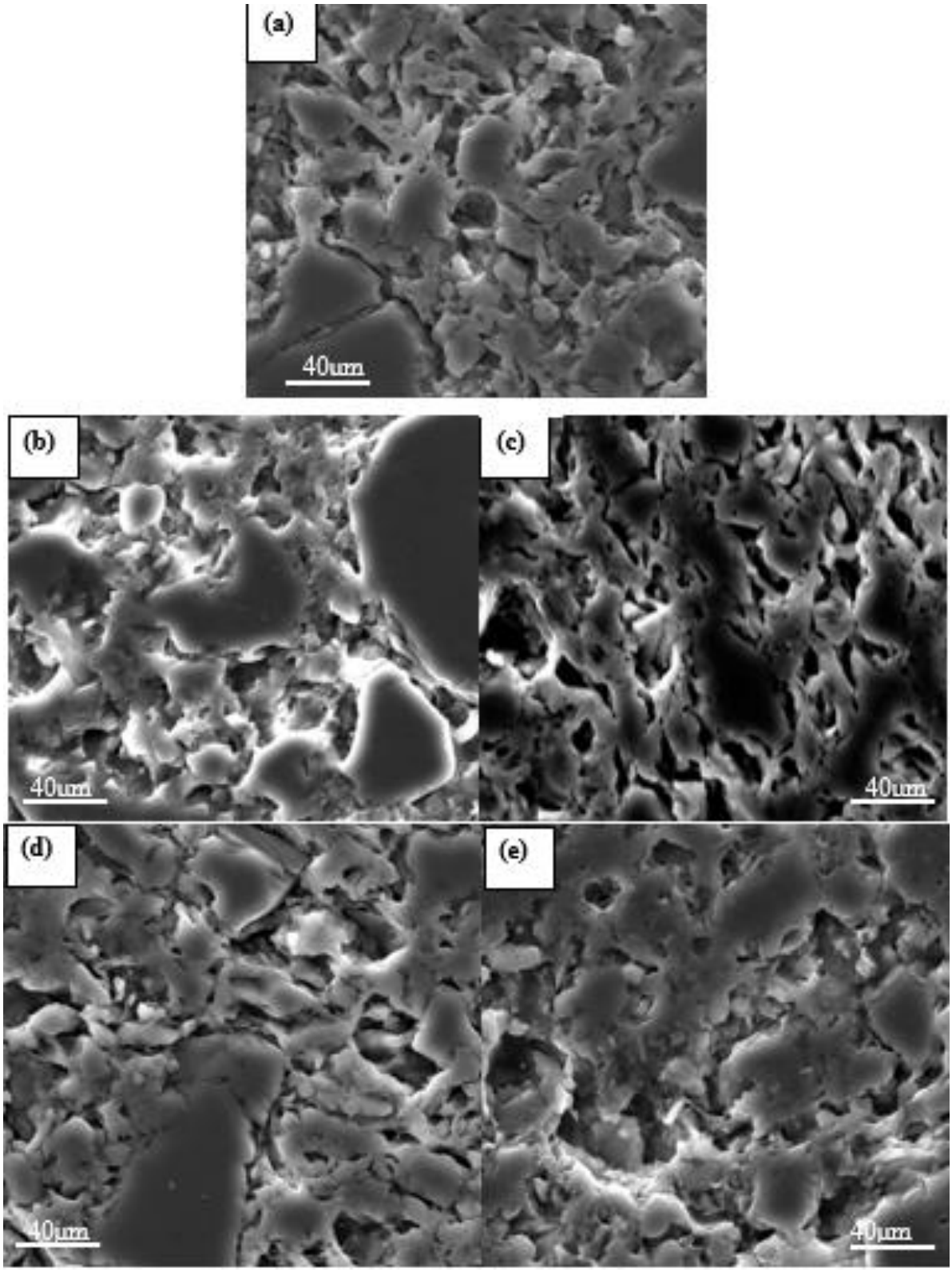

Figure 6-19: SEM images on (a) control (b)2wt% container glass(c) 4wt% rockwool (d) 4wt% slurry dust (e)4wt% filter cake body fired to 1040°C.

6.11 Discussions on Industrial Wastes

Introducing 2wt% or 4wt% industrial waste minerals (cullet/container glass waste, mineral wool, slurry dust and filter cake, respectively) to Weald clay positively and negatively affected the reformulated body. These are discussed in the sections below.

6.11.1 *Container glass waste (2wt.%)-CG2W effect in ceramic production*

One key advantage of using cullet is that it leaves no carbon footprint due to the secondary use of the material. The additional fluxes (Na and Ca) obtained from the cullet provided strong bonding with the clay on heating, especially to ceramics fired at 1040°C. The liquid phase formed improved densification, which was not separable from the shrinkage over the wide temperatures (**Figure 6-10**) and low levels of additives addition, and the crystalline phase (mullite forming in place of dehydrated muscovite).

The addition of a 2wt% level was used based on the studies conducted by Matteucci et al.,[261], who established that less than 5wt% soda lime glass waste was easy to alter and control the technological properties of ceramics. CG2W saw the highest shrinkage, ∼14%, when the clay body was fired to 950°C but reached 20% when the ceramic was heated to 1040°C. This was due to the glassy nature of the additive since, in practice, it was just a remelting of glass in a clay component. On the contrary, high shrinkage obtained can present serious product distortion and even stick to kiln cars if temperatures and additive levels are above certain limits due to high melts or even a collapse of packed bricks due to excessive dimensional changes[367]. According to Njindam et al.[384], this higher limit, that >30%, creates an adverse effect on porcelain bodies requiring incredibly low absorption value and higher strength. Previous studies have shown that adding a cullet for laboratory and industrial trials positively affects strength, water absorption and colour[263]. Smith [367] reported on work he titled “recycled glass

as a brick fluxing agent" that 60°C energy reduction can be achieved with 10% cullet addition to extruded Etruria marl by firing brick to 1040°C instead of 1100°C whilst maintaining brick quality as stated in BS EN771:2011 and reduce HF gas due to the early melt. Current findings with CG2W ceramics fired to 1040°C could only be useful for common brick or facial ceramic applications instead of engineering bricks due to additive level and shaping method. Lorvuenyoung et al.,[385] reported an adverse effect on incorporating higher (45wt%) glass inclusion resulting in strength~ 41MPa lower than the requirement for a Class B engineering and 2-3% water absorption due to glass flow to specimen surface for clay bricks fired to 1100°C.

Darkening in the colour of ceramics containing cullet has been reported with increased additive levels, firing temperature, and oxidising kiln atmosphere[313]. For glass to be effective, finer particle sizes are encouraged [313,367]. The 500μm particle size waste glass incorporated into Wealden clay increased reactivity[367] and promoted sintering in Weald clay, is classed as a low-fired material[313] and promoted surface scum due to the additive's rich Ca content (11.5%). However, the obtained darker colour of the sample was difficult to access due to the whitish scum stain. However, without any colour measuring device, the lower paramagnetic iron site and high magnetic site by Mössbauer spectroscopy could be used to assess the change in colour of ceramics over the control (**see Chapter 8, section 8.2, Table 8-3**).

Although the obtained boiling water absorption (BWA%) obtained was equivalent to the control (8.6%), the high shrinkage of 14% and 20% for samples fired at 950°C and 1040°C, respectively, were not in agreement with the theoretical principle, which states that higher shrinkages should result in lower absorption rate. But the SEM and MIP (Hg porosimetry) validate the benefit of this additive, showing more closed pores / reduced connectivity of porosity, which the Hg could not fill due to the glassy phase formed within the pores, so recorded lower Hg percentages over the control material (20.41-17.66% for samples fired

950°C and 18.30-14.12% for samples fired to 1040°C is recorded). The reason for the obtained result could be explained by (i) the inhomogeneity of pore structure within the ceramic, and the outer shell of the ceramic creates a large disparity in the result or (ii) the shaping method used does not correlate with the industrial extrusion method which removes pockets even before the secondary creation of pores within the ceramic on firing.

The developed phases, anorthite (Ca (Al_2SiO_2 O_8- ICCD No.01-076-0948), hematite (Fe_2O_3 ICCD No. 04-005-4630), mullite ($Al_{2.22}Si_{0.78}O_{4.89}$ ICCD No. 04-016-1586) and quartz (SiO_2- ICCD No. 01-087-2096) improved the mechanical strength of the body (i.e., by 5%, 12% and 15%) when compared to the other industrial wastes respectively (mineral wool and the quarry wastes). The formation of anorthite can be explained by the reaction of lime vs dehydroxylation of kaolinite or the reaction of quartz, mullite and lime (CaO)[384].

$SiO_2 + Al_2O_3 + CaO \longrightarrow CaO.\ Al_2O_3.\ 2SiO_2$- equation 1

$3Al_2O_3 + 2SiO_2 + 3CaO + 4SiO2 \longrightarrow 3(CaO + Al_2O_3.\ 2SiO_2)$ – equation 2

So clearly, in terms of the mineralogy, the new phase developed was anorthite from the waste glass(hence the XRF showed high CaO).

The clay body containing cullet reduced sintering temperature of 31°C was obtained by the 2wt% addition, which is far greater than what 4wt% mineral wool (20°C) or slurry dust provides (22°C) at the point where zero is crossed, as shown by the dilatometry measurement in **Figure 6-9 and Table 6-3**. For a large-scale trial, Smith [264] advises on practical factors different from the laboratory testing that affect product outcome negatively, suggesting a further reduction of at least 30°C for typical industrial testing to ensure quality produce. Typical industrial firing is usually different from a laboratory setting, for example, gas volumes, heat transfer rates, and volume of product within the kiln. The DTA trace shown in **Appendix 1** does not indicate sudden melting behaviour, and the Dilatometry also shows no sudden melting.

With such low dopant levels, the formation of liquid phases (i.e., melting) is not separable from the shrinkage effects that occur over a wide temperature range.

6.11.2 *4wt% Filter cake and Slurry dust (as granite waste) effect in ceramic production*

Recycling 4wt% Filter cake (F4W) and Slurry dust (S4W) has the advantages of minimizing clay use and landfill waste[236,264,386]. As stated earlier in **Chapter 3**, filter cake and slurry dust are products from granite washings and cuttings, respectively. The advantage of this waste is its high source of feldspar content which is a network modifier or (simply put) a good flux. Vasić et al.,[357] mentioned the tendency of granite waste to act as a filler to reduce shrinkage, which was evident in this study (**Figure 6-11**). The use of high granite waste (>20wt%) has been practically applied to stoneware[387] and porcelain[388] ceramic tiles and bricks[389] a cheap material to lower sintering temperature and water absorption by increased granite level content, which is environmentally friendly and not hazadous[386]. The use of granite in literature for stoneware and porcelain tiles is usually a combination of high granite waste (20-47.5wt%) and Na feldspar prepared by powder pressing and firing at a higher temperature (>1100 -1210°C) to achieve a zero /low porosity. Meanwhile, in this study, clay was replaced with 4wt% of the granite waste fired to 1040°C and its properties were examined. The key physical property, BWA% (**Figure 6-12**), was slightly lower due to the advantageous flux (Ca) and a reduced mechanical strength (<50Mpa, **Figure 6-13**). The low strength is explained by Torres et al.. [386] and Lougon et al.[390] as a formation of microcracks during quartz volume change occurs even for ceramics fired at 950°C.

Granite from a sedimentary rock source generally possesses different iron contents. Interestingly, the chemical analyses from this granite waste sourced from Wienerberger Ltd. are calcium-rich feldspar see **Table 6-1**, **Chapter 6**. The sourced granite wastes were high in Fe_2O_3 (~7.5%) and Fe in Weald clay. The Fe_2O_3 is responsible for the reddish colour of the

ceramic sample produced [265]. In contrast to the granite waste used in this study, Barreto et al. [316] reported its additive (granite) low in Fe_2O_3 1.3%. Both high /low percentages of Fe are still beneficial for ceramic colour in heavy brick manufacture. Although this granite waste was a Ca feldspar, no calcium phase formed from the reaction of meta kaolinite with calcium oxide according to the reaction: $Al_2O_3{\cdot}2SiO_2$ (meta Kaolinite) + CaO (calcium oxide) → CaO. $Al_2O_3{\cdot}2SiO_2$ (anorthite) [391] for 4wt% slurry and filter cake containing ceramic as depicted in **Figure 6-2** fired at 1040^{o}C

Mineralogically (**Figure 6-1 and 2**), phases in the reformulated composition (F4W, S4W) were similar to the 100% clay since the waste was also an inorganic material with additional fluxing content and was cheaper. This result agrees with Vieira et al.[266], who obtained no change in the crystalline phases compared to their control material. What was surprising from the granite waste findings were its recorded strengths compared with 100% clay. This was attributed to the lower shrinkages or possibly low dosage and increased median pore identified with Hg porosimetry (**Figures 6-14 and 15**), and volumetric change of quartz (**Figure 6-9**) has been reported by [266] to promote micro-cracks and pores, affecting ceramic strength. Unfortunately, the high Ca containing granite in this composition also increased scumming on firing, which can easily be addressed using $BaCO_3$.

In conclusion, the study reveals the possibility of reusing this low-cost material, rich in feldspar, in ceramic applications to reduce connectivity pores. Extruded reformulated samples containing granite waste have been reported to have superior properties over pressed; therefore, extruded ceramics for clay brick formulations could be adapted and increase the level of granite wastes used [386]. While one must be mindful of the microcracks that could affect strength, the obtained water absorption and compressive strength testing are still appropriate for common brick applications.

6.11.3 *4wt% Mineral wool additive effect in ceramic production*

Most studies conducted around Rockwool / mineral wool as secondary raw material in construction application is around cement and concrete, polymer composites, production of low-cost glass fibres, oil and gas absorbents and the waste chemical and physical property reviewed by Yap et al. [392] and only one source in the literature[393] talks of its incorporation in clay brick related to this study. Consistent with the literature, Rockwool has a high content of CaO[394].

In this laboratory study, M4W ceramic samples were found to reduce boiling absorption tests by 0.5% compared to the control. Volumetric shrinkage results for ceramics fired to 1040°C were lower than the Control but saw an increase when fired to 950°C. See **Figure 6-11**. This is possible because, at 950°C, sintering had just begun, and extreme bonding for a denser product has not been created yet due to decreased viscosity [395] which affects the crystalline phases formed. The total porosity measured with MIP (**Figures 6-14 and 15**) was 3 and 4% lower than that of the control depicting reduced interconnecting pores.

Contrary to expectations, where low porosity usually results in high strength, this study did not see that correlation; instead, lower strength (28MPa) than the control (81MPa) was recorded. The reason for this is unclear, but it may have something to do with the shaping of the clay body, where the pressing force of 7 tons was sometimes difficult to reach. Also, findings obtained by Kizinievicˇ et al. (2014) [393] on mineral wool waste in clay brick production reported the formation of diopside, a reaction of clay minerals and CaO caused low-fired shrinkages. The formation of anorthite and diopside formation in their [393] formulations is consistent with this study (**Figure 6-1 and 2**), except that albite ($NaAlSi_3O_8$) which is reported by Chen et al. and Gualtieri et al.[396,397].

Moreover, ceramics fired to 1080°C with 20wt% mineral wool attained a strength of 59MPa compared to 53MPa for only 4wt% additive fired to 1040°C. The 59MPa strength could be

associated with the hand moulding technique used by the author. The mineral wool's positive effect is its ability to check expansion, shown in the dilatometric diagram in **Figure 6-9** and porosity reduction (**Table 6-5**). But one of the main disadvantages of this additive was its increase in whitish stains/ scum on the ceramic surface, which Gualtieri et al..[396] reported as the effect of the high CaO. In summary, mineral wool is a recyclable material that can help promote a reduction in sintering temperature and porosity.

Chapter 7 Additives Effect Of Inorganic Mineral Additive On The Sintering, Microstructure And Properties Of A Class B Engineering Brick Inorganic mineral additives

7.1 Series 3 -Inorganic mineral additives (Background)

This section replaced up to 4wt% levels, four naturally occurring minerals with specific crystallinity and chemical composition complimentary to Weald Clay. They were chosen to provide additional fluxes in the body, which were otherwise lower in the control clay. The additives are:

- Colemanite ($2CaO.3B_2O_3.5H_2O$)
- Nepheline syenite ($K_{1.37}Na_6(AlSiO_4)_8$),
- Wollastonite ($CaSiO_3$) and
- Talc ($Mg_3Si_4O_{10}(OH)_2$)

Nine (9) characterization techniques have been used to understand the behaviour and effect of these additives on the project goal: reducing energy demand and CO_2 emissions. These were mixed with 96wt% Weald clay and fired to 950°C and 1040°C. The quantity of flux for individual composition is calculated by the sum of K_2O+CaO+MgO+Na_2O+$Fe_2O_{3/}$ +BaO (as taken from XRF results **Table 7-1**).

7.2 Sample Preparation

Series 3 additive composition is summarised in **Table 3-1.** Raw materials were separately dried in an oven at 120°C for 48hrs. 4 wt% was weighed and mixed with 96wt% dried clay, then

milled in Retzsch vibratory disc mill for 1 minute at 800 rpm to produce a fine powder. This powder was mixed with 20-23ml distilled water (21%) to provide sufficient plasticity for shaping. A hydraulic press with 7 tonnes of pressure was applied to the 8.3g wet weight of the composition to form a 20 mm x 5 mm cylindrical pellet. After shaping, the green body dimensions were recorded in the "as-pressed" condition. Samples were left on a bench and dried in an electric laboratory oven (105°C) for approximately 36 hrs to eliminate free water gradually. The effect of additives on the brick property was studied by firing samples to 950°C and 1040°C at a 1°C/minute heating rate and holding for 2hrs at the maximum temperatures before cooling at the same rate in an electric laboratory furnace.

7.3 Results and Discussions

7.4 Chemical analysis of inorganic minerals additive

All the inorganic minerals had lower levels of Fe_2O_3 <1%. The equipment PW2540 sample changer Philips MagiXPro used for this analysis cannot detect boron in $2CaO.3B_2O_3.5H_2O$ because the energy x-ray is light. Therefore, it is assumed that the boron may account for the higher LOI for Colemanite (29.5%). It is also the only mineral with 2.5% strontium oxide (SrO), with its overall fluxing totalling 76.1%. Colemanite is low in SiO_2 (18%). Na_2O and K_2O are the main fluxes in Nepheline syenite ($K_{1.37}Na_6(AlSiO_4)_8$), with 8 and 9% recorded as oxides; respectively calculated flux was 18.9%. The Al_2O_3 content in Talc ($Mg_3Si_4O_{10}(OH)_2$) and Wollastonite ($CaSiO_3$) is low, ranging from 0.1 and 0.2, respectively, with SiO_2 content of 67% and 52%. The main difference between these two is the amount of alkaline earth oxide. For example, $Mg_3Si_4O_{10}(OH)_2$ has 31.1% of MgO, whiles $CaSiO_3$ contains 45.7% CaO. Differences in loss of ignition and analysed oxides on the individual additives are shown in **Table 7-1**.

7.4.1 *Chemical analysis of inorganic minerals in clay body composition*

Table 7-1 summarises the XRF results of the inorganic additives. XRF results for the 4wt% additives of colemanite (C4W), nepheline syenite (N4W), and wollastonite (W4W) showed the same SiO_2 content of 72% except for 4wt% talc (T4W) which introduces additional silicon; therefore, the overall content (as SiO_2) goes up by 1%. Also, the Fe_2O_3 content decreases by 0.4 and 0.3% for W4W and T4W. Moreover, the 4wt% additives and the clay provide 11.3%, 5.1%, 6.6% and 5.6% flux to the clay body mixture for C4W, N4W, W4W and T4W, respectively. As expected, $CaSiO_3$ introduces more CaO to the composition at 2.3%. Meanwhile, talc and nepheline syenite recorded the least CaO (0.4%)

Table 7-1: X-ray fluorescence of analysed Weald clay (Wt%) replaced with 4wt% inorganic minerals fired to 1040°C

Oxide	Clays	Inorganic Minerals only				4wt% Inorganic Minerals added to Weald clay				
	Weald clay	Colemanite	Nepheline Syenite	Wollastonite	Talc	Fired Weald clay (1040°C)	C4W (1040°C)	N4W (1040°C)	W4W (1040°C)	T4W (1040°C)
SiO_2	73.5	18.0	55.7	52.1	66.8	71.0	71.8	72.0	71.7	72.6
Al_2O_3	15.4	2.0	24.3	0.2	0.1	15.9	14.9	15.7	14.8	14.7
Fe_2O_3	6.1	1.0	0.1	0.4	0.2	7.7	6.9	6.9	6.5	6.6
Mn_3O_4	0.1	0.0	0.0	0.1	0.0	0.1	0.2	0.2	0.1	0.1
TiO_2	1.5	0.3	0.2	0.0	0.1	1.5	1.5	1.3	1.4	1.4
Na_2O	0.0	0.1	8.0	0.0	0.0	0.2	0.2	0.5	0.2	0.2
K_2O	2.2	1.1	9.3	0.0	2.1	2.3	2.1	2.4	2.1	2.0
MgO	0.5	0.9	0.0	1.3	31.3	0.6	0.6	0.5	0.6	1.6
CaO	0.3	69.2	1.6	45.7	1.4	0.4	1.5	0.4	2.3	0.4
P_2O_5	0.1	0.0	0.1	0.0	0.1	0.1	0.1	0.1	0.1	0.1
BaO	0.1	0.0	0.4	0.1	0.0	0.1	0.1	0.1	0.1	0.1
SrO	-	2.5	0.4	0.0	0.0	0.0	0.0	0.0	0.0	0.0
ZrO_2	0.0	0.0	0.0	0.0	0.0	0.1	0.1	0.0	0.1	0.1
SO_3	0.2	0.3	0.0	0.0	0.1	0.0	0.0	0.0	0.0	0.0
SUM (%)	100	100	100	100	100	100	100	100	100	100
LOI (%)	16.75	29.50	5.80	8.32	12.49	4.83	5.62	6.49	5.62	5.30

Where flux = (K_2O+CaO+MgO+Na_2O+Fe_2O_3/ +BaO) and the symbols C4W=4wt% Colemanite,N4W= 4wt% Nepheline syenite, W4W=4wt% Wollastonite and T4W= 4wt% Talc

7.4.2 *Mineralogical assessment of clays with inorganic additives by XRD*

Samples containing nepheline syenite, talc, and wollastonite fired to 950°C do not promote mullite formation, which gives strength to fired bodies, instead dehydrated muscovite forms. However, the colemanite body (C4W) produces mullite at 950ºC, which is usually only seen in the raw clay when fired to 1040C. Anorthite also forms in C4W at 950°C. Quartz remains constant at all temperatures. Hematite, which influences brick colour, begins to appear but is more intense in the Colemanite sample. A diopside is formed with wollastonite, and the remaining phases ($KAl_3Si_3O_{11}$, $CaSO_4$, Fe_2O_3 and SiO_2) do not change. But in the nepheline syenite samples, microcline ($K_{0.95}Na_{0.05}$) $AlSi_3O_8$ - 01-084-1455) and orthoclase [potassium sodium aluminium silicate] a feldspar ($K_{0.94}Na_{0.06}$) ($AlSi_3O_8$)- 01-086-0437 forms in place of the dehydrated muscovite ($KAl_3Si_3O_{11}$) see **Figure 7-1**.

Colemanite ($2CaO.3B_2O_3.5H_2O$) body fired to 1040°C promote boro-mullite ($Al_9B_1O_{19}Si_{2-}$ 98-016-1811), anorthite ($Al_2Ca_1O_8Si_2$ - 98-002-2023), hematite (Fe_2O_{3-} 01-076-4579) and quartz (SiO_2 - 01-087-2096). The peak height of hematite is twice the intensity of fired Weald Clay without additive. Also, the hematite (Fe_2O_3) was found to enter the mullite structure well-distributed for all the additives shown in **Figure 7-2.**

Diopside or calcium magnesium aluminium silicate (Ca (Mg, Al) Si, $Al)_2O_6$)- 00-025-0154 forms only with 4wt% wollastonite (W4W) containing sample fired to 1040°C whilst talc ($Mg_3Si_4O_{10}(OH)_2$) promote spinel (Mg (Al_2O_4 -01-072-7248) formation along with mullite ($Al_{2.26}Si_{0.74}O_{4.87}$ - 04-016-1587), quartz (SiO_2 - 01-087-2096) and Hematite (Fe_2O_3 - 04-005-4630).

The 4wt% inorganic mineral additive promoted new phase formation except for nepheline syenite $K_{1.37}Na_6(AlSiO_4)_8$ for samples fired to 1040°C.

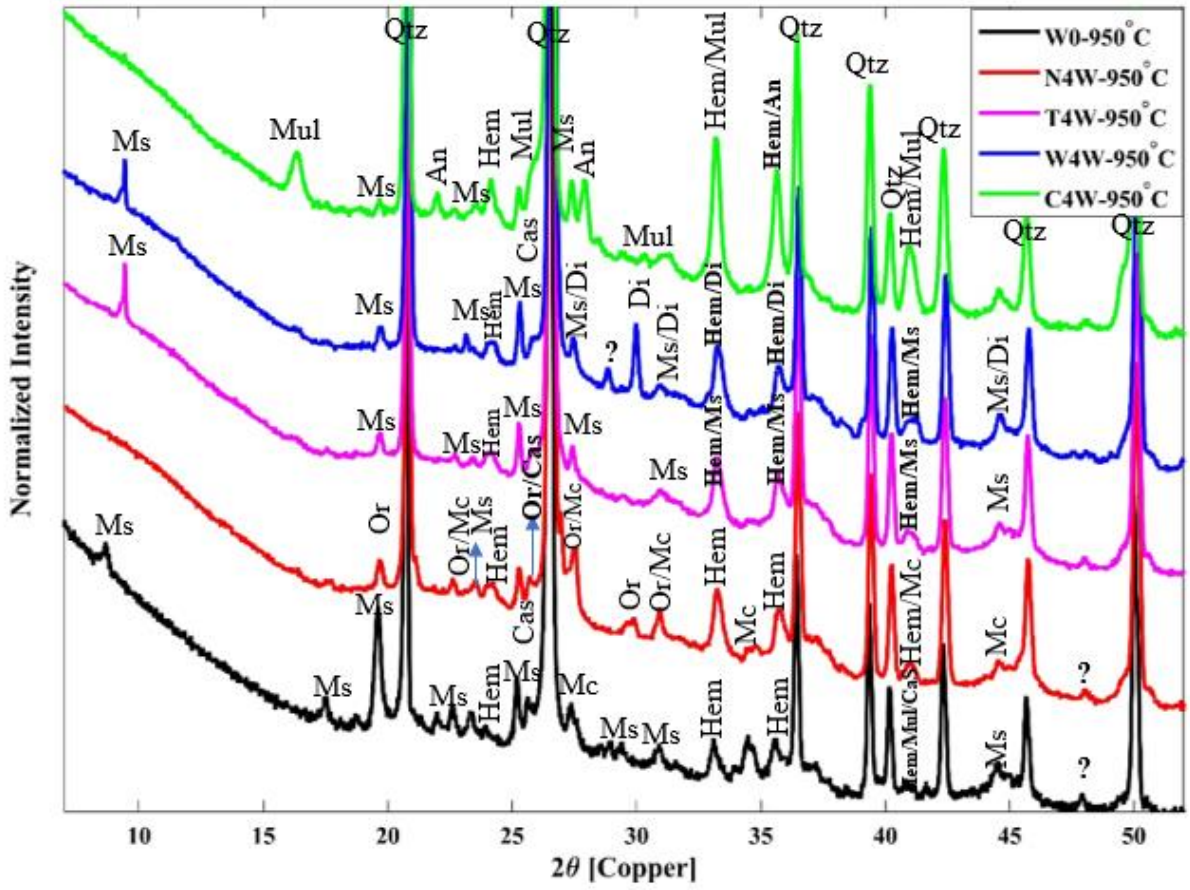

Figure 7-1: Crystalline phases of 4wt.% inorganic waste additive to Weald clay fired to 950°C. Symbols after Kretz 1983[343]. Phases present in

1. **Weald clay fired to 950°C:** Qtz- Quartz (SiO_2), Ms- dehydrated Muscovite ($KAl_3Si_3O_{11}$), Hem- Hematite (Fe_2O_3), Mc- Microcline ($KAlSi_3O_8$) and Calcium Sulfate ($CaSO_4$)
2. **4wt% Nepheline syenite [N4W-950°C]:** Qtz- Quartz (SiO_2), Ms- dehydrated Muscovite ($KAl_3Si_3O_{11}$), Hem- Hematite (Fe_2O_3), Mc- Microcline ($K_{0.95}Na_{0.05}AlSi_3O_8$), Or- orthoclase Potassium Sodium Aluminium silicate ($K_{0.94}Na_{0.06}$) ($AlSi_3O_8$)) and Calcium Sulfate ($CaSO_4$)

3. **4wt%Talc [T4W-950°C]:** Qtz- Quartz (SiO_2), Ms- dehydrated Muscovite ($KAl_3Si_3O_{11}$), Hem- Hematite (Fe_2O_3) and Calcium Sulfate ($CaSO_4$)
4. **4wt%Wollastonite [W4W-950°C]:** Qtz- (SiO_2), Hem- Hematite (Fe_2O_3), Ms- dehydrated Muscovite ($KAl_3Si_3O_{11}$), and Calcium Sulfate (CaSO4) and Di- Diopside (Ca (Mg, Al) Si, $Al)_2O_6$)
5. **4wt%Colemanite [C4W-950°C]:** Qtz- Quartz (SiO2), Ms- dehydrated Muscovite ($KAl_3Si_3O_{11}$), Hem- Hematite (Fe_2O_3), Mul-Boromullite ($Al_2(Al_{2.544}Si_{1.456})$ $O_{9.728}$ and An- anorthite sodian disordered (Ca, Na)(Si, $Al)_4O_8$

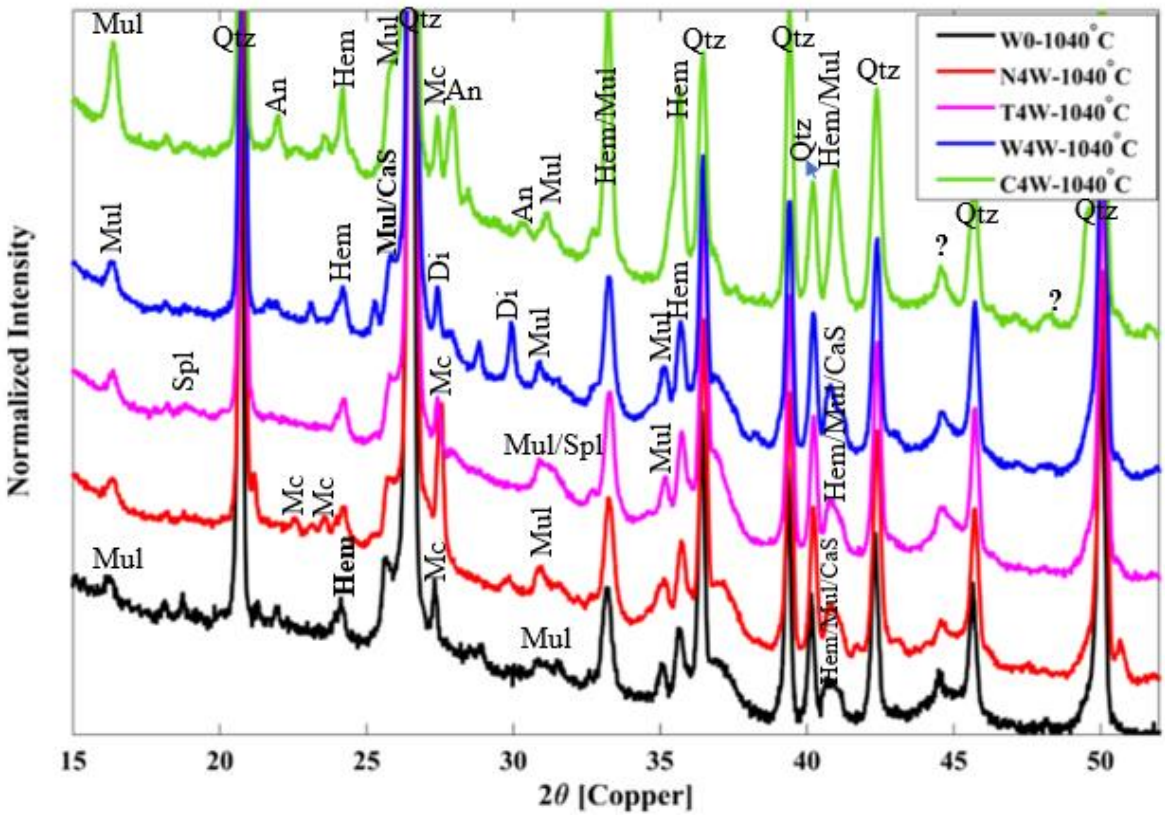

Figure 7-2: Crystalline phases of 4wt.% inorganic waste additive to Weald clay fired to 1040°C.Symbols after Kretz 1983[343]. Phases present in:

1. **Weald clay fired to 1040°C:** Qtz- (SiO_2), Mul- Mullite ($Al_{2.26}Si_{0.74}O_{4.87}$), Hem- Hematite ($Fe_2O_3$), Calcium Sulfate ($CaSO_4$) and Mc- Microcline ($KAlSi_3O_8$)
2. **4wt% Nepheline syenite [N4W-1040°C]:** Qtz- (SiO_2), Mul- mullite ($Al_{2.26}Si_{0.74}O_{4.87}$), Hem- Hematite ($Fe_2O_3$), Mc- Microcline ($K_{0.88}Na_{0.12}Si_3O_8$) and Calcium Sulfate ($CaSO_4$)
3. **4wt%Talc [T4W-1040°C]:** Qtz- (SiO_2), Mul- mullite ($Al_{2.26}Si_{0.74}O_{4.87}$), Hem- Hematite ($Fe_2O_3$), Spl- Spinel (Mg ($Al_2O_4$) and Calcium Sulfate ($CaSO_4$)
4. **4wt%Wollastonite [W4W-1040°C]:** Qtz- (SiO_2), Mul- mullite ($Al_{2.26}Si_{0.74}O_{4.87}$), Hem- Hematite ($Fe_2O_3$), Calcium Sulfate (CaSO4), Mc- Microcline ($KAlSi_3O_8$) and Di- Diopside (Ca (Mg, Al) Si, $Al)_2O_6$)
5. **4wt%Colemanite [C4W-1040°C]:** Qtz- (SiO_2), Mul- Boromullite ($Al_9B_1O_{19}Si_2$), Hem- Hematite (Fe_2O_3), and An-Anorthite ($Al_2Ca_1O_8Si_2$)

7.5 Thermogravimetry analysis coupled with mass spectroscopy on inorganic body compositions

The heating behaviour of inorganic mineral additives with clay is shown in **Figure 7-3**. The combined graph shows similar heating trends. The CO_2 removal is gradual and starts below, which is an endothermic reaction between 300°C- 600°C for all inorganic minerals. There's no evidence of the DTA of a liquid phase.

The derivative (DTG) of C4W depicts the breaking of borate chains and OH at lower temperatures[398] of 396°C -400°C an exothermic reaction shown in **Appendix 1b** and the decomposition of clay >400°C to release CO_2 (see **Figure 7-4** and **Figure 7-5**). The total weight loss recorded for C4W is 6.81%. The decomposition composition of the colemanite is written as $2CaB_3O_4(OH)_3.H_2O \rightarrow Ca_2B_6O_{11}+5H_2O$. N4W total weight loss is 7.16% greater than the control. T4W and W4W also have similar heating behaviour where the final weight

loss of T4W is 0.18% greater than W4W (7.02%) due to the removal of excess water (OH) beyond 600°C.

The decomposition of organics and carbonates in clays and additives associated with gas removal is detected at temperatures between 200-600°C except for colemanite, as discussed earlier. Thermogravimetry analyses coupled with mass spectroscopy (TG-MS) show the removal of absorbed H_2O and the chemical bonded water/ hydroxyl group (OH) (endothermic reaction) between 100-600°C. TG-MS of T4W shows a final water removal from the mass between 800°C-1000°C. Moreover, beyond 1000°C for all compositions, no further reactions were causing mass loss. See **Figure 7-4,** the derivative of the TGA.

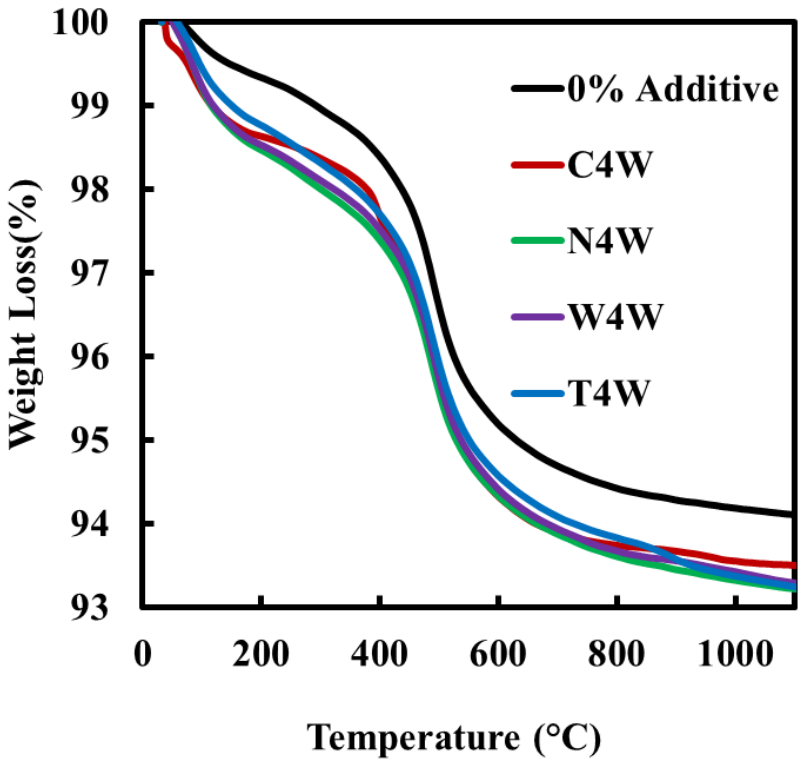

Figure 7-3: TGA of Weald clay body containing inorganic additives fired from 35°C -1100°C at 10°C/min in an alumina crucible. Where C4W= 4wt% colemanite, N4W= 4wt% nepheline syenite, W4W=4wt% wollastonite and T4W= 4wt% talc.

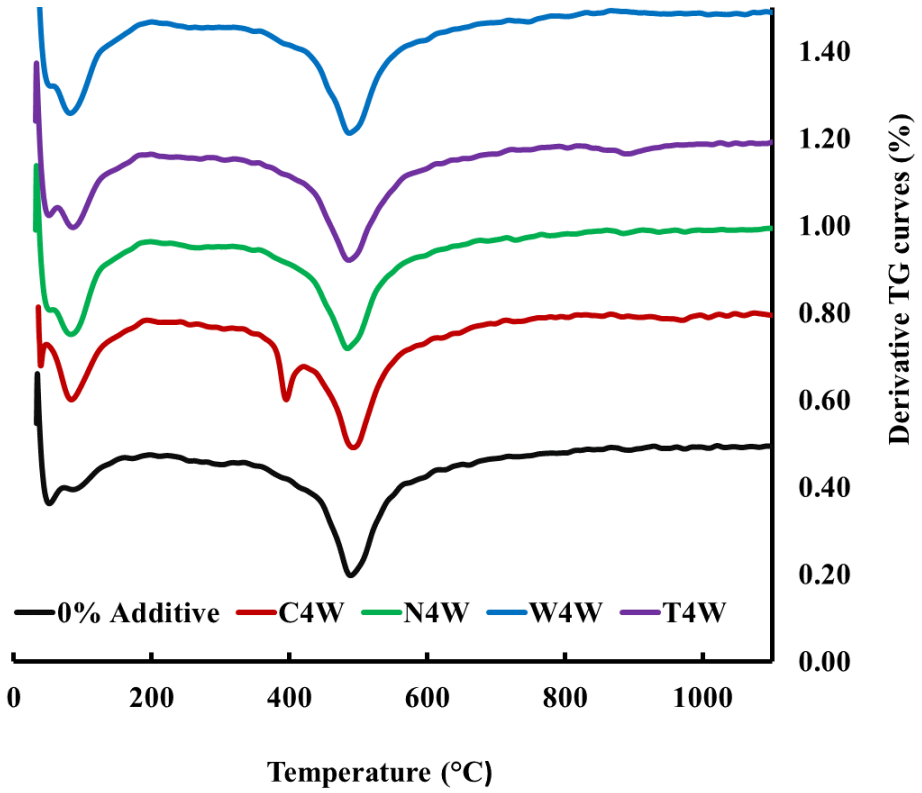

Figure 7-4: DTG of clay body containing inorganic additives fired from 35°C -1100°C at 10°C/min in an alumina crucible. Where C4W= 4wt% colemanite, N4W= 4wt% nepheline syenite, W4W=4wt% wollastonite and T4W= 4wt% talc.

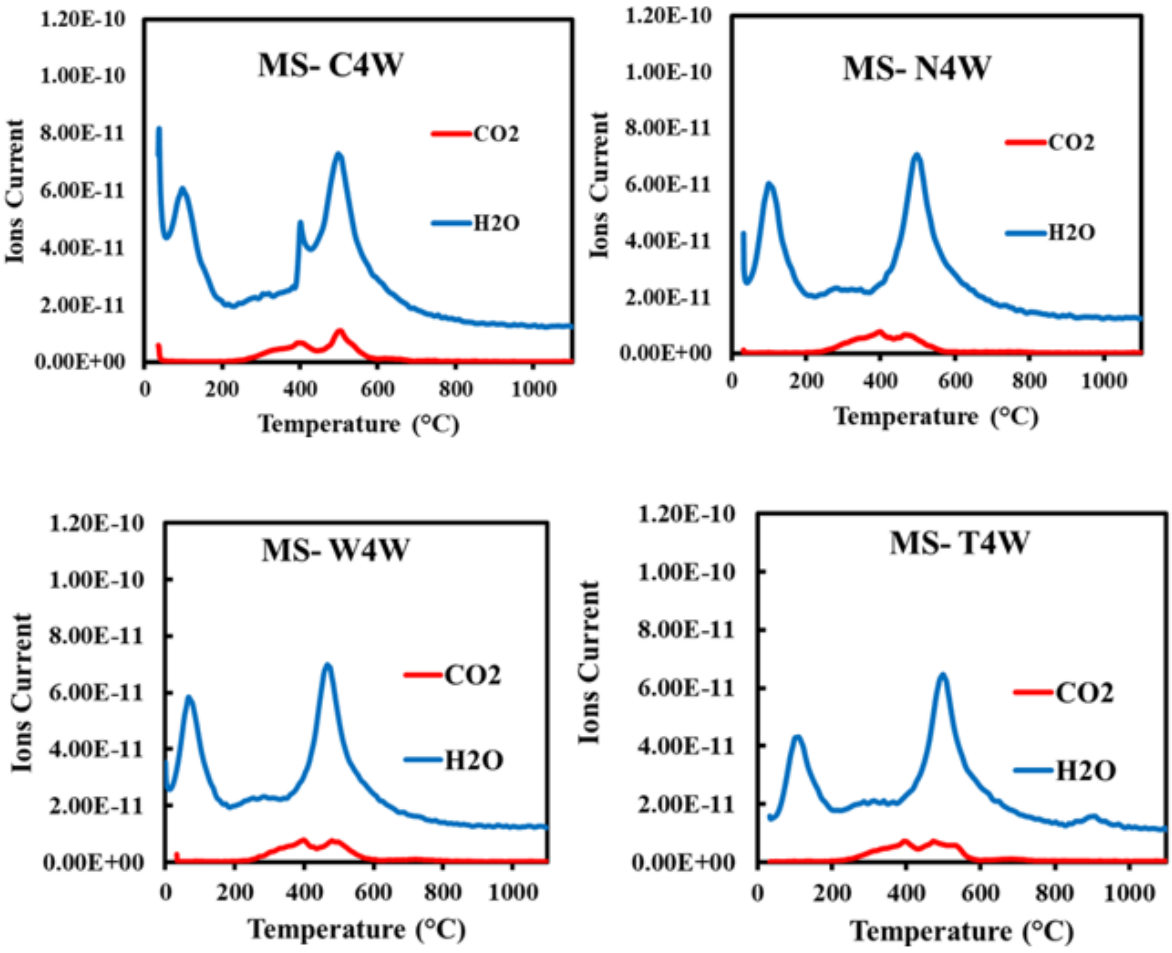

Figure 7-5: mass spectroscopy of 4wt% inorganic mineral additives body composition fired from 35°C -1100°C at 10°C/min in an alumina crucible.

7.5.1 *Dilatometry Analysis*

Figures 7-6 and Figure 7-7 show the dilatometric curves and its derivative when body compositions are heated. The derivative curves' sharply pointed peaks (150ºC and 250ºC) indicate vibrations on the bench or a heated-up furnace before the examination.

For the clay with colemanite additions, the maximum expansion on heating was 1.5%, 50% higher than for the control alone. The derivative curve shows two sharp peaks at 363°C and

380°C due to the decomposition of colemanite by removing the inter-crystallite water, leaving a glassy boron structure and rapidly expanding the body. Shrinkage begins at 700°C, and a shrinkage of 1% was achieved at a temperature of 875°C. At 1000°C, the sample had undergone 3% shrinkage.

Shrinkage began at 800°C, and 1% shrinkage was achieved at 972°C for 4wt% Nepheline syenite. At 1000°C, the sample had undergone 2.6% shrinkage. Wollastonite and Talc additions depicted a similar pattern to Nepheline syenite the control. The only difference is the potential shrinkage temperature reduction achieved by the additives. Thus, shrinkage temperatures observed with C4W, N4W, W4W and T4W are 95°C, 19,31 and 11°C, respectively. The shrinkage effects over a wide temperature range are not separable from the liquid phase formed from such low additive levels (4wt%); hence there's no evidence in the DTA depicting a melting phase see **Appendix 1b**.

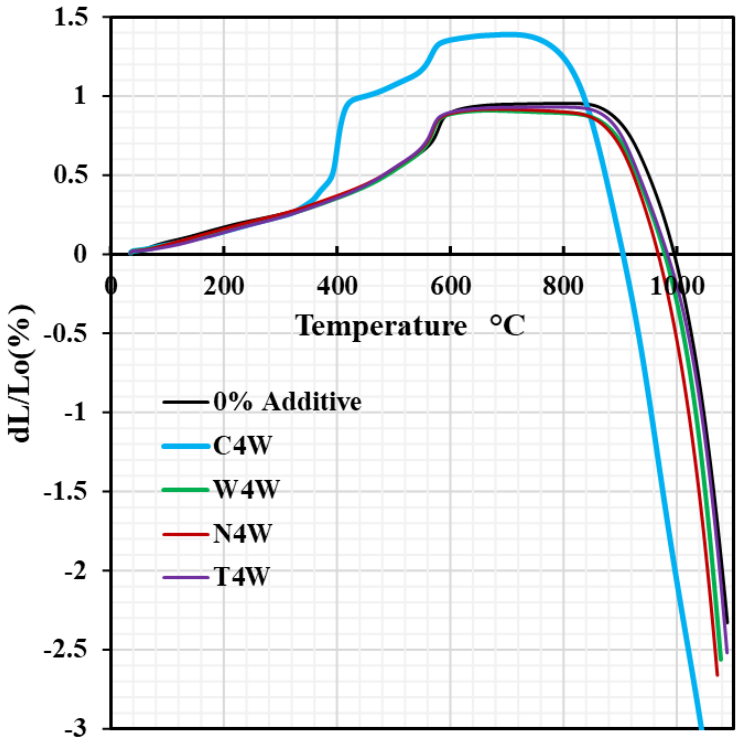

Figure 7-6: Comparable dilatometry curves of control and inorganic additive mixtures fired at 35-1100°Cat aa heating rate of 5°C/min.

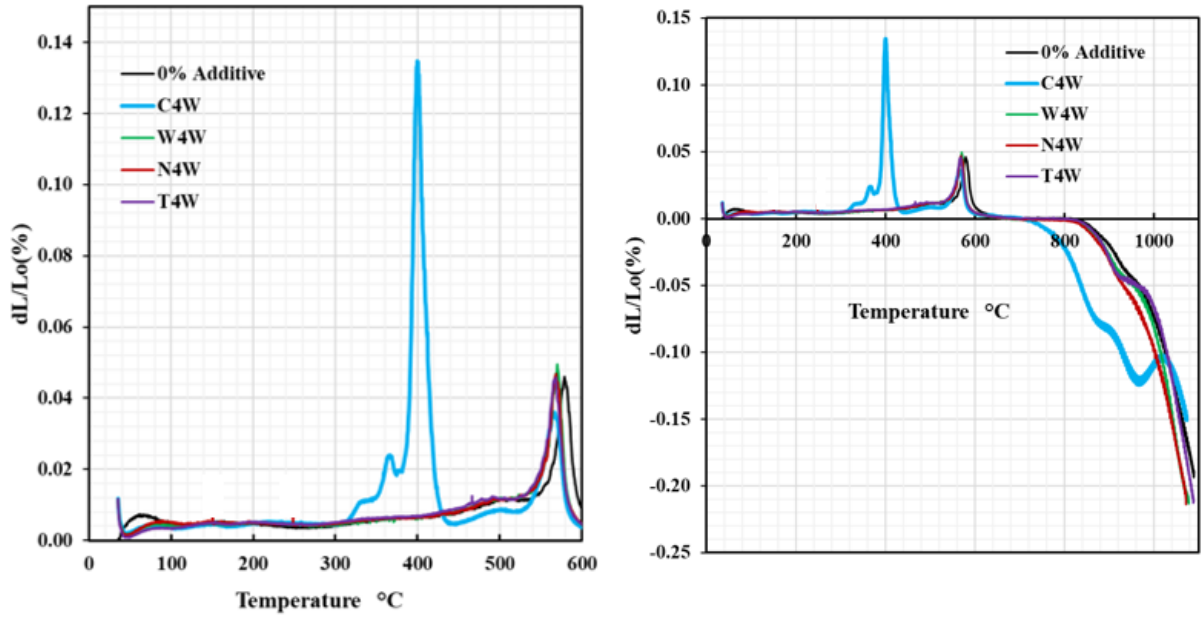

Figure 7-7: Dilatometry curve and its derivative for 4wt.% replacement inorganic mineral additives in weald clay fired to 1040°C at 5°C/min.

7.6 Fired images of inorganic mineral additives fired to 950°C and 1040°C

C4W samples minimised the surface stain found on the control. The rim of the fired body showed a yellowish stain, and the remaining surface a whitish stain. The additive also improved the fired colour, promoting a dark red hue similar to that observed with samples containing 4wt% $BaCO_3$ additive.

N4W and W4W samples fired to 950°C and 1040°C had a whitish stain on the ceramic surface caused by $CaSO_4$. T4W could not stop the stain's formation, as in the case of $MgCO_3$ in the Series 1 grouping (**Figure 5-52**). The surface stains make it impossible to distinguish fired colour at temperatures 1040°C and 950°C unless viewed at the opposite end of the ceramic pellet. This way, the effect of temperature and hue becomes relevant, an indicator of a well-burnt ceramic body.

Ultimately, none of these additives could stop the surface stain, thus reacting with soluble sulphate in Weald clay. **Figure 7-8** illustrates the effect of additives on a surface stain of clay products.

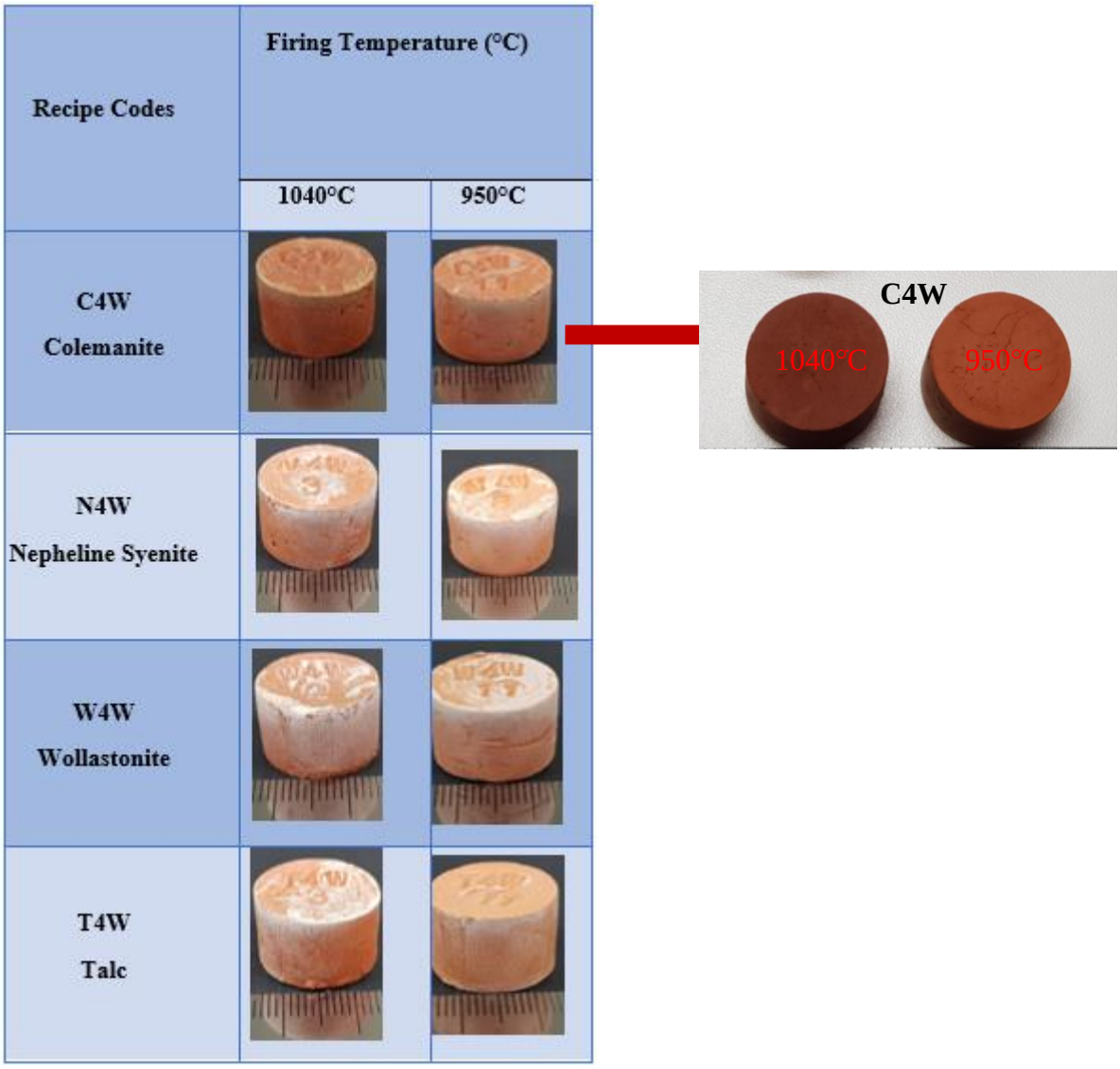

Figure 7-8: Effect of replacing 4wt% inorganic mineral additive to Weald clay and firing to 950°C and 1040°C.

7.7 Technological properties of replacing Weald Clay with 4wt% inorganic mineral additive

7.7.1 *Volumetric shrinkage (VS) and Boing Water Absorption (BWA)*

The volumetric shrinkage on body compositions fired to 950°C and 1040°C are shown in **Figure 7-9.** The additives had higher VS than the control at 950°C, but this did not happen at 1040C.

The base clay, or the control surprisingly, has the highest shrinkage when fired to 1040°C compared to the inorganic mineral additives with clay. T4W is 0.20% greater than W4W in shrinkage, followed by N4W with 8%. And the least VS recorded was C4W, with 4.9%.

For boiling-water absorption of clay body samples fired at 1040°C, W4W records the least absorption (7.2%) compared to the control (8.6%) and N4W (8.2%). C4W, on the other hand, marked the highest absorption at 10.6%. T4W's saturation was 1% higher than N4W's. The graphical presentation is shown in **Figure 7-9.** A summary table of volumetric shrinkage, boiling water absorption, and compressive strength is shown in **Table 7-2.**

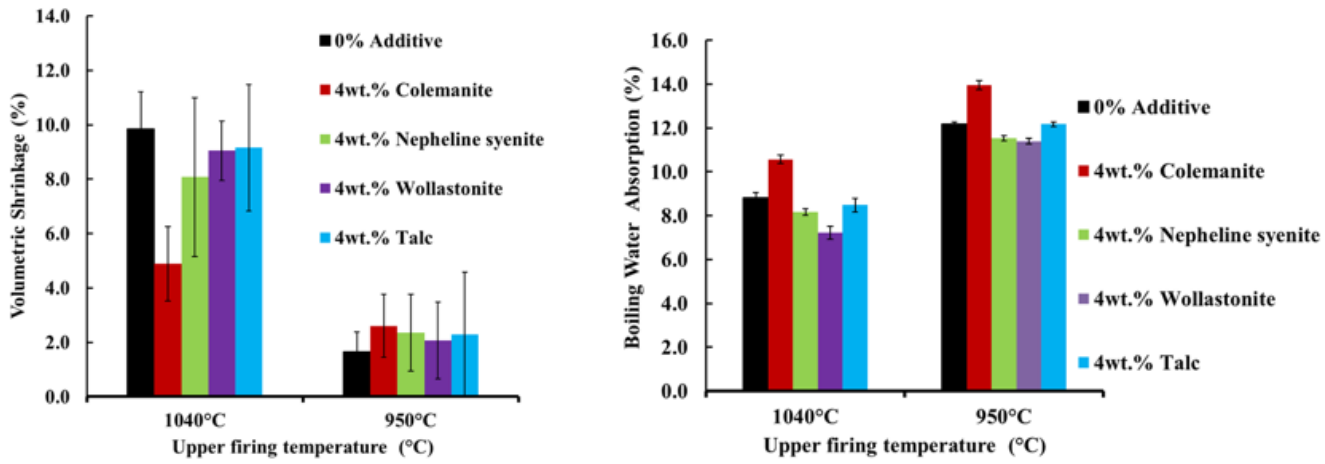

Figure 7-9: Volumetric shrinkages and boiling water absorption of inorganic minerals additives replaced with Weald clay fired to 950°C and 1040°C

Table 7-2: Summary of physical and mechanical testing on inorganic minerals additive level and temperature effect on ceramic mixture

Clay bodies fired to 1040°C			
Additive (%)	Shrinkage testing (%)	Boiling water absorption testing (%)	Compressive strength testing (MPa)
0% Additive	9.8	8.6	81.5
4wt% Colemanite	4.9	10.6	27.5
4wt% Nepheline Syenite	8.1	8.2	46.2
4wt% Wollastonite	9.0	7.2	72.5
4wt% Talc	9.2	8.5	60.5

7.7.2 *Compressive strength testing*

Figure 7-10 depicts the effects on compressive strength of adding 4wt% inorganic mineral additives to Weald clay. Generally, strength is increased by higher temperature firing. This is because ceramic densification is temperature-dependent. C4W has a detrimental effect on brick strength. The sample recorded the least strength at both temperatures (950°C and 1040°C), 26 MPa and 27MPa, respectively.

The highest strength was obtained with samples containing W4W fired to 950°C and 1040°C 52MPa and 72MPa, respectively. Samples containing talc fired to 1040℃ achieved the second-highest strength among the inorganic additive series, reading 60MPa, 10MPa lower than W4W.

However, N4W records 46MPa for samples fired to1040°C and 38MPa for clay samples fired to 950℃. However, it falls short when inorganic mineral additives are compared to the control (81.5MPa). This goes on to show the effect of the additive on brick properties.

None of the additives (inorganic) passed the BSI standard for Class B Engineering brick strength of 75MPa.

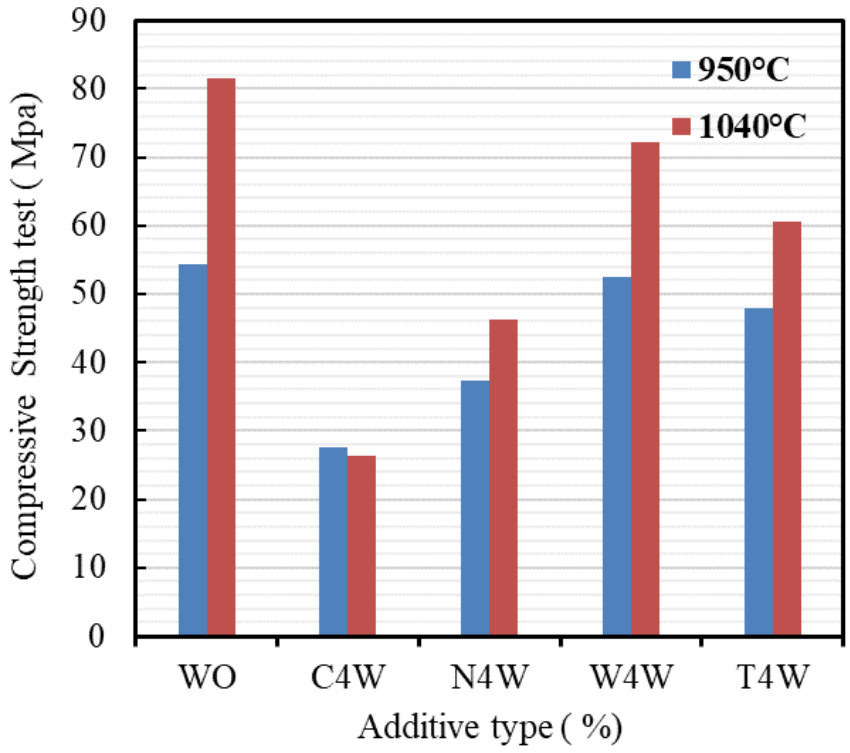

Figure 7-10: Compressive strength of incorporating 4wt% inorganic wastes into clay body for brick making at a loading rate of 5 MPa /s. Where C4W= 4wt% colemanite, N4W= 4wt% nepheline syenite, W4W= 4wt% wollastonite and T4W= 4wt% .Error margin ±2-14 (MPa) and ±0.2 (Boiling water absorption test)

7.7.3 *Mercury Intrusion Porosimetry analysis*

Pore diameter for samples fired to 950°C ranges from 0.01- 0.5µm except for the colemanite sample, whose pore size moved towards the macro-pore sizes (10µm). N4W containing samples records the least (17.58%) intrudable pore, whilst W4W and T4W containing samples read 18%. Also, the percentage of Hg porosity shows a higher % for C4W (18.44%) than any

other additive. Samples fired to 1040°C generally saw a reduction in the Hg % compared to the 950°C. At 1040°C, the pore sizes have now shifted from 0.5μm -1μm except for C4W, which went above 10μm. C4W again records the least porosity with 12.61%, and W4W obtains 13.65%, whilst T4W marks the highest Hg porosity (14.25%). These are shown in **Figures 7-11**.

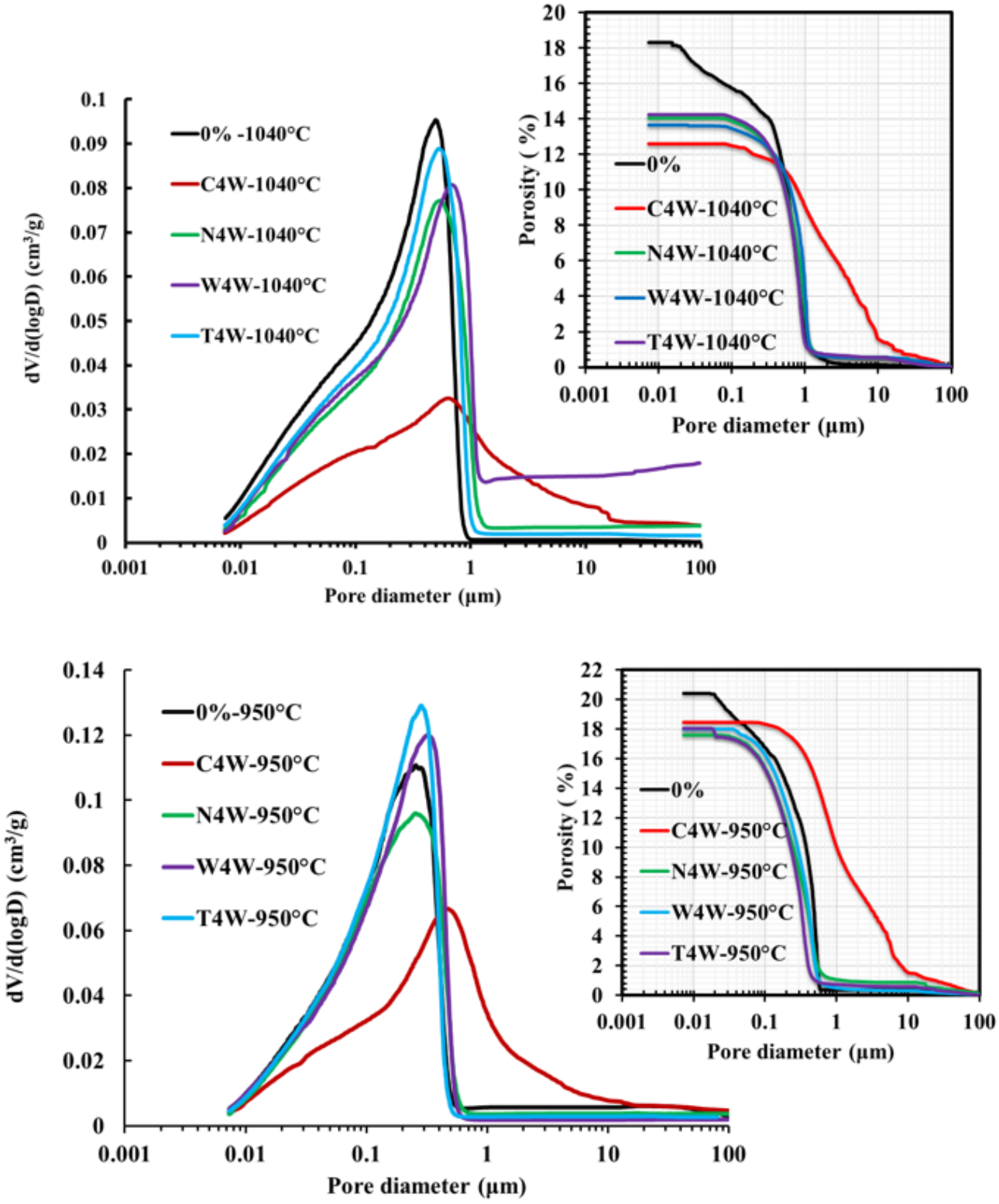

Figure 7-11*:* Pore diameter and porosity percentages of inorganic mineral additives containing body fired to 950°C and 1040°C.

7.7.4 *Predicting inorganic minerals admixture durability using the Maage equation*

Colemanite-containing samples fired to 950°C and 1040°C were predicted to be durable with >120 values. 4wt% Wollastonite, Nepheline syenite and Talc fired to 1040°C were found to be in the uncertainty region, whiles the low-fired replicates (950°C) of these samples were found to be non-durable (see **Appendix 3**).

7.7.5 *Scanning Electron Microscopy*

Generally, inorganic additive samples (C4W, N4W, T4W and W4W) fired to 950°C had a similar matrix with conglobation and pores present.

At 1040^{o}C, some individual particles and pores are present in all samples. N4W (b) and T4W (c) have a similar structure: sharp angular or needle-like pores. C4W (a) has even larger pores than the remaining three additives (N4W, W4W and T4W). The N4W, W4W and T4W microstructures are denser, with many closed pores and compact interconnectivity among particles and lone islands of quartz grains. These pores tend to be filled from the liquid-solid phase on chemical reaction (see **Figures 7-12 &13**). Generally, there is much more sintering with samples fired at 1040°C than with samples fired at 950°C.

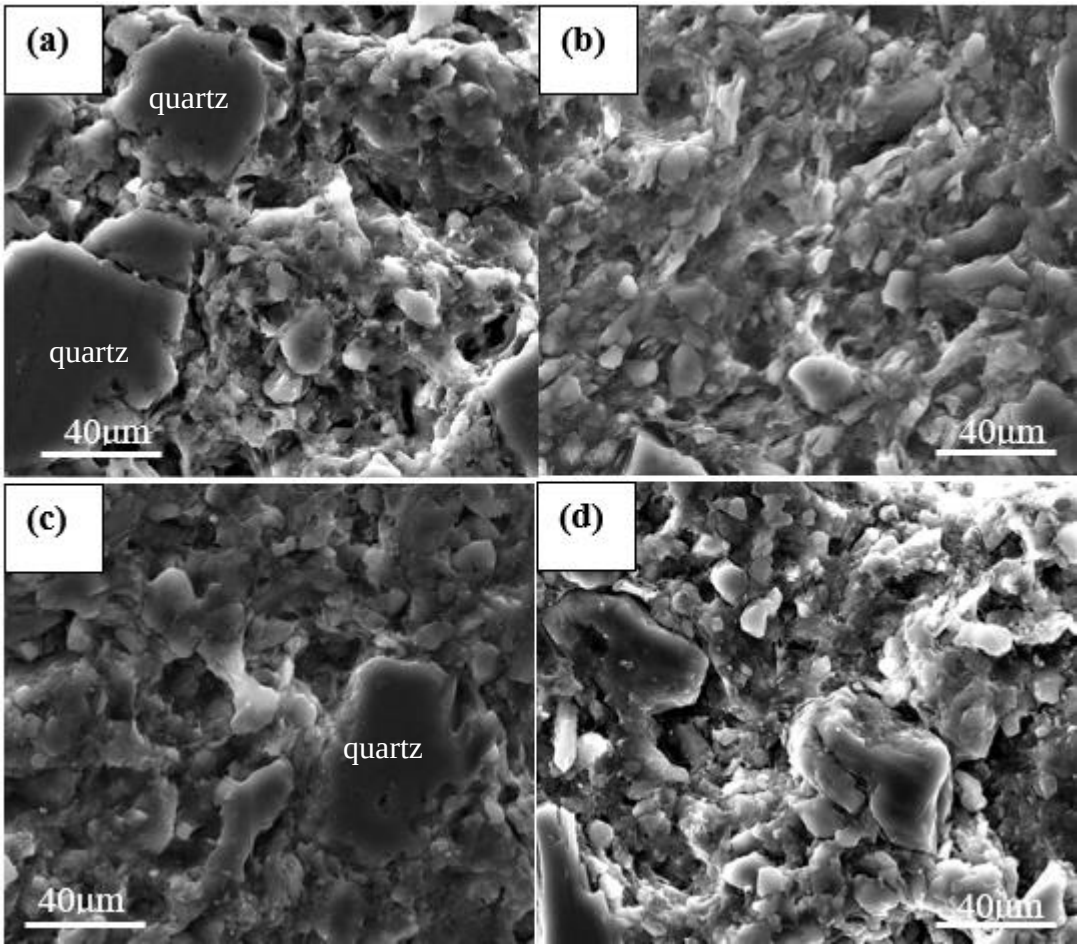

Figure 7-12: SEM images on 4wt% (a) Colemanite (b) Nepheline syenite (c) Talc (d)Wollastonite in Weald clay fired to 950°C.

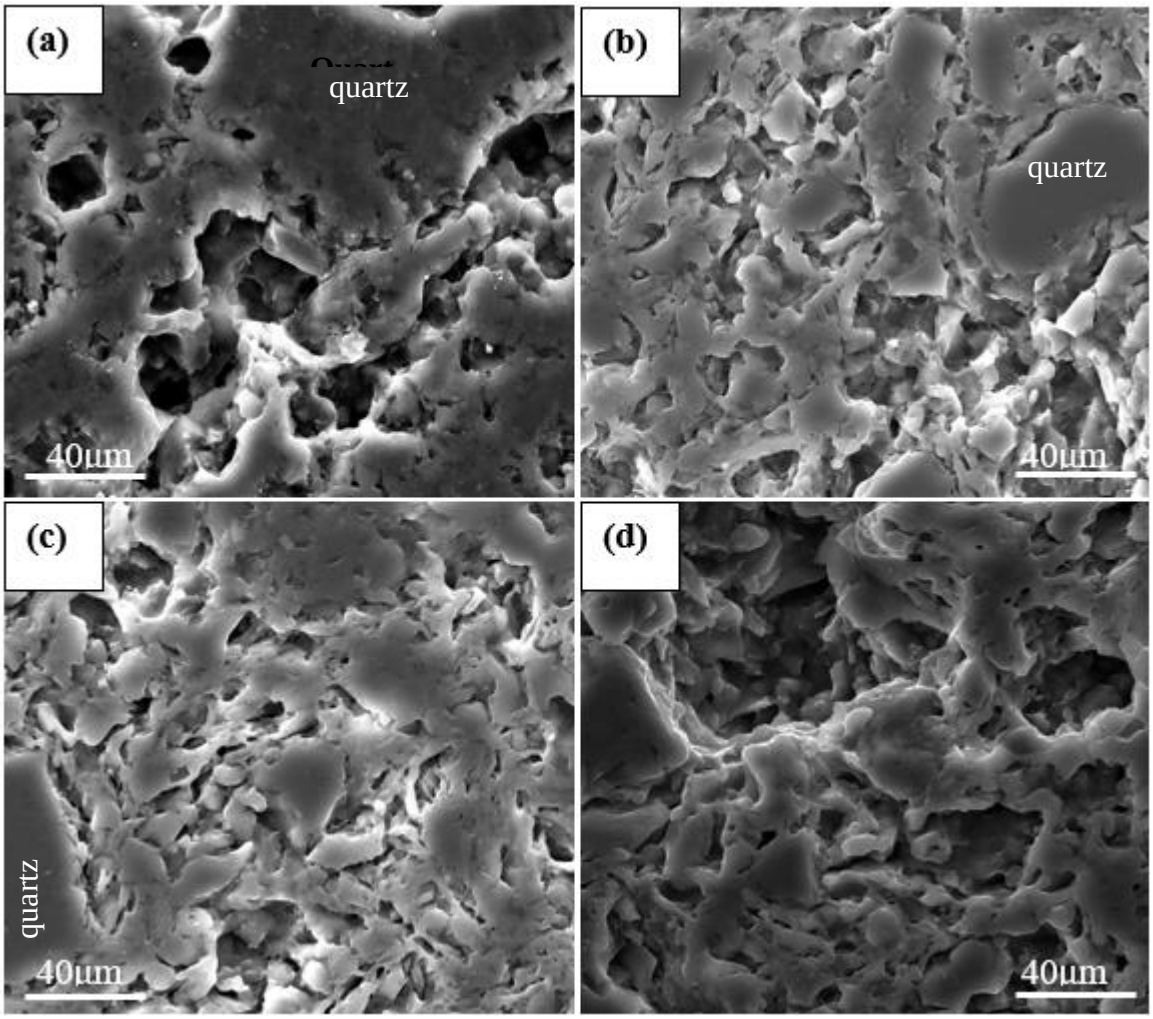

Figure 7-13: SEM images on 4wt% (a) Colemanite (b) Nepheline syenite (c) Talc (d) Wollastonite in Weald clay fired to 1040°C.

7.8 Dissussions of Inorganic mineral additives in the production of a Class B Enginerring Brick

7.8.1 *4wt% Colemanite additions effect in ceramic production*

The major fluxing additive in colemanite is boron, calcium, and strontium accounting for 76.1%. Although boron was not detected due to the instrument detection limit, the thermogravimetric and dilatometric examination detected the oxidation of the boron compound at temperatures between 363°C and 380°C, consistent with literature[398,399]. Expansion of the body doubled due to the boron compound's breakdown, causing bubbles and internal stresses in the form of microcracks within the body on heating (950°C and 1040°C), the highest shrinkage (3%) on the dilatometry curve. This internal stress affected the colemanite body's pore structure, resulting in the highest boiling water absorption (**Figure 7-9**) and Hg porosimetry shown in **Figures 7-11**.

The secondary electron image in **Figure 7-12/13** revealed a larger pore structure for ceramics containing colemanite fired to 950°C and 1040°C, consistent with values obtained with the water and Hg porosimetry**.** The mechanical strength was affected due to the pore structure, which was found to go towards a larger diameter (10μm). Another reason for the obtained low strength was the weak bond created by the boron (the glass phase viscosity). The crystalline phase mullite formed at 1040°C from the additive was found to contain boron (B^{3+}) substituting for Si^{4+} in the structure on heating.

What was surprising with this additive was the contradictory results obtained from the shrinkage by dilatometry measurement and volumetric shrinkage values. Thus a high shrinkage dilatometry measurement versus low volumetric shrinkage.

Aesthetically, the colemanite additive(4wt%) promoted the intensity of the colouring oxides, especially, Fe_2O_3 present in the clay from the decomposition of clay minerals[282] This effect was

comparable to the $BaCO_3$ additive added in high levels (4wt%). **Chapter 8**, **section 8.2.4** on Mössbauer studies, discusses this further.

The Ca in the Colmanite promoted the formation of anorthite, a characteristic of CaO reaction with metakaolin in samples fired to 950 and 1040^{o}C. Hematite (Fe_2O_3) formed as a free mineral from the anorthite phase promoting its strong reddish hue [135].

7.8.2 *4wt% Nepheline syenite additive effect in ceramic production*

The chemical composition obtained by XRF is consistent with the literature except for its high quartz content (55%)[400]. Dollase & Thomas [401] reported high silica- low alkalis content in some naturally occurring nepheline[401]. The high SiO_2 will mean this additive's melting temperature or activation energy will also increase.

In line with the hypothesis of using fluxing additives to reduce sintering temperature, the high $K_2O + Na_2O$ (see **Table 7-1**) achieved a 19% reduced sintering temperature by replacing 4wt% with Weald clay by dilatometry studies (**Figure 7-6**). Also, as mentioned earlier, the additive amount did not cause excessive shrinkage as expected compared to the 100% clay due to its high silica content. The volumetric shrinkage, boiling water absorption, and MIP results were lower than the control because of the low viscosity and closed pore developed during the cooling of the sample[402]. One would have expected that the lower boiling water absorption% would produce a higher strength; instead, the obtained strength for replacing 4wt% nepheline syenite and firing at 950°C and 1040°C was below the 75N/mm^2/MPa, for a class B Engineering, possibly because of the temperature at which the ceramic was fired at. Moreover, previous studies have found the additive to cause pyroplastic deformation of sanitary wares, higher shrinkages, and lower water absorption [293]. An adverse effect (more melts resulting in shape distortion) of the use of greater than 5% nepheline syenite in a porcelain body fired to

1260°C was reported by Esposito et al. [292]. In stoneware and porcelain bodies, nepheline syenite promoted ceramic microstructure[292] and low vitreous phase[403]. Processed nepheline syenite in magnesite glasses developed by Hamzawy and Khatar [297] was reported to impact glass colour. This colour included white, off-white and arrays of blue on a ceramic dielectric being improved by 50% additive due to the large liquid phases formed. How nepheline syenite affects brick colour has been explained using Mössbauer spectroscopy, discussed in **Chapter 8, section 8.2.6.2**. No change in the crystalline phase was obtained when compared to 100% clay fired to 950°C and 1040°C, but the melt formed provided a stronger bond, with the soaking time (2hrs) being advantageous[293].

7.8.3 *4wt% Wollastonite additive effect in ceramic production*

Wollastonite is a calcium silicate additive. It enters the composition for a ceramic product as both flux and a filler[404]. This is evidenced by the low boiling water absorption (8.2%) and high shrinkage (9%) but not greater than the 100% clay at a shrinkage (9.8%) due to its refractoriness and strength (60.5MPa) obtained (**Table 7-2**). The calcium oxide provides a resistive expansion on heating that is non-destructive for brick body composition. However, the excess lime (CaO) provided by the additive increased the surface stain found with the 100% clay fired to all temperatures. On drying, however, unlike the 100% clay, no whitish stain was detected due to its low solubility to deionized water.

Sintering from the dilatometry study shows that sintering starts after 900^{o}C with continual shrinkage. $CaSiO_3$ reacts with the clay at 1040^{o}C (**Figures 7-1&2**) to form mullite ($Al_{2.26}Si_{0.74}O_{4.87}$), quartz ($SiO_2$), hematite ($Fe_2O_3$) not incorporated into any phase, Calcium Sulfate ($CaSO_4$), Microcline ($KAlSi_3O_8$) and Di- Diopside (Ca (Mg, Al) Si, Al)$_2O_6$). At 950^{o}C, mullite does not form, affecting the obtained strength (52MPa) and boiling water absorption (12%).

Research has shown that wollastonite has a high melting point of 1450°C[404]. However, this elevated temperature in semi-vitreous wares[404,405] porcelain and stoneware bodies fires between 1180-1304°C due to the reaction of CaO. SiO_2 plus feldspar or sometimes a combination with waste glass form a eutectic melt at a lower temperature. The best-optimised levels of wollastonite for a semivitreous ceramic are reported to be between 1-4wt%[405]. Clays naturally contain traces of feldspars; therefore, in this current study, combining wollastonite with either alkali/alkaline felspar was not required. The 4wt% level recommended by Vukovich et al. [405] was used with the existing fluxes present in the clay, but in lower quantities, to react/ combine on firing to produce a low absorption body and high impart strength to the ceramics comparable to the control. One of the challenges emerging from using wollastonite relates specifically to ceramic surface stains increased by the additional CaO from wollastonite. However, this can be corrected by $BaCO_3$ /$MgCO_3$, as stated above.

7.8.4 *4wt% talc additive ($Mg_3Si_4O_{10}(OH)_2$) effect in ceramic production*

Talc has been reported to lower the firing temperature of porcelain to about 20°C[406] and 11°C was recorded in this study on dilatometry studies. The real effect of talc on ceramic body composition can best be viewed with the boiling water absorption and mechanical strength compared to the different additives and the control. The porosity from the MIP was a 4% reduction compared to the control material (18%); however, obtained strength was 20 MPa lower than the control (**Table 7-2**) yet better than N4W. Talc addition in ceramic applications has been constantly reported to decrease the strength[406,407] , especially if the dosage is greater than 3%. Njoya et al.[408]experimental findings of 40% Talc additions in porcelain tile fired >1200°C was found to decrease the growth of mullite for cordierite ($11MgO\ Al_2O_3$) which was reported to be the reason for the tile strength. Meanwhile, Sallam and Hennike [409] observed that

up to 5% talc increased the quantity of mullite just as Kaolinite will. However, in this current study, spinel, along with mullite, formed by the following reactions:

$Al_2O_3.SiO_2.H_2O + Mg_3Si_4O_{10}(OH)_2) \longrightarrow Al_2O_3SiO + Mg\ Al_20_4 + SiO_2$

Spinel ($Mg\ Al_20_4$)is the only new phase formed differently from the control material when the material is fired to 1040^{o}C.

Incorporating 4wt% talc in the ceramic application was disappointing based on the effect (scum removal) observed on $MgCO_3$-based samples (see **Figure 5-52**). This finding raises interesting questions regarding the chemistry of the two additives, the role of Akermanite, and whether this is the key reason that greater than 2wt% $MgCO_3$, there was no scum formation on fired ceramics even though the main fluxing in Talc is MgO. It is possible to hypothesise that talc, a magnesium source, does not stop whitish stains on ceramics, or the 4wt% could not be the optimal % for the mineral (Talc). Also, the flux, MgO, will reduce the sintering temperature by 2%, promote strength, minimize porosity, and promote shrinkage. Further research should be undertaken to investigate why changes in the mineral chemistry of the additive do not reduce or remove scum.

7.8.5 *Durability prediction on modified Weald clay using Maage equation*

Maage equation (3.2/PV)+(2.4*P3)[177] is undoubtedly a simple method for predicting brick and tiles frost resistance using the pore size distribution obtained by MIP. In the calculation, cumulative volume and volume distribution are considered[178]. However, results obtained show that admixtures that had previously shown excellent strength >60MPa all failed using the Maage equation, but surprisingly, samples that failed in ceramic strength due to larger pores and high porosity, as in the case of colemanite samples fired to 950°C, and 1040°C resulted in durable ceramic by Maage Equation. The results shown in **Appendix 3** suggest that the Maage

equation only favours larger pores. Nevertheless, factors reported affecting durability are mineralogy, base material composition, strength, porosity and pore size distribution which is a function of temperature [177,410]. Sveda et al.,[411] raised this concern of Maage favouring only larger pores when a failed sample recorded 28.2 passed a 155 cycle (direct durability testing), obtaining only a single crack. Therefore, although in the Maage equation, a larger portion of modified bodies failed in the prediction studies, direct durability testing (freeze and thaw) is necessary and the best approach for heavy clay ceramics testing.

Chapter 8 Surface Defects Of Admixtures

Surface stains on ceramics can be introduced intentionally (glazes, brick hearth, textured) or can appear as an unwanted occurrence from raw materials(efflorescence/ scum). Surface scum was first observed on Weald clay containing no additives on drying and after firing. See **Figure 4-9**. The level of scum that develops on drying was influenced by sulfate or soluble salt content in the clay and the water of plasticity needed to shape the cylindrical pellet [2,73,133,183,189,412]. The water present transports the stains (salts) to the surface and deposits them via evaporation. In some instances, stains will not be noticeable on drying but firing; they can become visible. Natural variation occurs within the stockpile received by the company. The unusual changes produced by six selected additives (alkali carbonates, alkaline earth carbonates, and inorganic wastes) on the incidence of staining are addressed in this chapter.

Additives such as 1wt% Li_2CO_3, 1wt% Na_2CO_3, and greater than 2wt% $MgCO_3$ resulted in ceramics that showed no scum on firing and $BaCO_3$[42,67,197,380], the traditional scum remover used by heavy clay manufacturing companies. In this section, three types of defects are discussed (i) defects in the form of patches caused by alkali carbonate type additives; (ii) whitish flaky stains caused by Na_2CO_3 on drying; and (iii) scum or white stain caused by $CaSO_4$.

8.1.1 *Defects on samples containing Li_2CO_3 and K_2CO_3 (Visual examination)*

Fired samples containing 1wt% Li_2CO_3 (L1) showed an unusual stain of dark brownish-red colour at the rim. This is due to ceramic temperature, steam removal from the ware on firing (900-1040°C) and the iron-bearing phase in the clay. At 2wt% Li_2CO_3 (L2), a mixture of dark patches and creamy-yellowish patches forms on half the top of the sample surface. The yellowish stain was not caused by vanadium or molybdenum[413] because these were not present

in the bulk chemical examination (XRF). This yellow stain became darker with increased additive-4wt% Li_2CO_3 (L4), with now what appears to be a whitish stain melting again at the rim. This is shown in **Figure 8-1**

Figure 8-1: Surface defects of ceramic samples containing Li_2CO_3 fired to 900°C-1040°C (a) 1wt% Li_2CO_3 (b) 2wt% Li_2CO_3 dark rim and creamy-yellowish patches, (c) 3wt% Li_2CO_3 and (d) 4wt% Li_2CO_3 darker rim and creamy-yellowish patches/melts

However, ceramic samples containing K_2CO_3 additive showed dark patches on the ceramic surface with an intense colour at the rim for 1wt% K_2CO_3 (K1) samples fired to 900°C, 1000°C and 1040°C. With 2wt%-4wt% of additives, this produced a lighter brown patch on the fired clay surface. Wilson[197] describes these patches as "irregular polychrome" caused by iron salt moving to ceramic products' surface on firing, especially when the brick is lighter in colour. However, the XRD showed no trace of $FeSO_4$ in the unfired clay except for the general report of Weald clay containing sulphate of calcium, magnesium and iron causes scum[320]. This

irregular colour scheme /surface patches can be added to the existing brick shade pallet for attractive construction designs. See **Figure 8-2** of the fired ceramic samples containing K_2CO_3.

Figure 8-2: Surface defects of ceramic samples containing K_2CO_3 fired to 900°C-1040°C (a) 1wt% K_2CO_3 darker -patches at the rim(b) 2wt% K_2CO_3 lighter shade patches (c) 3wt% K_2CO_3 lighter shade patches and (d) 4wt% K_2CO_3 lighter shade patches.

8.1.2 Stains found on ceramics containing 4wt% colemanite ($2CaO.3B_2O_3.5H_2O$)

Clay doped with the inorganic additive colemanite ($2CaO.3B_2O_3.5H_2O$) and fired to 1040°C showed a yellowish stain on the surface. See **Figure 8-3**. According to Palmer[413], in a paper on vanadium and molybdenum compound in clays, he reported that yellow stains found on heavy clay ceramics are due to vanadium and molybdenum compounds present in the clay, but this was not the case for the colemanite sample because there was no trace of molybdenum, vanadium or chromium in the clay or the additive. Weald clays high in CaO and have been

reported to form yellow spots on red-brown surfaces after firing[135]. Other studies have reported that uneven distribution of iron promotes firing red spots on yellow-fired bricks[414] . Additions of 2wt% CaO content in kaolinitic and illite/muscovite clays with iron content between 3-10wt% can occasionally lead to yellow-fired clays[135]. Although the lime (CaO) present in the colemanite ($2CaO.3B_2O_3.5H_2O$) is high (69%) per the XRF because the light energy X-ray could not detect BaO from boron. Also, the bulk chemical analysis revealed that the Weald clay is Ca-poor (0.3%), but Fe present in the clay(>6%) was within the range given by Kreimeyer[135] (2-4% CaO and 3-10% Fe_2O_3). Therefore, we can infer that the possible reason for the yellow stain on ceramics containing colemanite is the presence or proportion of > 2% CaO and > 6% Fe in the body composition reaction with clay. However, the colemanite additive's strontium oxide (2.5%) could also influence this yellow stain. Moreover, boron and sulphur react with metallic oxides in the clay to form a yellowish stain, and the temperature of 1040°C may have promoted this stain, too, because, at 950°C, the ceramic surface was only covered by a white stain. In glazes, iron oxide addition could transform colour tones from light yellow to dark brown in ceramics fired in an oxidising firing atmosphere[414]. The change in colour of the surface stain from white to yellow appeared temperature dependent since firing temperature was the only variable. Alternatively, a slight change in the furnace environment cannot be discounted. It is recommended that future studies examine if there is an atmospheric change in firing samples containing colemanite in an electric furnace and the possible effect that strontium carbonate (2-3%) will have on low calcareous clays high in Fe_2O_3 (3-10%).

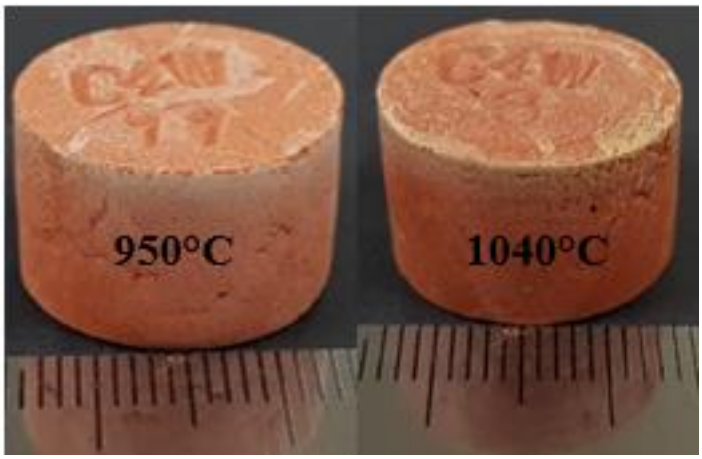

Figure 8-3: Surface stain following the addition of 4wt% colemanite to Weald clay and fired to 950°C and 1040°C.

8.1.3 Examination of surface stain on Weald clay using X-ray Diffraction

It is known that $CaSO_4$ is not decomposed until about 1200°C, which is above the maximum firing temperature for many red-firing clay wares reported by Wilson[197]. So, the stain found on the ceramic surface could result from incomplete burning of the causative compound ($CaSO_4$) by firing ceramics to 1040°C. This is why a fluxing additive, $BaCO_3$, is used to render the soluble salts insoluble within the industry.

The diffraction pattern of the whitish stain of Weald clay fired to 900°C was measured using X-rays from a cobalt source shown in **Figure 8-4**. The result indicates that the stains are crystalline. The stain is a mixture of quartz (Qtz), calcium sulphate (CaS) and calcium silicate (CS). Calcium sulphate was also present in the powdered samples of the control ceramic fired to 900, 950, and 1040°C studied using copper X-rays reported in **Figure 8-5**.

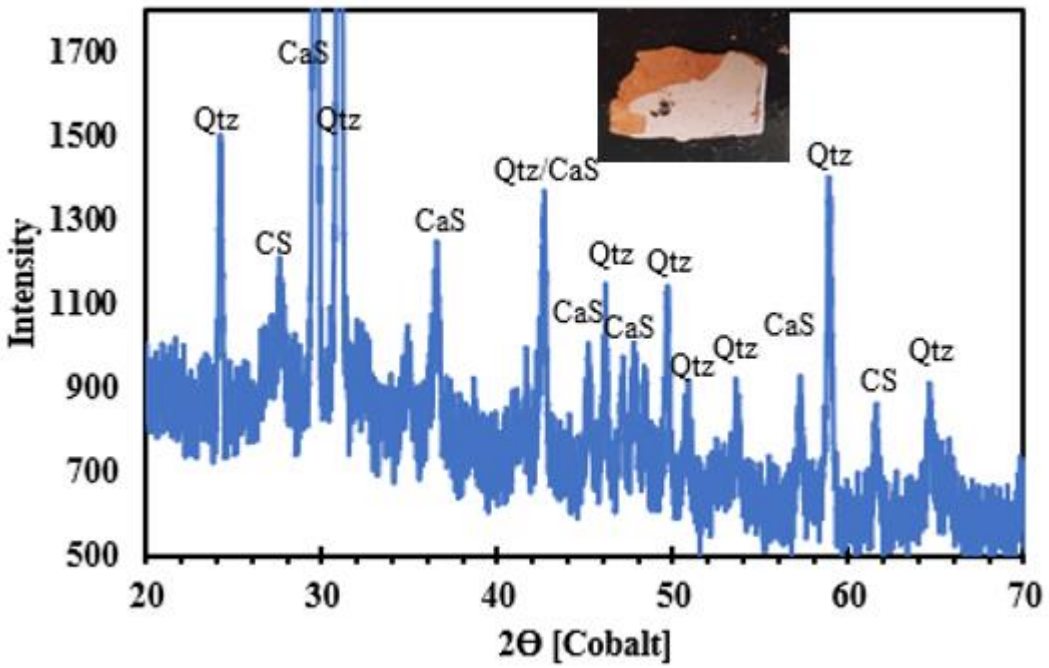

Figure 8-4: XRD pattern of Weald clay surface stain on ceramic sample fired to 900°C where Qtz= quartz, CaS= Calcium sulphate and CS=Calcium silicate

8.1.4 Raman spectroscopy of surface stain (scum) on Weald clay

This study was important to explain and support the cause of the whitish scum by the reaction of sulphate (S) and Ca^{2+} to form $CaSO_4$ on the fired ceramic surface shown in **Figure 8-5**. Raman spectra collected on the ceramic surface (monolithic) were between 100-1500$cm^{-1,}$ and $CaSO_4$ peaks detected from 416cm^{-1} to 1159cm^{-1} were found to be $CaSO_4$ and were consistent with anhydrite characterised by Berenblut et al.[415]. Sulphate main frequencies are reported to be under four vibrational modes by M. Lenoir et al.[416]. The strongest sulphate peak at 1016 cm^{-1} is assigned to the ν_1 symmetric S-O stretch band of the crystalline sulphate; most glass-doped sulphates obtained their strongest peak near this frequency[415–418]. The symmetric O-S-O bending modes are assigned to 416, 498 cm^{-1} for the second vibrational mode, also obtained by Berenblut et al.[415] on anhydrite. Raman bands at 1111, 1120 and 1159 cm^{-1} have been assigned

to ν3 asymmetric S-O stretch modes, once again consistent with Raman data for anhydite[415] with ± 1 changes in the obtained peak frequencies. Finally, vibrational modes for sulphates ν_4 are asymmetrical O-S-O bending modes near 608, 627 and 675 cm^{-1}. The weak peaks (100-320 cm^{-1}) have been assigned to Ca-O bonding modes[419]. This study of the cause of ceramic stains with Raman spectroscopy supports evidence from previous observations, especially [415] which concludes that the whitish stain on fired ceramics is $CaSO_4$. A summary table for the Raman peaks and their assigned origins, with corresponding references, is shown in **Table 8-1**. **Figures 8-8 to 8-10**, where inorganic and industrial wastes were added to Weald clay in 4wt%, were confirmed to be $CaSO_4$. No sulphate bands were found with samples containing 2wt% and 4wt% $BaCO_3$ and $MgCO_3$, explaining the scum-free surface after firing, as shown in **Figure 8-11**.

The SEM / EDX analysis of the whitish surface stain collected from the surface of the fired reveals that it is rich in Ca and S, as shown in **Figure 8-6**. However, the red parts of the sample surface (i.e., those not covered by whitish stains) showed low Ca and S contents. It may thus indicate low levels of Ca and S on the surface and/or in the clay matrix, such that only lower amounts of $CaSO_4$ are retained in the ceramic body. The majority is found at the surface. The sulphate retention in fired ceramics is in alignment with Brownel's[183] work.

Moreover, a visual examination of the fired samples stained with whitish pigments was found to be unequally distributed on the ceramic surface, as shown in **Figure 8-7,** along with SEM to see the spread. In the SEM image, some regions with more populated grains were denser than lighter regions, marked in a red rectangular box. That explains the uneven thickness of the stains on the body. Further studies are needed on what causes the concentration of stains to occur.

Table 8-1: Frequency region of $CaSO_4$ on a ceramic surface

Current work		
Wavenumbers (cm^{1}) obtained from this study	Assignments	Reference
416	ν_2- symmetric bend modes O-S-O	415,420
498	ν_2-symmetric O–S–O bend modes	415,420
608	ν_4-O-S-O Asymmetric bend mode	415,420
627	ν_4- Asymmetric O–S–O bend	415,420
675	ν_4-Asymmetric O–S–O bend	415,420
1016	ν_1 symmetric S–O stretching	416–418,420
1111	ν_3- Asymmetric S–O stretch modes	415
1128	ν_3-Asymmetric S–O stretch modes	415
1159	ν_3-Asymmetric S–O stretch modes	415
1322	Hematite band	421

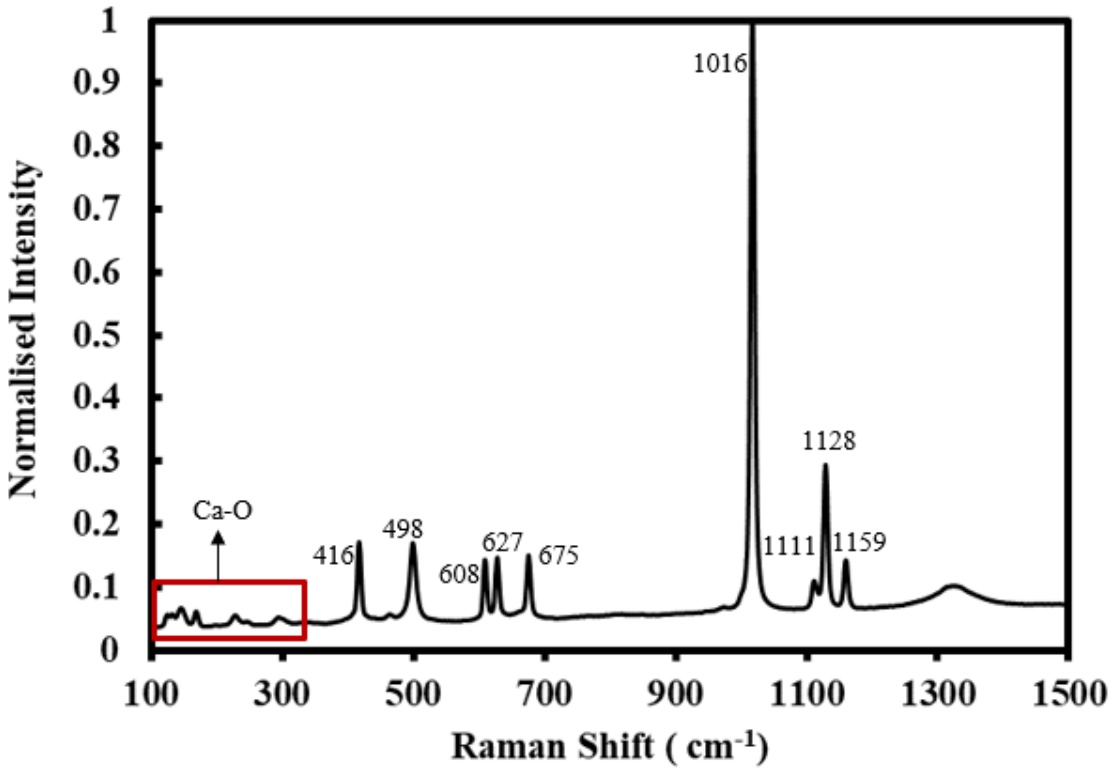

Figure 8-5: Raman spectra of surface scum on a solid piece of Weald clay fired to 900°C

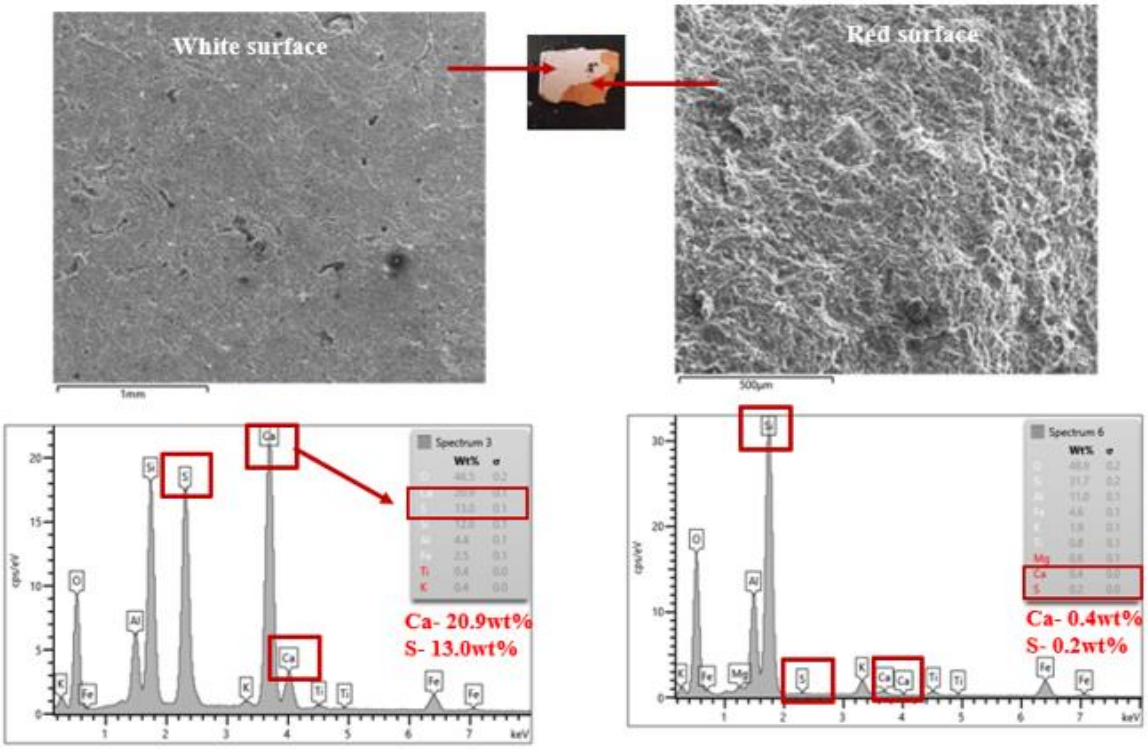

Figure 8-6: SEM/EDS on white and red surface of Weald clay fired to 900°C

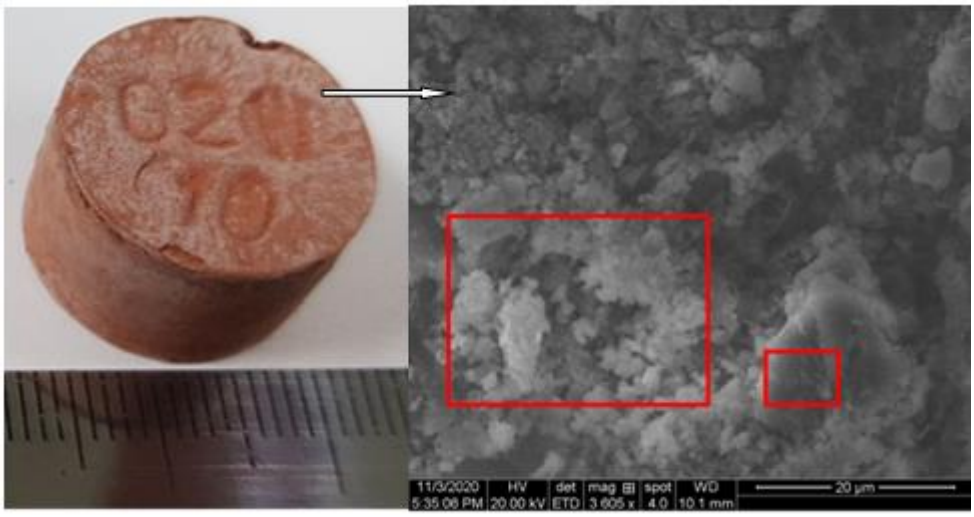

Figure 8-7: Uneven distribution of whitish stain on a ceramic surface containing 2wt% container glass fired to 950°C.

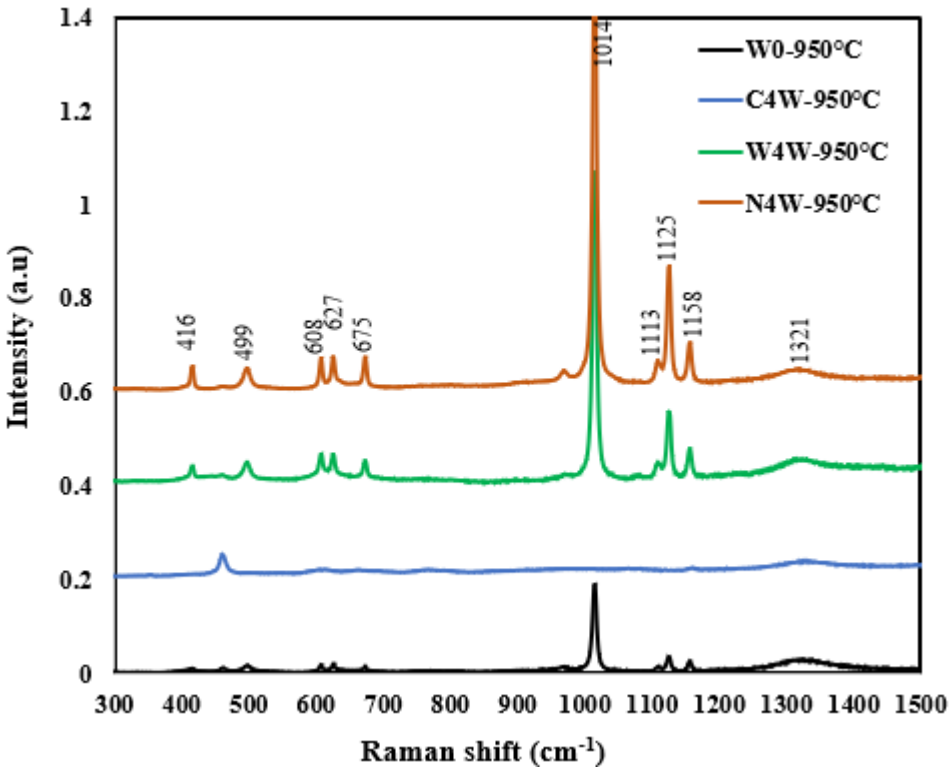

Figure 8-8: Raman spectra showing sulphate bands obtained with 4wt% inorganic wastes fired to 950°C compared to the 100% Weald clay sample.

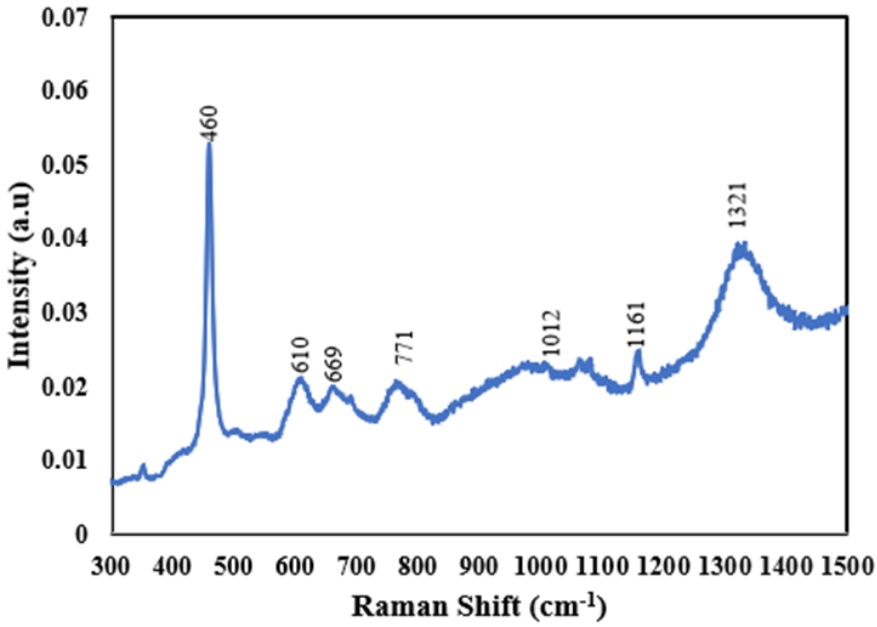

Figure 8-9*:* Raman spectrum showing sulphate bands obtained with 4wt% Colemanite sample fired to 950°C

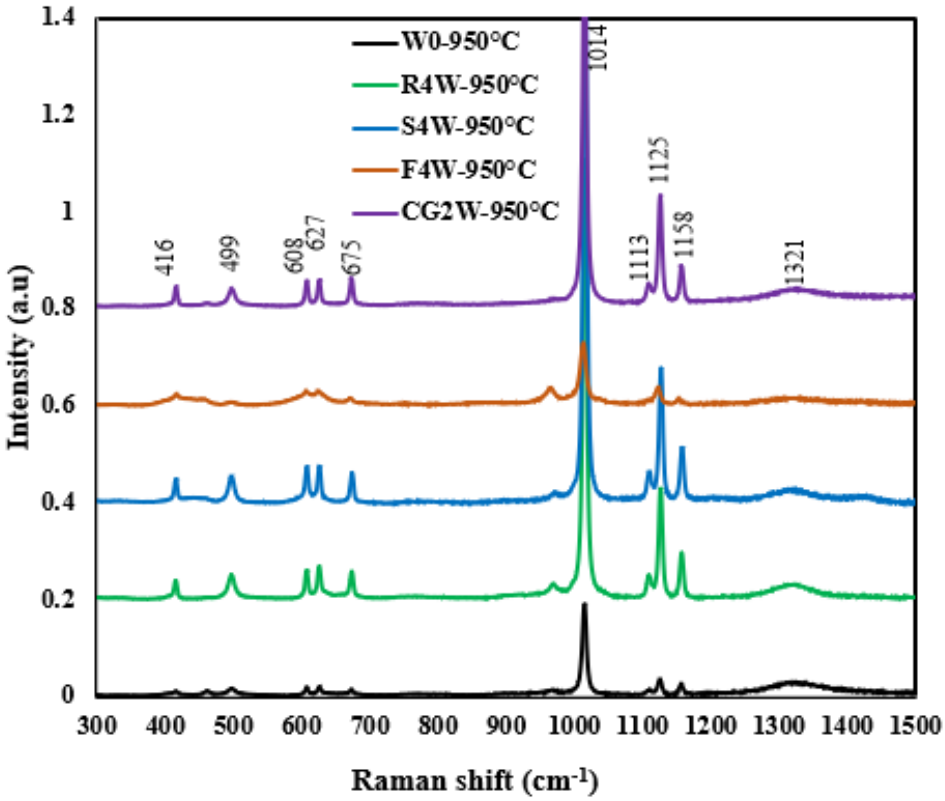

Figure 8-10: Raman spectrum showing sulphate bands obtained with 4wt% industrial wastes sample fired to 950°C compared to the Control.

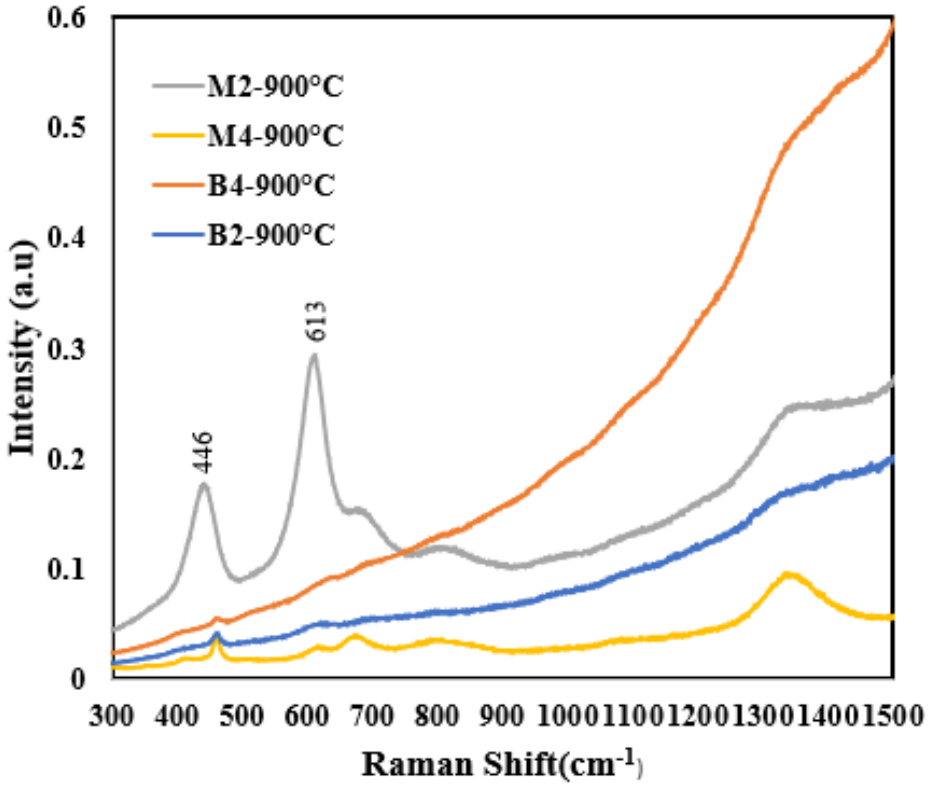

Figure 8-11: Raman spectrum showing no sulphate bands with samples containing 2wt% and 4wt% $BaCO_3$ and $MgCO_3$ samples

8.1.5 *Effect of additives on drying causing whitish stains on drying*

Chemical, mineralogy and microscopic analyses were conducted to examine the constituent of the flaky whitish stain obtained on samples containing >2wt% Na_2CO_3. The Na_2CO_3 additive promotes efflorescence on drying when levels of additive increase to >2wt%, forming a flaky white substance that could be scraped off from shaped clay on drying (see **Figure 8-13**). Because of the additive (Na_2CO_3) low melting temperature (851°C)[422] on firings, it melts and, depending on the temperature, produces a matt or glossy surface shown in **Figure 8-12**.

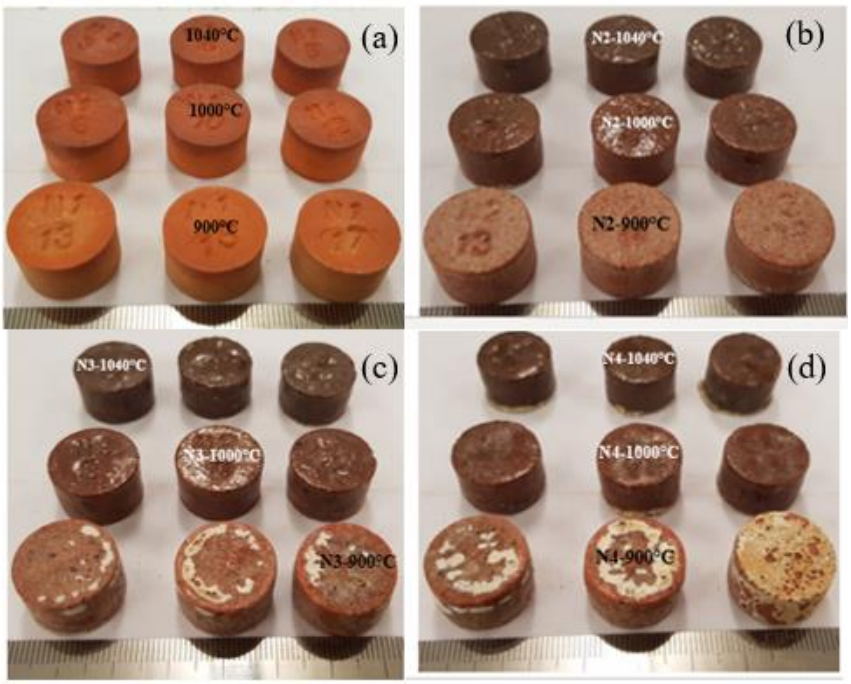

Figure 8-12: Surface defects of ceramic samples containing Na_2CO_3 fired to 900°C-1040°C (a) 1wt% Na_2CO_3 showing no stains; (b) 2wt% Na_2CO_3 showing matt surface at 900°C and a glossy surface at temperatures >1000°C; (c) 3wt% Na_2CO_3 showing a matt and white-stained surface at 900°C and a glossy surface at temperatures >1000°C; and (d) 4wt% Na_2CO_3 showing a matt and white stained surface at 900°C and a glossy surface at temperatures >1000°C.

The findings show that at 1wt% Na_2CO_3, the ceramic had no stains on the sample surface on drying. However, at greater than 2wt% Na_2CO_3, the salt crystallises or appears on the sample surface after forming. This is consistent with Brownel's[182] findings, in which he suggested that small additions of Na_2CO_3 can prevent scumming on clay products. The whitish stain mostly appeared at the rim exposed to air, then gradually distributed around the shaped or formed cylindrical test piece. Moreover, samples with 3-4wt% Na_2CO_3 developed stains even at the base of the cylindrical piece, as shown in **Figure 8-13.**

Oxide	Weight %
Na_2O	59.4
SiO_2	30.5
Al_2O_3	6.9
Fe_2O_3	3.4
K_2O	1.1
TiO_2	0.7
CaO	0.2
SO_3	0.1

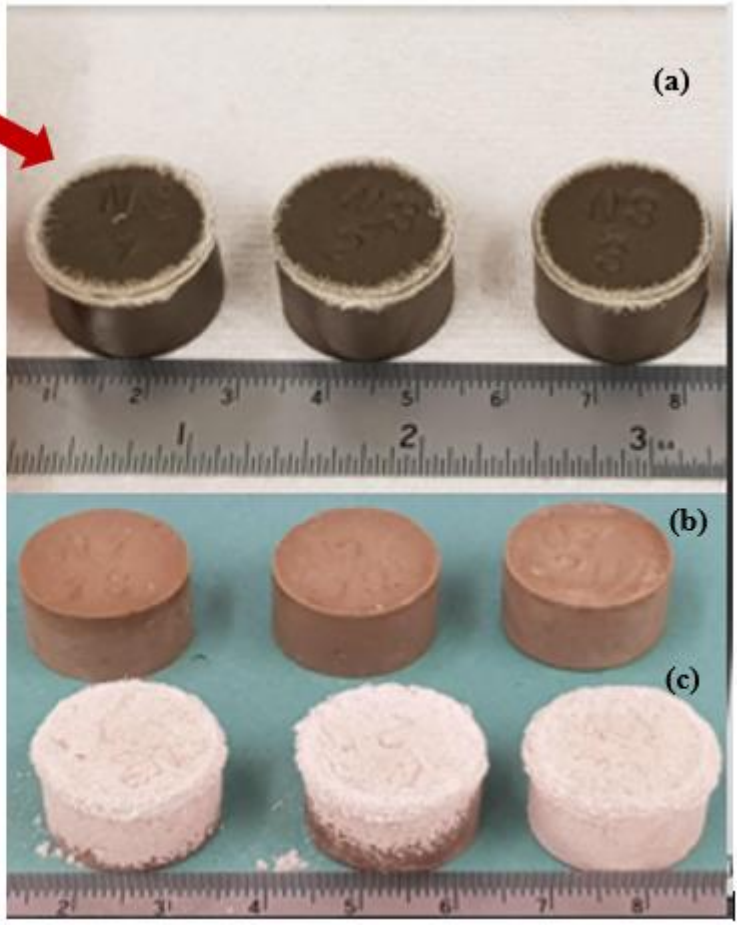

Figure 8-13: Whitish substance forms on Weald clay containing Na_2CO_3 additive (a) Wet clay sample with developed efflorescence after adding 3wt% Na_2CO_3 (b) Dry clay shaped sample containing 1wt% Na_2CO_3 and (c) bench drying of Na_2CO_3 containing the sample and its bulk chemical composition with XRF.

The chemical composition of the whitish substance formed on the clay body surface upon drying when Weald clay is doped with >2wt% Na_2CO_3 is depicted in **Figure 8-13**. The main constituent was a soluble compound of sodium (e.g. Na_2CO_3), with traces of impurities clearly from the clay -silica, alumina, iron, potassium, calcium and sulphur. Transportation of the whitish substance from the body surface is believed to be through the pores[190].

Mineralogical phases identified using XRD show that the whitish substance (scraped powder) on the cylindrical body contains approximately 30% Na_2CO_3, 1% $CaCO_3$, 41% muscovite, 5% kaolinite and 23% quartz, shown in **Figure 8-14**. The clay mineral only indicates contamination when the whitish stain is scraped from the green body (shaped unfired clay).

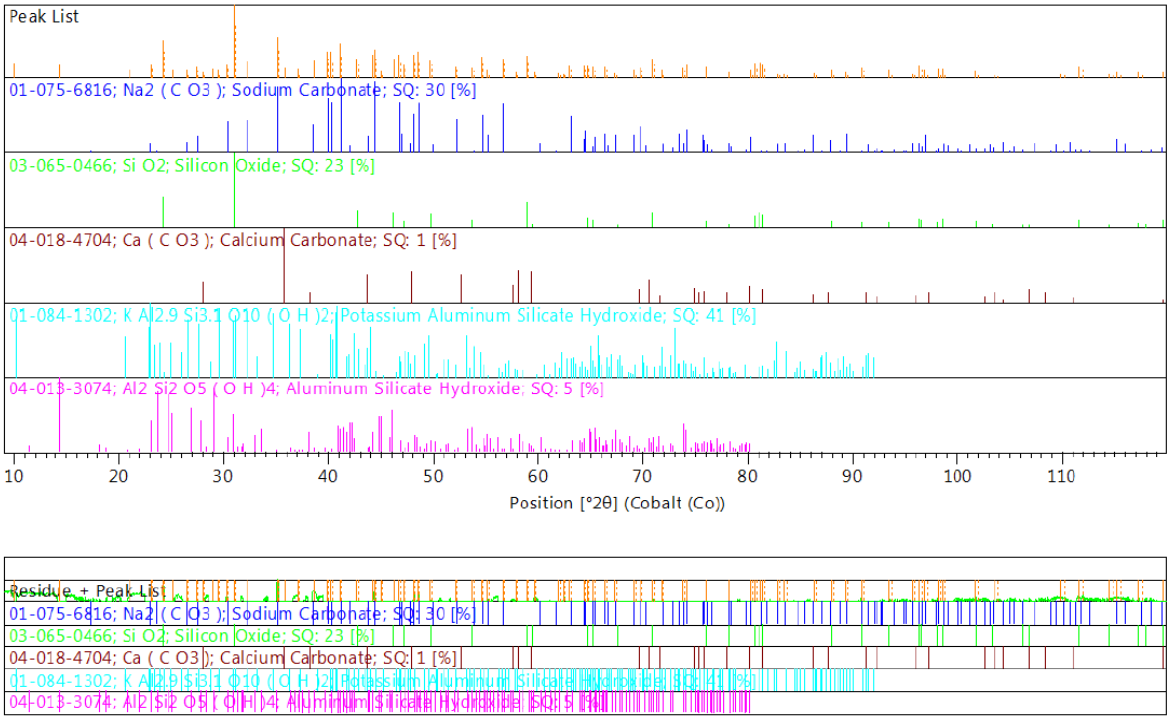

Figure 8-14: Mineralogical phases of whitish substance on Na_2CO_3 additive at levels greater than 2wt %.

8.1.6 *Morphology of efflorescence surface of clay containing Na_2CO_3*

Microstructural analysis by SEM / EDS was used as a complementary tool to XRD in verifying the whitish stain shown in **Figure 8-15.** The secondary electron images show needle-like elongated crystals scattered within the image and larger shapes populated by many particles. The composition revealed by EDS point analysis shows that Na_2CO_3 crystals dominate the stain, and the S content is very low, with Si and Al as possible contamination from scraping the whitish stain from the surrounding clay.

The fibrous nature of the needle-like shape structures was viewed more detail by increasing the magnification (point 5) and the same chemical information was discovered.

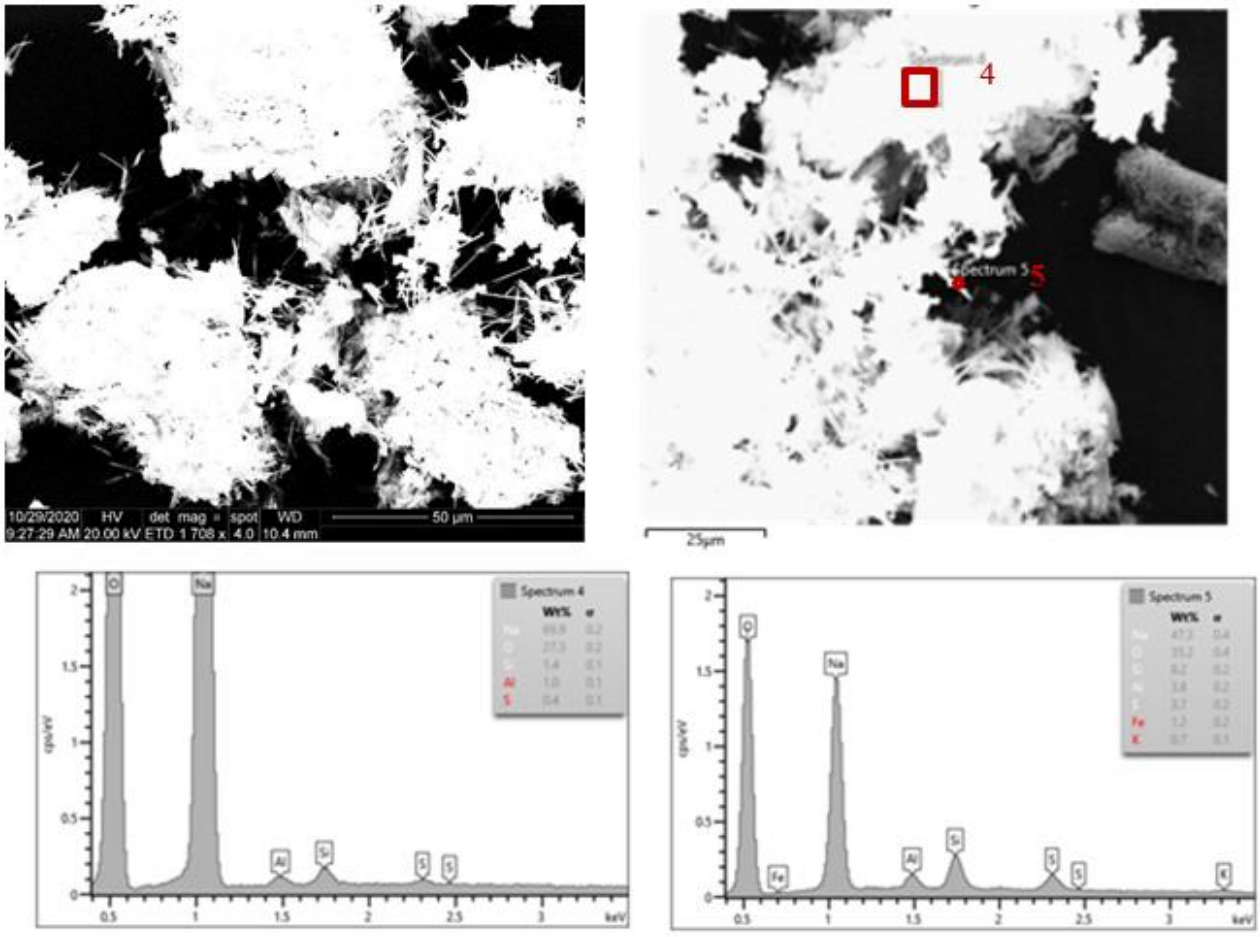

Figure 8-15: SEM/EDS studies of whitish stain on green ceramic body containing >2wt% Na_2CO_3.

8.1.7 *Conclusions*

In the current study, comparing surface stains obtained by incorporating alkali and alkaline earth additives and inorganic mineral additives into ceramic formulations, the following conclusions can be drawn:

1. The surface stain present on Weald clay after firing is caused by $CaSO_4$.
2. Greater than 2wt% $MgCO_3$ additive to Weald clay was an optimum level to facilitate precipitation of sulphate salts and discolour ceramic surface and provide a potentially viable, non-toxic alternative to using $BaCO_3$ in heavy clay ceramic manufacture.
3. Addition to Weald clay with 1wt% alkali (Li, Na, K) carbonate additives and firing to 1040°C surprisingly removed surface stains. However, a darker reddish or brownish colour was obtained at the rim of the ceramics.
4. Na_2CO_3 additive levels greater than 2wt% in the ceramic body mix produced efflorescence / drier scum after shaping and firing, producing a matt or glassy coating on the ceramic surface, depending on the firing temperature.

8.2 Mossbauer Spectroscopy

The colour of fired clay brick is associated with several factors: Fe content in the starting clay minerals, their reactivity upon firing, and the phases in the final material. Additional samples in which the clay was partially replaced by 4wt% colemanite ($Ca_2B_6O_{11}\cdot 5H_2O$) and another six (6) additives were also produced and compared to the fired clay and the unfired clay spectrum.

Upon firing, a noticeable colour change compared to the control sample. Results obtained from ^{57}Fe Mössbauer spectroscopy reveal that iron is present in all samples, predominantly as Fe^{3+} as hematite (Fe_2O_3), except for the unfired Weald clay, which had Fe^{2+} as well. Differences in Fe^{3+} partitioning and site populations between the seven samples were measured: these were consistent with observed differences in XRD patterns and can be related to colour differences of the fired ceramics. This range of ceramic colours can give brickmakers more flexibility in their product range. ^{57}Co Rhodium matrix 14.4eV source was used for the data collection.

8.2.1 *Interpreting Mössbauer spectra*

Mössbauer spectroscopy is used in ceramic studies to differentiate oxidation and coordination states of iron and identify specific iron environments affecting colour change. One key constraint is the technique's inability to quantify the number of Fe atoms in a specimen [339].

Non-Fe-bearing species, as part of a composition, only alter the specific Fe-site whilst decreasing the spectrum's intensity.

The main parameters for interpreting Mössbauer spectroscopy are the isomer shift (IS) read from the "difference between the midpoint of doublet and zero on the velocity scale, quadrupole splitting (QS) as the separation of two-component peaks/shift in energy levels caused by electric field gradient and a nearby electron and enables the identification of the valence state and occupancy of Fe sites." The hyperfine interactions or Zeeman effect, which usually shows as the six peaks called the sextet, is caused by the interaction between nuclear magnetic dipole and the magnetic field at the nucleus for magnetic materials[142,338,339]. Some common structures and clays parameters related to this study are summarised in **Table 8-2**.

Table 8-2: Mössbauer spectra of hematite, magnetite and clay containing structural iron and or oxyhydroxides

	IS	**QS(mm/s)**	**T**	**Valence state/ species**	**Reference**
Hematite	0.37	-0.20	51.8		339
Magnetite	0.26	-0.02	49		339
	0.67	0.00	46.0		339
Unfired clays	0.35	0.68	-	Fe^{3+}	423
	0.32	0.51		Fe^{3+}	
	1.13	2.62		Fe^{2+}	
	1.03	2.65	-	Fe^{2+}	424
	0.35	0.55		Fe^{3+}	
	0.37	-0.32	51.7	Fe^{3+}	

In a previous study, isomer shift values for Fe^{3+} are in the range: 0.10 - 0.30 mm/s for Fe^{3+} in tetrahedral site, 0.28 - 0.50 mm/s for Fe^{3+} in octahedral site[425]. A graphical presentation of assigning the Fe site and its valence state[339] is shown in **Figure 8-16**. Iron can be present in clays as structural iron, iron oxides/oxyhydroxides in the clay minerals or added hematite[169,338].

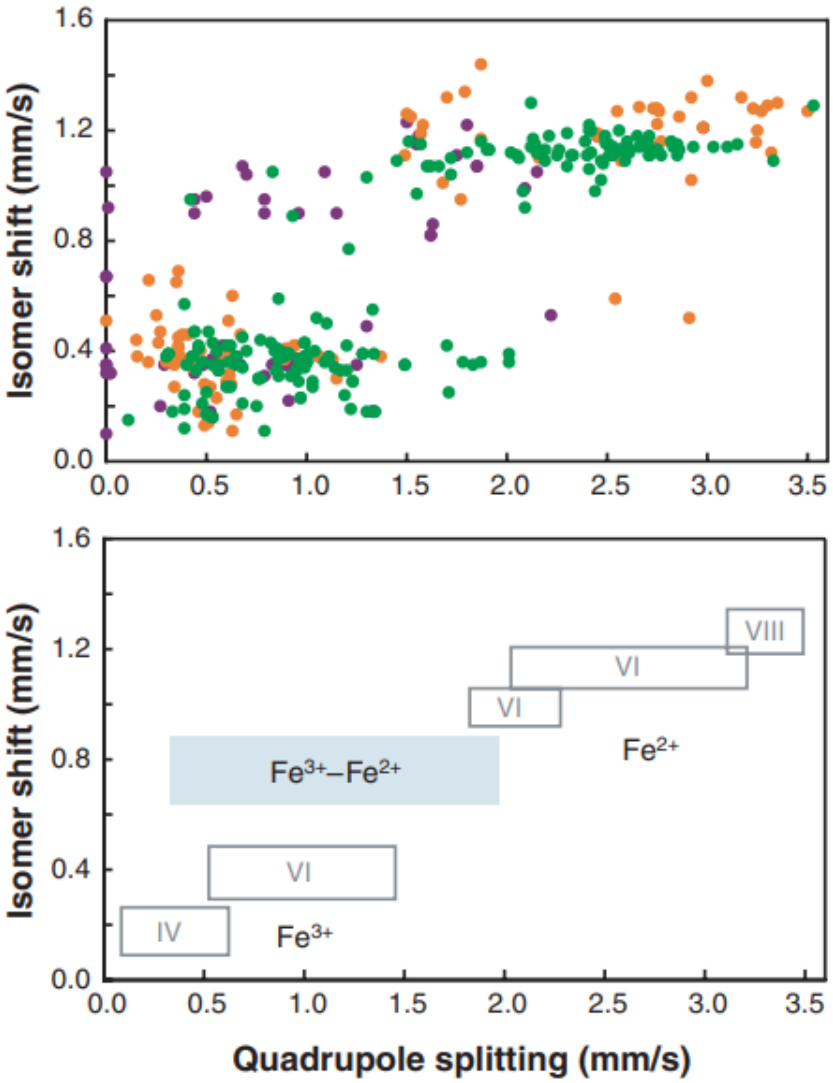

Figure 8-16: Graphical presentation of assigning Fe site and valence[339]

8.2.2 *Benchmark material*

Figure 8-17 shows the spectrum of unfired Weald clay at room temperature. The spectrum presents a quadrupole split doublet with no magnetically ordered phase similar to the spectrum of illite (NP 548 sample) obtained by Murad and Wagner[141].

Generally, a magnetic phase will appear as a sextet or a six-line spectrum[426]. This means hematite is not present until Weald clay is fired. The isomer shift of 0.25mm/s indicates the presence Fe^{3+} site and 1.24mm/s in the Fe^{2+} site, which is within values given by Dyar[170,339] (see **Table 8-3**) and Menil[425]. Al can substitute for Fe in the octahedral site resulting in a superparamagnetic phase which prevents a magnetic phase from forming at non-ambient temperatures[427,428] in silicate materials. In previous studies, the Fe^{2+} site identified with unfired clay was related to the presence of the clay minerals illite/muscovite[424] and chlorite[423,429]. This result is consistent with the XRD pattern shown in **Figure 4-2,** which shows no magnetic phase, hematite (Fe_2O_3) until the clay is fired (>900). Peters and Iberg[95] report that a complete decomposition of the clay mineral illite occurs above >700°C. The isomer shift obtained for Girininkai clay [424] shown in **Table 8-1** supports Dyar [170] (see **Figure 8-16**) and Menil [425]site range; hence the assigned site (Fe^{3+} and Fe^{2+}) for this current work is summarized in **Table 8-3**. Moreover, the two sites (Fe^{3+} and Fe^{2+}) have been reported to be present in silicate minerals with different surroundings and therefore have different energy[430] or distorted sites.

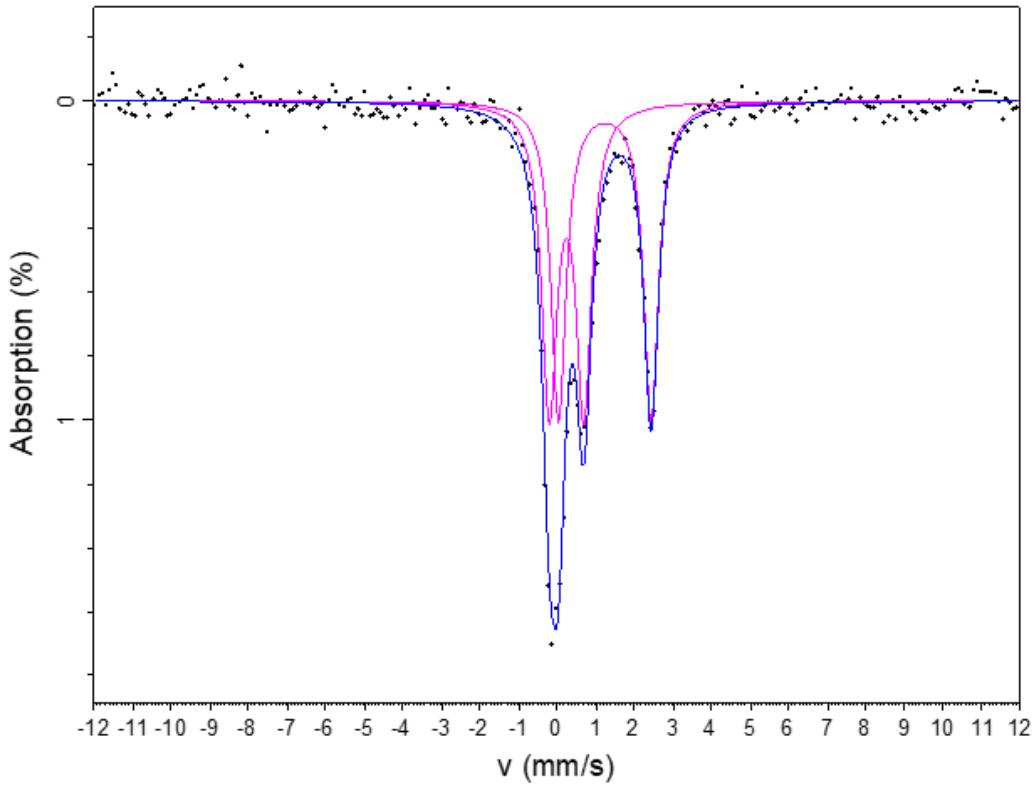

Figure 8-17: Mössbauer spectrum of unfired Weald clay fired measured at room temperature showing no signs of a magnetic phase.

Table 8-3: Room temperature Mössbauer parameters of unfired Weald clay relative to α-Fe; CS±0.02 mm/s; QS ± 0.02 mm/s; H ± 0.5T reduced $\chi^2 = 0.85903$

	CS (mm/s)	**QS/Δ (mm/s)**	**HWHM (mm/s)**	**Area (%)**	**Phases**
Doublet 1	0.26	0.89	0.24	49.6	$^{VI}Fe^{3+}$
Doublet 2	1.25	2.4	0.23	50.4	$^{VI}Fe^{2+}$

8.2.3 *Mössbauer's findings on the control fired to 1040°C*

The crystallographic site symmetry for Fe has often been drawn from the hyperfine parameters obtained from the Mössbauer spectrum. Menil[425] states that the usual isomer shift values for Fe^{3+} are in the following range: 0.10 - 0.30 mm/s for Fe $^{3+}$ in the tetrahedral site, 0.28 - 0.50 mm/s for Fe $^{3+}$in octahedral site. Site assignment for Fe^{3+} is still a debatable subject on Mössbauer spectroscopy[170,431,432].

Doublets form when the local environment of iron changes affecting the spectrum[433–438] from the decomposition of clay minerals. Fe content also increases with temperature[439] with the decrease of other species, which is why a six-line spectrum is formed when Weald clay is fired. The control or 100% fired clay sample has strong magnetic (Fe_2O_3) sites (54%) and a paramagnetic iron population of 46%, shown in **Figure 8-18**. Parameters for sextet are shown in **Table 8-4**, typical for hematite with the crystallographic environment of the Fe^{3+} corresponding to the octahedral.

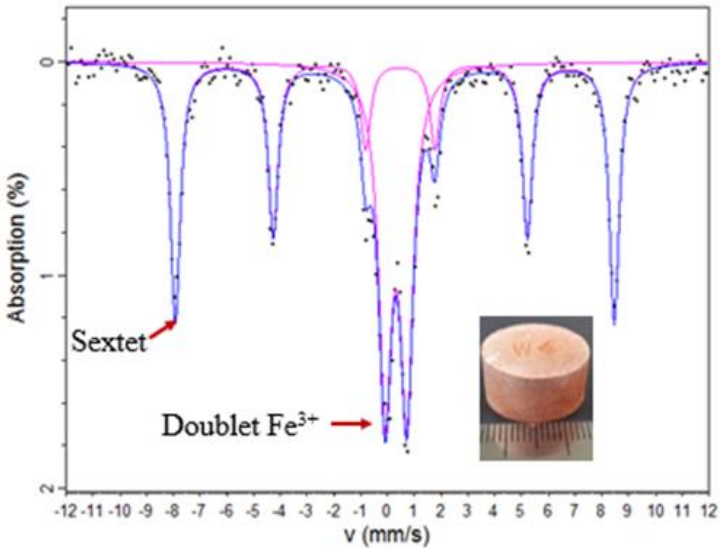

Figure 8-18: Mössbauer spectrum of 100% clay fired to 1040°C having a doublet and a sextet measured at room temperature.

Table 8-4: Room temperature Mössbauer parameters of 100% clay fired to 1040°C relative to α-Fe; CS±0.02 mm/s; QS ± 0.02 mm/s; H ± 0.5T reduced $\chi^2 = 1.05336$

	CS (mm/s)	**QS/Δ (mm/s)**	**HWHM (mm/s)**	**H (T)**	**Area (%)**	**Phases**
Doublet	0.32	0.80	0.29	-	45.8	$^{VI}Fe^{3+}$
Sextet	0.38	-0.10	0.22	50.1	54.2	$^{VI}Fe^{3+}$

8.2.4 *Alkaline Earth Findings*

8.2.4.1 *Colour & magnetic variation of 2wt% $BaCO_3$ (B2) fired to 1040°C*

The broad shape at the right-hand side suggests another sextet within the same region, which was not found in the fired weald clay/control. B2 shows a lower magnetic phase Fe^{3+} when compared to 100% clay. The Fe^{3+} is still in the octahedral site, according to Menil[425]. In the spectrum, it is just about 0.5% absorption compared with the control, which is 1.2%. However, from the parameter, the combined sextet is 38.3%, whiles the paramagnetic doublet population is 62%, higher than the 100% clay and 4wt% $BaCO_3$(B4). These are depicted in **Figure 8-19** and **Table 8-5**.

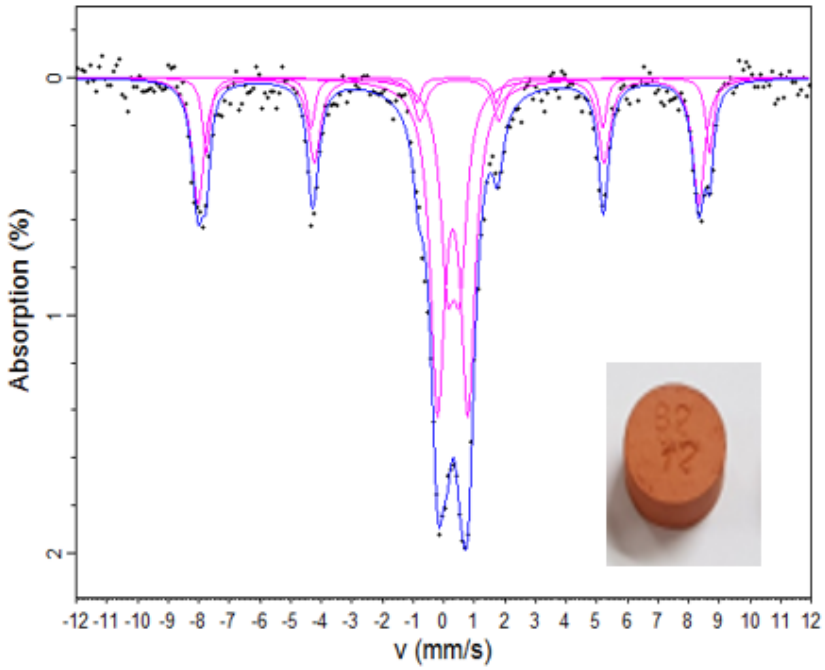

Figure 8-19: Mossbauer spectrum of ceramic containing 2wt% $BaCO_3$ fired to 1040°C having two doublets and two (2) sextets measured at room temperature**.**

Table 8-5: Room temperature Mössbauer parameters of a ceramic body containing 2wt% $BaCO_3$ (B2) fired to 1040°C relative to α-Fe CS±0.02 mm/s; QS ± 0.02 mm/s; H ± 0.5T reduced χ^2 =0.549891.

	CS (mm/s)	**QS/Δ (mm/s)**	**HWHM (mm/s)**	**H (T)**	**Area (%)**	**Phase**
Doublet 1	0.30	0.99	0.28	-	40.0	$^{VI}Fe^{3+}$
Doublet 2	0.33	0.41	0.27	-	22.0	$^{VI}Fe^{3+}$
Sextet 1	0.34	-0.18	0.24	50.7	27.6	$^{VI}Fe^{3+}$
Sextet 2	0.46	0.02	0.15	51.0	10.7	$^{VI}Fe^{3+}$

8.2.4.2 *Colour & magnetic variation of 4wt% $BaCO_3$ (B4) fired to 1040°C*

Fired colour containing 4wt% $BaCO_3$ additive produced a darker hue than the control 1040°C. Magnetic sites are higher (56%) than the 100% clay ceramic with 54% (**Table 8-6**). Furthermore, the paramagnetic iron population decreased to 45% with an increased additive level (4wt%). This means 4wt% of $BaCO_3$ promotes a higher magnetic phase (**Figure 8-20**) and a lower paramagnetic site affecting its darker hue, whilst the B2 magnetic phase is low (38%). According to Nordari et al.[440], the paramagnetic phase is related to amorphous liquid produced from clay minerals on decomposition during the firing of ceramics. Interestingly, the admixture containing 4wt% of the flux ($BaCO_3$) has contributed to these reduced paramagnetic sites resulting in its decreased area percentage at the Fe^{3+} site.

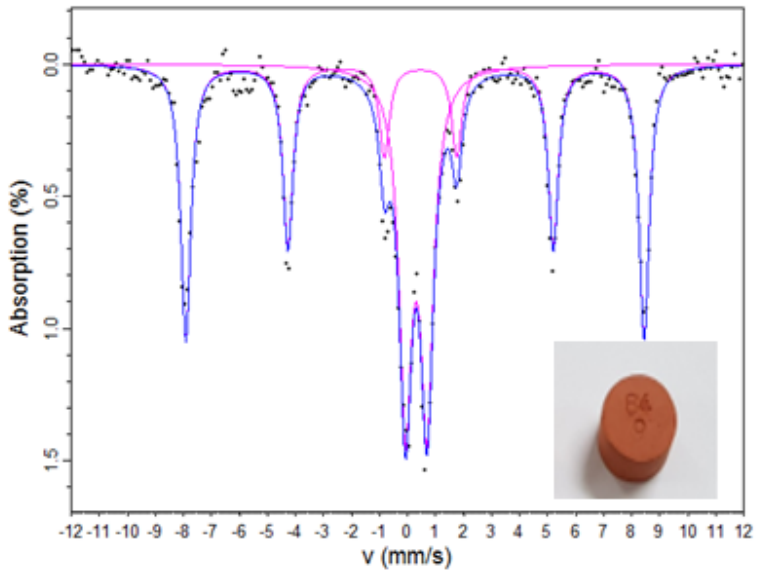

Figure 8-20: Mossbauer spectrum of ceramic containing 4wt% $BaCO_3$ fired to 1040°C having a doublet and a sextet measured at room temperature.

Table 8-6: Room temperature Mössbauer parameters of a ceramic body containing 4wt% $BaCO_3$ (B4) fired to 1040°C relative to α-Fe CS±0.02 mm/s; QS ± 0.02 mm/s; H ± 0.5T reduced $\chi^2 = 1.30834$

	CS (mm/s)	QS/Δ (mm/s)	HWHM (mm/s)	H (T)	Area (%)	Phases
Doublet	0.31	0.77	0.28	-	44.5	$^{VI}Fe^{3+}$
Sextet	0.37	-0.10	0.22	50.1	55.5	$^{VI}Fe^{3+}$

8.2.4.3 *Colour & magnetic variation of 2wt% $MgCO_3$ (M2) fired to 1040°C*

The quadrupole splitting is an indicator of melt species causing a paramagnetic phase[440] which is greater in B2 but similar to B4 with 56% area but not abundant with hematite Fe^{3+}. The magnesium additive spectrum seems to have more distorted symmetry. Spectrum is shown in **Figure 8-21** and Mössbauer parameters in **Table 8-7**.

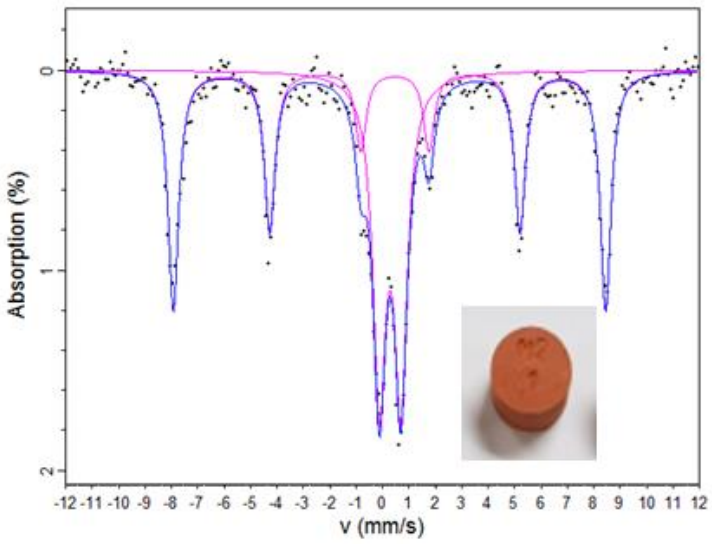

Figure 8-21: Mössbauer spectrum of ceramic containing 2wt% $MgCO_3$ fired to 1040°C having a doublet and a sextet measured at room temperature

Table 8-7: Room temperature Mössbauer parameters of a ceramic body containing 2wt% $MgCO_3$ (M2) fired to 1040°C relative to α-Fe CS±0.02 mm/s; QS ± 0.02 mm/s; H ± 0.5T reduced $\chi^2 = 0.945861$

	CS (mm/s)	QS/Δ (mm/s)	HWHM (mm/s)	H (T)	Area (%)	Phases
Doublet	0.29	0.82	0.30	-	44.5	$^{VI}Fe^{3+}$
Sextet	0.37	-0.10	0.24	50.8	55.5	$^{VI}Fe^{3+}$

8.2.5 Alkali Additive findings

8.2.5.1 *Colour & magnetic variation of 1wt% K_2CO_3 (K1) fired to 1040°C*

Sextet does not contribute to the doublet formed, so a sextet was perfect for this fit, as depicted in **Figure 8-22 and Table 8-8**. Strong magnetic Fe^{3+} sites of 54% were similar to the control, and a paramagnetic doublet area of 46% was obtained. Once again, one thing remained consistent with this additive after incorporating 1wt% K_2CO_3, a higher magnetic phase with a lower paramagnetic area due to melting produced darker hues in colour obtained[440].

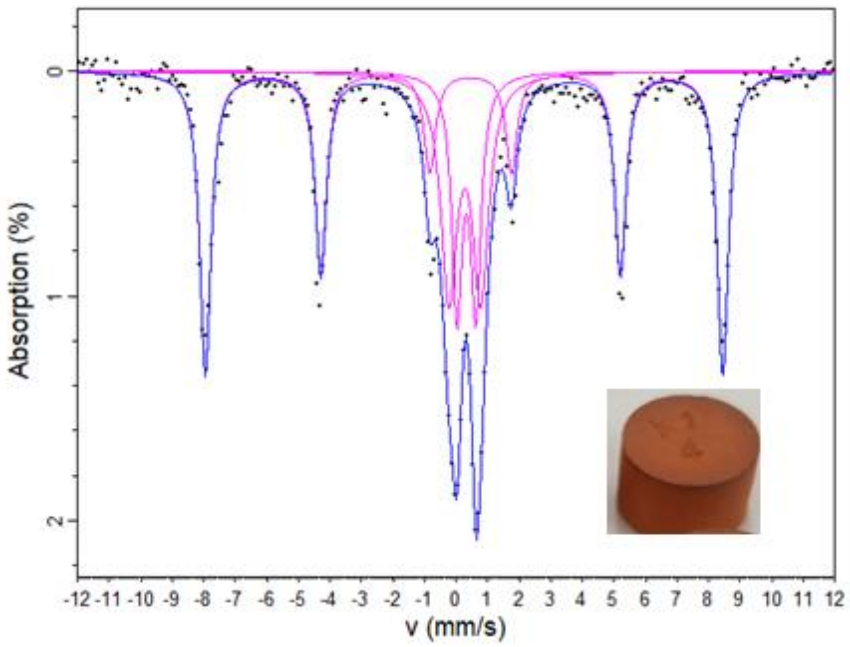

Figure 8-22: Mossbauer spectrum of the ceramic body containing 1wt% K_2CO_3 fired to 1040°C, having two doublets and a sextet measured at room temperature.

Table 8-8: Room temperature Mössbauer parameters of a ceramic body containing 1wt% K_2CO_3 fired to 1040°C relative to α-Fe CS±0.02 mm/s; QS ± 0.02 mm/s; H ± 0. reduced χ^2 =1.1545

	CS (mm/s)	**QS/Δ (mm/s)**	**HWHM (mm/s)**	**H (T)**	**Area (%)**	**Phases**
Doublet 1	0.28	1.01	0.31	-	27	$^{VI}Fe^{3+}$
Doublet 2	0.33	0.60	0.20	-	19	$^{VI}Fe^{3+}$
Sextet	0.36	-0.10	0.22	50.9	53.6	$^{VI}Fe^{3+}$

8.2.5.2 *Colour & magnetic variation obtained with 1wt% Li_2CO_3 (L1) fired to 1040°C*

Mössbauer spectrum of 1wt% Li_2CO_3 is shown in **Figure 8-23 and Table 8-9**. Additions of 1wt% Li_2CO_3 have a stronger magnetic site (57%), 1% greater than the Control (**Figure 8-18 and Table 8-3**) and a paramagnetic population site of 43% lower than ceramic containing 1wt% K_2CO_3 (46%) (see **Figure 8-22 and Table 8-8**). The primary brick clay used for the analysis is low in CaO (<0.3) see **Table 4-1**, therefore implying from De Bonis et al.,[441] on the role of low lime concentration in ceramics and the addition of 1% Li_2CO_3 with the firing temperature~1040°C could have been the main factor in promoting the slightly darker red colour for samples B4, K1, L1 and C4.

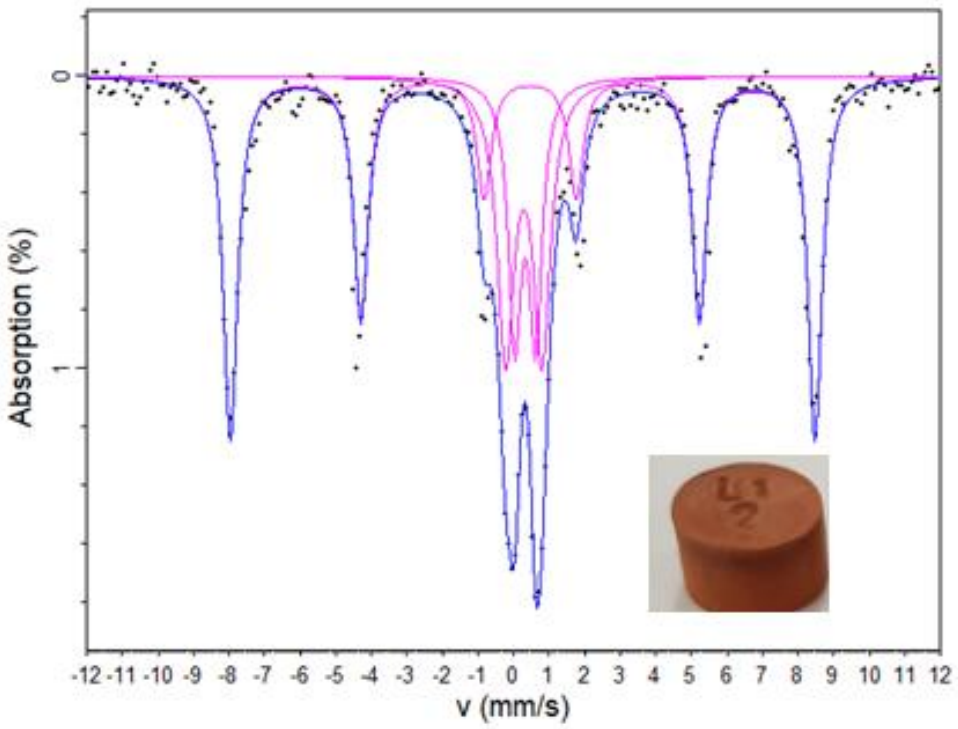

Figure 8-23: Mossbauer spectrum of the ceramic body containing 1wt% Li_2CO_3 fired to 1040°C, having two doublets and a sextet measured at room temperature

Table 8-9: Room temperature Mössbauer parameters of a ceramic body containing 1wt% Li_2CO_3 fired to 1040°C relative to α-Fe CS±0.02 mm/s; QS ± 0.02 mm/s; H ± 0. reduced χ^2 =2.32704

	CS (mm/s)	QS/Δ (mm/s)	HWHM (mm/s)	H (T)	Area (%)	Phases
Doublet 1	0.29	1.02	0.29	-	25	$^{VI}Fe^{3+}$
Doublet 2	0.33	0.59	0.22	-	18	$^{VI}Fe^{3+}$
Sextet	0.37	-0.11	0.24	51.0	56.8	$^{VI}Fe^{3+}$

8.2.5.3 *Colour & magnetic variation of 1wt% Na_2CO_3 (N1) fired to 1040°C*

The addition of N1 shows a low paramagnetic site of 44.5% and a magnetic site of 55.5% (**Figure 8-24**). The Magnetic site is slightly greater (~56%) than K1(~54%) depicted in **Table 8-10**. It is the area % of the sextet which affects the overall colour of the ceramic sample. Determination of $Fe^{3+/2+}$ was obtained by Menil's[425] and Dyar et al.[339] parameter range.

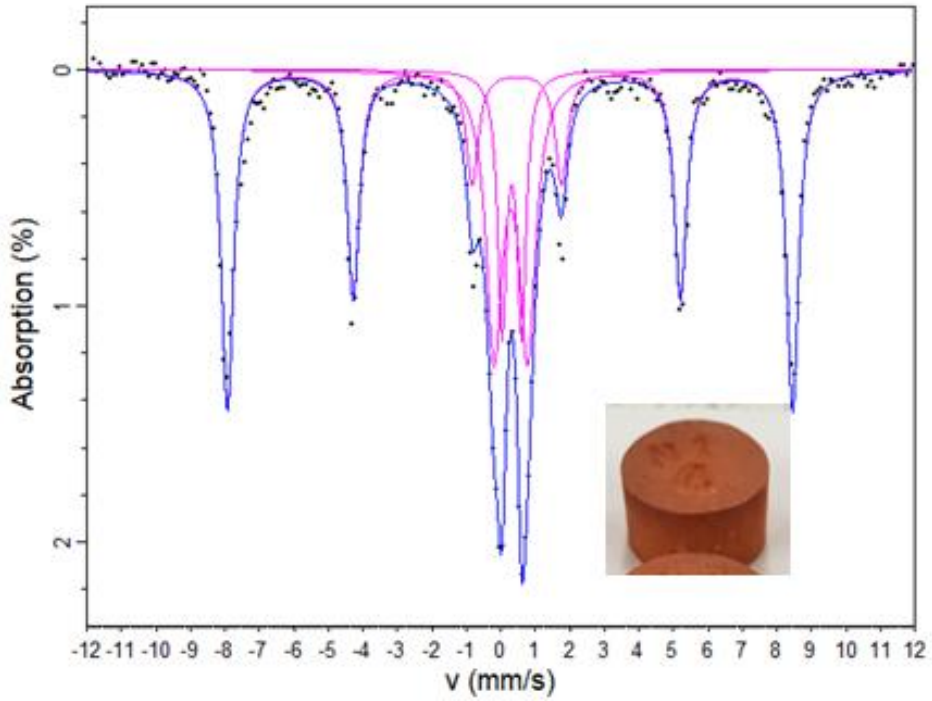

Figure 8-24*:* Mossbauer spectrum of the ceramic body containing 1wt% Na_2CO_3 fired to 1040°C, having two doublets and a sextet measured at room temperature.

Table 8-10: Room temperature Mössbauer parameters of a ceramic body containing 1wt% Na_2CO_3 fired to 1040°C relative to α-Fe CS±0.02 mm/s; QS ± 0.02 mm/s; H ± 0. reduced χ^2 =1.37752

	CS (mm/s)	**QS/Δ (mm/s)**	**HWHM (mm/s)**	**H (T)**	**Area (%)**	**Phases**
Doublet 1	0.29	0.97	0.28	-	29.7	$^{VI}Fe^{3+}$
Doublet 2	0.32	0.57	0.15	-	14.8	$^{VI}Fe^{3+}$
Sextet	0.37	-0.10	0.21	50.8	55.5	$^{VI}Fe^{3+}$

8.2.6 *Inorganic additive findings*

8.2.6.1 *Colour & magnetic variation of 4wt% colemanite containing sample fired to 1040°C*

More hematite was found in the ceramic sample containing 4wt% colemanite (C4W). The recorded population area is 74% greater (see **Figure 8-25** and **Table 8-11**) than the 54% recorded in 100% clay, with just over half the paramagnetic doublets sites (26%) than the control. This gives a potential cause for the darker shade of the ceramics. Moreover, the quadrupole splitting indicates the paramagnetic phase influenced site distortion caused by the glassy phase on clay mineral and additive decomposition and not forgetting the role of low calcium oxide in ceramic and firing temperature improving hematite intensity [440,441]. The XRD pattern is shown in **Figures 7-1 and 7-2,** the high hematite (Fe_2O_3) intensity in the colemanite ceramic body.

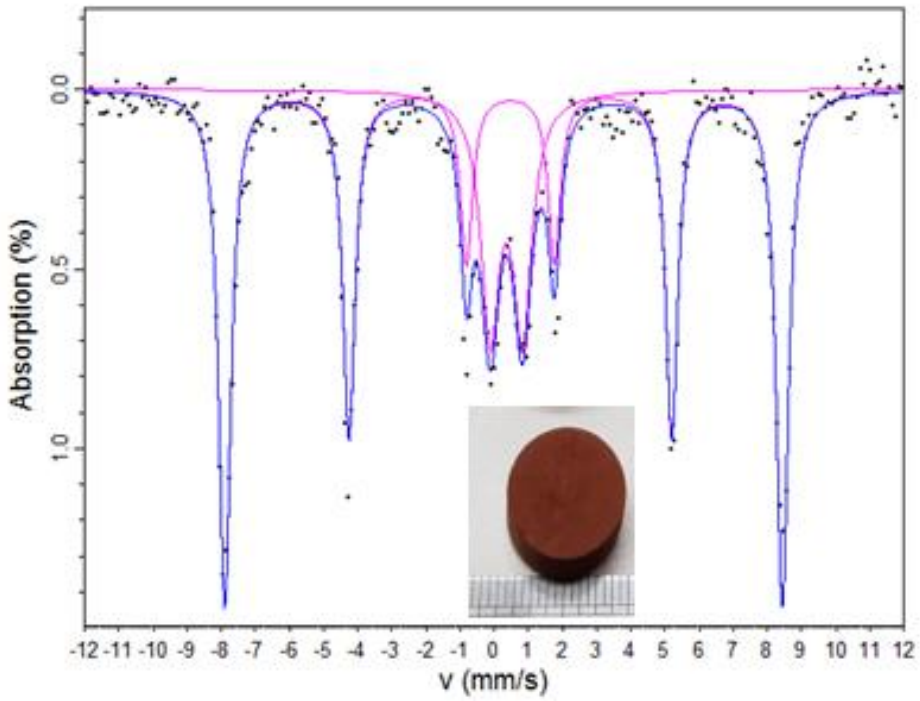

Figure 8-25: Mossbauer spectrum of the ceramic body containing 4wt% colemanite fired to 1040°C, having a doublet and a sextet measured at room temperature.

Table 8-11: Room temperature Mössbauer parameters of a ceramic body containing 4wt% colemanite fired to 1040°C relative to α-Fe CS±0.02 mm/s; QS ± 0.02 mm/s; H ± 0. reduced $\chi^2 = 0.660218$

	CS (mm/s)	QS/Δ (mm/s)	HWHM (mm/s)	H (T)	Area (%)	Phases
Doublet 1	0.36	0.94	0.33	-	25.6	$^{VI}Fe^{3+}$
Sextet	0.38	-0.10	0.22	50.6	74.4	$^{VI}Fe^{3+}$

8.2.6.2 *Colour & magnetic variation of 4wt% Nepheline syenite (N4W) containing sample fired to 1040°C.*

Figure 8-26 shows a magnetic phase obtained for N4W 3% higher than recorded in the control sample (54%) (**Table 8-12**). Also, the paramagnetic iron site (Fe^{3+}) recorded for the N4W sample was found to be greater (43%) than the amount recorded for colemanite samples (26%) **Table 8-11** and 3% lower than what was recorded for the control (46%) affecting the colour slightly. Therefore, we can conclude that a lower paramagnetic site with a higher magnetic phase produces a darker shade of red obtained from hematite (Fe_2O_3) formation.

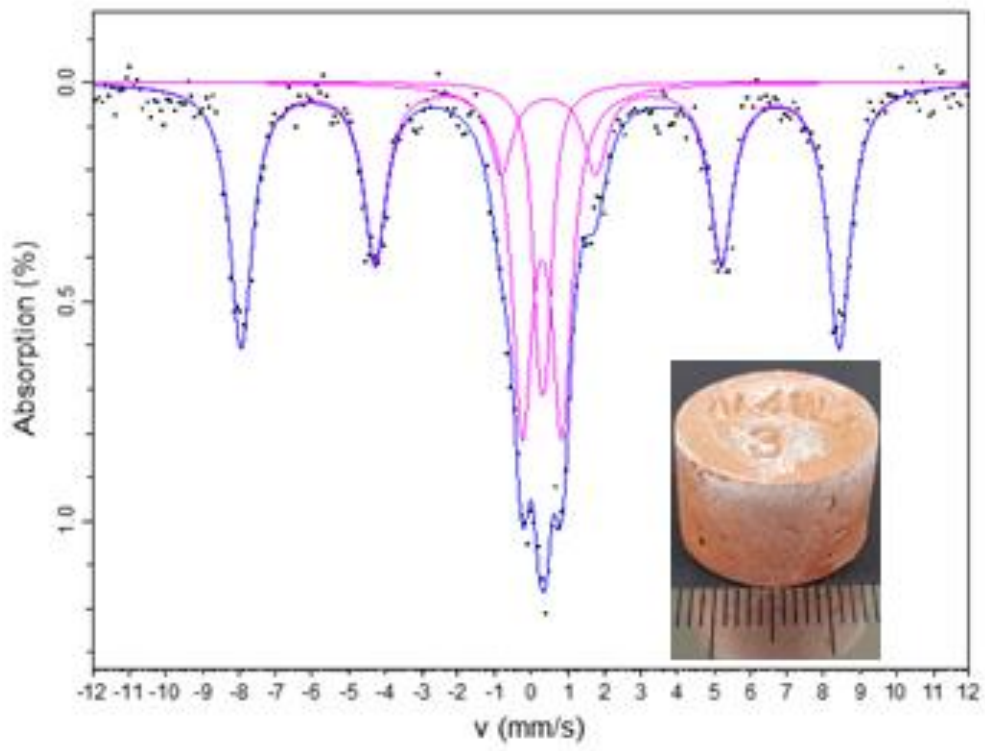

Figure 8-26: Mossbauer spectrum of the ceramic body containing 4wt% Nepheline syenite fired to 1040°C, having two doublets and a sextet measured at room temperature.

Table 8-12: Room temperature Mössbauer parameters of a ceramic body containing 4wt% Nepheline syenite fired to 1040°C relative to α-Fe CS±0.02 mm/s; QS ± 0.02 mm/s; H ± 0. reduced χ^2 = 1.16146.

	CS (mm/s)	**QS/Δ (mm/s)**	**HWHM (mm/s)**	**H (T)**	**Area (%)**	**Phases**
Doublet 1	0.33	0.20	0.22	-	12.0	$^{VI}Fe^{3+}$
Doublet 2	0.31	1.09	0.33	-	33.3	$^{VI}Fe^{3+}$
Sextet	0.37	-0.10	3.45	50.6	56.7	$^{VI}Fe^{3+}$

8.2.7 *Conclusions*

The following conclusions can be drawn from Mössbauer analysis conducted on fired clay containing different additives, producing varied colours on firing compared with clay without additives.

1. Sextets are only developed in clays by chemical reactions during firing.
2. Unfired fired clay (Weald) is not magnetically ordered, although the bulk chemical analysis shows high percentages of Fe ∼>6%.
3. The colemanite body produced a strong magnetic spectrum, affecting the ceramic colour. Hematite (Fe_2O_3) suggests darker red, orange, and brown colours. In the XRD pattern, a higher intensity of (Fe_2O_3) is observed, whilst the Mössbauer spectrum shows more hematite with an increased incidence area.
4. Generally, it was observed that lower paramagnetic sites and higher magnetic phases produced a darker shade of red obtained from the hematite. Likewise, the role of low CaO in Weald clay and flux derived from different additives promoted ceramic colour variation.
5. Differences in Fe^{3+} partitioning and site populations affect ceramic colour and provide an advantageous range of ceramic colours that can give brickmakers more flexibility in their product range.
6. Alkaline additives, 2wt% $BaCO_3$ ceramics fired to 1040°C reduced the magnetic absorption lines, whiles 4wt% $BaCO_3$ increased with stronger absorption lines.
7. Alkali additives included in ceramics in 1wt% levels slightly increase sextet lines observed to enhance ceramic colour.

Chapter 9 Industrial Sample Testing

9.1 Characterisation of brick clays and extruded fired clay bricks

Analyses on industrial standard-fired bricks included XRF, XRD IFM, SEM, MIP and Mössbauer spectroscopy.

9.1.1 *Chemical and mineralogical analysis of clay types and additives used at Wienerberger Ltd*

Figure 9-1 also shows the analysed chemical composition of fired bricks from Wienerberger. These were analysed using two different software, iQ Plus and Oxi programme. The differences between these two software are that the Oxi-programme allows the calibration of individual/ standard oxides with minimal errors while iQ Plus does not.

Fluxing distribution of each brick is different by different ratios. Abbeydale multi-red had the least SiO_2, with 17%. Higher percentages of Fe_2O_3 (>7% -38%) were recorded for the 13 other brick products.

Moreover, clays received from Wienerberger were grouped into six (6) based on industrial body composition (Group 1), Geographical location (Group 2), Similar thermal behaviour (Group 3), specified factory (Group 4), used as an additive-(Group 5 & 6). These were then made into a homogenous glass (fused bead). The chemical analyses are shown in **Table 9-1(a & b).** It depicts raw materials containing varying percentages of oxides in clays used for brick manufacturing—silica (SiO_2), mainly in larger quantities and other impurities which often function as flux. For example, the fluxing additive chalk in Group 6 sample is far greater than all the remaining samples constituting 95% of CaO.

XRD data shows that quartz (SiO_2) is present in all samples along with Kaolinite ($Al_4(OH)_8(Si_4O_{10})$), illite ($(K,H_3O)Al_2Si_3AlO_{10}(OH)_2$), and Saponite-

$CaO_{0.2}Mg_3(Si_3,Al)_4O_{10}(OH)_24H_2O)$ as the main clay minerals. According to the classified clay minerals by Durham [84] only three types were observed with the analysed materials, with Kaolinite and Illite frequently seen, as summarised in **Table 9-2**. **Figure 9-2** to **Figure 9-7** shows the XRD pattern for each group sample.

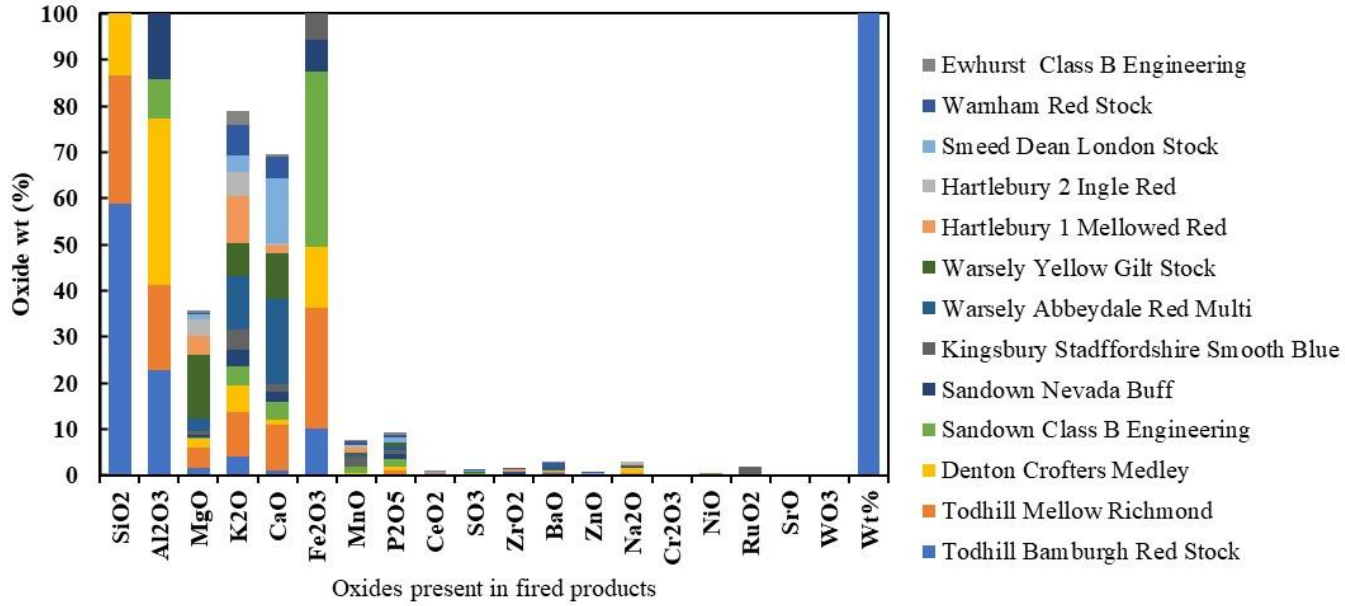

Figure 9-1: Analysed chemical composition of 13 fired bricks from Wienerberger

Table 9-1: (a) The chemical analysis is a typical example of the different distribution of clay composition of oxides for different clays or raw materials to produce brick and tiles in the UK (Wienerberger Ltd). using iQ^{+}and **(b)** XRF analyses of clay samples used in clay brick manufacture (tr., trace) using the new Oxi programm.

Oxides (a)	**GROUP 1**		**GROUP 2**				**GROUP 3**					**GROUP 4**		**GRP 5**	**GRP 6**
	Campions Wood	**Holly Bank**	**Eturia Marl**	**Ewhurst Weald**	**Warhnam Weald**	**Brick Earth Marl**	**Bridgenoth Marl**	**Keuper Marl**	**Carb. Marl**	**Donnington Fireclay**	**Glossop Clay**	**Kings. Deep Red**	**Kings. Deep Blue**	**Body Sand**	**Smead Dean - Chalk**
SiO_2	61.7	56.2	55.0	68.6	56.8	74.4	71.6	59.6	54.2	65.1	59.4	51.1	59.1	89.3	2.4
Al_2O_3	20.2	26.4	25.2	18.5	19.4	11.8	10.7	15.1	26.2	25.4	20.8	27.2	22.3	6.0	0.5
Fe_2O_3	13.0	13.5	13.3	8.1	10.8	8.0	6.3	7.1	11.8	3.0	9.3	16.4	14.5	1.6	1.1
P_2O_5	tr.	-	-	0.1	4.8	-	5.3	0.2	0.1	-	4.7	0.1	-	-	0.3
Na_2O	-	-	-	-	-	0.6	-	-	-	-	0.8	0.5	-	-	-
CaO	0.8	0.4	0.9	0.3	2.5	0.7	1.8	6.2	0.6	0.2	0.4	0.2	0.3	0.1	95.6
MgO	1.3	0.7	0.9	1.0	1.0	1.3	1.2	7.1	1.8	1.2	0.8	0.9	0.6	tr	tr.
K_2O	2.2	1.9	2.5	2.3	3.2	2.5	2.8	4.3	4.5	3.1	2.5	2.5	2.2	2.9	tr.
TiO_2	0.8	0.9	2.2	0.9	0.8	0.6	0.4	0.5	0.8	18	0.6	1.1	1.0	0.2	-
MnO	tr.	tr.	tr.	-	tr.	tr.	-	tr.	tr.	-	-	-	-	-	-
ZrO_2	0.1	0.1	0.1	0.1	0.1	0.2	0.1	0.1	0.1	0.1	0.1	0.1	0.1	-	-
SO_3	-	-	-	0.2	0.5	-	-	-	-	0.1	-	-	-	-	-(**Sr** 0.2)
SUM%	100	100	100	100	100	100	100	100	100	100	100	100	100	100	100
L.O.I	23.8	23.8	23.7	23.8	15.1	11.9	10.5	16.5	12.6	12.7	13.3	12.56	14.3	23.6	23.8

Oxides (b)	GROUP 1		GROUP 2				GROUP 3 Oxi programme					GROUP 4		GRP 5	GRP 6
	Campions wood	Holly Bank	Eturia Marl	Ewhurst Weald	Warhnam Weald	Brick Earth Marl	Bridgenoth Marl	Keuper Marl	Carb. Marl	Donnington Fireclay	Glossop Clay	Kings. Deep Red	Kings. Deep Blue	Body Sand	Smead Dean – Chalk
SiO_2	63.8	63.6	63.9	70.2	64.5	79.8	75.0	59.6	63.0	64.9	60.3	60.5	60.6	89.3	2.2
Al_2O_3	19.9	23.0	22.1	17.7	19.0	9.9	12.4	13.9	22.3	27.5	24.0	23.1	23.1	5.5	0.4
Fe_2O_3	10.0	8.9	8.7	6.2	6.9	4.9	4.7	5.1	7.3	2.2	7.4	11.1	11.0	1.2	0.2
P_2O_5	0.1	0.1	0.1	0.1	0.1	0.1	0.1	0.2	0.2	0.0	0.1	0.1	0.1	0.1	0.2
Na_2O	0.0	0.0	0.1	0.2	0.2	0.5	0.4	0.5	0.7	0.0	0.3	0.1	0.2	0.1	-0.1
CaO	1.1	0.5	0.7	0.3	2.8	0.8	2.4	7.5	0.6	0.2	0.6	0.3	0.4	0.1	96.3
MgO	1.1	0.7	0.9	0.8	1.0	0.9	1.1	8.0	1.6	0.7	1.8	0.6	0.5	0.3	0.4
K_2O	2.3	1.8	2.0	2.4	3.0	2.2	3.1	4.2	2.9	2.4	4.0	2.3	2.3	3.2	0.1
TiO_2	1.4	1.2	1.2	1.5	1.2	0.8	0.7	0.8	1.2	1.4	1.1	1.5	1.6	0.2	0.1
Mn3O4	0.1	0.1	0.1	0.1	0.1	0.1	0.1	0.1	0.1	0.0	0.1	0.1	0.0	0.0	0.1
BaO	0.1	0.1	0.1	0.1	0.1	0.1	0.1	0.1	0.1	0.1	0.1	0.1	0.1	0.0	0.0
ZrO_2	0.0	0.1	0.0	0.1	0.1	0.1	0.1	0.1	0.1	0.1	0.0	0.1	0.1	0.0	0.0
ZnO	0.0	0.0	0.0	0.0	0.0	0.0	0.0	0.1	0.1	0.0	0.0	0.0	0.0	0.0	0.0
SO_3	0.0	0.0	0.0	0.3	0.9	0.1	0.0	0.0	0.1	0.4	0.1	0.0	0.0	0.0	0.1
SUM%	100	100	100	100	100	100	100	100	100	100	100	100	100	100	100
L.O.I	14.7	14.7	14.7	11.6	15.0	11.9	10.1	16.8	13.5	13.1	13.0	12.1	13.8	23.7	10.51

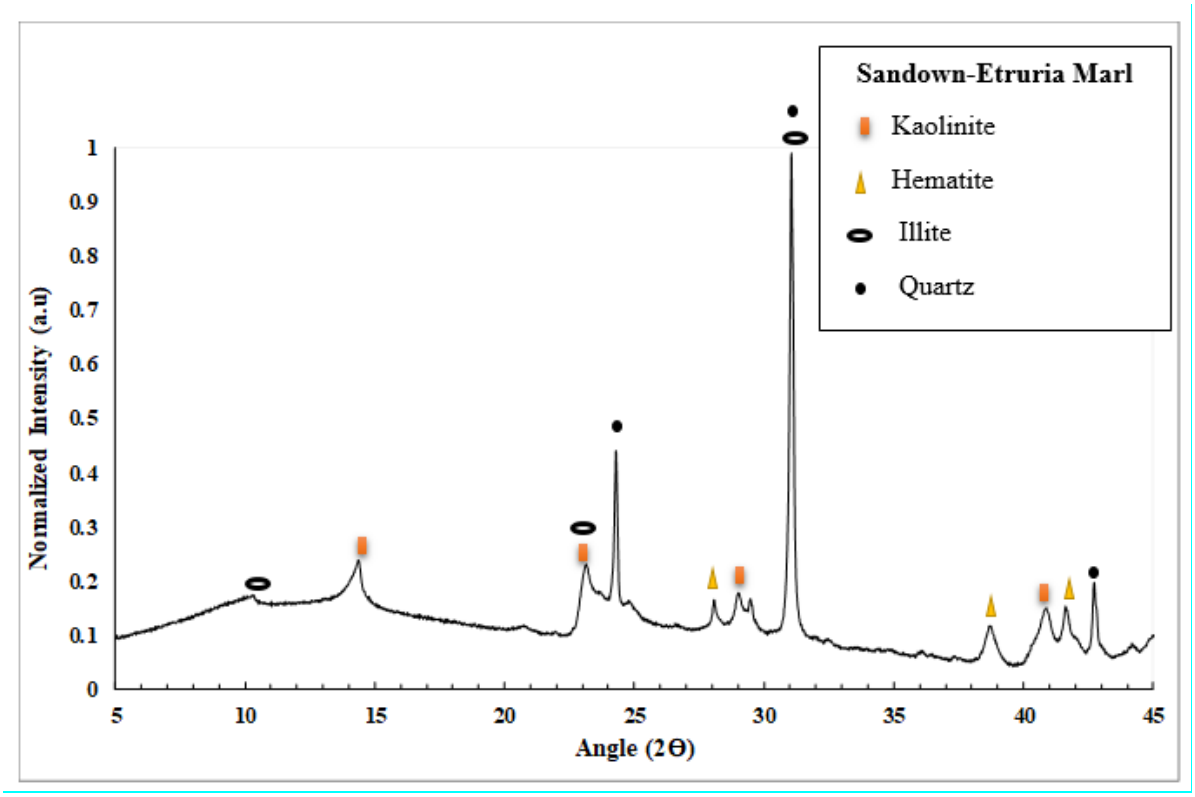

Figure 9-2: XRD pattern of Sandown -Eturia Marl sample-Group 1

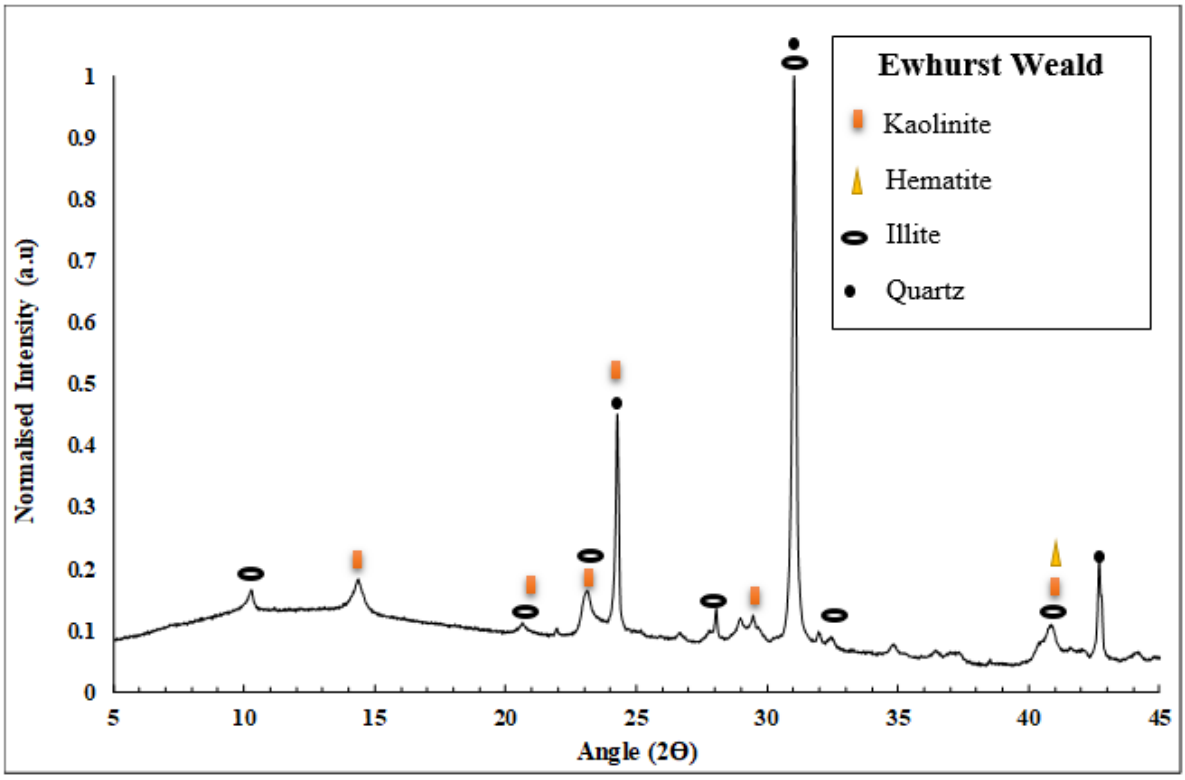

Figure 9-3: XRD pattern of Ewhurst sample -Group 2

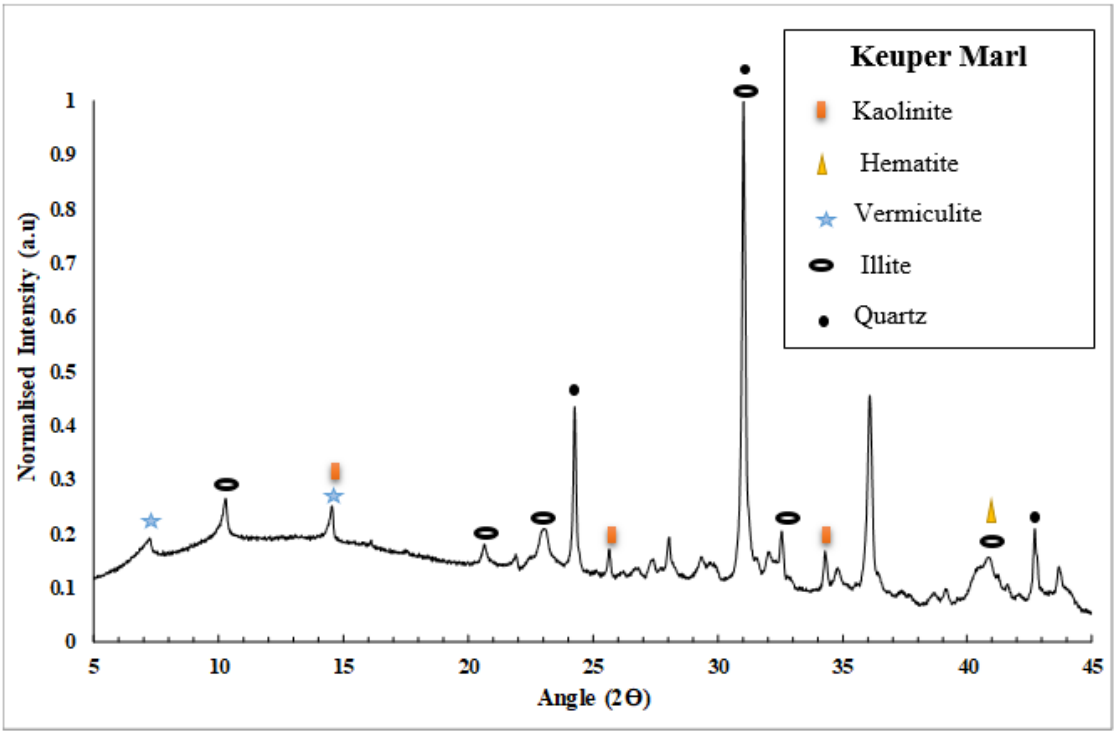

Figure 9-4: XRD pattern of Keuper Marl sample -Group 3

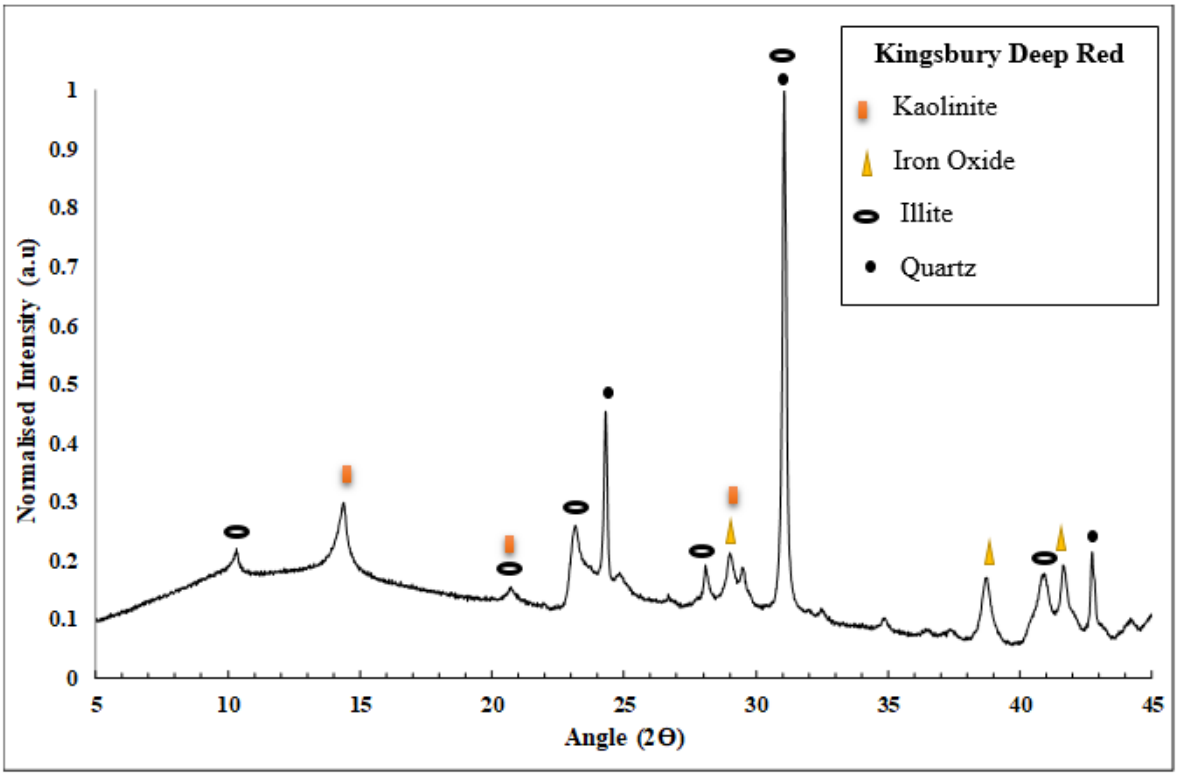

Figure 9-5: XRD pattern of Kingsbury Deep Red sample -**Group 4**

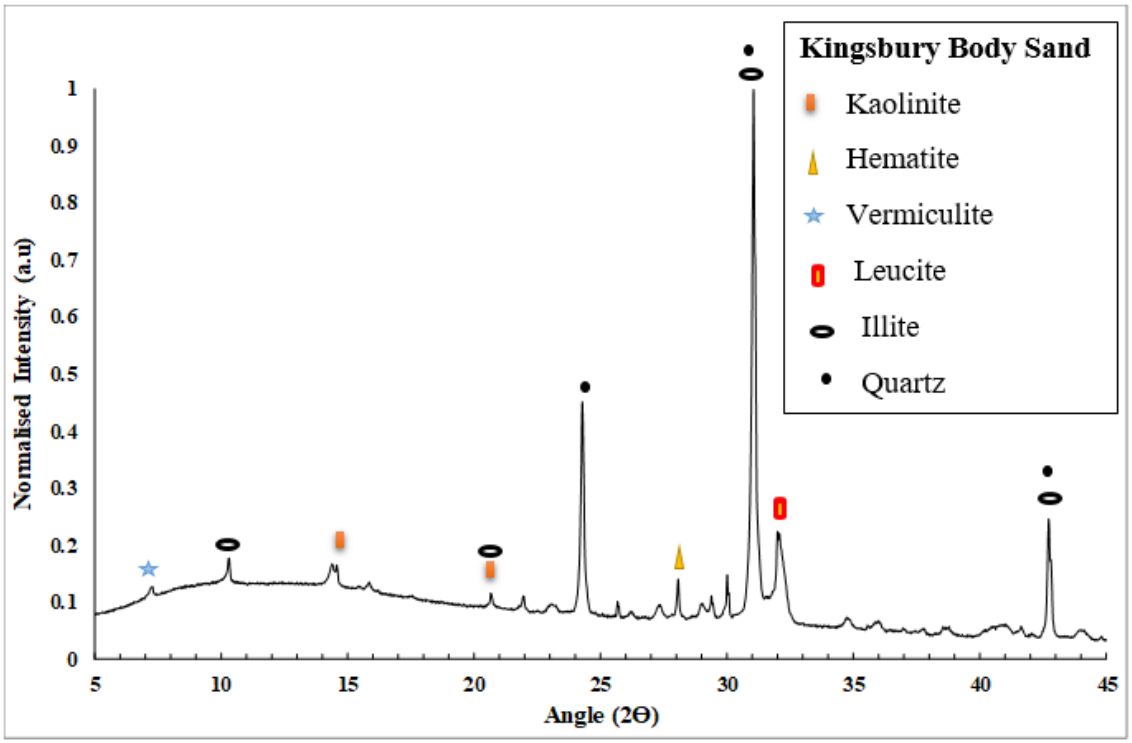

Figure 9-6: XRD pattern of Kingsbury Body Sand sample -Group 5

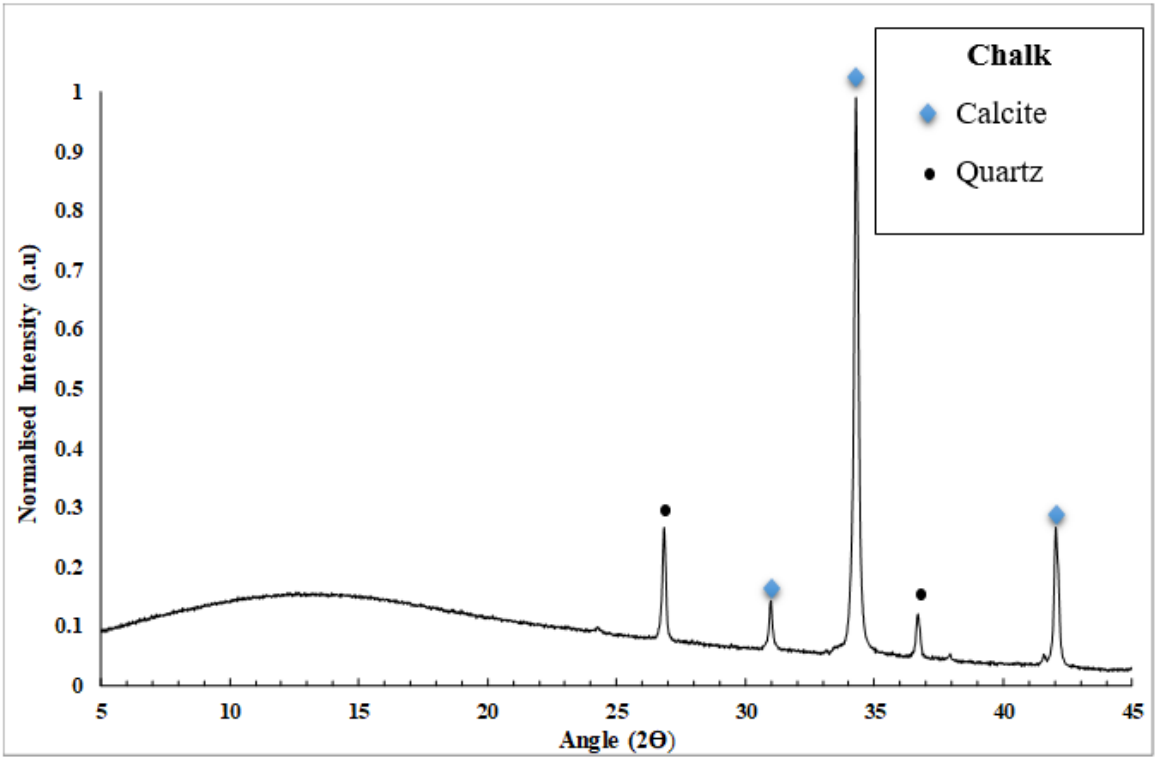

Figure 9-7: XRD pattern of Smead dean chalk sample -Group 6

Table 9-2: Mineralogy analyses of clay samples used in clay brick manufacture.

Clay Minerals	1	2	3	4	5	6	7	8	9	10	11	12	13	14	15
Kaolinite	*	*	*	*	*	-	*	*	*	*	*	*	*	*	-
Illite	*	*	*	*	*	*	*	*	*	*	*	*	*	*	-
Muscovite	*	*	-	-	-	-	-	-	-	-	-	-	*	-	-
Quartz	*	*	*	*	*	*	*	*	*	*	*	*	*	*	*
Hematite	*	*	*	*	*	*	*	*	*	*	*	*	*	*	-
Saponite	-	-	-	-	-	*	-	-	-	-	*	-	-	-	-
Montmorillonite	-	-	-	-	-	-	-	*	-	-	-	-	-	-	-
Pyrochorite	-	-	-	-	-	-	*	-	-	-	-	-	-	-	-
Calcite	-	-	-	-	-	-	-	-	-	-	-	-	-	-	*
Vermiculite	-	-	-	-	-	-	-	-	*	-	-	*	-	-	-
Calcium	-	-	-	-	-	-	*	-	-	-	-	-	-	-	-
Aluminium															
Hydroxide															
Hydrate															
Leucite	-	-	-	-	-	-	-	-	-	-	-	*	-	-	-
Gypsum	-	-	-	-	*	-	-	-	-	-	-	-	-	-	-
Magnetite	-	-	-	-	-	-	-	-	*	-	-	-	-	-	-

Relation:

1. Campions Wood
2. Holly Bank
3. Sandown Eturia Marl
4. Ewhurst Weald
5. Warnham Weald
6. Brick Earth Marl
7. Bridgenorth Marl
8. Keuper Marl
9. Carbonaceous Shale
10. Donnington Fireclay
11. Glossop
12. Kingsbury Deep Red
13. Kingsbury DeepBlue
14. Kingsbury Body Sand
15. Chalk

***** ***Present Mineral***

- ***Absent Mineral***

Table 9-3*:* Thermogravimetry analyses of clay samples of heating rate 10^{o}C/min

Group Number	Sample Name	Event 1			Event 2			Event 3			Event 4			Total Mass loss %
		Temp. ^{o}C	**Mass loss%**	**Evolved gas**	**Temp. ^{o}C**	**Mass loss%**	**Evolved gas**	**Temp. ^{o}C**	**Mass loss%**	**Evolved gas**	**Temp. ^{o}C**	**Mass loss%**	**Evolved gas**	
1	Eturia Marl	35-180	0.52	Surface water	249-358	0.10	Dehydroxylation of clay minerals and slight release of CO_2	365-722	1.82	Dehydroxylation of clay minerals and CO_2	-	-	-	**2.52**
2	Ewhurst Weald	35-192	1.69		198-849	5.11		-	-	-	-	-	-	**6.81**
3	Keuper Marl	35-159	1.02		504-594	1.47	CO_2, CO and dissociation of clay minerals	599-800	8.92	Dehydroxylation of clay minerals and CO_2	-	-	-	**12.60**
4	Kingbury Deep Red	35-140	1.58		277-352	0.34	Dehydroxylation of clay minerals and slight release of CO_2	377-864	5.63	Dehydroxylation of clay minerals and the release of CO_2	-	-	-	**8.06**
5	Kingbury Body Sand	35-1086	1.35		-	-	-	-	-	-	-	-	-	**1.35**
6	Chalk	623-867	42.19	CO_2	-	-	-	-	-	-	-	-	-	**42.19**

9.1.2 *Thermal analysis*

9.1.2.1 *Group 1. Sandown Etruria Marl*

The mass change of Sandown Etruria marl when heated from 35^{o}C - 200^{o}C resulted in a weight loss of 0.52%. In the first event, surface water is lost, and the second step results from dehydration. This is quickly followed by a larger peak-trough, believed to be the removal of structural water at temperatures above 400^{o}C - 650^{o}C and a release of CO_2 gas in **Figure 9-8** resulting from the decomposition of a carbonate substance which the XRD could not detect. After 750^{o}C, there is no further weight loss. The total mass loss is summarised in **Table 9-3**. The later event (decomposition) is irreversible as removing the (OH) group encourages the formation of new phases.

Mass loss is expressed in percentage as the initial weight of the sample minus the final weight divided by the initial weight multiplied by 100%.

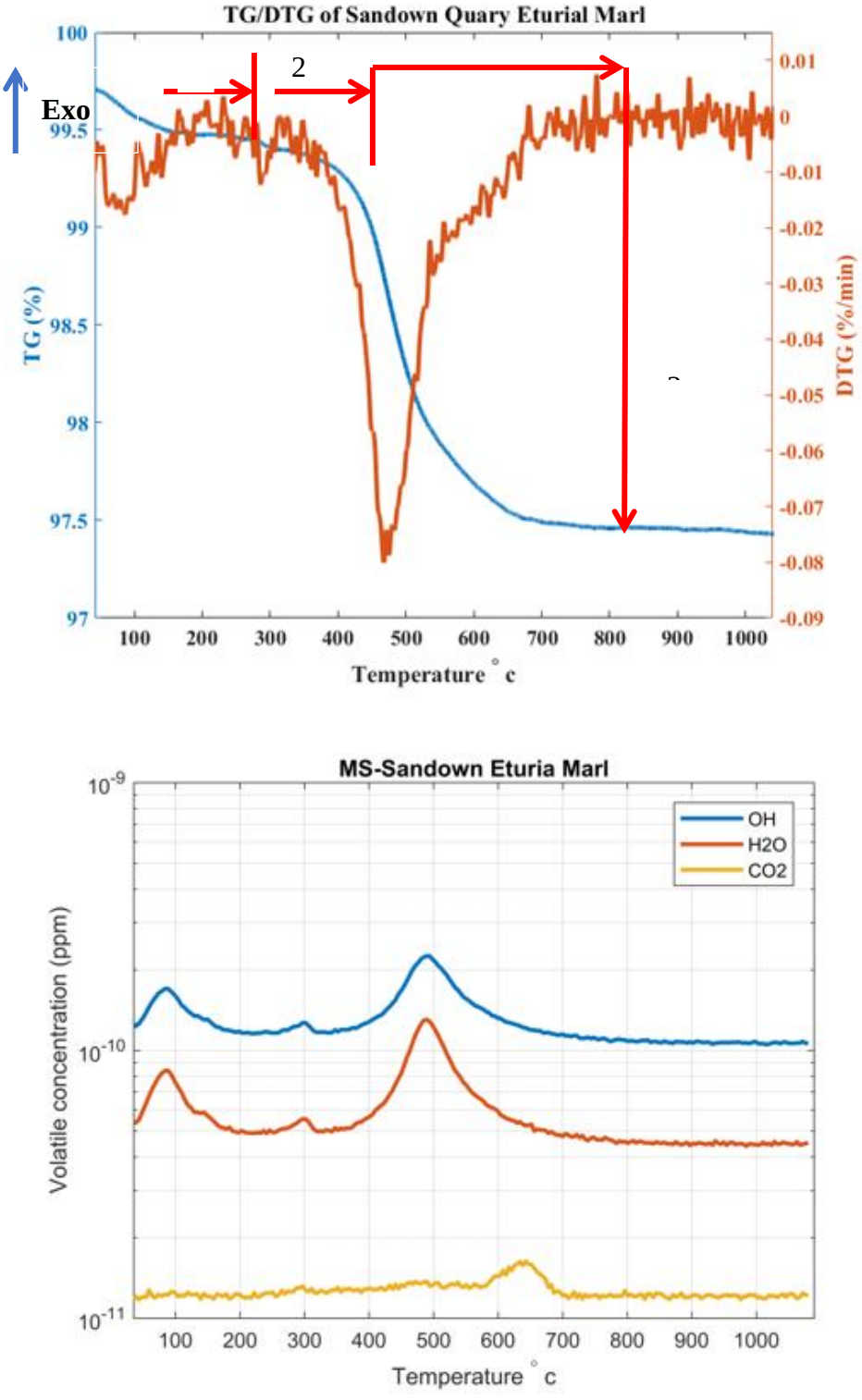

Figure 9-8: TG/DTG curves and evolved gas analysis (MS) for Sandown Quarry Eturial Marl clay, 0.5mg, Al crucible, 10°C/min, Air**.**

9.1.2.2 *Group 2. Ewhurst Clay*

Ewhurst samples again absorbed water removal at the earliest stages of the thermal treatment (35°C- 192°C) with a mass change of 1.69%. The second peak is a hydroxyl group (OH) released from clay minerals. From the mass spectrometer diagram in **Figure 9-9**, there is a gradual but continual release of CO_2 from 200^{o}C to 600^{o}C, accounting for the 5.11% weight loss for the second order. The total percentage loss is recorded in **Table 9-3**. According to the literature, Kaolinite decomposes after 450^{o}C - 550^{o}C and then transforms into metakaolin, an irreversible reaction. The TG curve obtained by Freeman[374] for Weald clay is the same as the reported curve.

9.1.2.3 *Group 3. Keuper Marl Clay*

The difference in weight for the Keuper marl sample resulted from the dehydration of absorbed water and OH groups from clay minerals and the decomposition of carbonaceous substances within the examined specimen indicated in **Figure 9-10**. From the TG curve, illite dehydroxylates at lower temperatures >300^{o}C, and the final OH removal occurs at temperatures > 780^{o}C. Unlike the other group's thermal behaviour, the mass spectrometer shows CO as one of the volatiles that evolved simultaneously with CO_2, the reason behind the larger peak being prominent in the derivative and resulting in the total weight loss of 12.60 % in **Table 9-3**. Above 780^{o}C, a constant weight plateau is observed, and the final removal of the OH from the clay mineral (illite). Studies conducted by Freeman[442] on ten British clays show that illite is principally the main mineral in Keuper marl clays in higher percentages. Similarly, it has been proven that illite under thermal treatment undergoes collapse of the octahedral and tetrahedral layers forming mullite around 950^{o}C and spinel structure above 750^{o}C, respectively.

The TG curve for pure illite on testing its AC conductivity with zeolite as an additive depicts a similar curve denoting both the lowest and final temperatures[443] of which illite

dehydroxylate proves that indeed Keuper marl clay is mostly of illitic mineral as Freeman confirmed[442]. It should be noted that the other mineral, Kaolinite, which is scantly present, can significantly alter or change the curve just around the first dehydroxylation of illitic clays due to metakaolin forming at 550^{o}C after the release of chemically bound water from kaolin.

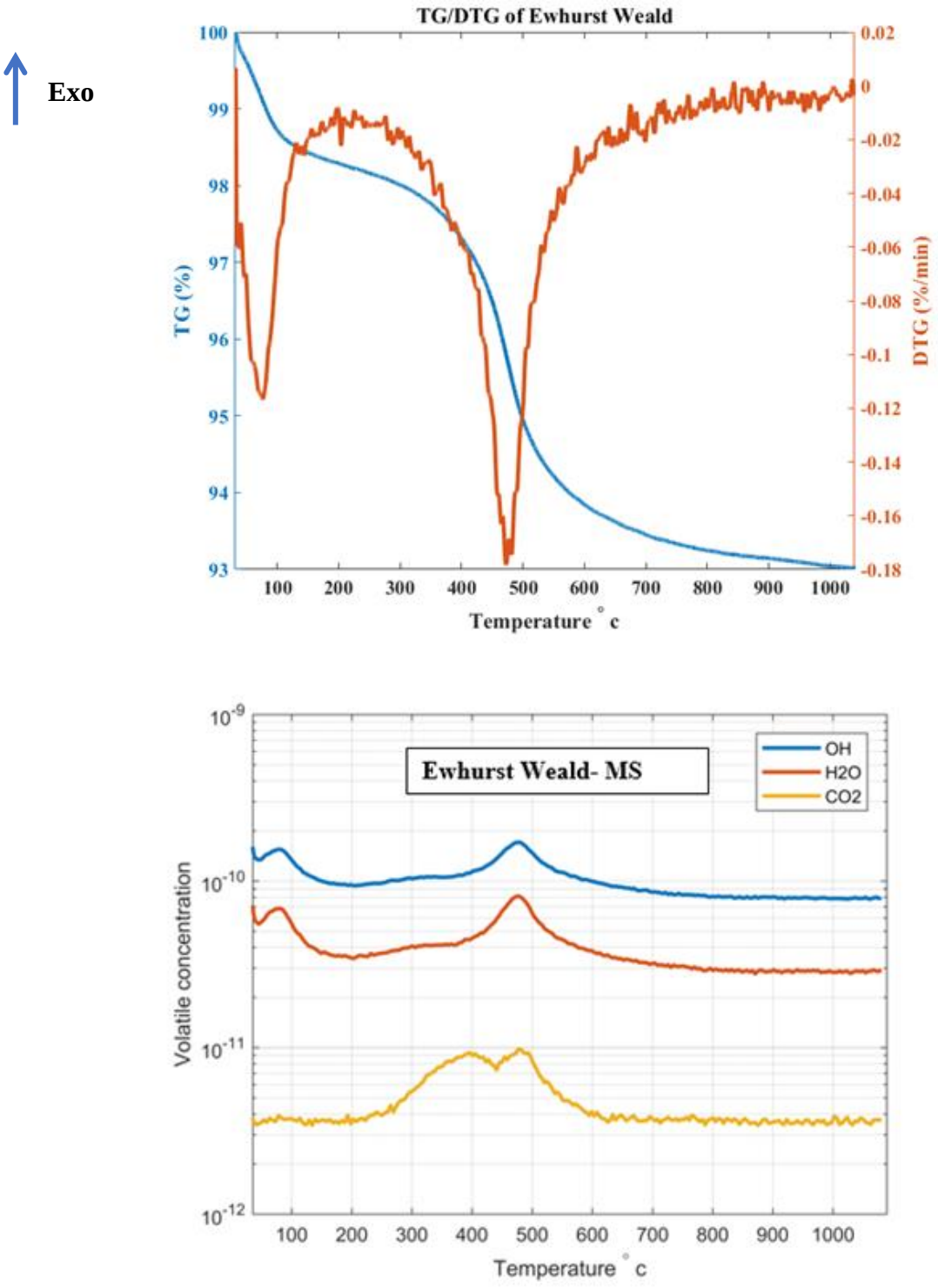

Figure 9-9: TG/DTG curves and evolved gas analysis (MS) for Ewhurst clay , 0.5mg,Al crucible, 10°C/min, Air

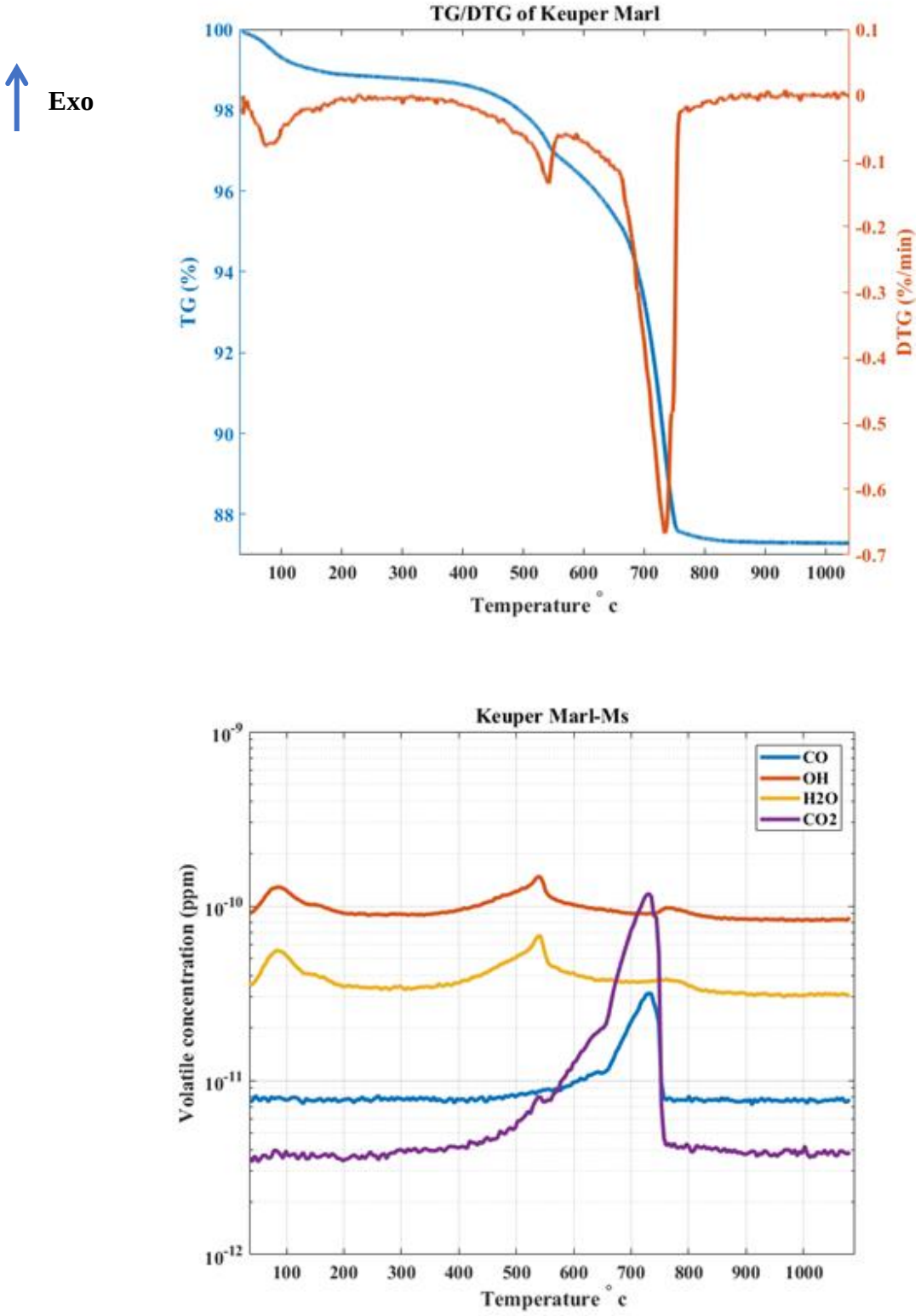

Figure 9-10: TG/DTG curves and evolved gas analysis (MS) for Keuper Marl clay, 0.5mg, Al crucible, 10°C/min, Air

9.1.2.4 *Group 4. Kingsbury Deep Red*

The TG/DTG curve depicted in **Figure 9-11** shows three event stages of mass loss. The first to third events release substantial intrinsic and absorbed water. CO_2 and OH leave the composition at 300°C to 600°C, and the reaction stays flat or uniform. Whiles this reaction is very similar to that of Sandown Eturia Marl, the total weight % loss for this clay is 8.06% due to its high alkali and carbonaceous content.

9.1.2.5 *Group 5. Kingsbury Body Sand*

Body sand is added to clays to reduce the plasticity and shrinkage of the product. The body sand's TG curve (**Figure 9-12**) shows a minor mass loss (1.36%) at 35^{o}C-1086^{o}C. The evolved gas analysis shows a little water removal. However, the sharp peaks in the derivative curves do not accurately represent clay minerals. However, the XRD measurement obtained kaolinite and illite. These clay minerals may be present in smaller percentages, and the observed reactions at the temperatures where kaolinite and illite structures break down are due to the OH removal.

9.1.2.6 *Group 6. Chalk*

Calcite ($CaCO_3$) is the main phase in chalk, followed by quartz, as shown in **Figure 9-13**. This group's TGA / DTG curve has a unique thermal reaction. In air, decomposition of $CaCO_3$ decomposition starts at temperatures above 680^{o}C. It is associated with the decomposition of $CaCO_3$ to release CO_2 gas at 623-867^{o}C to form calcium oxide. A total % weight loss of 42% for chalk is obtained after the measurement. The chemical reaction of this event is expressed as $CaCO_3$ (s) → CaO (s) + CO_2 (g). The colour of the chalk after firing in air changed from white to light pink due to the 1% Fe impurity.

The result obtained for the chalk incorporated in heavy clay production agrees with the experimentation conducted by Earnest [444] even though his heating rate was 10°C / min. The study confirms that the expected temperature at which chalk decomposes is 820°C.

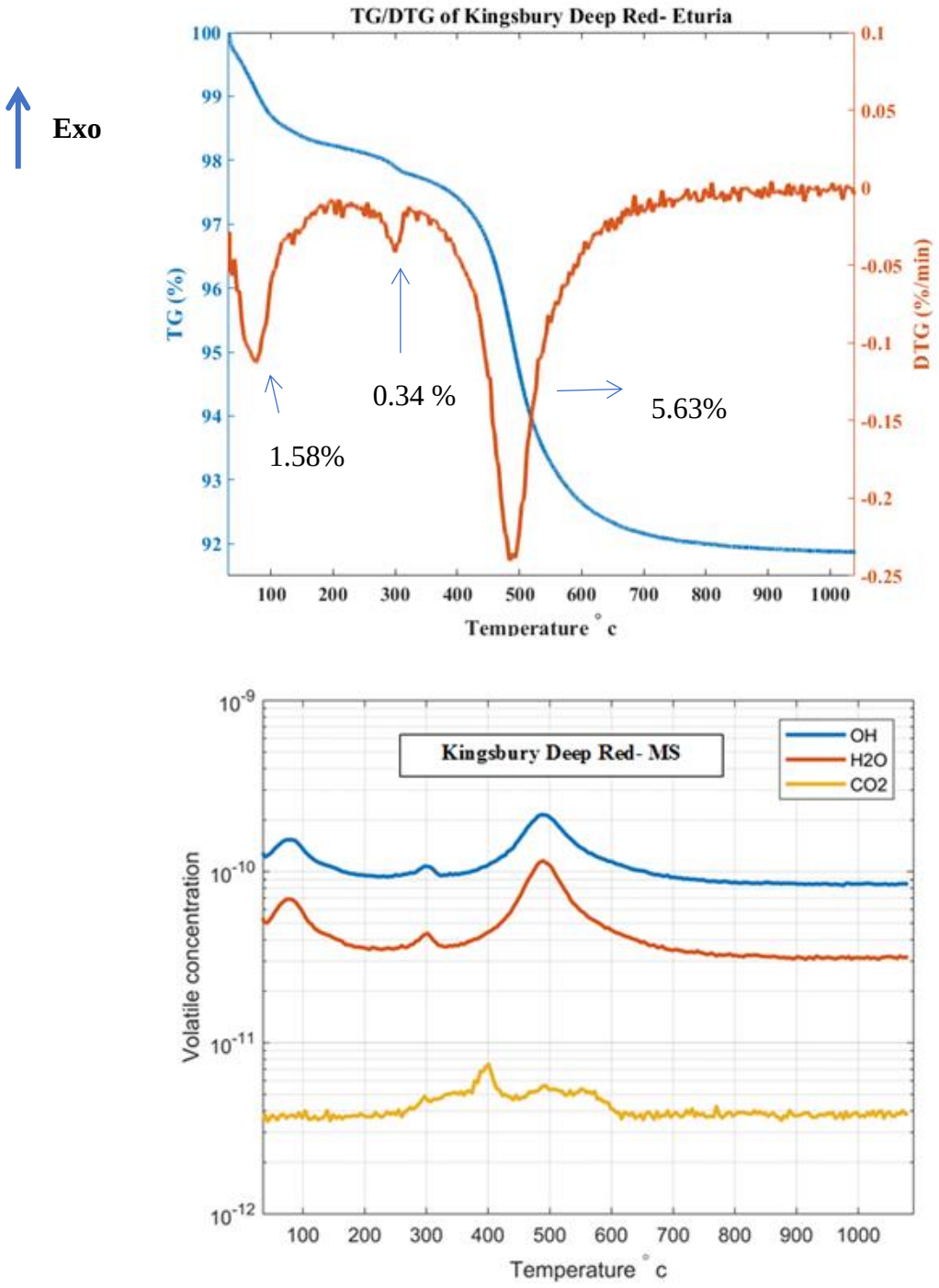

Figure 9-11: TG/DTG curves and evolved gas analysis (MS) for Kingsbury Deep Red clay, 0.5mg, Al crucible, 10°C/min, Air

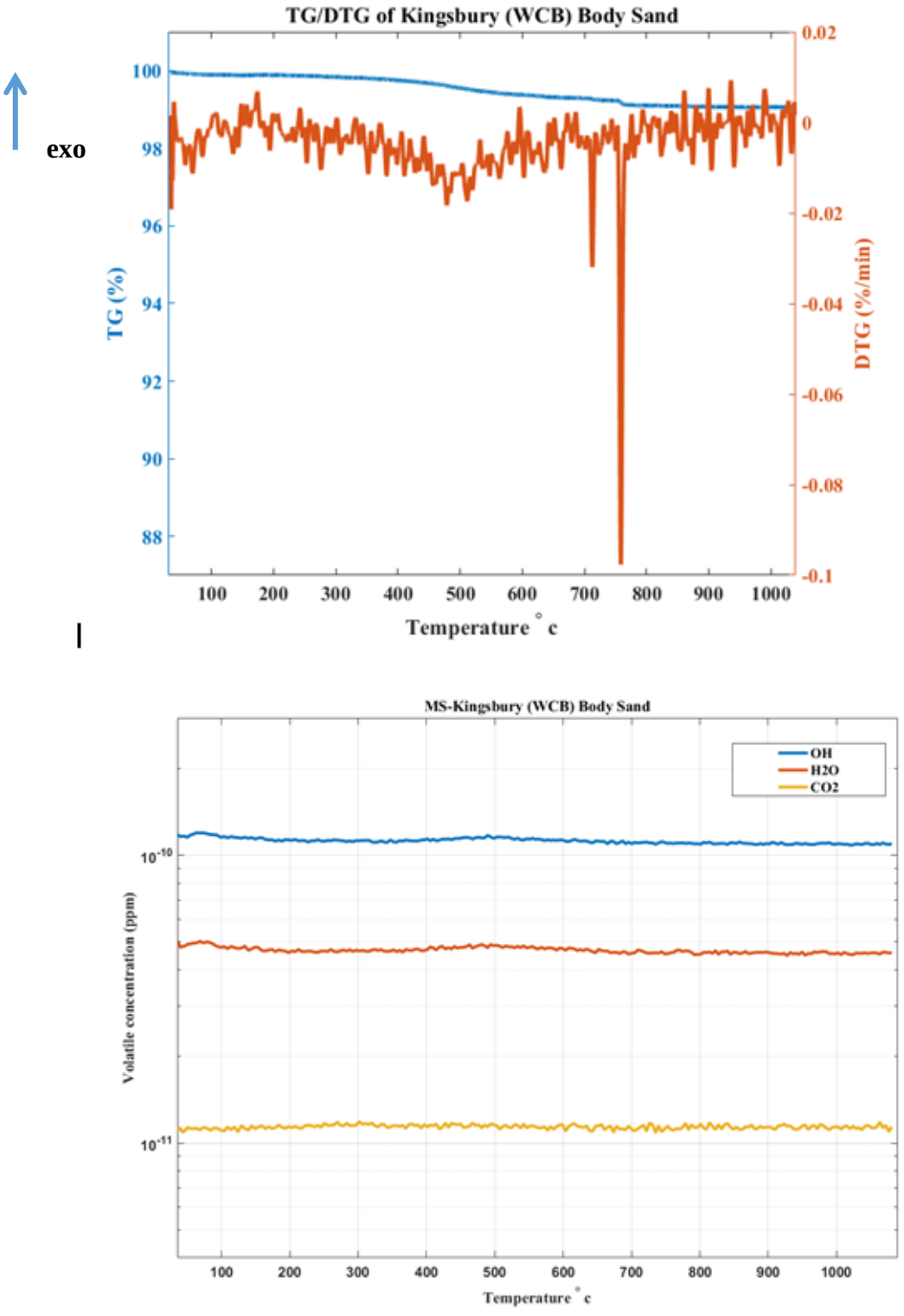

Figure 9-12: TG/DTG curves and evolved gas analysis (MS) for Kingsbury Body Sand, 0.5mg, Al crucible, 5ºC/min, Air

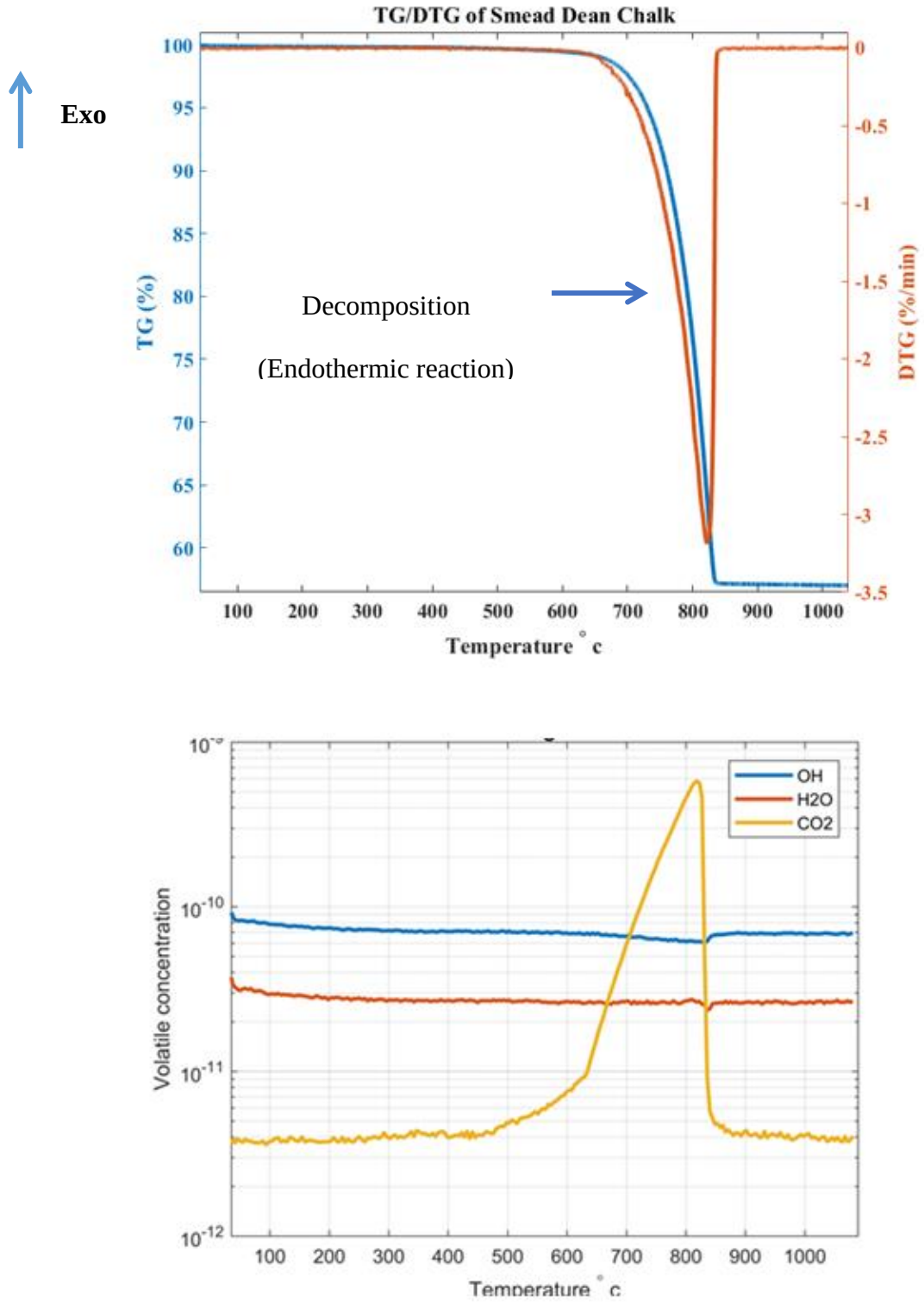

Figure 9-13: TG/DTG curves and evolved gas analysis (MS) for chalk, 0.5mg, Al crucible, 10°C/min, Air

9.1.3 *Dilatometry of Ewhurst Weald clay*

The dilatometry curve in **Figure 9-14** shows two samples of the same mineralogy, but one contains 2wt% ($BaCO_3$) into about 500 tons of clay to produce 42000 bricks per day. Clay dehydrates at temperatures just above the boiling point of water. However, after 200^oC, the sample begins to expand linearly to 538^oC with a difference in CTE 25.034 x 10^{-8} for the sample that contained $BaCO_3$. The CTE is 27.046 x 10-6 for Ewhurst clay without any additive. As the temperature increases, quartz inversion occurs for both samples at 581^oC. Holdridge[445] demonstrates that clays usually expand to 600^oC because of the quartz content evident in this study. Moreover, a similar linear curve was obtained in his studies when he measured the expansion of Etruria marl clay and its residue.

This is the first stage of shrinkage at 578°C, which is believed to be the temperature at which the Kaolinite structure breaks down completely. The onset temperature recorded is at 541.9^oC.

The first contraction curve after the quartz inversion may be attributed to removing OH and kaolinite breakdown, forming meta-kaolin. The quartz transition temperature for Ewhurst Weald clay without additive and Ewhurst Weald clay containing $BaCO_3$ is 581^oC. The second (2^{nd}) order of shrinkage starts at 850^oC for Ewhurst without $BaCO_3$ and 837^oC for $BaCO_3$ containing sample. This indicates the vitrification and contraction associated with the densification of the material at higher temperatures due to the formation of a liquid phase. Clay with $BaCO_3$ shrinks at 40^oC lower (shrinkage reduction temperature) than the sample without $BaCO_3$, which demonstrates the role of the sintering of the carbonate along with other fluxes such as Fe_2O_3, K_2O, Na_2O and MgO.

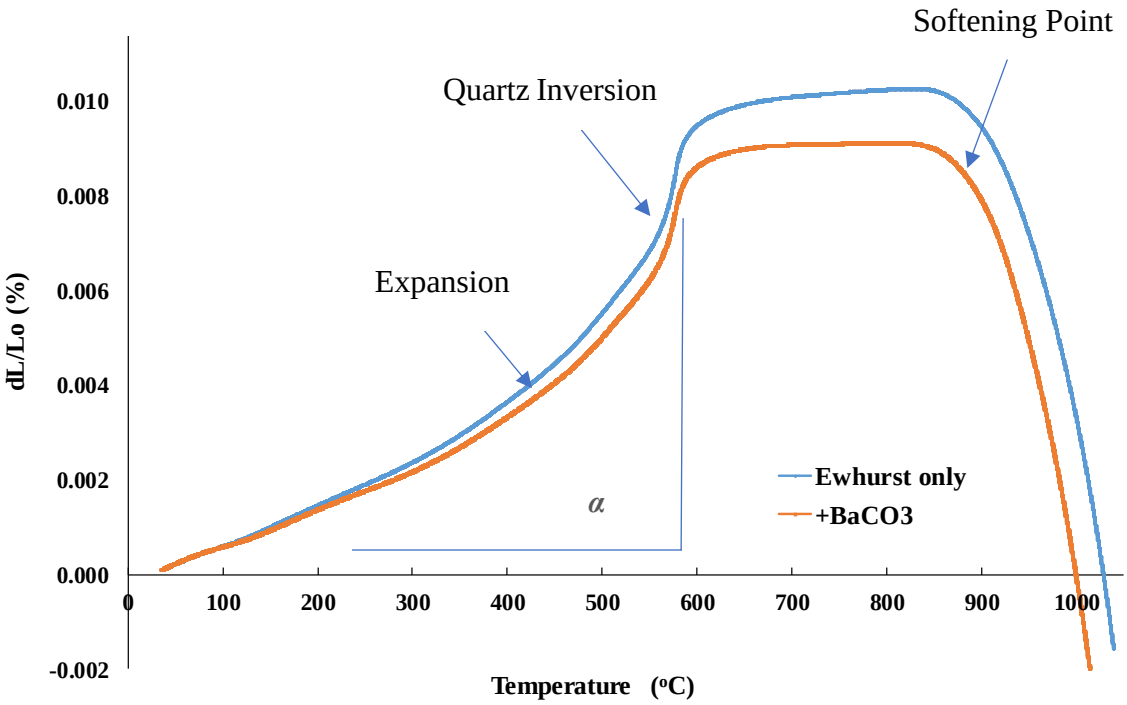

Figure 9-14: Dilatometry curves for Ewhurst clay with/without $BaCO_3$ heated to 1040°C at 5°C/min.

9.1.4 *Infinite focus microscopy*

IFM imaging of fired Weald (fractured and polished surface down to 1µm) reveals a compact surface structure of the thermally heated clay to 1050°C with occasional micro pores of 22.1µm (**Figure 9-15**). The deep brown spots are the pores that negatively affect the product's durability if present in large quantities.

Figure 9-15: Macro-surface of fired Weald clay under IFM.

9.1.5 *Scanning electron microscopy (SEM) / Energy dispersive spectroscopy (EDS)*

The image in **Figure 9-16** shows the formation of a new phase when the clay is fired to 1050^{o}C. The large clusters examined by EDS show that it is formed predominately of alumina and silicate (Al_2SiO_5), a mullite structure and iron silicate (Fe_2SiO_4) with occasional pores with sizes ranging from 22.1um - ≥ 4μm around those.

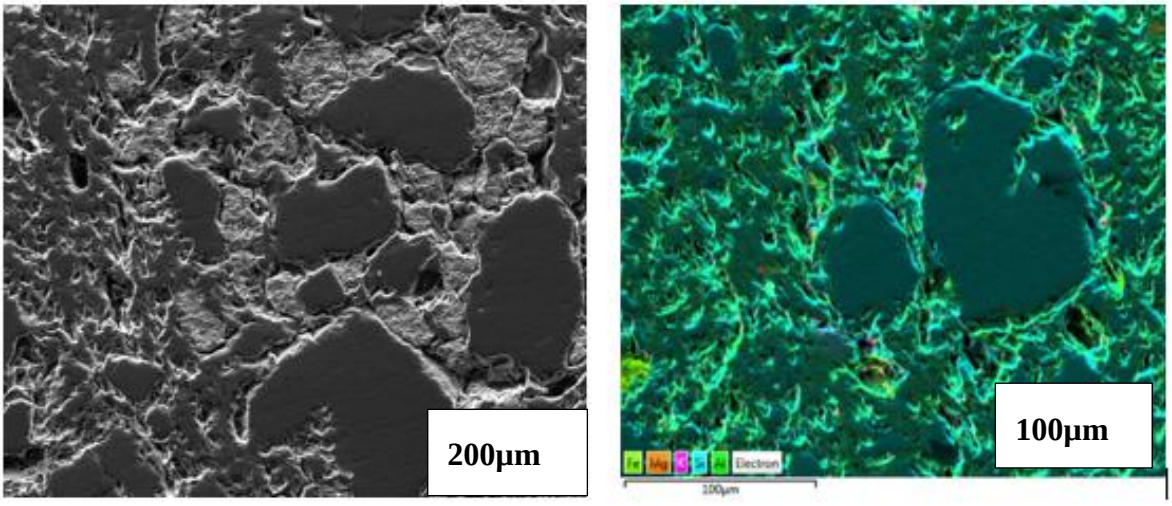

Figure 9-16: Secondary electron image of fired Ewhurst clay at 1050^{o}C and (b) the elemental analysis of the same Weald clay with large clusters forming Aluminosilicate and iron silicate.

The SEM image **(Figure 9-17)** shows the microstructure as an extruded brick whose composition is a mixture of Staffordshire clay, manganese and a secret additive fired to temperatures above 1100° to obtain a blue-fired brick for an engineering application. This vitrified brick, fired at 1120^{o}C under a reduced atmosphere, shows a porous structure which could result from the decomposition of carbonaceous content present in the composition and particle size of clay particles. Also, the microstructure reveals a glassy phase and solid or dense structure from the melting and bonding of particles on shaping and by firing temperature. The crack observed is due to the impact of the hammer to obtain a fracture for

the analysis and not an internal crack caused by either expansion on heating or cooling or even from the trapped gas.

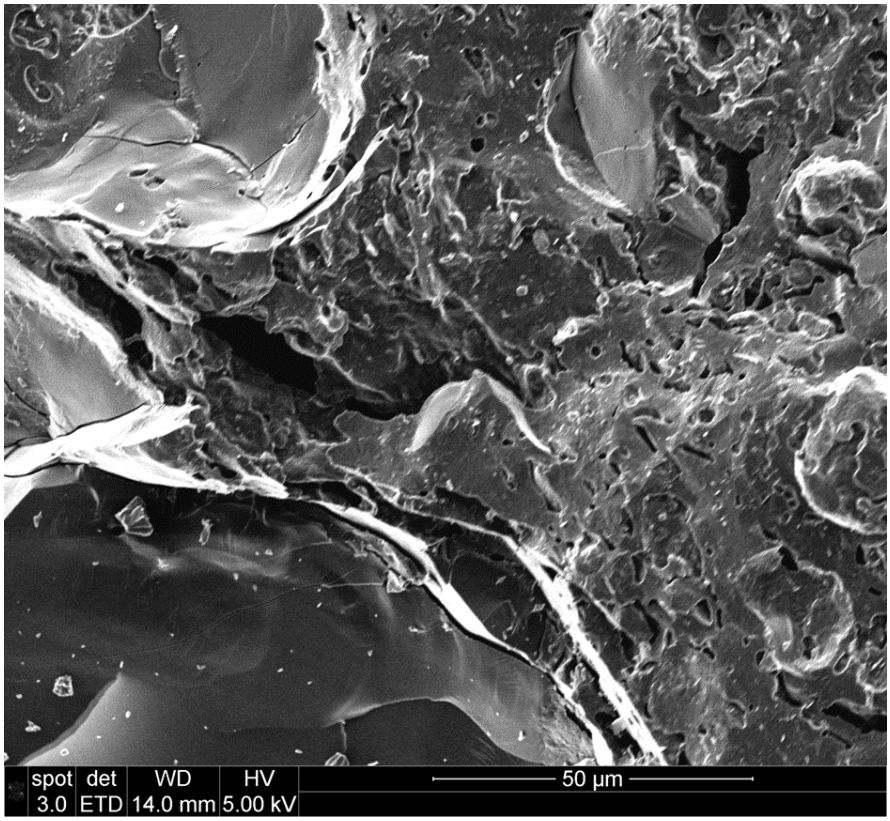

Figure 9-17: Secondary electron image of blue brick fired in a reduced atmosphere containing manganese to help improve the blue-black colour fired to 1120^{o}C.

9.1.6 *Mössbauer spectroscopy*

Mössbauer spectroscopy explains the coordination state of Fe in Blue Engineering brick and the different colouring effects obtained after firing the brick product. **Figure 9-18** shows the Mössbauer spectra (a) the Blue coloured brick section and (b) the red surface**.** The interior section of the same brick under the same reduced atmosphere depicts a non-identical spectrum to the exterior section. The XRD of this fired product revealed quartz (SiO_2) as the dominant phase, followed by mullite (Al), iron Oxide (Fe_2O_3) and spinel (Mg Fe)AlO_4). Fe_2O_3 is only found in the interior section **(Figure 9-18b**), along with mullite and quartz.

The first sextet denotes a paramagnetic phase with a tesla of 50.34, while the second is of a lower magnetic field, as summarised in **Figure 9-19,** with a doublet indicating the oxidation state of the iron.

Although the oxidation state of iron for the external section (**Figure 9-18a**) of the brick showed both the Fe^{2+} and Fe^{3+} per the fitting parameters of the spectrum, it also indicates that Fe^{2+} has the most populated site at 53% with a magnetic field of 48.34. So, as was expected, the reduced section of the brick piece changes from Fe^{3+} to Fe^{2+} when Oxygen is limited within the fired piece or the kiln.

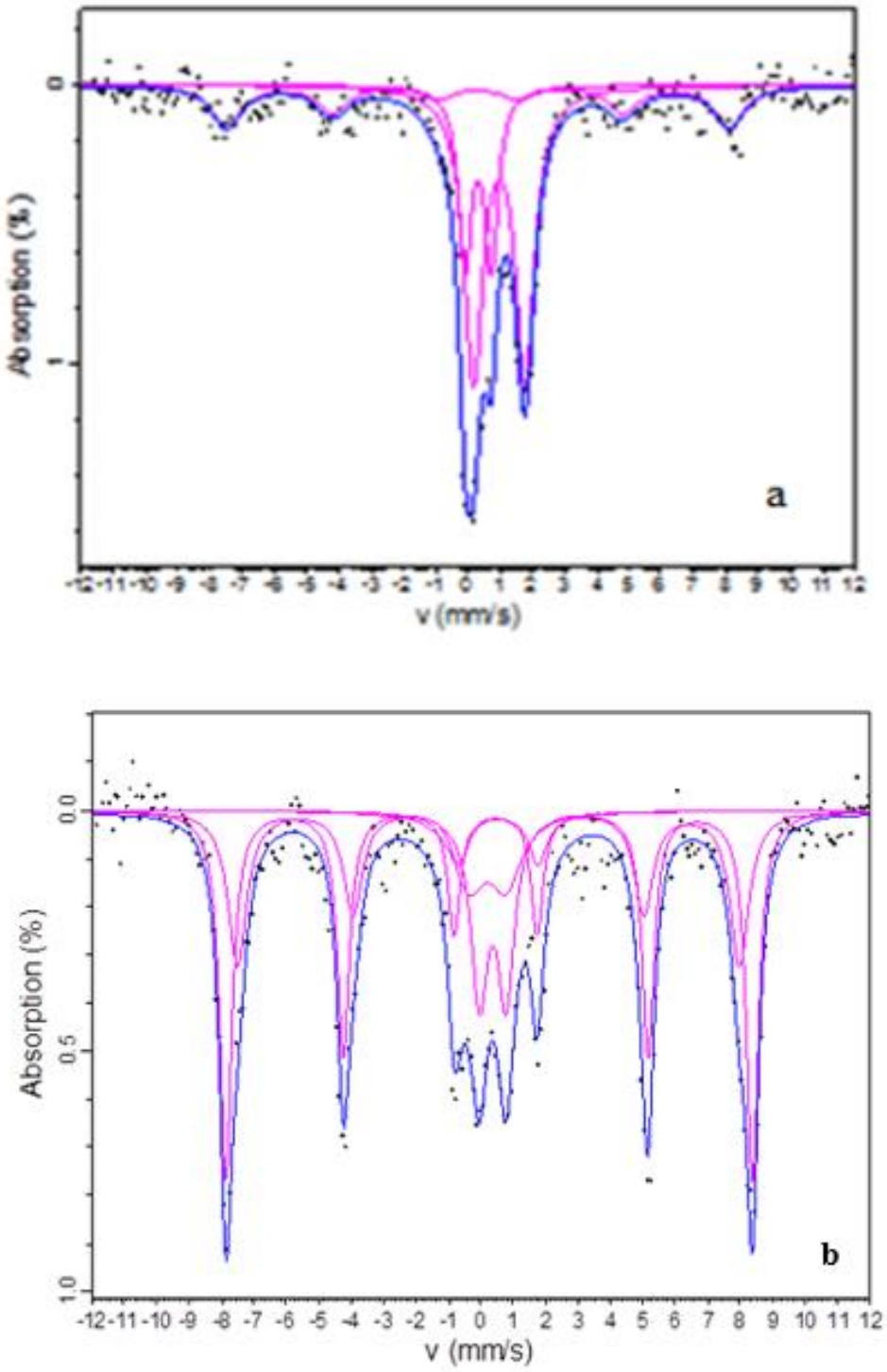

Figure 9-18: Mossbauer spectra of a reduced Engineering brick with two different shades of colour after firing (a) Exterior surface (Blue-black Colour) (b) Interior section (brownish-red colour)

ID	Spectral details	Centre Shift, CS (mm/s)	Quadruple splitting, QS (mm/s)	H (Tesla)	Linewidth, LW (mm/s)	Area %	Oxidation state
Exterior Surface (blue-black colour)	Doublet 1	0.32	0.82	-	0.25	22.5	Fe^{3+}
	Doublet 2	0.97	1.6	-	0.36	53.1	Fe^{2+}
	Sextet 1	0.31	0	48.34	0.56	24.4	
Interior section of same brick (brownish –red colour)	Doublet 1	0.34	0.88	-	0.41	25.9	Fe^{3+}
	Sextet 1	0.36	-0.1	50.37	0.23	45.1	-
	Sextet 2	0.39	-0.15	48.03	0.35	29	-

Figure 9-19: Fitted Mössbauer parameters of fired blue brick samples an engineering brick.

Chapter 10 Energy and CO_2 Estimation

10.1 Energy Requirements and CO_2 estimation for clay brick body formulations

Energy use is an important commodity for the ceramic sector to obtain desired fired properties. The quantity of energy for ceramic manufacture affects the overall product cost and CO_2 tariff [446]. Since fossil fuels account for the major energy use (70-80%)[8], CO_2 from these fuels will contribute to the total emissions and those produced by the carbonates in the raw material. The high demand for the product in the housing sector makes the heavy clay industry an energy-intensive industry. However, the 2020 sector sustainability report showed a reduction due to low demand for products caused by the pandemic[345].

Innovative technological approaches have been identified and reported in the 2017 decarbonisation roadmap[8]. Vogl[117] lists similar approaches to the 2050 decarbonisation map. Mezquita et al.[446] reported on energy savings in ceramic tile production by new installation designs based on the 2050 roadmap the European ceramic industry Association gave. Fradette[447] reports on understanding heat loss in vacuum furnaces by comparing different materials.

Research has shown that moving away from fuel that emits high CO_2 (e.g., coal, firewood, gas) to natural gas and green power (hydro, solar and wind) can help reduce emissions from ceramic manufacturing. Research has shown that moving away from fuel emitting high CO_2 (e.g., coal, firewood, gas) to natural gas and green power (hydro, solar and wind) can help reduces emissions from ceramic manufacturing[345]. For example, Ibstock reported a 6% energy reduction by switching to electricity [448].

Of all the four identified areas that can lead to energy efficiency[8], reducing emissions by reformulating body compositions is challenging due to the changes in clay chemistry and

mineralogy, and additives that are effective at lower emissions can produce sub-standard product quality. Since the primary raw material clay can be high /low in carbonates or organic matter, changing formulations may not be sufficient to reduce CO_2 emissions [449,450].

Complex models involving reactions during thermal treatment (mineralogical changes), enthalpies of reactions calculated from the enthalpies of formation, and organic burning have been used to estimate energy and CO_2 released in manufacturing [137,451,452] Minimising fuel will drastically affect the overall CO_2 reduction in ceramic production. Hence this study sort of modified clay brick composition to reduce fuel use. It becomes absolute that the manufacture of ceramics consists of clay and heat along with its CO_2 emissions, which is impossible to do without[117,345].

This chapter explores a simple model of calculating CO_2 emissions and reduced energy use derived from reformulated bodies containing alkali metals and alkaline earth carbonates.

For the model, the following assumptions were made:

1. Fuel use is constant for kiln operation
2. Enthalpy reactions that lead to phase change, ceramic bond, and texture are obtained at temperatures above 1000°C.
3. CO_2 from clay are all carbonates
4. The main sources of CO_2 are clay, additives and fuel used for firing and
5. No heat loss during firing

The calculation does not consider energy for clay mixing, shaping and drying. Additional parameters for the model are based on typical class B engineering bricks produced from Ewhurst Weald clay, provided by Wienerberger Ltd on April 7th 2021. 500kWh/ tonne was

given to fire class B engineering bricks (3-hole perforated brick) at 1090°C. Three tonnes of Weald clay is used to produce 1000 bricks; therefore, to produce 6336 bricks on one kiln car (provided by Wienerberger Ltd on April 7th 2021) for one batch firing, 19.008 tonnes of clay is required (this is shown in **Table 6-1**). Burning of natural gas releases is 0.185 kg CO_2 per kWh of natural gas[453]. Carbon % in Weald clay (without additives) was analysed using a carbon analyser. An average of six 2020 stockpiles was taken for this calculation (~0.26%)-provided by personal communication from Wienerberger on April 7th 2021. Equation (4) calculated the CO_2 percentage emitted in Weald clay during firing, which gives 181.08 kg.

Total CO_2 release is the sum of batch material emissions plus fuel for firing. The calculation based on Hu et al.,[454] is Total CO_2= CO_2 energy + CO_2 Batch. This is because the main sources of CO_2 emissions in clay brick production are the fuel and starting raw materials, including the decomposition of carbonates shown in equation (3).

Table 10-1: Summary data total CO_2 from fuel and clay without additives

Energy (kWh/t)	500
Clay needed to produce 6336 bricks if 3tonnes produce 1000 bricks/t	19.008
Energy required to fire 6336 bricks (kWh)	9504.00
CO_2 released from burning natural gas (kg)	1758.24
CO_2 in clay (kg)	181.08
Total CO_2 (kg)	**1939.32**

10.2 Method of Calculation

The equations (1)-(6) below were used to estimate CO_2 saving and energy reduction of laboratory-based ceramics containing Series 1 additives doped in 1-4wt% fired at 1000°C and 1040°C compared to industrial firing at 1090°C. See **Table 10-2**.

$$Mass\ fraction\ of\ CO_2\ from\ additive = \frac{(RMM\ CO_2)}{(RMM\ Carbonate)} \quad (1)$$

$$Mass_{batch} = \text{X (kg)} \quad (2)$$

$$Mass\ CO_2\ from\ additive\ per\ batch = \left(\frac{x}{100}\right) * additive(wt\%) * (eq.1) \quad (3)$$

$$CO_2\ from\ Clay\ (kg) = C\ wt\%\ in\ clay * \left(\frac{RMM\ CO_2}{RMM\ C}\right) \quad (4)$$

$$Energy\ required\ for\ temp\ x\ (kWh) = \frac{500\ kW * \ fired\ temperature\ (x)}{Kiln\ temperature\ (1090°)} \quad (5)$$

$$KgCO_2\ per\ ton/brick = 1000 * \left(\frac{Total\ \ CO_2}{mass\ of\ Clay\ (kg)}\right) \quad (6)$$

10.3 Estimated energy and CO_2 emissions

The obtained energy savings and total CO_2 emissions were calculated with body compositions containing carbonates (Li, Na, K, Mg, Ca and Ba in 1-4wt% levels), fired to 900°C, 950°C, 1000°C, 1040°C. and compared to the body composition containing 2wt% $BaCO_3$ fired at 1090°C assumed as the industrial standard. The energy use of the kiln is 500 kWh for 1090°C, and it has been assumed for simplicity that the required energy for firing reduces linearly with decreasing temperature from 1090°C to 900°C (Eqn 7). We have also

extrapolated back to 0°C. However, because we have assumed a linear relationship, the uncertainties are far greater than the uncertainties if we extrapolate to room temperature. See **Figure 10-1**.

$$y = 0.4589x \quad (7)$$

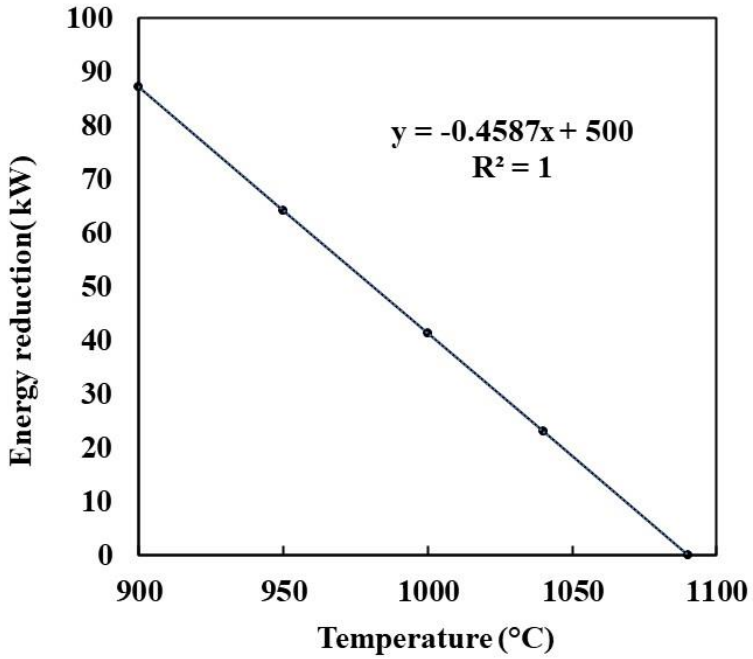

Figure 10-1: Energy reduction obtained when laboratory-based clay samples are fired below the 1090°C industrial firing regime. The model assumes a linear relationship between kiln energy use and operating temperature.

Table 10-2 shows the contribution of individual additive CO_2 and the total CO_2 with different energy use [kg per batch]. The model indicates that CO_2 released from brick-making is mostly from fuel combustion, and even for the worst-case scenario, 4wt% Li_2CO_3 fired at 1040°C contributes to only 20.22% and 5.75% for 1wt% additions to the total emissions.

Table 10-2: Estimated CO_2 emitted from additive only, Weald clay and the total CO_2 if fuel is 500kWh for ceramics fired to 1090°C, compared to 477.06 kWh (1040°C) and 458.72 kWh (1000°C) not including electricity. Total CO_2= energy CO_2 + batch CO_2 (CO_2 Kg [per batch])

Additives (2wt%)	**CO_2 emissions from additive (kg)**	**CO_2 emissions from additive and clay (kg)**	**Total emissions (fuel +batch) CO_2/kg [per batch]**		
			500kWh	477.06 kWh	458.72 kWh
$BaCO_3$	84.78	262.24	2020.48	1939.83	1875.30
$CaCO_3$	167.16	344.62	2102.86	2022.21	1957.68
Na_2CO_3	157.86	335.31	2093.55	2012.90	1948.37
K_2CO_3	121.06	298.52	2056.76	1976.10	1911.58
$MgCO_3$	198.44	375.90	2134.14	2053.48	1988.96
Li_2CO_3	226.43	403.89	2162.13	2081.48	2016.95

Table 10-3 shows a CO_2 emission of clay firing (kg CO_2 per kg) calculated per additive as kg per dry clay fired at 1040°C and 1000°C per kg of fired product from BDA 2015 results**.** The result shows that 0.228_e is obtained for the 2016 sustainability[7] emissions compared to the alkali and alkaline earth carbonates used in this study (producing lower CO_2 emissions). Additions of 2wt% $BaCO_3$ ceramics fired to 1040°C emit 0.102 CO_2 on firing. Moreover, CO_2 emissions from the 1wt% Li_2CO_3 additive are slightly higher (0.104 CO_2) than 2wt% $BaCO_3$ when fired at 1000°C (~0.097 CO_2). The 2016 sustainability report calculates electricity as part of its direct fuel, whiles this calculation only factored in fuel from natural gas. Overall, $BaCO_3$ records the least CO_2/tonne across all levels (1-4wt%).

Table 10-3: CO_2 emissions of clay firing (kg CO_2 per kg) calculated per additive as kg per dry clay fired at 1040 °C and 1000°C per kg of fired product from BDA 2015 results**.**

Additives	1040°C			1000°C	BDA 2015 (process and direct emissions)
	1wt%	2wt%	4wt%	1wt%	
$BaCO_3$	0.100	0.102	0.103	0.097	0.228
$CaCO_3$	0.102	0.106	0.112	0.099	
Na_2CO_3	0.102	0.106	0.111	0.098	
K_2CO_3	0.101	0.104	0.107	0.097	
$MgCO_3$	0.103	0.108	0.115	0.100	
Li_2CO_3	0.104	0.110	0.118	0.100	

$1m^2$ = 60 bricks, 2015 direct emissions =23.2KgCO_2 / m^2, process emissions =11KgCO_2 / m^2 and weight of brick =2.5kg (60*2.5)

For 1 m^2 = 60*2.5=150

For direct emissions, 23.2/150=0.155, and process emissions, 11/150=0.733

Therefore, process emissions + direct emissions equal 0.228 CO_2

The reference ceramic, 2wt% $BaCO_3$, contributes 106.11 kgCO_2 per ton/brick at 1090°C. However, if we replace $BaCO_3$ with 2wt% $MgCO_3$ to stop scumming (reported in **Chapter 5**), 112.09 kgCO_2 per ton/brick would be released when ceramics are fired to 1090°C. Assuming at this temperature of 1090^{o}C, a Class B Engineering property is achieved. This increase is a result of the atomic mass of the Mg, which is lighter than the Ba atom. The change in mass is also seen with the Ca, K and Na. However, when ceramics containing 2wt% $MgCO_3$ composition is fired at 1040°C (477kWh), the estimated emitted kgCO_2 per ton/brick is lower (~108.3) than ceramics fired at 1090°C (500kWh), due to energy input using Eqn (6). However, CO_2 and fuel consumption savings can be attained by using additives and firing bricks at 1000°C and 1040°C instead of 1090°C (shown in **Table 9-4**); not all the additives and all levels produce ceramics with acceptable brick-making

properties. For example, in the laboratory trials described in **Chapter 5**, Additions of 1-4wt% $CaCO_3$ containing ceramics or 1wt% $MgCO_3$ failed to prevent scumming. However, higher levels (2wt%,3wt% and 4wt% $MgCO_3$) prevented scumming, whereas 2wt% alkali carbonates resulted in patchy type staining (for > 2wt% K_2CO_3 / Li_2CO_3) and matt or glassy surfaces on firing (>2wt% Na_2CO_3 containing samples) at 1000°C and 1040°C. Higher boiling water absorption (**Figure 5-50**) (**~** >8%) was recorded for the alkaline earth, and lower boiling water absorption for the alkali metals (<7%) for ceramics fired at 1040°C. The compressive strength of ceramics improved with the alkali metals additives (>75MPa) compared to the alkaline earth (**Figure 5-86)**.

What is significant to this study is that we can obtain a class B engineering by firing ceramics doped with 1wt% Li_2CO_3 fired at 1000°C, with a CO_2 savings of 5.52% and 8.26% energy reduction compared to clay body fired to 1090°C at an industrial scale. Thus 90°C savings are made by firing the clay body (1wt% Li_2CO_3) to 1000°C—moreover, 2.32% CO_2 savings can be made for firing at 1040°C. Additions of 1wt% K_2CO_3 and 1wt% Na_2CO_3 containing ceramics fired at 1040°C are also viable for a desirable Class B engineering brick with estimated CO_2 savings of 4.93% and 4.02%, respectively (see **Table 10-5**). Meanwhile, at 1040°C, the energy savings is 4.58% or 24kWh. The CO_2 savings was calculated as Total CO_2 of additive/ Total CO_2 of standard (2wt% $BaCO_3$ fired at 1090°C) multiplied by 100.

The calculated amount of CO_2 released into the atmosphere is additive and temperature dependent. Additions of alkali and alkaline carbonates can bring down firing temperature and yet pass the class B engineering standard for brick masonry. In literature, >20% CO_2 savings have been achieved by incorporating steel slag[312], glass cullet[263,313] aquatic waste[157], biomass blend[316] into brick production with additive levels greater than 5wt%-30wt% and produced not a class B engineering brick with 7% or 17 % energy savings. While ceramics

fired to 900°C have a more considerable reduction in fuel savings, the quality of the product is negatively imparted for the specified brick in this study.

Sourcing Li, K and Na oxides from waste streams can save material cost and landfill tax and provide between 2.32%- 8.13% CO_2 savings on carbon price for firing bricks at 1040°C instead of 1090°C.

The estimated study demonstrates a saving of 64kWh and 23kWh energy by firing clay bodies at 1000°C and 1040°C. **Table 10-4** shows further energy reduction for ceramics fired at 1000°C (458.72kWh) compared to 1040°C (477.06kWh).

One advantage of body modification to minimise CO_2 from clay brick manufacture is materials efficiency. Therefore replacing 1-4wt% additives in Ewhurst Weald clay will reduce clay consumption by 80,000- 320,000t, based on Biggs' report of 8 million tonnes of winned clay used by the heavy clay industry[313]

Table 10-4: CO_2 emissions of clay firing (kg CO_2 per kg) calculated per additive as kg per dry clay fired at 1040 °C and 1000°C per kg of fired product from BDA 2015 results**:**
Total CO_2 savings when ceramics are fired at 1000°C (458.06 kWh) compared to 1040°C (477.06 kWh) for 1wt% additive [per batch]

Additives (1wt%)	**Total CO_2(fuel +batch) CO_2/kg**	
	477.06kWh	458.72 kWh
$BaCO_3$	1899.25	1834.72
$CaCO_3$	1940.44	1875.91
Na_2CO_3	1935.78	1871.26
K_2CO_3	1917.38	1852.86
$MgCO_3$	1956.07	1891.55
Li_2CO_3	1970.07	1905.54

Table 10-5: CO_2 emissions of clay firing (kg CO_2 per kg) calculated per additive as kg per dry clay fired at 1040 °C and 1000°C per kg of fired product from BDA 2015 results**:** Modelled CO_2 (%) savings for viable Class B engineering brick

Viable additives	CO_2 Saving at 1040°C	CO_2 Savings at 1000°C
1 wt% Li_2CO_3	2.32	5.52
1 wt% K_2CO_3	4.93	8.13
1 wt% Na_2CO_3	4.02	7.22
2 wt% $MgCO_3$*	-1.82	1.38
2wt% $BaCO_3$*	3.82	7.02

*Note: 2wt% $MgCO_3$ /2wt% $BaCO_3$ was included in the table based on its ability to stop scumming.

10.4 How does or to what extent do energy savings affect brick properties?

Direct energy savings in clay brick manufacture is tackled under four main streams: (i) modifying body compositions by introducing additives that promote early sintering, (ii) weight /mass reduction in brick, (iii) packing of green ceramic products for firing and finally (iv) a well-insulated furnace to minimise energy loss on firing. Fuel switching is directly related to its associated CO_2 emissions[8].

In considering the role of additives in achieving energy reduction, reference is made to **Chapters 4** to **7** of this thesis. For example, the mineralogical assessment (XRD- section 4.12) clearly showed that at 900°C, the clay mineral muscovite is still present with greater porosity compromising brick properties compared to ceramics fired at 1040°C; therefore, we can conclude that there is a direct correlation between firing temperature amount of

energy generated to obtain a specified clay brick property. From the experimental studies in **Chapter 5**, ceramics containing 2wt% $BaCO_3$ did not reach the requirement for class B engineering, possibly due to the limitation in forming the ceramic. Moreover, 1wt% K_2CO_3 and 1wt% Na_2CO_3 clay body fired at 1040°C give better CO_2 savings than ceramics containing 1wt% Li_2CO_3 fired at a lower temperature (1000°C) as shown in **Table 10-5** and yet retained the required properties for a Class B engineering standard. Therefore, it is recommended that potassium from waste streams could potentially replace using K_2CO_3. Also, energy saving / CO_2 must always be tailored to the product type and its properties.

10.5 Conclusions

Simple model energy and CO_2 estimations show that furnace temperature (1000°C and 1040°C) can be reduced using additives (1wt% Li_2CO_3, 1wt% K_2CO_3, and 1wt% Na_2CO_3) producing technically acceptable class B engineering bricks. Energy reductions of 8.3% and 4.6% can be made when ceramics are fired at 1000°C and 1040°C compared to the factory firing at 1090°C, offsetting the CO_2 emissions. The additive 1wt% K_2CO_3 gives better CO_2 savings than 1wt% Li_2CO_3 fired at a lower temperature. Furthermore, the estimated CO_2 from the batch materials was found to be low compared to the CO_2 contribution from the fuel.

Chapter 11 Conclusions and Recommendations

This chapter presents a summary of the conducted research and suggested future work.

11.1 Conclusions

11.1.1 *Effect of additives on ceramic properties.*

Modifying heavy clay ceramic compositions to promote lower fuel use in drying and firing, reducing CO_2 emissions from heavy clay ceramic manufacture, whilst maintaining product properties (in the context of ceramics class B engineering bricks) using Weald clay will help the industry solve the vital global problem of decarbonisation.

This study shows that types and levels of additives, shaping methods and firing temperature significantly change ceramic mineralogy, porosity, volumetric shrinkage, strength, microstructure and even colour when Ewhurst clay is fired.

The DTA trace does not indicate sudden melting behaviour; the Dilatometry also shows no sudden melting. With such low dopant levels, the formation of liquid phases (i.e., melting) is not separable from the shrinkage effects that occur over a wide temperature range. The differences in additives lie in the decomposition temperatures. Volatiles derived from this study were mainly: water of formation, intrinsic water and CO_2. Samples containing CaO greater than ~6% (Colemanite, filter cake, slurry dust, mineral wool, container glass waste and wollastonite) were more prone to form surface scum ($CaSO_4$) at all studied firing temperatures (900°C, 950°C and 1040°C) and the sulphate was derived from the starting material. However, adding greater than 2wt% $MgCO_3$ prevented scumming, as observed with the traditional use of $BaCO_3$. Although talc is MgO rich, talc additions were unsuccessful in preventing surface scum. Performance characteristics of the modified ceramics for class B Engineering bricks were limited by the laboratory-based clay precursor shaping method used in this study. Promising ceramic samples such as 2wt% $MgCO_3$, 1-

4wt% $CaCO_3$, 2wt% container glass, 4wt% wollastonite and 4wt% talc, revisited in strengths of between 60-74 MPa, which did not pass the limit for a Class B engineering brick. However, adding 1wt% of alkali's carbonates to ceramics (Li, Na and K) provides brick that passes the compressive strength and boiling water absorption tests (6-7% porosity). Boiling water absorption testing for ceramics produced with additions of alkaline earth, industrial wastes, and inorganic minerals exceeded the standard limit of ~7.0%.

Colemanite additive was found to impact colour (produce a darker red hue) and promote porosity due to the decomposition of the additive to amorphous B_2O_3 and CaO, which occurs at temperatures <600 °C. Additions of 2wt% $MgCO_3$ and 2wt% $BaCO_3$ to clay fired to 1040°C reduced the spectrums intensity, while additions of 4wt% $BaCO_3$ and colemanite promoted stronger magnetic intensity, which corresponds to the differences in XRD pattern intensities, and hence the observed ceramic colours obtained. Moreover, adding>2wt% Na_2CO_3 promoted efflorescence on drying and formed glassy and/or matt surfaces on firing. Also,1wt% of Li, Na and K carbonate additives slightly increased the sextet / magnetic lines affecting the fired colour. Hence the % area of the sextet or differences in Fe^{3+} partitioning and site populations can affect ceramic colour and may provide advantageous ranges of ceramic colours, giving manufacturers more flexibility in their product range.

11.2 Savings on fuel, CO_2 and material efficiency

Up to 50°C firing temperature reduction has been saved by firing ceramics to 1040°C instead of 1090°C per the simple energy calculation model. 90°C firing temperature reduction can be saved by replacing 1wt% Li_2CO_3 with Weald clay fired at 1000°C with a CO_2 reduction of 0.100 compared to the 2016 sustainability report (~0.228 CO_{2e}), achieving a suitable brick (i.e. Class B engineering standard). However, 1wt% K_2CO_3 containing ceramics fired at 1000°C /

1040°C has better CO_2 savings (4.93% and 8.13%) compared to 1wt% Li_2CO_3 fired at 1000°C (∼2.32%) and still passes the EN77-1-:2011 standard.

Regarding material efficiency, 80,000-320,000 tonnes can be saved by replacing clay with 1-4wt% additives for the overburden of virgin material if an average of about 8m of clay is consumed.

11.3 Recommendations for future work

1. Seven ceramic compositions are suggested for industrial trial by extrusion based on their properties: strength, porosity, shrinkage, and absence of surface stains. These are additions of 2wt% $MgCO_2$ (M2W), 1wt% K_2CO_3 (K1W), 1wt% Na_2CO_3 (N1W),1wt% Li_2CO_3 (L1W), 4wt% Wollastonite (W4W), 4wt% Mineral w ool (M4W) and 4wt% Talc (T4W). A summary of these is shown **in Table 11-1.**
2. Investigate why talc additive does not remove surface scum.
3. Conduct direct durability testing of recommended samples especially (>2wt% $MgCO_3$, 4wt% Wollastonite, 1wt% K_2CO_3, 1wt% Li_2CO_3, 4wt% Talc with >60MPa fired to 1040°C.
4. Establish the magnetic domain state of fired ceramics (the control, 4wt% Colemanite, 2wt% $MgCO_3$, 2wt% $BaCO_3$ and 4wt% $BaCO_3$) using superconducting quantum interference detector (SQUID) magnetometry and TEM if perhaps this influence ceramic colour.
5. Estimate the economic cost of firing temperature reduction of 50°C and 90°C.
6. Explore other waste streams for lithium and potassium instead of high-processed additives for ceramic manufacture.
7. Pilot testing for in-use efflorescence forming on finished products of $MgCO_3$ as an alternative to $BaCO_3$.

POTENTIAL ADDITIVE LIST FOR CLASS B ENGINEERING BRICK (PELLETS) FIRED TO 1040°C

ADDITIVES	ADDITIVE AMOUNT /LEVEL (Wt.%)	SAFETY DATA SHEET	PRODUCT PROPERTIES ON WEALDEN CLAY				ADDITIVE EMISSIONS (CO_2) (%)
			COLOUR	*STRENGTH (MPa)	*WATER ABSORPTION (%)	POTENTIAL TEMP. REDUCTION (°C) BASED ON DILATOMETRY	
$MgCO_3$	2	✓		71.5	11	12	1.81
Na_2CO_3	1	✓		87.5	7.3	5	0.73
Li_2CO_3	1	✓		107	6.3	23	1.04
K_2CO_3	1	✓		94	8.7	4	0.56
Mineral / Rockwool	4	✓		52.8	8.6	20	N/A

✓ A safety data sheet of used additives can be obtained from Sigma Aldrich.

*Water absorption and strength given based on laboratory-based pellet presser.

Scummed samples can be removed by $MgCO_3$/$BaCO_3$

Appendix 1:DTA Analysis Of Selected Samples

The DTA curves of selected Series 1 -3 samples

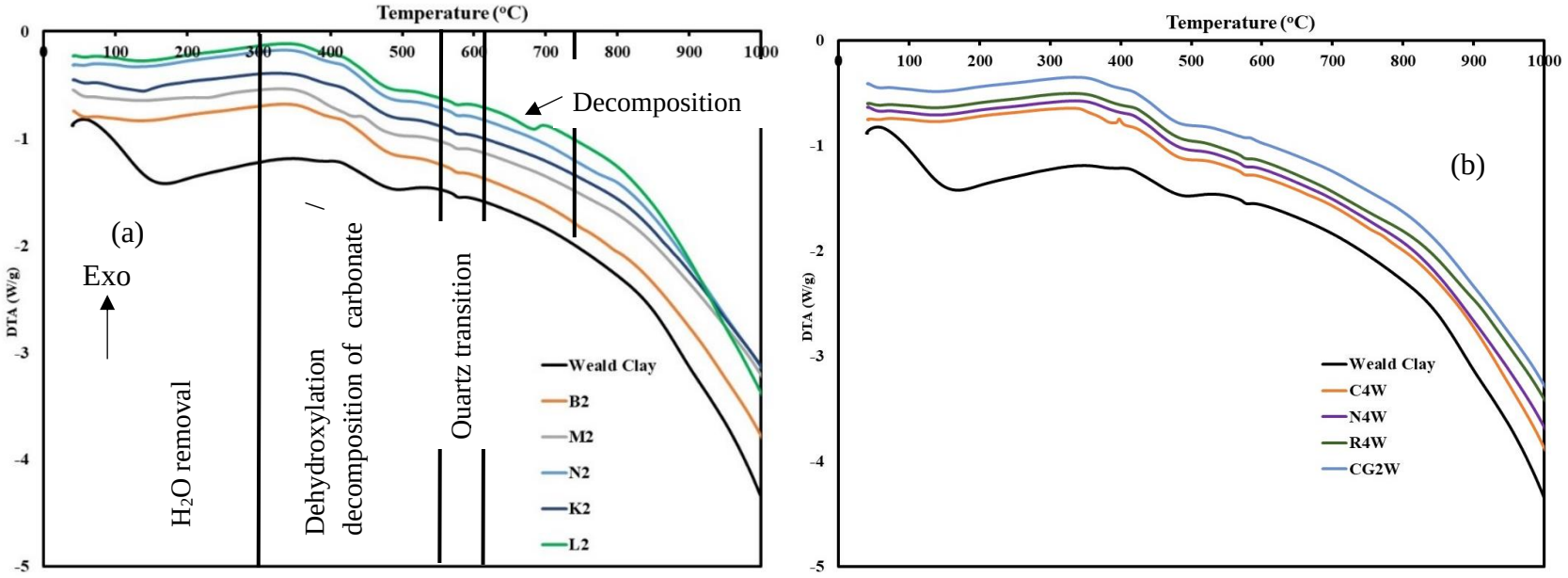

Differential thermal analyses of selected additives compared to Weald clay fired from room temperature to 1000°C at 10°C / min in an alumina crucible.

Appendix 2: Analysed XRF results of ceramics fired from 900°C and 950°C in weight percentages(wt%)

Control material fired to 900°C and 1040°C

Samples	SiO_2	Al_2O_3	Fe_2O_3	K_2O	TiO_2	BaO	MgO	CaO	Na_2O	MnO	SUM
W0-900°C	71.94	16.20	6.99	2.39	1.37	0.00	0.75	0.36	0.00	0.00	100.00
W0-950°C	77.03	13.61	7.20	2.16	0.00	0.00	0.00	0.00	0.00	0.00	100.00
Series 1- Additives (Alkaline Earths and Alkalis)											
C1-900°C	71.93	16.01	6.93	2.40	1.35	0.00	0.75	0.63	0.00	0.00	100.00
C2-900°C	70.25	16.04	6.79	2.33	1.35	0.00	0.72	2.53	0.00	0.00	100.00
C3-900°C	69.72	15.76	6.62	2.27	1.29	0.00	0.70	3.64	0.00	0.00	100.00
C4-900°C	68.86	15.49	6.53	2.22	1.33	0.00	0.71	4.86	0.00	0.00	100.00

Samples	SiO_2	Al_2O_3	Fe_2O_3	K_2O	TiO_2	BaO	MgO	CaO	Na_2O	MnO	SUM
B1-900°C	68.91	17.55	7.55	2.67	1.46	0.73	0.82	0.31	0.00	0.00	100.00
B2-900°C	68.31	17.29	7.15	2.53	1.48	2.51	0.73	0.00	0.00	0.00	100.00
B3-900°C	67.49	17.08	7.07	2.55	1.46	3.66	0.68	0.00	0.00	0.00	100.00
B4-900°C	72.15	15.45	6.64	2.31	1.33	1.12	0.68	0.33	0.00	0.00	100.00
M1-900°C	72.03	16.11	6.91	2.41	1.35	0.00	0.89	0.31	0.00	0.00	100.00
M2-900°C	70.65	16.01	6.94	2.38	1.33	0.00	2.31	0.37	0.00	0.00	100.00
M3-900°C	70.15	15.65	6.80	2.32	1.30	0.00	3.41	0.36	0.00	0.00	100.00
M4-900°C	69.38	15.58	6.81	2.31	1.33	0.00	4.23	0.36	0.00	0.00	100.00
L1-900°C	71.87	16.27	6.92	2.42	1.38	0.00	0.75	0.37	0.00	0.00	100.00
L2-900°C	72.16	16.13	6.89	2.38	1.35	0.00	0.72	0.37	0.00	0.00	100.00

Samples	SiO_2	Al_2O_3	Fe_2O_3	K_2O	TiO2	BaO	MgO	CaO	Na_2O	MnO	SUM
L3-900°C	72.62	15.83	7.00	2.42	1.37	0.00	0.75	0.00	0.00	0.00	100.00
L4-900°C	75.26	14.50	7.93	2.32	0.00	0.00	0.00	0.00	0.00	0.00	100.00
K1-900°C	71.58	16.14	6.91	2.94	1.36	0.00	0.73	0.35	0.00	0.00	100.00
K2-900°C	70.48	15.70	6.73	4.70	1.32	0.00	0.74	0.34	0.00	0.00	100.00
K3-900°C	69.78	15.59	6.55	5.73	1.30	0.00	0.71	0.35	0.00	0.00	100.00
N1-900°C	71.72	16.42	7.03	2.41	1.34	0.00	0.70	0.38	0.00	0.00	100.00
N2-900°C	72.00	16.12	7.05	2.37	1.38	0.00	0.73	0.35	0.00	0.00	100.00
N3-900°C	70.67	16.13	6.90	2.38	1.30	0.00	0.73	0.38	1.51	0.00	100.00
N4-900°C	69.87	16.31	6.75	2.34	1.36	0.00	0.72	0.38	2.27	0.00	100.00

Samples	SiO_2	Al_2O_3	Fe_2O_3	K_2O	TiO_2	BaO	MgO	CaO	Na_2O	MnO	SUM
Series 2-Industrial Wastes Additives											
R4W-950°C	**72.79**	**15.09**	**6.30**	**2.09**	**1.32**	**0.00**	**0.89**	**1.51**	**0.00**	**0.00**	**100.00**
F4W-950°C	73.94	14.84	6.38	2.21	1.31	0.00	0.76	0.57	0.00	0.00	100.00
S4W-950°C	73.94	15.56	5.78	2.06	1.24	0.00	0.83	0.59	0.00	0.00	100.00
CG2W-950°C	74.75	14.78	5.78	2.17	1.26	0.00	0.68	0.57	0.00	0.00	100.00
Series 3- Inorganic Mineral Additives											
C4W-950°C	73.69	14.53	6.12	2.20	1.30	0.00	0.71	1.46	0.00	0.00	100.00
W4W-950°C	73.03	14.75	5.85	2.12	1.21	0.00	0.70	2.35	0.00	0.00	100.00
N4W-950°C	73.90	15.74	5.68	2.50	1.24	0.00	0.58	0.36	0.00	0.00	100.00
T4W-950°C	74.20	14.36	5.89	2.11	1.23	0.00	1.86	0.36	0.00	0.00	100.00

Appendix 3- Durability prediction of Series 1-3 additives using Maage Equation

Sample	Filled Pore Volume PV (cm^3/g)	P3	Durability Factor	Assessment
Control -900°C	0.11621	0.2	28.1	Fail
Control -950°C	0.09799	8.9	54.0	Fail
Control -1000°C	0.09435	1.8	38.1	Fail
Control -1040°C	0.06786	3.6	55.8	uncertain
	SERIES 1 ADDITIVES			
C1-900°C	0.10956	2.0	34.0	Fail
C2-900°C	0.10998	0.9	31.3	Fail
C3-900°C	0.09443	1.0	36.2	Fail
C4-900°C	0.11682	0.5	28.7	Fail
C1-1040°C	0.07561	0.4	43.3	Fail
C2-1040°C	0.0889	2.0	40.9	Fail
C3-1040°C	0.09443	1.0	36.2	Fail
C4-1040°C	0.11024	2.1	34.2	Fail
B1-900°C	0.11921	5.5	40.0	Fail
B2-900°C	0.10026	8.5	52.2	Fail
B3-900°C	0.10852	2.0	34.3	Fail
B4-900°C	0.06845	1.6	50.6	Fail
B1-1040°C	0.08397	6.2	53.0	Fail

B2-1040°C	0.08946	16.6	75.5	Pass
B3-1040°C	0.09426	7.8	52.6	Fail
B4-1040°C	0.06845	1.6	50.6	Fail
M1-900°C	0.11346	0.0	28.2	Fail
M2-900°C	0.11847	0.0	27.0	Fail
M3-900°C	0.11034	0.1	29.2	Fail
M4-900°C	0.1164	0.0	27.5	Fail
M1-1040°C	0.07953	0.3	41.0	Fail
M2-1040°C	0.09181	0.0	34.9	Fail
M3-1040°C	0.09066	0.0	35.3	Fail
M4-1040°C	0.09954	0.0	32.1	Fail
L1-900°C	0.09671	1.1	35.7	Fail
L2-900°C	0.10828	1.7	33.7	Fail
L3-900°C	0.12205	3.2	33.9	Fail
L4-900°C	0.12385	6.2	40.8	Fail

Sample	Filled Pore Volume PV (cm^3/g)	P3	Durability Factor	Assessment
N1-1040°C	0.06217	4.0	61.0	Uncertainty
N2-1040°C	0.04937	6.5	80.3	Pass
N3-1040°C	0.03965	5.3	93.4	Pass
N4-1040°C	0.04211	46.6	187.9	Pass
SERIES 2-INDUSTRIAL WASTES ADDITIVES				
M4W-950°C	0.09488	3.2	41.4	Fail
M4W-1040°C	0.06992	2.3	51.2	Fail
F4W-950°C	0.09713	3.4	41.2	Fail
F4W-1040°C	0.06615	3.7	57.3	Uncertainty
S4W-950°C	0.09561	6.0	47.9	Fail
S4W-1040°C	0.07169	3.8	53.8	Fail
CG2W-950°C	0.09431	2.8	40.6	Fail
CG2W-1040°C	0.06882	2.6	52.8	Fail

SERIES 3- INORGANIC MINERAL ADDITIVES

Sample	Filled Pore Volume PV (cm^3/g)	P3	Durability Factor	Assessment
C4W-950°C	0.10121	31.5	107.3	Pass
C4W-1040°C	0.0654	44.7	156.3	Pass
W4W-950°C	0.09242	1.9	39.2	Fail
W4W-1040°C	0.06461	4.3	59.8	Uncertain
N4W-950°C	0.09104	5.0	47.1	Fail
N4W-1040°C	0.06844	4.4	57.4	Uncertain
T4W-950°C	0.09494	3.3	41.6	Fail
T4W-1040°C	0.07237	4.6	55.4	Uncertain

References

1. Heritage crafts https://heritagecrafts.org.uk/brick-making/.

2. Brownell, W. E. *Structural Clay Products*. *Springer Science and Business Media* vol. 9 (2012).

3. Lopez-Arce, P. & Garcia-Guinea, J. Weathering traces in ancient bricks from historic buildings. *Build Environ* **40**, 929–941 (2005).

4. Jin, P. jun, Zhang, Y., Wang, S., Yang, X. gang & Zhang, M. Characterization of the superficial weathering of bricks on the City Wall of Xi'an, China. *Constr Build Mater* **149**, 139–148 (2017).

5. Fernandes, F. M., Lourenço, P. B. & Castro, F. Chapter 3 Ancient Clay Bricks: Manufacture and Properties. *Materials, Technologies and Practice in Historic Heritage Structures* (2010) doi:10.1007/978-90-481-2684-2.

6. Leslie, K. C. The Ashburnham Estate Brickworks 1840-1968. *Journal of the sussex industrial archaeology study group* **1**, (1970).

7. Brick Development Association. BRICK Sustainability Report 2016. *Brick Development Association website* 45 (2016).

8. WSP PB, D. G. Decarbonisation, Industrial Roadmap, Energy Efficiency Plan, Action. (2017).

9. Barrett, J., Cooper, T., Hammond, G. P. & Pidgeon, N. Industrial energy, materials and products: UK decarbonisation challenges and opportunities. *Appl Therm Eng* **136**, 643–656 (2018).

10. WSP, Parsons Brinckerhoff & DNV-GL. Industrial Decarbonisation & Energy Efficiency Roadmaps to 2050| Ceramic Sector. (2015).

11. European Ceramic Industry Association. (2012). Paving the Way to 2050: the Ceramic Industry Road Map. doi:10.1049/et.2011.0303.

12. Al-Fakih, A., Mohammed, B. S., Liew, M. S. & Nikbakht, E. Incorporation of waste materials in the manufacture of masonry bricks: An update review. *Journal of Building Engineering* **21**, 37–54 (2019).

13. J.C, G. Structural Ceramic Products Fluxing Additives: A Critical Literature Review. *CERAM Research Spec.Publ.134,1990* (1990).

14. Zhang, L. Production of bricks from waste materials – A review. *Constr Build Mater* **47**, 643–655 (2013).

15. Dondi, M., Marsigli, M. & Fabbri, B. Recycling of Industrial and urban wastes in brick production : A review. *Tile & brick international* **13**, 302–315 (1997).

16. Muñoz Velasco, P., Morales Ortíz, M. P., Mendívil Giró, M. A. & Muñoz Velasco, L. Fired clay bricks manufactured by adding wastes as sustainable construction material - A review. *Constr Build Mater* **63**, 97–107 (2014).

17. EN. Specification for Masonry Units–Part 1: Clay Masonry Units. *BS1 Standard publication* 771–1 Preprint at (2015).

18. Changxue SHU. From the blue to the red: Changing technology in the brick industry of modern Shanghai. *The Proceedings of the Fifth International Congress on Construction History* **3**, 313–320 (2015).

19. Fiala, J., Mikolas, M. & Krejsova, K. Full Brick, History and Future. *IOP Conf Ser Earth Environ Sci* **221**, (2019).

20. Coronado, M., Blanco, T., Quijorna, N., Alonso-Santurde, R. & Andrés, A. *Types of waste, properties and durability of toxic waste-based fired masonry*

bricks. *Eco-efficient Masonry Bricks and Blocks: Design, Properties and Durability* (Elsevier Ltd, 2015). doi:10.1016/B978-1-78242-305-8.00007-3.

21. Murmu, A. L. & Patel, A. Towards sustainable bricks production: An overview. *Constr Build Mater* **165**, 112–125 (2018).

22. Nelson, T. *The Holy Bible, New King James Version*. (Thomas Nelson, Inc, 1982).

23. Hummel, R. E. No Ceramics Age? *Understanding Materials Science* 287–325 (2004) doi:10.1007/0-387-26691-7_15.

24. Clews, F. H. *Heavy clay technology*. (Academic Press, 1969).

25. Arbuckle, L. Clays and Clay Bodies. **6**, 1–7 (2010).

26. Fernandes, F. M., Lourenço, P. B. & Castro, F. Ancient Clay Bricks: Manufacture and Properties. *Materials, Technologies and Practice in Historic Heritage Structures* (2010) doi:10.1007/978-90-481-2684-2.

27. Vitruvius, M. P. The ten books on architecture, translated by Morris Hicky Morgan. (1960).

28. Fernandes, F. M. *Clay bricks*. *Long-term Performance and Durability of Masonry Structures: Degradation Mechanisms, Health Monitoring and Service Life Design* (Elsevier, 2018). doi:10.1016/B978-0-08-102110-1.00001-7.

29. Dalkılıç, N. & Nabikoğlu, A. Traditional manufacturing of clay brick used in the historical buildings of Diyarbakir (Turkey). *Frontiers of Architectural Research* **6**, 346–359 (2017).

30. Illustration of ancient brick making in Egypt. *https://www.bing.com/images/search?q=Illustration+of+historical+brick+production&form=HDRSC2&first=1&tsc=ImageBasicHover [Online] Available* (2021).

31. Lourenço, P. B., Fernandes, F. M. & Castro, F. Handmade clay bricks: Chemical, physical and mechanical properties. *International Journal of Architectural Heritage* **4**, 38–58 (2010).

32. Vitruvius Pollio M (1960) The ten books on architecture. (MH Morgan, Trans.) Courier Dover Publications, New York.

33. Introduction to Brick Kilns & Specific Energy Consumption Protocol for Brick Kilns Manual developed by :

34. Obeng, K., Ocran, K. A. G. & Anaba, D. Palm kernel shell as fuel for burning bricks. *Building Research & Information* **25**, 131–136 (1997).

35. Moedinger, F. Advances in the utilization of waste materials and alternative sources of energy in clay brick making A South Tyrolean case study investigating environmental and financial impacts. (2010).

36. Brownell, W. E. *Structural clay products*. vol. 9 (Springer Science & Business Media, 2012).

37. Moore, D. M. & J., R. C. R. *X-ray diffraction and the identification and analysis of clay minerals*. (Oxford University Press (OUP), 1989).

38. Wood, A. Capacity Rationalisation and Barriers To Exit: the British Brick Industry. *L* **44**, 0–26 (2003).

39. Andrew Smith. Clay Bricks a nd Clay Blocks: Resource Efficiency Action Plan. *The Green Construction Board* 1–47 (2013).

40. Mutsago, M. Technical Feasibility of Using Spent Lubricating Oil as a Body Fuel in Traditional Clay Brick Making Operations. 140 (2012).

41. Menezes, R. R., Ferreira, H. S., Neves, G. A., Lira, H. de L. & Ferreira, H. C. Use of granite sawing wastes in the production of ceramic bricks and tiles. *J Eur Ceram Soc* **25**, 1149–1158 (2005).

42. Savage, J. How to Reduce Scumming from Structural Bricks without Barium Carbonate? *2018, https://blog.biokeram.com/ acessed 20th April .2021*.

43. Ecofys. Methodology for the free allocation of emission allowances in the EU ETS post 2012. 38 (2009).

44. Terzić, A. *et al.* Influence of different bonding and fluxing agents on the sintering behavior and dielectric properties of steatite ceramic materials. *Ceram Int* **43**, 13264–13275 (2017).

45. Boltakova, N. v, Faseeva, G. R., Kabirov, R. R., Nafikov, R. M. & Zakharov, Y. A. Utilization of inorganic industrial wastes in producing construction ceramics. Review of Russian experience for the years 2000–2015. *Waste Management* **60**, 230–246 (2017).

46. Mutsago, M. Technical Feasibility of Using Spent Lubricating Oil as a Body Fuel in Traditional Clay Brick Making Operations. 140 (2012).

47. Andrew, S. S. Materials from Alternative, Recycled and Secondary Sources Survey (MARSS); the use of non primary clay raw materials in brick making in the UK 2005. *British Ceramic Confederation (BCC)* 6 (2005).

48. Mezquita, A., Monfort, E., Ferrer, S. & Gabaldón-Estevan, D. How to reduce energy and water consumption in the preparation of raw materials for ceramic tile manufacturing: Dry versus wet route. *J Clean Prod* **168**, 1566–1570 (2017).

49. Bonamartini Corradi, A., Leonelli, C., Manfredini, T., Pennisi, L. & Romagnoli, M. Quantitative determination of pyrite in, ceramic clay raw materials by DTA. *Thermochim Acta* **287**, 101–109 (1996).

50. Kadir, A. A., Sarani, N. A., Zaman, N. N. & Abdullah, M. M. A. B. Feasibility study on utilization of palm fibre waste into fired clay brick. *AIP Conf Proc* **1835**, 1–7 (2017).

51. Demir, I. Effect of organic residues addition on the technological properties of clay bricks. *Waste Management* **28**, 622–627 (2008).

52. Esharghawi, A., Penot, C. & Nardou, F. Contribution to porous mullite synthesis from clays by adding Al and Mg powders. *J Eur Ceram Soc* **29**, 31–38 (2009).

53. Waclawska, I. Thermal behaviour of mechanically amorphized colemanite: II. Internal structure reconstitution processes of ground colemanite. *Journal of Thermal Analysis* **48**, 155–161 (1997).

54. Wie-Addo G., Jones A.H., Palmer S., Starinieri V., Renshaw J., B. P. A. Reformulating Ceramic Body Composition to Improve Energy Efficiency in Brick Manufacture. in *Energy and Sustainable Futures: Proceedings of 2nd ICESF* p.257 (2020).

55. O, A. & G, K. Chemical and Thermodynamic Processes in Clay Brick Firing Technologies and Associated Atmospheric Emissions Metrics-A Review. *Journal of Pollution Effects & Control* **05**, (2017).

56. Jadambaa Temuujin*a, T. J. and S. H. Preparation of coloured facing brick from low melting clay under a water vapour atmosphere. in *Chapter 7* 2016–2030 (2012).

57. Kadir, A. A. & Mohajerani, A. Bricks: An excellent building material for recycling wastes - A review. *Proceedings of the IASTED International Conference on Environmental Management and Engineering, EME 2011* 108–115 (2011) doi:10.2316/P.2011.736-029.

58. Konta, J. Clay and man: clay raw materials in the service of man. *Appl Clay Sci* **10**, 275–335 (1995).

59. Guggenheim, S. *et al.* Definition of clay and clay mineral: Joint report of the AIPEA nomenclature and CMS nomenclature committees. *Clays Clay Miner* **43**, 255–256 (1995).

60. Barton, E. P. & J. Heavy Ceramic (Brick), Characterisation of Mineral Wastes, Resources and Processing technologies. Integrated waste management for the production of construction material. *(DEFRA Project Code WRT_177* 1–23 (2007).

61. Chemani, H. & Chemani, B. Valorization of wood sawdust in making porous clay brick. *Scientific Research and Essays* **8**, 609–614 (2013).

62. Elinwa, A. U. Effect of addition of sawdust ash to clay bricks. *Civil Engineering and Environmental Systems* **23**, 263–270 (2006).

63. ASTM C62 - 17 Standard Specification for Building Brick (Solid Masonry Units Made From Clay or Shale). (2017).

64. Petavratzi, C. D. E. & Wilson, S. Foundry sand in facing bricks.

65. Serra, M. F. *et al.* Talc, Spodumene and Calcium Carbonate Effect as Secondary Fluxes in Triaxial Ceramic Properties. *Procedia Materials Science* **1**, 397–402 (2012).

66. Celik, A. G., Depci, T. & Kilic, A. M. New lightweight colemanite-added perlite brick and comparison of its physicomechanical properties with other commercial lightweight materials. *Constr Build Mater* **62**, 59–66 (2014).

67. Kindrick, I. R. H. & Harrison, B. C. Extended BaCO3 for brick scum prevention. 3–7 (1980).

68. Gallacher Chris. Lignosulphonates the Heavy Clay conditioners.

69. Borovik, S. I., Lysova, G. A., & Chuklai, A. M.Borovik, S. I., Lysova, G. A., & Chuklai, A. M. Kinetic Aspects of the Thermal Degradation of a Temporary Binder Modified with Vitreous Molasses for Use in Making High-Temperature Periclase Refractories. *Refractories and Industrial Ceramics* **6**, 479-484. (2014).

70. Stefanov, S. Applications of borate compounds for the preparation of ceramic glazes. *Glass Technology* **41**, 193–196 (2000).

71. Cultrone, G., Aurrekoetxea, I., Casado, C. & Arizzi, A. Sawdust recycling in the production of lightweight bricks: How the amount of additive and the firing temperature influence the physical properties of the bricks. *Constr Build Mater* **235**, 117436 (2020).

72. de Matos, P. R., Sakata, R. D., Gleize, P. J. P., de Brito, J. & Repette, W. L. Eco-friendly ultra-high performance cement pastes produced with quarry wastes as alternative fillers. *J Clean Prod* **269**, 122308 (2020).

73. Veiga Simão, F., Chambart, H., Vandemeulebroeke, L. & Cappuyns, V. Incorporation of sulphidic mining waste material in ceramic roof tiles and blocks. *J Geochem Explor* **225**, (2021).

74. Lin, D. F., Chang, W. C., Yuan, C. & Luo, H. L. Production and characterization of glazed tiles containing incinerated sewage sludge. *Waste Management* **28**, 502–508 (2008).

75. Lin, D.-F., Luo, H.-L., Luo, H.-L. & Sheen, Y.-N. Glazed Tiles Manufactured from Incinerated Sewage Sludge Ash and Clay. *J Air Waste Manage Assoc* **55**, 163–172 (2005).

76. Anderson, M. Encouraging prospects for recycling incinerated sewage sludge ash (ISSA) into clay-based building products. *Journal of Chemical Technology & Biotechnology* **77**, 352–360 (2002).

77. Lu, J.-X. *et al.* Sustainable reuse of waste glass and incinerated sewage sludge ash in insulating building products: Functional and durability assessment. *J Clean Prod* **236**, 117635 (2019).

78. Ortelli , G. and Vincenzini, P. The use of waste glaze from floor and ceramic wall tile factories to prevent efflorescencet salt in heavy clay products. *CERAMURGIA Ceramurgia*, **13.6**, 241 (1983).

79. Sokolar, R. & Smetanova, L. Dry pressed ceramic tiles based on fly ash–clay body: Influence of fly ash granulometry and pentasodium triphosphate addition. *Ceram Int* **36**, 215–221 (2010).

80. Shakir, A. A., Naganathan, S. & Mustapha, K. N. Properties of bricks made using fly ash, quarry dust and billet scale. *Constr Build Mater* **41**, 131–138 (2013).

81. Worrall, W. E. *Clays and Ceramic Raw Materials*. vol. 49 (1986).

82. Christie, T., Thompson, B. & Brathwaite, B. Mineral Commodity Report 20 - Clays. *New Zealand Mining* **27**, 26–43 (2000).

83. Aras, A. The change of phase composition in kaolinite- and illite-rich clay-based ceramic bodies. *Appl Clay Sci* **24**, 257–269 (2004).

84. Dunham, A. C. Developments in industrial mineralogy: I. The mineralogy of brick-making. *Proceedings of the Yorkshire Geological Society* **49**, 95–104 (1992).

85. Shaw, D. B. & Weaver, C. E. The mineralogical composition of shales. *Journal of Sedimentary Research* **35**, 213–222 (1965).

86. Wedepohl, B. K. H. Environmental influences on the chemical composition of shales and clays. *Physics and Chemistry of the Earth*.

87. Odin, G. P., Belhadj, O., Cabaret, T., Foy, E. & Rouchon, V. Alterations of fossil-bearing shale (Autun, France; Permian), part III: Framboidal pyrite and sulfur as the main cause of efflorescence. *Annales de Paleontologie* **102**, 31–40 (2016).

88. Serra, M. F. *et al.* Thermal evolution of the mechanical properties of calcareous earthenware. *Ceram Int* **40**, 1709–1716 (2014).

89. Grimshaw, R. W., & Searle, A. B. (1971). The chemistry and physics of clays and allied ceramic materials, 4th edn,Ernest Benn limited,Ds 666.3Grim.

90. Morgan, D. J., Fanning, D. S. & Kodama, H. Definition of clay and clay mineral: Joint Report of the AIPEA and CMS Nomenclature Committees. *Clay Miner* 257–259 (1995).

91. Dollimore, D. The techniques and theory of thermal analysis applied to studies on inorganic materials with particular reference to dehydration and single oxide systems. *Selected Annual Reviews of the Analytical Sciences* **2**, 1–81 (1972).

92. Morgan, D. J. Thermal analysis - including evolved gas analysis - of clay raw materials. *Appl Clay Sci* **8**, 81–89 (1993).

93. Grim, R. E., & Bradley, W. F. Investigation of the effect of heat on the clay minerals illite and Montmorillonite. *Clay Miner* **23**, 242–248 (1939).

94. Flank, W. H. Behavior of Kaolinite Pellets At Elevated Temperatures. *Clays Clay Miner* **27**, 11–18 (1979).

95. Peters, T. Mineralogical changes during firing of calcium-rich brick clays. (1978).

96. McConville, C. J. & Lee, W. E. Microstructural development on firing illite and smectite clays compared with that in kaolinite. *Journal of the American Ceramic Society* **88**, 2267–2276 (2005).

97. Araújo, J. H. de, Silva, N. F. da, Acchar, W. & Gomes, U. U. Thermal decomposition of illite. *Materials Research* **7**, 359–361 (2004).

98. Murray, H. H. Traditional and new applications for kaolin, smectite, and palygorskite: A general overview. *Appl Clay Sci* **17**, 207–221 (2000).

99. Schomburg, J. Thermal reactions of clay minerals: their significance as ‘archaeological thermometers’ in ancient potteries. *Appl Clay Sci* **6**, 215–220 (1991).

100. Duminuco, P., Messiga, B. & Riccardi, M. P. Firing process of natural clays. Some microtextures and related phase compositions. *Thermochim Acta* **321**, 185–190 (1998).

101. Haldar, S. K. & Tišljar, J. *Basic Mineralogy*. *Introduction to Mineralogy and Petrology* (2014). doi:10.1016/b978-0-12-408133-8.00002-x.

102. Brigatti, M. F., Galán, E. & Theng, B. K. G. *Structure and Mineralogy of Clay Minerals*. *Developments in Clay Science* vol. 5 (2013).

103. M.S. Prasad a, K. J. R. H. H. M. Kaolin: Processing, Properties and Applications. *Appl Clay Sci* **6**, 1–264 (2018).

104. Yoder, H. S. & Eugster, H. P. Synthetic and natural muscovites. *Geochim Cosmochim Acta* **8**, (1955).

105. Falcone, R., Hreglich, S., Vallotto, M. & Verita, M. X-ray fluorescence analysis of raw materials for the glass and ceramic industries. *Glass Technology* **43**, 39–48 (2002).

106. Bell, A. M. T. *et al.* X-ray fluorescence analysis of feldspars and silicate glass: Effects of melting time on fused bead consistency and volatilisation. *Minerals* **10**, (2020).

107. Aboudi Mana, S. C., Hanafiah, M. M. & Chowdhury, A. J. K. Environmental characteristics of clay and clay-based minerals. *Geology, Ecology, and Landscapes* **1**, 155–161 (2017).

108. Odom, I. E. Smectite clay minerals: properties and uses. *Philos Trans R Soc Lond* 391–409 (1984) doi:10.1098/rsta.1984.0036.

109. Winchell, A. N. Studies in the mica group (abstract)1. *American Mineralogist* **10**, 52–54 (1925).

110. Sayers, C. M. & den Boer, L. D. The elastic anisotropy of clay minerals. *Geophysics* **81**, C193–C203 (2016).

111. Guven & N. Molecular aspects of clay-water interactions. *Clay-Water Interface and its Rheological Implications* 2–79 (1992).

112. *BS EN 771-1, BSI Standards Publ. Specification for Masonry Units Part 1 : Clay Masonry Units.* (2011).

113. British Ecological Society. An Introduction To Policy in the UK. *British Ecological Society* 1–4 (2017).

114. Malinauskaite, J. *et al.* Energy efficiency in industry: EU and national policies in Italy and the UK. *Energy* **172**, 255–269 (2019).

115. European Parliament. Revised energy efficiency directive. DG Energy Portal; 2017.

116. Council, F. E. *et al.* Energy and Climate Change Committee Consumption - Based Emissions Reporting.

117. Vogl. Ceramic roadmap 2050 - Whitewares' contribution. **90**, E34–E38 (2013).

118. Advani, A. *et al.* Energy use policies and carbon pricing in the UK IFS Report R84 Energy use policies and carbon pricing in the UK. (2013).

119. Leach, G. Policies to reduce energy use and carbon emissions in the UK. *Energy Policy* **19**, 918–925 (1991).

120. Baraldi, L. World production and consumption of ceramic tiles. *Ceramic world review* **113**, 48–61 (2015).

121. Ros-Dosdá, T., Celades, I., Monfort, E. & Fullana-i-Palmer, P. Environmental profile of Spanish porcelain stoneware tiles. *International Journal of Life Cycle Assessment* **23**, 1562–1580 (2018).

122. Ros-Dosdá, T., Fullana-i-Palmer, P., Mezquita, A., Masoni, P. & Monfort, E. How can the European ceramic tile industry meet the EU's low-carbon targets? A life cycle perspective. *J Clean Prod* **199**, 554–564 (2018).

123. Agrafiotis, C. & Tsoutsos, T. Energy saving technologies in the European ceramic sector: A systematic review. *Appl Therm Eng* **21**, 1231–1249 (2001).

124. Kurmus, H. & Mohajerani, A. Energy savings, thermal conductivity, micro and macro structural analysis of fired clay bricks incorporating cigarette butts. *Constr Build Mater* **283**, 122755 (2021).

125. Muñoz, P., Letelier, V., Bustamante, M. A., Marcos-Ortega, J. & Sepúlveda, J. G. Assessment of mechanical, thermal, mineral and physical properties of fired clay brick made by mixing kaolinitic red clay and paper pulp residues. *Appl Clay Sci* **198**, 105847 (2020).

126. WSP Parson Brinkerhoff; and DNV GL. Industrial Decarbonisation & Energy Efficiency Roadmaps to 2050: Cross Sector Summary. *London, UK: WSP Parsons Brinckerhoff* 31 (2015).

127. Cultrone, G. & Sebastián, E. Fly ash addition in clayey materials to improve the quality of solid bricks. *Constr Build Mater* **23**, 1178–1184 (2009).

128. Elias, M. L. & Cultrone, G. On the use of sodium chloride and calcined diatomite sludge as additives to improve the engineering properties of bricks made with a clay earth from Jun (Granada, Spain). *Minerals* **9**, (2019).

129. Aras, A. The differences between alkaline- and alkaline-earth-flux effects on high-temperature phase change of clay based ceramic. *Appl Clay Sci* **164**, 2–12 (2018).

130. Elimbi, A., Dika, J. M. & Djangang, C. N. Effects of Alkaline Additives on the Thermal Behavior and Properties of Cameroonian Poorly Fluxing Clay Ceramics. *Journal of Minerals and Materials Characterization and Engineering* **02**, 484–501 (2014).

131. Aras, A. & Demirhan, H. Firing behavior of alkaline earth flux in ceramic bodies: The effect of magnesite on firing mineralogy and physical properties. *Key Eng Mater* **264–268**, 1523–1526 (2004).

132. Houseman, J. E. & Koeing, C. J. Influence of Kiln Atmospheres in Firing Structural Clay Products: I, Maturation and Technological Properties. *Journal of the American Ceramic Society* **54**, 75–82 (1971).

133. Jackson, F. G. Oxidation of ceramic wares during firing.II. The decomposition various compounds of iron with Sulphur under simulated kiln conditions. *Journal of the American Ceramic Society* **1**, 141–143 (1918).

134. Stępkowska, E. T. & Jefferis, S. A. Influence of microstructure on firing colour of clays. *Appl Clay Sci* **6**, 319–342 (1992).

135. Kreimeyer, R. Some notes on the firing colour of clay bricks. *Appl Clay Sci* **2**, 175–183 (1987).

136. John F.Clifford. High Temperature Reactions And Colour Development In Brick Clays. *Department of Metallurgy and Materials Technology, University of Surrey - ProQuest Number: 10798335* (1984).

137. Ferrer, S., Mezquita, A., Gomez-Tena, M. P., Machi, C. & Monfort, E. Estimation of the heat of reaction in traditional ceramic compositions. *Appl Clay Sci* **108**, 28–39 (2015).

138. Pontikes, Y. & Angelopoulos, G. N. Effect of firing atmosphere and soaking time on heavy clay ceramics with addition of Bayer's process bauxite residue. *Advances in Applied Ceramics* **108**, 50–56 (2009).

139. Hauck, D., Krutzner-Brezynski, B. & Ruppik, M. Different firing chamber atmospheres for improvement of product properties. *ZI International* **48**, 851–859 (1995).

140. Denissen, J. Continuously reducing tunnel Kiln. *Klei/Glas/Keram.* **15**, 256–260 (1994).

141. Murad, E., & Wagner, U. The Mössbauer spectrum of illite. *Clay Miner* **1**, 1–10 (1994).

142. Murad, E. Mössbauer Spectroscopy. *Dev Clay Sci* **5**, 11–24 (2013).

143. Murad, E. Clays and clay minerals: What can Mössbauer spectroscopy do to help understand them? *Hyperfine Interact* **117**, 39–70 (1998).

144. He, C. Application of Mössbauer spectroscopy to fired clay products. *Silicates industriels* **61**, 247–250 (1994).

145. Fayçal El Fgaier , Zoubeir Lafhaj , Christophe Chapiseau, E. A. Effect of sorption capacity on thermo-mechanical properties of unfired clay bricks. *Journal of Building Engineering* **6**, 86–92 (2016).

146. Houseman, J. E. & Koenig, C. J. Influence of Kiln Atmospheres in Firing Structural Clay Products: II, Color Development and Burnout. *Journal of the American Ceramic Society* **54**, 82–89 (1971).

147. Beddiar, L., Sahnoune, F., Heraiz, M. & Redaoui, D. Thermal transformation of fired clay ceramics by dilatometric analysis. in *Acta Physica Polonica A* vol. 134 86–89 (Polish Academy of Sciences, 2018).

148. Dondi, M., Marsigli, M. & Venturi, I. Microstructure and mechanical properties of clay bricks: comparison between fast firing and traditional firing. *British Ceramic Transactions* **98**, 12–18 (1999).

149. Abdul Kadir, A. & Mohajerani, A. Effect of heating rate on gas emissions and properties of fired clay bricks and fired clay bricks incorporated with cigarette butts. *Appl Clay Sci* **104**, 269–276 (2015).

150. Ukwatta, A. & Mohajerani, A. Characterisation of fired-clay bricks incorporating biosolids and the effect of heating rate on properties of bricks. *Constr Build Mater* **142**, 11–22 (2017).

151. Gredmaier, L., Banks, C. J. & Pearce, R. B. Calcium and sulphur distribution in fired clay brick in the presence of a black reduction core using micro X-ray fluorescence mapping. *Constr Build Mater* **25**, 4477–4486 (2011).

152. Sohrabi Baba Heidary, D., Lanagan, M. & Randall, C. A. Contrasting energy efficiency in various ceramic sintering processes. *J Eur Ceram Soc* **38**, 1018–1029 (2018).

153. Charsley, E L; Warrington, S. B. [. *Thermal analysis - techniques and applications*. (1992).

154. Brown, M. Ewart. *Introduction to thermal analysis: techniques and applications. Vol. 1. Springer Science & Business Media, 2001.*

155. Dondi, M., Guarini, G. & Raimondo, M. Trends in the formation of crystalline and amorphous phases during the firing of clay bricks. *Tile & brick international* **15**, 176–183 (1999).

156. Cultrone, G., Sebastián, E. & De La Torre, M. J. Mineralogical and physical behaviour of solid bricks with additives. *Constr Build Mater* **19**, 39–48 (2005).

157. Rasmussen, K. L., de La Fuente, G. A., Bond, A. D., Mathiesen, K. K. & Vera, S. D. Pottery firing temperatures: A new method for determining the firing temperature of ceramics and burnt clay. *J Archaeol Sci* **39**, 1705–1716 (2012).

158. Fontes Vieira, C. M. & Monteiro, S. N. Firing behavior of the clay fraction of a natural kaolinitic clay: Are they different? *Materials Research* **22**, 1–9 (2019).

159. Goel, G. & Kalamdhad, A. S. A practical proposal for utilisation of water hyacinth: Recycling in fired bricks. *J Clean Prod* **190**, 261–271 (2018).

160. Rekecki, R., Ranogajec, J., Oszkó, A. & Kuzmann, E. Effects of firing conditions on the properties of calcareous clay roofing tiles. *Journal of Materials in Civil Engineering* **26**, 175–183 (2014).

161. Lee, W. E., Souza, G. P., McConville, C. J., Tarvornpanich, T. & Iqbal, Y. Mullite formation in clays and clay-derived vitreous ceramics. *J Eur Ceram Soc* **28**, 465–471 (2008).

162. Schneider, H., Fischer, R. X. & Schreuer, J. Mullite: Crystal Structure and Related Properties. *Journal of the American Ceramic Society* **98**, 2948–2967 (2015).

163. Nigay, P. M., Cutard, T. & Nzihou, A. The impact of heat treatment on the microstructure of a clay ceramic and its thermal and mechanical properties. *Ceram Int* **43**, 1747–1754 (2017).

164. Franke, L. & Schumann, I. *A brief history of brickmaking in Northern Germany*. (Donhead Publishing Ltd. United Kingdom, 1998).

165. Viani, A., Cultrone, G., Sotiriadis, K., Ševčík, R. & Šašek, P. The use of mineralogical indicators for the assessment of firing temperature in fired-clay bodies. *Appl Clay Sci* **163**, 108–118 (2018).

166. Daghmehchi, M., Rathossi, C., Omrani, H., Emami, M. & Rahbar, M. Mineralogical and thermal analyses of the Hellenistic ceramics from Laodicea Temple, Iran. *Appl Clay Sci* **162**, 146–154 (2018).

167. Miras, A., Galán, E., González, I., Romero-Baena, A. & Martín, D. Mineralogical evolution of ceramic clays during heating. An ex/in situ X-ray diffraction method comparison study. *Appl Clay Sci* **161**, 176–183 (2018).

168. Tourneret, L., Berger, F., Mavon, C. & Chambaudet, A. Calcium sulphate formation during the heat-up period: Some essential parameters. *Appl Clay Sci* **14**, 299–317 (1999).

169. Molera, J., Pradell, T. & Vendrell-Saz, M. The colours of Ca-rich ceramic pastes: Origin and characterization. *Appl Clay Sci* **13**, 187–202 (1998).

170. Dyar, M. D. Review of Mössbauer data on trioctahedral micas: Evidence for tetrahedral Fe2+/Fe3+ plus and cation ordering. *American Mineralogist* **72**, 102–112 (1987).

171. C67-08, A. Standard Test Methods for Sampling and Testing Brick and Structural Clay Tile," ASTM Standards on Disc,. **Vol. 4.05,**.

172. Eliche-Quesada, D. & Leite-Costa, J. Use of bottom ash from olive pomace combustion in the production of eco-friendly fired clay bricks. *Waste Management* **48**, 323–333 (2016).

173. Wu, J., Zhang, F., Li, H., Fang, B. & Xu, X. Preparation and reaction mechanism of red mud based ceramic simple bricks. *Journal Wuhan University of Technology, Materials Science Edition* **25**, 1001–1005 (2010).

174. Phonphuak, N. & Thiansem, S. Effects of charcoal on physical and mechanical properties of fired test briquettes. *ScienceAsia* **37**, 120–124 (2011).

175. BS EN 772-7:1998. Methods of test for masonry units — Part 7: Determination of water absorption of clay masonry damp proof course units by boiling in water.

176. Cultrone, G. *et al.* Influence of mineralogy and firing temperature on the porosity of bricks. *J Eur Ceram Soc* **24**, 547–564 (2004).

177. Maage, M. Frost resistance and pore size distribution of bricks. *ZI, Ziegelindustrie International/Brick and Tile Industry International* **43**, 345–350 (1984).

178. Winslow, D. Predicting the durability of paving bricks. *J Test Eval* **19**, 29–33 (1991).

179. ASTM C67/C67M-21. Standard Test Methods for Sampling and Testing Brick and Structural Clay Tile; ASTM International: West Conshohocken, PA, USA, 2021.

180. Ducman, V., Škapin, A. S., Radeka, M. & Ranogajec, J. Frost resistance of clay roofing tiles: Case study. *Ceram Int* **37**, 85–91 (2011).

181. Brownell, W. Efflorecence resulting from sulphates in clay raw material. *Journal of the American Ceramic Society.* **41(8)**, 310–314 (1958).

182. Brownell, W. E. Fundamental factors influencing efflorescence of clay products. *Journal of the American Ceramic Society* **32**, 376–389 (1949).

183. Brownell, W. E. Retention of Sulfates by Fired Clay Products. *Journal of the American Ceramic Society* **3**, 75–81 (1960).

184. Brownell, W. E. Application of New Techniques to the Solution of an Efflorescence Problem. *Journal of the American Ceramic Society* **33**, 360–363 (1950).

185. Brownell, W. E. Crystalline Phases in Fired Shale Products. *Journal of the American Ceramic Society* **33**, 309–313 (1950).

186. Brownell, W. E. Efflorescence Resulting from Pyrite in Clay Raw Materials. *Journal of the American Ceramic Society* **41**, (1958).

187. Mike, T. M. & Brownell, W. E. Effect of Sulfur Dioxide Atmospheres on Efflorescence. *Journal of the American Ceramic Society* **39**, 253–256 (1956).

188. F.G.Jackson. A descriptive bibliography of scummming and efflorescence. *Journal of the American Ceramic Society* **8(8)**, 376–401 (1925).

189. Palmer, L. A. *Cause and Prevention of kiln and dry- house scum and of efflorence on face-brick walls. US Government Printing Office* vol. 370 (1928).

190. Merrigan, M. Efflorescence: cause and control. *MASONRY SOC. J. Masonry Soc. J.* 2–5 (1986).

191. Zhang, Z., Wang, H., Provis, J. L. & Reid, A. Efflorescence : A Critical Challenge for Geopolymer Applications ? *In Concrete Institute of Australia's Biennial National Conference* (2013).

192. Yao, X., Yang, T. & Zhang, Z. Fly ash-based geopolymers: Effect of slag addition on efflorescence. *Journal Wuhan University of Technology, Materials Science Edition* **31**, 689–694 (2016).

193. Husbands, T. B. Efflorescence Study, Fort Leonard Wood, Missouri. *U.S. Army Corps of Engineers Waterways Experiment Station 3909 Halls Ferry Road Vicksburg, MS 39180-6199 Miscellaneous Paper SL-94-1 April 1994 Accesion* (1994).

194. Young, J. E. Backup Materials as a Source of Efflorescence. *Journal of the American Ceramic Society* **40**, 240–243 (1957).

195. Brocken, H. & Nijland, T. G. White Efflorescence on Brick Masonry: Towards Prediction of Efflorescence Risk. *13th International Brick and Block Masonry Conference* 1–10 (2004).

196. Schorr, J. R. & Everhart, J. O. Thermal Behavior of Pyrite and Its Relation to Carbon and Sulfur Oxidation in Clays. *Journal of the American Ceramic Society* **52**, 351–354 (1969).

197. Wilson, H. Progress report on the efflorescence and scumming of mortar materials. *Journal of the American Ceramic Society* **11**, 1–31 (1928).

198. Kaufmann, W. Cause, Action, and Prevention of Efflorescence. *Ziegelwelt* **71**, 165–167 (1940).

199. Bauleke M.P and Dodd C.M. Effect of Ammonium Salts on an Illitic Shale. *Journal of the American Ceramic Society* **40**, 325–334 (1957).

200. Bennett, A. L. & Goodrich, H. R. the Reactivity Test for Determining the Value of Barium Carbonate As a Scum Preventative. *Journal of the American Ceramic Society* **13**, 461–469 (1930).

201. COOKSON GROUP, C. & P. DIV. Chemical Additives for Heavy Clay Products. PT. 5. Scum and Efflorescence (CONT). *Cookson Mon.Bull.Ceram.Ind.* 2–4 (1990).

202. Netinger, I., Vračević, M., Ranogajec, J. & Vučetić, S. Evaluation of brick resistance to freeze / thaw cycles according to indirect procedures. *Gradjevinar* **66**, 197–209 (2014).

203. Andrés, A., Díaz, M. C., Coz, A., Abellán, M. J. & Viguri, J. R. Physico-chemical characterisation of bricks all through the manufacture process in relation to efflorescence salts. *J Eur Ceram Soc* **29**, 1869–1877 (2009).

204. Ciliberto, E., Ioppolo, S. & Manuella, F. Ettringite and thaumasite: A chemical route for their removal from cementious artefacts. *J Cult Herit* **9**, 30–37 (2008).

205. Utton, C. A., Gallucci, E., Hill, J. & Milestone, N. B. Interaction between BaCO3 and OPC/BFS composite cements at 20 °c and 60 °c. *Cem Concr Res* **41**, 236–243 (2011).

206. Carmona-Quiroga, P. M., Blanco-Varela, M. T., Martínez-Ramírez, S. & Lothenbach, B. *Thermodynamic modeling of sulfate-resistant cements with addition of barium compounds*. (CRC Press, 2013).

207. Carmona-Quiroga, P. M. & Blanco-Varela, M. T. Ettringite decomposition in the presence of barium carbonate. *Cem Concr Res* **52**, 140–148 (2013).

208. Lynch, G. C. J. Bricks: Properties and Classifications. *Structural Survey* **12**, 15–20 (1994).

209. Gillott, J. E. Clay Mineralogy in Biuliding Research. in *Eleventh International Conference on Clays and Clay Minerals* 296–298 (1963).

210.https://www.bing.com/images/search?view=detailV2&ccid=%2FHhmmoRI&id=029F8560F08DCE4B39C8B7B05872A255 (22/03/2022).

211. Fluminense, N. & Ribeiro, D. Incorporation of solid wastes in red ceramics – an updated review. *Revista Materia* 881–905 (2009).

212. Rehman, M. U., Ahmad, M. & Rashid, K. Influence of fluxing oxides from waste on the production and physico-mechanical properties of fired clay brick: A review. *Journal of Building Engineering* **27**, 100965 (2020).

213. Raut, S. P., Ralegaonkar, R. v & Mandavgane, S. A. Development of sustainable construction material using industrial and agricultural solid waste: A review of waste-create bricks. *Constr Build Mater* **25**, 4037–4042 (2011).

214. Vieira, C. M. F. & Monteiro, S. N. Incorporation of solid wastes in red ceramics: an updated review. *Matéria (Rio de Janeiro)* **14**, 881–905 (2009).

215. Specification for processed glass for selected secondary end markets.

216. Díaz-García, Almudena ; Martínez-García, Carmen ; Cotes-Palomino, T. Properties of Residue from Olive Oil Extraction as a Raw Material for SustainaDíaz-García, Almudena ; Martínez-García, Carmen ; Cotes-Palomino, T. (2017). Properties of Residue from Olive Oil Extraction as a Raw Material for Sustainable Construction Mater. *Peer Reviewed Journal* **10(2)**, (2017).

217. Mangesh V . Madurwar, S. A. . M. and R. V. . R. Use of sugarcane bagasse ash as brick material. **107**, 1044–1051 (2014).

218. Teixeira, S. R. *et al.* Valorization of sugarcane bagasse ash: Producing glass-ceramic materials. *J Environ Manage* **134**, 15–19 (2014).

219. Souza, A. E., Teixeira, S. R., Santos, G. T. A., Costa, F. B. & Longo, E. Reuse of sugarcane bagasse ash (SCBA) to produce ceramic materials. *J Environ Manage* **92**, 2774–2780 (2011).

220. Teixeira, S. R., Souza, A. E. de, de Almeida Santos, G. T., Peña, A. F. V. & Miguel, Á. G. Sugarcane Bagasse Ash as a Potential Quartz Replacement in Red Ceramic. *Journal of the American Ceramic Society* **91**, 1883–1887 (2008).

221. Mohajerani, A., Kadir, A. A. & Larobina, L. A practical proposal for solving the world's cigarette butt problem: Recycling in fired clay bricks. *Waste Management* **52**, 228–244 (2016).

222. Kurmus, H. & Mohajerani, A. Recycling of cigarette butts in fired clay bricks: A new laboratory investigation. *Materials* **13**, (2020).

223. Beal, B. *et al.* A Comparison of Thermal and Mechanical Properties of Clay Bricks Prepared with Three Different Pore-Forming Additives: Vermiculite, Wood Ash, and Sawdust. *Environ Prog Sustain Energy* **38**, (2019).

224. Liaw, C.-T., Chang, H.-L., Hsu, W.-C. & Huang, C.-R. A novel method to reuse paper sludge and co-generation ashes from paper mill. *J Hazard Mater* **58**, 93–102 (1998).

225. Council, D. county. Derbyshire and Derby Towards a Minerals Local Plan : Background Paper Brick Clay and Fireclay. *Background Paper Industrial Limestone* 1–28 (2018).

226. Asquini, L., Furlani, E., Bruckner, S. & Maschio, S. Production and characterization of sintered ceramics from paper mill sludge and glass cullet. *Chemosphere* **71**, 83–89 (2008).

227. Sutcu, M. & Akkurt, S. The use of recycled paper processing residues in making porous brick with reduced thermal conductivity. *Ceram Int* **35**, 2625–2631 (2009).

228. Njeumen Nkayem, D. E., Mbey, J. A., Kenne Diffo, B. B. & Njopwouo, D. Preliminary study on the use of corn cob as pore forming agent in lightweight clay bricks: Physical and mechanical features. *Journal of Building Engineering* **5**, 254–259 (2016).

229. Quaranta, N. *et al.* Addition of polymeric wastes as pore formers in ceramic lightweight bricks. *WIT Transactions on Ecology and the Environment* **128**, 447–458 (2010).

230. Aouba, L., Bories, C., Coutand, M., Perrin, B. & Lemercier, H. Properties of fired clay bricks with incorporated biomasses: Cases of Olive Stone Flour and Wheat Straw residues. *Constr Build Mater* **102**, 7–13 (2016).

231. Sutcu, M., Ozturk, S., Yalamac, E. & Gencel, O. Effect of olive mill waste addition on the properties of porous fired clay bricks using Taguchi method. *J Environ Manage* **181**, 185–192 (2016).

232. Borlini, M. C., Mendonça, J. L. C. da C., Vieira, C. M. F. & Monteiro, S. N. Influence of the sintering temperature in the physical, mechanical and microstructural properties of red ceramic incorporated with sugar cane bagasse ash. *Matéria (Rio de Janeiro)* **11**, 433–441 (2006).

233. Oliveira de paula, M., Ferreira tinoco, I. & Osorio Saraz, J. A. Sugarcane bagasse ash as a partial-port-land-cement-replacement material | Ceniza de bagazo de caña de azúcar como material de sustitución parcial del cemento portland. *DYNA (Colombia)* **77**, 47–54 (2011).

234. Kazmi, S. M. S., Abbas, S., Munir, M. J. & Khitab, A. Exploratory study on the effect of waste rice husk and sugarcane bagasse ashes in burnt clay bricks. *Journal of Building Engineering* **7**, 372–378 (2016).

235. Ukwatta, A. & Mohajerani, A. Characterisation of fired-clay bricks incorporating biosolids and the effect of heating rate on properties of bricks. *Constr Build Mater* **142**, 11–22 (2017).

236. Phonphuak, N. & Chindaprasirt, P. Types of waste, properties, and durability of pore-forming waste-based fired masonry bricks. Eco-efficient Masonry Bricks and Blocks: Design, Properties and Durability (Elsevier Ltd, 2015). doi:10.1016/B978-1-78242-305-8.00006-1.

237. Almeida, J. & Carvalho, J. A. L. Incorporation of petroleum waxes in clay bricks. *Industrie Ceramique* **11**, (1991).

238. Veiseh, S. & Yousefi, A. A. The use of polystyrene in lightweight brick production. *Iranian Polymer Journal (English Edition)* **12**, 323–329 (2003).

239. Al-shathr, B. S. Production of Lightweight Clay Bricks Using Polymer Wastes. *Engineering and Technology Journal* **36**, (2018).

240. Liu, P., Farzana, R., Rajarao, R. & Sahajwalla, V. Lightweight expanded aggregates from the mixture of waste automotive plastics and clay. *Constr Build Mater* **145**, 283–291 (2017).

241. Lingling, X., Wei, G., Tao, W. & Nanru, Y. Study on fired bricks with replacing clay by fly ash in high volume ratio. *Constr Build Mater* **19**, 243–247 (2005).

242. Yalçin, N. & Sevinç, V. Utilization of bauxite waste in ceramic glazes. *Ceram Int* **26**, 485–493 (2000).

243. Pérez-Villarejo, L., Corpas-Iglesias, F. A., Martínez-Martínez, S., Artiaga, R. & Pascual-Cosp, J. Manufacturing new ceramic materials from clay and red mud derived from the aluminium industry. *Constr Build Mater* **35**, 656–665 (2012).

244. Quijorna, N., Coz, A., Andres, A. & Cheeseman, C. Recycling of Waelz slag and waste foundry sand in red clay bricks. *Resour Conserv Recycl* **65**, 1–10 (2012).

245. Alonso-Santurde, R., Coz, A., Viguri, J. R. & Andrés, A. Recycling of foundry by-products in the ceramic industry: Green and core sand in clay bricks. *Constr Build Mater* **27**, 97–106 (2012).

246. Tittarelli, F. Waste foundry sand. Waste and Supplementary Cementitious Materials in Concrete: Characterisation, Properties and Applications (Elsevier Ltd, 2018). doi:10.1016/B978-0-08-102156-9.00004-3.

247. Quaranta, N. *et al.* Recycling of foundry sand residuals as aggregates in ceramic formulations for construction materials. *WIT Transactions on Ecology and the Environment* **122**, 503–512 (2009).

248. Hossiney, N., Das, P., Mohan, M. K. & George, J. In-plant production of bricks containing waste foundry sand—A study with Belgaum foundry industry. *Case Studies in Construction Materials* **9**, e00170 (2018).

249. Lin, D. F., Luo, H. L., Lin, J. D. & Zhuang, M. L. Characterizations of temperature effects on sintered ceramics manufactured with waste foundry sand and clay. *J Mater Cycles Waste Manag* **20**, 127–136 (2018).

250. Li, C. *et al.* Heavy metals leaching in bricks made from lead and zinc mine tailings with varied chemical components. *Construction and Building Materials* vol. 134 443–451 Preprint at https://doi.org/10.1016/j.conbuildmat.2016.12.076 (2017).

251. Suárez-Macías, J., Terrones-Saeta, J. M., Iglesias-Godino, F. J. & Corpas-Iglesias, F. A. Retention of contaminants elements from tailings from lead mine washing plants in ceramics for bricks. *Minerals* **10**, 1–21 (2020).

252. Alfonso, P. *et al.* Potential of tungsten tailings as glass raw materials. *Mater Lett* **228**, 456–458 (2018).

253. Liu, W., Wu, T., Li, Z., Hao, X. & Lu, A. Preparation and characterization of ceramic substrate from tungsten mine tailings. *Constr Build Mater* **77**, 139–144 (2015).

254. Pacheco-Torgal, F., Castro-Gomes, J. & Jalali, S. Tungsten mine waste geopolymeric binder: Preliminary hydration products investigations. *Constr Build Mater* **23**, 200–209 (2009).

255. Choi, Y. W., Kim, Y. J., Choi, O., Lee, K. M. & Lachemi, M. Utilization of tailings from tungsten mine waste as a substitution material for cement. *Constr Build Mater* **23**, 2481–2486 (2009).

256. Vieira, C. M. F. & Monteiro, S. N. Effect of grog addition on the properties and microstructure of a red ceramic body for brick production. *Construction and Building Materials* vol. 21 1754–1759 Preprint at https://doi.org/10.1016/j.conbuildmat.2006.05.013 (2007).

257. Mao, L., Guo, H. & Zhang, W. Addition of waste glass for improving the immobilization of heavy metals during the use of electroplating sludge in the production of clay bricks. *Constr Build Mater* **163**, 875–879 (2018).

258. Galán-Arboledas, R. J., Merino, A. & Bueno, S. Use of new raw materials and industrial wastes to improve the possibilities of using ceramic materials from Bailén (Jaén, southern Spain). *Materiales de Construccion* **63**, 553–568 (2013).

259. Lin, K. L., Lee, T. C. & Hwang, C. L. Effects of sintering temperature on the characteristics of solar panel waste glass in the production of ceramic tiles. *J Mater Cycles Waste Manag* **17**, 194–200 (2014).

260. Hwang, J.-Y., Huang, X., Garkida, A. & Hein, A. Waste Colored Glasses as Sintering Aid in Ceramic Tiles Production. *Journal of Minerals and Materials Characterization and Engineering* **05**, 119–129 (2006).

261. Matteucci, F., Dondi, M. & Guarini, G. Effect of soda-lime glass on sintering and technological properties of porcelain stoneware tiles. *Ceram Int* **28**, 873–880 (2002).

262. Kim, K., Kim, K. & Hwang, J. Characterization of ceramic tiles containing LCD waste glass. *Ceram Int* **42**, 7626–7631 (2016).

263. Silva, R. v, de Brito, J., Lye, C. Q. & Dhir, R. K. The role of glass waste in the production of ceramic-based products and other applications: A review. *J Clean Prod* **167**, 346–364 (2017).

264. Smith, A. To demonstrate commercial viability of incorporating ground glass in bricks with reduced emissions and energy savings To demonstrate commercial viability of incorporating ground glass in bricks with reduced emissions and energy savings . 0–35 (2004).

265. Ibrahim, D.M., Mostafa, A.A., Nour, W. M. N. Granite processing waste as a source of flux for the production of acid resistant sewage bricks. *Interceram.* **55**, 186–190 (2006).

266. Vieira, C. M. F., Soares, T. M., Sánchez, R. & Monteiro, S. N. Incorporation of granite waste in red ceramics. *Materials Science and Engineering: A* **373**, 115–121 (2004).

267. de' Gennaro, R. *et al.* Influence of zeolites on the sintering and technological properties of porcelain stoneware tiles. *J Eur Ceram Soc* **23**, 2237–2245 (2003).

268. Luz, A. P. & Ribeiro, S. Use of glass waste as a raw material in porcelain stoneware tile mixtures. *Ceram Int* **33**, 761–765 (2007).

269. Fatt, W. J., Xin, C. J., Hassan, A. bin, Mohamad, Z. binti & Othman, N. binti. Thermal and flammability properties of wollastonite-filled thermoplastic composites: a review. *J Mater Sci* (2020) doi:10.1007/s10853-020-05255-5.

270. Zakaria, M. Y., Sulong, A. B., Muhamad, N., Raza, M. R. & Ramli, M. I. Incorporation of wollastonite bioactive ceramic with titanium for medical applications: An overview. *Materials Science and Engineering C* **97**, 884–895 (2019).

271. Aly, I. H. M., Abed Alrahim Mohammed, L., Al-Meer, S., Elsaid, K. & Barakat, N. A. M. Preparation and characterization of wollastonite/titanium oxide nanofiber bioceramic composite as a future implant material. *Ceram Int* **42**, 11525–11534 (2016).

272. Li, H. & Chang, J. Fabrication and characterization of bioactive wollastonite/PHBV composite scaffolds. *Biomaterials* **25**, 5473–5480 (2004).

273. Sahin, T. Mechanical and thermal properties of colemanite filled polypropylene. *KGK Kautschuk Gummi Kunststoffe* **64**, 16–21 (2011).

274. Yadollahi, A., Nazemi, E., Zolfaghari, A. & Ajorloo, A. M. Optimization of thermal neutron shield concrete mixture using artificial neural network. *Nuclear Engineering and Design* **305**, 146–155 (2016).

275. Rusen, A. Investigation of structural behavior of colemanite depending on temperature. *Revista Romana de Materiale/ Romanian Journal of Materials* **48**, 245–250 (2018).

276. Wacławska, I. Thermal reactions of solid-state amorphized borates and borate glasses :A comparative study. *Journal of Thermal Analysis* **49**, 1337–1345 (1997).

277. Uysal, T., Mutlu, H. S. & Erdemoğlu, M. Effects of mechanical activation of colemanite (Ca2B6O11·5H2O) on its thermal transformations. *Int J Miner Process* **151**, 51–58 (2016).

278. Ediz, N. & Yurdakul, A. Characterization of porcelain tile bodies with colemanite waste added as a new sintering agent. *Journal of Ceramic Processing Research* **10**, 414–422 (2009).

279. Akpinar, S., Evcin, A. & Ozdemir, Y. Effect of calcined colemanite additions on properties of hard porcelain body. *Ceram Int* **43**, 8364–8371 (2017).

280. Karasu, B. Use of Borax Solid Wastes in Ceramics' World. *Proceedings of the 10th International Conference of the European Ceramic Society. Baden-Baden: Göller* 1773–1778 (2008).

281. Uslu, T. & Arol, A. I. Use of boron waste as an additive in red bricks. *Waste Management* **24**, 217–220 (2004).

282. Kurama, S., Kara, A. & Kurama, H. The effect of boron waste in phase and microstructural development of a terracotta body during firing. *J Eur Ceram Soc* **26**, 755–760 (2006).

283. Kavas, T. Use of boron waste as a fluxing agent in production of red mud brick. *Build Environ* **41**, 1779–1783 (2006).

284. Christogerou, A. *et al.* Use of boron wastes in the production of heavy clay ceramics. *Ceram Int* **35**, 447–452 (2009).

285. Şen, N., Demir, C., Demirbas, A. & Kar, Y. Obtaining of boron as an alternative fuel from borax with various methods. *Energy Sources, Part A: Recovery, Utilization and Environmental Effects* **31**, 509–515 (2009).

286. Bodian, S. *et al.* Thermo-mechanical behavior of unfired bricks and fired bricks made from a mixture of clay soil and laterite. *Journal of Building Engineering* **18**, 172–179 (2018).

287. Kangal, M. O., Bulut, G., Yeşilyurt, Z., Baştürkcü, H. & Burat, F. Characterization and production of Turkish nepheline syenites for industrial applications. *Physicochemical Problems of Mineral Processing* **55**, 605–616 (2019).

288. Negm Abdel Tawab, Abouzeid Abdel Zaher, Boulos Tawfik, A. H. Nepheline syenite processing for glass and ceramics industries. *physiochemical Problems of Mineral processing* **34**, 5–16 (2000).

289. Lewicka, E. Conditions of the feldspathic raw materials supply from domestic and foreign sources in Poland. *Gospodarka Surowcami Mineralnymi / Mineral Resources Management* **26**, 5–19 (2010).

290. Burat, F., Kangal, O. & Onal, G. An alternative mineral in the glass and ceramic industry: Nepheline syenite. *Miner Eng* **19**, 370–371 (2006).

291. Harben, P. W. *The industrial minerals handybook: a guide to markets, specifications, & prices*. (Metal Bulletin, 1999).

292. Esposito, L., Salem, A., Tucci, A., Gualtieri, A. & Jazayeri, S. H. The use of nepheline-syenite in a body mix for porcelain stoneware tiles. *Ceram Int* **31**, 233–240 (2005).

293. Salem, A., Jazayeri, S. H., Rastelli, E. & Timellini, G. Dilatometeric study of shrinkage during sintering process for porcelain stoneware body in presence of nepheline syenite. *J Mater Process Technol* **209**, 1240–1246 (2009).

294. John Everhart and John Lawson Felder. Process for fast-fire ceramic tile using nepheline syente and clay. (1972).

295. Pranckevičiene, J., Balkevičius, V. & Špokauskas, A. A. Investigations on properties of sintered ceramics out of low-melting illite clay and additive of fine-dispersed nepheline syenite. *Medziagotyra* **16**, 231–235 (2010).

296. Salem, S. & Salem, A. Effects of technical factors on dimensional stability of porcelain stoneware body during sintering process: Isothermal kinetic study, Part II. *Thermochim Acta* **598**, 82–90 (2014).

297. Hamzawy, E. M. A. & Khater, G. A. Crystallisation of processed nepheline syenite-magnesite glasses. *Advances in Applied Ceramics* **104**, 277–281 (2005).

298. Bauluz, B., Mayayo, M. J., Fernández-Nieto, C., Cultrone, G. & Gonzalez Lopez, J. M. Assessment of technological properties of calcareous and non-calcareous clays used for the brick-making industry of Zaragoza (Spain). *Appl Clay Sci* **24**, 121–126 (2003).

299. Tavangarian, F., Zolko, C. A., Sadeghzade, S., Fayed, M. & Davami, K. Fabrication, mechanical properties and in-vitro behavior of Akermanite bioceramic. *Materials* **13**, 1–13 (2020).

300. Poirier, M. *et al.* Mineralogical and crystal-chemical characterization of the talc ore deposit of Minzanzala, Gabon. *Clay Miner* **54**, 245–254 (2019).

301. Chauhan, V. S. & Bhardwaj, N. K. Efficacy of dispersion of magnesium silicate (talc) in papermaking. *Arabian Journal of Chemistry* **10**, S1059–S1066 (2017).

302. Zazenski, R. *et al.* Talc: Occurrence, characterization, and consumer applications. *Regulatory Toxicology and Pharmacology* vol. 21 218–229 Preprint at https://doi.org/10.1006/rtph.1995.1032 (1995).

303. Tothill, I. E., Best, D. J. & Seal, K. J. Studies on the inhibitory effect of paint raw materials on cellulolytic enzymes present in waterborne paint. *Int Biodeterior Biodegradation* **32**, 233–242 (1993).

304. Kocic Nikola, Kretschmer, Bastian Martin, H. P. The influence of Talc Nucleation Agent on the Nonisothermal Crystallization and Morphology of Isotactic Polypropylene: the Application of the Lauritzen-Hoffmann, Avrami , and Ozawa Therories. *J Appl Polym Sci* **126**, 1207–1217 (2012).

305. Mallet serge, Delord Patrick, Juin Herve', L. M. Effect of feed talc supplement on broiler performance. **54**, 485–492 (2005).

306. Trindade, M. J., Dias, M. I., Coroado, J. & Rocha, F. Mineralogical transformations of calcareous rich clays with firing: A comparative study between calcite and dolomite rich clays from Algarve, Portugal. *Appl Clay Sci* **42**, 345–355 (2009).

307. Kaftelen Odabaşı, H., Anıl, Ü. E., Odabaşı, A. & Kocabıyık, B. K. Effect of Barium Carbonate Addition on the Properties of Porcelain Ceramic Tile. *Nevşehir Bilim ve Teknoloji Dergisi* **7**, 41–48 (2018).

308. Santiago Manuel Rivera. *Brick and Mortar Research*. (2012).

309. Zhang, Z. Energy efficiency and environmental pollution of brickmaking in China. *Energy* **22**, 33–42 (1997).

310. Kajaste, R. & Hurme, M. Cement industry greenhouse gas emissions - Management options and abatement cost. *J Clean Prod* **112**, 4041–4052 (2016).

311. Oti, J. E. & Kinuthia, J. M. Stabilised unfired clay bricks for environmental and sustainable use. *Appl Clay Sci* **58**, 52–59 (2012).

312. Galán-Arboledas, R. J., Álvarez de Diego, J., Dondi, M. & Bueno, S. Energy, environmental and technical assessment for the incorporation of EAF stainless steel slag in ceramic building materials. *J Clean Prod* **142**, 1778–1788 (2017).

313. Biggs, A. *Full scale operational trials involving the use of recycled glass in the heavy clay industry (bricks and tiles). Business* (2005).

314. Rambaldi, E. Pathway towards a high recycling content in traditional ceramics. *Ceramics* **4**, 486–501 (2021).

315. Munir, M. J., Kazmi, S. M. S., Wu, Y. F., Hanif, A. & Khan, M. U. A. Thermally efficient fired clay bricks incorporating waste marble sludge: An industrial-scale study. *J Clean Prod* **174**, 1122–1135 (2018).

316. Sales Barreto, G. N., Babisk, M. P., Girondi Delaqua, G. C., Borlini Gadioli, M. C. & Fontes Vieira, C. M. Evaluation of the effect of the incorporation of blends of fuel and fluxing wastes in red clay ceramics. *Materials Research* **22**, 1–8 (2019).

317. Demir, I., Baspinar, M. S. & Orhan, M. Utilization of kraft pulp production residues in clay brick production. *Build Environ* **40**, 1533–1537 (2005).

318. Lawanwadeekul, S., Otsuru, T., Tomiku, R. & Nishiguchi, H. Thermal-acoustic clay brick production with added charcoal for use in Thailand. *Constr Build Mater* **255**, 119376 (2020).

319. Herrmann, H. & Bucksch, H. Brick Clay. *Dictionary Geotechnical Engineering/Wörterbuch GeoTechnik* 164–164 (2014) doi:10.1007/978-3-642-41714-6_23236.

320. Bessey, G. E. & LEA, F. M. The Distribution of Sulphates in Clay Soils and Groundwater. *Proceedings of the Institution of Civil Engineers* **2**, 159–181 (1953).

321. EN, BS. '771-1: 2011 Specification for masonry units—Clay masonry units.' (2011): 771-2.

322. West, A. R. *Solid state chemistry and its applications.* (John Wiley & Sons., 2014).

323. Brouwer, P. *Theory of XRF*. *Almelo: PANalytical BV* (2010).

324. Giles H.L, Hurley P.W, W. H. W. Simple Approach to the Analysis of Oxides, Silicates and Carbonates Using X-ray Fluoresence Spectrometry. *X-Ray Fluorescence Spectrometry (XRF) in Geoarchaeology* **24**, 205–218 (1995).

325. Martin, A. & Bell, T. Structural Studies using Synchrotron X-Ray Powder Diffraction and Other Techniques . By For the degree of Doctor of Philosophy in the University of Cambridge. (1998).

326. Shackley, M. S. *X-Ray Fluorescence Spectrometry (XRF) in Geoarchaeology*. *X-Ray Fluorescence Spectrometry (XRF) in Geoarchaeology* (2011). doi:10.1007/978-1-4419-6886-9.

327. International Centre for Diffraction Pattern https://www.icdd.com/.

328. Mccusker, L. B., von Dreele, R. B., Cox, D. E., Louër, D. & Scardi, P. Rietveld refinement guidelines. *J Appl Crystallogr* **32**, 36–50 (1999).

329. Plante, A. F., Fernández, J. M. & Leifeld, J. Application of thermal analysis techniques in soil science. *Geoderma* **153**, 1–10 (2009).

330. Meyer, K. & Klobes, P. Comparison between different presentations of pore size distribution in porous materials. *Fresenius J Anal Chem* **363**, 174–178 (1999).

331. Aligizaki, K. K. *Pore structure of cement-based materials: testing, interpretation and requirements*. (Crc Press, 2005).

332. Arvanitidis, I., Sichen, D. & Seetharaman, S. A study of the thermal decomposition of BaCO3. *Metallurgical and Materials Transactions B: Process Metallurgy and Materials Processing Science* **27**, 409–416 (1996).

333. Jankula, M., Šín, P., Podoba, R. & Ondruška, J. Typical problems in push-rod dilatometry analysis. *Epitoanyag-Journal of Silicate Based and Composite Materials* **65**, 11–14 (2013).

334. Giesche, H. Mercury porosimetry: A general (practical) overview. *Particle and Particle Systems Characterization* **23**, 9–19 (2006).

335. Hearn, N. & Hooton, R. D. Sample mass and dimension effects on mercury intrusion porosimetry results. *Cem Concr Res* **22**, 970–980 (1992).

336. Egerton, R. F. *Physical principles of electron microscopy*. *Materials Today* vol. 8 (2005).

337. Dunlap, M., & Adaskaveg, J. E. Introduction to the scanning electron microscope. *Microscopy and Microanalysis* **9**, 1556–1557 (1997).

338. Murad, E. Chapter 12.1 Mössbauer spectroscopy of clays and clay minerals. *Dev Clay Sci* **1**, 755–764 (2006).

339. Dyar, M. D., Agresti, D. G., Schaefer, M. W., Grant, C. A. & Sklute, E. C. Mössbauer spectroscopy of Earth and planetary materials. *Annu Rev Earth Planet Sci* **34**, 83–125 (2006).

340. D. Rancourt. Recoil Mössbauer Spectral Analysis Software. Preprint at (1988).

341. Rowden, E. *The firing of Bricks. Brick Development Association.* (1964).

342. George, B. *Crystal structures of clay minerals and their X-ray identification.Vol 5. the Mineralogical Society of Great Britain and Ireland*. (1982). doi:10.1098/rsta.1984.0025.

343. Kretz, R. Symbols for rock-forming minerals. *American Mineralogist* **68**, 277–279 (1983).

344. Udvardi, B. *et al.* Application of attenuated total reflectance Fourier transform infrared spectroscopy in the mineralogical study of a landslide area, Hungary. *Sediment Geol* **313**, 1–14 (2014).

345. Brick Development Assosiation. *Brick Sustainability Report 2021*. https://brick.org.uk/sustainability (2021).

346. Manoharan, C., Sutharsan, P., Dhanapandian, S. & Venkatachalapathy, R. Spectroscopic and thermal analysis of red clay for industrial applications from Tamilnadu, India. *J Mol Struct* **1027**, 99–103 (2012).

347. González-García, F., Romero-Acosta, V., García-Ramos, G. & González-Rodríguez, M. Firing transformations of mixtures of clays containing illite, kaolinite and calcium carbonate used by ornamental tile industries. *Appl Clay Sci* **5**, 361–375 (1990).

348. Jordán, M. M., Boix, A., Sanfeliu, T. & de La Fuente, C. Firing transformations of cretaceous clays used in the manufacturing of ceramic tiles. *Appl Clay Sci* **14**, 225–234 (1999).

349. Menezes, R. R. *et al.* Statistical design for recycling kaolin processing waste in the manufacturing of mullite-based ceramics. *Materials Research* **12**, 201–209 (2009).

350. Melhem, m. the effect of calcite additives on clay for ceramic tile manufactory. www.qualicer.org.

351. González, I. *et al.* A proposal for the formulation of high-quality ceramic "green" materials with traditional raw materials mixed with Al-clays. *Appl Clay Sci* **131**, 113–123 (2016).

352. Krakowiak, K. J., Lourenço, P. B. & Ulm, F. J. Multitechnique investigation of extruded clay brick microstructure. *Journal of the American Ceramic Society* **94**, 3012–3022 (2011).

353. Brick Development Association. The UK Clay Brickmaking Processing. (2017).

354. Traoré, K., Kabré, T. S. & Blanchart, P. Gehlenite and anorthite crystallisation from kaolinite and calcite mix. *Ceram Int* **29**, 377–383 (2003).

355. Ptáček, P., Opravil, T., Šoukal, F., Havlica, J. & Holešinský, R. Kinetics and mechanism of formation of gehlenite, Al-Si spinel and anorthite from the mixture of kaolinite and calcite. *Solid State Sci* **26**, 53–58 (2013).

356. Alarcon, O. E. & Pecanha, R. N. Effect of Carbonates on Firing Shrinkage and on Moisture Expansion of Porous Ceramic Tiles. 101–106.

357. Vasić, M. V., Mijatović, N. & Radojević, Z. Aplitic Granite Waste as Raw Material for the Production of Outdoor Ceramic Floor Tiles. *Materials* **15**, (2022).

358. Bazhenov, A. A., Miklushevskii, V. V., Vatulin, I. I., Kropacheva, E. N. & Bidylo, A. P. Study of the process of dissociation of lithium carbonate in the presence of aluminum powder. *Russian Journal of Non-Ferrous Metals* **51**, 44–48 (2010).

359. Gruver, R. M. Differential Thermal-Analysis Studies of Ceramic Materials: I, Characteristic Heat Effects of Some Carbonates. *Journal of the American Ceramic Society* **33**, 96–101 (1950).

360. Amaral, L. F. *et al.* Development of ceramic paver with ornamental rock waste. *Journal of Materials Research and Technology* **8**, 599–608 (2019).

361. Martirena, J. F., Day, R. L., Betancourt, D. & Diaz, Y. Improvement of Engineering Properties of Fired Clay Bricks Through the Addition of Calcite. *Test* 1–6.

362. Okada, K. *et al.* Effects of grinding and firing conditions on CaAl2Si2O8 phase formation by solid-state reaction of kaolinite with CaCO3. *Appl Clay Sci* **23**, 329–336 (2003).

363. Sikalidis, C. A., Zampetakis, Th. & Dagilas, C. The Effect of Magnesite Addition on the Properties and Production Process of Low Porosity Type Ceramics. *Grecian Magnesite* 0–8 (2003).

364. Chemani, H. To overcome the appearance of the efflorescences by magnesium carbonate addition in a mass for manufacture of bricks of construction. *AIP Conf Proc* **1315**, 289–294 (2010).

365. Li, J. G., Ikegami, T., Lee, J. H., Mori, T. & Yajima, Y. A wet-chemical process yielding reactive magnesium aluminate spinel (MgAl2O4) powder. *Ceram Int* **27**, 481–489 (2001).

366. Grubeša, I. N. *et al.* Influence of the size and type of pores on brick resistance to freeze-thaw cycles. *Materials* **13**, (2020).

367. Smith, A. S. Recycled Glass as a Brick Fluxing Agent. *Proceedings of Sustainable Waste Management and Recycling: Glass Waste* 149–165 (2004).

368. Katyal, N. K., Ahluwalia, S. C. & Parkash, R. Effect of barium on the formation of tricalcium silicate. *Cem Concr Res* **29**, 1857–1862 (1999).

369. Ersoy, B. *et al.* The effect of BaCO3 addition on the sintering behavior of lignite coal fly ash. *Fuel* **87**, 2563–2571 (2008).

370. Bouzidi, N., Bouzidi, A., Nunes, R. O. & Merabet, D. Study of the microstructure and mechanical properties of halloysite–kaolinite/BaCO 3 ceramic composites . *Clay Miner* **53**, 403–412 (2018).

371. Kwaambwa, H. M. Stability and phase separation behaviour of systems of particles in a medium with added polymer. *Water SA* **32**, 111–114 (2006).

372. Betz, G. C. Lithium Minerals and Compounds in Ceramics. *Journal of the American Ceramic Society* **21**, 189–191 (1938).

373. Martin, G., Rentsch, L., Höck, M. & Bertau, M. Lithium market research – global supply, future demand and price development. *Energy Storage Mater* **6**, 171–179 (2017).

374. Peng, L. & Qin, S. Sintering behavior and technological properties of low-temperature porcelain tiles prepared using a lithium ore and silica crucible waste. *Minerals* **9**, (2019).

375. Lemougna, P. N. *et al.* Recycling lithium mine tailings in the production of low temperature (700–900 °C) ceramics: Effect of ladle slag and sodium compounds on the processing and final properties. *Constr Build Mater* **221**, 332–344 (2019).

376. Mahmoudi, S., Srasra, E. & Zargouni, F. Composition and Ceramic Properties of Carbonate-Bearing: Illitic Clays from North-Eastern Tunisia. *Arab J Sci Eng* **39**, 5729–5737 (2014).

377. de La Casa, J. A. & Castro, E. Recycling of washed olive pomace ash for fired clay brick manufacturing. *Constr Build Mater* **61**, 320–326 (2014).

378. Faria, K. C. P., Gurgel, R. F. & Holanda, J. N. F. Recycling of sugarcane bagasse ash waste in the production of clay bricks. *J Environ Manage* **101**, 7–12 (2012).

379. Zamek_Jeff_Sodium_Carbonate_Vapor_Firing_1974_part1.pdf.

380. Wasanapiarnpong, T., Thueploy, A., Nilpairach, S. & Arayaphong, D. Treatment of scumming effects of pottery clay by sodium carbonate addition.

in *IOP Conference Series: Materials Science and Engineering* vol. 18 (Institute of Physics Publishing, 2011).

381. Kazmi, S. M. S., Abbas, S., Saleem, M. A., Munir, M. J. & Khitab, A. Manufacturing of sustainable clay bricks: Utilization of waste sugarcane bagasse and rice husk ashes. *Constr Build Mater* **120**, 29–41 (2016).

382. Falcone, R., Ceola, S., Daneo, A. & Maurina, S. The Role of Sulfur Compounds in Coloring and Melting Kinetics of Industrial Glass. *Rev Mineral Geochem* **73**, 113–141 (2011).

383. Sahar, M. R., Hamzah, K., Rohani, M. S., Samah, K. A. & Razi, M. M. The microstructural study of cullet-clay ceramics. *Phys Procedia* **22**, 125–129 (2011).

384. Njindam, O. R. *et al.* Effect of glass powder on the technological properties and microstructure of clay mixture for porcelain stoneware tiles manufacture. *Constr Build Mater* **170**, 512–519 (2018).

385. Loryuenyong, V., Panyachai, T., Kaewsimork, K. & Siritai, C. Effects of recycled glass substitution on the physical and mechanical properties of clay bricks. *Waste Management* **29**, 2717–2721 (2009).

386. Torres, P., Fernandes, H. R., Agathopoulos, S., Tulyaganov, D. U. & Ferreira, J. M. F. Incorporation of granite cutting sludge in industrial porcelain tile formulations. *J Eur Ceram Soc* **24**, 3177–3185 (2004).

387. El-Maghraby, H. F., El-Omla, M. M., Bondioli, F. & Naga, S. M. Granite as flux in stoneware tile manufacturing. *J Eur Ceram Soc* **31**, 2057–2063 (2011).

388. Torres, P., Fernandes, H. R., Agathopoulos, S., Tulyaganov, D. U. & Ferreira, J. M. F. Incorporation of granite cutting sludge in industrial porcelain tile formulations. *J Eur Ceram Soc* **24**, 3177–3185 (2004).

389. Menezes, R. R., Ferreira, H. C., Ferreira, H. S., Neves, G. A. & de L. Lira, H. Use of granite sawing wastes in the production of ceramic bricks and tiles. *J Eur Ceram Soc* **25**, 1149–1158 (2005).

390. Maria Catarina Menegucci Lougon α, C. T. D. B. A. σ & A. G. de S. G. Evaluation of the Effect of Natural Stone Processing Waste Incorporation on Red Ceramics Physical Properties London Journals Press. **19**, (2019).

391. Hojamberdiev, M., Eminov, A. & Xu, Y. Utilization of muscovite granite waste in the manufacture of ceramic tiles. *Ceram Int* **37**, 871–876 (2011).

392. Yap, Z. S., Khalid, N. H. A., Haron, Z., Mohamed, A. & Tahir, M. solutions. (2021).

393. Kizinievič, O., Balkevičius, V., Pranckevičiene, J. & Kizinievič, V. Investigation of the usage of centrifuging waste of mineral wool melt (CMWW), contaminated with phenol and formaldehyde, in manufacturing of ceramic products. *Waste Management* **34**, 1488–1494 (2014).

394. Cheng, A., Lin, W. T. & Huang, R. Application of rock wool waste in cement-based composites. *Mater Des* **32**, 636–642 (2011).

395. Fu, K., Wang, S., Wang, G. & Wang, Y. The effects of calcium oxide on fluorapatite crystal morphology and mechanical property of functional glass-ceramics. *Ceram Int* **44**, 20531–20538 (2018).

396. Gualtieri, A. F. *et al*. The thermal transformation of Man Made Vitreous Fibers (MMVF) and safe recycling as secondary raw materials (SRM). *J Hazard Mater* **162**, 1494–1506 (2009).

397. Chen, B., Wang, K., Chen, X. & Lu, A. Study of foam glass with high content of fly ash using calcium carbonate as foaming agent. *Mater Lett* **79**, 263–265 (2012).

398. Waclawska, I., Stoch, L., Paulik, J. & Paulik, F. Thermal decomposition of colemanite. *Thermochim Acta* **126**, 307–318 (1988).

399. Frost, R. L., Scholz, R., Ruan, X. & Lima, R. M. F. Thermal analysis and infrared emission spectroscopy of the borate mineral colemanite (CaB3O4(OH)3·H2O): Implications for thermal stability. *J Therm Anal Calorim* **124**, 131–135 (2016).

400. Micheal J Potters. *Feldspar and nepheline syenite*. (Minerals Yearbook 1 (1998): 3057, 1998).

401. Dollase, W. A., & Thomas, W. M. The crystal chemistry of silica-rich, alkali-deficient nepheline. *Contributions to Mineralogy and Petrology* **66(3)**, 311–318 (1978).

402. Salem, A., Jazayeri, S. H., Rastelli, E. & Timellini, G. Kinetic model for isothermal sintering of porcelain stoneware body in presence of nepheline syenite. *Thermochim Acta* **503–504**, 1–7 (2010).

403. Fluegel, A. Glass viscosity based on a glabal statistical modeling approach. *Glass Technology: European Journal of Glass Science Technology A* **48**, 13–30 (2007).

404. Azarov, G. M., Maiorova, E. v., Oborina, M. A. & Belyakov, A. v. Wollastonite raw materials and their applications (a review). *Glass and Ceramics* **52**, 237–240 (1995).

405. Vukovich, M. Effect of Wollastonite Substitutions in a Semivitreous Dinnerware Body. *Journal of the American Ceramic Society* **39**, 323–329 (1956).

406. Biasini, V. et al. Effect of talc and chlorite on sintering and technological behaviour of porcelain stoneware tiles. (2003).

407. Mukhopadhyay, T. K., Das, M., Ghosh, S., Chakrabarti, S. & Ghatak, S. Microstructure and thermo mechanical properties of a talc doped stoneware composition containing illitic clay. *Ceram Int* **29**, 587–597 (2003).

408. Njoya, D., Elimbi, A., Fouejio, D. & Hajjaji, M. Effects of two mixtures of kaolin-talc-bauxite and firing temperatures on the characteristics of cordierite-based ceramics. *Journal of Building Engineering* **8**, 99–106 (2016).

409. EM Sallam. Sallam, E. M. (1983). Effect of talc additions on The crystalline constituents and fired properties of alumina-porcelains. (1983).

410. Šveda, M. & Sokolář, R. The effect of firing temperature on the irreversible expansion, water absorption and pore structure of a brick body during freeze-thaw cycles. *Medziagotyra* **19**, 465–470 (2013).

411. Sveda, M., Kerestur, M., Sokolar, R., Nevrivova, L. & Uncik, S. Determination of suitable raw materials for preparation of frost resistant brick body and its evaluation according to pore size distribution. *Journal of the Ceramic Society of Japan* **123**, 868–873 (2015).

412. G.Fredrick, Jackson. The Oxidation of ceramic wares during firing III. The behaviour of calcium compounds in clays. 3–5 (1906).

413. PALMER, L. A. Vanadium and Molybdenum Compounds in Clays. *Journal of the American Ceramic Society* **12**, 37–47 (1929).

414. Gol, F. *et al.* Coloring effect of iron oxide content on ceramic glazes and their comparison with the similar waste containing materials. *Ceram Int* 1–9 (2021) doi:10.1016/j.ceramint.2021.10.001.

415. Berenblut, B. J., Dawson, P. & Wilkinson, G. R. A comparison of the Raman spectra of anhydrite (CaSO4) and gypsum (CaSO4).2H2O). *Spectrochim Acta A* **29**, 29–36 (1973).

416. Lenoir, M., Grandjean, A., Poissonnet, S. & Neuville, D. R. Quantitation of sulfate solubility in borosilicate glasses using Raman spectroscopy. *J Non Cryst Solids* **355**, 1468–1473 (2009).

417. Vaishnav, S., Hannon, A. C., Barney, E. R. & Bingham, P. A. Neutron Diffraction and Raman Studies of the Incorporation of Sulfate in Silicate Glasses. *Journal of Physical Chemistry C* **124**, 5409–5424 (2020).

418. McKeown, D. A., Muller, I. S., Gan, H., Pegg, I. L. & Kendziora, C. A. Raman studies of sulfur in borosilicate waste glasses: Sulfate environments. *J Non Cryst Solids* **288**, 191–199 (2001).

419. Buzgar Nicolae, Buzatu Andrei, S. I. V. The Raman Study on Certain Sulfates. (2009).

420. Schmid, T., Jungnickel, R. & Dariz, P. Insights into the CaSo4–H2O system: A raman-spectroscopic study. *Minerals* **10**, (2020).

421. de Faria, D. L. A. & Lopes, F. N. Heated goethite and natural hematite: Can Raman spectroscopy be used to differentiate them? *Vib Spectrosc* **45**, 117–121 (2007).

422. Devito, M. & Northrop, J. H. Drying and Decomposition of Sodium Carbonate. *Anal Chem* **30(5)**, 982–984 (1958).

423. Maritan, L., Nodari, L., Mazzoli, C., Milano, A. & Russo, U. Influence of firing conditions on ceramic products: Experimental study on clay rich in organic matter. *Appl Clay Sci* **31**, 1–15 (2006).

424. Valanciene, V., Siauciunas, R. & Baltusnikaite, J. The influence of mineralogical composition on the colour of clay body. *J Eur Ceram Soc* **30**, 1609–1617 (2010).

425. Menil, F. Systematic trends of the 57Fe Mössbauer isomer shifts in (FeOn) and (FeFn) polyhedra. Evidence of a new correlation between the isomer shift and the inductive effect of the competing bond T-X (→ Fe) (where X is O or F and T any element with a formal posit. *Journal of Physics and Chemistry of Solids* **46**, 763–789 (1985).

426. Lemine, O. M. *et al.* Rietveld analysis and Mössbauer spectroscopy studies of nanocrystalline hematite α-Fe2O3. *J Alloys Compd* **502**, 279–282 (2010).

427. W.B, J. Structural Iron in Smectites and in associated ancillary minerals. *Iron in Soils and Clay Minerals* 625–675 (1988) doi:10.1007/978-94-009-4007-9_17.

428. Jay, W. H. & Cashion, J. D. Raman spectroscopy of Limehouse porcelain sherds supported by Mössbauer spectroscopy and scanning electron microscopy. *Journal of Raman Spectroscopy* **44**, 1718–1732 (2013).

429. E. De Grave, J. V. & M. V. B. 57Fe Mössbauer spectroscopic analysis of chlorite. *Phys Chem Miner* **15**, 173–180 (1987).

430. Coey, J. M. D. Magnetic Properties of Iron in Soil Iron Oxides and Clay Minerals. *Iron in Soils and Clay Minerals* 397–466 (1988) doi:10.1007/978-94-009-4007-9_14.

431. Ncounr, D. G. R. Miissbauer spectroscopy of tetrahedral Fe3 * in trioctahedral micas-Reply. **78**, 669–671 (1993).

432. Dyar, M. D. Mössbauer spectroscopy of tetrahedral Fe3+ in trioctahedral micas—Discussion. *American Mineralogist*, 78(5–6), 665-668. (1993).

433. Murad, E. & Wagner, U. Pure and impure clays and their firing products. *Hyperfine Interact* **45**, 161–177 (1989).

434. Soro, N. *et al.* Role of iron in mullite formation from kaolins by Mössbauer spectroscopy and Rietveld refinement. *Journal of the American Ceramic Society* **86**, 129–134 (2003).

435. Hanzlicek, T. *et al.* Discoloration of fired kaolinitic clays (study of Fe3+ coordination by Mössbauer and UV-ViS-NIR spectroscopy). *Journal of the American Ceramic Society* **90**, 2843–2848 (2007).

436. Parmentier, J., Vilminot, S. & Dormann, J. L. Fe- and Cr-substituted mullites: Mössbauer spectroscopy and Rietveld structure refinement. *Solid State Sci* **1**, 257–265 (1999).

437. Vandenberghe, R. E., de Grave, E., de Geyter, G. & Landuydt, C. Characterization of goethite and hematite in a Tunisian soil profile by Mossbauer spectroscopy. *Clays Clay Miner* **34**, 275–280 (1986).

438. Ariskina, K. A., Mukhametzyanov, R. R., Salakhov, A. M., Vagizov, F. G. & Nikolaev, A. G. Study of ceramics color development on the basis of Nizhneuvelsky kaolin clay. *International Journal of Green Pharmacy* **12**, S716–S721 (2018).

439. D.C, Goodman. B. A. and B. Mossbeaur spectra of chlorite and their decomposition products. *The Macaulay Institute for Soil Research, Craigiebuckler, Aberdeen AB9 2QJ, (Scotland)* (1977).

440. Nodari, L., Marcuz, E., Maritan, L., Mazzoli, C. & Russo, U. Hematite nucleation and growth in the firing of carbonate-rich clay for pottery production. *J Eur Ceram Soc* **27**, 4665–4673 (2007).

441. de Bonis, A. *et al.* Different shades of red: The complexity of mineralogical and physico-chemical factors influencing the colour of ceramics. *Ceram Int* **43**, 8065–8074 (2017).

442. I.L., F. Mineralogy of ten British brick clays. *Clay Miner* **32**, 474–486.

443. Csáki, S. *et al.* AC conductivity of an illitic clay with zeolite addition after firing at different temperatures. *AIP Conf Proc* **1866**, (2017).

444. Earnest, C. M. The modern thermogravimetric approach to the compositional analysis of materials. In Compositional analysis by Thermogravimetry. *ASTM International* (1988).

445. Holdridge, B. D. A. Thermal expansion as a method for checkng thecomposition of ceramic clays and studying mineralogical changes during firing. 94–105 (1959).

446. Autors, A. & Gimeno, M. Reduction Of CO2 Emissions In Ceramic Tile Manufacture By Combining Energy-Saving Measures. (2014).

447. Fradette, R. J. Understanding Power Losses in Vacuum Furnaces. http://solaratm.com/uploads/2015/06/48_PowerLoss-5.pdf (2011).

448. *Sustainability Report 2020*. *Sustainability Report 2020* vol. 1 https://www.petronasgas.com/IR/Documents/3. Sustainability Report 2020.pdf%0Ahttps://wegreen.walisongo.ac.id/annual-report/ (2020).

449. Cultrone, G., Sidraba, I. & Sebastián, E. Mineralogical and physical characterization of the bricks used in the construction of the 'Triangul Bastion', Riga (Latvia). *Appl Clay Sci* **28**, 297–308 (2005).

450. García-Ten, J., Orts, M. J., Saburit, A. & Silva, G. Thermal conductivity of traditional ceramics: Part II: Influence of mineralogical composition. *Ceram Int* **36**, 2017–2024 (2010).

451. Peng, J., Zhao, Y., Jiao, L., Zheng, W. & Zeng, L. CO2 Emission Calculation and Reduction Options in Ceramic Tile Manufacture-The Foshan Case. *Energy Procedia* **16**, 467–476 (2012).

452. Carvalho M. de O. Madivate, Agostinho M. Malate, S. V. & Loubser, and M. Energy requirement for firing porcelain. **18**, 73–80 (2004).

453.https://www.google.co.uk/search?q=+is+to+kg+CO2+per+kWh+natural+gas&source=hp&ei=isQtY-7xJ7iFhbIP-oqomAk&iflsig=AJiK0e8AAAAAYy3SmlRPgoEklWgI30nlcli-8_JNCQa-&ved=0ahUKEwju3vLhkav6AhW4QkEAHXoFCpMQ4dUDCAk&uact=5&oq=+is+to+kg+CO2+per+kWh+natural+gas&gs_lcp=Cg.

454. Hu, P., Li, Y., Zhang, X., Guo, Z. & Zhang, P. CO2 emission from container glass in China, and emission reduction strategy analysis. *Carbon Manag* **9**, 303–310 (2018).